



Universitat Autònoma de Barcelona

**ADVERTIMENT.** L'accés als continguts d'aquesta tesi doctoral i la seva utilització ha de respectar els drets de la persona autora. Pot ser utilitzada per a consulta o estudi personal, així com en activitats o materials d'investigació i docència en els termes establerts a l'art. 32 del Text Refós de la Llei de Propietat Intel·lectual (RDL 1/1996). Per altres utilitzacions es requereix l'autorització prèvia i expressa de la persona autora. En qualsevol cas, en la utilització dels seus continguts caldrà indicar de forma clara el nom i cognoms de la persona autora i el títol de la tesi doctoral. No s'autoritza la seva reproducció o altres formes d'explotació efectuades amb finalitats de lucre ni la seva comunicació pública des d'un lloc aliè al servei TDX. Tampoc s'autoritza la presentació del seu contingut en una finestra o marc aliè a TDX (framing). Aquesta reserva de drets afecta tant als continguts de la tesi com als seus resums i índexs.

**ADVERTENCIA.** El acceso a los contenidos de esta tesis doctoral y su utilización debe respetar los derechos de la persona autora. Puede ser utilizada para consulta o estudio personal, así como en actividades o materiales de investigación y docencia en los términos establecidos en el art. 32 del Texto Refundido de la Ley de Propiedad Intelectual (RDL 1/1996). Para otros usos se requiere la autorización previa y expresa de la persona autora. En cualquier caso, en la utilización de sus contenidos se deberá indicar de forma clara el nombre y apellidos de la persona autora y el título de la tesis doctoral. No se autoriza su reproducción u otras formas de explotación efectuadas con fines lucrativos ni su comunicación pública desde un sitio ajeno al servicio TDR. Tampoco se autoriza la presentación de su contenido en una ventana o marco ajeno a TDR (framing). Esta reserva de derechos afecta tanto al contenido de la tesis como a sus resúmenes e índices.

**WARNING.** The access to the contents of this doctoral thesis and its use must respect the rights of the author. It can be used for reference or private study, as well as research and learning activities or materials in the terms established by the 32nd article of the Spanish Consolidated Copyright Act (RDL 1/1996). Express and previous authorization of the author is required for any other uses. In any case, when using its content, full name of the author and title of the thesis must be clearly indicated. Reproduction or other forms of for profit use or public communication from outside TDX service is not allowed. Presentation of its content in a window or frame external to TDX (framing) is not authorized either. These rights affect both the content of the thesis and its abstracts and indexes.



Universitat Autònoma  
de Barcelona

# Study of New Liposomes for the Delivery of Enzymes through Biological Membranes

Judit Tomsen Melero

Tesi Doctoral

Programa de Doctorat en Ciència dels Materials

Directores

Dr. Elisabet González Mira

Dr. Nora Ventosa Rull

Tutora

Dr. Nora Ventosa Rull

Departament de Física, Química i Geologia

Facultat de Ciències

2021

La present memòria es presenta per aspirar al Grau de Doctor per:

Judit Tomsen Melero

Vist i plau:

Dr. Elisabet González Mira

Dr. Nora Ventosa Rull

Bellaterra, maig de 2021



**ELISABET GONZÁLEZ MIRA**, Researcher of the Scientific Researcher of the Spanish Council of Research at the Institute of Materials Science of Barcelona (ICMAB-CSIC), and **NORA VENTOSA RULL** Scientific Researcher of the Spanish Council of Research at the Institute of Materials Science of Barcelona (ICMAB-CSIC),

CERTIFY:

That **Judit Tomsen Melero**, Master's degree in Biomedicine and Bachelor's Degree in Nanoscience and Nanotechnology, has performed, under their management, the research work entitled "**Study of new liposomes for the delivery of enzymes through biological membranes**". This work has been performed under the frame of the Materials Science Ph.D. program of the Physics and Chemistry Department of the Autonomous University of Barcelona.

And in witness whereof this is signed by

Directors

Dr. Elisabet González Mira

Dr. Nora Ventosa Rull

Bellaterra, May 2021





” *Have no fear of perfection; you'll never reach it.*

— Marie Curie



# Preamble

Great part of this PhD Thesis has been performed under the framework of collaborative projects. Therefore, besides the results obtained by the author, it has been decided to include some experiments obtained thanks to a collaborative effort of researchers belonging to other institutions, which complete and reinforce the work presented in this Thesis.





” *“Books! And cleverness! There are more important things –  
friendship and bravery...”*

— Harry Potter and the Philosopher’s Stone

## Agraïments

Per fi, amb la tesi quasi enllestida, a falta dels retocs finals, arriba un dels moments més macos de quan es completa una etapa: el de donar les gràcies. Perquè aquest camí no el recorrem soles, si no que són moltes les persones que el fan possible.

Primer de tot, m’agradaria començar donant les més sinceres gràcies a les meves dues directores de tesi, la Dr. Nora Ventosa i la Dr. Elisabet González. Nora, moltes gràcies per l’oportunitat de fer el doctorat amb vosaltres. T’estic molt agraïda per tota la confiança en mi que sempre m’has transmès, els consells i el gran treball científic que hem fet juntes. Eli, moltíssimes gràcies per ser-hi allà sempre, a les bones i a les dolentes. Em sento molt afortunada d’haver treballat amb tu tot aquest temps. Gràcies per la teva constància, amistat, professionalitat i responsabilitat cap al treball rigorós i ben fet. Durant aquests anys, les dues m’heu fet créixer com a científica i com a persona. Moltes gràcies per donar-me l’oportunitat de participar en projectes tan desafiants i estimulants com l’*Smart-4-Fabry*. Malgrat totes les dificultats, imprevistos, reptes, i algun que altre mal de cap, amb esforç i treball, juntes hem aconseguit arribar a fites que en un inici semblaven massa lluny. Gràcies!

Voldria expressar el meu agraïment al finançament rebut a través de la beca FI-AGAUR de la Generalitat de Catalunya i el Fons Social Europeu que m’ha permès realitzar aquesta tesi doctoral. Donar les gràcies també a en Jaume Veciana i a la Concepció Rovira per aquesta qualitat i bon ambient que han creat en el grup Nanomol.

Aquest treball de tants anys no hagués estat possible sense totes les científiques i científics amb les que he tingut la sort de col·laborar. Moltes gràcies Imma Ratera i Judith Guasch per aquesta col·laboració tan maca i constructiva, i sobretot un agraïment especial a en Xavi Rodríguez. Gràcies Xavi pel teu optimisme, per cuidar tan bé les cèl·lules i per compartir la bona sort que sempre t’acompanya quan fas els experiments!

M’agradaria seguir donant les gràcies a la Dr. Ibane Abasolo i al seu gran equip del VHIR. Marc, Vanessa, Natalia, Ibane, muchas gracias por todos los experimentos in vitro e in vivo que salen en esta tesis. Quiero agradecer también al Dr. Pepe Corchero toda su aportación y calidad trabajado con

proteínas así como por todas las medidas de cuantificación. Gràcies molt especials també a la Dr. Miriam Royo i al seu equip per tota la feinassa de síntesi i la sempre bona disposició a treballar plegades. Moltes gràcies Miriam, Edgar, Daniel i Kamil.

M'agradaria seguir donant les gràcies a la resta del consorci del projecte *Smart-4-Fabry*. Thank you very much for all the joined effort, the scientific discussions, and the hard work carried out during these last 4 years. I would like to specially thank to Dr. Thomas Birngruber and Thomas Kroath, from Joanneum Research, for all the studies related to the BBB. Thank you for accepting me for my stay abroad despite I could not enjoy it due to the COVID situation and thank you for the continuous collaboration. I would like to specially highlight the great collaboration with Prof. Dganit Danino group from Technion for the acquirement of such a nice cryoTEM images and with Prof. Jan Skov Pedersen group from Aarhus University for all the SAXS characterization. I would like to expand my gratitude to Dr. Hazel and her team for their professionalism and scientific work, as well as my thankfulness to the LeanBio team for all the work related to the production of GLA enzymes. Thank you also to the rest of the partners from the project, DDR, BioNanoNet, and Biopraxis.

Voldria agrair també al Servei de Microscopia de la UAB i als grans professionals que tenen, especialment a en Martí de Cabo i a l'Helena Montón. Mil gràcies Martí per totes les sessions de cryoTEM i per les imatges tan maques que hem aconseguit. Moltes gràcies Helena per aquestes sessions tan profitoses de confocal. Agrair també al servei Laboratori de Luminescència i Espectroscòpia de Biomolècules (LLEB) de la UAB, en especial a en Salvador Bartolomé. Gràcies també a la Pilar Tudela, de la Facultat de Biociències de la UAB, per deixar-me fer ús del vostre equip per realitzar les mesures d'osmolalitat. Gràcies a tot el personal del ICMA B que encara que molts cops des d'un segon pla feu possible totes les gestions. Gràcies especials a la Pietat i a la Sonia. I moltíssimes gràcies a la Carme Gimeno, una persona meravellosa que et cuida i et fa la vida més senzilla, sobretot quan hi ha tràmits, papers i burocràcia pel mig.

També voldria seguir donant les gràcies a totes aquelles persones que m'han donat un cop de mà sempre que ho he necessitat. David, per la destresa trobant i solucionant fugues. Ramon, no puc més que donar-te les gràcies per tota l'ajuda experimental, els ànims i tots els moments de lab compartits. Gràcies Aida, pel teu suport experimental sempre que ha calgut, tant en l'HPLC com en altres assajos. Moltes gràcies Judit M, Mariana, i Nathaly per la vostra ajuda, escalf i suport. I, com no, voldria agrair especialment a en Josep Merlo. Les paraules es queden curtes per donar-te les gràcies per tot el que hem compartit durant aquests anys. Mil gràcies per ser el meu company d'equip, amic i aliat, en aquest projecte tan desafiant. Els problemes són menys problemes si es comparteixen amb tu.

Voldria seguir agraint de manera especial a tota la família Nanomol Technologies. Gràcies Santi per donar-me l'oportunitat de formar part d'aquest grup on hi ha tanta qualitat, científica i personal, i a on m'he sentit integrada i valorada des del primer moment. Voldria seguir donant les gràcies també de

forma especial a l'Alba Córdoba per tot el suport i la implicació, i a l'Arnau G, Arnau G, Carla, Ivana, Josep, Lúdia, Lidia, Marta, Òscar, Teresa, per tots els bons moments dins i fora del laboratori.

També voldria destacar el bon ambient que sempre hi ha hagut al despatx. Nerea, Martí, Judit M, Carles, Albert, Jose, mil gràcies per fer el dia a dia més alegre, pels riures, i (sobretot) per guardar sempre xocolata en un calaix.

Finalment, aquesta tesi no hagués sigut la mateixa sense tota aquella gent que m'ha acompanyat dia a dia, fora i dins del laboratori. El doctorat és un camí llarg, empedregat, i amb trams de desnivell. La motxilla pesa, les botes fan mal i el cim molts cops es veu encara massa lluny. Guillem, David, Lúdia, Ramon, David, Francesc, Edu, Marta A, Albert R, Mario, Marc, Nerea, Xavi, Sara, Teresa, Adrián, Adri, Aida, Albert G, Àngel, Ari, Arnau G, Arnau G, Carla, Carles, Cristina, Fabião, Inés, Ivana, Jose, Josep, Judit M, Lamia, Lidia, Marc, Mariana, Mario, Marta A, Marta P, Miquel, Nathaly, Nerea, Òscar, Paula, Solène, Songbai, Sílvia, Simona, Toni, simplement gràcies. Gràcies per fer-me gaudir del camí i alleugerar-me la motxilla quan pesava massa. Tinc l'enorme sort d'haver coincidit en aquesta etapa amb persones meravelloses com vosaltres. Mil gràcies a totes!

I, com no podria ser d'altra manera, voldria agrair de tot cor a aquelles amb qui ens vam atrevir per primer cop a fer travessa juntes en aquest món de la ciència i la nanotecnologia. Bernat, Laura V, Albert, Unai, Laura A, Marc, Anna, Aina, Oriol. Espero seguir tenint la sort de compartir aquest viatge amb vosaltres durant molts anys més!

Després estan aquelles persones que podríem dir que són ja quasi de tota la vida, que saps que estan allà sempre pel que necessitis. Però sempre va bé recordar-ho: Laura, Andreu, gràcies.

I per acabar, voldria donar les gràcies a la meva família, als meus pares i a la meva germana Elia el seu constant suport i inesgotable confiança. Les paraules es queden curtes per expressar tot el que he après d'ells; a ser constant, forta i valenta.

I, ara sí, sembla que ja s'entreveu el cim.



# Abstract

Liposomes are lipid-based nanovesicles widely explored as nanocarriers for the transport of biomolecules or drugs of interest to the place of action and for the development of new nanomedicines. This Thesis is devoted to the study of liposomal systems functionalized with targeting-ligands, with the final goal to be used as nanocarriers of therapeutically active enzymes. The new liposomal formulations have been specifically investigated and developed for the effective transportation of  $\alpha$ -galactosidase A enzyme through cellular and blood brain membranes, and for the achievement of a new liposomal intravenous pharmaceutical product for the treatment of Fabry disease.

Fabry disease is a rare disease which belongs to the group of lysosomal storage disorders, currently without a definitive cure. It characterizes by the deficiency in  $\alpha$ -galactosidase (GLA) enzyme activity which results in the cellular accumulation of neutral glycosphingolipids (mainly Gb3) with multisystemic organ affection, such as kidneys, heart, and nervous system. The current treatment is the enzyme replacement therapy, in which free GLA recombinant protein is administered intravenously to patients. This treatment shows several drawbacks including poor biodistribution, low stability, limited efficacy, high immunogenicity, and low capacity to cross biological barriers, such as cell membranes and the blood-brain barrier. An attractive strategy to overcome these problems is the use of nanocarriers for encapsulating enzymes.

Nanoliposomes functionalized with RGD-peptide have already emerged as a good platform to protect and deliver GLA to endothelial cells. However, this initial GLA-nanoconjugate was still far from the preclinical testing. Several issues must be addressed for transforming this initial GLA-nanoformulation (or nanoGLA) into a pharmacological product. To achieve this transformation, a deep understanding and control of the nanoliposomal vehicle at the molecular and supramolecular level is unavoidable. In this Thesis, the relation between the physicochemical properties and biological behavior of targeted liposomes have been addressed, to get knowledge and gain control of liposomal systems for enzyme delivery, especially for the delivery of GLA enzyme for Fabry disease treatment.

Small and uniform nanoGLA liposomes, functionalized with targeting-peptides, were successfully prepared by DELOS-susp, showing high GLA entrapment efficiency, enhanced enzymatic activity, and superior

efficacy. NanoGLA formulation for the treatment of Fabry disease was successfully optimized with the required amount and quality to advance towards the preclinical evaluation in vivo. NanoGLA demonstrated superior efficacy compared to current treatment (Replagal®) and non-nanoformulated GLA in a Fabry KO mouse model in terms of higher reduction of Gb3 levels in all tested tissues, including brain. Further, the regulatory preclinical stage of development for this novel nanoGLA formulation was achieved for first time with GLP toxicity studies in rodent. Finally, alternative new ligand-targeted functionalized nanoliposomes prepared by the CO<sub>2</sub>-based DELOS-susp technology were explored for blood-brain barrier crossing applications.

In summary, the results achieved in this Thesis support the strong potential of targeted liposomal systems for nanomedicine and drug delivery application. The successful development and optimization of the nanoGLA product for improving the current enzymatic replacement therapy in Fabry disease especially contributes as an example of translational and interdisciplinary research.

# Content

Preamble.....	7
Agraïments .....	9
Abstract .....	13
Content .....	15
List of Abbreviations.....	21
1 Introduction .....	27
1.1. Introduction to Biotherapeutics .....	27
1.2. Routes for drug administration and distribution.....	29
1.3. Nanoparticles for Drug Delivery .....	30
1.3.1. Liposomes as molecular self-assembled structures for drug delivery .....	32
1.3.2. Other non-liposomal lipid-based types of vesicles.....	35
1.4. Methods for the preparation of vesicles .....	37
1.4.1. Preparation of vesicles by conventional methods.....	37
1.4.2. Preparation of vesicles by compressed fluid-based technologies.....	39
1.4.3. Preparation of nanovesicles by DELOS-susp.....	40
1.4.4. Purification by microfiltration using Tangential Flow Filtration .....	41
1.5. Lysosomal Storage Disorders and their treatment: Special focus on Fabry Disease.....	43
1.5.1. Fabry Disease .....	44
1.5.2. GLA-loaded nanoliposomes as drug delivery system for Fabry Disease.....	46
1.6. References .....	49
2 Objectives.....	56



3	Impact of chemical composition on nanostructure and biological activity of $\alpha$ -Galactosidase-loaded nanovesicles for Fabry disease treatment .....	57
3.1.	Introduction .....	57
3.1.1.	Increase of cationic character of the nanovesicles as strategy for improving entrapment efficiency and colloidal stability .....	58
3.2.	Impact of MKC on physicochemical characteristics of GLA-loaded nanovesicles .....	59
3.2.1.	Studying the impact of MKC addition on morphology and lamellarity of nanovesicles 66	
3.3.	Impact of MKC addition on the specific enzymatic activity of GLA .....	70
3.4.	In vitro efficacy and in vivo toxicological profile of HLP-GLA hybrid-liposomes.....	73
3.4.1.	In vitro efficacy and safety assays.....	73
3.4.2.	In vivo repeated dose toxicity assay with non-GLA hybrid-liposomes .....	76
3.5.	Summary and Conclusions .....	79
3.6.	References .....	81
4	Effect of modifying the liposomal surface on the intracellular delivery .....	85
4.1.	Importance of nanoparticle-cell interaction for cell uptake.....	85
4.2.	Impact of chol-PEG <sub>400</sub> -RGD density in liposomes' characteristics .....	88
4.2.1.	Quantification of membrane components .....	89
4.2.2.	Supramolecular physicochemical characterization .....	91
4.2.3.	Fluorescent labeling of liposomes for in vitro cell studies .....	94
4.3.	Impact of RGD density on liposomes surface in their interaction with integrin-expressing U2OS cells	98
4.4.	Summary and Conclusions .....	103
4.5.	References .....	105
5	Development of nanoGLA liposomes for Fabry disease treatment with the requirements for advancing towards a preclinical phase .....	107
5.1.	General development of pharmaceutical products .....	107
5.1.1.	Translation of GLA-loaded nanoliposomes to improve the treatment of Fabry disease 108	
5.2.	Towards an optimized nanoGLA suitable for preclinical testing.....	109

5.2.1.	Change of GLA protein model to GLAcmycHis for nanoGLA development .....	109
5.2.2.	Identification of the Critical Quality Attributes (CQA) of the nanoGLA product .....	111
5.2.3.	Increase of nanoGLA batch-size from small- to intermediate-lab plant .....	115
5.2.4.	Impact of formulation parameters of intermediate nanoGLA on CQA.....	117
5.2.5.	Concentration of nanoGLA formulation to be suitable for intravenous dosing .....	127
5.2.6.	Isosmolality adjustment of nanoGLA formulation.....	132
5.3.	Summary and Conclusions .....	150
5.4.	References .....	152
6	Preclinical evaluation of nanoGLA liposomes for Fabry disease treatment .....	157
6.1.	Introduction to preclinical efficacy and toxicology studies in drug development process.....	157
6.1.1.	Pharmacokinetics and Toxicokinetics .....	158
6.1.2.	Safety studies to evaluate toxicity .....	160
6.1.3.	Current state in nanoGLA drug development: milestones achieved to start the preclinical phase	163
6.2.	PK of GLA-free liposomes: MKC as a useful indicator of in vivo liposomal presence .....	164
6.3.	Selection of the final nanoGLA candidate for entering in the preclinical evaluation .....	166
6.3.1.	Substitution of GLAcmycHis protein for a new tag-free rh-GLA .....	166
6.3.2.	Evaluation of two nanoGLA candidates containing different RGD densities: nanoGLA <sub>3%RGD</sub> and nanoGLA <sub>6%RGD</sub> .....	167
6.3.3.	In vivo studies in a Fabry mouse model .....	174
6.3.4.	Implementation of HPLC quantification method for GLA quantification .....	181
6.4.	Preparation of large nanoGLA batches with high quality level for non-regulatory and early GLP regulatory in vivo testing.....	182
6.4.1.	First large batch production of nanoGLA and empty-liposomes .....	183
6.4.2.	Second large batch production of nanoGLA and empty-liposomes .....	189
6.4.3.	Chemical composition of both high batch productions .....	195
6.4.4.	Analysis of the reproducibility between both large-batch productions .....	197
6.4.5.	Aseptic-like processing, aliquoting, and generation of certificates of analysis.....	198
6.5.	Preclinical in vivo repeated dose efficacy in mice .....	200
6.6.	Pharmacokinetic profile in rat .....	203

6.7.	NanoGLA designed as Orphan Drug by the European Medicines Agency .....	206
6.8.	Toxicology studies.....	207
6.9.	Summary and Conclusions .....	208
6.10.	References .....	210
7	New targeted-liposomes for the transport across the Blood-Brain Barrier .....	213
7.1.	Intra-brain delivery of drugs: a real challenge for CNS disease treatment.....	213
7.1.1.	Structure of brain and blood-brain barrier.....	214
7.1.2.	Transport pathways for nutrient delivery at the BBB.....	215
7.1.3.	Nanocarriers as a strategy to enhance drug delivery to the brain .....	218
7.1.4.	Experimental methods to evaluate drug delivery across the BBB .....	219
7.2.	Evaluation of RGD-liposomes capability to cross the BBB.....	224
7.2.1.	PK of RGD-liposomes vehicle in plasma and cerebral ISF .....	224
7.3.	Development of alternative-ligand targeted-liposomes to enhance BBB crossing .....	226
7.3.1.	Incorporation of Alanine and T7 ligands into nanoliposomes .....	227
7.3.2.	In vivo evaluation of Alanine-liposomes and T7-liposomes.....	232
7.4.	Exploration of dual-targeted liposomes.....	238
7.5.	Cell viability of targeted liposomes in HeLa cells.....	239
7.6.	Optimization of ligand-targeted liposomes and in vitro hemocompatibility evaluation .....	240
7.7.	Summary and Conclusions .....	243
7.8.	References .....	245
8	General Conclusions.....	249
9	Experimental Methods .....	251
9.1.	Materials.....	251
9.2.	Preparation of nanovesicles by DELOS-susp.....	252
9.2.1.	Equipment at lab-scale .....	252
9.2.2.	Experimental procedure.....	255
9.2.3.	Formulations prepared by DELOS-susp .....	256
9.3.	Microfiltration by Tangential Flow Filtration .....	262
9.3.1.	Aseptic-like conditions.....	264

9.4.	Freeze-drying of nanovesicles .....	264
9.5.	Physicochemical characterization of nanovesicles .....	265
9.5.1.	Size, PDI, $\zeta$ -potential, and particle concentration .....	265
9.5.2.	pH measurements .....	267
9.5.3.	Osmolality measurements .....	267
9.5.4.	Quantification of membrane components .....	267
9.5.5.	Morphological analysis by cryoTEM .....	269
9.5.6.	Lamellarity determination by SAXS .....	270
9.5.7.	Theoretical number of GLA per vesicle .....	272
9.5.8.	Optical characterization of DiD-labeled liposomes .....	274
9.5.9.	Stability studies .....	274
9.6.	Synthesis and characterization of bioactive compounds .....	275
9.6.1.	Production of cholesterol-PEG <sub>n</sub> - derivatives .....	275
9.6.2.	Synthesis of GLAcm <sup>y</sup> His and rh-GLA enzymes .....	278
9.6.3.	Quantification of GLA and Entrapment Efficiency (EE%) calculation .....	281
9.7.	Biological activity of GLA .....	283
9.7.1.	Specific enzymatic activity .....	283
9.7.2.	In vitro enzymatic efficacy by Gb3 reduction in MAEC .....	284
9.8.	In vitro cell internalization of RGD-liposomes in U2OS cells .....	285
9.8.1.	Preparation of substrates: Cleaning and Fibronectin coating .....	285
9.8.2.	Cell culture, Seeding, and Immunostaining .....	285
9.8.3.	Confocal Imaging .....	286
9.9.	In vitro safety assays .....	287
9.9.1.	Cytotoxicity in HeLa and HMEC-1 .....	287
9.9.2.	Hemocompatibility .....	288
9.10.	In vivo studies in Fabry mouse model .....	289
9.10.1.	Single dose efficacy study and enzymatic activity biodistribution in tissue .....	289
9.10.2.	Repeated dose efficacy study .....	289
9.11.	Pharmacokinetics of nanoGLA and free rh-GLA in rat .....	289

9.12.	Preliminary toxicity of MKC-liposomes in mice .....	291
9.13.	Toxicology studies in rat .....	291
9.14.	BBB crossing studies.....	291
9.15.	Quantification of analytes in biological samples.....	292
9.15.1.	Quantification of MKC in plasma and cOFM samples by LC-MS .....	292
9.15.2.	Quantification of MKC from nanoGLA samples in PK study .....	294
9.15.3.	Quantification of GLA from nanoGLA samples in PK study .....	294
9.15.4.	Quantification of Gb3 levels in tissue samples by LC-HRMS.....	294
9.16.	Sterilization studies .....	295
9.16.1.	Gamma-radiation of nanovesicles .....	295
9.16.2.	Syringe filtration of nanovesicles.....	295
9.16.3.	NanoGLA aliquoting in sterile vials for preclinical studies .....	295
9.17.	Statistical analysis .....	295
9.17.1.	Design of experiments (DoE) and data processing .....	295
9.18.	Figures.....	296
9.19.	References .....	297
	Scientific Contributions.....	299
	Annex I – Sterilization study.....	I
	Annex II – CoA.....	IX
	Annex III – Scientific contributions .....	XV

# List of Abbreviations

<b>A</b>	<b>Å</b>	Angstrom
	<b>Abs</b>	Absorption
	<b>AcOH</b>	Acetic acid
	<b>ADA</b>	Anti-drug antibodies
	<b>ADME</b>	Absorption, distribution, metabolism, and excretion
	<b>Ala</b>	Alanine
	<b>API</b>	Active pharmaceutical ingredient
	<b>APTT</b>	Partial prothrombin time
	<b>atm</b>	Standard atmosphere pressure
	<b>AUC</b>	Area under the curve
<b>B</b>	<b>BBB</b>	Blood-brain barrier
	<b>BSA</b>	Bovine serum albumin
<b>C</b>	<b>C14 or C18</b>	14 or 18 carbon chain length
	<b>CA</b>	Cellulose acetate
	<b>CF</b>	Compressed fluids
	<b>CF</b>	Concentration factor
	<b>CHO</b>	Chinese hamster ovary
	<b>Chol</b>	Cholesterol
	<b>CIBER-BBN</b>	Centro de Investigación Biomédica en Red – Bioingeniería, Biomateriales y Nanomedicina
	<b>CL</b>	Clearance
	<b>CMA</b>	Critical material attributes
	<b>CNS</b>	Central nervous system
	<b>CO<sub>2</sub></b>	Carbon dioxide
	<b>CoA</b>	Certificate of analysis
	<b>cOFM</b>	Cerebral open flow microperfusion
	<b>Conc</b>	Concentrated sample by TFF
	<b>CPP</b>	Critical process parameters
	<b>CQA</b>	Critical Quality Attributes
	<b>c-RGDfK</b>	Cyclo pentapeptide Arginine-Glycine-Aspartic acid-D-phenylalanine-Lysine
	<b>CryoTEM</b>	Cryogenic transmission electron microscopy
	<b>CSF</b>	Cerebrospinal fluid
	<b>CSIC</b>	Consejo Superior de Investigaciones Científicas
	<b>CTAB</b>	Cetyltrimethylammonium bromide

<b>D</b>	<b>D</b>	Spacing between layers by SAXS
	<b>d.nm</b>	Diameter in nm
	<b>D5W</b>	Dextrose 5 % w/v
	<b>Da</b>	Dalton
	<b>DDS</b>	Drug delivery systems
	<b>DELOS</b>	Depressurization of an expanded organic solution
	<b>DELOS-susp</b>	Depressurization of an expanded organic solution-suspension
	<b>DFF</b>	Direct flow filtration
	<b>Diaf</b>	Diafiltrated sample by TFF
	<b>DiD</b>	1,1'-dioctadecyl-3,3,3',3'-tetramethylindodicarbocyanine perchlorate dye
	<b>DLS</b>	Dynamic light scattering
	<b>DMSO</b>	Dimethyl sulfoxide
	<b>DNA</b>	Deoxyribonucleic acid
	<b>DoE</b>	Design of experiments
	<b>DOX</b>	Doxorubicin
	<b>DPPC</b>	Dipalmitoylphosphatidylcholine
<b>E</b>	<b>e.g.</b>	For example
	<b>EA</b>	Specific enzymatic activity
	<b>ECM</b>	Extracellular matrix
	<b>ECS</b>	Brain extracellular space
	<b>EE%</b>	Enzyme entrapment efficiency
	<b>EGF</b>	Epidermal growth factor
	<b>ELS</b>	Electrophoretic light scattering
	<b>ELSD</b>	Evaporative light scattering detector
	<b>Em</b>	Emission
	<b>EMA</b>	European Medicines Agency
	<b>EPR</b>	Enhanced permeability and retention
	<b>ERT</b>	Enzyme replacement therapy
	<b>EtOH</b>	Ethanol
	<b>EU</b>	European Union
	<b>Exc</b>	Excitation
	<b>F</b>	<b>f</b>
<b><i>f<sub>single</sub></i></b>		Unilamellarity fraction by SAXS
<b>FA</b>		Formic acid
<b>FBS</b>		Fetal Bovine Serum
<b>FD</b>		Fabry disease
<b>FDA</b>		Food and Drug Administration
<b>FTO</b>		Freedom-to-operate
<b>G</b>		<b>Ga</b>
	<b>Gb3</b>	Globotriaosylceramide
	<b>GLA</b>	$\alpha$ -galactosidase A enzyme
	<b>Glc</b>	Glucose
	<b>GLP</b>	Good laboratory practices
	<b>Gly</b>	Glycine
	<b>GMP</b>	Good manufacturing practices
	<b>GT</b>	Gene therapy
	<b>GUV</b>	Giant unilamellar vesicles

<b>H</b>	<b>h</b>	Hours
	<b>His</b>	Histidine
	<b>His-tag</b>	Polyhistidine tag
	<b>HLP</b>	Hybrid liposomes
	<b>HMEC-1</b>	Human microvascular endothelial cells
	<b>h-MKC</b>	High concentration MKC
	<b>HPLC</b>	High performance liquid chromatography
	<b>HSCT</b>	Hematopoietic stem cell transplantation
<b>I</b>	<b>i</b>	Initial
	<b>i.e.</b>	That is
	<b>IBB</b>	Institut de Biotecnologia i de Biomedicina
	<b>ICAM</b>	Intercellular adhesion molecule
	<b>ICH</b>	International Council for Harmonisation of Technical Requirements for Pharmaceuticals for Human Use
	<b>ICMAB</b>	Institut de Ciència de Materials de Barcelona
	<b>ID</b>	Identification
	<b>Incub</b>	Incubation
	<b>Intrmed</b>	Intermediate samples after DELOS-susp
	<b>IQAC</b>	Institut de Química Avançada de Catalunya
	<b>ISF</b>	Interstitial fluid
	<b>ISTD</b>	Internal standard solution
	<b>IV</b>	Intravenous administration
	<b>K</b>	<b>KO</b>
<b>L</b>		Liposomes
<b>L</b>	<b>LB</b>	Buffer composed of mannitol, sodium phosphate monobasic monohydrated, and sodium phosphate dibasic heptahydrated
	<b>LC-MS</b>	Liquid chromatography-mass spectroscopy
	<b>I-MKC</b>	Low concentration MKC
	<b>LOQ</b>	Limit of quantification
	<b>LP</b>	Liposomes without MKC
	<b>LSD</b>	Lysosomal storage disorders
	<b>LUV</b>	Large unilamellar vesicles
	<b>M</b>	<b>M6P</b>
<b>MAEC</b>		Mouse aortic endothelial cells
<b>MeOH</b>		Methanol
<b>min</b>		Minutes
<b>miRNA</b>		MicroRNA
<b>MKC</b>		Miristalkonium chloride
<b>MLV</b>		Multilamellar vesicles
<b>MP</b>		Mobile phase
<b>mPES</b>		Polyethersulfone
<b>MPS</b>		Mucopolysaccharidoses
<b>MQ</b>		MKC-based quatsomes
<b>mRNA</b>		Messenger RNA
<b>MVV</b>		Multivesicular vesicles
<b>MW</b>		Molecular weight



<b>N</b>	<b>n</b>	Number of replicates	
	<b>N<sub>layer</sub></b>	Average number of layers by SAXS	
	<b>N<sub>2</sub></b>	Nitrogen	
	<b>NA</b>	Not applicable	
	<b>Naf</b>	Sodium fluorescein	
	<b>nanoGLA</b>	GLA-loaded liposomes	
	<b>NBD</b>	Nitrobenzoxadiazole fluorophore	
	<b>ND</b>	Not determined	
	<b>n.s.</b>	Not significant	
	<b>No</b>	Number	
	<b>NOAEL</b>	No observed adverse effect level	
	<b>NTA</b>	Nanoparticle tracking analysis	
	<b>O</b>	<b>Osm</b>	Osmolality
	<b>P</b>	<b>p</b>	statistical p-value
<b>Pa</b>		Pascal	
<b>PBS</b>		Phosphate-buffered saline	
<b>P<sub>c</sub></b>		Critical pressure	
<b>PCT</b>		Pharmacological chaperone therapy	
<b>PD</b>		Pharmacodynamics	
<b>PDI</b>		Polydispersity index	
<b>PEG</b>		Polyethylene glycol	
<b>PES</b>		Polyethersulfone	
<b>pI</b>		Isoelectric point	
<b>PK</b>		Pharmacokinetics	
<b>PT</b>		Prothrombin time	
<b>PVDF</b>		Polyvinylidene fluoride	
<b>P<sub>w</sub></b>		Working pressure	
<b>px</b>		pixel	
<b>Q</b>		<b>q</b>	modulus of scattering vector in SAXS
		<b>QbD</b>	Quality by Design
<b>R</b>	<b>RES</b>	Reticuloendothelial system	
	<b>RGD</b>	Tripeptide Arginine-Glycine-Aspartic acid	
	<b>rh</b>	Recombinant human	
	<b>RNA</b>	Ribonucleic acid	
	<b>ROI</b>	Region of interest	
	<b>RP</b>	Reversed-phase	
	<b>RT</b>	Room temperature	
<b>S</b>	<b>s</b>	Seconds	
	<b>S4F</b>	Smart-4-Fabry project	
	<b>SAXS</b>	Small-angle X-ray scattering	
	<b>SD</b>	Standard deviation	
	<b>SDS-PAGE</b>	Sodium dodecyl sulphate-polyacrylamide gel electrophoresis	
	<b>SEM</b>	Standard error of the mean	
	<b>SLC</b>	Solute carriers	
	<b>STR</b>	Substrate reduction therapy	

	<b>Suc</b>	Sucrose
	<b>SUV</b>	Small unilamellar vesicles
<b>T</b>	<b>T</b>	Bilayer thickness by SAXS
	<b>t<sub>1/2</sub></b>	Half-life
	<b>T7</b>	Septapeptide Histidine-Alanine-Isoleucine-Tyrosine-Proline-Arginine-Histidine
	<b>T<sub>c</sub></b>	Critical temperature
	<b>TFF</b>	Tangential flow filtration
	<b>TGX</b>	Tris-Glycine eXtended
	<b>Theor</b>	Theoretical
	<b>TJ</b>	Tight junctions
	<b>TK</b>	Toxicokinetics
	<b>TMC</b>	Trimethyl chitosan
	<b>TMP</b>	Transmembrane pressure
	<b>Tre</b>	Trehalose
	<b>TRL</b>	Technology readiness level
	<b>TSI</b>	Turbiscan stability index
	<b>TT</b>	Thrombin time
	<b>T<sub>w</sub></b>	Working temperature
<b>U</b>	<b>U2OS</b>	Human osteosarcoma cells
	<b>UAB</b>	Universitat Autònoma de Barcelona
	<b>UV-vis</b>	Ultraviolet-visible spectroscopy
<b>V</b>	<b>v/v</b>	Volume/volume
	<b>VHIR</b>	Vall Hebron Institut de Recerca
	<b>Vol.</b>	Volume
<b>W</b>	<b>w/o</b>	Water/oil
	<b>w/v</b>	Weight/volume
	<b>WT</b>	Wild-type
<b>X</b>	<b>X<sub>CO2</sub></b>	CO <sub>2</sub> molar fraction
<b>Z</b>	<b>ζ-pot</b>	ζ-potential
<b>#</b>	<b>λ</b>	Wavelength
	<b>χ<sup>2</sup></b>	Reduced weighted chi-square
	<b>%ID</b>	Percentage of injected dose
	<b>°C</b>	Celsius
	<b>4-MU</b>	4-methylumbelliferone
	<b>4-MUG</b>	4-methylumbelliferyl α-D-galactopyranoside



” Wonderful ideas cannot spring out of nothing. They build on a foundation of other ideas.

— Eleanor Duckworth

# 1

## Introduction

### 1.1. Introduction to Biotherapeutics

Pharmacology was initially considered as a sister concern to other medical fields such as physiology, pathology, and chemistry. However, pharmacology as an independent medical subject started at the middle of the 19<sup>th</sup> century. It was mainly due to the first discovery of potential drugs such as alkaloids (e.g. purified morphine from opium in 1805 by Friedrich Sertürner) and anesthetics (e.g., ether in 1846 by William Morton or chloroform in 1847 by James Simpson), as well as the discovery that it was possible to artificially synthesize organic molecules in the laboratory (synthesis of urea in 1828 by Friedrich Wöhler).<sup>1</sup>

According to World Health Organization (WHO) definition, *drug* can be defined as the active substance that is used or intended to be used to modify or explore physiological systems or pathological states for the benefit of the recipient, such as diagnosis, prevention, treatment, or cure of a disease.

Pharmacological drugs have evolved during the last decades. In early stages, classical pharmacology was based on the screening and discovery of new small molecule drugs. These compounds were generally synthesized or modified through chemical reactions between organic or/and inorganic compounds. Classical molecular drugs (e.g., aspirin, ibuprofen, etc.) have small size, and usually can be fully described in terms of their molecular structure and purity.<sup>2</sup> Although these discoveries supposed important advances in the pharmacology field, many conventional molecular drugs share several limitations, such as low selectivity, poor efficacy, and high toxicity due to off-target effects.

Besides, in the past three decades, biotherapeutics emerged as an improved strategy to overcome small molecule drug limitations thanks to advances in the biotechnology field. Biopharmaceuticals (also named biologics) are defined as therapeutic products derived from biological sources (e.g., microorganisms, plants, and animals) generally produced using biotechnological tools, including genetic engineering or hybridoma technique.<sup>3</sup> Biopharmaceutical drugs include biomolecules such as enzymes, vaccines, monoclonal antibodies, cytokines, hormones, recombinant blood products, hematopoietic growth factors, nucleic acid-based products (DNA and RNA), and gene- and cell-based therapeutics.<sup>3</sup> Unlike small molecular drugs, biologics tend to be larger and more structurally complex, often showing potentially higher specificity, efficacy, and better targeting ability with reduced side effects. They can act providing complex set of functions that cannot be mimicked by simple chemical compounds (Table 1.1).<sup>4,5</sup>

The first commercially approved biological drug was a recombinant protein therapeutic, the human insulin, approved in 1982 by the United States Food and Drug Administration (FDA) for the treatment of diabetes mellitus. This new recombinant protein therapeutic drug supposed a major advance of diabetes mellitus patients, since overcome the limitations of the existing treatment, based on the injection of insulin purified from bovine and porcine pancreas, with clear related issues, such cost and immunological reaction to animal insulin.<sup>4</sup>

**Table 1.1.** Major differences between small molecular drugs and biologics. Adapted from <sup>5-7</sup>.

	<b>Small molecules</b>	<b>Biologics</b>
<b>Size</b>	Low molecular weight (0.1 – 1 kDa)	High molecular weight (typically, 1 – 500 kDa)
<b>Structure</b>	Small, simple, well-defined	Large, complex, heterogenous
<b>Physicochemical properties and characterization</b>	Mostly well-defined	Complex (e.g., 3D conformation, stability, pots-translational modifications...)
<b>Manufacturing process</b>	Produced by predictable and precise chemical processes, identical copies in batches. Mostly process-independent	Living cell-based complex technology, batch to batch variation. Strongly process-dependent
<b>Stability</b>	Stable	Mostly unstable
<b>Mode of administration</b>	Usually amenable to ingestion	Usually requires injection or infusion
<b>Immunogenicity</b>	Mostly non-immunogenic	Immunogenic

## 1.2. Routes for drug administration and distribution

The accessibility of pharmaceutical drugs to reach their respective target site is strongly dependent on the route of administration used. Briefly, pharmaceutical drugs can be administered into the body using two types of administration routes: systemic, when drugs have the potential to reach the entire body, and local, when the effect of the drug is more localized (e.g., topical administration). In turn, systemic routes can be classified in enteral (oral, sublingual, and rectal) or parenteral (intravascular, intramuscular, subcutaneous, and inhalation) administration.

Apart from the route of administration, i.e., how the drug is given, the bioavailability of the drug is also a crucial factor for reaching its intended site of action in the body. The bioavailability is defined as the proportion of an administered drug that reaches the systemic circulation and is therefore available for distribution to the intended site of action. The rate at which a drug reaches its site of action depends on its adsorption, distribution, metabolism, and elimination profiles.

Intravenous administration (IV) shows the best bioavailability, since drugs are directly injected into blood circulation. The IV is the most rapid-acting route and drugs can be administered either in a bulk dose (bolus) or as a continuous infusion.<sup>1</sup> Besides, drugs administered by other extravascular routes, e.g., the oral route, first need to overcome an initial barrier to be absorbed into the bloodstream, showing notably less bioavailability. This process is named *first-pass metabolism*, and it is characterized by a first drug loss and subsequent reduction of its bioavailability, generally because of the passage of the drug through the gut and liver, which contain several metabolic enzymes, before reaching the systemic circulation (**Figure 1.1**). For small molecule drugs, absorption often occurs in the gastrointestinal tract after an oral administration, whereas biologics, in general, are poorly absorbed after an oral route due to a poor permeation across the gastrointestinal wall. Therefore, since biologics are generally more affected by the first-pass effect, they are usually administered intravenously.<sup>5</sup>

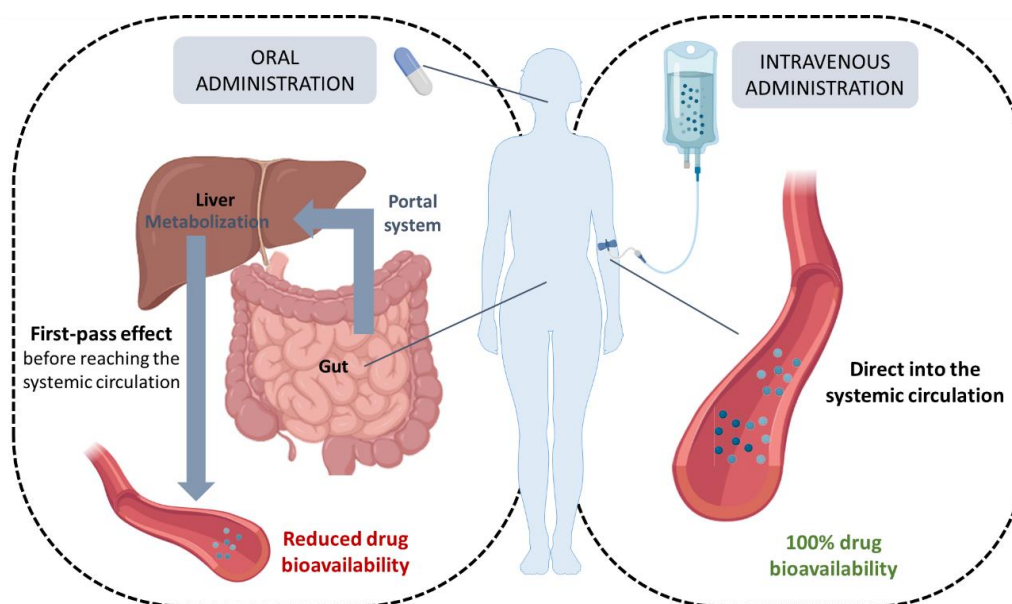


**Figure 1.1.** Differences in bioavailability of drugs administered by oral or intravenous route.

Once drugs have entered the systemic circulation, distribution varies depending on the nature of the drug, kinetics, and mechanism. The distribution of small molecule drugs tends to be modulated by diffusion, with uptake and/or efflux transporters expressed in certain tissues.<sup>8</sup> In contrast, the distribution of biotherapeutic drugs into tissues highly depends on their size, and can be mediated by convection from the vascular space into the interstitial tissue space through paracellular pores, or by an uptake enhanced by some receptor-mediated processes.<sup>8</sup>

The last process is the elimination of drugs from the body. Small molecules are usually eliminated by renal clearance (kidney filtration) and liver metabolism (by metabolic enzymes). Elimination of biotherapeutics strongly depends on its molecular weight and can be removed also by renal clearance (small biological drugs, < 60 kDa) or by catabolic endo-lysosomal pathway after cell uptake.<sup>5,8</sup>

### 1.3. Nanoparticles for Drug Delivery

Nowadays, drug therapy is continuously advancing toward a more precise delivery of biomolecules or drugs of interest, more specifically, the specific delivery of active pharmaceutical ingredient (API) to the intended site of action.<sup>9</sup> Nanotechnology applied in the biomedicine field has become a successful tool to achieve this goal, searching for the improvement of conventional drug therapies, specially introducing the concept of drug delivery systems (DDS). In DDS, the biomolecule or drug of interest is incorporated into a carrier (usually a nanocarrier, i.e., with sizes in the nanometric scale) and transported to the place of action. It can open the door to a great number of alternative strategies for drug transport and delivery, overcoming limiting factors of conventional drug application. Despite the considerable progress in recent years in the treatment of a large number of diseases (e.g., cancers, hematological

problems, immune diseases, metabolic diseases)<sup>3</sup>, a considerable number of constraints in conventional treatments are still present, such as a low sensitivity, limited specificity, poor biodistribution, drug toxicity, and severe side effects. For example, many therapeutic drugs present a narrow action window, in which the therapeutic dose (i.e., the quantity of drug required to produce the optimal effect) is not much lower than a toxic one. A change on the temporal and spatial biodistribution of the drug, e.g., using an appropriate DDS, can lead to a reduced toxicity and an improved efficacy.<sup>10</sup> Moreover, DDS can provide additional functions, such as protection from rapid degradation or clearance, improvement of drug's solubility, and enhancement of drug concentration in target tissues, requiring lower doses of drug.<sup>11</sup>

The most efficient route for DDS is by IV administration, since, as biologicals, DDS have a low permeation if they are administered through extravascular delivery (e.g., oral route). Once in circulation, nanocarriers can take advantage of both passive and active targeting. Passive mechanisms can include the accumulation of DDS to vascular tissue in presence of specific pathologies, e.g., as in the case of cancer tumors, mainly due to the enhanced permeability and retention effect (EPR). The EPR is based on an increased permeability in inflamed tissues or tumor environments, leading to the passive accumulation of small nanoparticles (< 150 nm) which are then able to cross these vessels and accumulate in the affected tissue.<sup>12,13</sup> Otherwise, active targeting can be achieved by the attachment of ligands or molecules (e.g., peptides, antibodies, nucleic acids, etc.) on the nanoparticle surface, with specific affinity for some cellular receptor. Recognition of these ligands by target cells or tissues, can show an enhanced uptake at sites of target expression. Finally, unlike small molecule or biological drugs, the predominant elimination route of DDS is clearance by the reticuloendothelial system (RES) of some tissues, such as the liver, spleen, bone marrow, and lung.<sup>5,10,14</sup> Phagocytic cells (e.g., macrophages) of these tissues can remove nanocarriers from circulation since they recognize DDS as foreign entities. Moreover, opsonization of the nanoparticles by serum proteins (e.g., antibodies and complement proteins) can enhance this process.<sup>5</sup>

A wide range of different types of delivery systems has been investigated as potential drug carriers for biomedical application. Nanocarriers can be classified based on different criteria, such as surface functionality, size, shape, or nanoparticle nature. However, nanoparticles are usually classified based on their composition (**Figure 1.2**), including: polymeric-based nanocarriers (e.g., polymeric nanoparticles, polymeric micelles, dendrimers, or nanogels), lipid-based nanoparticles (e.g., liposomes, non-liposomal vesicles, micelles, solid-lipid nanoparticles, or exosomes), protein-based nanoparticles (e.g., protein-complexes, or virus-like particles), but also inorganic-based nanocarriers (e.g., metallic, magnetic, and silica nanoparticles, quantum dots, or carbon nanotubes) or other types of materials such as metal-organic framework (MOF) composites.<sup>9,15,16</sup>



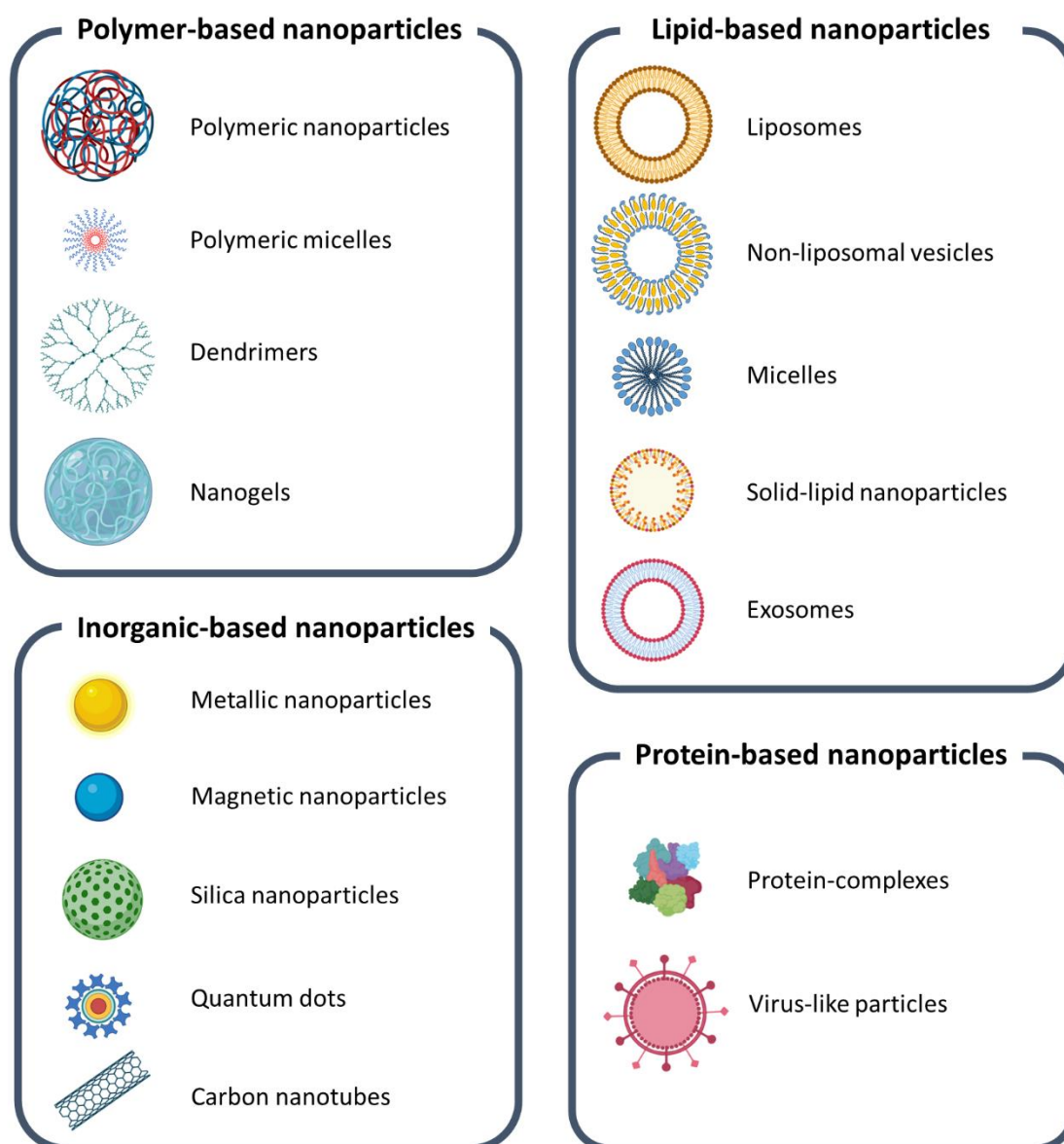


**Figure 1.2.** Schematic illustration of different nanoparticle-based carriers for drug delivery, classified depending on their composition. Adapted from Gu et al.<sup>15</sup>

### 1.3.1. Liposomes as molecular self-assembled structures for drug delivery

Among lipid-based nanovesicles, liposomes are one of the main promising carriers for nanomedicine applications. Liposomes were discovered by Alec Bangham in the 1960s, after observing that phospholipids in aqueous systems can form self-closed bilayered structures.<sup>17</sup> Liposomes have been extensively investigated, since from the very beginning they have shown excellent potential to become a pharmaceutical carrier due to good biocompatibility and biodegradability, and their great versatility in size, composition, surface properties, and capacity to entrap both hydrophilic and/or hydrophobic compounds.<sup>14</sup> The ability to entrap water-soluble pharmaceutical agents into their internal water cavity as well as water-insoluble pharmaceuticals into the membrane can overcome common issues in

conventional drug therapy, e.g., increasing drug solubilization, offering protection against degradation, decreasing nonspecific side-effects, or improving the selectivity to targeted cells and organs.<sup>14</sup>

As explained before, liposomes are spherical nanovesicles composed by amphiphilic molecules, predominantly phospholipids, that self-assemble in one or several concentric closed lipid bilayers. Amphiphilic molecules, like phospholipids, have a hydrophilic region (e.g., polar head group) and a hydrophobic section (e.g., non-polar tail) that can spontaneously organize into vesicles, exposing their polar groups towards the water phase and protecting the hydrophobic tails into the bilayer (**Figure 1.3**).<sup>18</sup>

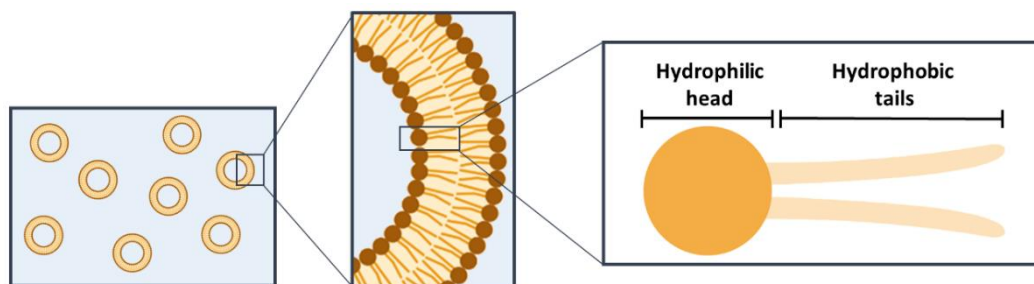


**Figure 1.3.** Scheme of an amphiphilic-like molecule, such as a phospholipid, and their self-organization in water forming vesicular structures.

Vesicles, and liposomes among them, can be classified according to their size and lamellarity (i.e., number of bilayers) (**Figure 1.4**).<sup>19</sup> Regarding size, vesicles can be small (< 200 nm), large (200–1000 nm), or giant (> 1000 nm), and regarding lamellarity they can be unilamellar (single bilayer) or multilamellar (several concentric bilayers). When several small vesicles are entrapped into a larger one, it is named multivesicular vesicles. Among all these types of vesicles, small unilamellar vesicles (SUVs) are particularly interesting for medical use. Liposomes with small size (usually in 100 – 200 nm range) are compatible with intravenous administration, are big enough to avoid rapid clearance through kidneys, and small enough to show a minimal uptake by the cells of the reticuloendothelial system (RES), leading to extended circulation time.<sup>19,20</sup>

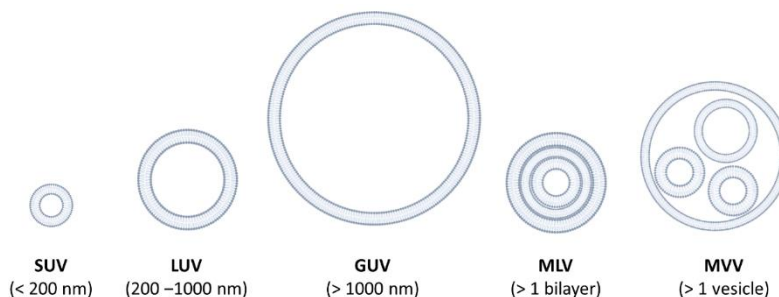


**Figure 1.4.** Schematic representation of vesicles classified regarding their size and lamellarity: SUV, small unilamellar vesicles; LUV, large unilamellar vesicles; GUV, giant unilamellar vesicles; MLV, multilamellar vesicles; and MVV, multivesicular vesicles. Adapted from Grimaldi et al.<sup>19</sup>

### 1.3.1.1. Evolution of liposomal structures for drug delivery

Liposomes for drug delivery have evolved from their discovery until the present (**Figure 1.5**). Early traditional plain liposomes composed exclusively of phospholipids with some water- or lipid-soluble drug lead to the “first-generation” of liposomes.<sup>14</sup> They showed some evident limitations, especially regarding stability and fast clearance from bloodstream. To improve the physical stability of liposomes, cholesterol was added as an additional membrane component. Cholesterol increases membrane rigidity, enhancing liposomal colloidal stability and decreasing membrane permeability. The presence of cholesterol induces a denser packing of phospholipids, preventing drug leakage.<sup>10,19</sup>

Additionally, other molecules, such as polyethylene glycol (PEG), can be anchored to membrane liposome components, e.g., cholesterol. Modification on the nature and ratio of phospholipids, addition of cholesterol, or additional decoration of the liposomal surface (e.g., with PEG) have a strong effect on physico-biochemical properties of liposomes and their *in vitro* and *in vivo* behavior, obtaining the “second-generation” of liposomes.<sup>18,21</sup> With the addition of PEG, “stealth” liposomes or “long-circulating” liposomes are obtained. PEG is a hydrophilic, inert, low immunogenicity, and biocompatible polymer widely used for the protection of nanoparticles and prolongation of the *in vivo* circulation time.<sup>22</sup> PEGylation of liposomes (i.e., coating the liposomal surface with PEG polymer) grants protection against recognition by opsonins, i.e., the adsorption of blood proteins to particle surface, and, therefore, subsequent clearance of liposomes from the bloodstream by the RES.<sup>14,23</sup> Currently, PEGylated liposomes are widely used in the majority of liposomes which have reached the clinical phase. However, the PEG coating of liposomal surface not only protects the nanoparticle, but can limit the cellular uptake and endosomal escape, reducing the final therapeutic effect.<sup>24</sup> Another strategy to overcome the difficulties of conventional liposomes is the use of stimuli-responsive liposomes, aiming to obtain a triggered drug release profile. A triggered chemical component sensitive to an external (e.g., heat, light, ultrasound, magnetic field) or internal (e.g., pH, enzymes) stimulus is incorporated to the liposome composition. Stimuli-responsive liposomes protect drug from degradation and unspecific delivery, and only release the compound of interest in response to the stimuli, that generally destabilize the liposomal membrane provoking the drug release.<sup>21</sup>

Moreover, “third-generation” or ligand-targeted liposomes combine several additional functionalities to produce higher and more selective therapeutic activity, by incorporating specific ligands to liposome surface.<sup>22</sup> Targeting moieties include peptides, receptor ligands, growth factors, glycoproteins, carbohydrates, monoclonal antibodies or fragments, and can be added directly to the nanoparticle surface or through a PEG molecule acting as a linker.<sup>14</sup> When ligand-targeted liposomes arrive at the target location, they interact by complementary affinity with the ligand receptor, increasing the drug accumulation in the targeted site.<sup>22</sup>

Finally, theranostic liposomes can be considered the “fourth-generation” of liposomes, referring to the approach of facilitating simultaneously the therapy and the diagnosis. These new and complex liposomes try to combine several additional functionalities, such as the delivery of a therapeutic agent by the encapsulation of a pharmaceutical drug, a site-specific targeting by the incorporation of a targeting ligand, and complementary bioimaging capability by the addition of an imaging agent.<sup>21</sup>

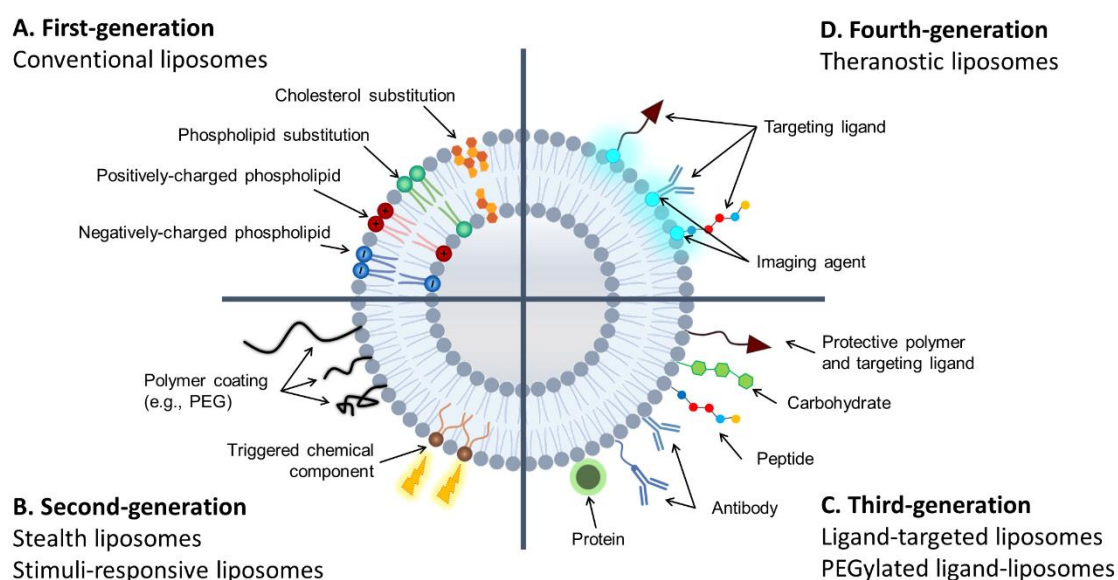


**Figure 1.5.** Schematic representation of the different generations of liposomes: (A) first-generation (conventional liposomes), (B) second-generation (stealth and stimuli-responsive liposomes), (C) third-generation (ligand-targeted liposomes), and (C) fourth-generation (theranostic liposomes). Adapted from Sercombe et al.<sup>25</sup>

Consequently, breakthrough developments in the area during the past decades have resulted in some approval nanomedicines. The first liposomal pharmaceutical product, Doxil<sup>®</sup>, was approved in 1995 by the US Food and Drug Administration (FDA). Doxil<sup>®</sup> consists of the entrapment of the doxorubicin chemotherapy drug in liposomes, for the treatment of ovarian cancer and AIDS-related Kaposi’s sarcoma. This nanomedicine was followed by other liposomal products that reach the market in following years. Currently, there are about 15 liposomal-based drugs approved for clinical use, and more than one hundred in various stages of clinical trials, representing more than 50% of the clinical trials involving nanoparticles.<sup>17,26,27</sup>

### 1.3.2. Other non-liposomal lipid-based types of vesicles

Despite the extended research development in the use of liposomes for drug delivery applications, other non-liposomal types of lipid-based nanovesicles have also emerged to try to overcome the limitations showed by liposomes. Non-liposomal lipid-based nanovesicles can be classified based on their

membrane components nature, where at least one of them is a natural and/or a synthetic lipid.<sup>19</sup> The main characteristics on each type of system are described in **Table 1.2**.

**Table 1.2.** Examples of non-liposomal lipid-based nanovesicles, compared to liposomes\* systems. Adapted from Grimaldi et al.<sup>19</sup>.

<b>Non-liposomal lipid-based nanovesicles</b>	<b>Main chemical composition</b>	<b>Description/Application</b>
<b>Liposomes*</b>	Phospholipids (and cholesterol)	Aqueous core enclosed by single or multiple concentric phospholipid bilayers.
<b>Niosomes</b>	Cholesterol Non-ionic surfactants	Use of surfactants, which are cheaper and more stable alternatives to phospholipids.
<b>Transfersomes</b>	Phospholipids Surfactants	Highly deformable and elastic systems used for enhanced transdermal delivery.
<b>Ethosomes</b>	Phospholipids Alcohols	Include high amount of alcohol, used for skin permeation and delivery.
<b>Sphingosomes</b>	Cholesterol Sphingolipids	Show better resistance to hydrolysis than liposomes as well as better drug retention.
<b>Ufasomes</b>	Fatty acids Surfactants	Improved stability, better drug entrapment efficiencies, cheaper and more available membrane components. Used for topical delivery.
<b>Pharmacosomes</b>	Phospholipids Drugs	Drugs are covalently bound to the phospholipid, increased entrapment efficiency without leakage.
<b>Virosomes</b>	Phospholipids Viral envelope proteins	Viral envelope proteins are integrated into liposomes to acquire fusogenic capacity.
<b>Quatsomes</b>	Cholesterol-derivatives Cationic surfactants	Constituted by quaternary ammonium surfactants and sterols in defined molar ratios.

### 1.3.2.1. Quatsomes

Quatsomes are non-liposomal lipid-based nanovesicles developed and extensively studied by Nanomol group (ICMAB-CSIC) during the last years. Quatsomes are composed by the association of ionic surfactants (generally cationic surfactants) with sterol derivatives (mostly cholesterol).<sup>28</sup> These vesicles have a great colloidal stability regarding size, morphology, and lamellarity.<sup>19</sup>

Quatsomes composed of the quaternary ammonium surfactant CTAB (cetyltrimethylammonium bromide) and cholesterol are thermodynamically stable,<sup>29</sup> and one of the most studied quatsomal systems.<sup>28-31</sup> Cholesterol in water forms crystals, whereas the CTAB in water self-assemble in micelles (**Figure 1.6**). However, both components placed together in water in an equimolar ratio self-assemble

forming small and high homogenous nanovesicles, named quatsomes. These nanovesicles showed attracting characteristics, such as high level of homogeneity in size and unilamellarity, they can be stable for several months and even years, and their morphology is maintained upon rising temperature or dilution.<sup>28,32,33</sup> Further studies by molecular dynamic simulations showed that both molecules, CTAB and cholesterol, self-assemble in a bimolecular synthon, that works as a single entity to form the nanovesicular membrane (**Figure 1.6**).

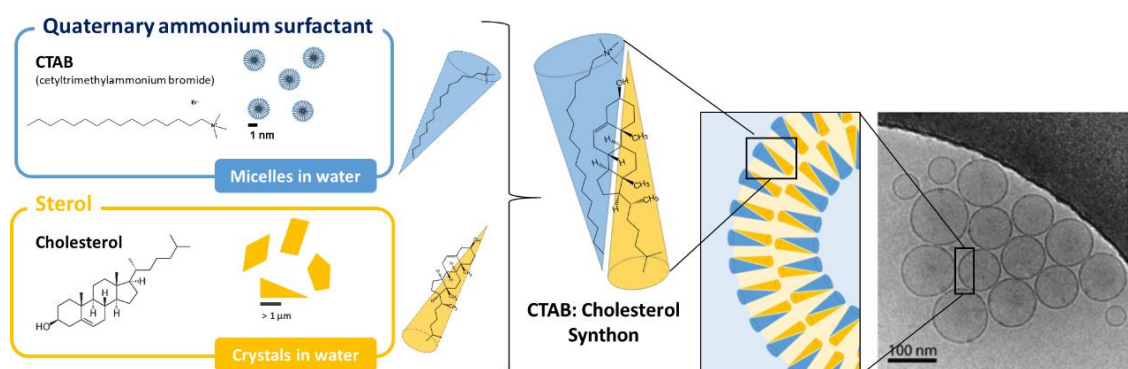


**Figure 1.6.** Schematic representation of quatsomes composed by CTAB and cholesterol. Both components self-assemble in equimolar ratio forming a synthon, which in turn is organized forming the membrane bilayer of a small nanovesicle. Adapted from Ferrer-Tasies et al.<sup>28</sup>.

Quatsomes are an attractive platform for entrapping both hydrophilic and hydrophobic compounds for pharmaceutical and bioimaging applications.<sup>34,35</sup> Quatsomes have been already applied for entrapping hydrophobic fluorescent dyes (e.g., carbocyanine, diketopyrrolopyrroles, and fluorenyl dyes),<sup>30,36–39</sup> small hydrophilic molecules (e.g. fluorescein), large biomolecules, such as rh-EGF (recombinant human-epidermal growth factor)<sup>40</sup> and BSA (bovine serum albumin) proteins,<sup>41,42</sup> and oligonucleotides, such as miRNA for gene therapy.<sup>43</sup>

## 1.4. Methods for the preparation of vesicles

The optimal performance of a formulation composed of supramolecular entities, such as vesicles, is completely related to their structural characteristics. Ensuring a strong control over the supramolecular structure is something of great importance. The shape, size, surface features, lamellarity, and homogeneity of supramolecular entities are structural parameters strongly influenced by the preparation method.

### 1.4.1. Preparation of vesicles by conventional methods

Nanocarriers are usually built following a bottom-up strategy, starting from their constituent units (macromolecules, molecules, atoms) by self-assembly procedures. Conventional methods to produce

nanocarriers (e.g., nanovesicles) tend to show difficulties in the well-control of the self-assembling of the molecules for constituting the system, leading to materials with high structural heterogeneity.<sup>10,44</sup> Some of the most used conventional techniques include thin-film hydration method (i.e. the dissolution of lipid components in organic solvents, the obtainment of a thin film by evaporation of the organic solvent, finally followed by a rehydration step of the thin film in an aqueous media), reverse-phase evaporation (i.e., the preparation of a w/o emulsion dissolving the lipid in water-immiscible solvent and further addition of an aqueous solution, followed by the organic solvent removal under vacuum), ethanol injection (i.e., the dissolution of lipids into an organic phase and next injecting the lipid solution into aqueous solution), and freeze-drying.<sup>44,45</sup> The poor homogeneity obtained by these techniques, especially in terms of size and lamellarity, can be improved by additional process steps, e.g., extrusion, sonication, and high-pressure homogenization, for achieving better vesicle-to-vesicle structural homogeneity (**Figure 1.7**).<sup>10</sup> These multi-step procedures are time-consuming, not easily scalable, and can increase the risk of losing or damaging the functionality of bioactive molecules.<sup>46</sup> Furthermore, some of these conventional procedures include an intermediate solvent-free state, e.g., film hydration methods, hindering to obtain stable cholesterol-based supramolecular vesicles due to the formation of cholesterol-rich domains.<sup>33</sup> Additionally, conventional methods are also limited due to their poor entrapment ability.<sup>47</sup> Moreover, these conventional methods tend to need large amount of organic solvents, with an associate toxic residue in many cases, that can be difficult to remove not only at lab scale but also at large scale production.<sup>46</sup>

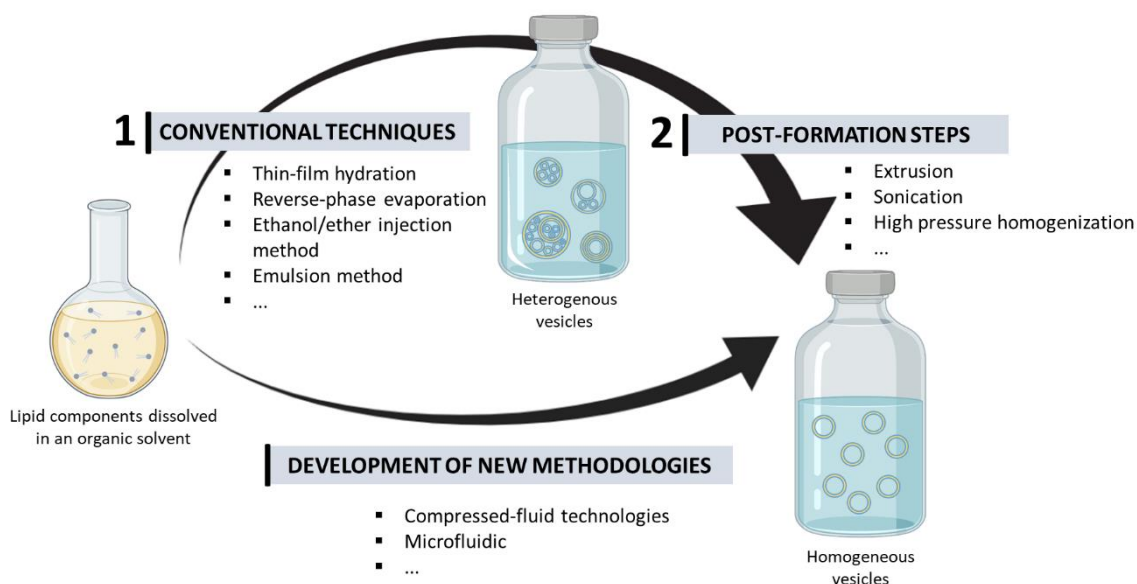


**Figure 1.7.** Different production methods to obtain homogeneous vesicles.

Consequently, the development of new methodologies for the processing and preparation of multi-molecular nanocarriers, with larger control of molecular self-assembling, and environmentally respectful become something of extreme interest. These new methodologies should allow the

preparation of supramolecular materials in a well-controlled process and the obtainment of systems with well-established characteristics.

#### 1.4.2. Preparation of vesicles by compressed fluid-based technologies

Compressed fluid-based preparation processes have been considered as an interesting alternative to conventional methods to produce vesicles. The use of compressed fluids (CF or also named dense gas) tends to overcome some of the concerns of conventional production methods, being less toxic, inert, economical, and more environmentally friendly.<sup>48</sup>

The term dense gas is generally used to refer to a substance in conditions surrounding its critical point. The supercritical region is one of the states of matter, where substances can share the best features of gases (i.e., low viscosity and high diffusivity) and liquids (high density and solvating power).<sup>48</sup> Thus, small changes in pressure or temperature can lead into significant impact on the density or solvent power of these compressed fluids, either in the liquid or supercritical state.<sup>44,49</sup> It has been proved that this special behavior starts to be observable at conditions below but near the critical point (named as subcritical region), which allows to work at milder conditions of pressure and temperature, reducing the costs related to work with elevated pressures. Among compressed-fluids, CO<sub>2</sub> is the most widely used dense gas, especially in the pharmaceutical industry. CO<sub>2</sub> is considered as safe solvent by the FDA, and their critical parameters ( $T_c = 31.1\text{ }^\circ\text{C}$ ,  $P_c = 72.8\text{ atm}$ ) (**Figure 1.8**) make it easily accessible.<sup>46,49</sup>

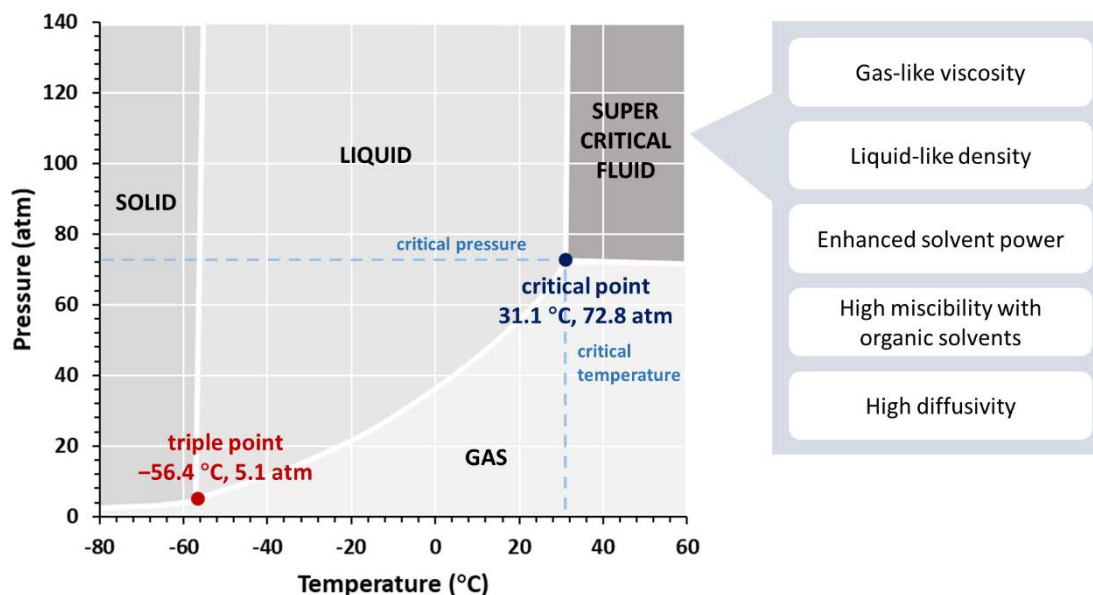


**Figure 1.8.** Phase diagram of carbon dioxide (CO<sub>2</sub>) and list of its properties in supercritical conditions. The critical point is defined by a critical temperature ( $T_c$ ) and a critical pressure ( $P_c$ ). Adapted from <sup>49,50</sup>.

Several CO<sub>2</sub>-based methodologies are currently implemented to produce drug delivery systems with better homogeneity regarding nanoparticle size distribution, decreased number of process steps, and



potential reduction of the amount of organic solvent required by conventional methods. Moreover, CF-based methodologies can provide sterile operating conditions and potential for transferring to larger scale productions.<sup>46,48</sup>

### 1.4.3. Preparation of nanovesicles by DELOS-susp

A new procedure based on the use of compressed CO<sub>2</sub> to produce micron and submicron-sized crystalline particles with high polymorphic purity was developed and patented by Nanomol group (ICMAB-CSIC) two decades ago, named depressurization of an expanded organic solution (DELOS).<sup>51,52</sup> In DELOS process, CO<sub>2</sub> acts as a completely miscible co-solvent at a given pressure and temperature conditions with an organic solution, that contains the solute of interest to be crystallized. When depressurized, this CO<sub>2</sub>-expanded organic solution experiences a fast, large, and extremely homogeneous cooling of the solution, due to the CO<sub>2</sub> evaporation from the solution. The homogeneous decrease of temperature over all the solution causes and homogeneous increase of the solution supersaturation and the straightforward production of crystalline material with small particle size and high polymorphic purity.<sup>52</sup> The requirements of DELOS process are milder than other compressed fluid-based methodologies ( $\leq 10$  MPa,  $\leq 35$  °C), allowing its use with heat-labile compounds as well as the cost is reduced.<sup>51,52</sup> Later on, a novel and improved procedure based on the DELOS process was developed for the preparation of colloidal suspensions, e.g., cholesterol-rich nanovesicles like liposomes or quatsomes. This new method, named Depressurization of an Expanded Organic Solution-Suspension (DELOS-susp) allows the one-step preparation of multifunctional cholesterol-rich nanovesicles, including the obtention of nanovesicles-bioactive conjugates.<sup>41,53-55</sup> In comparison to other nanovesicle processing techniques, DELOS-susp allows the preparation of nanovesicles with high batch-to-batch consistency and easy scalability, which are essential requirements for clinical translation.<sup>54,56</sup>

All the nanovesicles produced in this Thesis were prepared by DELOS-susp method, performed according to the following procedure, schematically represented in **Figure 1.9**. Briefly, the DELOS-susp procedure includes:

- (i) Loading of an organic solution (usually ethanol) containing hydrophobic membrane components (e.g., cholesterol, cholesterol-derivatives, phospholipids, etc.) into a high-pressure vessel at working temperature ( $T_w = 35$  °C) and atmospheric pressure.
- (ii) Addition of liquid compressed CO<sub>2</sub> and formation of a CO<sub>2</sub>-expanded solution with all the membrane components dissolved, at  $T_w = 35$  °C and working pressure,  $P_w = 10$  MPa; The expanded-system is kept for achieving a complete homogenization and to attain thermal equilibration.
- (iii) Depressurization of the CO<sub>2</sub>-expanded solution into an aqueous solution (usually water), which can contain water-soluble components and/or hydrophilic (bio)molecules. A flow of

nitrogen ( $N_2$ ) at working pressure  $P_w = 11$  MPa is used to plunge the  $CO_2$ -expanded solution from the reactor, maintaining a constant pressure inside the vessel during depressurization.

Similarly to the DELOS process, during the depressurization step, the expanded organic solution experiences a large, abrupt, and homogeneous decrease in temperature, produced by the change of state of the  $CO_2$  to gas. It could be one possible reason why this procedure provides more vesicle-to-vesicle homogeneity and supramolecular organization, compared to conventional procedures.<sup>32,41</sup>

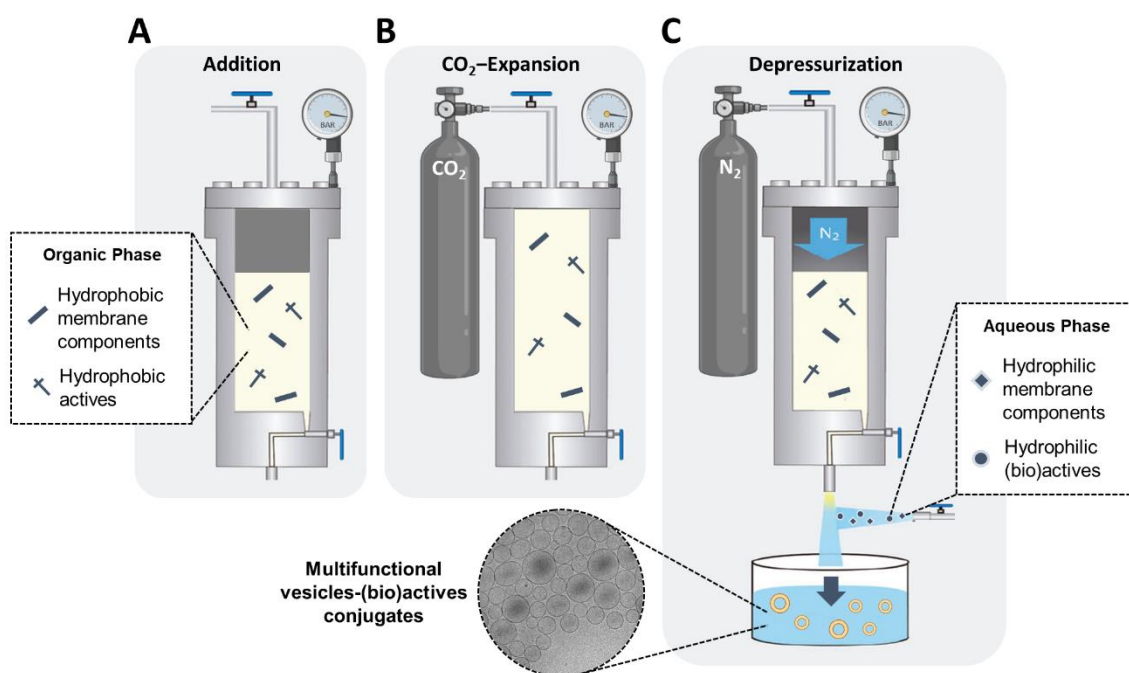


**Figure 1.9.** Schematic procedure of the preparation of nanovesicles by DELOS-susp technology, including: (A) addition of the membrane components dissolved in an organic solvent, (B) expansion of the solution by the addition of compressed  $CO_2$  acting as cosolvent, and (C) depressurization of the  $CO_2$ -expanded solution over an aqueous solution, which can contain hydrophilic (bio)molecules. More detailed explanations of DELOS-susp process can be found in the **Chapter 9.2**.

DELOS-susp has demonstrated to be a powerful tool for the preparation of a variety of nanovesicles that can be conjugated to (bio)molecules of interest, with high structural homogeneity and controlled process parameters that allows the potential translation of these new nanomedicines candidates.<sup>41</sup>

#### 1.4.4. Purification by microfiltration using Tangential Flow Filtration

After nanovesicles' production, a purification step is necessary to remove the non-incorporated components (i.e., free GLA, non-incorporated small molecules...), as well as the remained organic solvent (added during the preparation by DELOS-susp).

Microfiltration membranes, with pores sizes typically between 0.1 – 10  $\mu\text{m}$ , are widely used as separation technique to differentiate components based on size. Two main membrane filtration modes can be distinguished (**Figure 1.10**): (A) Direct Flow Filtration (DFF) or dead-end filtration, that applies the feed stream perpendicular to the membrane face and attempts to pass 100% of the fluid through the membrane, and (B) Tangential Flow Filtration (TFF) or crossflow filtration, where the feed stream passes parallel to the membrane face as one portion passes through the membrane (permeate) while the remainder (retentate) is recirculated back to the feed sample reservoir. TFF can be faster and more efficient than DFF for size separation, since the crossflow prevents buildup of molecules at the surface that can cause fouling, as well as prevents the rapid decline in flux rate seen in DFF, allowing a greater volume to be processed per unit area of membrane surface. For this reason, TFF has become a widely used technique for the separation of biomolecules in the biological field. Independently of the membrane filtration mode, the driving force for permeation is based on transmembrane pressure (TMP), related to the pressure difference between the feed and the permeate.

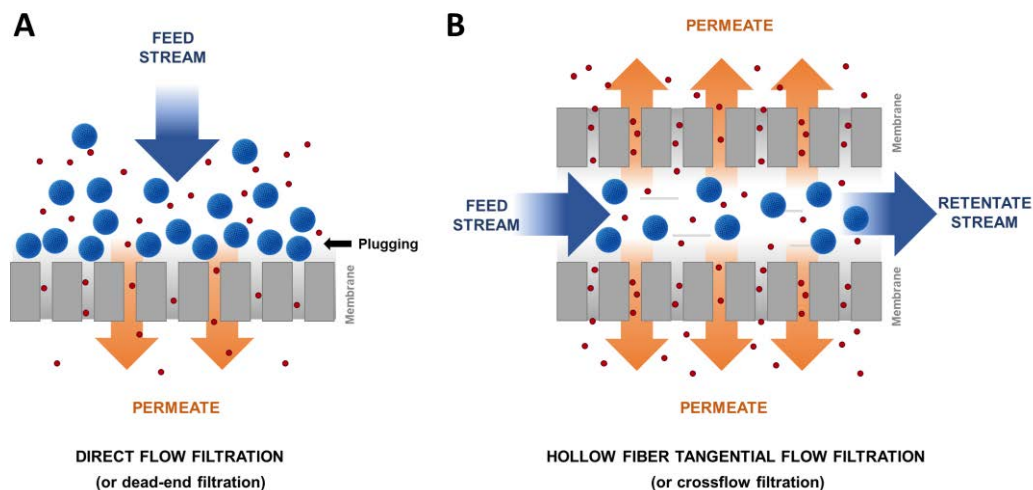


**Figure 1.10.** Differences of (A) direct flow filtration, and (B) tangential flow filtration.

In this thesis, the purification step after DELOS-susp production of nanovesicles was based on TFF (see **Chapter 9.3**). Three different operating modes were used, depending on the aimed objective:

- (i) **Diafiltration:** Purification step for removing components with a size below pore size, maintaining a constant sample volume; the eliminated volume through the permeate was immediately replaced by the same amount of volume from the buffer reservoir (usually water).
- (ii) **Buffer exchange:** Same concept than in the diafiltration mode, but here not only the samples were purified, but also the original media was replaced for the new one (placed in the buffer reservoir), always maintaining a constant sample volume.

- (iii) **Batch concentration:** Concentration step; when the material retained by the membrane contains the desired product, the sample was recirculated through the membrane and back to the sample reservoir without connecting the buffer reservoir. This allowed the sample to become more concentrated as volume was being removed. The degree of concentration (Concentration Factor, CF) corresponds to the initial volume ( $V_i$ ) divided into the final volume ( $V_f$ ),  $CF = V_i / V_f$ .

## 1.5. Lysosomal Storage Disorders and their treatment: Special focus on Fabry Disease

Lysosomal storage disorders (LSD) are a group of more than 50 diseases caused by a lysosomal dysfunction usually due to a deficiency of a single enzyme required for the metabolism of macromolecules, such as lipids, glycoproteins, or mucopolysaccharides, resulting in accumulation of the undegraded substrates.<sup>57,58</sup> The majority of LSD are characterized by a progressive course, usually resulting in severe disease manifestations and early death.<sup>57</sup> Individually, LSD are considered rare diseases, since their incidences are really low, less than 1: 100,000 of live births. However, overall as a group, its incidence has been estimated as 1: 7,000 – 1: 8,000, representing a serious global health problem.<sup>57</sup>

Lysosomes are generally spherical and membrane-limited subcellular organelles in eukaryotic cells, involved in multiple cellular processes specially related to the intracellular digestion and degradation of macromolecules, such as proteins, nucleic acids, glycosphingolipids, mucopolysaccharides, and glycogen, as well as other foreign substances.<sup>57,59</sup> Lysosomes contain more than two hundred lysosomal-resident proteins, and among them, around 60 are part of a mixture of acidic hydrolytic enzymes.<sup>60</sup> In LSD, lysosomal hydrolases are one of the most affected enzymes, resulting in an accumulation of specific substrates due to the inability to degrade them. Clinically, lysosomal diseases are generally classified according to the major storage compound. Thus, LSD includes mucopolysaccharidoses (MPS) (e.g., Hunter disease and Sanfilippo disease), sphingolipidoses (e.g., Fabry disease and Gaucher disease), oligosaccharidosis and glycoproteinoses, and glycogenosis (e.g., Pompe disease).<sup>61</sup>

Although there is not a definitive cure for LSD, several specific treatments have been developed to correct the metabolic defect and to reduce the pathophysiological effect of substrate accumulation into lysosome (**Figure 1.11**).<sup>62,63</sup> Among them, enzyme replacement therapy (ERT) is currently considered the standard treatment for several LSD, and consists of the exogenous administration of the deficient lysosomal enzyme. Substrate reduction therapy (STR) is based on reducing the accumulated substrate by the inhibition of an enzyme responsible of its synthesis. Another strategy is the pharmacological chaperone therapy (PCT), based on the use of small molecule drugs that improve the stability and activity of the defective enzyme, although is only useful for mutant enzyme proteins with residual

activity. Finally, other therapies that can allow constant delivery of a therapeutic protein to the whole body include hematopoietic stem cell transplantation (HSCT) and gene therapy, although the majority of gene therapy-based treatments are still in clinical trials.<sup>60,62,64</sup>

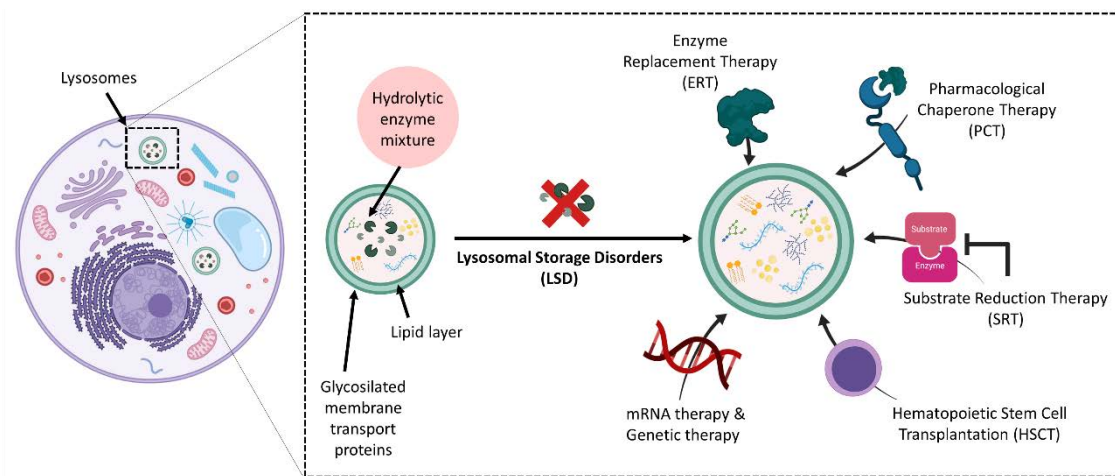


**Figure 1.11.** Therapeutic treatments for LSD, including enzyme replacement therapy (ERT), substrate reduction therapy (SRT), pharmacological chaperone therapy (PCT), hematopoietic stem cell transplantation (HSCT) and gene therapy (GT). Adapted from Leal et al.<sup>62</sup>

### 1.5.1. Fabry Disease

Fabry disease (FD) is an X-linked LSD disease caused by a deficiency or absence of the  $\alpha$ -galactosidase A (GLA) lysosomal enzyme, and whose incidence has been estimated at 1: 40,000 to 1: 117,000 live births.<sup>65</sup>

GLA is a glycosylated enzyme, produced in the endoplasmic reticulum, modified with mannose-6-phosphate recognition markers in the Golgi apparatus, packed into secretory vesicles, and delivered to the late endosomes/lysosomes.<sup>63,66,67</sup> Moreover, after their passage through Golgi apparatus, a variable fraction of the newly synthesized GLA can also be secreted from the cell and be endocytosed and transported to the lysosomes of neighboring cells, through plasma membrane located mannose-6-phosphate receptors.<sup>63</sup> Glycosylation is essential for GLA water-solubility, activity, stability, and correct transport to the lysosome.<sup>68</sup>

The missing GLA activity leads to the accumulation of its neutral glycosphingolipid substrates, mainly globotriaosylceramide (Gb3), within lysosomes of a wide variety of cell types including vascular endothelial cells, podocytes, cardiomyocytes, and nerve cells.<sup>65</sup> Endothelial cells are among the most affected cell types, playing an important role in the disease pathophysiology. Substrate accumulation in endothelial cells impairs multiple cellular activities such as energy metabolism, oxidative stress, and transport across ions channels. Early manifestations start in childhood and adolescence, including neuropathic pain, gastrointestinal symptoms, and skin injuries (e.g., angiokeratoma), followed by renal

disfunction, cardiac manifestations, and cerebrovascular events (e.g., ischemic attacks and stroke) in adulthood, leading to multi-organ pathologies and early death of untreated patients.<sup>65,69–71</sup>

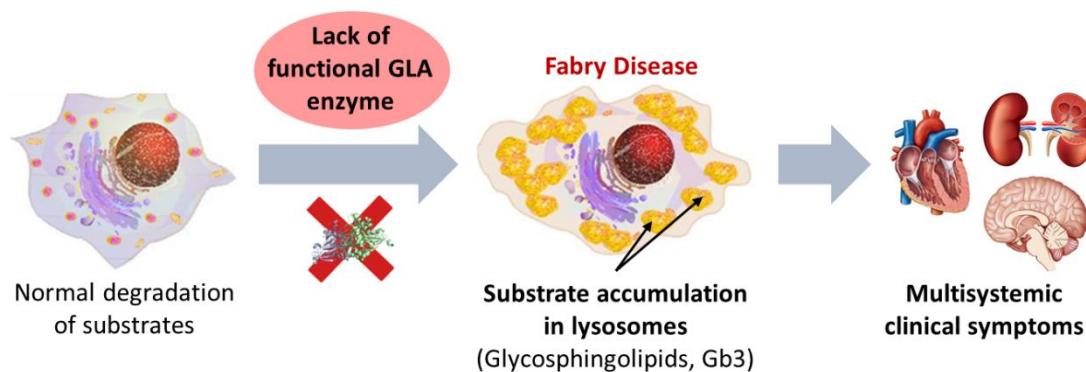


**Figure 1.12.** Fabry disease is characterized by a lack of  $\alpha$ -galactosidase A (GLA) activity which results in the accumulation of non-degraded glycosphingolipids, mainly globotriaosylceramide (Gb3) inside the lysosomes of the cells.

The principal treatment of Fabry patients is enzyme replacement therapy (ERT), which relies on the intravenous infusion of exogenous recombinant human GLA every other week.<sup>70,72</sup> Nowadays, there are two enzymes approved for ERT in FD: agalsidase beta (Fabrazyme<sup>®</sup>, Sanofi-Genzyme) produced in CHO (Chinese hamster ovary) cells, and agalsidase alfa (Replagal<sup>®</sup>, Shire-Takeda) produced in a lineage of human fibroblasts, administered at  $1 \text{ mg kg}^{-1}$  and  $0.2 \text{ mg kg}^{-1}$ , respectively. Both products contain recombinant human GLA with identical biochemical properties, showing only minor differences in glycosylation, composition, and mannose-6-phosphate receptor mediated cellular uptake, which can be mainly attributed to the difference in the used production cell line.<sup>70,73</sup>

Although both compounds reduce Gb3 accumulation in tissues,<sup>74,75</sup> neither treatment seems to completely reverse the disease, especially in advanced stages. Moreover, ERT showed several potential limitations: (i) limited efficacy, generally due to a poor biodistribution (liver sequestration) and the developing of anti-drug antibodies (ADA) with neutralizing effect; (ii) no crossing of the blood-brain barrier (BBB), complicating the treatment of brain affectation; (iii) low stability of the enzyme, resulting in rapid degradation and short circulation time; (iv) high immunogenicity issues, leading to infusion-associated reactions; and (v) inconvenience of lifelong therapy, requiring biweekly intravenous administration and resulting in expensive treatment costs.<sup>64,71,73</sup>

Additionally to these two ERT approved therapies (available since 2001), a pharmacological chaperone therapy, migalastat (Galafold<sup>®</sup>, Amicus Therapeutics), was recently approved (2016) only for Fabry patients with amenable mutations. Some non-classical patients show mutated enzymes with some residual activity but they are prematurely degraded.<sup>71</sup> Chaperones, as migalastat, are small molecules that can enhance enzyme folding, stability, and trafficking of the enzyme to the appropriate functional

site.<sup>76</sup> Migalastat shows several potential advantages, such as an oral administration, non-immunogenic response, and potential to cross the BBB, although it can be only profitable for patients with some residual enzymatic activity.

Therefore, several new strategies are currently under research, including new forms of ERT (pegunigalsidase alfa), substrate reduction therapy, mRNA therapy, and genetic therapy.<sup>73</sup> Pegunigalsidase alfa (PRX-102, Protalix Biotherapeutics) is currently being evaluated for efficacy in clinical trials (III phase). It is a chemically modified version of the GLA with attached chains of PEG, which has showed significant extension of the enzyme's half-life and lower generation of anti-drug antibodies (ADA).<sup>77</sup>

Novel formulations should protect the active biomolecules from degradation, reduce enzyme immunogenicity, enhance enzyme cellular internalization, and significantly improve the treatment efficacy.<sup>78,79</sup> This clearly indicates that there is still room to improve ERT formulations for treating Fabry disease, as well as other LSD.

### 1.5.2. GLA-loaded nanoliposomes as drug delivery system for Fabry Disease

One attractive strategy to improve an ERT formulation is to design a robust enzyme delivery nanoformulation. In the field of nanomedicine, biomolecules can be encapsulated in different types of delivery systems with the aim to improve the efficacy and reduce the adverse effects of the treatment.<sup>14,27,72</sup> For instance, targeted-polystyrene nanocarriers coated with antibodies against intercellular adhesion molecule 1 (anti-ICAM-1) and loaded with GLA have shown an enhanced enzymatic activity to organs as well as an improved targeting to endothelial cells, resulting in an efficient Gb3 degradation.<sup>80,81</sup> Another example of nanoparticles for GLA delivery are the ionically cross-linked polyelectrolyte complexes (PEC) composed of trimethyl chitosan (TMC) and GLA, with greater in vitro efficacy.<sup>64,82</sup>

Widely used nanocarriers are vesicular systems, especially liposomal systems, which in general have shown promising in vitro and in vivo results for drug delivery applications.<sup>13,53</sup> Nanomol group (ICMAB-CSIC), together with other CIBER-BBN teams, previously developed a liposomal nanovesicle system containing an in-house produced recombinant GLA (**Figure 1.13**),<sup>54,83</sup> in the frame of a synergic and multidisciplinary collaboration initially financed by CIBER-BBN (Centro de Investigación Biomédica en Red – Bioingeniería, Biomateriales y Nanomedicina, Spain) and further by Nanofabry project financed by *Marató de TV3* telethon.

This liposomal system (**LP**) was composed of the phospholipid DPPC (dipalmitoylphosphatidylcholine), cholesterol, and an RGD unit (tripeptide Arginine-Glycine-Aspartic acid) linked to the cholesterol moiety through a polyethylene glycol (PEG, 200 Da) chain (chol-PEG<sub>200</sub>-RGD).<sup>84</sup> The chol-PEG<sub>200</sub>-RGD compound was developed and synthesized by Dr. Miriam Royo group

from the IQAC-CSIC (Barcelona). Importantly, the cholesterol is bound to the PEG linker through an ether bond instead of a carbamate one, as it is generally done. Then, the RGD was coupled to this unit through a carbamate bond. The chol-PEG<sub>200</sub>-RGD conjugate was incorporated into the liposomes to favor the recognition of  $\alpha_v\beta_3$ -integrins, expressed in endothelial cells. Considering that injured endothelial cells overexpress  $\alpha_v\beta_3$ -integrins<sup>85</sup> and their levels are increased in kidneys of Fabry disease patients,<sup>86</sup> RGD-mediated internalization pathway is a promising alternative to the mannose-6-phosphate (M6P) one. Among the different types of RGD peptides available, the c-RGDfK (i.e., the cyclic pentapeptide Arginine-Glycine-Aspartic acid-D-phenylalanine-Lysine) was chosen to functionalize the nanoliposomes due to the advantages brought by its cyclic structure (e.g., improved selectivity and stability).<sup>87</sup> The incorporation of a chol-PEG<sub>200</sub>-RGD moiety within the nanoliposomes translated into a higher cellular uptake compared to the plain liposomes with the same membrane composition but without RGD, emphasizing the importance of incorporating this targeting unit.<sup>54</sup> The addition of this peptide did not alter the enzymatic activity of the GLA, but improved its delivery into lysosomes of target cells, since the incorporation of the RGD contributed to a significant enhancement of the cell functionality in comparison with the free drug.<sup>54</sup> Theoretical analysis with atomistic resolution of the interaction of the GLA protein with the liposomes pointed out that such enzymatic activity increase was caused by the enzyme-liposome association through electrostatic interactions, which oriented the enzyme in a “site-specific” manner in the lipid bilayer exposing its active site to the exterior aqueous phase.<sup>54</sup> Additionally, these vesicles were produced by compressed-CO<sub>2</sub> DELOS-susp technique, that as explained in the previous section, allows the preparation of nanovesicles with high batch-to-batch consistency and easy scalability, in comparison to other nanovesicle processing techniques, which are essential requirements for clinical translation.<sup>54,56</sup> The resulting RGD-liposomal platform is protected by several international patents.<sup>88,89</sup>

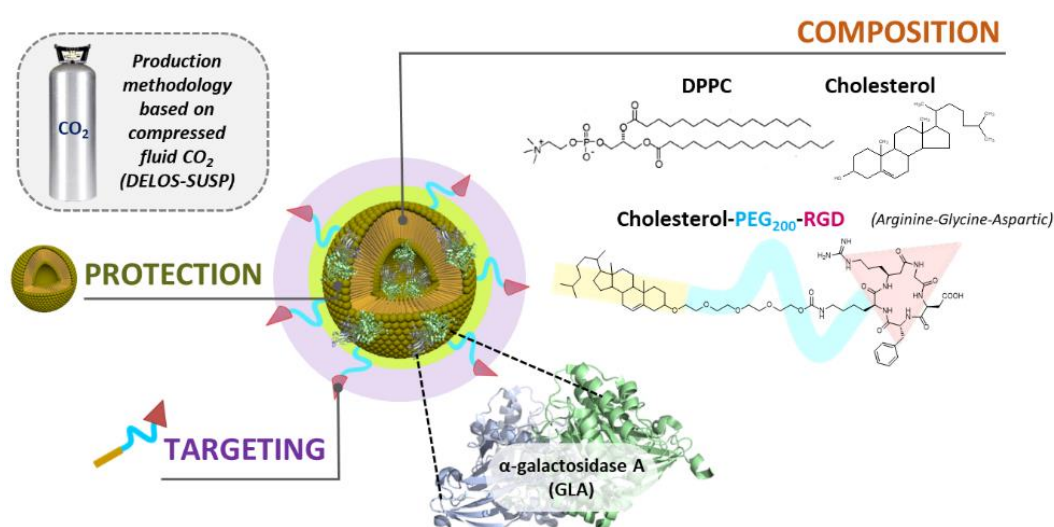


**Figure 1.13.** Peptide-targeted liposomal nanocarrier for the transport and delivery of the  $\alpha$ -galactosidase A (GLA) enzyme, initially developed in the frame of a synergic collaboration by CIBER-BBN.



Overall, DELOS-susp process has demonstrated its potential to prepare a variety of nanovesicle-biomolecule conjugates of great interest for the development of new nanomedicine candidates. Nanoliposomes functionalized with RGD-peptide emerged as a potential drug delivery platform for the protection and delivery of enzymes and open the door to further physicochemical and biological exploration. To highlight, initial results of these nanoliposomes to protect and deliver the GLA enzyme point out the potential of this strategy to improve the enzymatic replacement therapy of Fabry disease patients. However, this initial GLA-nanoconjugate was still far from the preclinical testing. Several issues must be addressed for transforming this initial GLA-nanoformulation into a pharmacological product. To achieve this transformation, a deep understanding and control of the nanoliposomal vehicle at the molecular and supramolecular level is unavoidable. In this Thesis, the relation between the physicochemical properties and biological behavior of targeted liposomes have been addressed, to get knowledge and gain control of liposomal systems for enzyme delivery, with special focus on the delivery of GLA enzyme for Fabry disease treatment.

## 1.6. References

1. Raj, G. M. *Introduction to Basics of Pharmacology and Toxicology. Introduction to Basics of Pharmacology and Toxicology* vol. 1 (Springer, 2019).
2. Crommelin, D. J. A. *et al.* Shifting paradigms: Biopharmaceuticals versus low molecular weight drugs. *Int. J. Pharm.* **266**, 3–16 (2003).
3. Zeb, A. *et al.* Potential and applications of nanocarriers for efficient delivery of biopharmaceuticals. *Pharmaceutics* vol. 12 (2020).
4. Leader, B., Baca, Q. J. & Golan, D. E. Protein therapeutics: A summary and pharmacological classification. *Nat. Rev. Drug Discov.* **7**, 21–39 (2008).
5. Glassman, P. M. & Muzykantov, V. R. Pharmacokinetic and pharmacodynamic properties of drug delivery systems. *J. Pharmacol. Exp. Ther.* **370**, 570–580 (2019).
6. Makurvet, F. D. Biologics vs. small molecules: Drug costs and patient access. *Med. Drug Discov.* **9**, 100075 (2021).
7. Wan, H. An overall comparison of small molecules and large biologics in ADME testing. *ADMET DMPK* **4**, 1–22 (2016).
8. Crommelin, D. J. A., Sindelar, R. D. & Meibohm, B. *Pharmaceutical biotechnology: Fundamentals and applications. Pharmaceutical Biotechnology: Fundamentals and Applications* (Springer, 2019). doi:10.1007/978-3-030-00710-2.
9. Aminu, N. *et al.* The influence of nanoparticulate drug delivery systems in drug therapy. *J. Drug Deliv. Sci. Technol.* **60**, 101961 (2020).
10. Bozzuto, G. & Molinari, A. Liposomes as nanomedical devices. *Int. J. Nanomedicine* **10**, 975–999 (2015).
11. Wilczewska, A. Z., Niemirowicz, K., Markiewicz, K. H. & Car, H. Nanoparticles as Drug Delivery Systems. *Pharmacol. Reports* **64**, 1020–1037 (2012).
12. Juskiewicz, K., Sikorski, A. F. & Czogalla, A. Building blocks to design liposomal delivery systems. *Int. J. Mol. Sci.* **21**, 1–22 (2020).
13. Yetisgin, A. A., Cetinel, S., Zuvin, M., Kosar, A. & Kutlu, O. *Therapeutic Nanoparticles and Their Targeted Delivery Applications. Molecules* (2020).
14. Torchilin, V. Recent Advances with Liposomes as Pharmaceutical Carriers. *Nat. Rev.* **4**, 145–160 (2005).

15. Gu, Z., Biswas, A., Zhao, M. & Tang, Y. Tailoring nanocarriers for intracellular protein delivery. *Chem. Soc. Rev.* **40**, 3638–3655 (2011).
16. Qin, X. *et al.* Rational Design of Nanocarriers for Intracellular Protein Delivery. *Adv. Mater.* **31**, 1–32 (2019).
17. Chang, H. I. & Yeh, M. K. Clinical development of liposome-based drugs: Formulation, characterization, and therapeutic efficacy. *Int. J. Nanomedicine* **7**, 49–60 (2012).
18. Inglut, C. T. *et al.* Immunological and toxicological considerations for the design of liposomes. *Nanomaterials* **10**, (2020).
19. Grimaldi, N. *et al.* Lipid-based Nanovesicles for Nanomedicine. *Chem. Soc. Rev.* **45**, 6520–6545 (2016).
20. Petros, R. A. & Desimone, J. M. Strategies in the design of nanoparticles for therapeutic applications. *Nat. Rev. Drug Discov.* **9**, 615–627 (2010).
21. Islam Shishir, M. R., Karim, N., Gowd, V., Zheng, X. & Chen, W. Liposomal delivery of natural product: A promising approach in health research. *Trends Food Sci. Technol.* **85**, 177–200 (2019).
22. Immordino, M. L., Dosio, F. & Cattell, L. Stealth liposomes: Review of the basic science, rationale, and clinical applications, existing and potential. *Int. J. Nanomedicine* **1**, 297–315 (2006).
23. Cattell, L., Ceruti, M. & Dosio, F. From conventional to stealth liposomes a new frontier in cancer chemotherapy. *Tumori* **89**, 237–249 (2003).
24. Nosova, A. S. *et al.* Diversity of PEGylation methods of liposomes and their influence on RNA delivery. *Medchemcomm* **10**, 369–377 (2019).
25. Sercombe, L. *et al.* Advances and challenges of liposome assisted drug delivery. *Front. Pharmacol.* **6**, 1–13 (2015).
26. Germain, M. *et al.* Delivering the power of nanomedicine to patients today. *J. Control. Release* **326**, 164–171 (2020).
27. Bulbake, U., Doppalapudi, S., Kommineni, N. & Khan, W. Liposomal Formulations in Clinical Use: An Updated Review. *Pharmaceutics* **9**, 1–33 (2017).
28. Ferrer-Tasies, L. *et al.* Quatsomes: Vesicles formed by self-assembly of sterols and quaternary ammonium surfactants. *Langmuir* **29**, 6519–6528 (2013).
29. Ferrer Tasies, L. P. Cholesterol and compressed CO<sub>2</sub>: a smart molecular building block and

- advantageous solvent to prepare stable self-assembled colloidal nanostructures. *TDX (Tesis Doctorals en Xarxa)* (2016).
30. Ardizzone, A. *et al.* Nanostructuring Lipophilic Dyes in Water Using Stable Vesicles, Quatsomes, as Scaffolds and Their Use as Probes for Bioimaging. *Small* **14**, 1–6 (2018).
  31. Gumí-Audenis, B. *et al.* Insights into the Structure and Nanomechanics of a Quatsome Membrane by Force Spectroscopy Measurements and Molecular Simulations. *Nanoscale* **10**, 23001–23011 (2018).
  32. Elizondo, E., Veciana, J. & Ventosa, N. Nanostructuring Molecular Materials as Particles and Vesicles for Drug Delivery, Using Compressed and Supercritical Fluids. *Nanomedicine* **7**, 1391–1408 (2012).
  33. Elizondo, E. *et al.* Influence of the preparation route on the supramolecular organization of lipids in a vesicular system. *J. Am. Chem. Soc.* **134**, 1918–1921 (2012).
  34. Vargas-Nadal, G. *et al.* MKC-Quatsomes: a Stable Nanovesicle Platform for Bio-imaging and Drug-Delivery Applications. *Nanomedicine Nanotechnology, Biol. Med.* **24**, 102136 (2020).
  35. Vargas Nadal, G. Novel Quatsome nanovesicles, prepared using CO<sub>2</sub>, for the development of advanced nanomedicines. (Universitat de Barcelona (UB), 2020).
  36. Ardizzone, A. New Fluorescent Nanovesicles, by Self-assembly of Organic Fluorophores, Sterols and Surfactants, as Probes for Bioimaging. (Universitat Autònoma de Barcelona (UAB), 2017).
  37. Morla-Folch, J. *et al.* Dye-Loaded Quatsomes Exhibiting FRET as Nanoprobes for Bioimaging. *ACS Appl. Mater. Interfaces* **12**, 20253–20262 (2020).
  38. Liu, X. *et al.* Fluorenyl-Loaded Quatsome Nanostructured Fluorescent Probes. *ACS Omega* **2**, 4112–4122 (2017).
  39. Ardizzone, A. *et al.* Highly stable and red-emitting nanovesicles incorporating lipophilic diketopyrrolopyrroles for cell imaging. *Chem. - A Eur. J.* **24**, 11386–11392 (2018).
  40. Ferrer-Tasies, L. *et al.* Recombinant human epidermal growth factor/quatsome nanoconjugates: A robust topical delivery system for complex wound healing. *Adv. Ther.* **2000260**, 1–14 (2021).
  41. Cabrera, I. *et al.* Multifunctional Nanovesicle-Bioactive Conjugates Prepared by a One-Step Scalable Method Using CO<sub>2</sub>-Expanded Solvents. *Nano Lett.* **13**, 3766–3774 (2013).
  42. Cabrera, I. Nanovesicle-bioactive conjugates to be used as nanomedicines, prepared by a one-step scalable method using CO<sub>2</sub>-expanded solvents. *Tesis doctoral* (Universitat Autònoma de

- Barcelona (UAB), 2013).
43. Ariadna, B. Quatsomes as a Novel Nanocarrier for Clinical Delivery of Small RNA. (Universitat Autònoma de Barcelona (UAB), 2019).
  44. Liu, G., Hou, S., Tong, P. & Li, J. Liposomes: Preparation, Characteristics, and Application Strategies in Analytical Chemistry. *Crit. Rev. Anal. Chem.* **0**, 1–21 (2020).
  45. Shah, S., Dhawan, V., Holm, R., Nagarsenker, M. S. & Perrie, Y. Liposomes: Advancements and innovation in the manufacturing process. *Adv. Drug Deliv. Rev.* **154–155**, 102–122 (2020).
  46. Meure, L. A., Foster, N. R. & Dehghani, F. Conventional and Dense Gas Techniques for the Production of Liposomes: A Review. *AAPS PharmSciTech* **9**, 798–809 (2008).
  47. Has, C. & Sunthar, P. A comprehensive review on recent preparation techniques of liposomes. *J. Liposome Res.* **30**, 336–365 (2020).
  48. Chakravarty, P., Famili, A., Nagapudi, K. & Al-Sayah, M. A. *Using supercritical fluid technology as a green alternative during the preparation of drug delivery systems. Pharmaceutics* vol. 11 (2019).
  49. William, B., Noémie, P., Brigitte, E. & Géraldine, P. Supercritical fluid methods: An alternative to conventional methods to prepare liposomes. *Chem. Eng. J.* **383**, (2020).
  50. Chemistry LibreText. Phase Diagrams. <https://chem.libretexts.org/@go/page/24249> (2020).
  51. Ventosa, N., Sala, S. & Veciana, J. DELOS process: A crystallization technique using compressed fluids - 1. Comparison to the GAS crystallization method. *J. Supercrit. Fluids* **26**, 33–45 (2003).
  52. Ventosa, N., Sala, S., Veciana, J., Torres, J. & Llibre, J. Depressurization of an Expanded Liquid Organic Solution (DELOS): A New Procedure for Obtaining Submicron- Or Micron-Sized Crystalline Particles. *Cryst. Growth Des.* **1**, 299–303 (2001).
  53. Cano-Sarabia, M. *et al.* Preparation of uniform rich cholesterol unilamellar nanovesicles using CO<sub>2</sub>-expanded solvents. *Langmuir* **24**, 2433–2437 (2008).
  54. Cabrera, I. *et al.*  $\alpha$ -Galactosidase-A Loaded-Nanoliposomes with Enhanced Enzymatic Activity and Intracellular Penetration. *Adv. Healthc. Mater.* **5**, 829–840 (2016).
  55. Ventosa, N., Veciana, J., Sala, S., Cano, M. & (Nanomol Technologies SL). Procedure for the Obtainment of Micro- and Nano-disperse Systems. *WO2006/079889*, (2005).
  56. Eaton, M. A. W. Improving the Translation in Europe of Nanomedicines (a.k.a. Drug Delivery) from Academia to Industry. *J. Control. Release* **164**, 370–371 (2012).

57. Nair, V., Belanger, E. C. & Veinot, J. P. Lysosomal storage disorders affecting the heart: a review. *Cardiovasc. Pathol.* **39**, 12–24 (2019).
58. Sun, A. Lysosomal storage disease overview. *Ann. Transl. Med.* **6**, 476–476. (2018).
59. Ratko, T., Marbella, A., Godfrey, S. & Aronson, N. Enzyme-Replacement Therapies for Lysosomal Storage Diseases. 107 (2013).
60. Parenti, G., Medina, D. L. & Ballabio, A. The rapidly evolving view of lysosomal storage diseases. *EMBO Mol. Med.* **13**, 1–21 (2021).
61. Ballabio, A. & Gieselmann, V. Lysosomal disorders: From storage to cellular damage. *Biochim. Biophys. Acta - Mol. Cell Res.* **1793**, 684–696 (2009).
62. Leal, A. F. *et al.* Lysosomal storage diseases: current therapies and future alternatives. *J. Mol. Med.* **98**, 931–946 (2020).
63. Beck, M. New Therapeutic Options for Lysosomal Storage Disorders: Enzyme Replacement, Small Molecules and gene Therapy. *Hum. Genet.* **121**, 1–22 (2007).
64. Abasolo, I. *et al.* Nanotechnology-based Approaches for Treating Lysosomal Storage Disorders, a Focus on Fabry Disease. *Wiley Interdiscip. Rev. Nanomedicine Nanobiotechnology* 1–18 (2020).
65. Zarate, Y. A. & Hopkin, R. J. Fabry's Disease. *Lancet* **372**, 1427–1435 (2008).
66. Kornfeld, S. & Mellman, I. The Biogenesis of Lysosomes. *Annu. Rev. Cell Biol.* **5**, 483–525 (1989).
67. Coutinho, M. F., Prata, M. J. & Alves, S. Mannose-6-phosphate Pathway: A Review on its Role in Lysosomal Function and Dysfunction. *Mol. Genet. Metab.* **105**, 542–550 (2012).
68. Ioannou, Y. A., Zeidner, K. M., Grace, M. E. & Desnick, R. J. Human  $\alpha$ -Galactosidase A: Glycosylation Site 3 is Essential for Enzyme Solubility. *Biochem. J.* **332**, 789–797 (2015).
69. Anastasakis, A., Papatheodorou, E. & Steriotis, A. Fabry Disease and Cardiovascular Involvement. *Curr. Pharm. Des.* **19**, 5997–6008 (2013).
70. Alipourfetrati, S., Saeed, A. & Norris, J. M. A Review of Current and Future Treatment Strategies for Fabry Disease : A Model for Treating Lysosomal Storage Diseases. *J Pharmacol Clin Toxicol* **3**, 1051 (2015).
71. Miller, J. J., Kanack, A. J. & Dahms, N. M. Progress in the understanding and treatment of Fabry disease. *Biochim. Biophys. Acta - Gen. Subj.* **1864**, 129437 (2020).

72. Solomon, M. & Muro, S. Lysosomal Enzyme Replacement Therapies: Historical Development, Clinical Outcomes, and Future Perspectives. *Adv. Drug Deliv. Rev.* **118**, 109–134 (2017).
73. Azevedo, O., Gago, M. F., Miltenberger-Miltenyi, G., Sousa, N. & Cunha, D. Review fabry disease therapy: State-of-the-art and current challenges. *Int. J. Mol. Sci.* **22**, 1–16 (2021).
74. Fervenza, F. C., Torra, R. & Warnock, D. G. Safety and Efficacy of Enzyme Replacement Therapy in the Nephropathy of Fabry Disease. *Biol. Targets Ther.* **2**, 823–843 (2008).
75. Siatskas, C. & Medin, J. A. Gene Therapy for Fabry Disease. *J. Inherit. Metab. Dis.* **24**, 25–41 (2001).
76. Felis, A., Whitlow, M., Kraus, A., Warnock, D. G. & Wallace, E. Current and Investigational Therapeutics for Fabry Disease. *Kidney Int. Reports* **5**, 407–413 (2020).
77. Schiffmann, R. *et al.* Pegunigalsidase Alfa, a Novel PEGylated Enzyme Replacement Therapy for Fabry Disease, Provides Sustained Plasma Concentrations and Favorable Pharmacodynamics: A 1-year Phase 1/2 Clinical Trial. *J. Inherit. Metab. Dis.* **42**, 534–544 (2019).
78. Ibraheem, D., Elaissari, A. & Fessi, H. Administration Strategies for Proteins and Peptides. *Int. J. Pharm.* **477**, 578–589 (2014).
79. Bosio, V. E., Islan, G. A., Martínez, Y. N., Durán, N. & Castro, G. R. Nanodevices for the Immobilization of Therapeutic Enzymes. *Crit. Rev. Biotechnol.* **36**, 447–464 (2016).
80. Hsu, J. *et al.* Enhanced Endothelial Delivery and Biochemical Effects of  $\alpha$ -Galactosidase by ICAM-1-Targeted Nanocarriers for Fabry Disease. *J. Control. Release* **149**, 323–331 (2011).
81. Hsu, J., Bhowmick, T., Burks, S. R., Kao, J. P. Y. & Muro, S. Enhancing biodistribution of therapeutic enzymes in vivo by modulating surface coating and concentration of ICAM-1-targeted nanocarriers. *J. Biomed. Nanotechnol.* **10**, 345–354 (2014).
82. Giannotti, M. I. *et al.* Highly Versatile Polyelectrolyte Complexes for Improving the Enzyme Replacement Therapy of Lysosomal Storage Disorders. *ACS Appl. Mater. Interfaces* **8**, 25741–25752 (2016).
83. Ventosa Rull, L. *et al.* Functionalised Liposomes Useful for the Release of Bioactive Compounds. *WO2014/001509*, (2012).
84. Cabrera, I. *et al.* Multifunctional Nanovesicle-Bioactive Conjugates Prepared by a One-Step Scalable Method Using CO<sub>2</sub>-Expanded Solvents. *Nano Lett.* **13**, 3766–3774 (2013).
85. Sajid, M. & Stouffer, G. A. The Role of  $\alpha v \beta 3$  Integrins in Vascular Healing. *Thromb. Haemost.*

- 87**, 187–193 (2002).
86. Utsumi, K., Sakuraba, H., Iino, Y. & Katayama, Y. Urinary Excretion of the Vitronectin Receptor (integrin  $\alpha\beta 3$ ) in Patients with Fabry Disease. *Clin. Exp. Nephrol.* **3**, 41–45 (1999).
87. Temming, K., Schiffelers, R. M., Molema, G. & Kok, R. J. RGD-based Strategies for Selective Delivery of Therapeutics and Imaging Agents to the Tumour Vasculature. *Drug Resist. Updat.* **8**, 381–402 (2005).
88. Ventosa Rull, L. *et al.* Functionalised Liposomes Useful for the Release of Bioactive Compound. (2012).
89. Ventosa, N. *et al.* Liposomes and its use for enzyme delivery. *EP 21382062.4-1112* (2021).



# 2

## Objectives

This Thesis is devoted to the study of liposomal systems functionalized with targeting-ligands, with the final goal to be used as nanomedicines. Translation from the laboratory to the clinical is a challenging road, and the present PhD Thesis is part of this effort.

In this frame, the following specific objectives have been pursued:

1. Study of GLA-loaded liposomes functionalized with an RGD peptide, named nanoGLA, at molecular and supramolecular level. Determination of the impact of their physicochemical properties, on their in vitro cell behavior, as well as on their in vivo performance.
2. Development and rational optimization of the nanoGLA with the appropriate physicochemical and biological characteristics to advance this nanoformulation from the experimental proof of concept to the pharmaceutical preclinical evaluation for Fabry disease treatment.
3. Exploration of new targeted-nanoliposomes able to cross the blood-brain barrier to be used as nanocarriers for brain delivery applications.

” *I am among those who think that science has great beauty.*

— Marie Curie

# 3

## Impact of chemical composition on nanostructure and biological activity of $\alpha$ -Galactosidase-loaded nanovesicles for Fabry disease treatment

### 3.1. Introduction

In this Chapter, it is described the testing performed to optimize the GLA-loaded targeted-liposomes initially developed in the Nanomol group (ICMAB-CSIC) in collaboration with CIBER-BBN and reported by Cabrera et al.<sup>1</sup> Continue development of these initial nanoformulation is essential to overcome its limitations and moving towards a future effective translation into a novel product of Fabry disease treatment.

In the initial GLA-loaded liposomal system (**LP-GLA**), the enzyme entrapment efficiency was around 40 % (i.e., the amount of GLA attached and/or contained inside nanoliposomes compared with the total amount of added GLA), resulting in an insufficient drug concentration for achieving in vivo therapeutic doses.<sup>1</sup> Accordingly, to continue with the preclinical development of the liposomal GLA system and guarantee the arrival of this innovative enzyme nanoformulation to the clinics, GLA entrapment, as well as the colloidal stability of the nanoformulation, had to be improved. A higher percentage of drug entrapment could potentially reduce the manufacturing cost and increase the GLA concentration in the final nanoformulation, allowing therefore for greater flexibility in dosing.<sup>2</sup> Additionally, a high enzyme

entrapment efficiency implies a reduced or null presence of free enzyme in the liposomal formulation which might induce unwanted destabilization phenomena, e.g., liposome aggregation and/or formation of enzyme aggregates. Both types of instabilities may contribute to the activation of the complement system in vivo that could, in turn, reduce the bioavailability of the nanomaterial<sup>3</sup> and induce hypersensitivity (allergic) reactions and anaphylaxis,<sup>4</sup> as previously shown for other types of liposomes.<sup>5,6</sup>

### 3.1.1. Increase of cationic character of the nanovesicles as strategy for improving entrapment efficiency and colloidal stability

In this first section, it was examined if an increase in the cationic character of the nanovesicles could promote a better electrostatic interaction with the negatively charged GLA at the pH in which the nanovesicles are self-assembled (**Figure 3.1A**). This would lead to higher enzyme entrapment as previously described for other proteins,<sup>7-9</sup> and enhanced colloidal stability of the nanoformulation. Indeed, human GLA, a homodimeric enzyme with a monomer weight of 48.8 kDa and one active site per monomer, is an unstable protein having a negative net charge close to neutral pH and a theoretical isoelectric point (pI) of 5.1.<sup>10</sup>

In this Chapter, two different RGD-targeted lipid-based nanovesicles for the intracellular delivery of GLA were explored: (i) non liposomal nanovesicles, known as quatsomes,<sup>11,12</sup> and (ii) liposomes with various concentrations of a cationic surfactant in their membrane, named here hybrid liposomes. Both systems contain the quaternary ammonium surfactant miristalkonium chloride (MKC) in high (> 50 mol % of the total membrane components, h-MKC) and low (< 5 mol % of the total membrane components, l-MKC) amounts, respectively, and they were produced using the DELOS-susp method based on the use of compressed CO<sub>2</sub>, described in detail in **Chapter 9**.<sup>13-15</sup>

MKC is the C14 homolog of a benzalkonium chloride. Surfactants of the benzalkonium chloride family are widely used as antimicrobial preservatives in many medicinal products with different administration routes. For example, they are found in approved parenteral formulations of corticosteroids (Celestone Soluspan, Schering-Plough) at a concentration of 0.02 % w/v, as well as in products for the enteral route that are used to ease the penetration of drugs, such as lorazepam.<sup>16,17</sup> In addition, as it was explained in **Chapter 1**, quatsomes with high MKC levels were shown to be stable for several years, keeping stability upon rising temperature and dilution and displaying high homogeneity in terms of nanovesicle size and lamellarity.<sup>18,19</sup> However, there are no studies on the impact of high MKC concentrations on the stability and activity of enzymes such as GLA.

Our objective was to compare h-MKC-based quatsomes (**MQ**), with hybrid liposomes (**HLP**) containing low MKC levels, as vehicles for GLA delivery. From a regulatory perspective, **HLP** could present an advantage over **MQ** since their formulations are closer to the well-studied **LP** and, additionally, because lower MKC concentrations will preclude future safety concerns.

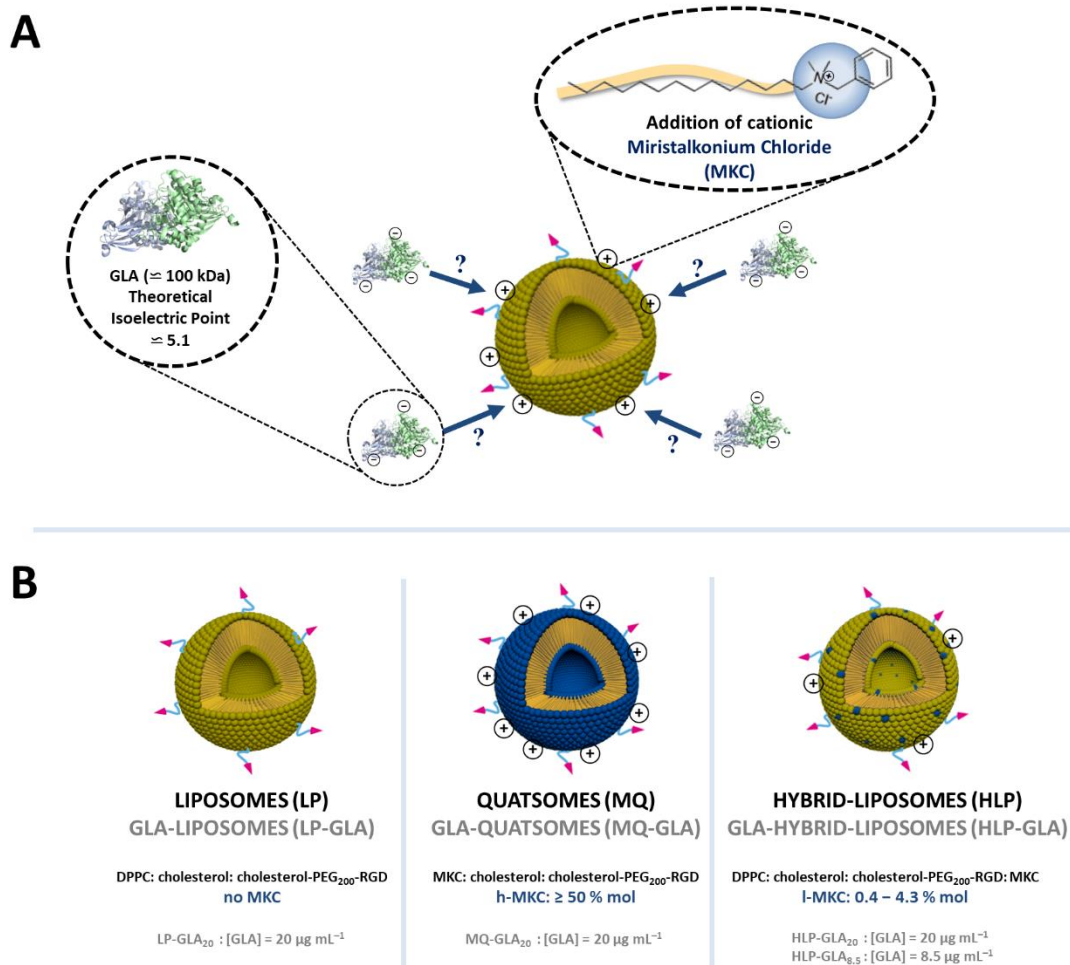


**Figure 3.1.** (A) Proposed strategy for increasing the GLA entrapment efficiency into nanovesicles, through the electrostatic interaction between the negatively charged GLA enzyme and the positively charged MKC-containing vesicle membranes; (B) Nomenclature and chemical composition of the different nanovesicle systems: liposomes, quatosomes, and hybrid liposomes, in which MKC is contributing in different ways for each system. Moreover, for each system, the blank prototype (without GLA) and the GLA-loaded version (with GLA) were produced. For hybrid-liposomes, two different GLA concentrations (i.e., 20 and 8.5  $\mu\text{g mL}^{-1}$ ) were tested, resulting in **HLP-GLA<sub>20</sub>** and **HLP-GLA<sub>8.5</sub>**, respectively.

### 3.2. Impact of MKC on physicochemical characteristics of GLA-loaded nanovesicles

GLA-nanovesicle systems were prepared using three different membrane compositions (**Figure 3.1B**). All formulations contained chol-PEG<sub>200</sub>-RGD, to achieve a RGD peptide surface functionalization which could allow the recognition of  $\alpha_v\beta_3$ -integrins overexpressed in endothelial cells.<sup>1,20</sup> The chol-PEG<sub>200</sub>-RGD used for the preparation of all formulations described in this Chapter is not commercially available, since it was synthesized by the team of Dr. Miriam Royo from the IQAC-CSIC (Barcelona). The first formulation was constituted of DPPC, cholesterol, and chol-PEG<sub>200</sub>-RGD yielding liposomes

**(LP)**. The second formulation was composed of cholesterol, chol-PEG<sub>200</sub>-RGD, and h-MKC, that formed quatsomes **(MQ)**. Further, three types of hybrid-liposomes **(HLP)** were prepared, which were mainly composed of DPPC, cholesterol, and chol-PEG<sub>200</sub>-RGD, and contained different low amounts of cationic surfactant MKC, l-MKC, at 0.4, 2.2, and 4.3 mol % (which, in mass, corresponded to 0.004, 0.02, and 0.04 mg mL<sup>-1</sup> of MKC in the nanoformulation).

All the GLA-loaded systems (named **LP-GLA<sub>20</sub>**, **MQ-GLA<sub>20</sub>**, and **HLP-GLA<sub>20</sub>**, respectively) were prepared using the same initial theoretical GLA concentration, i.e., 20 µg mL<sup>-1</sup>. An additional **HLP-GLA<sub>8.5</sub>** system was prepared at the lower GLA concentration of 8.5 µg mL<sup>-1</sup>, to yield the same enzyme and membrane components ratio of 3.4 µg µmol<sup>-1</sup>, as in **MQ-GLA<sub>20</sub>** (see **Table 3.1**).

All the nanovesicles were prepared with the DELOS-susp production method described in **Chapter 9** and schematized in **Figure 3.2**. In this process, first, membrane components (cholesterol, cholesterol-derivative chol-PEG<sub>200</sub>-RGD, DPPC and/or MKC) were dissolved in a mixture of ethanol (EtOH) and dimethyl sulfoxide (DMSO). Although cholesterol, DPPC, and MKC showed high solubility in ethanol, it was not possible to completely solubilize the chol-PEG<sub>200</sub>-RGD. For this reason, a mixture of EtOH/DMSO was used to achieve a practically complete dissolution of all the components. Both solvents, EtOH and DMSO, belong to solvents in Class 3 of the ICH guideline Q3C (R6) Impurities: guideline for residual solvents from the European Medicines Agency (EMA), considered low toxic and of lower risk to human health if remain as residual solvents, being adequate for their use during the manufacturing of pharmaceutical formulations.<sup>21</sup> Then, the organic solution containing all the membrane components was loaded into a high-pressure vessel and volumetrically expanded with compressed CO<sub>2</sub>. The system was maintained at working conditions ( $P_w$  10 MPa, 35 °C) to achieve a complete homogenization and thermal equilibration and then, it was depressurized into a water solution. For GLA-loaded nanovesicles, GLA at the desired concentration was previously dissolved in the aqueous solution. Further, to determine the GLA entrapment efficiency, the non-conjugated free GLA enzyme was separated from the GLA-loaded liposomes using a diafiltration TFF process.

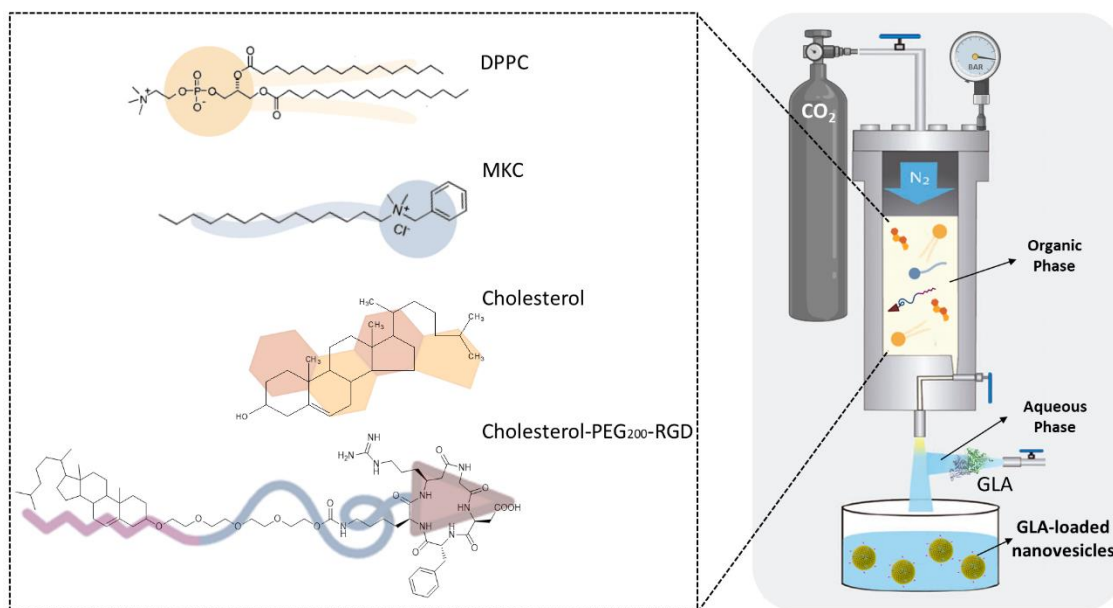


**Figure 3.2.** Chemical structure of membrane components and schematic representation of the depressurization step of the DELOS-susp process to obtain GLA-loaded nanovesicles, composed by cholesterol, chol-PEG<sub>200</sub>-RGD, MKC and/or DPPC.

The physicochemical characteristics of blank vesicles and GLA-loaded vesicles were assessed by measurements of the particle size, size distribution, polydispersity, and  $\zeta$ -potential using dynamic light scattering (DLS) and electrophoretic light scattering (ELS), as detailed in **Chapter 9.5.1**. The results are summarized in **Table 3.1**.

**Table 3.1.** Physicochemical characteristics of the GLA nanoformulations, the next day after production.

Nanovesicle system	Size (nm) ( $\pm$ SD)	PDI ( $\pm$ SD)	$\zeta$ -potential (mV) ( $\pm$ SD)	GLA concentration ( $\mu\text{g mL}^{-1}$ )	GLA per vesicle <sup>†</sup> (theor.)	Ratio GLA per nanovesicle <sup>‡</sup> ( $\mu\text{g } \mu\text{mol}^{-1}$ )
LP	152 $\pm$ 1	0.41 $\pm$ 0.02	26 $\pm$ 1	–	–	–
LP-GLA <sub>20</sub>	550 $\pm$ 40* (310 $\pm$ 20)*	0.77 $\pm$ 0.02* (0.50 $\pm$ 0.10)*	-6.3 $\pm$ 0.2 (-25.2 $\pm$ 0.8)	20 $\pm$ 1 (7 $\pm$ 2)	ND	8.3
MQ	69 $\pm$ 1	0.19 $\pm$ 0.01	64.2 $\pm$ 0.7	–	–	–
MQ-GLA <sub>20</sub>	69 $\pm$ 3 (65 $\pm$ 3)	0.19 $\pm$ 0.02 (0.20 $\pm$ 0.01)	61.0 $\pm$ 0.9 (58.0 $\pm$ 0.6)	18 $\pm$ 1 (15.1 $\pm$ 0.3)	ND	3.4
(0.4%MKC)-HLP	107 $\pm$ 1	0.23 $\pm$ 0.02	36 $\pm$ 4	–	–	–
(0.4%MKC)-HLP-GLA <sub>20</sub>	141 $\pm$ 6 (140 $\pm$ 4)	0.18 $\pm$ 0.02 (0.17 $\pm$ 0.01)	17 $\pm$ 1 (17 $\pm$ 1)	12 $\pm$ 2 (2.8 $\pm$ 0.2)	3	8.3
(2.2%MKC)-HLP	112 $\pm$ 1	0.24 $\pm$ 0.01	59 $\pm$ 2	–	–	–
(2.2%MKC)-HLP-GLA <sub>20</sub>	123 $\pm$ 1 (124 $\pm$ 3)	0.17 $\pm$ 0.01 (0.17 $\pm$ 0.02)	36 $\pm$ 2 (42.3 $\pm$ 0.1)	11 $\pm$ 2 (6 $\pm$ 1)	6	8.3
(2.2%MKC)-HLP-GLA <sub>8.5</sub>	108 $\pm$ 2 (112 $\pm$ 1)	0.18 $\pm$ 0.01 (0.20 $\pm$ 0.01)	51 $\pm$ 2 (46 $\pm$ 1)	4.9 $\pm$ 0.4 (4.6 $\pm$ 0.2)	4	3.4
(4.3%MKC)-HLP	113 $\pm$ 1	0.23 $\pm$ 0.02	63.6 $\pm$ 0.7	–	–	–
(4.3%MKC)-HLP-GLA <sub>20</sub>	126 $\pm$ 1 (123 $\pm$ 1)	0.19 $\pm$ 0.01 (0.17 $\pm$ 0.01)	46.8 $\pm$ 0.7 (49 $\pm$ 1)	12.1 $\pm$ 0.9 (12 $\pm$ 1)	11	8.3

Values in parentheses are for diafiltrated nanoformulations. Results are shown as the average of two independent productions for each system; <sup>†</sup> Theoretical number of GLA per vesicle (see calculation in **Chapter 9**); <sup>‡</sup> Theoretical ratio mass of GLA per mole of membrane component; \* Not reliable data; sample showed some sedimentation.

First, GLA-loaded liposomes (**LP-GLA<sub>20</sub>**) similar to those described by Cabrera et al.<sup>1</sup> were prepared, but using the commercially available agalsidase alfa (Replagal<sup>®</sup>) as the model enzyme of high-quality, free-tag, and already approved and commercialized GLA instead of the in-house-produced His-tag GLA, obtaining similar low enzyme entrapment efficiency but less stability than the previously reported system. Entrapping the commercial GLA, **LP-GLA<sub>20</sub>** showed higher mean particle size and wider size distribution compared to **LP** and the previous evaluated systems, also reflected by a notably higher polydispersity index (PDI). The PDI value acts as indicator of the particle size dispersity of a given

sample, and ranges from 0.00 (low disperse) to 1.00 (high disperse). In addition, **LP-GLA<sub>20</sub>** showed low-negative  $\zeta$ -potential values, a fact that had a direct negative impact on their stability. Specifically, these **LP-GLA<sub>20</sub>** liposomes sedimented few days after production, indicating the necessity of improvement (**Figure 3.3**).

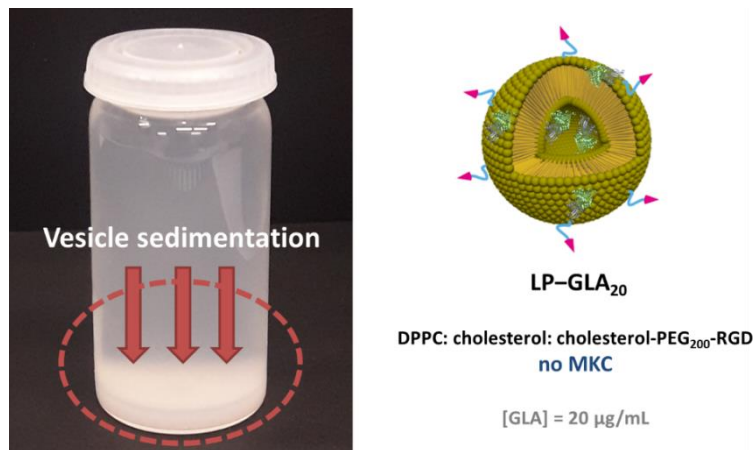


**Figure 3.3.** Sedimentation of **LP-GLA<sub>20</sub>** system few days after production, corresponding to liposomes loaded with GLA (agalsidase alfa, Replagal<sup>®</sup>) and free of MKC.

In comparison, **MQ** formulations showed a narrow size distribution and a considerable smaller mean size of around 70 nm. Notably, their physicochemical properties were also maintained when GLA was incorporated into the system (**MQ-GLA<sub>20</sub>**).

All three **HLP** systems (see **Table X**), with different content of surfactant MKC, formed small vesicles around 110 nm in diameter, slightly larger than the **MQ** vesicles, but still with a narrow size distribution. The  $\zeta$ -potential values directly correlated with the MKC concentration, increasing when more MKC was present in the liposomal structure. The addition of MKC maintained high and positive  $\zeta$ -potential values even when the GLA was entrapped (**HLP-GLA<sub>20</sub>** systems), although values were slightly below those obtained in the absence of GLA (**HLP**). This decrease in the  $\zeta$ -potential value could reflect the electrostatic nature of the interaction between the negatively charged enzyme and the positively charged vesicle. The  $\zeta$ -potential represents the electrical charge on the nanovesicle surface, which is also an important parameter that allows prediction of the physical stability. In theory, higher  $\zeta$ -potential values, either positive or negative, tend to stabilize particle dispersions. Usually, particle aggregation is less likely to occur for charged particles with a pronounced  $\zeta$ -potential due to the electrostatic repulsion between particles with the same electrical charge.<sup>22</sup> This effect on the nanoformulation stability was clearly observed when **MQ-GLA<sub>20</sub>** and **HLP-GLA<sub>20</sub>** containing the cationic MKC surfactant were compared with the non-MKC-containing **LP-GLA<sub>20</sub>** system, since no vesicle sedimentation was observed up to 1 month after production for the first systems. The remarkable stability of MKC-containing systems could also be observed by monitoring the evolution of their size, PDI, and  $\zeta$ -potential over time (**Figure 3.4**).



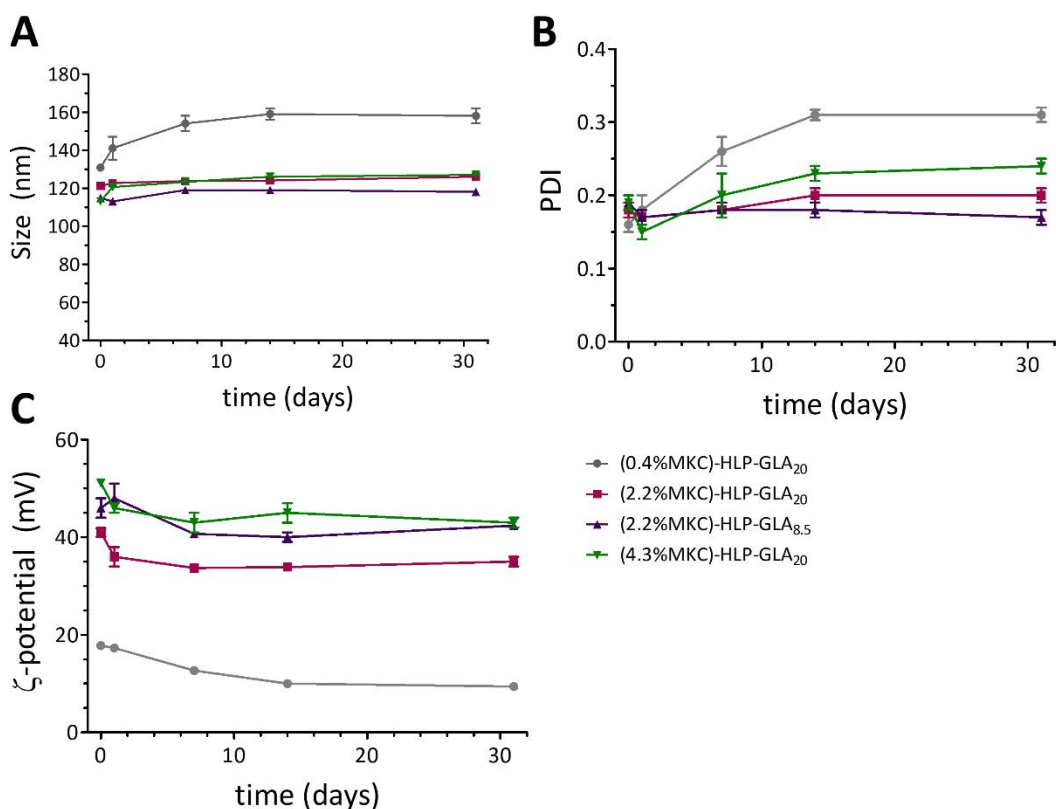


**Figure 3.4.** Stability of **HLP-GLA** nanovesicles in terms of diameter size, PDI and  $\zeta$ -potential measured at different time points (day 0, 1, 7, 14, and 31 after production) after being stored at  $5 \pm 2$  °C (see **Chapter 9.5.9.1**). The shown data corresponds to the mean  $\pm$  SD of three independent measurements of the same batch per each system.

Next, the concentration of GLA in the nanovesicles was quantified by SDS-PAGE (Sodium dodecyl sulphate-polyacrylamide gel electrophoresis) and TGX (Tris-Glycine eXtended) densitometry analysis. These assays were performed by Dr. Jose Luís Corchero from the IBB-UAB (Barcelona) as explained in **Chapter 9.6.3.1**. The GLA concentration for each nanovesicle system is shown in **Table 3.1** and based on it, the entrapment efficiency (EE%) and GLA loading were determined (see **Chapter 9.6.3.4**). The correlation between both parameters, the EE% and GLA loading, and the MKC content is represented in **Figure 3.5**.

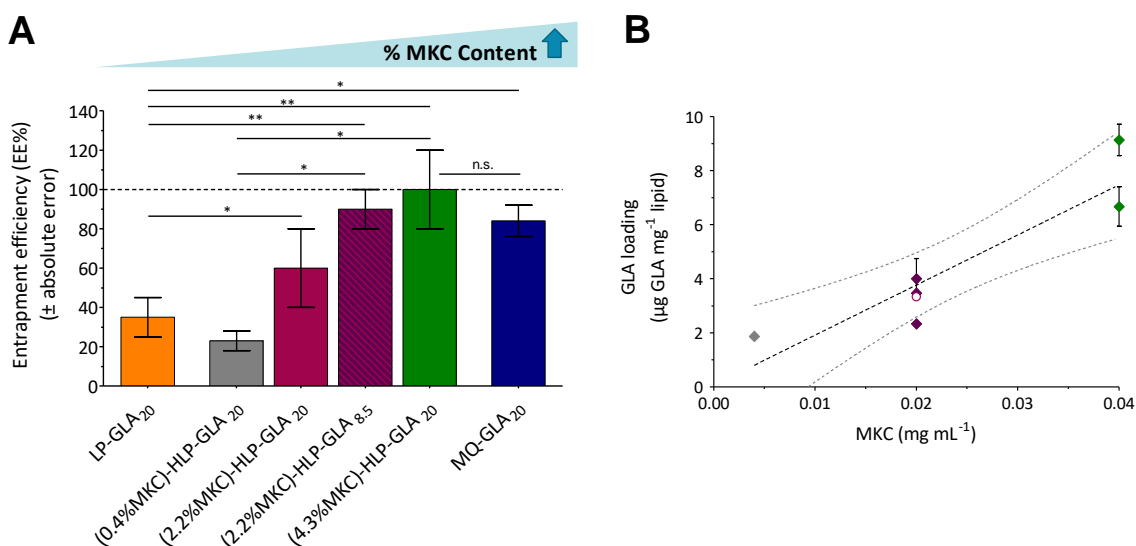


**Figure 3.5.** (A) GLA entrapment efficiency of all the tested systems, and (B) GLA loading in relation to MKC amount (in mg mL<sup>-1</sup> of formulation) for hybrid-liposomes (see **Chapter 9.6.3.4**). Samples represented with bulk symbols correspond to systems prepared with the same GLA initial concentration (**HLP-GLA<sub>20</sub>**). The empty circle corresponds to the system with lower GLA initial concentration (**HLP-GLA<sub>8.5</sub>**). The results correspond to the average of two or three independent assays. GLA was measured by SDS-PAGE plus TGX by Dr. J. L. Corchero from IBB-UAB (Barcelona) (see **Chapter 9.6.3.1**).

As expected, MKC played an important role in the integration capacity of GLA into the nanoformulations. Significantly higher entrapment efficiency was achieved in **MQ-GLA<sub>20</sub>** (EE% > 80 %) in comparison to the MKC-free **LP-GLA<sub>20</sub>** (EE% ≈ 30%). As aforementioned, the quaternary ammonium surfactant MKC was the main membrane component of **MQ-GLA<sub>20</sub>** formulations, and consequently, it led to higher cationic surface charge in the membrane, which induces higher entrapment of GLA by electrostatic interactions.

Similar effects were found in the hybrid-liposomal systems as shown in **Figure 3.5**; in **HLP-GLA<sub>20</sub>** systems, EE% and GLA loading directly correlated with the amount of MKC present. For the **(0.4%MKC)-HLP-GLA<sub>20</sub>** (the lowest MKC concentration) an entrapment efficiency of 23 ± 5 % was obtained, comparable to **LP-GLA<sub>20</sub>**, suggesting that despite the improvement of physicochemical characteristics (size, PDI, and stability) given by MKC addition, more electrostatic interactions are needed to achieve the improvement of EE. In the formulations with higher MKC levels, **(2.2%MKC)-HLP-GLA<sub>20</sub>** and **(4.3%MKC)-HLP-GLA<sub>20</sub>**, with considerably improved EE% values of up to 60 ± 20 and 100 ± 20 %, respectively, were detected. However, the difference between EE% of **(4.3%MKC)-HLP-GLA<sub>20</sub>** and **MQ-GLA<sub>20</sub>** was not statistically significant at this specific GLA concentration of 20 μg mL<sup>-1</sup>, indicating that the electrostatic interactions provided by MKC concentrations ≥ 4.3 mol % are enough to entrap this amount of GLA.

Interestingly, as shown in **Figure 3**, both (2.2%MKC)-HLP-GLA<sub>20</sub> and (2.2%MKC)-HLP-GLA<sub>8.5</sub> showed similar GLA loading despite being formulated at two different GLA concentrations, suggesting that, at this MKC concentration, nanovesicles reach the maximum enzyme loading capacity with 8.5  $\mu\text{g mL}^{-1}$  GLA. These findings provide a better understanding of the effect of MKC.

### 3.2.1. Studying the impact of MKC addition on morphology and lamellarity of nanovesicles

To gain further understanding of changes in the liposome morphology, the different nanovesicular formulations described in the previous section were characterized by small-angle X-ray scattering (SAXS) in collaboration with Prof. Jan Skov Pedersen group from Aarhus University (Denmark).

SAXS is a useful characterization technique to study the structure of materials and colloidal systems on the molecular scale, since it is non-invasive, non-destructive, and can give statistical data. This technique measures the time-average intensity of the scattered X-rays as a function of the scattering angle (**Figure 3.6**) and, when applied to soft materials and specifically to nanovesicles, SAXS can give structural information such as membrane thickness, lamellarity, ordering, or contribution of some component.<sup>23–25</sup>

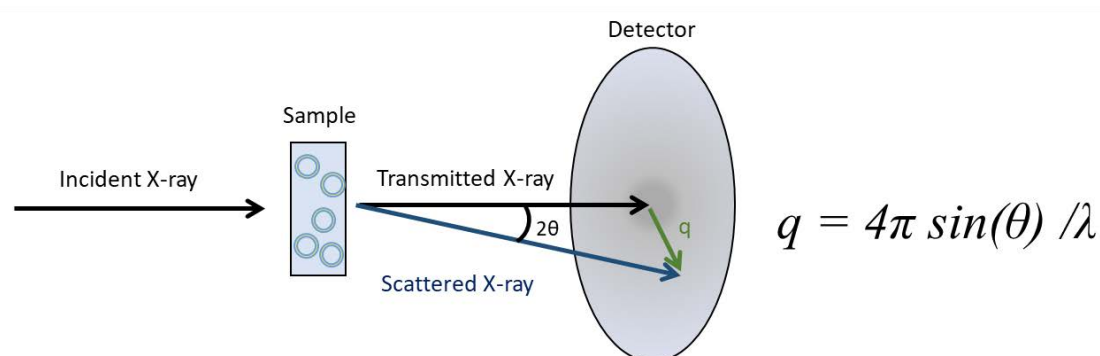


**Figure 3.6.** SAXS measurement. The modulus of the scattering vector is defined as  $q$ , the scattering angle as  $2\theta$ , and the X-ray wavelength as  $\lambda$ .

First, the scattering from an aliquot of the commercial GLA was investigated since GLA could contribute significantly to the total scattering signal in the GLA-loaded liposome samples. The SAXS data of the pure enzyme could be fitted with a rigid-body refined dimer structure<sup>26</sup> based on the known dimeric crystal structure of GLA (PDB: 1r46<sup>10</sup>,  $\chi^2 = 1.8$ ) (**Figure 3.7A**). Fitting was done on an absolute scale yielding a concentration estimate of 1.10  $\text{mg mL}^{-1}$  (assuming that all GLA is on dimer form), which was slightly higher than the concentration of 1  $\text{mg mL}^{-1}$ , corresponding to the nominal value of the commercial stock GLA. A small increase in intensity at low scattering vector moduli,  $q$ , could suggest slight aggregation in the sample, resulting in a somewhat elevated concentration estimate.

For the nanoformulations, the SAXS data showed a characteristic minimum at intermediate  $q$ , typical for liposomes, arising from the variations in electron density across the cross-section profile of the bilayer membranes. Unfortunately, quatsomal systems (**MQ** and **MQ-GLA<sub>20</sub>**) could not be analyzed with SAXS, since MKC shows an electron density close to that of water, and therefore, is not possible to get good data for samples with high MKC concentrations.

The data was fitted with a paracrystalline model<sup>27</sup> based on Pabst et al.<sup>23,28</sup> where the average number of layers ( $N_{\text{layers}}$ ) and the bilayer thickness ( $T$ ) can be determined. Experimental details are in **Chapter 9.5.6**. When fitting the data, it was observed that an additional contribution from polymer scattering had to be included to obtain good fits (**Figure 3.7B** and **Table 3.2**). For the samples without GLA (**LP** and **HLP**), this scattering contribution was constant and probably arises from the flexible chol-PEG<sub>200</sub>-RGD on the membranes surface. For samples containing GLA, the polymer scattering was therefore fixed at an average value obtained from the GLA-free fits. In **LP-GLA<sub>20</sub>** and **HLP-GLA<sub>20</sub>**, GLA also contributed to the scattering patterns and, thus, the theoretical signal from free GLA was added to the liposome scattering through a linear combination with its own individual scale factor. Even though the scattering contributions from the polymer and GLA were small and to some extent correlated, it was still possible by this approach to determine the GLA concentrations with SAXS, which corresponded fairly well with the theoretically calculated GLA concentrations (**Table 3.2**).

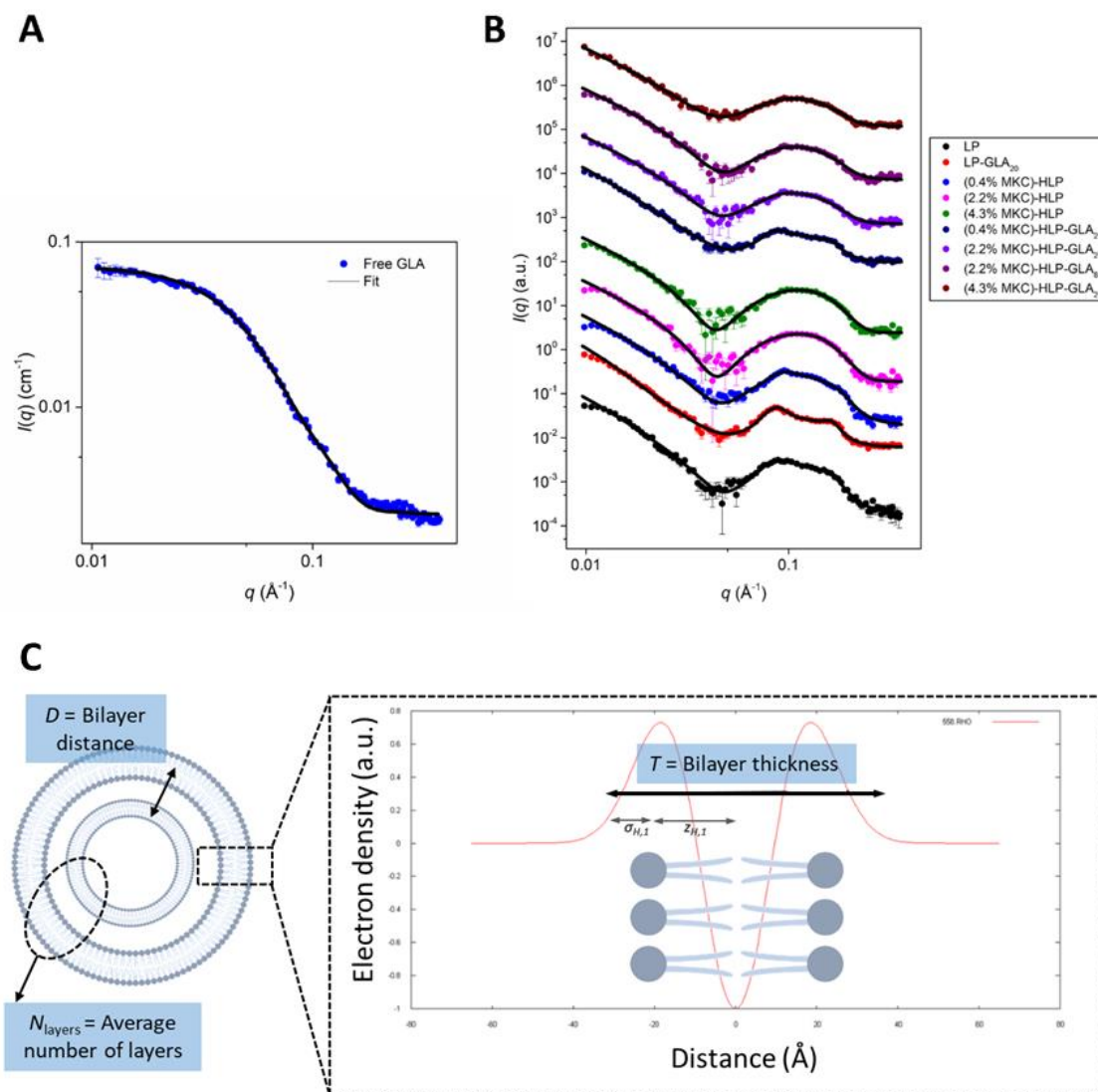


**Figure 3.7.** (A) SAXS data of free GLA and (B) the unloaded and GLA-loaded nanoformulation samples. Assay corresponds to a single representative experiment for each system, replicated in three independent assays, performed by Prof. J. S. Pedersen from Aarhus University (Denmark). (C) Scheme of the nanovesicle parameters and a representative cross-section profile which could be determined after SAXS data modelling:  $N_{\text{layers}}$  is the average number of layers in liposomes,  $T$  is the bilayer thickness, and  $D$  is the distance between bilayers in multilamellar liposomes (see **Chapter 9.5.6**).

**Table 3.2.** SAXS data of the nanoformulations.

Nanovesicle systems	$\chi^2$ <sup>†</sup>	Polymer	Concentration		$N_{layers}$ <sup>‡</sup>	$T$ <sup>§</sup> (Å)
		scale (10 <sup>-4</sup> )	GLA <sub>theor.</sub> (µg mL <sup>-1</sup> )	GLA <sub>fitted</sub> (µg mL <sup>-1</sup> )		
LP	1.1	4.6 ± 0.8	–	–	1.5 ± 0.1	51.5 ± 0.3
LP-GLA <sub>20</sub>	1.1	4.2 <sup>d)</sup>	20	13 ± 2	2.0 ± 0.1	51.0 ± 0.2
(0.4%MKC)-HLP	2.2	4.2 ± 0.8	–	–	1.3 ± 0.1	48.9 ± 0.3
(2.2%MKC)-HLP	1.5	3.4 ± 0.7	–	–	1.0 ± 0.1	48.6 ± 0.3
(4.3%MKC)-HLP	1.5	4.4 ± 0.8	–	–	1.0 ± 0.1	48.5 ± 0.4
(0.4%MKC)-HLP-GLA <sub>20</sub>	1.2	4.2 <sup>*</sup>	20	22 ± 3	1.1 ± 0.1	50.7 ± 0.3
(2.2%MKC)-HLP-GLA <sub>20</sub>	1.5	4.2 <sup>*</sup>	20	18 ± 3	1.1 ± 0.1	50.2 ± 0.5
(2.2%MKC)-HLP-GLA <sub>8.5</sub>	1.6	4.2 <sup>*</sup>	8.5	8 ± 4	1.1 ± 0.1	49.9 ± 0.4
(4.3%MKC)-HLP-GLA <sub>20</sub>	0.9	4.2 <sup>*</sup>	20	16 ± 3	1.1 ± 0.1	49.3 ± 0.3

Single representative experiment for each system, replicated in three independent assays (mean ± SD), performed by Prof. J. S. Pedersen from Aarhus University (Denmark). <sup>†</sup>  $\chi^2$  is the reduced weighted chi-square; <sup>‡</sup> Average number of layers in liposomes; <sup>§</sup> Bilayer thickness defined as  $T = 2(z_{H,1} + \sigma_{H,1})$ , where  $z_{H,1}$  is the distance from the center of the bilayer to the centers of the Gaussian used to describe the headgroup and  $\sigma_{H,1}$  is the width of this Gaussian; Details in **Chapter 9.5.6.1**. \* Not fitted value.

Increasing MKC concentrations slightly decreased the bilayer thickness ( $T$ ) for both GLA-containing (from 51.0 Å to 49.3 Å) and GLA-free (from 51.5 Å to 48.5 Å) liposomes. Furthermore, for samples with MKC,  $T$  was slightly higher when GLA was added, suggesting that the protein possibly binds to the positively charged liposome surface and therefore increase the apparent bilayer thickness. Both **LP** and **LP-GLA<sub>20</sub>** showed some multilamellarity that diminished as MKC was introduced into the liposomes, probably an effect of the general lower stability and early sedimentation observed for **LP** and **LP-GLA<sub>20</sub>** in comparison with **HLP** and **HLP-GLA<sub>20</sub>**.

Cryogenic transmission electron microscopy (cryoTEM) images were acquired in collaboration with the team of Prof. Dganit Danino (Institute of Technology, Israel) (see **Chapter 9.5.5**). Direct observation of the nanovesicles with cryoTEM was fully consistent with the SAXS analysis. **Figure 3.8** presents as examples characteristic data for the **LP-GLA<sub>20</sub>**, **MQ-GLA<sub>20</sub>** and **HLP-GLA<sub>8.5</sub>** systems. The nanoformulations were largely unilamellar as expected and with reduced dispersity in size and morphology. **LP-GLA** and **HLP-GLA<sub>8.5</sub>** nanovesicles were about 120 nm in diameter, and **MQ-GLA<sub>20</sub>** nanovesicles were smaller and on average 60 – 70 nm in diameter, all in excellent agreement with the

DLS data shown in **Table 3.1**. Because cryoTEM is showing individual nanovesicles, certain polydispersity with some double-layer structures was recognized, but overall and in agreement with the SAXS analysis, the vesicular formulations showed a low degree of dispersity.

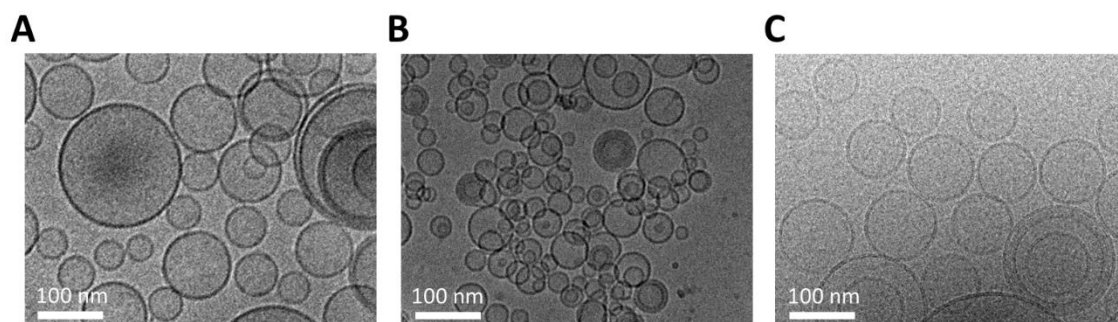


**Figure 3.8.** CryoTEM images of the three different nanoformulations: (A) non-MKC-containing liposomes (**LP-GLA<sub>20</sub>**), (B) quatsomes (**MQ-GLA<sub>20</sub>**) and (C) hybrid liposomes (**HLP-GLA<sub>8.5</sub>**). Images were acquired by the team of Prof. Dganit Danino from Technion (Israel).

Overall, the physicochemical properties showed that both quatsomes and hybrid-liposomes are promising systems for further exploration as potential carriers of the GLA enzyme. The increase in their membrane positive charge due to the presence of the cationic surfactant leads to a narrower and less disperse size distribution, with a marked improvement in the colloidal stability. This amends the earlier destabilization phenomena seen in the MKC-free system (**LP-GLA<sub>20</sub>**) and makes **MQ-GLA<sub>20</sub>** and **HLP-GLA** systems suitable for further examination. Especially important is the two-fold increase in GLA entrapment efficiency compared with **LP-GLA<sub>20</sub>**. This is a major advancement in enzyme nanoformulations, where it is often very challenging to obtain high or full incorporation of big biomacromolecules into the nanovesicles.

### 3.3. Impact of MKC addition on the specific enzymatic activity of GLA

The specific enzymatic activity of the GLA enzyme conjugated to the nanovesicles was measured in collaboration with Dr. Ibane Abasolo group from Vall Hebron Institut de Recerca (VHIR, Barcelona) using a fluorescence assay following Cabrera et al.<sup>12</sup> The enzymatic activity assay is based on the conversion of a non-fluorescent substrate (4-MUG) in a fluorescent product (4-MU) when active GLA is present (**Figure 3.9**). Since the GLA is a lysosomal enzyme, the enzymatic activity assay needs to occur at acidic pH conditions, similar to those of cell lysosomes, where GLA operates most efficiently.<sup>10</sup> To be sure that the enzyme activity was measured over the non-altered encapsulation patterns, we confirmed the stability of the nanostructured formulations in the acidic media of the assay conditions, before performing the enzyme assays. The integrity of the nanovesicles in the assay conditions (pH 4.5,





were only significant when comparing **(0.4%MKC)-HLP-GLA<sub>20</sub>** to other **HLP-GLA** containing higher MKC content (\*\*p = 0.004).

As previously reported, molecular dynamics calculations pointed out that GLA-liposome association occurs through electrostatic interactions, which could orient the enzyme in a “site-specific” manner in the lipid bilayer, exposing its active site to the exterior aqueous phase.<sup>1</sup> So it seems reasonable that the presence of small amounts of the cationic MKC surfactant in the **HLP-GLA** membrane enhances this effect in comparison to **LP-GLA**, with similar membrane composition but free of MKC.

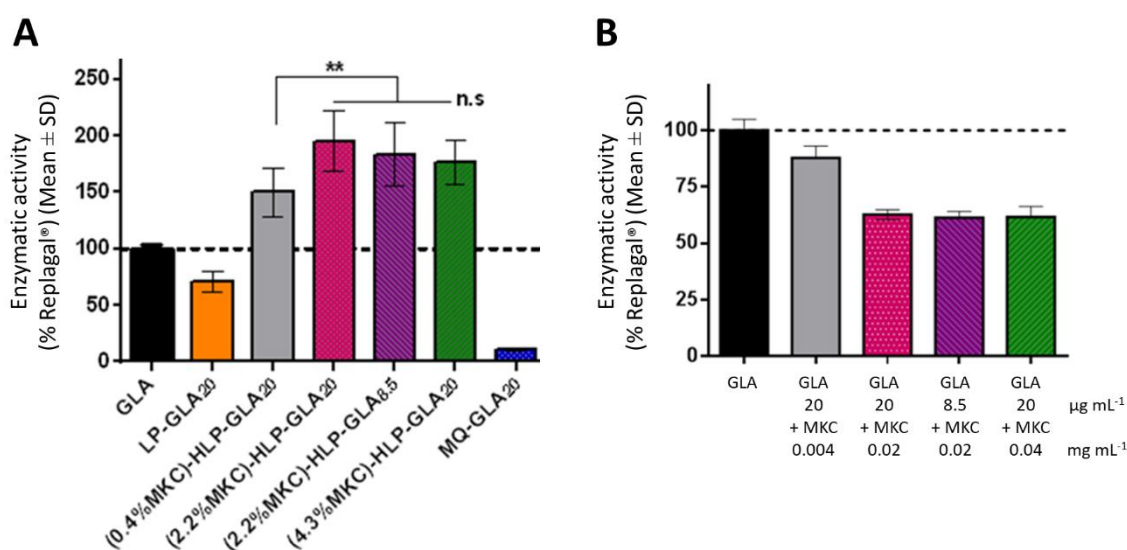


**Figure 3.10.** Specific enzymatic activity: (A) in liposomes (**LP-GLA**), quatsomes (**MQ-GLA**), and hybrid liposomes containing MKC (**HLP-GLA**). All values were normalized by their GLA concentration and referred to the enzymatic activity of the free GLA (Replagal®) as a reference. Average of three independent assays using two different batches per each system. (B) Enzymatic activity of GLA (Replagal®) in presence of free MKC, reproducing the same concentrations than in **HLP-GLA** systems. Single representative experiment, replicate in two independent assays. Assays performed by Dr. I. Abasolo team from VHIR (Barcelona)

The enzymatic activity of GLA, measured in the presence of pure MKC at equivalent surfactant concentrations to those in **HLP-GLA** formulations, was lower than the one measured for the corresponding formulations (see **Figure 3.10B**). This result points out that the enzymatic activity enhancement is related to the entrapment of GLA in **HLP-GLA** liposomes, containing l-MKC in their membrane, and not only due to the presence of this surfactant in the formulation. Further, enzymatic activity of GLA in presence of pure MKC at even higher concentration, h-MKC, equivalent to those in **MQ-GLA** formulation, was also measured. This time, the enzymatic activity was even lower, around

20 % compared to the control, suggesting that the membrane structural differences between hybrid-liposomes and quatsomes might be the reason of a different mode of interaction with the enzyme. Besides, the **LP-GLA** and **HLP-GLA** liposomes used in the present work for the encapsulation of GLA are constituted by DPPC phospholipids and have a high content of cholesterol, which, as it is well known, yields rigid liposomal nanovesicles with mechanically stable gel-phase bilayers.<sup>30</sup> In a recent work, it was reported that quatsome non-liposomal lipid nanovesicles, although having also a high cholesterol content, are flexible nanovesicles, formed by a bilayer membrane with comparable structural properties to fluid-like lipid bilayers.<sup>31</sup> These differences on the membrane phase state between liposomes and quatsomes might cause a different type of enzyme-nanovesicle association and explain the different enzyme activities under different types of encapsulation patterns. It has been reported that the way proteins interact with lipid membranes depends not only on the surface charge of the membrane but also on the phase state.<sup>32</sup>

Although quatsomes were shown to be appropriate nanocarriers for other drug models,<sup>19</sup> the loss of enzymatic activity made them unfit for GLA delivery. Thus, further biological studies were only performed with the hybrid-liposomal systems due to their promising results, in terms of improved GLA loading and physicochemical stability, as well as the higher enzymatic activity of conjugated GLA.

### 3.4. In vitro efficacy and in vivo toxicological profile of HLP-GLA hybrid-liposomes

#### 3.4.1. In vitro efficacy and safety assays

Further in vitro assays were performed in collaboration with Dr. Ibane Abasolo group from VHIR (Barcelona) to assess the efficacy and safety of the nanoformulations. First, the capacity of **HLP-GLA** to enter cells and reduce the Gb3 deposits within the lysosomes was measured by adding a fluorescent-labeled Gb3 (NBD-Gb3).<sup>1,33</sup> In this assay, mouse aortic endothelial cells (MAEC) from Fabry KO mice, with no endogenous GLA activity, were challenged with different concentrations of **HLP-GLA**. Consequently, total Gb3 loss was solely attributed to the action of the enzyme carried by the nanovesicles after cell internalization and lysosomal localization, where the low pH allowed enzyme activity.

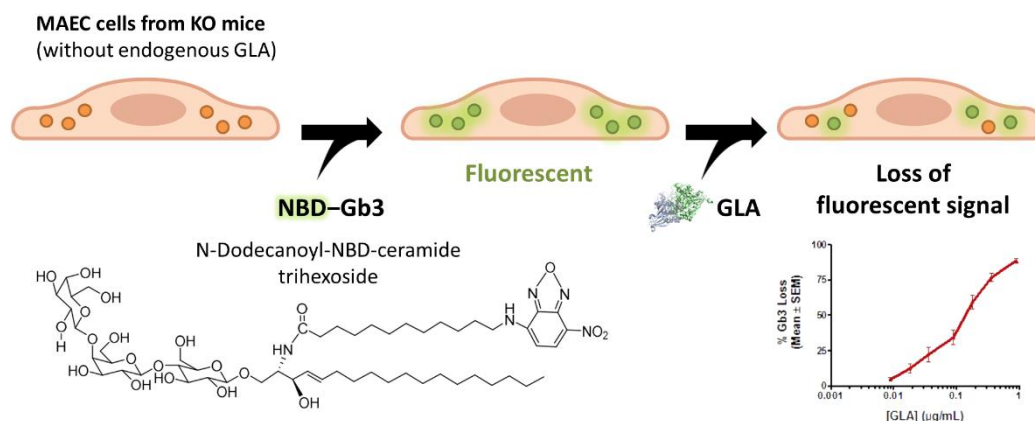


**Figure 3.11.** Scheme of the in vitro efficacy assay performed in cellular models, using mouse aortic endothelial cells (MAEC). Efficacy of GLA is proportional to the loss of Gb3 substrate. Experimental details in **Chapter 9.7.2**.

Results showed better efficacy of nanoformulated enzymes compared to experiments with free GLA (**Figure 3.12**), in accordance with the previously described increase in the intrinsic specific enzymatic activity.

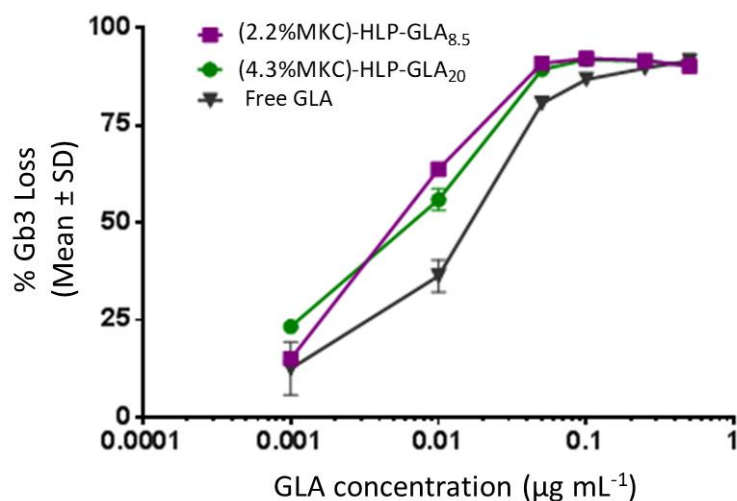


**Figure 3.12.** In vitro efficacy assays measured as loss of Gb3 (due to its hydrolysis by GLA) in primary endothelial cells derived from Fabry KO mice. Incubation with GLA or liposomal systems was performed at 37 °C for 48 h. Assay corresponds to a single batch per system replicated in three independent assays, performed by Dr. I. Abasolo team from VHIR (Barcelona) (see **Chapter 9**).

Therefore, these new **HLP-GLA** systems with enhanced colloidal stability and higher EE% ( $\geq 90\%$ ) and, thus of better quality, have demonstrated to be as effective in vitro as the previous published GLA-loaded liposomal system.<sup>1</sup> These results validate this nanoformulation optimization work since the

present developed hybrid liposomes overall fulfill the physicochemical and biological requirements to warrant their progress to an advanced stage of preclinical development.

The higher efficacy of nanoformulated GLA compared to experiments with free GLA could be explained by (i) the enzyme conjugation to nanoliposomes, which are well known nanocarriers for intracellular delivery, and (ii) the presence of RGD peptide in the nanoliposomal membrane, which we previously demonstrated allows a rapid mediated-internalization in endothelial cells.<sup>1,34</sup> The impact of GLA nanoformulation on efficacy was also observed when using other types of nanoparticles, such as ICAM-1-targeted polystyrene nanocarriers.<sup>35</sup>

To characterize the safety and toxicological profile of the **HLP-GLA** systems, several in vitro assays were performed. First, HeLa cells were exposed to different concentrations of **HLP-GLA**, and cell viability was measured after 72 h incubation by the MTT assay as explained in **Chapter 9.9.1**. Cell viabilities were kept above 75 % in all cases, indicating that integration of MKC into the hybrid liposomes was not inducing any dose-dependent cytotoxicity (**Figure 3.13A**).

Further, it was also tested whether the **HLP-GLA** could be safely administered intravenously, using well-established hemocompatibility studies. First, the impact of different nanoformulations in red blood cell fragility was studied by using hemolysis tests in murine blood samples. This assay determines the erythrocytes breakage in presence of the testing sample, as a measure of hemoglobin release, measured by absorbance (see **Chapter 9.9.2.1**). None of the tested **HLP-GLA** systems induced relevant hemolysis and the values measured never surpassed 5 % total hemolysis (see **Figure 3.13B**).

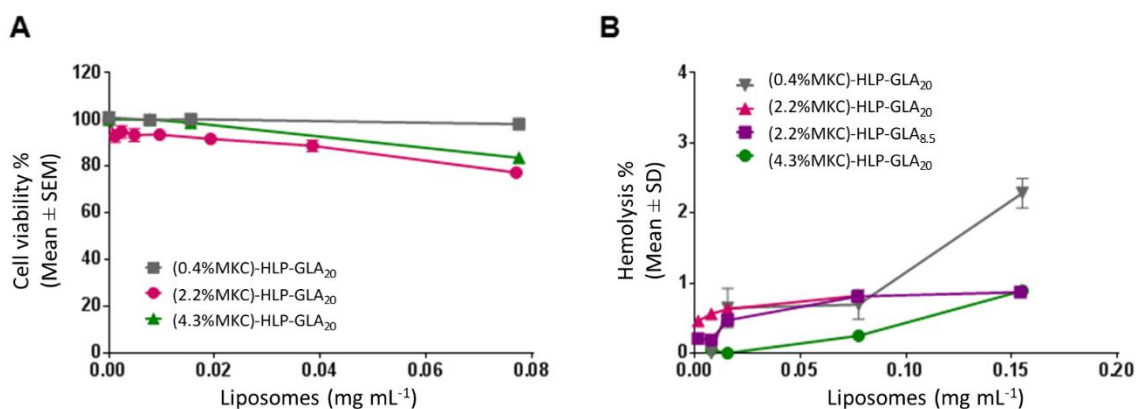


**Figure 3.13.** In vitro safety assays of different **HLP-GLA** formulations: (A) Cell viability in HeLa cells treated during 72 h at 37 °C with up to 0.08 mg mL<sup>-1</sup> in lipids. Values of three independent experiments of a single representative batch per each system; (B) Hemolysis of mouse red blood cells with different **HLP-GLA** systems, incubated 1 h at 37 °C. Values of a single representative batch per each system. Assays performed by Dr. I. Abasolo team from VHIR (Barcelona).

Similarly, plasma coagulation times in human plasma were measured in collaboration with Dr. I. Abasolo team (VHIR, Barcelona), as prothrombin time (PT), activated prothrombin time (APTT), and thrombin time (TT) in presence of 0.154 mg mL<sup>-1</sup> **(2.2%MKC)-HLP-GLA<sub>20</sub>**. According to manufacturer's protocol (see **Chapter 9.9.2.2**), prolongation  $\geq 2$ -fold versus untreated control is generally considered physiologically significant, suggesting then that the testing substance either depletes or inhibit coagulation factors. Our results showed no significant variations in plasma coagulation times at the tested concentration, since results were within the normal expected range (**Table 3.3**).

**Table 3.3.** Plasma coagulation times measured as prothrombin time (PT), activated partial prothrombin time (APTT) and thrombin time (TT) after incubation with (2.2%MKC)-HLP-GLA<sub>20</sub> liposomes.

Sample*	PT (s) (± SD)	APTT (s) (± SD)	TT (s) (± SD)
Normal coagulation time range	≤ 13.4	≤ 34.1	≤ 21
Control plasma	12.3 ± 0.1	33.6 ± 0.1	16.4 ± 0.7
Vehicle	12.4 ± 0.0 (12.3 ± 0.1)	34.4 ± 0.4 (34.3 ± 0.3)	16.2 ± 0.2 (16.6 ± 0.1)
(2.2%MKC)-HLP-GLA <sub>20</sub>	12.6 ± 0.1 (12.3 ± 0.0)	33.9 ± 0.1 (33.9 ± 0.0)	16.0 ± 0.0 (16.2 ± 0.4)

Values into brackets correspond to diafiltrated nanoformulations. Non-treated plasma (control plasma) and the nanoformulation without liposomes (vehicle) were used as controls. Mean of two independent measurements, performed by Dr. I. Abasolo group from VHIR (Barcelona) (see **Chapter 9.9.2.2**).

### 3.4.2. In vivo repeated dose toxicity assay with non-GLA hybrid-liposomes

Once the **HLP-GLA** demonstrated to be safe in vitro, an in vivo repeated dose toxicity assay was performed with just the vehicle (without GLA, **(2.2%MKC)-HLP** hybrid-liposomes). The rationale behind this preliminary in vivo study was to evaluate the plausibility of using MKC-containing liposomes and thus identify potential toxicities caused by the vehicle in vivo. It should be pointed out, that the interest of **HLP** as nanocarriers is not limited to GLA transportation, and that they might be further explored for the delivery of other actives, such as other enzymes related to LSD diseases.

Prior to administration, concentration experiments of the liposomal system were needed to reach the desired doses, mimicking the concentration factor that is required to reach the sufficient GLA concentration in the nanoformulation for achieving a therapeutic dose in vivo. To concentrate the samples, the same experimental configuration process specified in **Chapter 9.3** for TFF diafiltration

was used, with the exception that in this case, the buffer reservoir was not connected to the system. This allowed the sample to become more concentrated as the aqueous phase was being removed. The degree of concentration (Concentration Factor, CF) corresponds to the initial volume ( $V_i$ ) of the liposomal formulation divided into the final volume ( $V_f$ ),  $CF = V_i / V_f$ . Samples used for the hereafter described in vivo toxicology assay have been concentrated by  $CF = 12$ , reaching a theoretical concentration of  $18.0 \text{ mg mL}^{-1}$  of lipid.

Physicochemical characteristics (size, PDI, and  $\zeta$ -potential) of the liposomal system were determined by DLS after the concentration step, to ensure that the procedure itself has no relevant impact on the nanovesicular structure. No significant changes were observed after concentration in terms of size ( $p = 0.169$ ), PDI ( $p = 0.903$ ), and  $\zeta$ -potential ( $p = 0.116$ ) since liposomes maintained a nanoscopic size (below 250 nm) and low polydispersity ( $PDI < 0.35$ ) (**Figure 3.14A**). Morphology inspected by cryoTEM imaging showed spherical and mostly unilamellar vesicles, with the size in the nanometric range and in agreement with DLS results (**Figure 3.14B**). So, this concentration step did not induce any significant change in physicochemical properties of the system and 12-fold concentrated samples were obtained.

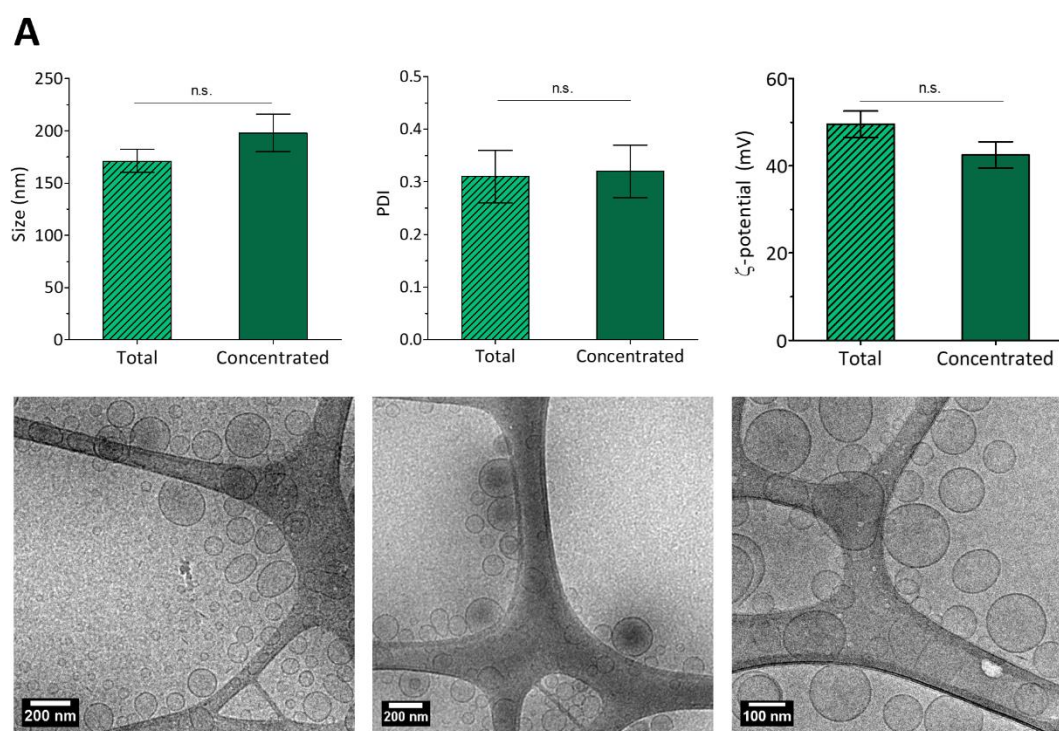


**Figure 3.14.** (A) DLS measurements in terms of size, PDI, and  $\zeta$ -potential of the (2.2%MKC)-HLP system after DELOS-SUSP preparation (Total) and after 12-fold concentration (Concentrated). Values correspond to the average of three different independent batches  $\pm$  SD. (B) Representative cryoTEM images of (2.2%MKC)-HLP sample after 12-fold concentration (see **Chapter 9.5.5**).

Additionally, the stability of 12-fold concentrated (2.2%MKC)-HLP in human serum (37 °C) was assessed by turbidity measurements, that allows the monitoring of changes in the system over time. By turbidimetrical methods, it is possible to measure the transmissivity and hence the attenuation of light. Changes in transmissivity over time, can act as indicator of changes in the suspension, e.g., if sedimentation or increasing of nanoparticles size occurs. Turbidity can be then assessed by absorbance since the absorbance has a logarithmic relationship to the transmittance.<sup>2</sup>

The 12-fold concentrated (2.2%MKC)-HLP system was incubated with two different concentrations of human serum, 75 % and 90 % (vol. %), at 37 °C in orbital shaker agitation, and stability over time was studied. At each time-point, the absorbance of samples was read ( $\lambda = 300$  nm), with the corresponding amount of serum alone as reference. Relative turbidity was determined dividing the sample turbidity by the turbidity at time zero (Chapter 9.5.9.3), without relevant changes (Figure 3.15A). Moreover, vesicle integrity was also confirmed after 1 h of incubation with human serum (37 °C), without changes in macroscopic appearance and preservation of liposomal structure as cryoTEM shows (Figure 3.15B and C).

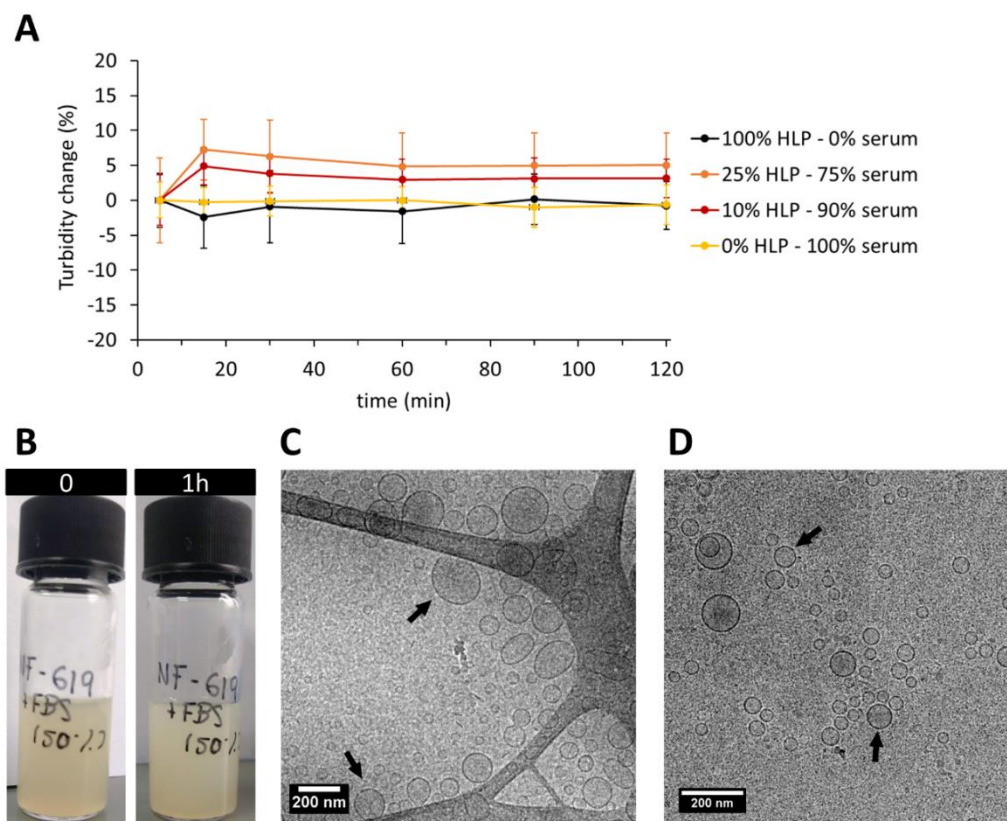


**Figure 3.15.** Stability of 12-fold concentrated (2.2%MKC)-HLP in presence of human serum: (A) measured by changes in turbidity ( $\lambda = 300$  nm); (B) Macroscopic appearance at two time-points (just after human serum addition, time 0, and after 1 h agitation at 37 °C); (C) CryoTEM images of concentrated (2.2%MKC)-HLP w/o human serum as control, and (D) in presence of human serum (50 % – 50 % vol). Details in Chapter 9.5.9.3.

Accordingly, C57BL6 wild-type mice were treated twice a week during 4 weeks with three different doses (0.37, 1.22, and 3.67 mg of lipid per injection, which corresponded approximately to 12, 41, and 105 mg kg<sup>-1</sup> lipid) of non-GLA **(2.2%MKC)-HLP** hybrid liposomes. This assay was performed in collaboration with Dr. I. Abasolo group (VHIR, Barcelona), as detailed in **Chapter 9.12**.

The treatment schedule was aimed at mimicking that of efficacy assays with GLA in Fabry mice, where repeated administrations of the enzyme are required to ensure a sustained effect. The overall welfare of the animals (general appearance, drinking/eating behavior, and response to stimuli) as well as weight was monitored for 5 weeks (4 weeks of treatment plus an additional week of surveillance), with no significant alterations of any of the monitored parameters (see **Figure 3.16** for body-weight monitoring) demonstrating a good tolerability of the **HLP** system upon repeated administrations.

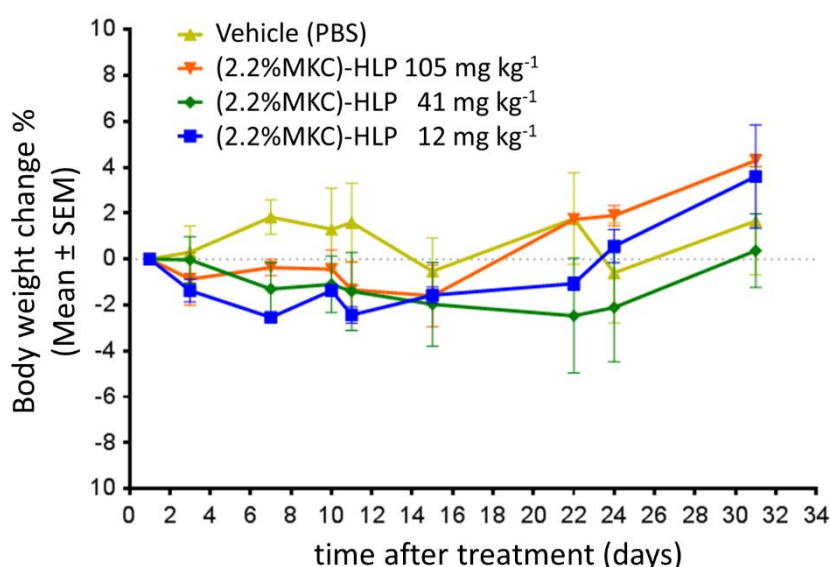


**Figure 3.16.** Body-weight changes in animals administered with concentrated **(2.2%MKC)-HLP**. Mice were treated repeatedly with a total of eight intravenous administrations over 4 weeks, with three different doses of **(2.2%MKC)-HLP**. Injection of PBS media (vehicle) was used as control. Weight gain on day 31 of the different treatment groups was not significantly different ( $p = 0.3747$ , by Kruskal–Wallis test). Assay performed by Dr. I. Abasolo group from VHIR (Barcelona).

### 3.5. Summary and Conclusions

In this Chapter, it was explored the use of two different RGD-targeted lipid-based nanovesicles for GLA enzyme entrapment, with distinct MKC surfactant content, i.e., non-liposomal nanovesicles, known as quatsomes, which contain high MKC concentrations (> 50 mol % of the total membrane components), and hybrid-liposomes that contain low MKC concentrations (< 5 mol % of the total membrane components). Previously reported similar RGD-targeted lipid-based nanovesicles, without MKC, were included in all studies for comparison purposes.



Both systems were successfully prepared using the DELOS-susp procedure, confirming the suitability of this technique for the preparation of multifunctional nanovesicles with a low dispersity.

Membrane composition of these vesicles strongly impacted both the physicochemical and biological characteristics of the nanoformulations. As expected, the addition of positive charges to the membrane by incorporating MKC improved the colloidal stability of the nanoformulation. Moreover, the amount of positive charge added to the system had a direct impact on the ability to entrap the enzyme, which is negatively charged at neutral pH. Consequently, quatsomes showed high entrapment efficiencies, but surprisingly, hybrid liposomes, with lower levels of MKC, achieved enzyme entrapment efficiencies similar to quatsomes. However, despite the high entrapment efficiency and good colloidal stability, quatsomes completely abolished the activity of the GLA enzyme. This underlines the relevance of obtaining a good balance between physicochemical properties of the carrier and the biological activity of the encapsulated drug, which must be tuned for each type of nanocarrier/drug combination.

In vitro, I-MKC hybrid-liposomes (0.4 – 4.3 mol % of the total membrane components) were shown to be non-cytotoxic and non-hemolytic. Moreover, the entrapment of GLA into these hybrid liposomes enhanced the efficacy of the enzyme and showed greater reduction of lysosomal Gb3 than the free administered GLA. Good tolerability and no adverse side effects were observed in mice after repeated administrations of MKC-containing liposomes, paving the way for future in vivo efficacy assays of such systems.

Overall, the improvements achieved by the incorporation of surfactant MKC in liposomal membrane, in relation to MKC-free RGD-targeted liposomes, resulted in an enhancement of colloidal stability, entrapment efficiency, and biological activity of GLA. The results described in this Chapter represent a first optimization step towards an effective translation of these promising nanoformulation into a novel product for improving the current enzymatic replacement therapy in Fabry disease treatment.

### 3.6. References

1. Cabrera, I. *et al.*  $\alpha$ -Galactosidase-A Loaded-Nanoliposomes with Enhanced Enzymatic Activity and Intracellular Penetration. *Adv. Healthc. Mater.* **5**, 829–840 (2016).
2. Porfire, A. *et al.* Pharmaceutical Development of Liposomes Using the QbD Approach. *Liposomes - Adv. Perspect.* 1–20 (2019) doi:10.5772/intechopen.85374.
3. Dobrovolskaia, M. A., Aggarwal, P., Hall, J. B. & McNeil, S. E. Preclinical Studies To Understand Nanoparticle Interaction with the Immune System and Its Potential Effects on Nanoparticle Biodistribution. *Mol. Pharm.* **5**, 487–495 (2008).
4. Szebeni, J. Complement Activation-related Pseudoallergy: A New Class of Drug-Induced Acute Immune Toxicity. *Toxicology* **216**, 106–121 (2005).
5. Barenholz, Y. Doxil® - The First FDA-approved Nano-drug: Lessons Learned. *J. Control. Release* **160**, 117–134 (2012).
6. Szebeni, J. *et al.* Liposome-induced Complement Activation and Related Cardiopulmonary Distress in Pigs: Factors Promoting Reactogenicity of Doxil and AmBisome. *Nanomedicine Nanotechnology, Biol. Med.* **8**, 176–184 (2012).
7. Colletier, J., Chaize, B., Winterhalter, M. & Fournier, D. Protein Encapsulation in Liposomes: Efficiency Depends on Interactions Between Protein and Phospholipid Bilayer. *BMC Biotechnol.* **2**, (2002).
8. Shimizu, T., Mori, T., Tomita, M. & Tsumoto, K. pH Switching That Crosses over the Isoelectric Point (pI) Can Improve the Entrapment of Proteins within Giant Liposomes by Enhancing Protein–Membrane Interaction. *Langmuir* **30**, 554–563 (2014).
9. Hwang, S. Y. *et al.* Effects of Operating Parameters on the Efficiency of Liposomal Encapsulation of Enzymes. *Colloids Surfaces B Biointerfaces* **94**, 296–303 (2012).
10. Garman, S. C. & Garboczi, D. N. The Molecular Defect Leading to Fabry Disease: Structure of Human  $\alpha$ -Galactosidase. *J. Mol. Biol.* **337**, 319–335 (2004).
11. Ferrer-Tasies, L. *et al.* Quatsomes: Vesicles Formed by Self-Assembly of Sterols and Quaternary Ammonium Surfactants. *Langmuir* **29**, 6519–6528 (2013).
12. Grimaldi, N. *et al.* Lipid-based Nanovesicles for Nanomedicine. *Chem. Soc. Rev.* **45**, 6520–6545 (2016).
13. Cabrera, I. *et al.* Multifunctional Nanovesicle-Bioactive Conjugates Prepared by a One-Step Scalable Method Using CO<sub>2</sub>-Expanded Solvents. *Nano Lett.* **13**, 3766–3774 (2013).

14. Elizondo, E., Veciana, J. & Ventosa, N. Nanostructuring Molecular Materials as Particles and Vesicles for Drug Delivery, Using Compressed and Supercritical Fluids. *Nanomedicine* **7**, 1391–1408 (2012).
15. Ventosa, N., Veciana, J., Sala, S., Cano, M. & (Nanomol Technologies SL). Procedure for the Obtainment of Micro- and Nano-disperse Systems. *WO2006/079889*, (2005).
16. European Medicines Agency. Benzalkonium Chloride Used as an Excipient. *Comm. Hum. Med. Prod.* EMA/CHMP/495737/2013 (2017).
17. Pramanick, S., Singoidia, D. & Chandel, V. Excipient Selection In Parenteral Formulation Development. *Pharma Times* **45**, 65–77 (2013).
18. Ferrer-Tasies, L. *et al.* SI - Quatsomes: Vesicles Formed by Self-Assembly of Sterols and Quaternary Ammonium Surfactants. *Langmuir* **29**, 6519–6528 (2013).
19. Vargas-Nadal, G. *et al.* MKC-Quatsomes: a Stable Nanovesicle Platform for Bio-imaging and Drug-Delivery Applications. *Nanomedicine Nanotechnology, Biol. Med.* **24**, 102136 (2020).
20. Cabrera, I. *et al.* Multifunctional Nanovesicle-Bioactive Conjugates Prepared by a One-Step Scalable Method Using CO<sub>2</sub>-Expanded Solvents. *Nano Lett.* **13**, 3766–3774 (2013).
21. European Medicines Agency. ICH guideline Q3C (R6) on impurities: Guideline for Residual Solvents. *International Conference on Harmonization of Technical Requirements for Registration of Pharmaceuticals for Human Use, EMA/CHMP/ICH/82260/2006* vol. 31 24 [https://www.ema.europa.eu/en/documents/scientific-guideline/international-conference-harmonisation-technical-requirements-registration-pharmaceuticals-human-use\\_en-33.pdf](https://www.ema.europa.eu/en/documents/scientific-guideline/international-conference-harmonisation-technical-requirements-registration-pharmaceuticals-human-use_en-33.pdf) (2019).
22. Moore, T. L. *et al.* Nanoparticle Colloidal Stability in Cell Culture Media and Impact on Cellular Interactions. *Chem. Soc. Rev.* **44**, 6287–6305 (2015).
23. Pabst, G. *et al.* Structural Analysis of Weakly Ordered Membrane Stacks. *J. Appl. Crystallogr.* **36**, 1378–1388 (2003).
24. Lyngsø, J. & Pedersen, J. S. A high-flux automated laboratory small-angle X-ray scattering instrument optimized for solution scattering. *J. Appl. Crystallogr.* **54**, 295–305 (2021).
25. Schwamberger, A. *et al.* Combining SAXS and DLS for Simultaneous Measurements and Time-Resolved Monitoring of Nanoparticle Synthesis. *Nucl. Instruments Methods Phys. Res. Sect. B Beam Interact. with Mater. Atoms* **343**, 116–122 (2015).
26. Steiner, E. M. *et al.* The Structure of the N-terminal Module of the Cell Wall Hydrolase RipA and its Role in Regulating Catalytic Activity. *Proteins Struct. Funct. Bioinforma.* **86**, 912–923

- (2018).
27. Hosemann, R. & Bagchi, S. N. Direct Analysis of Diffraction by Matter. *Science* **141**, (1963).
  28. Pabst, G., Rappolt, M., Amenitsch, H. & Laggner, P. Structural Information from Multilamellar Liposomes at Full Hydration: Full q-range Fitting with High Quality X-ray Data. *Phys. Rev. E - Stat. Physics, Plasmas, Fluids, Relat. Interdiscip. Top.* **62**, 4000–4009 (2000).
  29. Agency European Medicines, Replagal - EMEA/H/C/000369 - IAIN/0096, <https://www.ema.europa.eu/en/medicines/human/EPAR/replagal#product-information-section>, accessed: November, 2019. <https://www.ema.europa.eu/en/medicines/human/EPAR/replagal#product-information-section> (2019).
  30. Redondo-Morata, L., Giannotti, M. I. & Sanz, F. Influence of Cholesterol on the Phase Transition of Lipid Bilayers: A Temperature-Controlled Force Spectroscopy Study. *Langmuir* **28**, 12851–12860 (2012).
  31. Gumí-Audenis, B. *et al.* Insights into the Structure and Nanomechanics of a Quatsome Membrane by Force Spectroscopy Measurements and Molecular Simulations. *Nanoscale* **10**, 23001–23011 (2018).
  32. Crespo-Villanueva, A. *et al.* Casein Interaction with Lipid Membranes: Are the Phase State or Charge Density of the Phospholipids Affecting Protein Adsorption? *Biochim. Biophys. Acta - Biomembr.* **1860**, 2588–2598 (2018).
  33. Giannotti, M. I. *et al.* Highly Versatile Polyelectrolyte Complexes for Improving the Enzyme Replacement Therapy of Lysosomal Storage Disorders. *ACS Appl. Mater. Interfaces* **8**, 25741–25752 (2016).
  34. Abasolo, I. *et al.* Nanotechnology-based Approaches for Treating Lysosomal Storage Disorders, a Focus on Fabry Disease. *Wiley Interdiscip. Rev. Nanomedicine Nanobiotechnology* 1–18 (2020).
  35. Hsu, J. *et al.* Enhanced Endothelial Delivery and Biochemical Effects of  $\alpha$ -Galactosidase by ICAM-1-Targeted Nanocarriers for Fabry Disease. *J. Control. Release* **149**, 323–331 (2011).



” *Science makes people reach selflessly for truth and objectivity; it teaches people to accept reality, with wonder and admiration, not to mention the deep awe and joy that the natural order of things brings to the true scientist.*

— Lise Meitner

# 4

## Effect of modifying the liposomal surface on the intracellular delivery

### 4.1. Importance of nanoparticle-cell interaction for cell uptake

When nanocarriers intended to be used as drug delivery systems in the nanomedicine field enter the body, they find several biological barriers, both extracellular and intracellular. On the one hand, extracellular barriers can include several clearance pathways, e.g., opsonization and activation of the mononuclear phagocyte system, depuration by organs such as kidney, liver or spleen, extravasation, and enzymatic degradation. On the other hand, there also exist intracellular barriers before reaching the cell cytosol, such as the biological plasmatic cell membrane, or the endosomal vesicle compartment.<sup>1</sup> Special attention should also be paid when targeting more complex localizations, such as the central nervous system and the brain, since special and characteristic biological protective structures are found in these cases, e.g., the blood-brain barrier (BBB). Since this important biological obstacle deserves a special attention, **Chapter 7** is focused specifically on BBB assessment.

For successful development of nanobased-drug delivery systems, knowledge in the relation between nanoparticle structure and cell interaction is important, since plays a key role. This understanding is necessary for the proper design of nanocarriers with the desired physicochemical characteristics for

intracellular delivery. Nanoparticle characteristics such as size, shape, geometry, core-corona structure, surface chemistry, or presence of ligands are crucial parameters for optimal cell interaction.<sup>2,3</sup>

Cells own several pathways for uptake and internalize substances (i.e., small molecules, biomolecules, ions, etc.). Although small molecules or ions can be easily internalized both by passive and active pathways, endocytosis became the main internalization route in the case of bigger biomacromolecules. Likewise, nanoparticles are often internalized by endocytosis pathway as well, although some specialized cells can also use the phagocytosis pathway.

First, phagocytosis mechanism is only used by phagocytic cells, including several immune cells (e.g., macrophages, neutrophils, dendritic cells, or monocytes) and other non-specialized phagocytes (e.g., fibroblast or epithelial and endothelial cells) against exogenous elements. This process includes as a first instance an opsonization of the external agent, adhesion and ingestion, phagosome formation, and phago-lysosome formation.<sup>1</sup> Opsonization and posterior sequestration of nanomaterials by phagocytic cells is one of the main causes of clearance of nanosystems. It is known that nanoparticle-cell interactions can influence several cellular uptake pathways. In this sense, the binding of serum protein to nanoparticles could be decreased by the PEGylation of the nanomaterial, minimizing its recognition (and thus, the internalization) by phagocytic cells.<sup>4</sup>

Besides, the rest of non-phagocytic cells (i.e., the majority of cells) use endocytic pathways, generally consisting in the cell membrane deformation and surrounding of the introduced particle in an energy-dependent way.<sup>2</sup> Endocytic pathways are the principal route of entry of nanoparticles into cells,<sup>5</sup> and can be mainly divided in four different mechanisms, represented in **Figure 4.1**: clathrin-mediated endocytosis, caveolae-mediated endocytosis, other clathrin- and caveolae-independent endocytosis, and macropinocytosis.<sup>1,6</sup>

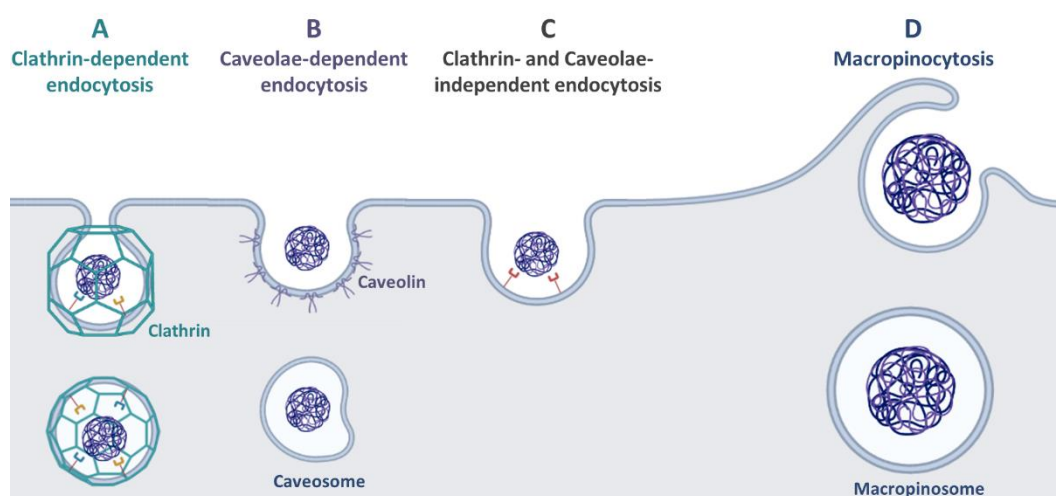


**Figure 4.1.** Mechanisms for endocytic-based cellular internalization, including (A) clathrin-dependent endocytosis, caveolae-dependent endocytosis, (C) clathrin- and caveolae-independent endocytosis, and (D) macropinocytosis. Adapted from Torres-Vanegas et al.<sup>1</sup>

Among those, the most studied internalization pathway is the clathrin-mediated endocytosis. This process involves a first step of binding of cell membrane receptors (e.g., receptors for transferrin, low-density lipoprotein, epidermal growth factor...) to nanoparticle surface ligands. This is followed by a clustering process, including the nucleation of cytosolic proteins to form a coated cage, followed by a membrane invagination, and its final pinch off to obtain an intracellular vesicle, of sizes around 100 – 200 nm.<sup>1,7</sup> Clathrin-mediated endocytosis process is a widely shared route for the internalization of several nanoparticle systems.<sup>6</sup> Then, the second most studied internalization route is the caveolae-mediated endocytosis. In this pathway, particles bind to cell plasma membrane and move to caveolae invaginations, cell structures characterized by comprising caveolin proteins with scaffolding features. Particles are incorporated into the intracellular vesicles (around 50 – 100 nm) by receptor-ligand interactions.<sup>1</sup> However, there exist also internalization pathways independent from clathrin or caveolin. Although in many cases the exact mechanism still is unclear, intracellular vesicles about 90 nm are usually formed. Besides, another pathway for cell uptake is the macro-pinocytosis route, typically used for the internalization of larger particles (0.5 – 5  $\mu\text{m}$ ), e.g., viruses, bacteria, or cell fragments.<sup>1</sup> Finally, direct translocation of the plasma membrane is possible for some particles, but this route is highly influenced by charge and size, limited to cationic particles usually smaller than 20 nm.<sup>1</sup>

The internalization pathway for each type of nanoparticle strongly depends on cell type and nanoparticle characteristics. This knowledge is very relevant for the efficient design of nanoparticles as drug nanocarriers towards specific cells. However, the identification of the exact cell internalization pathway of nanoparticles is still challenging. For example, the use of inhibitors of particular well-known internalization pathways can be utilized in cell culture models, although several times cells can compensate the lack of the intended inhibit pathway by the modulation of another one.<sup>5</sup> Besides, uptake of nanoparticles is usually investigated by fluorescence-based techniques, as flow cytometry or confocal microscopy.<sup>5</sup> On the one hand, quantitative-based techniques such as flow cytometry (fluorescence-activated cell sorting or FACS) allow an accurate quantification of fluorescence per cell,<sup>8</sup> although it cannot distinguish if a particle is just bounded to the cell membrane or if it is properly internalized inside.<sup>5</sup> Therefore, microscopic imaging, such as confocal imaging, can provide complementary information in a qualitative or semi-quantitative way.<sup>9</sup>

Overall, since the biological behavior of nanoparticles with cell surface strongly depends on their physicochemical characteristics, the robust determination of nanoparticle' characteristics, e.g., composition or surface functionalization, becomes of great importance. Therefore, in this Chapter, a deeper characterization of RGD-targeted liposomes is studied, as well as the impact of small functionalization changes on the interaction with cells.



## 4.2. Impact of chol-PEG<sub>400</sub>-RGD density in liposomes' characteristics

Small surface composition changes can have an important effect in physicochemical properties of liposomes, as seen for example in the previous Chapter, in which liposomes with a small addition of MKC could lead into large physicochemical properties' changes (e.g., the important increase in EE% and colloidal stability).

The liposomal vehicle presented in the previous **Chapter 3** was composed by DPPC, cholesterol, small amount of MKC, and the targeting unit chol-PEG<sub>200</sub>-RGD. It means that, in this system, the length of the PEG linker between cholesterol and RGD peptide ligand was considerably short, of 200 Da. As consequence, as mentioned in the beginning of **Chapter 3**, the whole chol-PEG<sub>200</sub>-RGD compound showed a limited solubility in ethanol and the addition of DMSO to the ethanolic phase was required for the correct solubilization of all the membrane components before the DELOS-susp process.

Despite this improvement because of DMSO, previous work done in the group with chol-PEG<sub>200</sub>-RGD liposomes showed generally low recoveries (< 50%) of this component after the DELOS-susp process, indicating a possible precipitation into the reactor as the most probable cause of material loss. Increasing the solubility of the cholesterol-(PEG)<sub>n</sub>-RGD unit will permit increasing its integration in the liposomes and favoring the reproducibility of the process. Therefore, a new chol-PEG-RGD compound was synthesized by Dr. Miriam Royo group from IQAC-CSIC (Barcelona), increasing the PEG length from 200 Da to 400 Da. In general, the longer the polyethylene glycol chain length, the higher hydrophilicity, so this longer PEG chain compound (chol-PEG<sub>400</sub>-RGD) was expected to show better solubility properties in polar solvents, as well as longer PEGs tend to provide better nanoparticles' stability and longer blood-circulation times. Therefore, it was decided to formulate nanoliposomes with chol-PEG<sub>400</sub>-RGD instead of chol-PEG<sub>200</sub>-RGD (**Figure 4.2**).

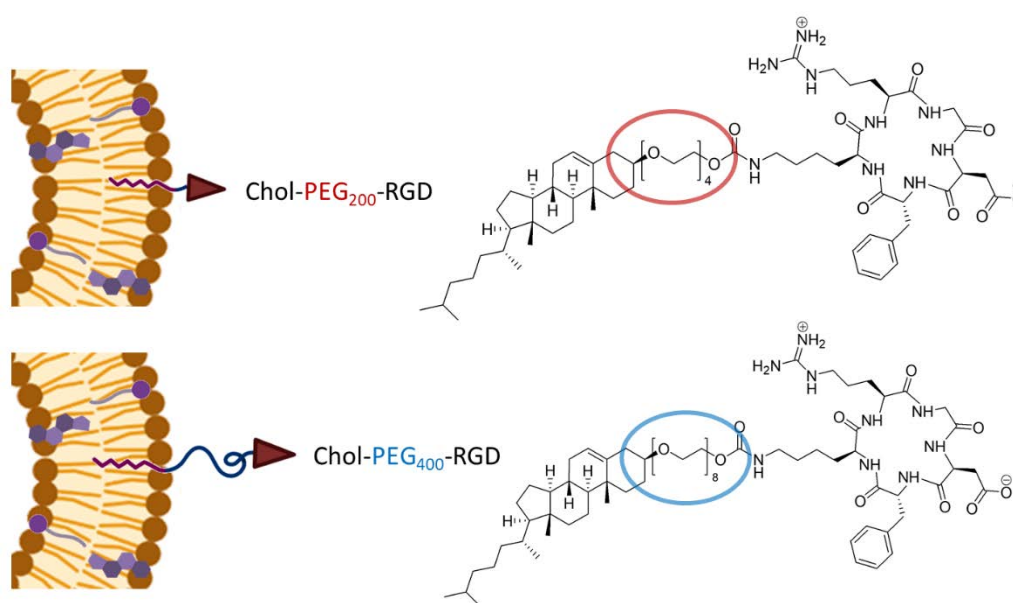


**Figure 4.2.** Scheme of liposomes composed by DPPC, cholesterol, MKC, and chol-PEG<sub>n</sub>-RGD, being n = 4 (top) or n = 8 (bottom). See chemical details of chol-PEG<sub>200</sub>-RGD and chol-PEG<sub>400</sub>-RGD in **Chapter 9.6.1**.

The impact of RGD density (i.e., chol-PEG<sub>400</sub>-RGD density) in liposomal surface in the physicochemical characteristics was then studied, as well as the robustness of the DELOS-susp process to produce nanovesicles with controlled functionalization ratio. Hence, three different RGD densities were compared: 0 mol %, 3 mol %, and 6 mol % of chol-PEG<sub>400</sub>-RGD in relation to the total mol of membrane components (**Figure 4.3**).

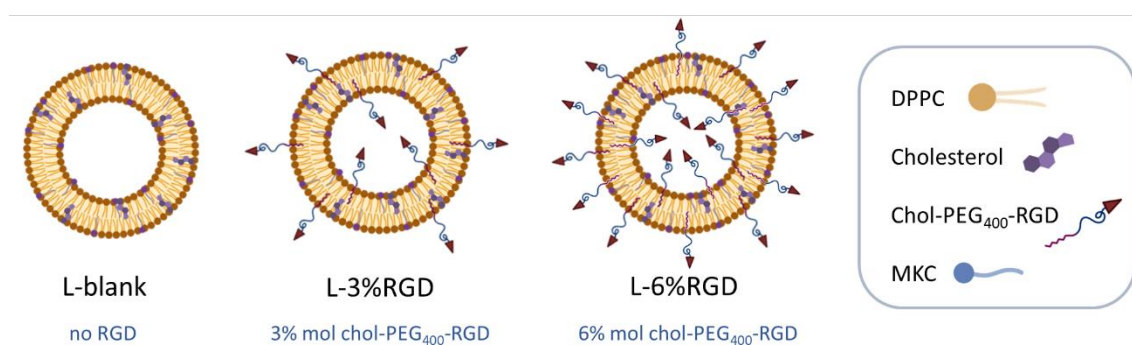


**Figure 4.3.** Scheme of the three liposomal systems prepared, containing three different RGD densities: 0 mol % (blank), 3 mol %, and 6 mol % in relation to the rest of membrane components.

Systems were produced by DELOS-susp in the small-lab scale equipment, and then were submitted to a TFF diafiltration process in water to remove the non-incorporated components as well as eliminate the remaining organic solvents. Then, a deep physicochemical characterization was done, in terms of chemical composition, nanoparticle size, PDI, and  $\zeta$ -potential, as well as morphological and lamellarity analysis by SAXS (experimental protocols described in **Chapter 9**).

#### 4.2.1. Quantification of membrane components

Several properties of drug delivery systems (DDS) are directly related to the chemical composition, as well as the supramolecular self-assembled structure, such as its efficacy, stability, pharmacokinetics, and drug-release properties. Moreover, the quality of lipid components can affect the quality and performance of the liposome drug product. Therefore, medicine regulatory agencies, such as the FDA and the EMA, dictate that one requirement for the successful development of any DDS is the definition and measurement of its chemical composition.<sup>10</sup>

Thus, the development of sensitive and quantitative analytical methods for the analysis of chemical composition of nanovesicles is an important requirement, to ensure the robustness in the manufacturing process and to demonstrate that characteristics batch-to-batch are comparable and similar to the expected ones.

Real concentration of DPPC, cholesterol, and chol-PEG<sub>400</sub>-RGD present in liposomes were quantified by High Performance Liquid Chromatography (HPLC), both after DELOS-susp process and after TFF diafiltration step (**Table 4.1**). Briefly, samples were lyophilized in replicates for removing water and organic solvents, and the dry product was solubilized in methanol for later injection to HPLC (detailed in **Chapter 9.4** and **Chapter 9.5.4.2**).

**Table 4.1.** Quantification of DPPC (DP), cholesterol (CH), chol-PEG<sub>400</sub>-RGD (CH-RGD) by HPLC in liposomal samples\*, containing also low amount of MKC (not quantified).

System ID	Concentration (mg mL <sup>-1</sup> ) (± SD)			Component ratio (mol %) (± SD)		
	DP	CH	CH-RGD	DP	CH	CH-RGD
L-blank	0.71 + 0.04 (0.81 + 0.07)	0.282 + 0.002 (0.285 + 0.022)	–	57.1 + 1.5 (59.9 + 0.3)	42.9 + 1.5 (40.1 + 0.3)	–
L-3%RGD	0.64 + 0.01 (0.70 + 0.01)	0.253 + 0.005 (0.230 + 0.001)	0.064 + 0.002 (0.062 + 0.002)	55.3 + 0.2 (59.8 + 0.4)	41.7 + 0.0 (37.4 + 0.3)	3.0 + 0.1 (2.9 + 0.1)
L-6%RGD	0.57 + 0.02 (0.61 + 0.02)	0.217 + 0.009 (0.189 + 0.005)	0.125 + 0.006 (0.115 + 0.004)	54.2 + 0.3 (59.2 + 0.3)	39.0 + 0.1 (34.8 + 0.2)	6.4 + 0.1 (6.0 + 0.1)

\* Values correspond to the average of two independent batches for each system, expressed in mass concentration and mol % ratio. In parenthesis, samples after diafiltration.

These data allowed to calculate some parameters, such as the real mol proportion of each membrane component (**Table 4.1**), the yield of each step (DELOS-susp, diafiltration, and the overall, **Eq. 4.1 – Eq. 4.3**), and RGD incorporation efficiency (**Eq. 4.4**). In these equations, Lipid<sub>DELOS</sub> is the sum of total lipid (DP, CH, and CH-RGD) quantified by HPLC in intermediate samples (obtained after DELOS-susp), Lipid<sub>DIAF</sub> is the sum of total lipid quantified by HPLC in diafiltrated samples (after TFF diafiltration process), and Lipid<sub>THEOR</sub> corresponds to the theoretical lipid concentration used in the preparation.

$$\text{Recovery DELOS-susp (R}_{\text{DELOS}}\text{) (\%)} = \frac{\text{Lipid}_{\text{DELOS}} \text{ (mg mL}^{-1}\text{)}}{\text{Lipid}_{\text{THEOR}} \text{ (mg mL}^{-1}\text{)}} \times 100 \quad (\text{Eq. 4.1})$$

$$\text{Recovery Diafiltration (R}_{\text{DIAF}}\text{) (\%)} = \frac{\text{Lipid}_{\text{DIAF}} \text{ (mg mL}^{-1}\text{)}}{\text{Lipid}_{\text{DELOS}} \text{ (mg mL}^{-1}\text{)}} \times 100 \quad (\text{Eq. 4.2})$$

$$\text{Recovery Overall (R}_{\text{OVERALL}}\text{) (\%)} = \frac{\text{Lipid}_{\text{DIAF}} \text{ (mg mL}^{-1}\text{)}}{\text{Lipid}_{\text{THEOR}} \text{ (mg mL}^{-1}\text{)}} \times 100 \quad (\text{Eq. 4.3})$$

Results confirmed the robustness of the DELOS-susp methodologies for the preparation of nanovesicles, with high batch-to-batch reproducibility. The RGD functionalization ratio of each system (mol %) fitted very well with the theoretical one, obtaining  $2.9 \pm 0.1$  % and  $6.0 \pm 0.1$  % mol for the L-3%RGD and L-6%RGD system, respectively (**Table 4.1**). Additionally, comparing the Chol-PEG<sub>400</sub>-RGD

concentration in the intermediate sample (obtained after DELOS-susp) with the final sample (after diafiltration step) high RGD incorporation efficiencies were achieved,  $97 \pm 1 \%$  and  $92 \pm 1 \%$  (**Eq. 4.4**). These results indicate that the chol-PEG<sub>400</sub>-RGD was well incorporated into the liposomal bilayer.

$$\text{RGD incorporation efficiency (\%)} = \frac{\text{Ch-RGD}_{\text{DIAF}} \text{ (mol)}}{\text{Ch-RGD}_{\text{DELOS}} \text{ (mol)}} \times 100 \quad (\text{Eq. 4.4})$$

Additionally, high recoveries ( $> 75 \%$ ) after the whole process were obtained (**Table 4.5**). On the one hand, the amount of lipid lost from the DELOS-susp process can be attributed to material lost during the preparation, e.g., due to be in contact with laboratory material, or the walls and tubes of the high-pressure vessel. These recoveries (76 – 83%) were considered high enough to consider DELOS-susp methodology as a good procedure to prepare nanovesicular systems and yields from this technology have the potential to be even larger when using higher production plants. On the other hand, the TFF diafiltration step showed recoveries around 100 %, indicating practically no loss of non-incorporated free molecules during the TFF process.

**Table 4.5.** Lipid concentration (sum of DPPC, cholesterol, and chol-PEG<sub>400</sub>-RGD) and samples after diafiltration in parenthesis. Mass recoveries of each production step: DELOS-susp ( $R_{\text{DELOS}}$ ), diafiltration ( $R_{\text{DIAF}}$ ), and whole process ( $R_{\text{OVERALL}}$ ).

System ID*	Lipid (mg mL <sup>-1</sup> ) (± SD)	R <sub>DELOS</sub> (%) (± SD)	R <sub>DIAF</sub> (%) (± SD)	R <sub>OVERALL</sub> (%) (± SD)
L-blank	1.00 + 0.03 (1.09 + 0.09)	83 + 3	109 + 5	91 + 8
L-3%RGD	0.95 + 0.02 (0.99 + 0.01)	79 + 1	104 + 1	83 + 1
L-6%RGD	0.91 + 0.03 (0.92 + 0.03)	76 + 3	101 + 0.1	76 + 3

\* Values correspond to the average of two independent batches for each system. The initial theoretical lipid concentration was 1.2 mg mL<sup>-1</sup>.

#### 4.2.2. Supramolecular physicochemical characterization

Once the chemical composition was analyzed, analysis was moved to supramolecular and nanoscopic characteristics, such as size, PDI, and  $\zeta$ -potential, measured by DLS (see **Chapter 9.5.1**). After production, liposomes showed small size ( $\sim 125$  for total, and  $\sim 135$  nm for diafiltrated), narrow PDI ( $< 0.3$ ) and high  $\zeta$ -potential ( $> +40$  mV), as **Table 4.6** summarizes. Moreover, any appreciable difference in size was observed between the three systems. Besides, the  $\zeta$ -potential values of RGD-containing liposomes was lower than plain liposomes without RGD. This decrease can be attributed to the surface charge masked effect due to the PEG-RGD coating of the liposomal surface.

**Table 4.6.** Size, PDI, and  $\zeta$ -potential by DLS, 0 – 2 days after production by DELOS-susp\*.

System ID	Size (nm) ( $\pm$ SD)	PDI ( $\pm$ SD)	$\zeta$ -potential (mV) ( $\pm$ SD)
L-blank	127 $\pm$ 2	0.18 $\pm$ 0.01	64 $\pm$ 2
	(139 $\pm$ 2)	(0.25 $\pm$ 0.01)	(61 $\pm$ 0)
L-3%RGD	123 $\pm$ 1	0.19 $\pm$ 0.01	55 $\pm$ 2
	(132 $\pm$ 1)	(0.23 $\pm$ 0.01)	(43 $\pm$ 2)
L-6%RGD	127 $\pm$ 1	0.21 $\pm$ 0.01	41 $\pm$ 5
	(132 $\pm$ 2)	(0.23 $\pm$ 0.01)	(41 $\pm$ 1)

\*In parenthesis, samples after diafiltration. Values correspond to the average of two independent batches for each system.

Then, the impact of chol-PEG<sub>400</sub>-RGD density in the lamellarity and bilayer structure of liposomes was deeper analyzed by SAXS in collaboration with Prof. Jan Skov Pedersen group from Aarhus University (Denmark). As in samples previously described in this Thesis (**Chapter 3, Figure 3.7**), SAXS data showed a characteristic minimum at intermediate  $q$ , typical for liposomes, attributed to the electron density variations across the cross-section profile of the bilayer membranes.

First, broad bumps from SAXS data showed that liposomes were mainly unilamellar, with only small structural changes between the three systems (**Figure 4.4A**). Then, data were modelled and fitted with the same paracrystalline model<sup>11</sup> based on Pabst et al.<sup>12,13</sup> used in the previous **Chapter 3**, where different structural parameters can be determined, such as the average number of layers ( $N_{layers}$ ), the bilayer thickness ( $T$ ), the degree of unilamellarity ( $f_{single}$ ), and the spacing between the layers ( $D$ ) (**Table 4.7**). A schematic representation of these parameters was previously presented in **Figure 3.7**.

**Table 4.7.** SAXS data of systems containing three different chol-PEG<sub>400</sub>-RGD densities, 0 mol %, 3 mol %, and 6 mol %.

System ID <sup>†</sup>	$\chi^2$	$f_{single}$ ( $\pm$ SD)	$\sigma_N$	$N_{layers}$	$z$ ( $\text{\AA}$ ) ( $\pm$ SD)	$T$ ( $\text{\AA}$ ) ( $\pm$ SD)	$D$ ( $\text{\AA}$ ) ( $\pm$ SD)
L-0%RGD	0.69	0.92 $\pm$ 0.03	5*	1.3	31.2 $\pm$ 0.2	72.4 $\pm$ 0.4	67.9 $\pm$ 1.0
	0.85	0.91 $\pm$ 0.02	5*	1.4	31.4 $\pm$ 0.2	72.8 $\pm$ 0.4	67.6 $\pm$ 0.7
L-3%RGD	0.86	0.95*	5*	1.2	32.5 $\pm$ 0.2	75.0 $\pm$ 0.4	73.1 $\pm$ 1.9
	0.72	0.95*	5*	1.2	32.6 $\pm$ 0.1	75.2 $\pm$ 0.2	76.0 $\pm$ 1.1
L-6%RGD	0.80	0.95*	5*	1.2	33.8 $\pm$ 0.2	77.6 $\pm$ 0.4	76.6 $\pm$ 1.3
	0.81	0.95*	5*	1.2	33.9 $\pm$ 0.2	77.8 $\pm$ 0.4	78.8 $\pm$ 1.9

<sup>†</sup> For each system, data of two independent batches. Values correspond to diafiltrated samples, 11 days after production;  $\chi^2$  is the reduced weighted chi-square;  $f_{single}$  is the fraction of single layers;

$\sigma_N$  is the sigma value of the Gaussian of the distribution;  $N_{\text{layers}}$  is the average number of layers in liposomes;  $z$  is the distance from the center of the bilayer to the centers of the Gaussian used to describe the headgroup;  $T$  is the bilayer thickness defined as  $T = 2(z + \sigma_N)$ ;  $D$  is the distance between the centers of the layers; \*Fixed values.

First, data indicated a high level of single-layered liposomes, since the average number of layers and degree of unilamellarity parameters ( $N_{\text{layer}}$  and  $f_{\text{single}}$ ) were close to 1. Moreover, looking at the bilayer thickness  $T$  (related to the headgroup-to-headgroup distance,  $z_H$ ), there was found a linear correlation with the chol-PEG<sub>400</sub>-RGD loading in the liposome phospholipid membranes (**Figure 4.4B**). The highest amount of chol-PEG<sub>400</sub>-RGD in the liposome, the thicker apparent liposomal bilayer, confirming the different contribution effect that PEG coating density can have. Additionally, some non-unilamellar liposomes (i.e., having more than one concentric lipid bilayer) were also found in low proportion, and interestingly, a correlation between the space between the bilayers (related to  $D$ ) was observed, probably due to the steric effect of having more PEG density (**Figure 4.4B**).

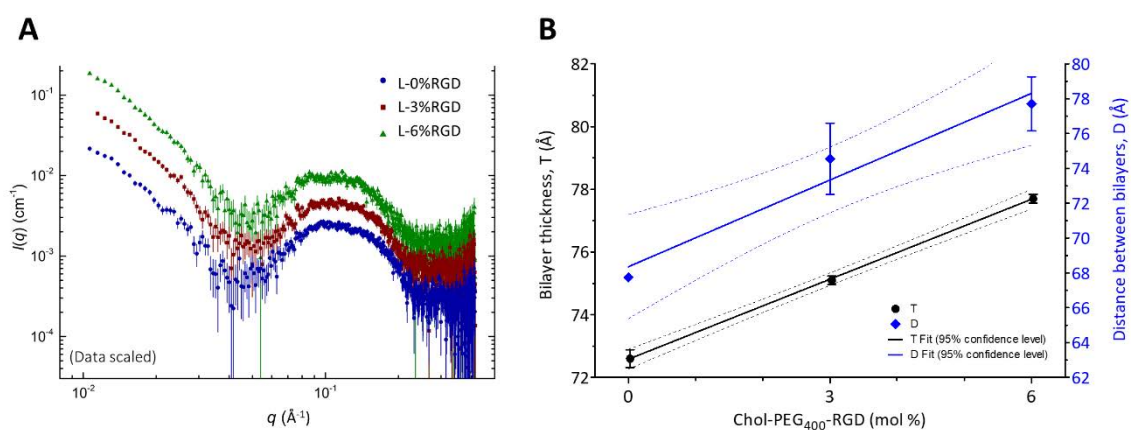


**Figure 4.4.** (A) SAXS data of liposomes with different RGD density; (B) Effect of chol-PEG<sub>400</sub>-RGD loading in bilayer thickness ( $T$ , black line) and distance between bilayers ( $D$ , blue line), average of two independent batches for each system. Measures performed by Prof. J. S. Pedersen from Aarhus University (Denmark).

Overall results showed that DELOS-susp technique allows the obtaining of nanovesicles with a robust peptide-functionalization. Small changes in the functionalization ratio can have an impact on the surface of the nanovesicles. Although no appreciable difference in the supramolecular structure of nanovesicles was observed by DLS, SAXS technique reveals to be an interesting technique for study deeply the liposomal surface. The data obtained by SAXS suggested a thickening of the liposomal membrane when it contains more proportion of chol-PEG<sub>400</sub>-RGD. Additionally, chemical composition values obtained by HPLC confirm the easier incorporation of chol-PEG<sub>400</sub>-RGD in the liposomal membrane, in comparison with chol-PEG<sub>200</sub>-RGD. Therefore, in next sections, RGD liposomal functionalization will be always given by the chol-PEG<sub>400</sub>-RGD instead of the chol-PEG<sub>200</sub>-RGD.

### 4.2.3. Fluorescent labeling of liposomes for in vitro cell studies

Liposomal systems containing different RGD-targeting densities were successfully achieved and characterized, confirming the difference in RGD density composition. Then, the possible impact that this difference can have in the interaction with cells was investigated. However, many in vitro assays, and especially those related with cell internalization assessment, require the use of fluorescent molecules to monitor and track the compound of interest. Therefore, the labelling of liposomes with fluorescent labels was required.

In the frame of previous work done in Nanomol group (ICMAB-CSIC), the integration of hydrophobic fluorescent indocyanine dyes in nanovesicles was studied for the development of optical probes for bioimaging applications.<sup>14-16</sup> These hydrophobic dyes (e.g., DiD and DiI) were successfully loaded between the nanovesicle bilayers without leakage, and leading to high extinction coefficient in non-aqueous environment. In this Thesis, the DiD dye was selected as the fluorophore for labelling our liposomal systems. DiD (i.e., 1,1'-dioctadecyl-3,3,3',3'-tetramethylindodicarbocyanine perchlorate) contains two long aliphatic chains (C18) that can be ideal to be inserted into the hydrophobic membrane of the liposomes (**Figure 4.5A**).

DiD is an organic solvent-soluble fluorescent dye, which shows the absorption maximum ( $\lambda_{\text{abs}}$ ) at 649 nm and its emission ( $\lambda_{\text{em}}$ ) at 674 nm when it is solubilized in ethanol. On the contrary, DiD is a water-insoluble dye, thus the dye tends to self-aggregate when it is dispersed in aqueous media. Aggregation phenomena leads into a change in their spectroscopic properties, losing its fluorescent emission due to self-quenching.<sup>17</sup> As represented in **Figure 4.5B**, the presence of non-fluorescence aggregates results in an increase of the absorption shoulder ( $\sim 600$  nm), whereas the fluorescence molecule in monomer form has a characteristic absorption peak at 649 nm.

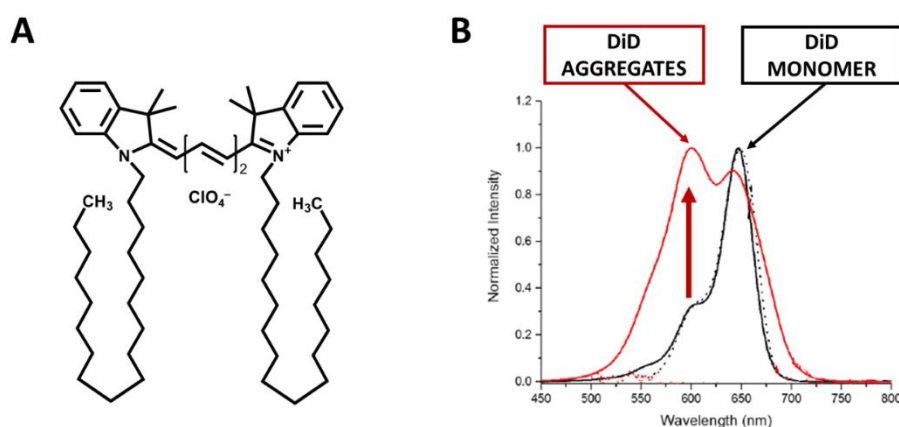


**Figure 4.5.** (A) Chemical structure of 1,1'-dioctadecyl-3,3,3',3'-tetramethylindodicarbocyanine perchlorate (DiD) fluorescent dye, and (B) Normalized absorption

spectra of DiD in ethanol (well-dispersed) and in water (aggregated). Adapted from Ardizzone PhD thesis <sup>17</sup>.

Two strategies were studied for the incorporation of DiD into the liposomal samples: (i) DiD addition post-production of liposomal formulation by incubation, or (ii) DiD added during the production by DELOS-susp incorporated together with the rest of components (**Figure 4.6**). In both cases, the obtained liposomes samples were followed by a diafiltration step, to remove the non-incorporated molecules (e.g., free dye not inserted into the membrane) and remained organic solvent (e.g., EtOH and DMSO). To confirm that the fact of containing RGD did not affect, both liposomes without functionalization (L-blank) and with RGD targeting (L-RGD, containing 3 mol % of chol-PEG<sub>400</sub>-RGD) were evaluated. Besides, in vitro internalization assays only require a small concentration of dye, so it was started trying 100 nM of DiD, corresponding to 0.004 mol % in relation to the rest of membrane components. This concentration was similar of those used in previous in vitro cell internalization experiments.<sup>18</sup>

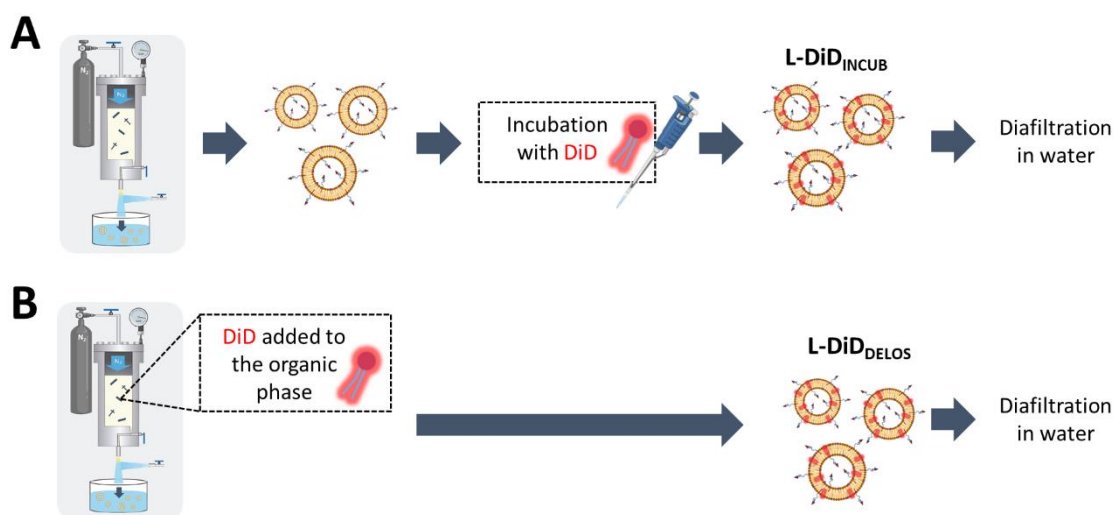


**Figure 4.6.** Strategies for DiD-labelling of liposomal systems, by (A) standard production by DELOS-susp and posterior incubation with the dye, and (B) by direct addition to the organic phase with the rest of membrane components, during the DELOS-susp process. In both cases, samples were TFF diafiltrated in water for removing the non-incorporated components.

Fluorescence spectra of the resulting DiD-labeled liposomes was recorded directly, without any modification or dilution (see experimental details **Chapter 9.5.8.2**). Both excitation and emission profiles were recorded. The excitation spectrum gives information about the wavelengths responsible to cause the fluorescence emission at a specific wavelength, i.e., excitation is scanned over all the wavelengths of the spectrum at a determined emission wavelength. Besides, the emission spectrum of a fluorophore is determined by the excitation at a determined wavelength (near the maximum of absorption) and the recording of the fluorescence emission intensity over the wavelength spectra.



Emission intensity at the wavelength of the maximum intensity peak corresponded to the recorded signal in many fluorescent experiments.

An adequate fluorescent signal was observed for samples in which DiD was incorporated by DELOS-susp (L-blank-DiD<sub>DELOS</sub> and L-RGD-DiD<sub>DELOS</sub>), independently of RGD presence. On contrast, a notable decrease on intensity was observed for samples in which DiD was incorporated by incubation (L-blank-DiD<sub>INCUB</sub> and L-RGD-DiD<sub>INCUB</sub>) (**Figure 4.7**). This lower fluorescent signal in incubated samples could be attributed to a lower concentration of dye, due to either a lower incorporation in the liposomal membrane and, then, a higher loss during the diafiltration step, or a self-aggregation of the dye in the aqueous media, leading consequently in a fluorescent quenching. Comparison of these samples with samples previous diafiltration (**Figure 4.7**, dotted lines) reveals a similar fluorescence signal, pointing out that the low fluorescence intensity was probably due to a fluorescent quenching and not to a dye loss or chemical degradation. The carbocyanine dye family, in which DiD belongs, is characterized by showing very low water-solubility, as well as the loss of fluorescent properties in an aqueous environment, so the addition of dye over already prepared nanovesicles (i.e., by incubation) can hinder the integration of these molecules into the lipid bilayer, leading to the aggregation and precipitation of the dye. In contrast, the incorporation of the fluorescence labelling by DELOS-susp allowed a good dissolution of DiD together with the rest of membrane components in the CO<sub>2</sub>-expanded ethanolic phase. Subsequently, during the depressurization, liposomes were self-assembled incorporating the DiD molecules into the liposomal bilayer during the process. The dye was well integrated in a lipid-environment, given by the lipid bilayer, and could maintain its spectroscopic properties.

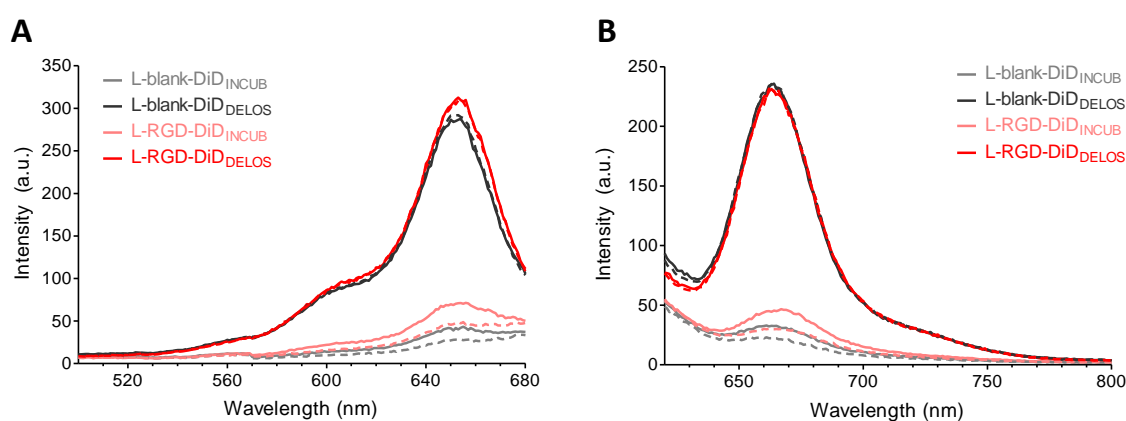


**Figure 4.7.** (A) Excitation spectra ( $\lambda_{em} = 700$  nm) and (B) Emission spectra ( $\lambda_{ex} = 585$  nm) of blank (no RGD targeting) and RGD-functionalized liposomes, after DiD-labelling by incubation (INCUB) or DELOS-susp (DELOS). Liposomes before (dotted lines) and after (solid lines) diafiltration are represented.

The measurement of real DiD concentration in vesicles is usually performed by absorbance, diluting 1:10 first the sample in ethanol to provoke the disruption of the vesicles and the release of the dye, for a more accurately estimation. However, the concentration of DiD in these liposomal systems was too low for performing this additional dilution in ethanol and being within the detection limit. Therefore, a rough estimation of DiD concentration was done by first lyophilizing the sample for removing the solvent, then resuspending the cake in EtOH for complete DiD solubilization, and, finally, determination of the absorbance through the Lambert-Beer Law (see **Chapter 9.4** and **Chapter 9.5.8.1**). Values suggested similar DiD content in all the samples, around 50 nM (**Table 4.8**). However, due to the low DiD concentration and some issues in subtracting the absorbance signal (because of an alteration in the absorbance spectra due to lipid scattering), this value may be underestimated.

**Table 4.8.** DiD concentration in liposomes estimated by absorbance ( $\lambda_{\text{Abs}} = 646 \text{ nm}$ ) after lyophilization and solubilization in ethanol\*.

System ID	Method for DiD incorporation	DiD concentration (nM)
L-blank-DiD	Incubation	~ 42
	DELOS-susp	~ 55
L-RGD-DiD	Incubation	~ 44
	DELOS-susp	~ 59

\* Experimental details in **Chapter 9.4** and **Chapter 9.5.8.1**.

These results showed that the way of incorporating the fluorescent labelling into nanovesicles impact on their optical properties. Incorporation of DiD in liposomes by DELOS-susp presented an advantage over the incubation method, showing higher fluorescence intensity and greater batch-to-batch robustness. Moreover, fluorescence was maintained after dilution in water, showing a linear relation between liposome concentration and fluorescence emission (**Figure 4.8A** and **B**). No DiD release was observed over time, since the maximum emission fluorescence intensity was maintained over time, indicating that samples were optically stable at least 2 months (**Figure 4.8C**).

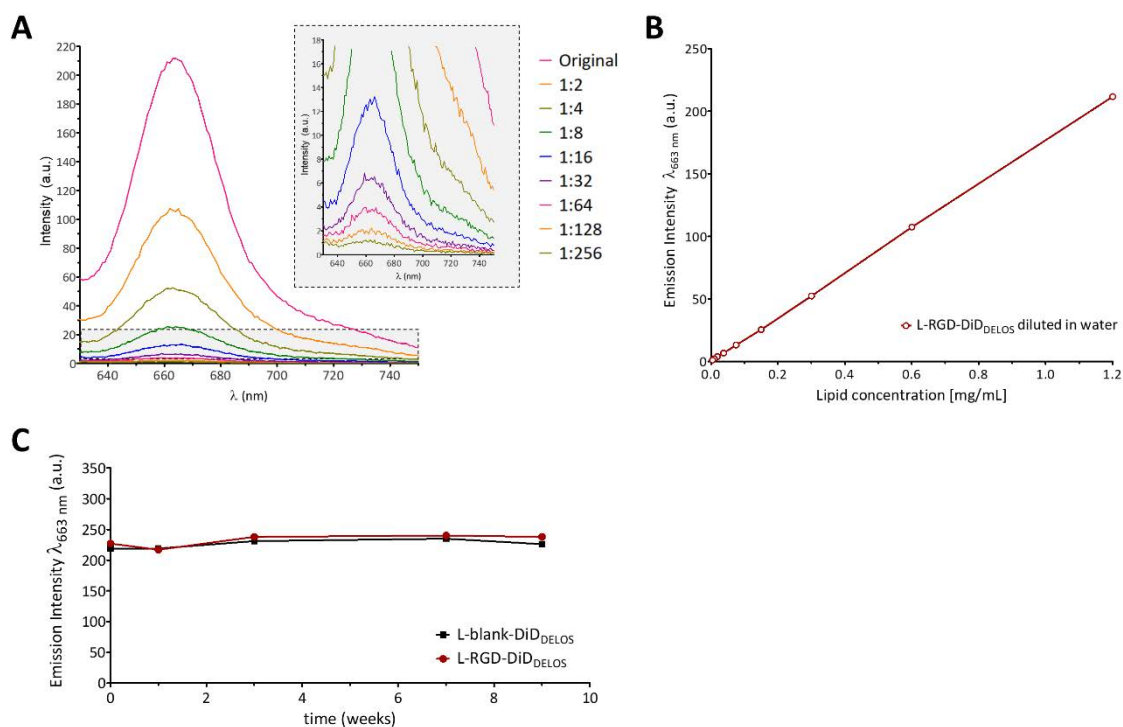


**Figure 4.8.** (A) Fluorescence emission spectra and (B) maximum fluorescence emission intensity of L-RGD-DiD<sub>DELOS</sub> upon dilution in water, and (C) fluorescence emission signal stability of blank and RGD DiD-labeled liposomes over time.

### 4.3. Impact of RGD density on liposomes surface in their interaction with integrin-expressing U2OS cells

After obtaining well-characterized liposomes with demonstrated different RGD-targeting functionalization density and able to be fluorescently labeled, an in vitro cell internalization study was carried out, in close collaboration with Dr. Imma Ratera and Dr. Judith Guasch from ICMAB-CSIC (Barcelona). The objective of this study was to evaluate if small changes in composition or supramolecular characteristics of nanovesicles could modify their biological interaction with cells, as well as to obtain better knowledge of the role of the RGD targeting unit in the internalization process with integrin-expressing cells. Therefore, three different liposomal systems, containing 0 mol %, 3 mol %, or 6 mol % of chol-PEG<sub>400</sub>-RGD, were seeded with human osteosarcoma cells (U2OS).

U2OS is an immortal human cell line derived from osteosarcoma cells. It is reported the expression of  $\alpha_v\beta_3$  and  $\alpha_5\beta_1$  integrins, related to cell adhesion, as well as the positive interaction with RGD motifs.<sup>19,20</sup> Integrins are cell-surface adhesion receptors, presented as transmembrane glycoprotein heterodimers and formed by the non-covalently association of  $\alpha$  and  $\beta$  subunits. The different combination of these subunits association leads to the integrin superfamily, which in humans includes around 24 distinct integrin types (e.g.,  $\alpha_v\beta_3$ ,  $\alpha_v\beta_5$ ,  $\alpha_5\beta_1$ ...).<sup>21</sup> Integrins can recognize ligands of the extracellular matrix (ECM), at the same time as they are in contact with cell cytoskeleton and interact with signaling proteins,

regulating many pathological and physiological cellular processes.<sup>21</sup> Several integrins recognize ECM proteins by short peptide sequences, such as the RGD motif (i.e., arginine-glycine-aspartic acid).<sup>22</sup> RGD peptide sequence can be recognized by integrins such as the  $\alpha_v\beta_3$  and the  $\alpha_v\beta_5$ , related to cell adhesion, cell migration, or angiogenesis processes. Besides, it is reported that integrin-mediated endocytosis can be favored by RGD peptides, so RGD motif has been widely explored as targeting unit in nanoparticles.<sup>23–27</sup>

Therefore, the internalization of RGD-targeted liposomal systems into integrin-expressing U2OS cells was evaluated by confocal microscopy. Since liposomes were fluorescently labeled, this technique allowed their direct visualization in the cell culture, providing information about localization.

The experimental procedure is schematically summarized in **Figure 4.9**. Briefly, human osteosarcoma cells (U2OS) were seeded into fibronectin-coated glass substrates and incubated for 3 hours (37 °C, 5 % CO<sub>2</sub>) with a fixed amount of DiD-labeled liposomes containing different RGD density in their membrane surface. Internalization of liposomes into U2OS was studied by confocal microscopy, after fixation and the immunostaining of cells. Apart from DiD fluorescence coming from liposomes (red signal), cells were stained with Hoechst for nucleus labelling (blue signal), and with phalloidin conjugated to Alexa fluor 488 dye (green signal). Phalloidin can bind to actin filaments, and its staining allows the visualization of the cell cytoskeleton. Details of the experimental methodologies related to sample preparation and immunostaining are described in **Chapter 9.8**.

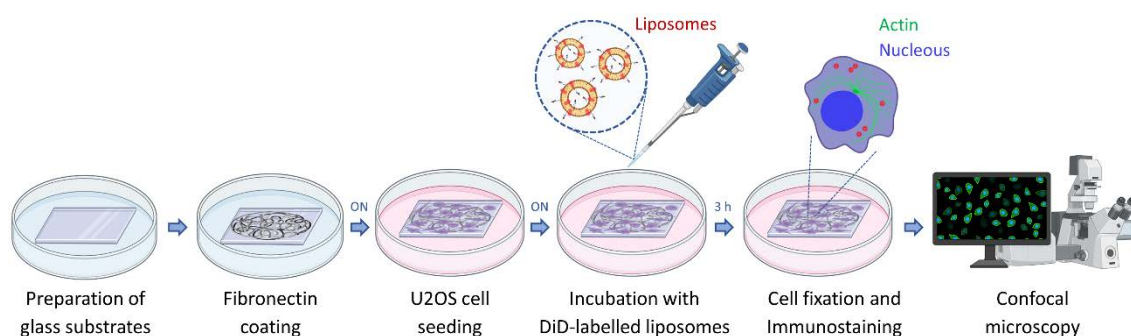


**Figure 4.9.** Scheme illustrating the experimental procedure described in this section for the internalization studies by confocal imaging, see details in **Chapter 9.8**.

After cell immunostaining and mounting of the substrates onto glass slides, confocal imaging was performed for cell internalization analysis. Different representative captures of each system were taken from several glass substrates prepared in three independent sets of experiments. The ImageJ software was used for quantification studies.

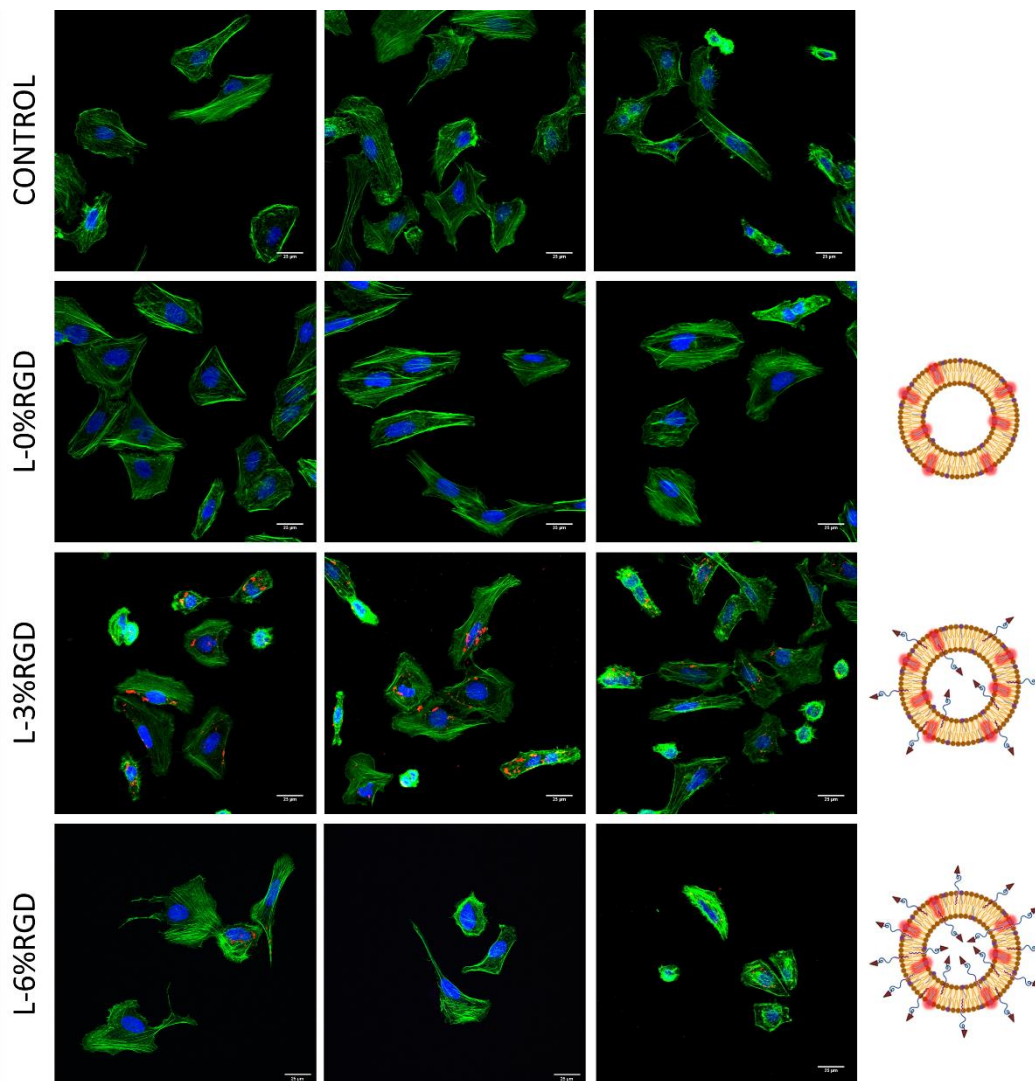


**Figure 4.10.** Representative fluorescence confocal images of U2OS cells treated with L-0%RGD, L-3%RGD, and L-6%RGD ( $0.3 \text{ mg mL}^{-1}$ ); fluorescence labelling includes actin cytoskeleton (green), nucleus (blue), and liposomes (red). Scale bars represent  $25 \mu\text{m}$ .

The proper fixation and staining of cells were confirmed, as seen in representative images of each system (**Figure 4.10**). The cells were successfully stained, since blue signal corresponding to cell nucleus was clearly observed, as well as green signal from the stained actin filaments.

The morphology of cells could be divided into a mixture of well spread cells, and other ones with more rounded shape, which can be attributed to a not completely adherence on the substrate. This finding was more frequently observed in L-6%RGD group. Interestingly, an important difference in DiD red signal coming from liposomes can be distinguished between all the treated groups. First, liposomes without RGD functionalization (L-0%RGD) showed a practically null red signal. Some residual DiD signal was observed in few L-0%RGD treated cells, but this fact was not predominant. However, cells treated with L-3%RGD showed remarkably higher DiD signal, suggesting a better internalization. The cross-section

of some representative pictures confirmed that liposomes were indeed inside cells or interacting with the cell membrane (**Figure 4.11**).

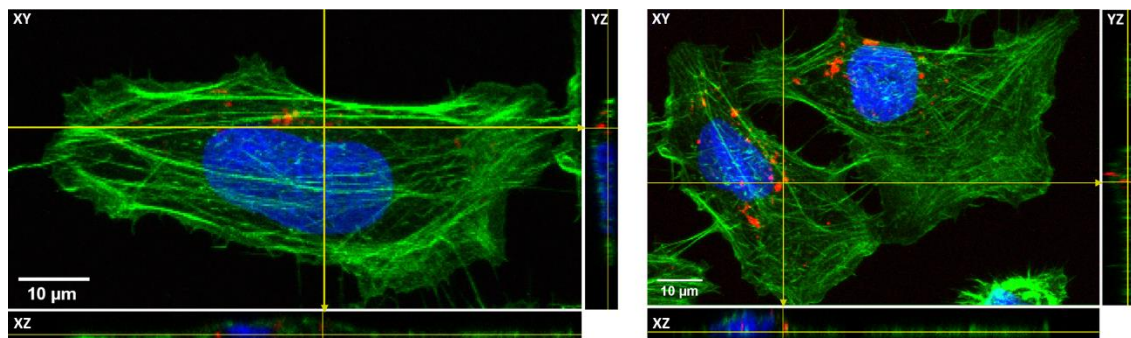


**Figure 4.11.** Some representative confocal cross-sections of U2OS cells treated with L-3%RGD ( $0.3 \text{ mg mL}^{-1}$ ), labelling actin cytoskeleton (green), nucleus (blue), and L-3%RGD liposomes (red). Scale bars represent  $10 \mu\text{m}$ .

These general trends were further confirmed with a more detailed quantification analysis using the ImageJ software, whose schematized protocol is represented in **Figure 4.12** (and detailed in **Chapter 9.8.3.2**). Briefly, cell area as well as DiD fluorescence signal coming from the liposomes were contoured and measured. For quantifying this signal, first, a threshold was applied for background subtraction. Then, particles were analyzed, obtaining the area and intensity of fluorescence signal coming from the liposome' dye, as well as the number of particles per cell. This last parameter (number of particles) does not refer to number of individual liposomes, but to rounded DiD-labeled spherical structures observed in cells, probably corresponding to aggregates of liposomes.

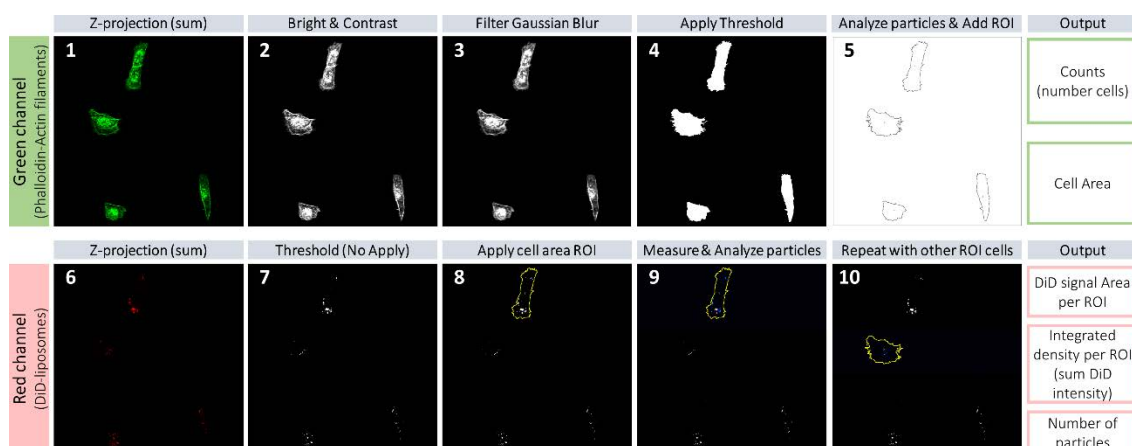


**Figure 4.12.** Example of image treatment for extraction of information concerning cell area and DiD signal: (1) z-projection of green channel, (2) bright & contrast, (3) filter gaussian blur, (4) thresholded image, (5) analysis of particles and regions of interest (ROI) added to manager, (6) z-projection of Red channel, (7) thresholded image, (8) ROI superposition on the image, (9) measure and analyze particles (limit to threshold) in each ROI (i.e., cell area),

(10) Repeat steps 8 and 9 for each cell. Outputs corresponded to the number of cells, cell area, DiD signal area and integrated density per cell, and number of particles.

First, the mean cell area of each group was represented in **Figure 4.13**. Similar cell area was obtained in all the treated groups compared to the control, except for L-6%RGD treated group, which showed slightly lower cell area. This finding correlates well with the less spread and more rounded morphological trend previously detected in this group.

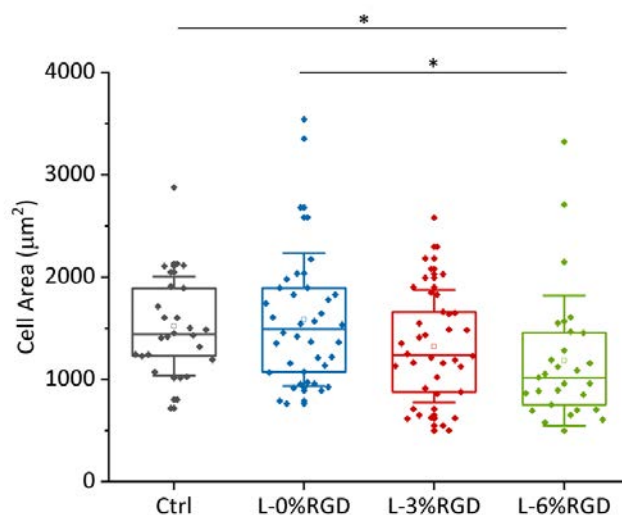


**Figure 7.13.** Cell area of control U2OS cells (Ctrl), and after incubation with L-0%RGD, L-3%RGD, and L-6%RGD liposomes (3 h, 37 °C, 5 % CO<sub>2</sub>). Individual cells are represented by solid dots (number of cells per group 26 – 38); boxes show the 25 – 75 % percentile, central line the median, whiskers 1-fold standard deviation, and empty square the average.

Next, quantification of DiD signal was done by measuring: (A) the area corresponding to liposome signal and normalizing it to the whole cell area, (B) the liposome fluorescence intensity per cell (corresponding to the integrated signal density, i.e., the sum of DiD intensities of each pixel in the selected area), and (C) the number of particles per cell (**Figure 7.14**). The three different analysis correlates well between them. Whereas practically null liposomal signal was found in L-0%RGD group, a greater presence of liposomes was detected in L-3%RGD and L-6%RGD group. Between them, L-3%RGD showed the highest fluorescence signal per cell, as well as the higher % area of DiD signal in relation to the cell area. This finding was more evident in the analysis of number of particles per cell (**Figure 7.14C**). Cells treated with L-3%RGD showed statistically higher DiD-labeled spherical structures corresponding to aggregates of liposomes.

These findings confirm the capacity of chol-PEG<sub>400</sub>-RGD functionalization for enhancing the cellular internalization, as well as confirm that small physicochemical changes in the liposomal surface, in this case the chol-PEG<sub>400</sub>-RGD density, impact on the nanoparticle-cell surface interaction. Further, results

suggest a better in vitro cell uptake for liposomes containing 3 mol % of chol-PEG<sub>400</sub>-RGD in U2OS cell line. Nevertheless, although some general behaviors can be observed, these findings are mainly dependent on the cell type and its specific integrin expression and, thus, may not be exactly extrapolated to other cell lines.<sup>5,20</sup>

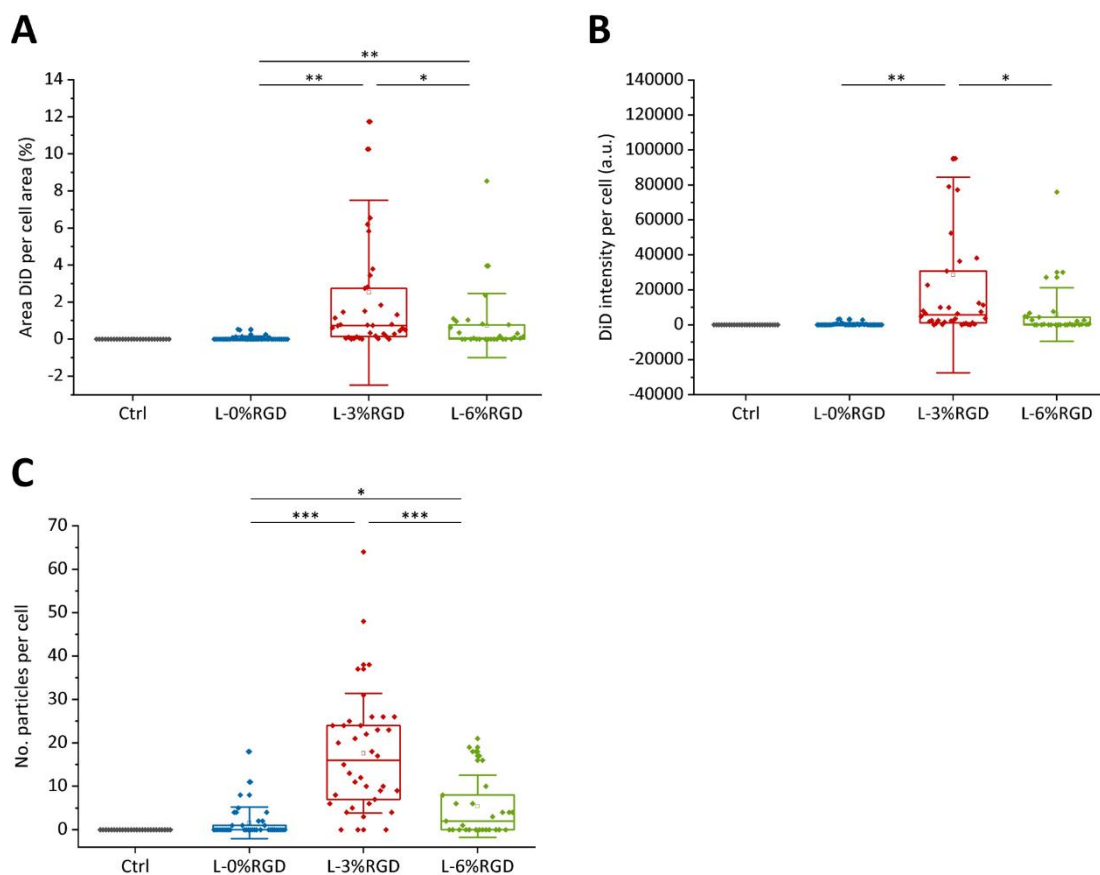


**Figure 7.14.** Quantification of liposome (DiD) signal by: (A) area of liposome DiD signal referred to the whole cell area, (B) liposome fluorescence intensity per cell (i.e., integrated signal density), and (C) number of particles per cell. U2OS cells (Ctrl) were incubated with L-0%RGD, L-3%RGD, and L-6%RGD liposomes (3 h, 37 °C, 5% CO<sub>2</sub>). Individual cells are represented by solid dots (number of cells per group 26 – 38); boxes show the 25 – 75 % percentile, central line the median, whiskers 1-fold standard deviation, and empty square the average.

#### 4.4. Summary and Conclusions

In this Chapter, the structural and biological impact of modifying liposome surface composition with different densities of RGD peptide on cellular internalization was assessed.

First, a cholesterol-PEG<sub>n</sub>-RGD moiety containing a PEG linker (n = 400 Da) was successfully incorporated in the liposomal system, obtaining a great performance in terms of physicochemical characteristics, chemical composition, and process yields. The achieved results promoted the change



from cholesterol-PEG<sub>200</sub>-RGD to cholesterol-PEG<sub>400</sub>-RGD, which will be the one used from now on for RGD-functionalization. Additionally, liposomes decorated with three different RGD-functionalization densities (0, 3, and 6 mol %) were achieved, with RGD ratios close to the theoretical ones. Further, these liposomes could be fluorescently labeled with carbocyanine DiD dye, and results corroborate the suitability of DELOS-susp as a suitable methodology to add new functionalities to nanovesicular systems.

Further, *in vitro* internalization studies with U2OS cells corroborate the functionality of chol-PEG<sub>400</sub>-RGD containing liposomes for enhancing cellular internalization. Liposomes were uptaken to a greater extent when functionalized with 3 mol % of RGD. This finding demonstrates the huge importance of establishing well-controlled methodologies for nanoconjugates' manufacturing processes, as well as robust techniques for their physicochemical characterization.

## 4.5. References

1. Torres-Vanegas, J. D., Cruz, J. C. & Reyes, L. H. Delivery systems for nucleic acids and proteins: Barriers, cell capture pathways and nanocarriers. *Pharmaceutics* **13**, 1–38 (2021).
2. Sabourian, P. *et al.* Effect of physico-chemical properties of nanoparticles on their intracellular uptake. *Int. J. Mol. Sci.* **21**, 1–20 (2020).
3. Rejman, J., Oberle, V., Zuhorn, I. S. & Hoekstra, D. Size-dependent internalization of particles via the pathways of clathrin-and caveolae-mediated endocytosis. *Biochem. J.* **377**, 159–169 (2004).
4. Xin, Y. W., Ishida, T., Ichihara, M. & Kiwada, H. Influence of the physicochemical properties of liposomes on the accelerated blood clearance phenomenon in rats. *J. Control. Release* **104**, 91–102 (2005).
5. Rennick, J. J., Johnston, A. P. R. & Parton, R. G. Key principles and methods for studying the endocytosis of biological and nanoparticle therapeutics. *Nat. Nanotechnol.* **16**, 266–276 (2021).
6. Hillaireau, H. & Couvreur, P. Nanocarriers' entry into the cell: Relevance to drug delivery. *Cell. Mol. Life Sci.* **66**, 2873–2896 (2009).
7. Kaksonen, M. & Roux, A. Mechanisms of clathrin-mediated endocytosis. *Nat. Rev. Mol. Cell Biol.* **19**, 313–326 (2018).
8. Semmling, M. *et al.* A novel flow-cytometry-based assay for cellular uptake studies of polyelectrolyte microcapsules. *Small* **4**, 1763–1768 (2008).
9. Gottstein, C., Wu, G., Wong, B. J. & Zasadzinski, J. A. Precise Quantification of Nanoparticle Internalization. *ACS Nano* **7**, 4933–4945 (2013).
10. Zhou, Y., Gong, X. J. & Yang, J. B. Introduction to the guidance for industry on liposome drug products: chemistry, manufacturing, and controls; human pharmacokinetics and bioavailability; and labeling documentation issued by FDA. *Chinese J. New Drugs* **27**, 1835–1840 (2018).
11. Hosemann, R. & Bagchi, S. N. Direct Analysis of Diffraction by Matter. *Science* **141**, (1963).
12. Pabst, G., Rappolt, M., Amenitsch, H. & Laggner, P. Structural Information from Multilamellar Liposomes at Full Hydration: Full q-range Fitting with High Quality X-ray Data. *Phys. Rev. E - Stat. Physics, Plasmas, Fluids, Relat. Interdiscip. Top.* **62**, 4000–4009 (2000).
13. Pabst, G. *et al.* Structural Analysis of Weakly Ordered Membrane Stacks. *J. Appl. Crystallogr.* **36**, 1378–1388 (2003).
14. Ardizzone, A. *et al.* Nanostructuring Lipophilic Dyes in Water Using Stable Vesicles,

- Quatsomes, as Scaffolds and Their Use as Probes for Bioimaging. *Small* **14**, 1–6 (2018).
15. Morla-Folch, J. *et al.* Dye-Loaded Quatsomes Exhibiting FRET as Nanoprobes for Bioimaging. *ACS Appl. Mater. Interfaces* **12**, 20253–20262 (2020).
  16. Vargas-Nadal, G. *et al.* MKC-Quatsomes: a Stable Nanovesicle Platform for Bio-imaging and Drug-Delivery Applications. *Nanomedicine Nanotechnology, Biol. Med.* **24**, 102136 (2020).
  17. Ardizzone, A. New Fluorescent Nanovesicles, by Self-assembly of Organic Fluorophores, Sterols and Surfactants, as Probes for Bioimaging. (Universitat Autònoma de Barcelona (UAB), 2017).
  18. Cabrera, I. *et al.*  $\alpha$ -Galactosidase-A Loaded-Nanoliposomes with Enhanced Enzymatic Activity and Intracellular Penetration. *Adv. Healthc. Mater.* **5**, 829–840 (2016).
  19. Guasch, J. *et al.* Segregation Versus Colocalization: Orthogonally Functionalized Binary Micropatterned Substrates Regulate the Molecular Distribution in Focal Adhesions. *Adv. Mater.* **27**, 3737–3747 (2015).
  20. Sales, A. *et al.* Cell Type-Dependent Integrin Distribution in Adhesion and Migration Responses on Protein-Coated Microgrooved Substrates. *ACS Omega* **4**, 1791–1800 (2019).
  21. Withofs, N. & Hustinx, R. Integrin  $\alpha\beta 3$  and RGD-based radiopharmaceuticals. *Med. Nucl.* **40**, 41–54 (2016).
  22. Danhier, F., Breton, A. Le & Préat, V. RGD-based strategies to target alpha(v) beta(3) integrin in cancer therapy and diagnosis. *Mol. Pharm.* **9**, 2961–2973 (2012).
  23. Zhao, J., Santino, F., Giacomini, D. & Gentilucci, L. Integrin-targeting peptides for the design of functional cell-responsive biomaterials. *Biomedicines* **8**, (2020).
  24. Kemker, I., Feiner, R. C., Müller, K. M. & Sewald, N. Size-Dependent Cellular Uptake of RGD Peptides. *ChemBioChem* **21**, 496–499 (2020).
  25. Paul, N. R., Jacquemet, G. & Caswell, P. T. Endocytic Trafficking of Integrins in Cell Migration. *Curr. Biol.* **25**, R1092–R1105 (2015).
  26. Xu, X., Zhang, S., Zhang, S., Ma, Y. & Fu, S. RGD peptide-based non-viral gene delivery vectors targeting integrin  $\alpha\beta 3$  for cancer therapy. *J. Drug Target.* **27**, 1–11 (2018).
  27. Temming, K., Schiffelers, R. M., Molema, G. & Kok, R. J. RGD-based Strategies for Selective Delivery of Therapeutics and Imaging Agents to the Tumour Vasculature. *Drug Resist. Updat.* **8**, 381–402 (2005).

” *“The moment of discovery” does not always exist: the scientist’s work is too tenuous, too divided, for the certainty of success to crackle out suddenly in the midst of his laborious toil like a stroke of lightening, dazzling him by its fire.*

— Marie Curie

# 5

## Development of nanoGLA liposomes for Fabry disease treatment with the requirements for advancing towards a preclinical phase

### 5.1. General development of pharmaceutical products

There is a growing need for researchers to be much more involved in the proof of concept process for new therapeutics and diagnostics, and not only to explore all technical and scientific possibilities of a drug delivery formulation.<sup>1</sup> This would allow a better translational research, i.e., the translation of basic science research into clinical applications, which is a crucial step in bringing basic research into clinical reality. Unfortunately, less than 10 % of basic research is nowadays leading into a translation to a clinical application, becoming a real and important challenge.<sup>2</sup>

The Technology Readiness Level (TRL) scale allows a more effective assessment and communication regarding the maturity and progression of the development of a new product or technology, which can be applied to any project as a planning tool for innovation management. Therefore, when applied to pharmaceutical drug discovery field, the following TRL can be distinguished (**Figure 5.1**).

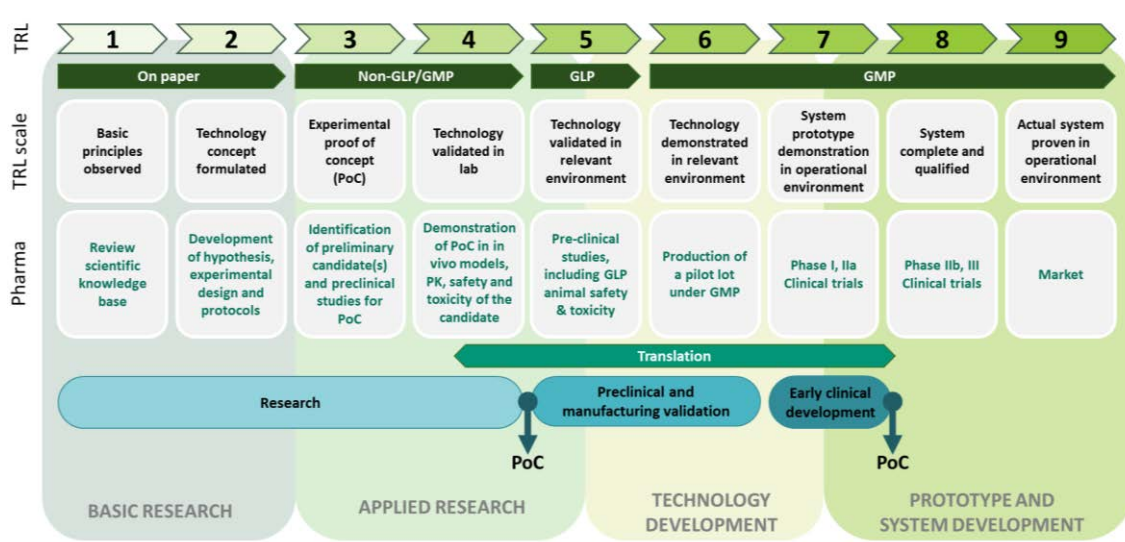


**Figure 5.1.** Technology Readiness Levels (TRLs) and representative research and development milestones of a pharmaceutical product. Adapted from<sup>3,4</sup>.

First TRL stages (TRL-1 and TRL-2) are based on basic research i.e., first hypothesis and preliminary studies to design, synthesize, and identify candidate and technology concepts, as well as the development of protocols and methodologies.<sup>4</sup> Then, TRL-3 is achieved by testing the hypothesis and collecting data to set the initial experimental proof of concept, based on in vitro and in vivo research models, to prove the feasibility of the candidate. In TRL-4, a proof of concept and safety of the candidate is demonstrated in assays including in vivo models, pharmacokinetic, safety, and toxicity studies.

Further steps enter in the development phase. In TRL-5 pilot batches of the drug formulation candidate are produced for further development and assays, including good laboratory practice (GLP) animal safety and toxicity studies in animal model, and additional preclinical studies such as pharmacokinetics and pharmacodynamics. Finally, the last stages of development include a production in pilot plants under good manufacturing practices (GMP), the beginning of clinical trials phase I/II (TRL-6 and TRL-7), clinical trial phase III (TRL-8), and finally the product launch and marketing (TRL-9).

### 5.1.1. Translation of GLA-loaded nanoliposomes to improve the treatment of Fabry disease

One of the main objectives of this Thesis is related to the optimization of the initial version of GLA-nanoformulation (i.e., GLA-loaded nanoliposomes) as a potential nanomedicine candidate to treat Fabry disease. The final goal was obtaining a nanoGLA formulation with optimal physicochemical properties and biological performance, to advance this innovative nanoGLA from the experimental proof of concept to preclinical regulatory phase. In the TRL scale explained before, it could be considered as the progress of the nanoGLA from TRL-3 to TRL-5.

In this Chapter, there are described the studies and improvement processes performed to overcome some product barriers to continue nanoGLA development from an experimental proof of concept to initial preclinical regulatory studies. In this regard, some issues should be considered in any nanomedicine development, such as evaluating if the new formulation could substantially help patients with a specific disease, if there is freedom to operate (i.e., no Intellectual Property problems or a plan to deal with this issue), the feasibility to adapt the production technology to scaling up process, or the necessity that all the procedures were in line with regulatory agencies and good manufacturing practices (GMP) requirements. In this sense, consultations with regulatory agencies (e.g., the EMA or the FDA) are strongly recommended from early product development process, to help in specific scientific and regulatory questions relevant to the nanotechnology product, as well as to address better issues related to safety, effectiveness, or regulatory status of the product.<sup>5</sup> Therefore, during the development of the nanoGLA formulation performed in the frame of this Thesis and the EU project Smart4Fabry (H2020, ID 720942), contact with EMA was established through a Scientific Advice procedure, to address specific questions concerning quality and preclinical development, and asking for advice, together with supportive documentation.

Overall, the final objective of the work presented in this Chapter is obtaining a nanoGLA with the needed requirements (e.g., appropriate physicochemical/biological characteristics for the intended intravenous administration route, with appropriate enzyme concentration, and suitable batch size production) to advance this nanoformulation from the solid experimental proof of concept to an advance preclinical stage of development.

## 5.2. Towards an optimized nanoGLA suitable for preclinical testing

### 5.2.1. Change of GLA protein model to GLAcmycHis for nanoGLA development

As explained in the first chapter, the system used as starting point of this Thesis, reported on Cabrera et al.,<sup>6</sup> contained an in-house GLA produced by Dr. Jose Lu s Corchero from IBB (Barcelona). This recombinant human (rh) GLA was obtained by a transient gene expression-based production method, using HEK 293 F cell line.<sup>7</sup> Compared to the clinically approved versions of the GLA, this latter in-house version of GLA, named GLA-His, contained a tag of histidine (His-tag) that permitted its rapid and efficient purification, retaining 70 % of the enzymatic activity of the clinically available proteins, and allowed the development of the first nanoGLA liposomes.

Moreover, previously in **Chapter 3**, it is described the substitution of GLA-His by the commercially GLA agalsidase alfa (Replagal<sup>®</sup>). Together with the incorporation of a small amount of MKC to the liposomal formulation, an important milestone was achieved, allowing the improvement of the colloidal stability of the system, as well as the entrapment efficiency increase of the GLA into liposomes. Besides, in **Chapter 4** it was demonstrated a high control in the liposomal functionalization and composition.

Moreover, the PEG length from the chol-PEG-RGD moiety was optimized, allowing higher incorporation efficiencies of the RGD targeting unit, as well as good cellular internalization, when PEG 400 Da was used as a linker.

However, although Replagal® is one of the GLA products approved for ERT treatment for Fabry Disease, it was not feasible to use this commercial GLA for further optimization and development of our nanoGLA product, due to the unaffordable high cost and, secondly, because of the lack of freedom-to-operate (FTO) status. For these reasons, two other GLA proteins were developed in the frame of S4F project. Both proteins derived from the human GLA gene and were produced using a stable expression method (**Table 5.1**): (i) the GLAcmycHis for research and development purposes, explained in the present Chapter and produced by Dr. J. L. Corchero from IBB-UAB (Barcelona) or LeanBio SL (Barcelona), and (ii) tag free rh-GLA using a new FTO cell line for preclinical studies, explained in the next Chapter, and produced by Leanbio SL (Barcelona) partner of S4F project. In the following experiments, one of these two GLA versions were used for loading into liposomes, and Replagal® was only used in some experiments as a reference for comparing our nanoGLA formulation with a commercial approved treatment.

**Table 5.1.** Comparison between commercially available GLA products already in the market (†) and GLA versions used for the development of the nanoGLA formulation (‡).

Protein and supplier	Production cell line	Production method	Tags	Buffer media	Physical form and storage conditions
<b>Replagal®</b> † agalsidase alfa <sup>8</sup> (Shire, USA)	Human cells	Stable	–	Sodium phosphate monobasic monohydrate, polysorbate 20, sodium chloride, sodium hydroxide	Liquid soluble (2 – 8 °C)
<b>Fabrazyme®</b> † agalsidase beta <sup>9</sup> (Genzyme, USA)	Chinese Hamster Ovary (CHO)	Stable	–	Mannitol, sodium phosphate monobasic monohydrate, sodium phosphate dibasic heptahydrate	Lyophilized cake (2 – 8 °C)
<b>GLA-His</b> Dr. J.L.Corchero <sup>7</sup> (IBB-UAB, Barcelona)	Human Embryonic Kidney (HEK 293F)	Transient	-His	Acetic acid (0.01 M, pH 4.5)	Liquid soluble (Frozen)
<b>GLAcmycHis</b> ‡ Dr. J.L.Corchero (IBB-UAB, Barcelona)	Chinese Hamster Ovary (CHO DG44)	Stable	-His -cmyc	Acetic acid (0.01 M pH 5.5)	Liquid soluble (Frozen)
<b>tag free rh-GLA</b> ‡ Leanbio SL (Barcelona)	Chinese Hamster Ovary (CHO Celonic)	Stable	–	Mannitol, sodium phosphate monobasic monohydrate, sodium phosphate dibasic heptahydrate	Liquid soluble (Frozen)

‡ Produced by Dr. J.L. Corchero from IBB-UAB (Barcelona) or LeanBio SL (Barcelona) as explained in **Chapter 9.6.2**

The new GLA version used in this Chapter, named hereafter GLAcmycHis, consisted of a new in-house GLA which contained two tags, c-myc and His-tag, produced by a stable expression method using a CHO cell line, and complying with all the appropriate quality requirements. The glycosylation pattern was comparable to Fabrazyme®, since posttranslational modifications depends on the cell line, and also showed appropriate enzymatic activity and protein purity. Moreover, GLAcmycHis showed to be as effective as Replagal® in reducing the Gb3 in an in vitro assay. The production of GLAcmycHis by a stable expression method allows to overcome the limited production yield and the inter-batch variability that the transient expression production method offers.

Therefore, the Replagal® or the GLA-His used so far for the preparation of nanoGLA samples, were substituted by the GLAcmycHis. For the nanoformulation of this new GLA, the already optimized liposomal composition described in **Chapter 3** and **Chapter 4** was used, which contain a small amount of surfactant MKC and chol-PEG<sub>400</sub>-RGD (using a PEG 400 Da linker for the attachment of RGD peptide to a certain number of cholesterol units of liposomal membrane). In all the experimental of this Chapter, the GLAcmycHis enzyme was used as an intermediate GLA model for R&D purposes.

## 5.2.2. Identification of the Critical Quality Attributes (CQA) of the nanoGLA product

### 5.2.2.1. Introduction to Quality by Design (QbD)

In this section, we applied the Quality by Design (QbD) approach to determine formulation and process parameters that could have an important impact on nanoGLA attributes when prepared by DELOS-susp. The QbD methodology is described in Guidelines of the International Council for Harmonization of Technical Requirements for Pharmaceuticals for Human Use (ICH), and it is strongly encouraged by the FDA and the EMA as a suitable methodology to develop robust drug manufacturing and control methods.<sup>10-12</sup> Pharmaceutical QbD is a systemic approach drug development that aims to ensure the quality of medicines, identifying characteristics that are critical to quality from the patients' perspective, translating them into the product Critical Quality Attributes (CQA), and establishing a relationship between manufacturing variables and CQA through a Design of Experiments (DoE). The goals of the pharmaceutical QbD may include the achievement of meaningful product quality specifications as well as the reduction of product variability and defects, to increase efficiencies and to enhance root cause analysis.<sup>13</sup>

### 5.2.2.2. Identification of the Critical Quality Attributes (CQA) of the nanoGLA product

During the development of liposomal drug products, the identification and pertinent characterization of CQA of liposomal drug products is one of the main challenges from the quality point of view, together with the definition of proper control strategies. A critical quality attribute (CQA) can be understood as a property, either physical, chemical, biological, or microbiological, that may influence the quality or performance of the finished product.<sup>10,14</sup> Liposomal products are complex formulations and small



changes in their physicochemical attributes can have notable effects in their in vivo performance. Thus, a suitable definition of CQA and control strategies may allow a faster and more efficient drug product development.<sup>14</sup>

The definition of the CQA for the final nanoGLA (or GLA-loaded nanoliposomes) product has considered the ICH recommendations, as well as the FDA and EMA guidelines.<sup>12,15</sup> The CQA selected as well as their justification are the following ones:

- **Macroscopic Appearance:** It must be a homogeneous opalescent dispersion without sedimentation. Sedimentation could indicate poor colloidal stability.
- **Mean Particle Size:** Particle size and particle size distribution are major CQA for nanoparticle-based systems, playing an important role in determining their in vivo absorption and distribution, drug loading, drug release, and targeting ability. Therefore, robust control of particle size is one of the crucial parameters for further in vivo application of liposomal drug products. Their size can range from few nanometers to several micrometers, although liposomes applied to pharmaceutical use are usually in the 50 – 400 nm range.<sup>16</sup>
- **Polydispersity Index (PDI):** PDI reflects the heterogeneity of the particle size, indicating how wide is the particle size distribution. The lower the PDI, the higher the homogeneity of the dispersion. Generally, polydispersity index below 0.5 are reported to be acceptable.
- **ζ-potential:** Important parameter in the evaluation of colloidal system's stability. Particles with a high negative or positive ζ-potential value repel each other, indicating that the colloidal system is stable. On the contrary, decreasing the ζ-potential value to nearly neutral could lead to liposomal aggregation. The liposome surface charge can also influence drug loading, cellular uptake, tissue distribution, and clearance. Positive ζ-potential values higher than + 20 mV can be considered inside the specification range for nanoGLA.
- **Particle morphology and lamellarity:** Vesicles must be spheroidal and, mostly, unilamellar. Lamellarity can affect drug loading and release, thus, impacting the enzyme delivery.
- **GLA entrapment efficiency/Free drug substance:** Free drug substance may have side effects and impact into pharmacokinetic profile. Besides, a high and reproducible percentage of drug entrapment could reduce manufacturing costs and increase drug concentration in the final formulation allowing greater flexibility in dosing. Depending on the pharmacokinetics, higher drug concentration can result in increased dosing intervals and hence improved patient compliance.

- **Total GLA content:** Since the enzyme is the active principle, the concentration of the GLA must be enough to reach efficacy levels in vivo, as well as to not exceed the maximum volume feasible for intravenous administration.
- **Specific enzymatic activity (EA):** The bioactivity of the integrated enzyme must be preserved in the nanoformulation since it is the active pharmaceutical ingredient. However, experimental observations showed quite variability in the assay used for determining the EA. Therefore, it was established that the EA ratio of nanoGLA to control should be higher than 0.5, using as control the agalsidase alfa (Replagal®).
- **Integration efficiency of chol-PEG<sub>400</sub>-RGD in the vesicular membrane:** Since it is the targeting moiety, the amount of targeting peptide moiety integrated in the nanoliposomal membrane must be high to allow the nanoGLA to interact with cells and facilitate the uptake by the tissue of interest, limiting the exposure to unwanted areas of the body.
- **Dispersion stability:** At this stage of development, final nanoGLA must be enough stable for carrying the proposed preclinical assays, which depending on the experiment can range from 2 to 8 weeks.
- **pH:** pH can affect dispersion stability, drug loading and release, and cell uptake among others. A suitable pH range is from 6.0 to 7.0.
- **Osmolality:** Parenteral products should be isosmotic with body fluids, therefore with osmolality valued between 260 – 300 mOsm kg<sup>-1</sup>.
- **Lipid and GLA degradation products:** Chemical stability of the lipid components in the liposome as well as the chemical stability of the contained drug substance is important. This parameter is not a priority in the current stage of development and will be considered at further stages.
- **Sterility and Bacterial endotoxins:** As a parenteral dosage form, liposomal products must be sterile and pyrogen-free.

Despite the importance of all the selected CQA, some of these parameters (e.g., degradation products, sterility, or bacterial endotoxins) were not considered as a priority in the current stage of development and will be considered at further stages. The specific range for each CQA of the final nanoGLA was summarized in **Table 5.2**. Further, these established CQA were validated by the EMA by means of a Scientific Advice procedure (Procedure No.: EMEA/H/SA/4167/1/2019/SME/III). This procedure can be requested by the developer at any stage of a medicine's development to ask guidance and direction

from EMA on specific questions, e.g. quality aspects, non-clinical or clinical aspects, or methodological issues.<sup>17</sup>

**Table 5.2.** Critical Quality Attributes (CQA) defined for the final nanoGLA liposomal dispersion.

CQA	Specification range
Macroscopic Appearance	Homogeneous aqueous dispersion without sediment and opalescent macroscopically appearance
Mean Particle Size	50 – 300 nm
Polydispersity Index (PDI)	≤ 0.45
ζ-potential	≥ + 20 mV
Particle morphology and lamellarity	Spheroidal vesicles and mostly unilamellar
GLA entrapment efficiency /Free drug substance	High entrapment efficiency (≥ 70 %) and low free drug substance
Total GLA content	≥ 0.2 mg mL <sup>-1</sup>
Specific enzymatic activity (EA)	Bioactive (ratio referred to the EA of Replagal® ≥ 0.5)
Integration efficiency of chol-PEG <sub>400</sub> -RGD in the vesicular membrane	High entrapment efficiency (≥ 70 %)
Dispersion stability	Enough stability for carrying out the further preclinical studies, which depending on the assay can range from 2 to 8 weeks. In terms of turbidimetry stability, the Turbiscan Stability Index (TSI) should be less than 10.0 at 24 h
pH	6.0 – 7.0
Osmolality	260 – 300 mOsm kg <sup>-1</sup>
Lipid and GLA degradation products	NA*
Sterility and bacterial endotoxins	NA*

\* These will be considered at further stages of development.

The process flow diagram of the whole nanoGLA manufacturing process is presented in **Figure 5.2**. First, membrane components, solvents, and gases, as well as the GLA protein, were processed using DELOS-susp to obtain an intermediate nanoGLA dispersion. Then, an additional step based on TFF is required to be able to reach a final nanoGLA product with the required specifications.

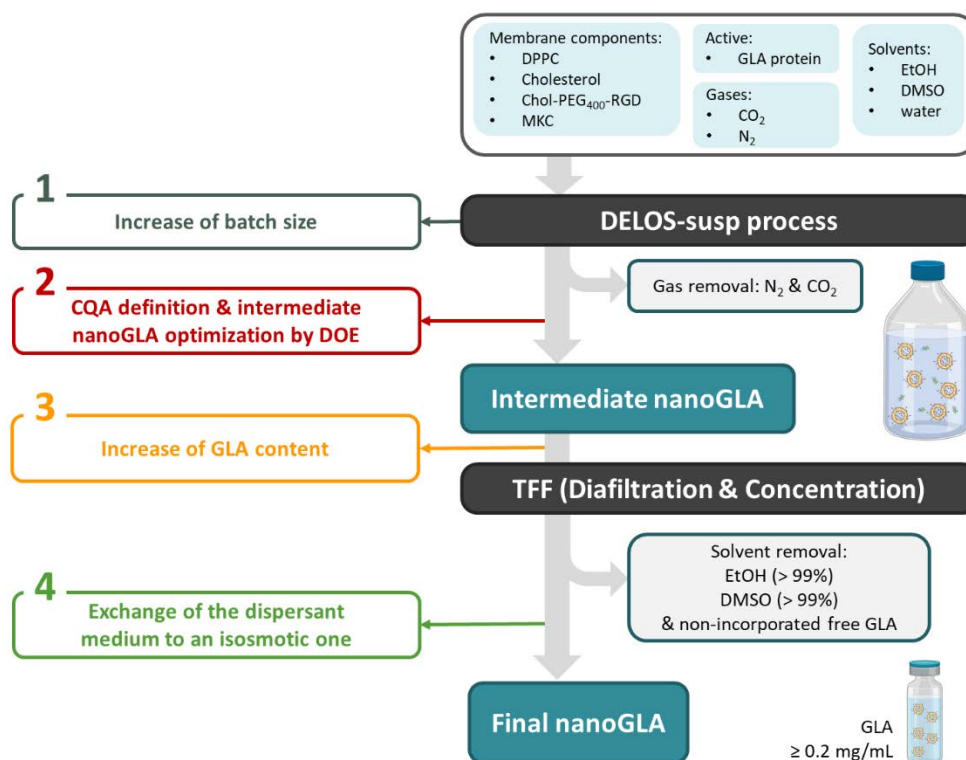


**Figure 5.2.** Process Flow Diagram to produce the final nanoGLA, including the raw materials and the materials leaving the process. On the left, the optimization activities (framed in different colors) carried out in each phase of the manufacturing process. These optimization activities are explained in detail in the next sections of this Chapter.

### 5.2.3. Increase of nanoGLA batch-size from small- to intermediate-lab plant

To produce vesicles at industrial scale, it is needed a methodology which allows obtaining vesicle-based formulations with batch-to-batch reproducible characteristics, involving a minimum number of steps and equipment, and meeting the requirements of the pharmaceutical industry and GMP. The use of production methodologies, since the beginning of a nanoformulation development, compatible with a scaling up, facilitates the further translation from the bench-scale to the preclinical or clinical scale. Otherwise, the difficulty to adapt the laboratory experimental production to larger-scale production is one of the main challenges in nanopharmaceuticals.<sup>1,4</sup> As previously mentioned during this thesis, DELOS-susp methodology for the preparation of nanovesicles showed many advantages, and among them, its easy potential scalability.

In early GLA-liposomal development stage, formulations were produced in the DELOS-susp small lab-scale plant, equipped with a 7.5 mL high-pressure vessel and allowing to produce vesicles with batch size in the 20 – 40 mL range (see **Chapter 9.2.1**).<sup>6</sup> However, for the translation of nanoGLA formulation from basic research to preclinical assays, it was needed to perform a first scaling up step, from the small lab-scale to an intermediate lab-scale, to be able to obtain enough nanoformulation quantities for the preclinical in vivo studies.

During this thesis, a knowledge transfer was done to Nanomol Technologies SL, and, for the first time, GLA-liposomal nanoformulation was scaled up from previous work<sup>6</sup> by a 20-fold factor. To do that, a new high-pressure laboratory plant was installed in Nanomol Technologies SL (Barcelona) facilities. Nanomol Technologies SL was founded in 2010 by researchers of Nanomol group (ICMAB-CSIC), and it is currently scaling up DELOS platforms for their implementation at industrial scale.

The new set up presented several differences with the small-lab plant used until that moment. Firstly, the capacity of the high-pressure vessel was increased from 7.5 mL (small-lab plant) to 50 mL (intermediate-lab plant) (see detailed configurations in **Chapter 9.2.2**). Besides, this new 50 mL high-pressure vessel could be exchanged by a 25 mL one, allowing a great flexibility in the produced batch size, that can range within 150 – 900 mL (**Figure 5.3**). Moreover, during the plant validation studies, the influence of CO<sub>2</sub> molar fraction ( $X_{CO_2}$ ) used during the DELOS-susp manufacturing on liposomal characteristics was evaluated, demonstrating a wide co-solvency range in ethanol-CO<sub>2</sub> mixtures at  $P_w$  and  $T_w$ , allowing to work in  $X_{CO_2}$  within the range 0.50 – 0.85.

Other improvements of the new set up, using a larger high-pressure vessel, included a better control in the process parameters (e.g., monitoring of temperature and pressure inside) and better homogenization inside the reactor. The better mixing was achieved installing a mechanical stirrer inside the high-pressure vessel, in a way that allows a quicker thermal equilibration of the CO<sub>2</sub>-expanded solution in the system, followed by a depressurization in an aqueous solution also under continuous magnetic mixing. Overall, it allowed the reduction of time per experiment, from 1 h to 15 – 25 min per batch, and the improvement of the batch-to-batch reproducibility.

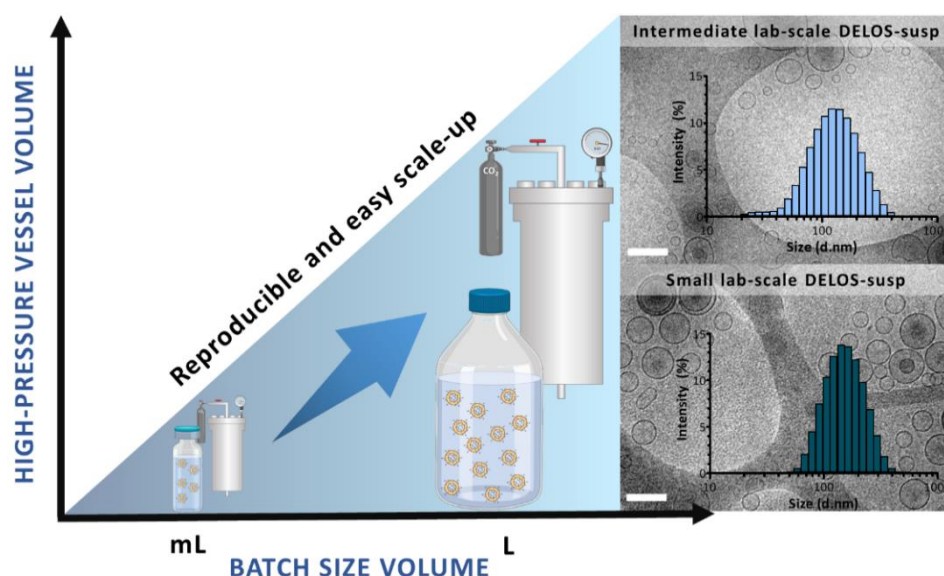


**Figure 5.3.** Scale up of DELOS-susp methodology, allowing the obtaining of enough quantities for nanoGLA translation from the bench to the preclinical phase. CryoTEM and size distribution corresponded to empty RGD-liposomes produced in the small and in the new intermediate lab-scale DELOS-susp equipment.

## 5.2.4. Impact of formulation parameters of intermediate nanoGLA on CQA

The goal of the QbD approach is in-depth understanding of the formulation and process variables, and of the relationship between them, in order to obtain a drug product with consistent desired characteristics.<sup>18</sup> Therefore, the impact of the formulation variables, material attributes, and process parameters on the critical quality attributes (CQA) of the intermediate nanoGLA product was studied in close collaboration with Nanomol Technologies SL team (Barcelona), in order to find which of them are critical, and establish a design space that ensures desired product specifications.

### 5.2.4.1. Design of Experiments (DoE) for intermediate nanoGLA optimization

Design of experiments (DoE) is a methodological technique useful for planning experiments and analyzing the resulted information in an optimized way, obtaining sufficient information using a minimum number of experiments, in which several experimental parameters (or hereafter named factors,  $X_n$ ) are simultaneously varied. Then, a mathematical model based on the obtained data is created, to understand the influence of the experimental factors included in the design on the outcome data.<sup>19</sup>

The first step involves the decision and selection of the factors to be included in the DoE, as well as the definition of the relevant responses to be measured, which, in our case, were previously defined during the identification of the CQA (**Table 5.2**). Therefore, the use of risk assessment becomes a valuable science-based process used in quality risk management that can help in the identification of those factors, i.e., material attributes, and process parameters, that can potentially influence in CQA of the product, and thus, worth including them in the DoE.<sup>13,20</sup> An Ishikawa diagram for intermediate nanoGLA was created to illustrate the potential risk factors and causes that could have an influence over the CQA, identified through risk analysis (**Figure 5.4**).

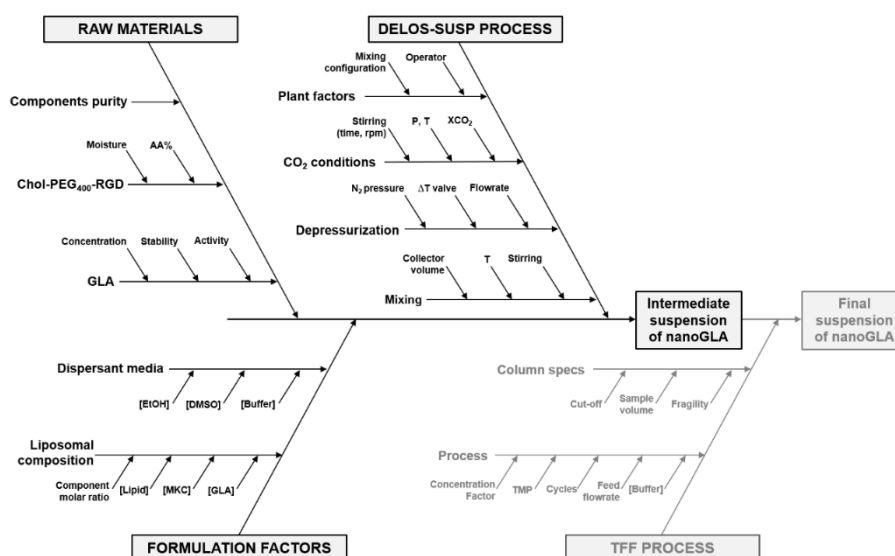


**Figure 5.4.** Ishikawa diagram (also named cause-and-effect diagram) illustrating the critical process parameters (CPP) and critical material attributes (CMA) that could impact on the critical quality attributes (CQA) of intermediate nanoGLA.

For each factor, a detailed risk analysis assessment was performed (see **Annex C**, Merlo-Mas et al. **Table C.1**). As a result, 4 formulation factors (independent variables,  $X_n$ ) were considered relevant to be included in the DoE analysis to study their influence on the physicochemical properties (dependent variables or responses, CQA) of intermediate nanoGLA obtained by DELOS-susp: GLA concentration ( $X_1$ ), lipid concentration ( $X_2$ ), peptide content in the liposomal membrane ( $X_3$ ), and ethanol concentration ( $X_4$ ). For each factor, its potential impact on CQA of intermediate nanoGLA was described, and for each factor low and high levels were selected, ranging based on previous data:

- **$X_1$ -GLA concentration:** Protein concentration plays a key role on dispersion stability. It has been reported that increasing the loading and charge of protein will impact on size distribution and aggregation rate of the liposomal system.<sup>16,21</sup> The range studied in the DoE included from 7 to 27  $\mu\text{g mL}^{-1}$  of enzyme, moving up and down of previously tested concentrations (e.g., **Chapter 3**).
- **$X_2$ -Lipid concentration:** Besides the molar ratio between membrane components (cholesterol and phospholipid), the total lipid concentration in liposomal systems will impact on its mean size, particle distribution and stability, as well as on its loading capacity.<sup>22,23</sup> The range studied in the DoE included from 1.2 to 5.0  $\text{mg mL}^{-1}$ , moving up from previously tested concentrations in similar nanoformulations.
- **$X_3$ -Chol-PEG<sub>400</sub>-RGD molar ratio:** PEGylation of liposomes improves the stability and circulation time<sup>24</sup> and the RGD peptide the active targeting towards endothelial cells, which are one of the most affected cell type in Fabry disease (by means of the RGD affinity for integrins). The range studied in the DoE included from 1 mol % to 3 mol % of molar ratio in relation to the total amount of lipid components, according to previous studies.
- **$X_4$ -Ethanol concentration:** Solvent concentration could have a direct impact on shape, solubility, and electrostatic interactions between the liposomal bilayer and the loaded protein. The range studied in the DoE included from 5 % to 10 % v/v, a low range, since higher quantities are not recommended for intravenous administration, although in some products the presence of organic solvents can be evaluated and justified.<sup>25</sup>

The matrix of the experimental design is presented in **Table 5.3**. Accordingly, ten GLA-loaded liposomal systems were produced by DELOS-susp, using the new intermediate lab-scale setup, and following the matrix of experimental design previously defined (**Table 5.3**). Batch size was ranging from 290 to 500 mL, while the rest of process parameters were kept constant for all experiments, e.g., the  $X_{CO_2}$  molar fraction to 0.55, the MKC content to 2.2 mol % in relation to the rest of lipid components, and the DMSO content to 2 % v/v.

**Table 5.3.** Matrix of experimental design. The sample codes consider the randomized order of experiments.

Factor	X <sub>1</sub>	X <sub>2</sub>	X <sub>3</sub>	X <sub>4</sub>
Experimental run	GLA concentration (µg mL <sup>-1</sup> )	Lipid concentration (mg mL <sup>-1</sup> )	Chol-PEG <sub>400</sub> -RGD ratio (mol %)	EtOH concentration (% v/v)
DOE-001	27	1.2	1	10.0
DOE-002	7	1.2	3	10.0
DOE-003	17	3.1	2	7.5
DOE-004	27	5.0	1	5.0
DOE-005	7	5.0	3	5.0
DOE-006	27	1.2	3	5.0
DOE-007	17	3.1	2	7.5
DOE-008	7	1.2	1	5.0
DOE-009	27	5.0	3	10.0
DOE-010	7	5.0	1	10.0

The responses of the experimental design were the critical quality attributes (CQA) for each nanoGLA intermediate dispersion: particle mean size, polydispersity index,  $\zeta$ -potential, turbidimetry stability index, ratio of monolayered liposomes, entrapment efficiency, enzymatic activity, and pH. Furthermore, macro- and microscopic appearance (i.e., particle morphology) were analyzed, but these two CQA were not included in the design because of their qualitative nature. In relation to the rest of CQA showed previously in **Table 5.2**, such as sterility and apyrogenicity, these are CQA which must be considered in the final formulation. However, they are not considered as CQA at this stage of formulation development since it is an intermediate product.

#### 5.2.4.2. Characterization of CQA from DoE experiment

First, all intermediate nanoGLA batches obtained by DELOS-susp presented a homogenous, whitish, opalescent macroscopic appearance without presence of sediment, except DOE-001, DOE-006, and DOE-009 which presented a small and dusty sedimentation. Besides, microscopy analysis of the nanoGLA samples by cryoTEM indicated that nanovesicular structures were obtained for all experiments (**Figure 5.5**), being mostly unilamellar and spherical, and ranging between 100 and 200 nm, with the presence of some larger vesicles around 500 nm, especially in those samples with some sedimentation or instability issue.



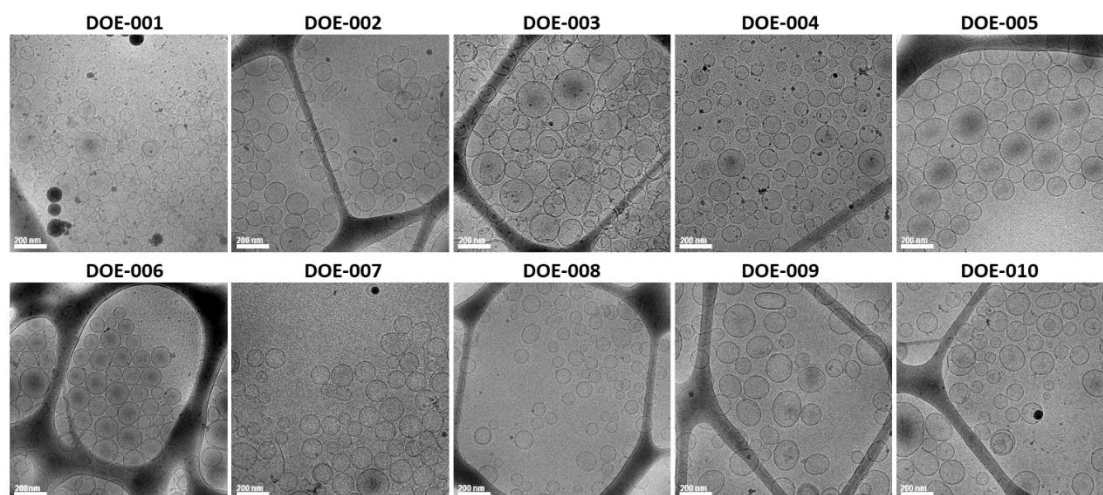


**Figure 5.5.** Representative cryoTEM images of intermediate nanoGLA DoE samples, 1 week after production. Scale bar 200 nm. Images were acquired by Prof. D. Danino from Technion (Israel).

A summary of the characterization results of the DoE samples which were considered for the statistical analysis is shown in **Table 5.4**. They include particle size, polydispersity, and  $\zeta$ -potential (using DLS and ELS), turbidimetry stability (by Turbiscan), level of unilamellarity (by SAXS, performed by Prof. J. S. Pedersen from Aarhus University, Denmark), entrapment efficiency (EE%, based on GLA concentrations determined by SDS-PAGE plus TGX performed by Dr. J. L. Corchero from IBB-UAB, Barcelona), and GLA enzymatic activity (EA, performed by Dr. I. Abasolo from VHIR, Barcelona).

The three out of ten batches (DOE-001, DOE-006, and DOE-009), that presented small sedimentation and aggregation, also showed a higher Turbiscan stability index (TSI) indicating the dispersion instability. Besides, those samples in which aggregation and sedimentation were observed, presented also higher size, PDI and lamellarity. Furthermore, the mean particle size and PDI of DOE-001, DOE-006, and DOE-009 significantly increased with time after production. On the other side,  $\zeta$ -potential, EE%, and EA values did not correlate with macro and microscopic characteristics of the samples, but in all the cases high  $\zeta$ -potential ( $> + 30$  mV) were achieved. Moreover, all the samples presented pH in the range 4.3 – 5.0 (see **Chapter 9.5.2**). This slightly acidic pH was due to the residual CO<sub>2</sub> dissolved in the aqueous phase after the depressurization step.

All the formulations showed enzymatic activity (EA), varying from 0.8 to 1.7 ratio to control referred to the enzymatic activity of a commercially available free GLA (Agalsidase alfa, Replagal<sup>®</sup>) included in the analysis, as also shown in **Table 5.4**. These results indicate an excellent enzymatic activity in all cases, compliant with preliminary specifications. Then, entrapment efficiencies (EE%) were above 50 % in all the systems although no clear correlation with the studied parameters was observed. GLA quantifications were determined by SDS-PAGE plus TGX, which sometimes can show an important

inter- and intra-sample variability, and can be responsible of the poor correlation with variables. Nevertheless, since in all the samples the MKC content was 2.2 mol % in relation to the rest of membrane components, results suggested that an increase of this excipient concentration would be required if higher GLA concentrations would be entrapped.

**Table 5.4.** Characterization of intermediate nanoGLA CQA after 1 week of production.

Sample ID	Size <sup>†</sup> (nm) (± SD)	PDI <sup>†</sup> (± SD)	ζ-pot <sup>†</sup> (mV) (± SD)	Turbidimetry stability <sup>‡</sup> (TSI)	Unilamellarity <sup>§</sup> ( $f_{single}$ ) (± SD)	EE% <sup>  </sup> (%) (± SD)	EA <sup>¶</sup> (± SEM)
DOE-001*	143 ± 6	0.45 ± 0.08	35 ± 2	11.5	0.88 ± 0.01	60 ± 5	1.7 ± 0.2
DOE-002	88 ± 2	0.17 ± 0.01	36 ± 2	0.6	0.99 ± 0.01	53 ± 10	1.2 ± 0.1
DOE-003	142 ± 3	0.12 ± 0.05	34 ± 1	1.2	0.95 ± 0.00	59 ± 8	1.4 ± 0.1
DOE-004	175 ± 1	0.32 ± 0.05	45 ± 1	8.2	0.93 ± 0.00	45 ± 8	1.6 ± 0.1
DOE-005	158 ± 4	0.24 ± 0.03	45 ± 6	1.9	0.93 ± 0.00	42 ± 16	0.8 ± 0.1
DOE-006*	202 ± 4	0.46 ± 0.05	32 ± 1	6.6	0.85 ± 0.02	68 ± 8	1.5 ± 0.1
DOE-007	146 ± 2	0.11 ± 0.05	35 ± 1	1.2	0.99 ± 0.01	53 ± 3	1.2 ± 0.2
DOE-008	100 ± 1	0.17 ± 0.02	38 ± 1	1.8	1.00 ± 0.01	84 ± 18	0.8 ± 0.1
DOE-009*	172 ± 5	0.22 ± 0.02	38 ± 1	12.0	0.94 ± 0.01	53 ± 5	1.1 ± 0.1
DOE-010	134 ± 2	0.13 ± 0.02	46 ± 2	0.6	0.93 ± 0.00	84 ± 13	1.4 ± 0.2

\* DOE-001, DOE-006, and DoE-009 presented sedimentation; † Measured by DLS and ELS (see **Chapter 9.5.1**);

‡ Measured by Turbiscan (see **Chapter 9.5.9.2**); § Measured by SAXS by Prof. J. S. Pedersen team from Aarhus University (Denmark) (see **Chapter 9.5.6.3**); || Enzyme entrapment efficiency, measured by SDS-PAGE plus TGX by Dr. J. L. Corchero from IBB-UAB (Barcelona) (see **Chapter 9.6.3.1**); ¶ Specific enzymatic activity referred to Replagal®, measured by Dr. I. Abasolo team from VHIR (Barcelona) (see **Chapter 9.7.1**).

In addition to these parameters, SAXS analysis also revealed an interesting correlation between the liposomal bilayer thickness (related to the  $z$  head parameter, see **Chapter 9.5.6.3**) and the amount of chol-PEG<sub>400</sub>-RGD added (**Figure 5.6**), similar to the result obtained for empty liposomes in **Chapter 4**.

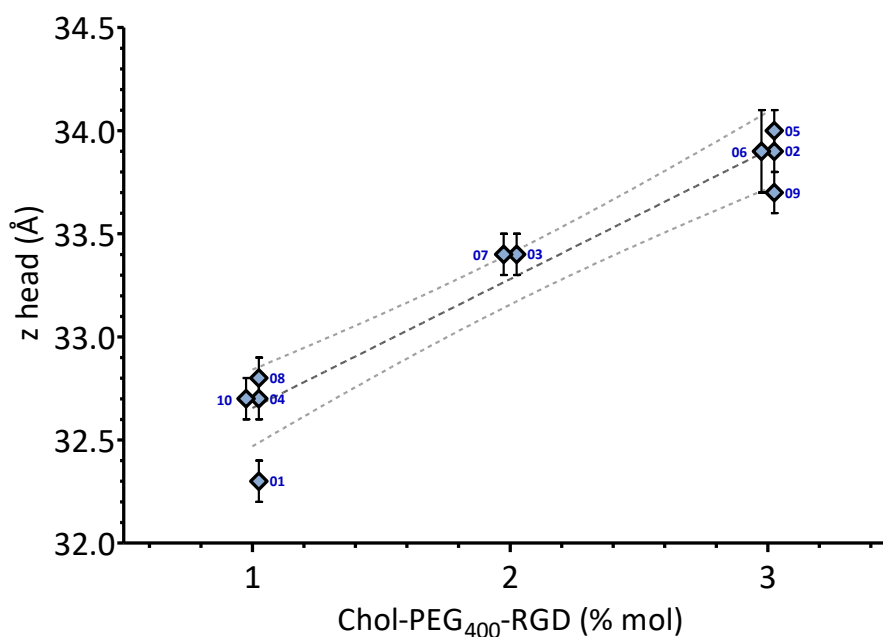


**Figure 5.6.** SAXS data representing bilayer thickness and amount of chol-PEG<sub>400</sub>-RGD (in mol % in relation to the rest of lipid components). Bilayer thickness ( $T$ ) is related to  $z$  parameter, where  $z$  is the distance from center of bilayer to modelled maximum intensity of the headgroup (see **Chapter 9.5.6.3**). Numbers correspond to ID sample. Measures performed by Prof. J. S. Pedersen from Aarhus University (Denmark).

#### 5.2.4.3. Analysis of the influence of the factors on CQA by data modelling

The influence of the four factors ( $X_1 - X_4$ ) was studied for the rest of dependent variables, i.e., CQA. The acceptance of the obtained responses was evaluated by means of the statistical parameters predicted by the software: (i)  $R^2$ , and (ii)  $Q^2$ . First,  $R^2$  represented the percent of the variation of the response explained by the model, i.e., how well the model fits the data. Besides,  $Q^2$  was the percent of the variation of the response predicted by the model according to cross validation, i.e., it can give information about how well the model can predict new data.

For each CQA, data collected from the experimental results were evaluated by means of  $R^2$  and  $Q^2$  statistical parameters, indicated in **Table 5.5**. Among them, only three CQA, i.e., mean particle size,  $\zeta$ -potential, and unilamellarity, could be statistically fitted, and were subsequently included in the prediction model. However, the rest of attributes showed a bad correlation, indicating a poor predictive ability of the model, so they were not further analyzed. An analysis and discussion for each quantifiable and fitted CQA is described below.

**Table 5.5.** Statistical parameters, modelling, and data fitting for the investigated intermediate nanoGLA CQA.  $R^2$  and  $Q^2$  ranges from 0 to 1, where 1 means the best value.

CQA	$R^2$	$Q^2$	Fitting and model (if apply) <sup>†</sup>
Mean particle size	0.937	0.661	Yes, size = $2.0 \cdot X_1 + 10.6 \cdot X_2 + 11.7 \cdot X_3 - 2.2 \cdot X_4 + 86$
Polydispersity index	0.437	0.200	No, bad correlation and poor predictive ability of the model were obtained.
$\zeta$ -potential	0.791	0.550	Yes, $\zeta$ -pot = $-19 \cdot X_1 + 2.1 \cdot X_2 - 10.9 \cdot X_3 - 24.5 \cdot X_4 + 41$
Turbidimetry stability	0.636	0.200	No, bad correlation and poor predictive ability of the model were obtained.
Unilamellarity	0.858	0.498	Yes, $f_{\text{single}} = 3.3 \cdot 10^{-4} \cdot X_1 - 1.8 \cdot 10^{-2} \cdot X_2 - 1.1 \cdot 10^{-7} \cdot X_3 - 5.7 \cdot 10^{-9} \cdot X_4 + 1.0$
Entrapment efficiency	0.420	0.200	No, bad correlation and poor predictive ability of the model were obtained.
Enzymatic activity	0.625	0.040	No, it could be explained by the high measurement related variability.

<sup>†</sup>  $X_1$  = GLA concentration,  $X_2$  = lipid concentration,  $X_3$  = chol-PEG<sub>400</sub>-RGD, and  $X_4$  = EtOH concentration, in the used level (-1, 0, +1). Analysis done using Modde software (Umetrics), in collaboration with Nanomol Technologies SL (Barcelona).

According to the data presented in **Table 5.4**, the mean particle size of the nanoGLA dispersions varied from 90 to 200 nm. These differences could be explained because of the aggregation and fusion of liposomal vesicles that could occur 1 week after preparation. The coefficients of the equation describing the influence of the factors on nanoGLA particle size are shown in **Figure 5.7A**. According to this figure, the size of nanoGLA liposomes is significantly influenced by GLA concentration ( $X_1$ ) and the lipid concentration ( $X_2$ ). Thus, a significant size increase is obtained when the concentration of GLA and lipid increase. The size increase with the increase of GLA and lipid concentrations could be explained by the occurrence of physical aggregation of the vesicles. The influence of GLA and lipid concentration is also illustrated by the contour plot for size in **Figure 5.7D**.

As shown in **Table 5.4**,  $\zeta$ -potential ranged from 32 to 46 mV for intermediate nanoGLA liposomes. The influence of studied factors on  $\zeta$ -potential is shown as coefficients of the regression equation plot in **Figure 5.7B**. According to this plot, lipid concentration ( $X_2$ ) was the only factor that had a significant positive effect on the  $\zeta$ -potential of the dispersions obtained. This could be explained because when lipid concentration increases, MKC (a cationic surfactant used as excipient in the nanoformulation) concentration also increases, giving more positive charges to the liposomal system. The influence of lipid concentration is also illustrated by the contour plot for size in **Figure 5.7E**.

Monolayered liposomes fractions varied from 0.88 to 1.00, as shown in **Table 5.4** by  $f_{single}$  values obtained by SAXS. According to **Figure 5.7C**, lipid concentration was the only factor affecting this CQA significantly, showing a larger difference in comparison to the rest of factors. As can be seen in **Figure 5.7F**, GLA concentration had an insignificant influence on the monolayer ratio of liposomes, but it was strongly affected by the lipid concentration. The explanation can be the same as the effect of lipid concentration on vesicle size: aggregation and fusion of the vesicles when lipid concentration increases could be responsible of this behavior.

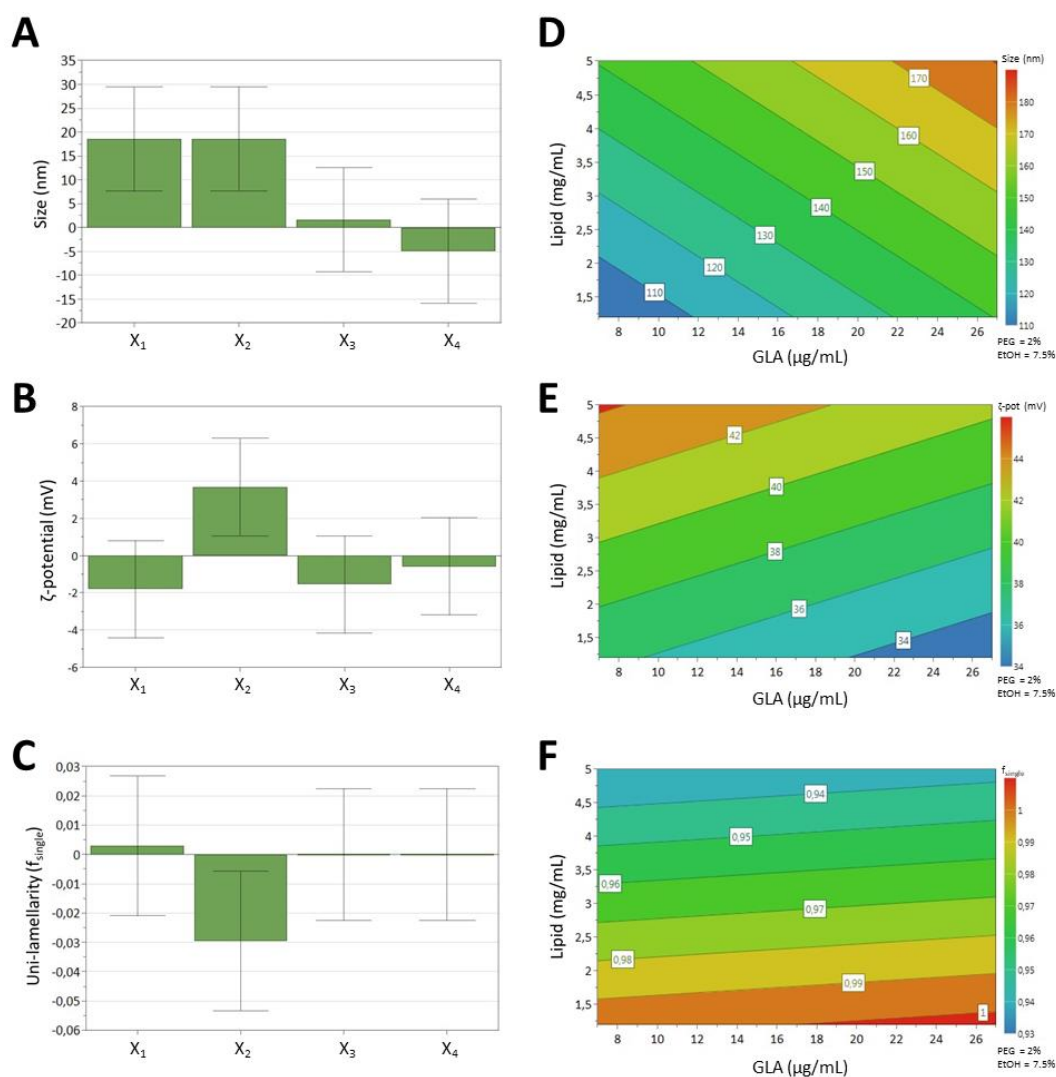


**Figure 5.7.** A–C: scaled and centered coefficients of the regression equations describing the influence of formulation parameters  $X_1$ -GLA concentration,  $X_2$ -lipid concentration,  $X_3$ -Chol-PEG<sub>400</sub>-RGD molar ratio,  $X_4$ -EtOH concentration, on the (A) liposomes size, (B)  $\zeta$ -potential, and (C) unilamellarity of intermediate nanoGLA. D–F: contour plots for the same CQA of the nanoGLA intermediate dispersion. Molar ratio of chol-PEG<sub>400</sub>-RGD to lipid and EtOH concentration were kept constant at 2 mol % and 7.5 % v/v, respectively. Analysis done using Modde software (Umetrics), in collaboration with Nanomol Technologies SL (Barcelona).

#### 5.2.4.4. Evaluation of the Design Space

Among all the factors studied, GLA concentration ( $X_1$ ) and lipid concentration ( $X_2$ ) were found to have a significant influence on some of the responses. Thus, the design space for intermediate nanoGLA was constructed using these factors which significantly influenced the quality of the nanoformulation.

The design space is defined as the multidimensional combination and interaction of input variables and process parameters that have been demonstrated to provide assurance of quality.<sup>10</sup>

On the one hand, increase of GLA and lipid concentration had a negative influence on liposomal mean particle size because of the size increase promoted by aggregation. On the other hand, as the lipid concentration increased, and, consequently, the amount of MKC surfactant was higher,  $\zeta$ -potential (which is related to the electrical charge at the liposomes surface) also increased due to the formal positive charge provided by this cationic surfactant. Nevertheless, this  $\zeta$ -potential increase was not correlated with a higher colloidal stability of the nanoformulation as also confirmed by an unilamellarity decrease. It seems that this MKC amount is not enough to stabilize such highly concentrated samples. However, higher MKC concentrations, although could improve the stability of these concentrated samples, it also could entail a toxicological concern as well as the abolishment of the enzymatic activity of the GLA, as was seen in **Chapter 3** of this Thesis.

The other CQA such as polydispersity index, TSI turbidimetry stability, GLA entrapment efficiency, and enzymatic activity could not be fitted in any reliable model because of the sedimentation observed in some batches and the high characterization variability, due to the use of SDS-PAGE plus TGX as a reference method for GLA quantification (a semi-quantitative analytical technique). Results could be improved in the future using a HPLC method for the quantification of GLA. Hence, the space design was determined using particle size,  $\zeta$ -potential, and unilamellarity.

The design space obtained is shown as the green region in **Figure 5.8** and shows the combination of factors for which the intermediate nanoGLA obtained by DELOS-susp will meet the specifications in terms of CQA, specified in **Table 5.6**, with a probability of failure less than 1 %. As criteria, it was decided to maximize the unilamellarity, as well as target 150 nm as size (with a minimum of 50 nm).

**Table 5.6.** The desired CQA of the intermediate nanoGLA introduced in the design space explorer and their values.

Response	Criterion	Min.	Target	Max.
Size (nm)	Target	50	150	250
$\zeta$ -potential	Excluded	–	–	–
Unilamellarity ( $f_{\text{single}}$ )	Maximize	0.95	1.00	–

Analysis done using Modde software (Umetrics) in collaboration with Nanomol Technologies SL (Barcelona).

The combination inside the design space which is pointed out by the black arrows indicates the robust setpoint (17.7  $\mu\text{g mL}^{-1}$  GLA concentration, 2.97  $\text{mg mL}^{-1}$  lipid concentration, 1.3 mol % chol-PEG<sub>400</sub>-RGD, and 6.2 % v/v EtOH) corresponding to the formulation for which the prediction errors are the lowest.

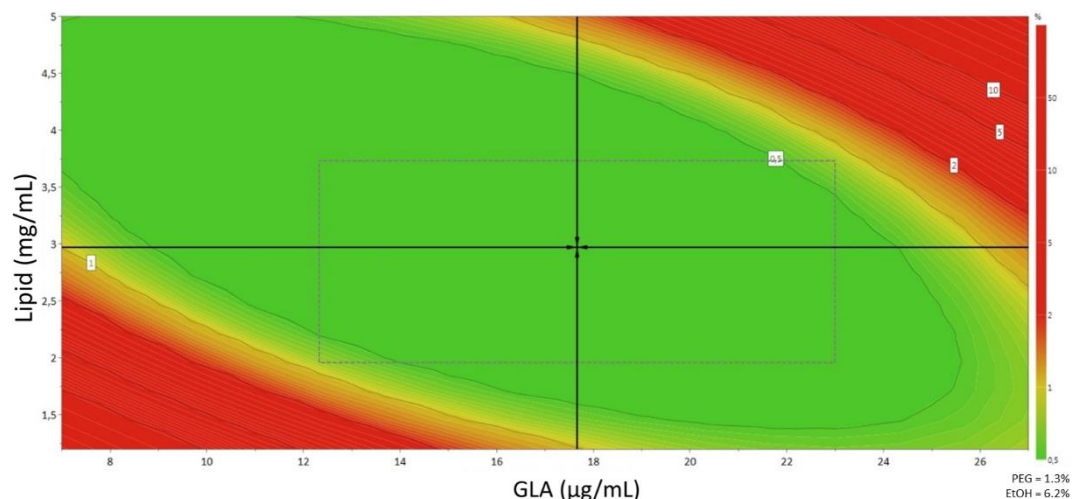


**Figure 5.8.** The design space for nanoGLA intermediate liposomal dispersion that meets the specifications in terms of CQA, expressed as the probability of failure (%). Analysis done using Modde software (Umetrics) in collaboration with Nanomol Technologies SL (Barcelona).

Overall, the results from the DoE performed for intermediate nanoGLA indicate a relationship between lipid and protein concentration, affecting size,  $\zeta$ -potential, and unilamellarity. The design space obtained suggested that an increase of lipid concentration as well as GLA concentration provoke a negative influence on liposomal mean particle size, that can lead to instability and aggregation. This model indicates that intermediate nanoGLA would escape from the acceptance limits in these conditions of high lipid and high GLA concentration. Otherwise, although the red zone in the lower left corner indicates a certain failure of having liposomes with the target values, this was not found empirically. Therefore, although it was supposed that the failure can come from a certain probability of having liposomes smaller than the target value, it was considered this region of the model little useful for our intentions.

Therefore, this preliminary design space gave the trend to reduce lipid concentration to 1.2  $\text{mg mL}^{-1}$ , so that the GLA concentration could be increased up to 35  $\mu\text{g mL}^{-1}$ , obtaining an intermediate nanoGLA by DELOS-susp meeting the required specifications. To ensure high enzyme entrapment efficiencies, MKC will be increased from 2 mol % to 5 mol % in next experiments.

### 5.2.5. Concentration of nanoGLA formulation to be suitable for intravenous dosing

The maximum protein concentration tested in the DoE for intermediate nanoGLA formulation was still too low to enter in vivo efficacy testing. To ensure a minimal effective dose, GLA concentration should be increased up to  $150 \mu\text{g mL}^{-1}$ , preferably  $\geq 0.2 \text{ mg mL}^{-1}$ . Otherwise, the volume of nanoformulation needed to reach therapeutic doses will be above the maximum tolerable volume for an intravenous administration ( $5 \text{ mL kg}^{-1}$  in rodent).<sup>26,27</sup> Thus, the challenge was to obtain a stable nanoGLA formulation containing at least  $0.2 \text{ mg mL}^{-1}$  of GLA, suitable for in vivo testing.

Considering the trend given by the Design Space, low lipid concentration in intermediate sample must be maintained to guarantee appropriate vesicle size and stability and, thus, two approaches were explored to increase the GLA concentration in the final sample:

1. Produce the nanoGLA with low lipid concentration but with higher cargo of GLA by DELOS-susp preparation.
2. Concentrate the current intermediate nanoGLA prototype by tangential flow filtration (TFF).

In both cases, nanoGLA must accomplish the specifications of the established quality attributes, paying special attention to the polydispersity and the stability over time.

#### 5.2.5.1. Increase the GLA cargo of nanoGLA by DELOS-susp

It was started producing DELOS-susp batches by fixing a low lipid concentration ( $1.2 \text{ mg mL}^{-1}$ ) and increasing the GLA concentration from  $35 \mu\text{g mL}^{-1}$  to  $75 \mu\text{g mL}^{-1}$ , since these GLA concentrations were out of the range explored in the previous DoE design space. The macroscopic appearance of the batch with high GLA concentration (L-GLA<sub>75</sub>) was quite opaque than normally, from the first moment just after the DELOS-susp depressurization processing step. Sample sedimented the next day after production, since large amount of sedimentation appeared at the bottom of the vial. Physicochemical characterization corroborated this instability, with more than one population peak, and PDI above 0.4 (**Figure 5.9** and **Table 5.7**). It suggested that GLA concentration ( $75 \mu\text{g mL}^{-1}$ ) was too high to entrap it into liposomes at that specific lipid concentration directly in the DELOS-susp production step, despite the MKC concentration was increased from 2 mol % to 5 mol %. Besides, liposomes within intermediate GLA concentration (L-GLA<sub>50</sub>) showed physicochemical characteristics in the limit of the acceptance requirements just after production, but its short-term colloidal stability was also compromised the next day after production, since showed higher PDI, aggregation and sedimentation. Finally, the lowest GLA concentration (L-GLA<sub>35</sub>) maintained acceptable criteria few days after production.



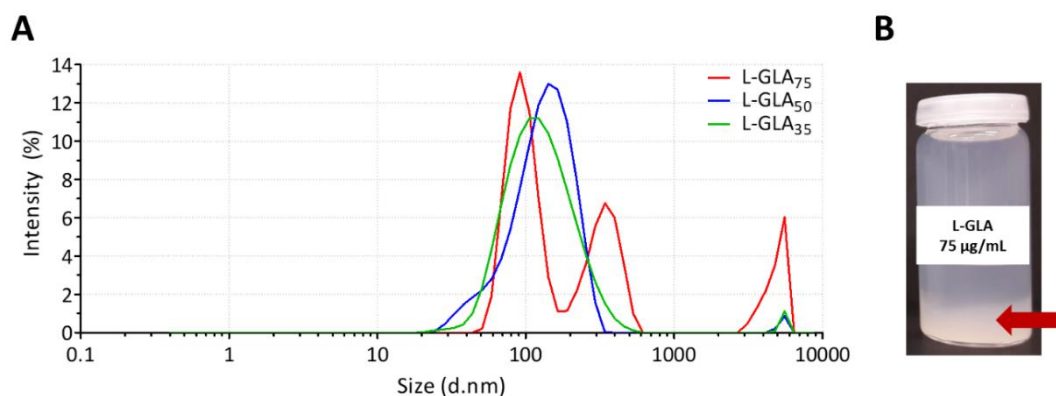


**Figure 5.9.** (A) Size distribution of intermediate liposomes containing GLA at 35, 50, and 75  $\mu\text{g mL}^{-1}$  (L-GLA<sub>35</sub>, L-GLA<sub>50</sub>, and L-GLA<sub>75</sub>, respectively), just after production by DELOS-susp process. (B) Macroscopic appearance of L-GLA<sub>75</sub> the next day after production.

**Table 5.7.** Physicochemical characterization of GLA-liposomes containing three different GLA concentrations just after their production by DELOS-susp, measured by DLS and ELS.

System ID	GLA [ $\mu\text{g mL}^{-1}$ ]	Size [nm]	PDI	$\zeta$ -potential [mV]
L-GLA <sub>35</sub>	35	139 $\pm$ 4	0.38 $\pm$ 0.02	40 $\pm$ 2
L-GLA <sub>50</sub>	50	135 $\pm$ 4	0.41 $\pm$ 0.04	38 $\pm$ 2
L-GLA <sub>75</sub>	75	256 $\pm$ 23	0.80 $\pm$ 0.04	ND

#### 5.2.5.2. Increase GLA by concentration of nanoGLA by TFF process

The option of increasing the GLA concentration  $> 35 \mu\text{g mL}^{-1}$  in the first production step was discarded due to the poor colloidal stability of the resulted systems. Intermediate nanoGLA liposomes at  $35 \mu\text{g mL}^{-1}$  of GLA were produced by DELOS-susp (named L-GLA<sub>INTRMED</sub>), and then, next day after production, they were submitted to TFF process following different approaches: (i) concentration without changing the dispersant media (L-GLA<sub>CONC</sub>), (ii) diafiltration changing the dispersant media and followed by a concentration step (L-GLA<sub>DIAF+CONC</sub>), and (iii) diafiltration of the nanoGLA by changing the dispersant media (L-GLA<sub>DIAF</sub>) (see TFF details in **Chapter 9.3**). The change of dispersant media to only water allows the removal of the remained organic solvents (EtOH and DMSO), and the non-incorporated molecules (e.g., free GLA), resulting in liposomes only dispersed in pure water. Besides, the concentration step consisted of the removal of media while sample became more concentrated, in a  $\sim (5 - 6)$ -fold factor.

From the beginning, differences in physicochemical characteristics between the distinct TFF processes were observed. All samples met the established specifications at time zero, with mean vesicle size below 220 nm, PDI below 0.4, and  $\zeta$ -potential above +20 mV, excepting the L-GLA<sub>CONC</sub>, whose polydispersity was higher than the desired (**Figure 5.10**). The other three samples, apart from meeting size distribution requirements, also showed a small and unilamellar liposomal morphology (**Figure 5.10**).

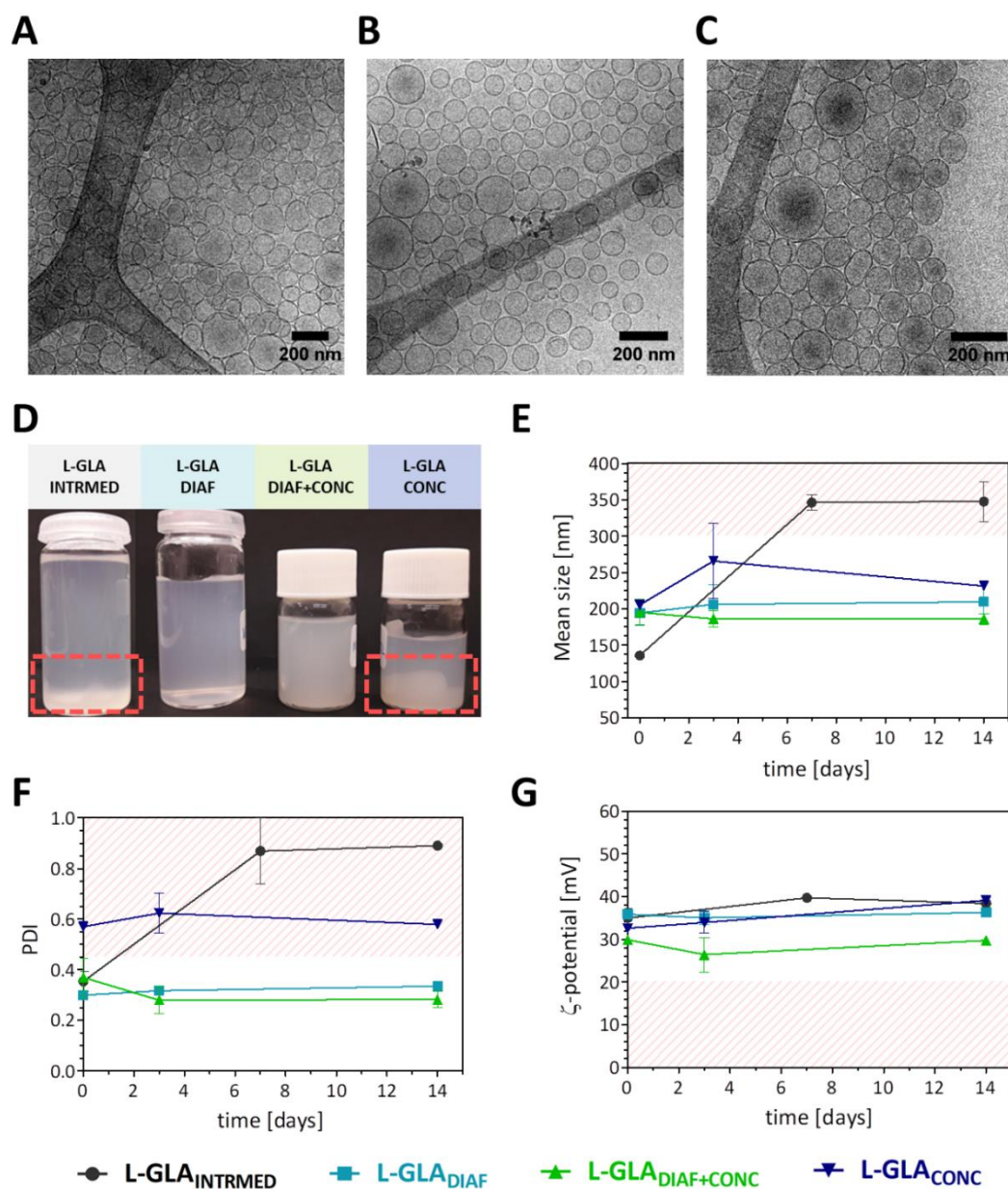


**Figure 5.10.** Morphology of nanoGLA by cryoTEM, two days after production: (A) L-GLA<sub>INTRMED</sub>, original sample obtained after DELOS-susp; (B) L-GLA<sub>DIAF</sub>, after diafiltration in water; and (C) L-GLA<sub>DIAF+CONC</sub>, after diafiltration in water and 5 or 6-fold concentration. (D) Macroscopic appearance of initial nanoGLA (L-GLA<sub>INTRMED</sub>) and after diafiltration and/or concentration processes, 1 week after production; and physicochemical characterization by DLS, in terms of (E) size, (F) PDI, and (G)  $\zeta$ -potential. Red area was marked for characteristics out of the specified range criteria.

The short-term stability of nanoGLA also became an important parameter. One week after production, L-GLA<sub>DIAF</sub> and L-GLA<sub>DIAF+CONC</sub> remained homogeneous and without apparently sedimentation. The L-GLA<sub>DIAF+CONC</sub> showed an expected slightly milkier macroscopic appearance due to the higher lipid content. However, the initial sample (L-GLA<sub>INTRMED</sub>) started to sediment, like the aforementioned L-GLA<sub>CONC</sub>, confirming the instability of these two samples (**Figure 5.10**). Interestingly, both samples still contained the production media (water with small amount of EtOH and DMSO) and the free GLA, since no diafiltration process was performed in these two samples. These results suggest that one or more of these components were affecting the nanoGLA stability, and that the purification step by diafiltration previous concentration of the sample could improve the stability of the samples that contained high amount of GLA. As shown in **Figure 5.10**, these samples met the physicochemical requirements and were stable at least 14 days, ensuring a minimum time between production and the in vivo administration date.

Finally, regarding GLA concentration, L-GLA<sub>DIAF+CONC</sub> reached the minimum desired concentration of  $\geq 150 \mu\text{g mL}^{-1}$  (**Table 5.8**) to allow a further in vivo efficacy study.

**Table 5.8.** GLA concentration in initial and diafiltration-processed samples. Two replicates per each system were prepared.

Samples	GLA concentration* ( $\mu\text{g mL}^{-1}$ ) ( $\pm$ SD)	EE (%)
L-GLA <sub>INTRMED</sub>	36 $\pm$ 4	-
L-GLA <sub>DIAF</sub>	27 $\pm$ 1	75 %
L-GLA <sub>DIAF+CONC</sub>	150 $\pm$ 30	79 %
L-GLA <sub>CONC</sub>	ND	ND

\* Quantified by SDS-PAGE plus TGX, performed by Dr. J. L. Corchero from IBB-UAB (Barcelona) (see **Chapter 9**).

To confirm the obtained results, an additional trial was performed, this time with an increased concentration factor (7.5-fold). Once again, liposomes with the required concentration of GLA and acceptable nanoGLA attributes were achieved through the preparation of an intermediate nanoGLA batch with low lipid concentration ( $1.2 \text{ mg mL}^{-1}$ ) and intermediate GLA concentration ( $35 \mu\text{g mL}^{-1}$ ) followed by a diafiltration and concentration step by TFF. The resulting sample met the requirements to go to future in vivo preclinical assays (**Table 5.9**). A good colloidal stability was observed for the concentrated final nanoGLA, composed mainly by single lamellar liposomes (**Figure 5.11**). This time, some structural effects were noticeable by cryoTEM after over-concentrating the GLA-loaded liposomes. Images revealed the formation of some multilamellar complexes, where the GLA can be identified between liposomal layers as well as inside the vesicles (**Figure 5.11**, arrows), forming structures resembling lipoplexes.<sup>28</sup> Interestingly, the high concentration of GLA ( $330 \mu\text{g mL}^{-1}$ ) after the

concentration process where these structures were identified was quite above the minimum required value for in vivo trials ( $200 \mu\text{g mL}^{-1}$ ).

**Table 5.9.** Critical quality attributes for optimized intermediate nanoGLA, diafiltrated and concentrated 7.5-fold.

Attributes	After DELOS-susp	After diafiltration and concentration
	L-GLA <sub>INTRMED</sub>	L-GLA <sub>DIAF+CONC</sub>
Stability	NA	$\geq 2$ weeks
Particle mean size (nm) <sup>†</sup>	$138 \pm 7$	$165 \pm 3$
Polydispersity index (PDI) <sup>†</sup>	$0.38 \pm 0.03$	$0.41 \pm 0.02$
$\zeta$ -potential (mV) <sup>†</sup>	$40 \pm 1$	$35 \pm 1$
Enzymatic activity (ratio to control) <sup>‡</sup>	$1.1 \pm 0.2$	$0.9 \pm 0.1$
GLA concentration ( $\mu\text{g mL}^{-1}$ ) <sup>§</sup>	$34 \pm 2$	$330 \pm 20$

<sup>†</sup> Measured by DLS, see **Chapter 9.5.1**; <sup>‡</sup> Referred to Replagal® (normalized to 1), measured by Dr. I. Abasolo group from VHIR (Barcelona), see **Chapter 9.7.1**; <sup>§</sup> Measured by SDS-PAGE plus TGX by Dr. J. L. Corchero from IBB-UAB (Barcelona), see **Chapter 9.6.3.1**.

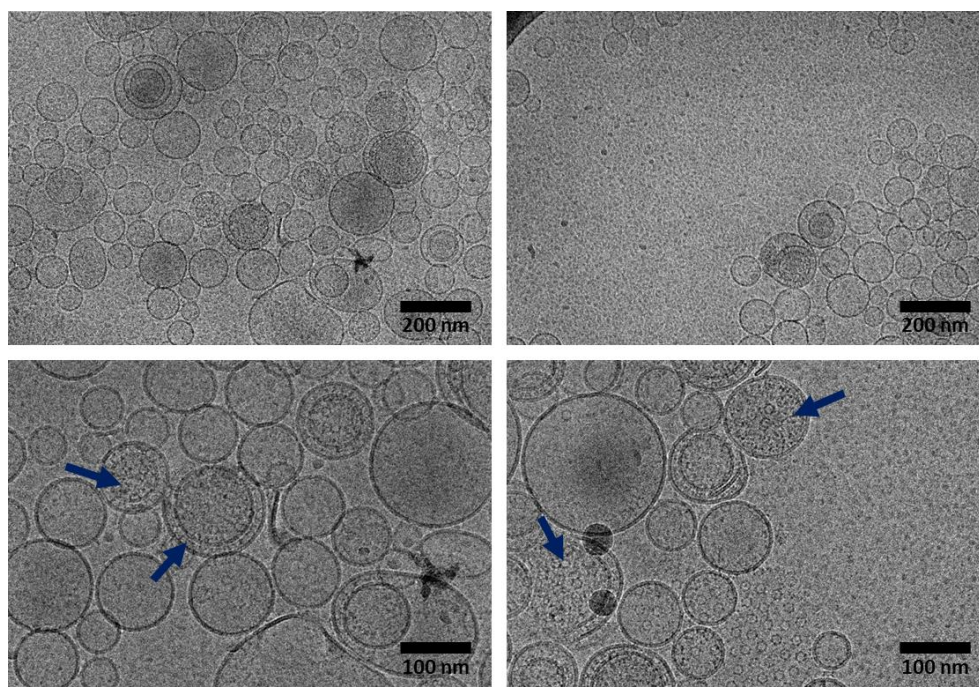


**Figure 5.11.** CryoTEM images of optimized nanoGLA prototype after concentration, two days after production. Images acquired by Prof. D. Danino team at Technion (Israel).

To sum up, diafiltration followed by a concentration step, ~ (5 – 6)-fold, allowed the obtaining of GLA concentration > 150 µg mL<sup>-1</sup> in nanoGLA, that also met the established physicochemical specifications (mean vesicle size ≤ 300 nm, PDI ≤ 0.5, ζ-potential ≥ + 20 mV and EE% ≥ 70 %) with a colloidal stability of at least 14 days. It opens the door to move forward and perform the first in vivo efficacy study.

### 5.2.6. Isosmolality adjustment of nanoGLA formulation

Parenteral formulations should preferably be isosmotic and isotonic with human plasma to prevent rupture or contraction of the liposomal structure as well as avoid damage to the tissues. These drugs that are not isosmotic at their recommended dose require the addition of adjusting agents to the formulation, to prevent hemolysis or crenation (blood cells dehydration) after administration. To be isosmotic to blood, solutions should have an osmolality value of 260 – 300 mOsm kg<sup>-1</sup>. A 0.9 % (w/v) sodium chloride or 5 % (w/v) dextrose solutions are examples of isosmotic solutions with human plasma.<sup>29</sup>

#### 5.2.6.1. Definition and calculation of osmolality

Osmolality and osmolarity are measures that are technically different but refer to the same concept, a measure of the osmotic pressure exerted by a solution across a perfect semi-permeable membrane, which allows free passage of water and completely prevents movement of solute(s).<sup>30</sup> Whereas osmolality is defined as the number of osmoles (Osm) of solute per kilogram of solvent (Osm kg<sup>-1</sup>), osmolarity is defined as the number of osmoles of solute per litre of solution (Osm L<sup>-1</sup>). Osmolality and osmolarity become very similar at low concentrations of solute since the mass of the solute is negligible compared to the mass of the solvent. Besides, tonicity is a measure of the osmotic pressure that a substance can exert across a cell membrane if the cell was placed into the solution. Tonicity should be understood as a behavioural term, and thus cannot be measured on an osmometer since it has no units, meaning that the tonicity of a solution depends on what type of cell we are comparing it.<sup>31</sup>

On the one hand, from the theoretical point of view, osmolality can be calculated with the next equation (**Eq. 5.1**), where for each solute (*i*), there are the contribution of the osmotic coefficient ( $\varphi$ ) which accounts for the degree of non-ideality of the solution (e.g., degree of dissociation of the solute, electrostatic effects...), the number of particles (*n*) of dissociation (e.g., ions), and the molal concentration of the solute (*C*):<sup>30</sup>

$$\text{osmolality} = \sum_i \varphi_i n_i C_i \quad (\text{Eq. 5.1})$$

On the other hand, from an experimental point of view, osmolality can be measured using an osmometer, which measures colligative properties (properties of solutions that depend on the ratio of the number of solute particles to the number of solvent molecules in a solution, and not on the nature of the chemical species present) such as freezing-point depression, vapor pressure or boiling-point elevation. For our

studies, it has been used an osmometer based on the freezing-point calibrated using water for the zero point, and a 0.9 % sodium chloride (NaCl) (w/v) solution as a 300 mOsm kg<sup>-1</sup> calibration point (**Chapter 9.5.3**). The principle of working is based on a comparison between the freezing point of the pure water (0 °C) with the sample to measure, since a solution of 1 Osm kg<sup>-1</sup> leads to a -1.858 °C decrease of the freezing-point (**Figure 5.12**).

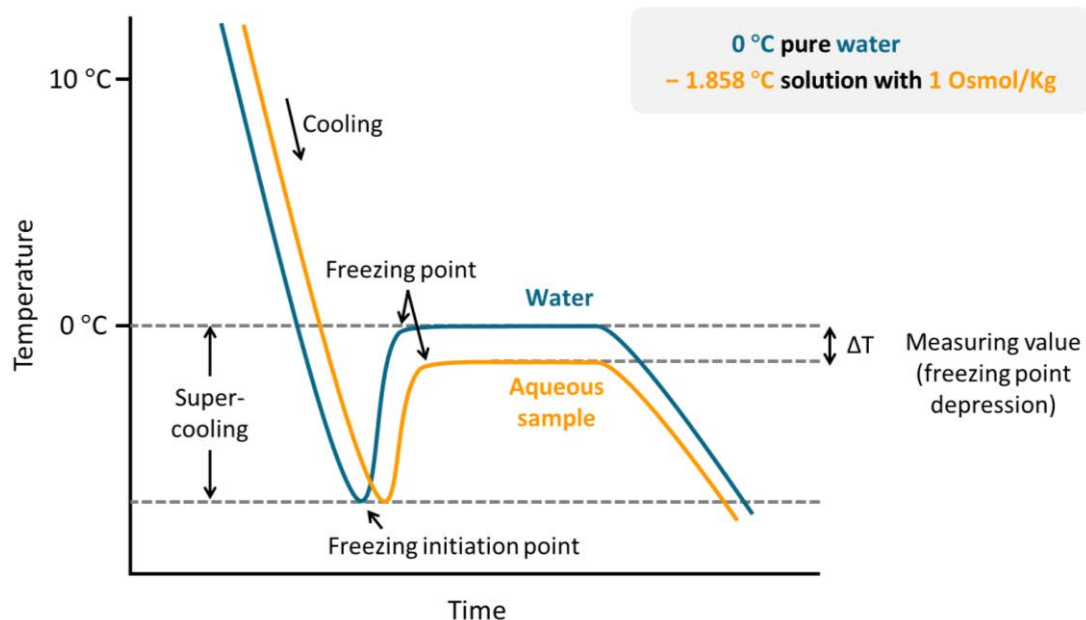


**Figure 5.12.** Standard cooling curve characteristic of water (blue line) and an aqueous solution with dissolved solute particles (orange line). The freezing point depression  $\Delta T$  is related to the osmolality of a solution. Adapted from <sup>32</sup>.

### 5.2.6.2. Initial osmolality of liposomal samples

Thus, osmolality control in a formulation become an important parameter to consider, especially when parental administration is intended to be used. First, to see in which range our formulations were moving, different prototypes of liposomes were analysed (**Table 5.10**). All the prototypes were far from blood osmolality, thus far from being isosmolar to blood, a desired parameter for intravenous administration. On the one hand, samples, just after their preparation by DELOS-susp, showed a very high osmolality (close to 800 mOsm kg<sup>-1</sup>). On the other hand, osmolality fell to zero in samples after diafiltration process (thus, after removing the remained solvent such as EtOH and DMSO, free GLA, and other non-incorporated molecules). These values proved the necessity of studying the addition of tonicity agents to adjust the osmolality of the liposomal samples, since current formulations are hyperosmotic (total samples after DELOS-susp) or hypoosmotic (diafiltrated samples in water).

It seemed that the reason of the high osmolality values found in samples after their production were mainly due to the presence of traces of organic solvents used during the production to solubilize the components. Despite these quantities were low in relation with the aqueous proportion (4 – 5 % vol.

EtOH and 0.8 – 1.2 % vol. DMSO), they could have an impact on the osmolality, as the osmolality measurement of the solvent alone indicated. Both organic solvents, ethanol and DMSO, increased the osmolality of the dispersion.

**Table 5.10.** Osmolality of the current GLA-liposomal formulations and the organic solvents used during the production process (EtOH, DMSO, and water).

System	Production step	Solvent	Osmolality (mOsm kg <sup>-1</sup> ) (± SD) <sup>†</sup>
GLA-loaded liposomes	After DELOS-susp	Ethanol (4 – 5 % vol) and DMSO (0.8 – 1.25 %)	790 ± 70
GLA-loaded liposomes	After diafiltration x1	Water	4 ± 1
Solvent solution	–	Ethanol (4 – 5 % vol)	≈ 800
Solvent solution	–	DMSO (0.8 – 1.25 % vol)	≈ 120
Solvent solution	–	Water (100 % vol)	≈ 0

<sup>†</sup> Average of two independent batches, determined by freezing-point (see **Chapter 9.5.3**).

This effect is also known and observed in the clinical field, especially in alcohol intoxications. As ethanol and non-ethanol alcohols behave osmotically active, physicians often rely on the measurement of the serum osmolality.<sup>33,34</sup> This value is usually compared with the calculated one (based on the serum's primary osmotically active components, mainly sodium, glucose, and blood urea nitrogen) (**Table 5.11**). The difference between the measured and calculated osmolar value (known as “osmol gap”) can be used to determine the presence of a possible toxic alcohol ingestion or evidences for other certain types of diseases (e.g., dehydration or hyperglycemia).<sup>30</sup>

**Table 5.11.** Typical human serum osmolality values in normal conditions. In the effective osmolality the contribution of components osmotically active but without impact in tonicity is rested<sup>†</sup>. Adapted from Oster et al.<sup>34</sup>.

Blood component	Concentration (mmol L <sup>-1</sup> )	Calculated osmolality (mOsm kg <sup>-1</sup> )	Effective osmolality (mOsm kg <sup>-1</sup> )
Sodium	140		
Glucose	5	290	285
Blood urea nitrogen <sup>†</sup>	5		

Additionally, since membrane liposomal components or GLA did not significantly contribute to the osmolality of the formulation, and assuming that all the contribution comes from the organic solvents, osmolality measurements could proportionate an indirect/general estimation of % of solvent that remains in the liposomal sample, allowing their control (**Figure 5.13**). Osmolality showed a linear relation with the concentration of organic solvent. This is an important fact, since small or uncontrolled amounts of remained organic solvents could have a high impact on osmolality.

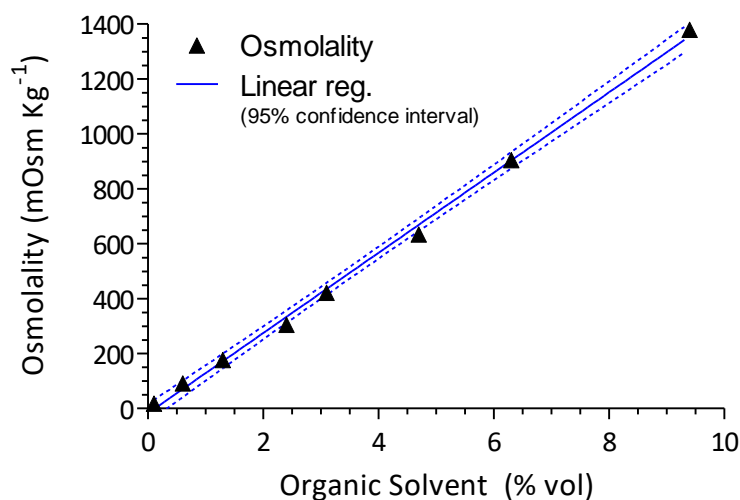


**Figure 5.13.** Correlation between organic solvent (without liposomes) and osmolality. Organic solvent was a mixture of EtOH and DMSO (in a 4:1 volume ratio) in water, mimicking the conditions used in liposomes, measured as detailed in **Chapter 9.5.3**.

For that, it can be concluded that for obtaining isosmotic liposomal formulations it is mandatory the elimination of the remained organic solvents, making the TFF diafiltration step a crucial part of the process, not only for removing free GLA, but also for the elimination of remained amounts of EtOH and DMSO.

### 5.2.6.3. Impact of the process methodology for media exchange

#### Production of blank liposomes in PBS

Results from the previous section clearly show the necessity of adding some isosmotic agents to adjust the osmolality of the samples. First, phosphate-buffered saline (PBS) 100 mM buffer (composed by sodium chloride and phosphates) was used as alternative dispersion medium. Two different methods were used for the preparation of GLA-unloaded liposomes in PBS medium: (i) during DELOS-susp preparation, by direct depressurization of the organic solution in an aqueous solution containing PBS instead of only pure water, and (ii) during diafiltration step, by medium exchange placing PBS in the buffer reservoir instead of pure water (**Figure 5.14**)



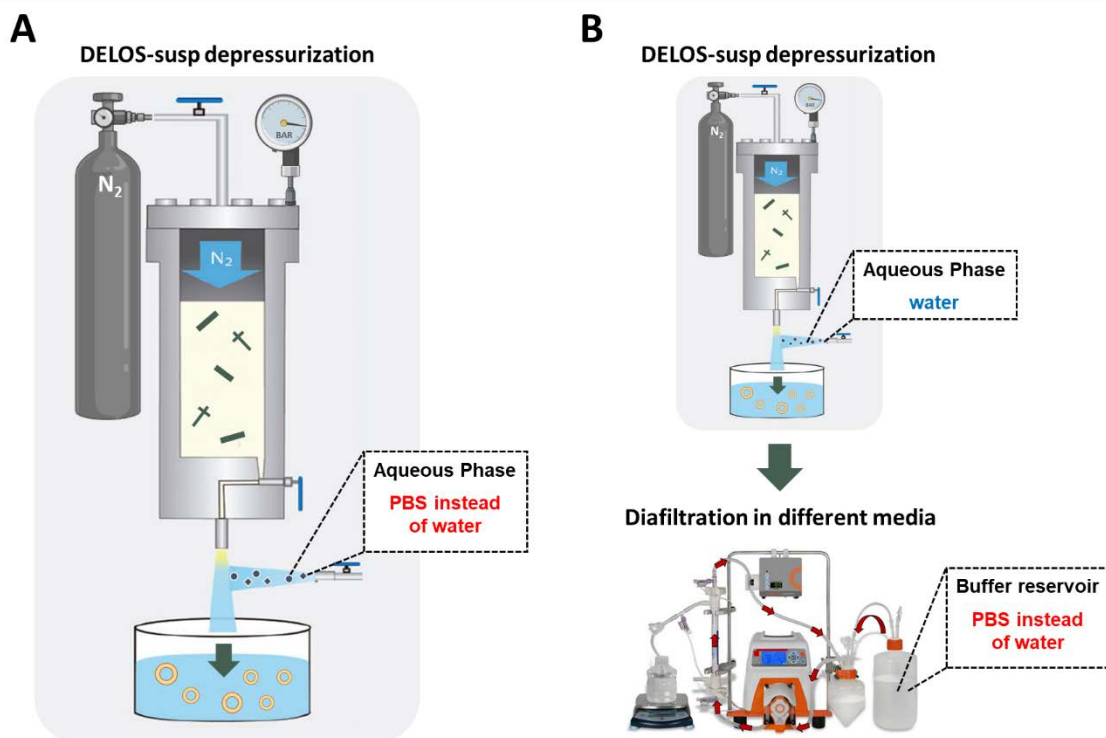


**Figure 5.14.** Scheme of the two different approaches for incorporating isosmotic media: (A) during DELOS-susp procedure, direct depressurization of the organic solution into an aqueous solution containing the PBS instead of pure water, and (B) after preparation of liposomes by DELOS-susp (depressurizing into pure water as usually), diafiltration using PBS instead of water for media exchange (see **Chapter 9.3**).

Considering the first option, the methodology of preparation was identical as when batches were prepared in water, excepting that the depressurization was performed in PBS (100 mM) solution instead of pure water. Unloaded GLA-liposomes were obtained, in water ( $L_{\text{DELOS-water}}$ ) or in PBS ( $L_{\text{DELOS-PBS}}$ ).

Control sample, depressurized in water, showed a good size distribution with narrow PDI, and high  $\zeta$ -potential (**Figure 5.15A**). Nevertheless, formulation depressurized directly in PBS showed undesired physicochemical characteristics, in terms of size, PDI, and colloidal stability. The size distribution showed a peak in the micrometric range, suggesting liposomal aggregation (**Figure 5.15B**). It correlated with a milky and cloudy macroscopic appearance, and liposomal sedimentation few hours later.

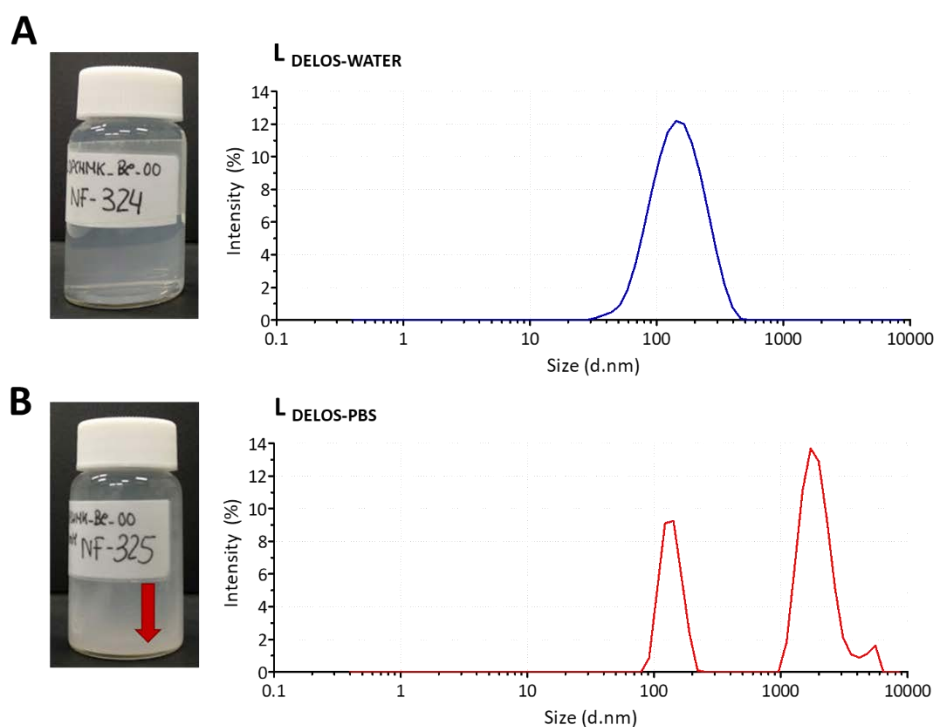


**Figure 5.15.** Size distribution and macroscopic appearance of blank liposomes depressurized in (A) water (control), and in (B) PBS 100 mM, 2 h after their preparation. Measured by DLS, see **Chapter 9.5.1**.

Next, considering the second option, GLA-unloaded liposomes were prepared by DELOS-susp as usually (depressurizing into pure water) ( $L_{\text{DELOS-water}}$ ), but this step was followed by diafiltration using PBS instead of water for media exchange. Liposomes were obtained diafiltrated in water ( $L_{\text{DIAF-water}}$ ) and in PBS ( $L_{\text{DIAF-PBS}}$ ).

The size distribution of liposomes diafiltrated in PBS showed only one population, with similar size to original liposomes before diafiltration (**Figure 5.16**). The obtained vesicles were in the nanometric size, and uniform in terms of size. Diafiltration in PBS tended to form a sample with more heterogeneity in morphology, with some peanut-like vesicles and oligo-lamellar vesicles, that were not observed in the original sample (**Figure 5.16**). A reduced PDI was observed for liposomes in PBS, result confirmed also by NTA, since a narrower peak was observed for PBS-diafiltrated sample. All samples showed good stability at short-time, at least one week. Regarding pH, diafiltrated samples (both in water and in PBS) showed a neutral pH (**Table 5.12**), more closed to the physiological pH than after DELOS-susp, which showed a more acidic pH. The acidic value is because of the depressurization with  $\text{CO}_2$ , which remains dissolved in the sample provoking this pH reduction. Time or agitation can help to release the dissolved  $\text{CO}_2$ .

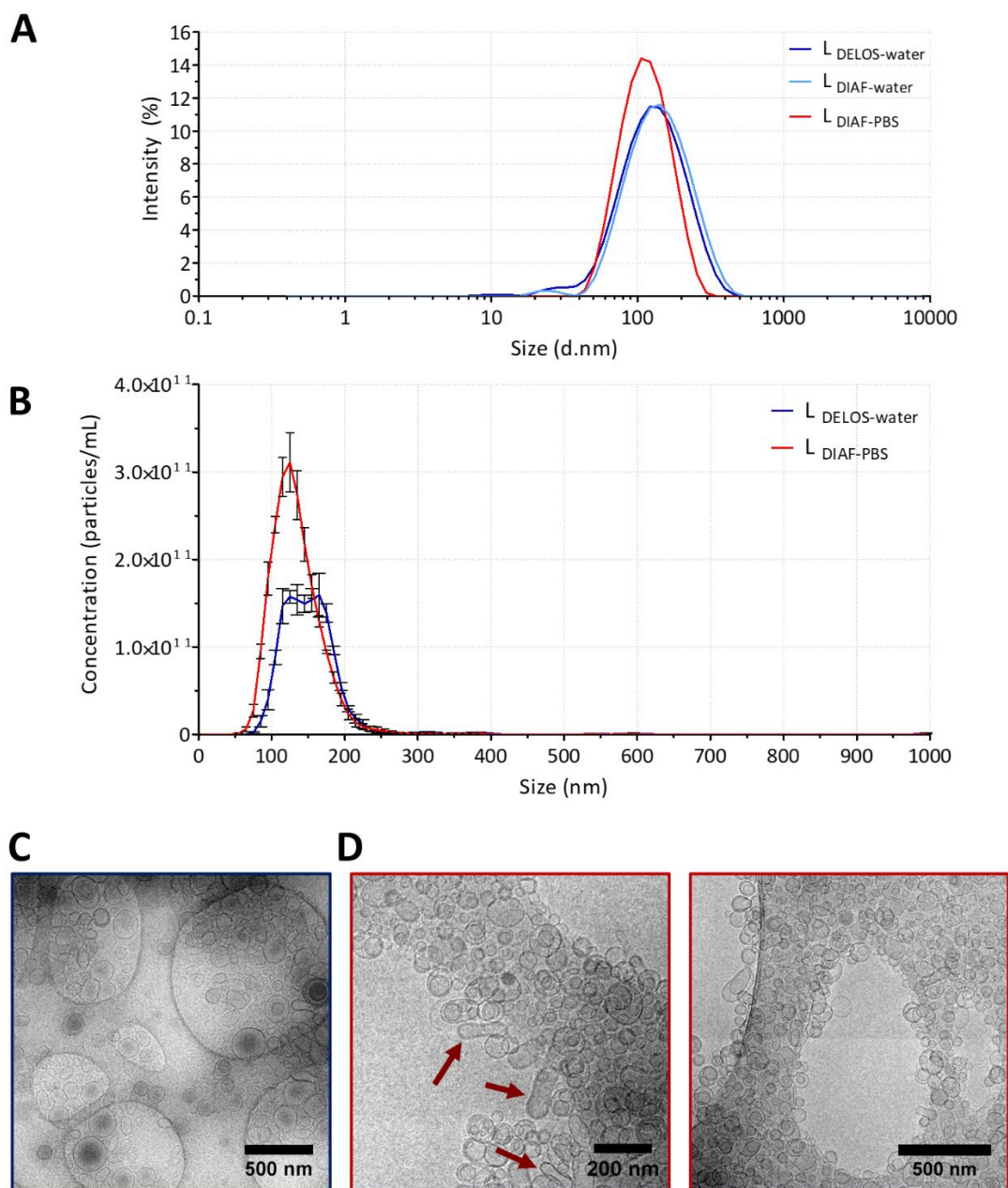


**Figure 5.16.** Size distribution of liposomes after DELOS-susp (depressurized in water,  $L_{\text{DELOS-water}}$ ), after diafiltration in water ( $L_{\text{DIAF-water}}$ ) or after diafiltration in PBS ( $L_{\text{DIAF-PBS}}$ ) by (A) DLS and by (B) NTA. Morphology by cryoTEM of (C)  $L_{\text{DELOS-water}}$  and (D)  $L_{\text{DIAF-PBS}}$  systems. See experimental details in **Chapter 9.5.1** and **Chapter 9.5.5**.

**Table 5.12.** Physicochemical characteristics at time 0 and in parenthesis at time 1 week after production.

System ID	Media	Size <sup>†</sup> (nm) (± SD)	PDI <sup>†</sup> (± SD)	No. particles <sup>‡</sup> (mL <sup>-1</sup> ) (± SD)	pH <sup>§</sup> (± SD)	Osmolality <sup>  </sup> (mOsm kg <sup>-1</sup> ) (± SD)
L <sub>DELOS-water</sub>	EtOH 5% /DMSO 1%	107.2 ± 0.5	0.23 ± 0.01	2.2 ± 0.1 × 10 <sup>12</sup>	4.92 ± 0.02	881 ± 5
L <sub>DIAF-water</sub>	Water	133 ± 1 (118 ± 1)	0.25 ± 0.01 (0.23 ± 0.01)	ND	6.1 ± 0.02	1 ± 5
L <sub>DIAF-PBS</sub>	PBS	105 ± 1 (109 ± 1)	0.12 ± 0.01 (0.15 ± 0.02)	4.4 ± 0.1 × 10 <sup>12</sup>	7.14 ± 0.01	190 ± 5
Buffer	PBS	–	–	–	7.16 ± 0.01	187 ± 5

† Measured by DLS (see **Chapter 9.5.1**); ‡ Measured nanoparticle tracking analysis (NTA) (see **Chapter 9.5.1**);

§ Measured by a pH meter (see **Chapter 9.5.2**); || Measured by freezing-point (see **Chapter 9.5.3**).

As introduced before, osmolality measurements could provide information regarding the % of organic solvent that remained in the sample, since EtOH and DMSO are osmotically active substances. To check the assumption that all the organic solvent was removed by diafiltration, the process of media exchange was monitored taking aliquots every two cycles and measuring the osmolality of the sample. The plotted results (**Figure 5.17**) showed a starting point with high osmolality, due to the presence of ethanol EtOH and DMSO (L<sub>DELOS-water</sub>). As sample is diafiltrating, the osmolality is decreasing, suggesting the remove of these organic solvents and its exchange with PBS buffer or water. Finally, the resulted sample showed the same osmolality than the media alone, indicating the complete exchange after at least 4 diafiltration cycles.

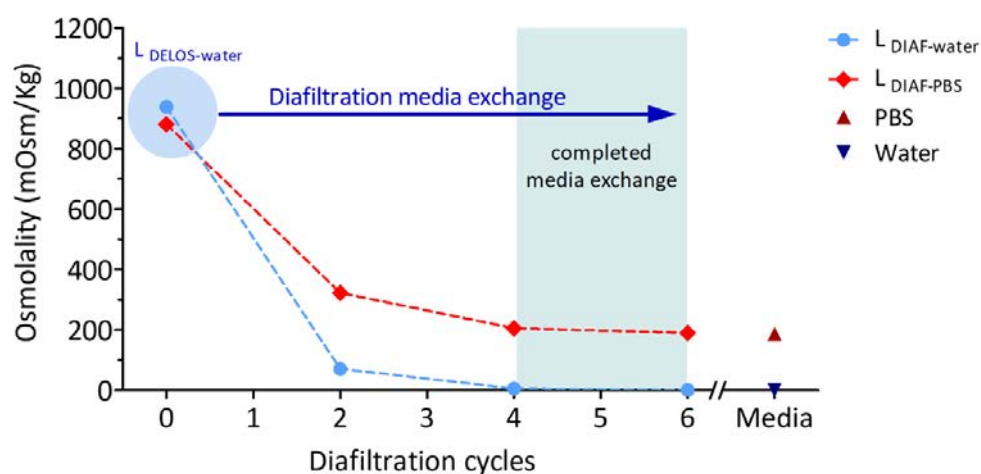


**Figure 5.17.** Evolution of the liposomal osmolality during the buffer exchange by diafiltration, in PBS or in water, measured by freezing-point (see **Chapter 9.5.3**). Media referred to PBS and water alone.

These results illustrated the importance of the media incorporation way to liposomes since this can influence the stability and self-assembling of liposomal molecular components. Whereas direct depressurization in PBS leads to an unstable liposomal sample, results supported the feasibility of the TFF diafiltration as a method to remove organic solvents and free molecules while exchanging the media to an isosmotic one.

### Production of GLA-liposomes in PBS

After the good results obtained for GLA-unloaded liposomes (i.e., without GLA) diafiltrated in PBS, the same process was repeated but this time incorporating the GLA. The usual DELOS-susp procedure depressurizing in GLA-containing water was performed. Then, in the diafiltration step, sample was submitted to diafiltration using PBS instead of water as usually.

First, the macroscopic appearance was slightly whiter just after the diafiltration, and some sedimentation was observed after two days, followed by a PDI increase. But the most important fact was that GLA quantification showed that all GLA in GLA-L<sub>DIAF-PBS</sub> was lost during the diafiltration, leading to a fall of the entrapment efficiency to zero (Table 5.13).

**Table 5.13.** Physicochemical characteristics of GLA-loaded liposomes at time 1 – 2 days after production.

System ID	Size <sup>†</sup> (nm) (± SD)	PDI <sup>†</sup> (± SD)	GLA <sup>‡</sup> (µg mL <sup>-1</sup> ) (± SD)	EE% <sup>§</sup> (%) (± SD)
GLA-L <sub>DELOS-water</sub>	126 ± 1	0.24 ± 0.02	13.5 ± 0.9	–
GLA-L <sub>DIAF-water</sub>	123 ± 1	0.18 ± 0.01	13.7 ± 0.9	102 ± 13
GLA-L <sub>DIAF-PBS</sub>	134 ± 4	0.30 ± 0.01	< LOQ*	0

\* Limit of detection (LOQ); † Measured by DLS (see Chapter 9.5.1); ‡ SDS-PAGE plus TGX, performed by Dr. J. L. Corchero from IBB-UAB (Barcelona) (see Chapter 9.6.3.1); § Enzyme entrapment efficiency (see Chapter 9.6.3.4).

This effect was not observed with GLA-L<sub>DIAF-water</sub>, which was able to retain the protein with high EE%. The hollow fiber cut-off used for the diafiltration was bigger enough to remove the free GLA, but small enough to ensure no crossing of liposomes.

The different behaviour of GLA-L<sub>DIAF-water</sub> and GLA-L<sub>DIAF-PBS</sub> liposomes illustrates that the selected aqueous medium not only could have an impact on the physicochemical properties of the liposomes (as higher PDI for liposomes in PBS), but also in the electrostatic interaction of the GLA with the liposome.

The presence of PBS salts and, thus, the addition of ions (i.e., phosphates and sodium chloride) could shield charged groups and lead to a reduction of the electrostatic interaction between the enzyme and the liposomal bilayer, provoking the final release of GLA from the nanovesicle. This decrease of the

entrapment efficiency (EE%) in presence of ionic salts is in line with the hypothesis that encapsulation is mainly due to an electrostatic interaction between the lipid membrane and the GLA enzyme.<sup>23,35</sup> For that, the study of GLA-loaded liposomes in different media alternative to PBS became important, to ensure good physicochemical characteristics as well as the preservation of their GLA entrapment and biological activity.

To sum up this section, the direct depressurization in an isosmotic media during DELOS-susp process was discarded, and the best strategy seems to be the media exchange in an isosmotic media by diafiltration process. Moreover, results also support the fact that EtOH and DMSO should be removed, since they were contributing to overly increase the osmolality of the suspension. The use of PBS was discarded, since provoked a loss of GLA due to a reduction of its electrostatic interactions with the liposomal membrane, leading to a fall of entrapment efficiency to zero. Results showed the necessity of finding alternative isosmotic media for nanoGLA system.

#### **5.2.6.4. Screening of isosmotic media suitable for the GLA-loaded liposomes**

Nowadays, there are around 15 liposomal-based nanomedicines approved for intravenous administration.<sup>36,37</sup> Among them, only systems with spherical morphology and nanometric size were considered for summarizing in **Table 5.14** some of their parameters, e.g., size, type of API, or physical form, including the media components used for osmolality adjustment. From them, the use of salts composed by small ions (e.g., phosphates, sodium) was widely used, but not the unique. Besides, sugars were commonly used for tonicity adjustment (e.g., sucrose, glucose), as well as some amino acids. It was also common to find specification regarding media incompatibilities, e.g., precipitation in saline, or dilution exclusively in dextrose (i.e., glucose), indicating the importance of the used media in liposomal formulations for maintaining their characteristics.

Therefore, GLA-loaded liposomes were prepared in water by DELOS-susp, and then water was exchanged by a battery of different isosmotic media in the diafiltration step (schematized in **Figure 5.18**), based on the compounds found in literature. These media were composed by sugars (trehalose, glucose, sucrose), in addition to some amino acids (histidine, glycine), salts as sodium chloride, and a mix of sodium phosphates and mannitol, similar to Fabrazyme<sup>®</sup> composition (named hereafter LB buffer). First, the concentration of each media was adjusted to a 260 – 300 mOsm kg<sup>-1</sup> range, to be isosmotic to blood, as indicated in **Table 5.15**.

**Table 5.14.** Formulation media in commercially available nanoliposomal formulations, approved for intravenous administration and presented as a lyophilized power (lyoph.) or as an aqueous dispersion (aq.). Adapted from <sup>36,37</sup>.

Liposomal product	Active agent and MW	Liposome size	Physical form	Media	Cautions
<b>Ambisome®</b>	Amphotericin B (0.9 kDa)	100 nm	Lyoph.	Sucrose	Do not reconstitute or mix with saline
<b>DaunoXome®</b>	Daunorubicin citrate (0.7 kDa)	45 nm	Aq.	Sucrose, glycine	Do not mix with saline, only use with D5W (dextrose 5 %)
<b>Doxil®</b> <b>Caelyx®</b> <b>Doxoves®</b> <b>Lipo-Dox®</b>	Doxorubicin (0.5 kDa)	80 – 100 nm	Aq.	Histidine (10 mM, pH 6.5), sucrose (10 % w/v)	Do not use with any diluent other than D5W (dextrose 5 %)
<b>Marqibo®</b>	Vincristine (0.8 kDa)	100 nm	Aq.	Mannitol, sodium phosphate, sodium chloride	–
<b>Mepact®</b>	Mifamurtide (1.2 kDa)	< 100 nm	Lyoph.	Sodium chloride (0.9 % w/v)	–
<b>Myocet®</b>	Doxorubicin (0.5 kDa)	190 nm	Lyoph.	Sodium carbonate	–
<b>Onivyde®</b>	Irinotecan (0.6 kDa)	110 nm	Aq.	HEPES, sodium chloride	–
<b>Visudyne®</b>	Verteporfin (1.4 kDa)	150 – 300 nm	Lyoph.	Lactose	Do not use sodium chloride solutions or other parenteral solutions since it precipitates
<b>Vyxeos®</b>	Daunorubicin (0.5 kDa) /cytarabine (0.2 kDa)	100 nm	Lyoph.	Sucrose	–

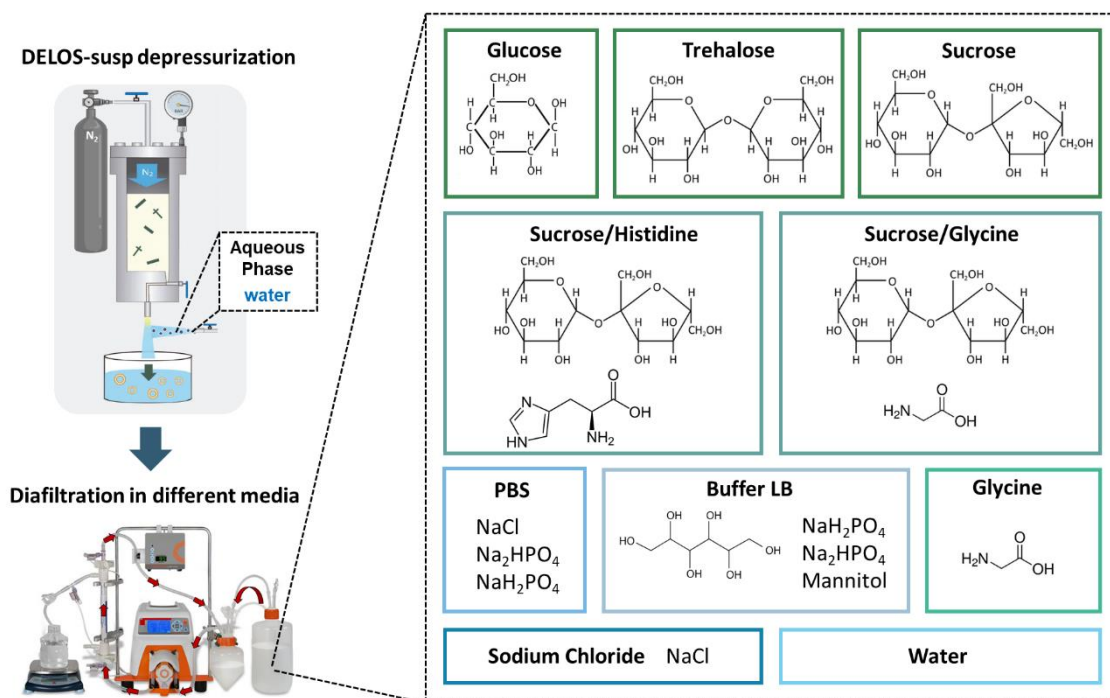


**Figure 5.18.** Scheme of the preparation of isosmotic GLA-loaded liposomal formulation, by media exchange in the diafiltration step. The screening of media contained sugars (glucose, trehalose, sucrose), amino acids (histidine, glycine), and salts (sodium chloride, phosphates).

**Table 5.15.** Composition of the media tested for osmolality adjustment.

Media	Components (% w/v)	Osmolality <sup>†</sup> (mOsm kg <sup>-1</sup> )	pH <sup>‡</sup>
Water	MilliQ water	-	~ 6 – 7
Glc	Glucose (5 %)	302 ± 5	~ 6 – 7
Tre	Trehalose (10 %)	305 ± 5	~ 6 – 7
Suc	Sucrose (10 %)	295 ± 5	~ 6 – 7
Suc/His	Histidine (10 mM, pH 7), sucrose (10 %)	288 ± 5	~ 7
Suc/Gly	Sucrose (8.5 %), glycine (0.4 %)	286 ± 5	ND
Gly	Glycine (2.5 %)	299 ± 5	ND
NaCl	Sodium chloride (0.9 %)	300 ± 5	ND
LB	Mannitol (3 %), sodium phosphate monohydrated (0.3 %), sodium phosphate dibasic heptahydrated (0.8 %)	277 ± 5	~ 7

<sup>†</sup> Osmolality by freezing-point determination (see **Chapter 9.5.3**), values represent a single representative measurement per system; <sup>‡</sup> pH estimated by pH indicator strips (see **Chapter 9.5.2**).



Characterization of size, PDI, and  $\zeta$ -potential, assessed by DLS; GLA concentration in diafiltrated samples was quantified by SDS-PAGE plus TGX and compared to the GLA concentration initially present in the liposomal samples. Entrapment efficiency (EE%) was calculated to see if diafiltration caused the loss of GLA as seen for the PBS. Results were summarized in **Table 5.16**.

**Table 5.16.** Summary of physicochemical characterization of GLA-liposomes diafiltrated in different isosmotic media at time 1 – 2 days or in parenthesis at 2 weeks after production.

Diafiltration media	Size <sup>  </sup> (nm) ( $\pm$ SD)	PDI <sup>  </sup> ( $\pm$ SD)	Z-potential <sup>  </sup> (mV) ( $\pm$ SD)	GLA <sup>¶</sup> ( $\mu$ g mL <sup>-1</sup> ) ( $\pm$ SD)	Osmolality <sup>#</sup> (mOsm kg <sup>-1</sup> ) ( $\pm$ SD)
L-DELOS	121 $\pm$ 2 (125 $\pm$ 5) <sup>†</sup>	0.26 $\pm$ 0.02 (0.27 $\pm$ 0.01) <sup>†</sup>	61 $\pm$ 1 (56 $\pm$ 1)	21 $\pm$ 1	1049 $\pm$ 10
L-Water	138 $\pm$ 3 (134 $\pm$ 7)	0.29 $\pm$ 0.02 (0.26 $\pm$ 0.01)	41 $\pm$ 8 (35 $\pm$ 4)	19.6 $\pm$ 0.4	0 $\pm$ 2
L-Glc	113 $\pm$ 4 (110 $\pm$ 3)	0.21 $\pm$ 0.01 (0.20 $\pm$ 0.01)	47 $\pm$ 1 (49 $\pm$ 3)	21 $\pm$ 1	294 $\pm$ 5
L-Tre	120 $\pm$ 1 (122 $\pm$ 1)	0.25 $\pm$ 0.01 (0.23 $\pm$ 0.01)	38 $\pm$ 1 (35 $\pm$ 5)	17.8 $\pm$ 0.2	324 $\pm$ 23
L-Suc	132 $\pm$ 8 (148 $\pm$ 14) <sup>‡</sup>	0.23 $\pm$ 0.01 (0.25 $\pm$ 0.02) <sup>‡</sup>	29 $\pm$ 2 (22 $\pm$ 4)	19 $\pm$ 2	284 $\pm$ 4
L-Suc/His*	232 $\pm$ 2 <sup>‡</sup> (300 $\pm$ 15) <sup>§</sup>	0.43 $\pm$ 0.06 <sup>‡</sup> (0.49 $\pm$ 0.06) <sup>§</sup>	15 $\pm$ 2 (14 $\pm$ 1)	23.1 $\pm$ 0.2	291 $\pm$ 5
L-Suc/Gly*	143 $\pm$ 3 (174 $\pm$ 1) <sup>‡</sup>	0.24 $\pm$ 0.01 (0.25 $\pm$ 0.02) <sup>‡</sup>	26 $\pm$ 3 (30 $\pm$ 2)	17.1 $\pm$ 0.1	282 $\pm$ 5
L-Gly*	128 $\pm$ 1 (124 $\pm$ 1)	0.26 $\pm$ 0.01 (0.23 $\pm$ 0.01)	35 $\pm$ 1 (35 $\pm$ 2)	21.6 $\pm$ 0.6	297 $\pm$ 5
L-NaCl*	125 $\pm$ 1 (134 $\pm$ 1) <sup>§</sup>	0.25 $\pm$ 0.01 (0.41 $\pm$ 0.03) <sup>§</sup>	6 $\pm$ 1 (7 $\pm$ 1)	< LOD	256 $\pm$ 5
L-LB*	125 $\pm$ 1 (123 $\pm$ 1)	0.19 $\pm$ 0.01 (0.20 $\pm$ 0.01)	13 $\pm$ 1 (14 $\pm$ 1)	< LOD	275 $\pm$ 5

Average of one\* or two independent batches; † Some sediment but resuspended well; ‡ Milky appearance; § Milky appearance and some sedimentation; || Measured by DLS and ELS (see **Chapter 9.5.1**); ¶ Measured by SDS-PAGE plus TGX, performed by Dr. J. L. Corchero from IBB-UAB (Barcelona) (see **Chapter 9.6.3.1**); # Measured by freezing-point (see **Chapter 9.5.3**).

First, GLA-loaded liposomes after DELOS-susp (L-DELOS) and diafiltration in water (L-water) were hyper- and hypoosmotic, as expected, but the osmolality of rest of the samples were within the isosmotic range (260 – 300 mOsm kg<sup>-1</sup>). This time, two interestingly trends were observed regarding the GLA entrapment efficiencies: On the one hand, GLA was well incorporated when sugars or amino acids were used as osmotic agents, since it was kept after the diafiltration. In this case, high entrapment efficiencies were obtained (EE% > 85 %), as seen in GLA-loaded liposomes diafiltrated in glucose, trehalose, sucrose, glycine, and sucrose/glycine (**Figure 5.19**). On the other hand, when salts were used (e.g., sodium chloride, or phosphates), they provoked a separation of the GLA from the liposomes, leading to its loss during the diafiltration. This effect was seen in samples diafiltrated in LB buffer and sodium chloride, like in PBS as was previously observed.

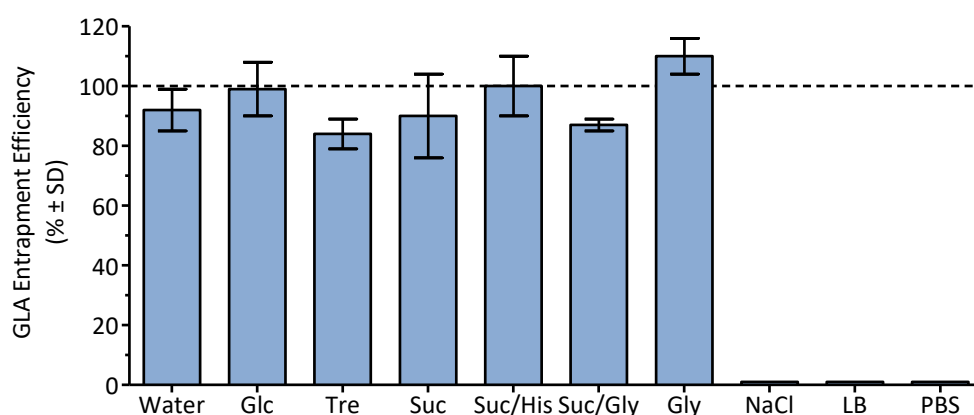


**Figure 5.19.** Entrapment efficiencies of GLA-loaded liposomes diafiltrated in different isosmotic media. GLA was measured by SDS-PAGE plus TGX by Dr. J. L. Corchero from IBB-UAB (Barcelona), see **Chapter 9.6.3.1**.

Formulations with good physicochemical characteristics were obtained when sugars were used as osmotic agents (i.e., glucose, trehalose, and sucrose), with similar size to the original L-DELOS, and low PDI, specially for GLA-liposomes in glucose. The three samples were stable after two weeks, but the macroscopic appearance of liposomes in sucrose tended to become whitish with time, although no sedimentation was obtained and PDI was not affected. It can be attributed to a slightly increase in size, maybe due to lower  $\zeta$ -potential, that it is well know that can influence on colloidal stability. Morphology of GLA-loaded liposomes in these media was varied, assessed by cryoTEM and summarized in **Figure 5.20**. In water, liposomes were mainly structured as spherical small unilamellar vesicles. Some multilamellar small vesicles were also observed in small proportion, with a characteristic stacking of several lipid bilayers. When sugars were used, morphology turned to some changes. In presence of glucose, liposomes showed a similar structuration than in water, with a majority of unilamellar vesicles. Surprisingly, some vesicles appeared not-well closed, although entrapment efficiencies did not indicate a loss of GLA. No aggregates were detected, in agreement with the low PDI. On the other hand,

diafiltration in trehalose provoked an elongation of some vesicles, as well as an apparently thicker membrane bilayer. Trehalose in small amounts is a commonly used lyoprotection agent, acting as a stabilizer agent which can interact with lipid bilayer and prevent rupture or fusion after freezing or lyophilization, stabilizing and maintaining the vesicle structuration,<sup>38</sup> and can be a possible explanation for such increase in the membrane thicker. On the contrary, liposomes in sucrose showed a majority of small unilamellar vesicles, although some of them appeared with a slightly elongated or oval shape, but all in the nanometric range without aggregates.

However, sucrose in combination with histidine leads to a sharper decrease in  $\zeta$ -potential, which was not high enough to prevent the sedimentation of the sample, correlated with higher PDI. Otherwise, sucrose with another amino acid, glycine, showed again a milky appearance and bigger sizes but without sediment. Thus, combination of sucrose with histidine or glycine amino acids was discarded for our system, as well as the option of glycine alone since morphology looked very heterogeneous. Curiously, for glycine, another widely used cryoprotectant, a similar thickening in lipid bilayer was detected as in the case of trehalose.

On the other hand, GLA-liposomes in sodium chloride sedimented with time, leading to a high PDI after two weeks. CryoTEM analysis also revealed the presence of such big structures in combination to small vesicles. Finally, vesicles in LB buffer (which contained sodium, phosphates, and mannitol) showed nice and narrow size distribution, but the loss of GLA made this buffer inappropriate.

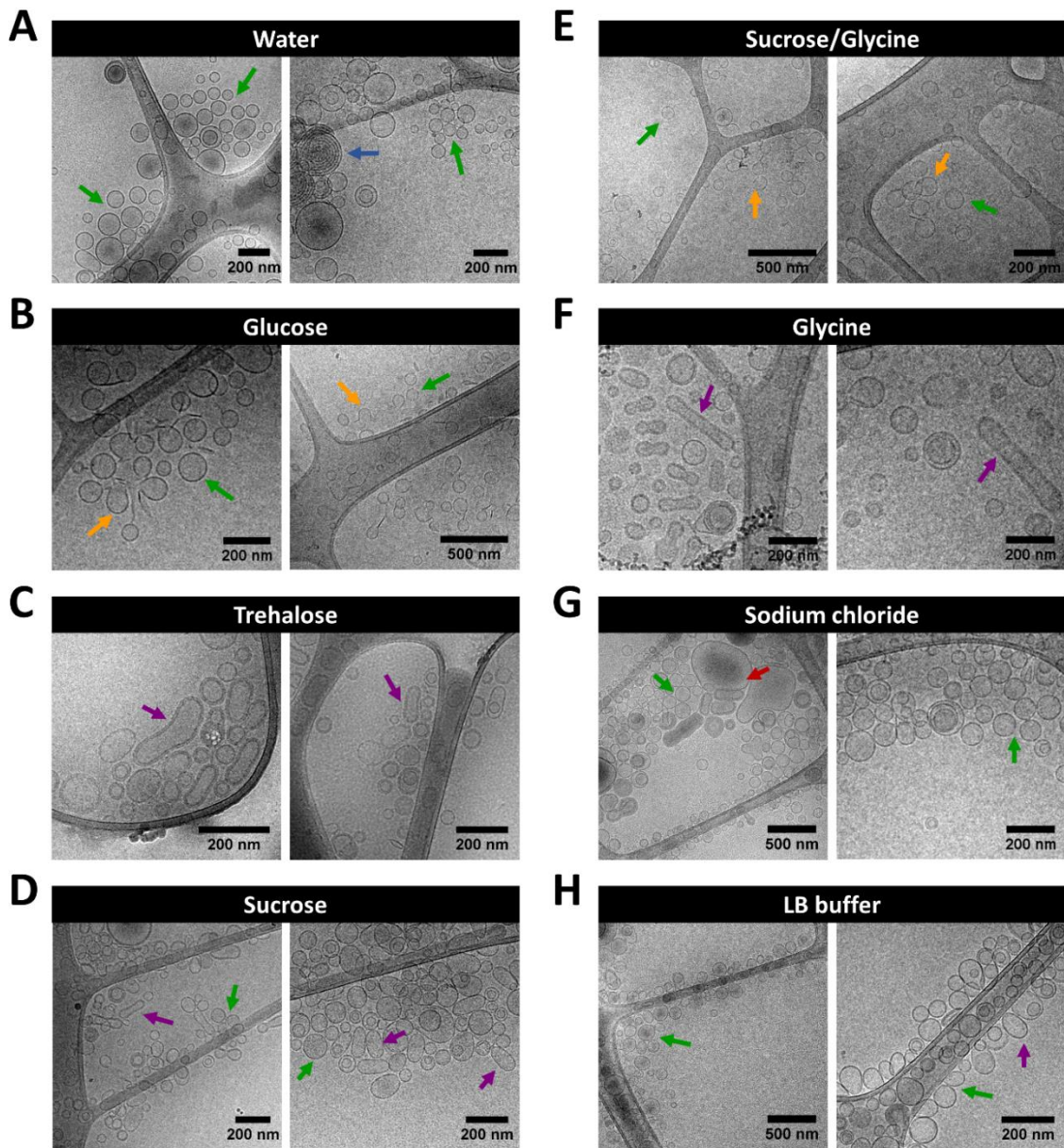


**Figure 5.20.** Morphology of GLA-loaded liposomes diafiltrated in (A) water, (B) glucose, (C) trehalose, (D) sucrose, (E) sucrose/glycine, (F) glycine, (G) sodium chloride, and (H) LB buffer. Small unilamellar vesicles (green arrows), “open vesicles” (orange arrows), multilayered small vesicles (blue arrows), elongated or oval vesicles, (purple arrows), big structures and aggregates (red arrows) can be distinguished.

Not only it is important to have the high entrapment efficiencies, but also GLA enzymatic activity preservation becomes crucial. The GLA enzymatic activity of the above-described samples was assessed by with Dr. I. Abasolo team from VHIR (Barcelona), as described in **Chapter 9.7.1**. The results of GLA specific enzymatic activity in the liposomal samples were presented in **Figure 5.21**, after correction by GLA concentration and normalization by the control (Replagal®).

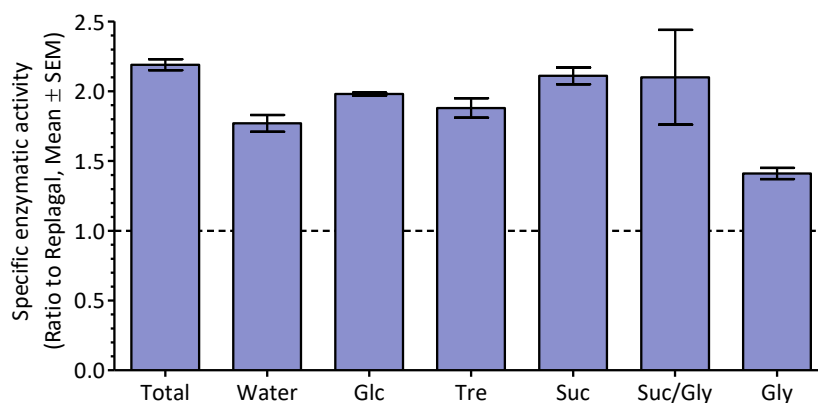


**Figure 5.21.** Specific enzymatic activity of GLA-loaded liposomes, in relation to the control (commercial Replagal® was normalized to 1). Values correspond to a single batch per system, replicated in 2 independent assays performed by Dr. I. Abasolo team from VHIR (Barcelona).

Whereas intermediate sample after DELOS-susp production showed a high enzymatic activity (more than the double than the commercial standard Replagal®), diafiltration in water showed a slightly decrease (1.77) in relation to the intermediate. The GLA specific enzymatic activity was maintained in liposomes diafiltrated in the different media, and, in all the samples, values were higher than the commercial standard Replagal®. Only glycine 2.5 % seemed to show a slightly less activity than the rest of samples probably because of the pH of this media. GLA is a lysosomal enzyme whose optimal working pH is more in the acidic range.

After this screening of media, the two more promising isosmotic media for GLA-loaded liposomes were glucose 5 % and sucrose 10 %, since liposomes in these media maintained good physicochemical characteristics, unilamellar morphology, and stability, as well as retained GLA with high entrapment efficiencies and enzymatic activity. Then, the in vitro efficacy of GLA-loaded liposomes in these media were tested in MAEC cells in collaboration with Dr. I. Abasolo team from VHIR (Barcelona), following the protocol described in **Chapter 9.7.2**. GLA-liposomes in glucose showed an efficacy closer to free GLA, whereas liposomes in sucrose showed a lower in vitro reduction of Gb3 (**Figure 5.22**).

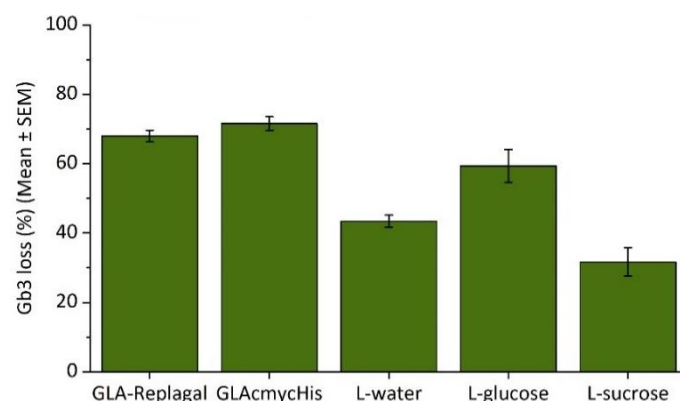


**Figure 5.22.** In vitro efficacy assay measured as loss of Gb3 in MAEC cells derived from Fabry KO mice. Incubation with GLA (Replagal® or GLAcmycHis) or GLA-liposomes at 37 °C for 48 h, at 0.01  $\mu\text{g mL}^{-1}$  GLA concentration. A single batch per system, performed by Dr. I. Abasolo team from VHIR (Barcelona).

Thus, glucose 5 % was selected as the best isosmotic media for GLA-loaded liposomes. A last trial was performed to reach doses suitable for in vivo testing. GLA-loaded liposomes were produced and submitted to a 7-fold concentration step followed by a diafiltration process in glucose, in three independent replicates. The obtained system was stable over time, showed a nanometric and narrow size distribution, and contained high concentration of GLA ( $\geq 150 \mu\text{g mL}^{-1}$ , EE%  $\geq 90$  %) (Table 5.17 and Figure 5.23A). Morphology of GLA-loaded liposomes in glucose after 7-fold concentration was maintained mainly spherical and unilamellar (Figure 5.23B). Finally, their capability of reducing the Gb3 deposits was measured in an in vitro efficacy assay in primary cells from Fabry KO mice (Figure 5.23C) in collaboration with Dr. I. Abasolo team from VHIR (Barcelona).

**Table 5.17.** Summary of physicochemical characterization of GLA-liposomes after 7-fold concentration and diafiltration in glucose (three independent replicates, #), at time 1 – 2 days or in parenthesis two weeks after production.

System ID	Size <sup>†</sup> (nm) (± SD)	PDI <sup>†</sup> (± SD)	$\zeta$ -pot <sup>†</sup> (mV) (± SD)	GLA <sup>‡</sup> ( $\mu\text{g mL}^{-1}$ ) (± SD)	EE% <sup>§</sup> (%) (± SD)	EA <sup>  </sup> (± SD)	Osm <sup>¶</sup> (mOsm $\text{kg}^{-1}$ ) (± SD)
L-Glu x7 #1	130 ± 2 (123 ± 1)	0.21 ± 0.01 (0.18 ± 0.01)	40 ± 1 (40 ± 1)	202 ± 7	125 ± 8	1.40 ± 0.07	294 ± 5
L-Glu x7 #2	131 ± 1 (126 ± 2)	0.28 ± 0.01 (0.22 ± 0.01)	45 ± 1 (47 ± 1)	161 ± 16	95 ± 17	0.90 ± 0.01	283 ± 5
L-Glu x7 #3	131 ± 1 (127 ± 3)	0.26 ± 0.01 (0.22 ± 0.01)	48 ± 1 (47 ± 1)	170 ± 12	100 ± 15	0.88 ± 0.04	282 ± 5

<sup>†</sup> Measured by DLS and ELS (see Chapter 9.5.1); <sup>‡</sup> Measured by SDS-PAGE plus TGX, performed by Dr. J. L. Corchero from IBB-UAB (Barcelona) (see Chapter 9.6.3.1); <sup>§</sup> Enzyme entrapment efficiency; <sup>||</sup> Specific enzymatic activity as a ratio to Replagal® (normalized to 1) performed by Dr. I. Abasolo team from VHIR (Barcelona) (see Chapter 9.7.1); <sup>¶</sup> Measured by freezing-point (see Chapter 9.5.3).

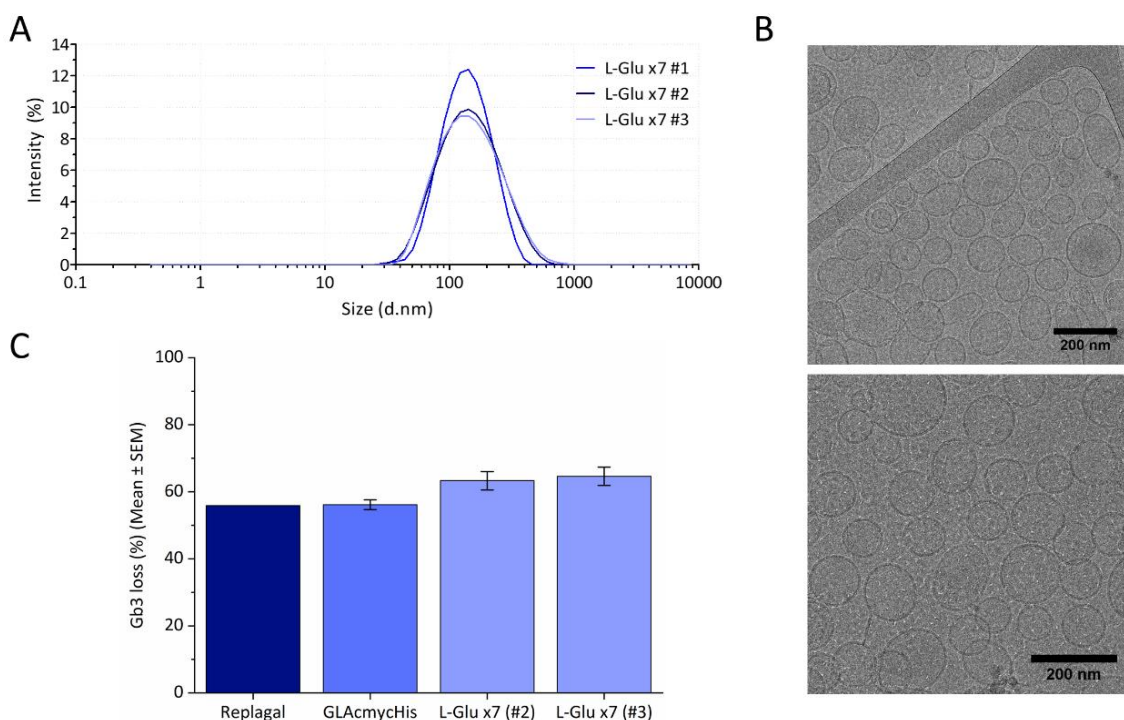


**Figure 5.23.** GLA-liposomes after 7-fold concentration and diafiltration in glucose: (A) size distribution (three independent replicates, #) by DLS two weeks after production (see **Chapter 9.5.1**); (B) morphology by cryoTEM, images acquired by Prof. D. Danino from Technion (Israel); and (C) in vitro efficacy assay as loss of Gb3 in MAEC cells derived from Fabry KO mice (incubation at 37 °C for 48 h, at 0.01  $\mu\text{g mL}^{-1}$  GLA concentration, single batch per system replicated in three independent assays), performed by Dr. I. Abasolo team from VHIR (Barcelona) (see **Chapter 9.7.2**).

### 5.3. Summary and Conclusions

In this chapter, some aspects to continue the nanoGLA development were addressed.

First, the critical quality attributes (CQA) for GLA-loaded nanoliposomal formulation (nanoGLA) were defined, as the relevant physicochemical and biological properties critical to product quality. Further, the established CQA were validated by the European Medicine Agency (EMA) by means of a Scientific Advice procedure.

Then, it was possible to first scaling up the nanoGLA production, from 25 mL to 150–900 mL per batch, with great potential flexibility in the produced batch size, confirming the suitability of the DELOS-susp platform for the preparation of robust nanoconjugates. Moreover, a successful application of the QbD approach to DELOS-susp production method was performed, and the influence of some formulation parameters on the CQA were determined by using a DoE methodology. Among the studied formulation factors, the analysis revealed that GLA concentration and lipid concentration were the two most important parameters to control for the quality of intermediate nanoGLA. Besides, the obtained

design space suggested that an increase of both lipid and GLA concentration provoke a negative impact on their physicochemical requirements.

Finally, using a TFF procedure, it was possible to reach the required concentration of GLA in the nanoGLA formulation, allowing the in vivo dosing. Different isosmotic media were tested, revealing a high impact of the media in the enzyme entrapment capacity of the liposomes. Lastly, glucose 5% was the selected isosmotic media for nanoGLA.

Overall, a successful optimization of the nanoGLA was done, allowing the advance of this nanoformulation to an advance stage of preclinical development.



## 5.4. References

1. Eaton, M. A. W. Improving the Translation in Europe of Nanomedicines (a.k.a. Drug Delivery) from Academia to Industry. *J. Control. Release* **164**, 370–371 (2012).
2. Satalkar, P., Elger, B. S., Hunziker, P. & Shaw, D. Challenges of clinical translation in nanomedicine: A qualitative study. *Nanomedicine Nanotechnology, Biol. Med.* **12**, 893–900 (2016).
3. Eaton, M. A. W., Levy, L. & Fontaine, O. M. A. Delivering nanomedicines to patients: A practical guide. *Nanomedicine Nanotechnology, Biol. Med.* **11**, 983–992 (2015).
4. Souto, E. B. *et al.* Nanopharmaceutics: Part II—production scales and clinically compliant production methods. *Nanomaterials* **10**, (2020).
5. Havel, H. *et al.* Nanomedicines: From Bench to Bedside and Beyond. *AAPS J.* **18**, 1373–1378 (2016).
6. Cabrera, I. *et al.*  $\alpha$ -Galactosidase-A Loaded-Nanoliposomes with Enhanced Enzymatic Activity and Intracellular Penetration. *Adv. Healthc. Mater.* **5**, 829–840 (2016).
7. Corchero, J. L. *et al.* Integrated approach to produce a recombinant, His-tagged human  $\alpha$ -galactosidase A in mammalian cells. *Biotechnol. Prog.* **27**, 1206–1217 (2011).
8. Agency European Medicines, Replagal - EMEA/H/C/000369 - IAIN/0096, <https://www.ema.europa.eu/en/medicines/human/EPAR/replagal#product-information-section>, accessed: November, 2019. <https://www.ema.europa.eu/en/medicines/human/EPAR/replagal#product-information-section> (2019).
9. Agency European Medicines, Fabrazyme - EMEA/H/C/000370 - II/0116, <https://www.ema.europa.eu/en/medicines/human/EPAR/fabrazyme>, accessed: January, 2021. (2020) doi:10.1163/187103210x528192.
10. European Medicine Agency. ICH guideline Q8 (R2) on pharmaceutical development. *EMA/CHMP/ICH/167068/2004 Committee for Human Medicinal Products ICH* vol. 8 [http://www.ema.europa.eu/docs/en\\_GB/document\\_library/Scientific\\_guideline/2009/09/WC500002872.pdf](http://www.ema.europa.eu/docs/en_GB/document_library/Scientific_guideline/2009/09/WC500002872.pdf) (2009).
11. European Medicine Agency. ICH guideline Q9 on quality risk management. *EMA/CHMP/ICH/24235/2006 Committee for Human Medicinal Products ICH* vol. 44 [https://www.ema.europa.eu/en/documents/scientific-guideline/international-conference-harmonisation-technical-requirements-registration-pharmaceuticals-human-use\\_en-3.pdf](https://www.ema.europa.eu/en/documents/scientific-guideline/international-conference-harmonisation-technical-requirements-registration-pharmaceuticals-human-use_en-3.pdf)

- (2017).
12. European Medicines Agency. ICH guideline Q10 on Pharmaceutical Quality System. *EMA/CHMP/ICH/214732/2007 Committee for Human Medicinal Products ICH* vol. 44 1–20 [http://www.ema.europa.eu/docs/en\\_GB/document\\_library/Scientific\\_guideline/2009/09/WC500002871.pdf](http://www.ema.europa.eu/docs/en_GB/document_library/Scientific_guideline/2009/09/WC500002871.pdf) (2015).
  13. Porfire, A., Muntean, D. M., Rus, L., Sylvester, B. & Tomuță, I. A quality by design approach for the development of lyophilized liposomes with simvastatin. *Saudi Pharm. J.* **25**, 981–992 (2017).
  14. Kapoor, M., Lee, S. L. & Tyner, K. M. Liposomal Drug Product Development and Quality: Current US Experience and Perspective. *AAPS J.* **19**, 632–641 (2017).
  15. Zhou, Y., Gong, X. J. & Yang, J. B. Introduction to the guidance for industry on liposome drug products: chemistry, manufacturing, and controls; human pharmacokinetics and bioavailability; and labeling documentation issued by FDA. *Chinese J. New Drugs* **27**, 1835–1840 (2018).
  16. Bozzuto, G. & Molinari, A. Liposomes as nanomedical devices. *Int. J. Nanomedicine* **10**, 975–999 (2015).
  17. European Medicines Agency. Scientific advice and protocol assistance. <https://www.ema.europa.eu/en/human-regulatory/research-development/scientific-advice-protocol-assistance>.
  18. Porfire, A. *et al.* Pharmaceutical Development of Liposomes Using the QbD Approach. *Liposomes - Adv. Perspect.* 1–20 (2019) doi:10.5772/intechopen.85374.
  19. GE Healthcare Life Sciences. Design of Experiments in Protein Production and Purification Handbook. *GE Healthc. Handbooks* 426 (2014).
  20. Xu, X., Costa, A. P., Khan, M. A. & Burgess, D. J. Application of quality by design to formulation and processing of protein liposomes. *Int. J. Pharm.* **434**, 349–359 (2012).
  21. European Medicine Agency. Reflection paper on the data requirements for intravenous liposomal products developed with reference to an innovator liposomal product. *EMA/Committee Hum. Med. Prod. 806058/2009/Rev. 02* **44**, 1–13 (2013).
  22. Shaker, S., Gardouh, A. & Ghorab, M. Factors affecting liposomes particle size prepared by ethanol injection method. *Res. Pharm. Sci.* **12**, 346–352 (2017).
  23. Colletier, J., Chaize, B., Winterhalter, M. & Fournier, D. Protein Encapsulation in Liposomes: Efficiency Depends on Interactions Between Protein and Phospholipid Bilayer. *BMC Biotechnol.* **2**, (2002).

24. Torchilin, V. Recent Advances with Liposomes as Pharmaceutical Carriers. *Nat. Rev.* **4**, 145–160 (2005).
25. European Medicines Agency. ICH guideline Q3C (R6) on impurities: Guideline for Residual Solvents. *International Conference on Harmonization of Technical Requirements for Registration of Pharmaceuticals for Human Use, EMA/CHMP/ICH/82260/2006* vol. 31 24 [https://www.ema.europa.eu/en/documents/scientific-guideline/international-conference-harmonisation-technical-requirements-registration-pharmaceuticals-human-use\\_en-33.pdf](https://www.ema.europa.eu/en/documents/scientific-guideline/international-conference-harmonisation-technical-requirements-registration-pharmaceuticals-human-use_en-33.pdf) (2019).
26. Boersen, N., Lee, T. & Hui, H. W. Development of Preclinical Formulations for Toxicology Studies. in *A Comprehensive Guide to Toxicology in Preclinical Drug Development* 69–86 (Elsevier Inc., 2013). doi:10.1016/B978-0-12-387815-1.00004-6.
27. Neervannan, S. Preclinical formulations for discovery and toxicology: Physicochemical challenges. *Expert Opin. Drug Metab. Toxicol.* **2**, 715–731 (2006).
28. Dan, N. & Danino, D. Structure and kinetics of lipid-nucleic acid complexes. *Adv. Colloid Interface Sci.* **205**, 230–239 (2014).
29. Pramanick, S., Singoidia, D. & Chandel, V. Excipient Selection In Parenteral Formulation Development. *Pharma Times* **45**, 65–77 (2013).
30. Wang, W. Tolerability of hypertonic injectables. *Int. J. Pharm.* **490**, 308–315 (2015).
31. Silverthorn, D. U. Isosmotic is not always isotonic: The five-minute version. *Adv. Physiol. Educ.* **40**, 499–500 (2016).
32. KNAUER Wissenschaftliche Geräte GmbH. The Theory of Osmolality and Freezing Point Measurement. *News-Medical* (2020).
33. Carstairs, S. D. *et al.* Contribution of serum ethanol concentration to the osmol gap: A prospective volunteer study. *Clin. Toxicol.* **51**, 398–401 (2013).
34. Oster, J. R. & Singer, I. Hyponatremia, hyposmolality, and hypotonicity: Tables and fables. *Arch. Intern. Med.* **159**, 333–336 (1999).
35. Rezaei Sani, S. M., Akhavan, M. & Jalili, S. Salt-induced effects on natural and inverse DPPC lipid membranes: Molecular dynamics simulation. *Biophys. Chem.* **239**, 7–15 (2018).
36. Bulbake, U., Doppalapudi, S., Kommineni, N. & Khan, W. Liposomal Formulations in Clinical Use: An Updated Review. *Pharmaceutics* **9**, 1–33 (2017).
37. Beltrán-Gracia, E., López-Camacho, A., Higuera-Ciapara, I., Velázquez-Fernández, J. B. &

Vallejo-Cardona, A. A. *Nanomedicine review: Clinical developments in liposomal applications*. *Cancer Nanotechnology* vol. 10 (Springer Vienna, 2019).

38. Chen, C., Han, D., Cai, C. & Tang, X. An overview of liposome lyophilization and its future potential. *J. Control. Release* **142**, 299–311 (2010).



” *For a research worker the unforgotten moments of his life are those rare ones which come after years of plodding work, when the veil over nature's secret seems suddenly to lift, and when what was dark and chaotic appears in a clear and beautiful light and pattern.*

— Gerty Cori

# 6

## **Preclinical evaluation of nanoGLA liposomes for Fabry disease treatment**

### **6.1. Introduction to preclinical efficacy and toxicology studies in drug development process**

The safety, efficacy, and initial dosing of potential new nanomedicines during drug development must be assessed before clinical phases, i.e., trials with humans, according with scientific, ethical, and regulatory requirements. Accordingly, preclinical studies, including efficacy, pharmacodynamics (PD), pharmacokinetics (PK), and toxicology studies of new potential drugs are required.<sup>1</sup> In this investigation stage, animal models are used to predict human response, since usually they have in common similar pathways or molecular targets with humans, in spite of existing ethical controversies about the use of experimental animals discussed over the years.<sup>2</sup>

Although two rodent species (usually mice and rats) are generally utilized for carrying out in vivo evaluation, most preclinical studies require the testing in a second additional non-rodent species, to increase the sensitivity of the test for human applications.<sup>2</sup> Frequent non-rodent species in preclinical testing includes dogs, minipigs, or rabbits. These species tend to show better genetic homology and organ similarity with humans, allow greater sequential sampling since are bigger animals, and show

other advantages regarding lifespan or metabolism. However, they also showed some issues related to less available background data, higher ethical concerns, and more difficult availability, housing, handling, maintenance and breeding, which are easier for rodent species.<sup>2</sup> However, in spite of some similarities to humans, all species differ in some biological behavior, and these differences should be always taken into account in the design study.

### 6.1.1. Pharmacokinetics and Toxicokinetics

First, pharmacokinetic (PK) studies are used to evaluate the absorption, distribution, metabolism, and excretion (ADME) of drugs, concepts explained in the introduction Chapter of this Thesis. By plasma sampling and analysis of the testing compound at appropriate time points, it is possible to calculate PK parameters, e.g., clearance (CL), volume of distribution ( $V_d$ ), half-life ( $t_{1/2}$ ) and exposure (area under the curve, AUC, or maximum concentration observed,  $C_{max}$ ), as represented in **Figure 6.1**.<sup>3</sup> These PK parameters can be affected by several variables to take into account, as methodological (administration route, dose...) or formulation (physicochemical characteristics, excipients...) changes.<sup>1</sup> Besides, the use of nanocarriers can play an important role in the modification of the PK profile of the entrapped biomolecules.

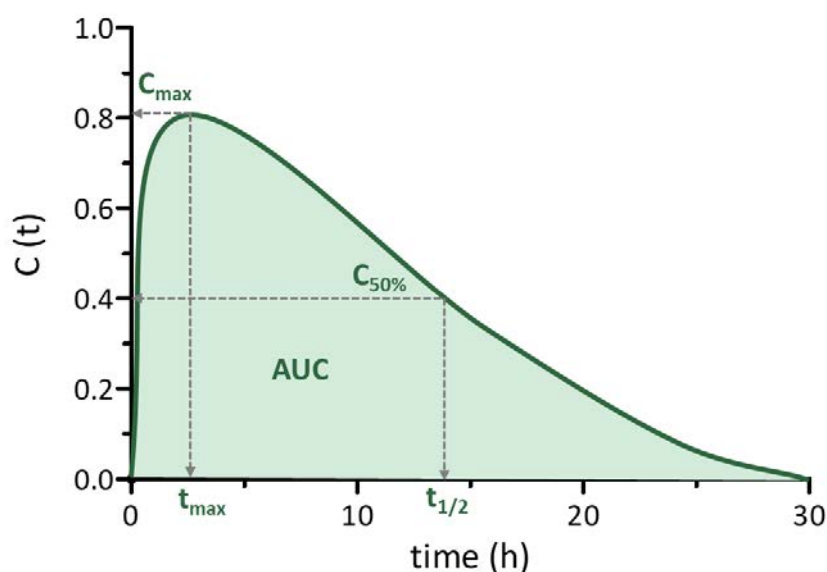


**Figure 6.1.** Generic PK profile, including some PK parameters, e.g., area under the curve (AUC), half-life ( $t_{1/2}$ ), or maximum concentration ( $C_{max}$ ). Adapted from Glassman et al.<sup>4</sup>

Generally, most preclinical PK studies use a non-compartmental approach for data analysis. This approach is versatile and robust, and allows to evaluate several PK parameters (e.g., CL,  $V_d$ ,  $t_{1/2}$ , and AUC) without assuming or understanding the mechanistic properties of the drug within the body.<sup>3</sup> Among these parameters, here below the most relevant ones are introduced.

Interestingly, plasma concentration vs time plots can exhibit different shapes, depending on the distribution of the drug. When the compound is mainly located in the central compartment (i.e., blood, plasma, or well perfused organs such as liver and kidneys), the PK profile shows a semi-log plot with only one decline tendency region, as illustrate in **Figure 6.2A**. Otherwise, when the decline in concentration shows two tendency regions (as in **Figure 6.2B**), this shape suggests a distribution of the drug between central and peripheral compartments.<sup>3</sup>

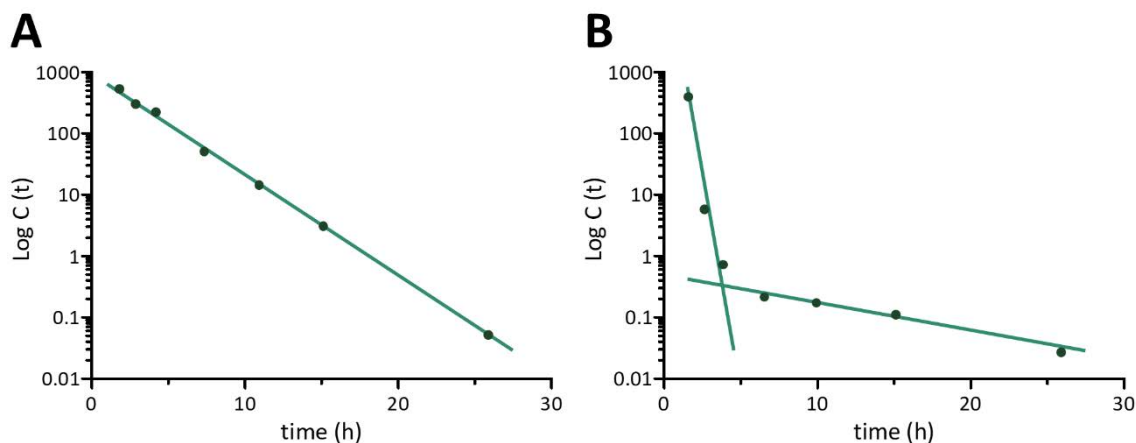


**Figure 6.2.** Example of PK profiles, representing concentration of drug in plasma over time, in (A) a monophasic profile, or in a (B) bi-phasic profile. Adapted from <sup>3,5</sup>.

First, from concentration vs time representations, one important parameter which can be extracted is the half-life ( $t_{1/2}$ ), defined as the amount of time required for the drug concentration measured in plasma to be reduced to exactly half of the starting concentration.<sup>3</sup> This reduction in plasma concentration is mainly due to distribution and elimination processes. In a biphasic decline profile (**Figure 6.2B**), the first region characterized by a fast reduction can be mainly attributed to distribution, whereas the later region is usually slower and can be primarily attributed to elimination process. Then, close related to half-life, other interesting PK parameters are clearance (CL) and distribution volume at steady state ( $V_{ss}$ ). First, clearance (CL, units of volume  $\text{time}^{-1}$ ) can be defined as the rate of removal of a drug from an apparent volume of fluid (usually plasma), and directly reflects in vivo elimination mechanisms. In a non-compartmental analysis, CL is estimated from the amount administered as IV dose, divided by the area under the curve (AUC). Besides, the distribution volume at steady state ( $V_{ss}$ , units of volume) is a parameter related to the volume of blood and tissue into which a drug is distributed, assuming the equilibrium state (same input than output rates) and can generally be useful to describe an average extent of distribution of the drug from plasma to the tissues.<sup>3,5</sup>

Besides, integrated into toxicity studies, there are the toxicokinetic (TK) studies which can be defined as the relation between in vivo drug concentration at various doses and observable toxicity effects.<sup>6</sup> Although TK can be included as an extension of PK field, both studies differ in the doses which are



analyzed.<sup>3</sup> Therefore, in TK studies doses are generally higher than those used in PK studies, and describes the drug concentrations required to induce undesirable side effects. The obtained TK data may differ from PK parameters (same drug at safer doses) since higher doses can push drug absorption and elimination processes to the limit and can alter the compound kinetics or introduce non-linearity.

Therefore, toxicokinetics allow to: (i) establish relations between the exposure received in toxicological studies with results of such studies, (ii) justify the animal model and administration regime selection in preclinical toxicology studies, and (iii) obtain complementary information to toxicology results to help the design of subsequent preclinical studies.<sup>7</sup> For that, TK studies should be conducted in accordance with the GLP rules.

### 6.1.2. Safety studies to evaluate toxicity

Therefore, there exist several kind of toxicity studies to evaluate the safety of a new compound during the preclinical phase of the drug development process, including general toxicology, safety pharmacology, genotoxicity, reproductive toxicity, and carcinogenicity studies, among others (Figure 6.3).

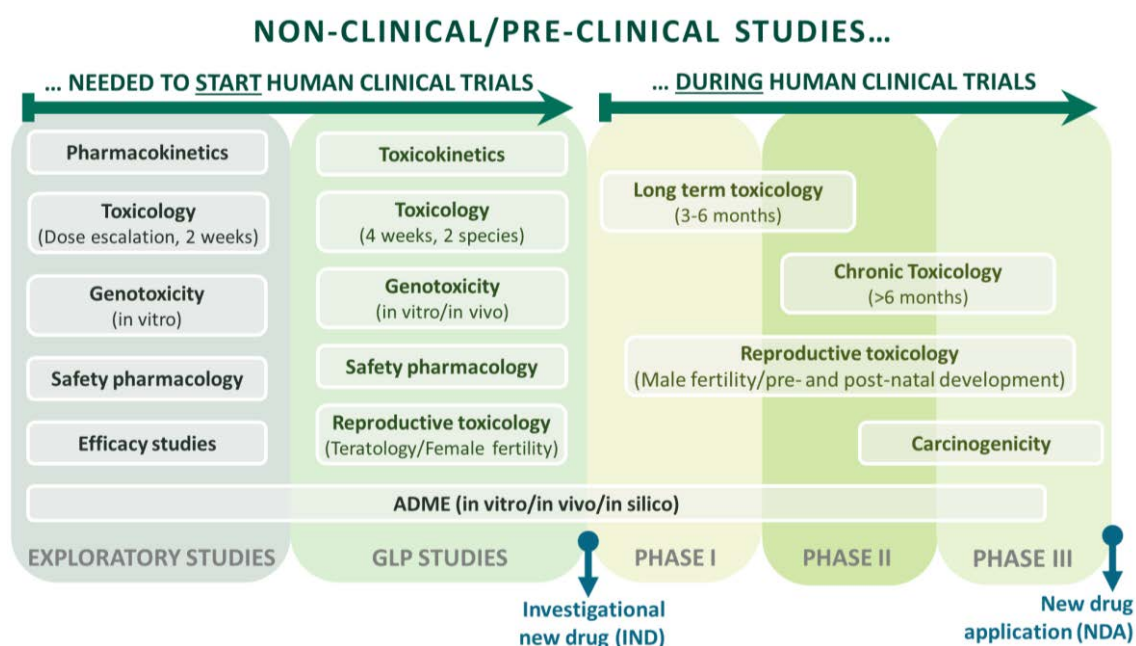


**Figure 6.3.** Scheme of the main required non-clinical studies, divided in those needed before starting human clinical trials, and those which can be conducted in parallel. Adapted from Andrade et al.<sup>6</sup>.

#### 6.1.2.1. Preclinical exploratory toxicology studies

In the initial stages of development, preliminary exploratory safety screening tests are usually assessed to detect possible toxic effects. These initial exploratory tests are generally performed in vitro, or with a minimal animal number, and they do not need to follow regulatory requirements. Some examples are

found in the previous chapters of this thesis, e.g., in vitro hemocompatibility assays. Additionally, genotoxicity effects, i.e., if the testing substance can provoke genetic alterations, are usually assessed in vitro (e.g., by Ames test in bacteria or micronucleous assay) at preliminary stage, especially in the testing of new chemical compounds.<sup>6</sup>

Further, the first in vivo exploratory toxicity study for a new potential drug is generally a dose range-finding study in rodents. In dose-ranging studies, different doses of the testing compound are tested to establish a first knowledge regarding which dose is less harmful or can potentially work best. This first exploration of possible adverse effects is commonly performed in rodent species, before testing in non-rodent species, due to scientific and welfare reasons, as well as to collect more information (e.g., adjustment of dose, or greater monitoring of specific observed adverse effects).

#### **6.1.2.2. Preclinical regulatory toxicology studies before clinical phase**

The toxicity level of the testing substance must be evaluated in terms of regulatory toxicology studies during the drug development process. This evaluation is characterized by the use of protocols that follow the requirements from the guidelines recommended to perform non-clinical studies of pharmaceutical products, as well as the compliance with the GLP (Good Laboratory Practice) principles, which assure to regulatory authorities that the data are a true reflection of the study results. In addition, for GLP-studies the testing substance should be in its final formulation (i.e., in the same formulation that will be used to treat humans during the clinical phase) and have a complete chemical certificate of analysis (CoA).<sup>6</sup>

After the preliminary toxicity studies, the GLP studies should be carried out using two animal species, and their design should be based on the efficacy and toxicity data obtained during the exploratory studies. At the end, the goal of the regulatory toxicity set of studies should be the translation of animal responses into an understanding of the risk for human subjects.

Although there is certain flexibility in the design and schedule organization of this preclinical regulatory phase, before starting in human testing it is recommended to perform a study of dose selection and repeated-dose toxicity (28-days), as well as genotoxicity studies (both in vitro and in vivo, under GLP).<sup>6</sup> The outcomes of these assays are indispensable for evaluating the toxicity of the test article, as well as providing a relationship between the dose-response and toxicity data. This relation allows to determine the “no observed adverse effect level” (NOAEL).

The NOAEL parameter represents the highest dose of tested article in animal that does not produce significant adverse effects when compared to the control group,<sup>6</sup> and this dose in animals ( $\text{mg kg}^{-1}$ ) is the one used to calculate the human equivalent dose (HED).<sup>8</sup> For a proper dose transposing between species, as from small animals to humans, there is not a linear transposition but it has to be considered

the body surface area, to know the equivalent dose between species. Examples of some species are illustrated in **Table 6.1**.

**Table 6.1.** Conversion of some animal doses to human equivalent doses, based on body surface area. Adapted from Andrade et al.<sup>6</sup>.

Species	To convert mg kg <sup>-1</sup> dose to mg m <sup>-2</sup> dose <sup>†</sup>	To convert animal dose (mg kg <sup>-1</sup> ) to human equivalent dose <sup>‡</sup> (mg kg <sup>-1</sup> )
	Multiply by	Divide animal dose by
Human	37	–
Mouse	3	12.3
Rat	6	6.2
Dog	20	1.8
Monkey	12	3.1
Minipig	35	1.1

† Related to body surface area; ‡ Assuming a 60 kg human.

After that, permission to regulatory agencies for starting the test in human can be requested, submitting a summary of the results from pharmacokinetic, efficacy, safety pharmacology, and substance chemical characterization studies.

### 6.1.2.3. Additional preclinical regulatory toxicology studies in parallel to clinical phase

Further, other non-clinical toxicity studies should be performed, e.g., sub-chronic and chronic studies, reproductive toxicology tests, and carcinogenicity tests, but they can be carried out in parallel to clinical studies.<sup>6</sup> First, sub-chronic and chronic studies are characterized by studying the toxicity effects during longer periods of time (30 – 90 days and > 90 days, respectively). Next, reproductive toxicology test along with the teratogenic (i.e., toxicity effect on embryo-fetal development) potential evaluation are very rigorous tests applied by regulatory agencies (e.g., FDA), which must be studied before the approval of new drugs. Further, carcinogenicity tests are usually required in some cases, e.g., for drugs belonging to a carcinogenic group, intended for continuous treatment ( $\geq 6$  months), or when substances are retained in the organism for a long period. This is one of the most expensive non-clinical study, since it is necessary to include a high number of specific pathogen-free animals per group and gender, evaluation for long period of time, and involves a large number of histopathology analysis and tissue samples.<sup>6</sup> Furthermore, depending on the observed effects in the standard toxicological studies, other tests could be required, e.g., immunogenicity studies. Therefore, although all these additional non-clinical toxicity studies can be performed during the clinical testing, they should be completed, when required, before new drugs reach the market.

Additional studies belonging to the safety pharmacology field can be integrated in the general toxicology studies. Safety pharmacology studies are intended to determine undesirable effects of the test substance on physiological functions of organ systems with relevance to human safety, specially of vital organs such as those related to cardiovascular, respiratory, and central nervous systems, although other complex physiological systems can also be included (gastrointestinal, renal, immune, etc.).<sup>6,9</sup> These studies should be generally performed at initial toxicology stages and before clinical phase, and can include a core battery of tests with the execution of *in vitro*, *ex vivo*, and *in vivo* preliminary tests of relatively low costs (preliminary tests usually do not need to follow the GLP requirements). The results should help to early detection of potential risk for humans, as well as contribute with the decision about continuing the development phase or not.

Overall, toxicology evaluations require high responsibility from all the involved teams, both non-clinical and clinical teams, and should be adapted for each tested substance. Moreover, continuous, and direct contact with regulatory agencies is again very recommended, for establishing the most appropriate strategies and studies at every stage of development. It allows to keep in mind the practical regulatory endpoint that has to be achieved once the studies are completed, besides considering the scientific approaches.<sup>9</sup>

### 6.1.3. Current state in nanoGLA drug development: milestones achieved to start the preclinical phase

All the composition optimization and characterization studies done in the previous sections were focused on obtaining a final GLA-nanoformulation (nanoGLA), with optimal physicochemical properties and biological performance in line to the regulatory perspective, to advance this innovative nanoGLA form the experimental Proof of Concept (TRL-3) to preclinical regulatory phase (TRL-5).

GLA-nanoformulation developed in the frame of this Thesis overcomes many limitations of previous GLA-liposomal formulations described in **Chapter 1**. Among these improvements, explained deeply in previous Chapters, it is important to highlight: (i) the increase of the GLA entrapment efficiency and the improvement of the colloidal stability by addition of small percentage of MKC surfactant, (ii) the better control of RGD-peptide targeting incorporation by the change from chol-PEG<sub>200</sub>-RGD to chol-PEG<sub>400</sub>-RGD, by means of enhanced solubility of this compound with the rest of membrane components, (iii) the definition of the critical quality attributes (CQA) for nanoGLA product, (iv) the increase of batch size by scaling-up from the small lab-scale to the intermediate lab-scale DELOS-susp plant, (v) the nanoGLA concentration for *in vivo* dosing in the range of therapeutic observable doses by TFF process, and (vi) the finding of a proper isosmotic medium (glucose 5% in water) able to keep the physicochemical, entrapment, and biological properties of nanoGLA, leading the formulation more convenient for intravenous administration.

Therefore, during this Chapter the final production of high size lab-scale batches with the required quality criteria previously defined, as well as the early non-regulatory and regulatory preclinical testing, are presented.

## 6.2. PK of GLA-free liposomes: MKC as a useful indicator of in vivo liposomal presence

First, although GLA enzyme is the active principle in the nanoGLA formulation, drug delivery systems are complex systems and, therefore, the study of PK parameters not only for the active, but from the vehicle point of view, can be also desirable to better understanding the biological behavior of the whole nanoGLA conjugate.

For monitoring the presence of nanoGLA liposomes in biological fluids (e.g., plasma), miristalkonium chloride (MKC), a membrane component of the nanoliposomes, was selected. Unlike other liposomal membrane components (e.g., cholesterol, or phospholipid DPPC), MKC quaternary ammonium surfactant is a compound which is not present in animal organisms in a natural way. The absence of a basal level of this molecule makes it virtually ideal for tracking liposomes in biological matrix.

To confirm the suitability of this strategy, a first preliminary in vivo pharmacokinetics study of empty-liposomes (i.e., without GLA) was performed, in collaboration with Dr. T. Birngruber group from Joanneum Research (Austria). The objective of this assay was triple: (i) confirm the suitability of using MKC as strategy for liposomal vehicle tracking, (ii) develop an analytical method for the detection of MKC in biological samples, and (ii) obtain preliminary information regarding plasma half-life of nanoliposomes in rats.

Empty-liposomes were prepared following the same protocol as previously explained; they were produced by DELOS-susp, followed by a TFF step, consisting in a diafiltration in water and 7.5-fold concentration (see **Chapter 9.2** and **Chapter 9.3**). Thus, the resulting empty-liposomes were composed by DPPC, cholesterol, cholesterol-PEG<sub>400</sub>-RGD, and MKC, with a theoretical concentration of 9.0 mg mL<sup>-1</sup> of liposomes, corresponding to 0.30 mg mL<sup>-1</sup> of MKC (5 mol % of the total composition). More experimental details could be found in **Chapter 9**. The resulted system showed very narrow vesicle size distribution in the nanometric range, as well as spherical and mostly unilamellar morphology (**Figure 6.4A** and **B**).

Then, wild type rats were assigned to two groups, and were dosing either with concentrated empty-liposomes at 30 mg kg<sup>-1</sup> of liposomes (equivalent to 1 mg kg<sup>-1</sup> of MKC), or with free MKC at the equivalent concentration (**Table 6.2**), as experimentally detailed in **Chapter 9.14**.

**Table 6.2.** IV dosing of the two different animal groups (n = 5 male rats/group) according to MKC content of the formulation, as detailed in **Chapter 9.14**.

Group	Stock concentration	Liposome dose level (mg liposomes <sup>-1</sup> kg <sup>-1</sup> )	Equivalent MKC dose level (mg MKC <sup>-1</sup> kg <sup>-1</sup> )
Empty-liposomes	9.0 mg mL <sup>-1</sup> liposomes (containing 0.30 mg mL <sup>-1</sup> MKC)	30	1
Free MKC	0.30 mg mL <sup>-1</sup> MKC	–	1

Concentration of MKC was quantified by a LC-MS methodology (see **Chapter 9.15.1**) and was plotted over time in **Figure 6.4C**. Preliminary PK results evidence the different behavior of MKC in plasma when it was integrated into the liposomal membrane or when it was dosed as free molecule. On the one hand, free MKC was rapidly removed from circulation, with a short plasma half-life of less than 15 min. This result was expected, since MKC, as free compound, at 0.30 mg mL<sup>-1</sup> (equivalent to MKC concentration in the liposomal stock sample) is below its critical micelle concentration (CMC), which is around 2.16 mM at 25 °C (this equals to 0.79 mg mL<sup>-1</sup>). The CMC of a surfactant is related to the self-assembling state of free surfactant molecules dissolved in water; below the CMC, surfactant molecules are found as monomers, whereas above the CMC, surfactant molecules self-assembled in micelles, exposing the polar head region of the molecule, and hiding the hydrophobic chains. In the case of free MKC in the stock solution before administration to rats, MKC concentration was below CMC, and thus, as monomer. Later dilution in blood during the administration also accentuates this dilution effect. It is known that small molecules, as hydrophilic MKC, can be rapidly removed from circulation after renal clearance or hepatic elimination.<sup>4,10</sup>

On the contrary, MKC from empty-liposomes (L-RGD) showed a sustained presence in the rat plasma, with a half-life of 96 min. This difference suggests that MKC is travelling in a different way than as free molecule, most likely retained in the liposome.

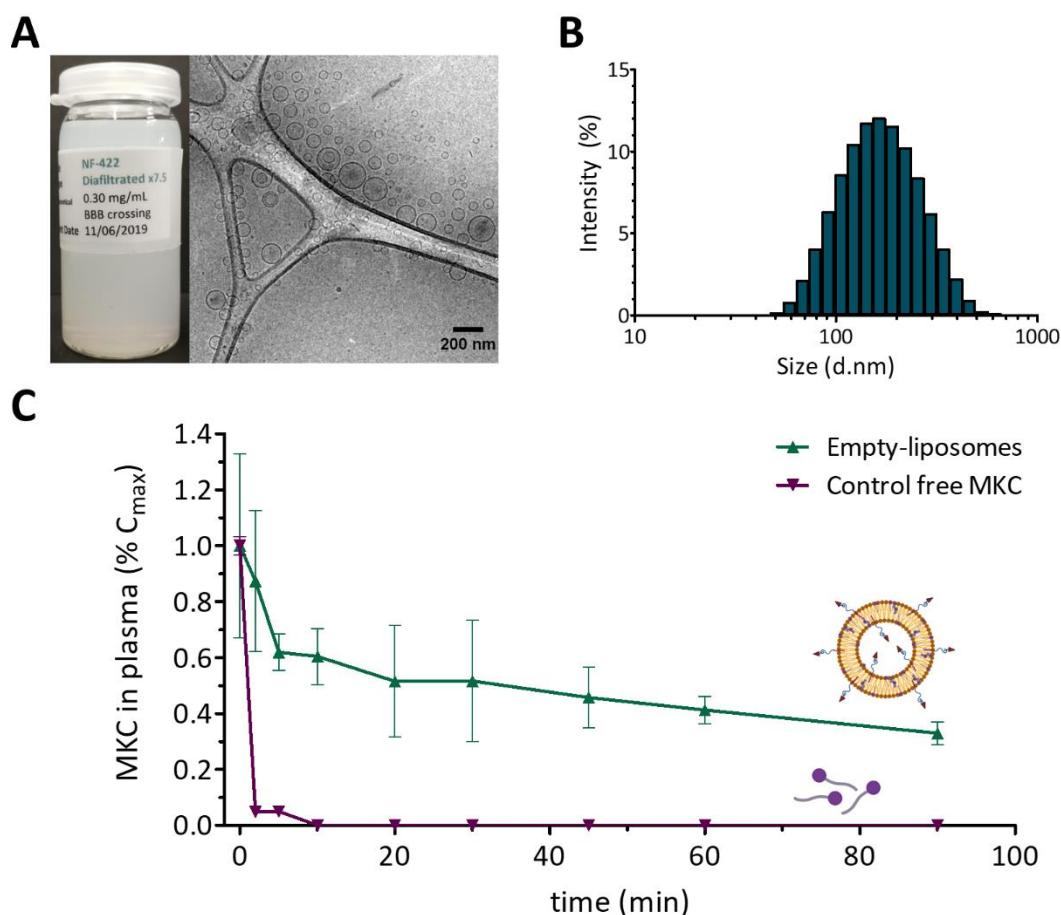


**Figure 6.4.** (A) Macroscopic appearance and microscopic morphology by cryoTEM; (B) Size distribution of concentrated empty-liposomes system in water, measure by DLS; (C) Concentration of MKC vs time in plasma, determined by LC-MS after IV dosing rats with empty-liposomes or free MKC, performed by Dr. T. Birngruber group from Joanneum Research (Austria) (see **Chapter 9.14** and **Chapter 9.15.1**)

This increased plasma half-life for empty-liposomes confirms the suitability of the strategy of tracking MKC as representation of the whole liposomal vehicle, as well as shows the extended blood circulation time of the unloaded RGD-functionalized liposomes when administered in rats.

## 6.3. Selection of the final nanoGLA candidate for entering in the preclinical evaluation

### 6.3.1. Substitution of GLAcmycHis protein for a new tag-free rh-GLA

During the optimization of the nanoGLA deeply developed in the previous **Chapter 5**, a GLAcmycHis protein consisting of a GLA with two tags (–His and –myc) and produced by Dr. J. L. Corchero from IBB-UAB (Barcelona) was used as GLA protein model (see **Chapter 9.6.2.1**). Although this GLAcmycHis was produced by a stable production method, unlike the initial GLA-His,<sup>11</sup> and it

supposed a major advance, GLAcmycHis protein owned some limitations: (i) a lack of free-of-operate status (FTO), related to intellectual properties (ID), and (ii) the presence of tags, whose avoidance is recommended since, in general, tagged proteins are found to be highly immunogenic.<sup>12</sup>

Therefore, a final change in the used GLA protein for its conjugation to the nanoliposomes was performed. A new recombinant human GLA, hereafter named rh-GLA, was produced by LeanBio SL (Barcelona) to bring this novel nanoGLA formulation towards the preclinical phases. The rh-GLA was produced by a stable expression production method in CHO cells, with free-of-operate status (i.e., without ID limitations for further exploitation issues), and tag-free (i.e., without any tags). A single large batch of the novel rh-GLA was produced and used for the experiments presented in this Chapter, showing high level of quality: high purity (~ 90 % by RP-HPLC), good stability (up to 7 months, stored at -80 °C), and low level of high molecular weight variants and stable over time (further detailed characterization can be found in **Chapter 9.6.2.2**).

Therefore, next sections are related to the production and characterization of final nanoGLA candidates containing the new tag-free rh-GLA, the selection of the definitive nanoGLA prototype to continue with the next drug development stages, and the in vivo preclinical evaluation.

### 6.3.2. Evaluation of two nanoGLA candidates containing different RGD densities: nanoGLA<sub>3%RGD</sub> and nanoGLA<sub>6%RGD</sub>

At that step, two nanoGLA candidates were produced substituting the GLAcmycHis version by the final rh-GLA (tag-free and with a free-to-operate status).

The two nanoGLA candidates' composition differed in the % mol of ch-PEG<sub>400</sub>-RGD content regarding the rest of mol of lipid membrane components, obtaining nanoGLA with the 3% mol (nanoGLA<sub>3%RGD</sub>) or with the 6% mol (nanoGLA<sub>6%RGD</sub>). It was decided to evaluate whether small modifications of the targeting peptide density in the nanoliposome surface could have a significant impact on the in vivo performance. The PEG content is well known to present a key role in circulation time, biodistribution, and cell uptake, and several times it is difficult to properly correlate the results found in vitro and in vivo.

For that, the two nanoGLA candidates were evaluated to select the best ch-PEG<sub>400</sub>-RGD density in the nanovesicles, according to the in vivo performance impact.

#### 6.3.2.1. Production of nanoGLA<sub>3%RGD</sub> and nanoGLA<sub>6%RGD</sub> by DELOS-susp and TFF

Each nanoGLA formulation was prepared by DELOS-susp in the intermediate lab-scale equipment, able to produce 150 – 900 mL of formulation, at 30 µg mL<sup>-1</sup> of rh-GLA, obtaining 225 mL batch size. Then, each intermediate nanoGLA sample was submitted to a TFF process: a first 7-fold concentration step to reach higher GLA concentrations (> 0.2 mg mL<sup>-1</sup>), followed by a diafiltration step in glucose 5 % (w/v) to exchange the media to an isotonic one, remove non-incorporated molecules (free-GLA, free components, etc.), as well as remove the remained organic solvent from the sample, obtaining the final



nanoGLA<sub>3%RGD</sub> and the final nanoGLA<sub>6%RGD</sub>. Two additional controls were also produced, diafiltrating the intermediate nanoGLA in water ( $D_{\text{water}}$ ) or in glucose 5% ( $D_{\text{glc}}$ ), without the concentration step. **Figure 6.5** provides a schematized overview of the different steps of the manufacturing process of the two nanoGLA systems and their versions.

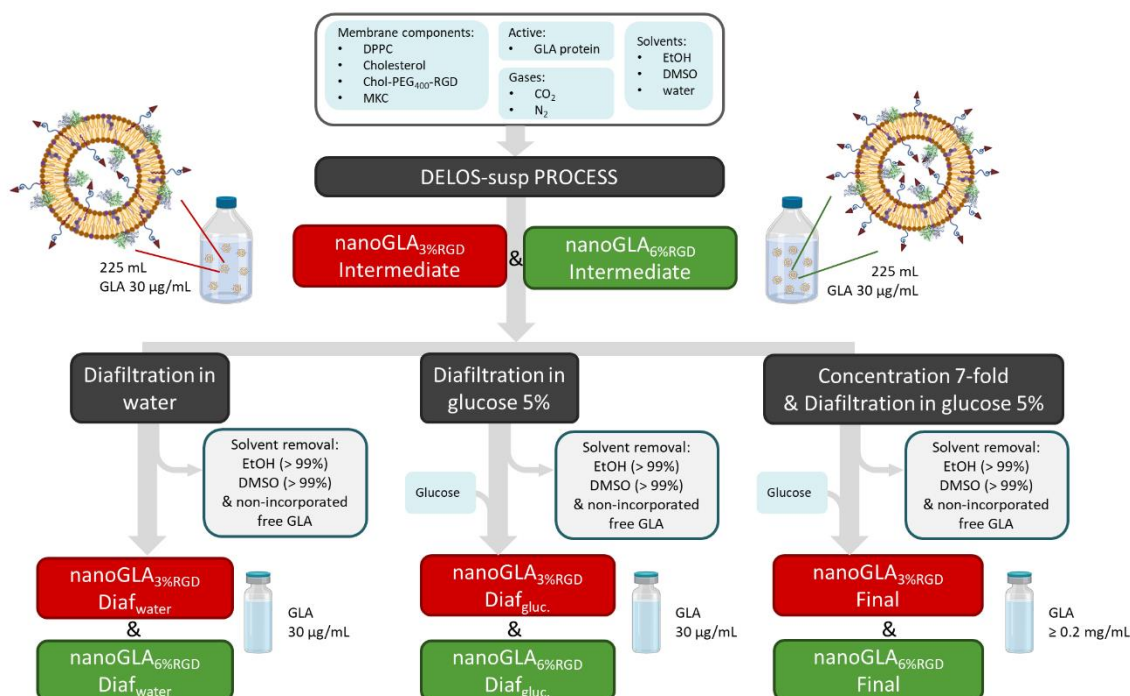


**Figure 6.5.** Process flow diagram to produce nanoGLA<sub>3%RGD</sub> and nanoGLA<sub>6%RGD</sub> including the intermediate products, two controls (diafiltrated in water and diafiltrated in glucose medium), and the final (concentrated x7 & diafiltrated in glucose medium) for each sample. Raw materials and the materials leaving the process are also represented.

### 6.3.2.2. Physicochemical and in vitro biological characterization of nanoGLA<sub>3%RGD</sub> and nanoGLA<sub>6%RGD</sub>

The relevant physicochemical and biological properties that are critical to product quality were characterized for the intermediate and the final nanoGLA products, as well as for the diafiltrated controls.

First, results showed that both final nanoformulations kept optimal physicochemical properties with the critical quality attributes (CQA) within the specifications established in **Chapter 5**: mean vesicle size < 300 nm, PDI ≤ 0.45, ζ-pot > + 20 mV (**Table 6.3**). Interestingly, the substitution of the enzyme version from GLAcmycHis to the novel tag-free rh-GLA resulted in even better physicochemical characteristics, as illustrated by a lower PDI and a better visual appearance than in the previous experiments with GLAcmycHis.

Moreover, samples after submitting to media exchange by TFF which contained glucose, showed an osmolality within the isosmotic range (260 – 300 mOsm kg<sup>-1</sup>), meeting as well with the requirement to be isosmotic with body fluids. High entrapment efficiencies were obtained again, similar to those found in the previous **Chapter 5** with GLAcmycHis, confirming the suitability of glucose 5 % as an isosmotic medium for the nanoGLA formulation, independently of the nature of the GLA model.

**Table 6.3.** Physicochemical characteristics of nanoGLA<sub>3%</sub> RGD and nanoGLA<sub>6%</sub> RGD, containing the novel tag-free rh-GLA, including the intermediate and the final products, and the controls in water and glucose, at time one day after production.

Prototype	Size <sup>†</sup>	PDI <sup>†</sup>	ζ-pot <sup>†</sup>	GLA <sup>†</sup>	EE% <sup>§</sup>	Osm <sup>  </sup>	
	(nm) (± SD)	(± SD)	(mV) (± SD)	(μg mL <sup>-1</sup> ) (± SD)	(%) (± SD)	(mOsm kg <sup>-1</sup> ) (± SD)	
NanoGLA <sub>3% RGD</sub>	Intermediate	128 ± 3	0.14 ± 0.02	47 ± 1	20 ± 1	–	–
	Diaf. water	123 ± 2	0.17 ± 0.02	45 ± 2	20 ± 1	96 ± 7	–
	Diaf. glucose	112 ± 1	0.15 ± 0.01	50 ± 2	21 ± 1	105 ± 9	277 ± 5
	Final	125 ± 2	0.15 ± 0.01	49 ± 1	167 ± 6	117 ± 9	291 ± 5
NanoGLA <sub>6% RGD</sub>	Intermediate	152 ± 2	0.16 ± 0.02	43 ± 1	23 ± 2	–	–
	Diaf. water	140 ± 1	0.16 ± 0.02	47 ± 1	24 ± 1	116 ± 9	–
	Diaf. glucose	126 ± 1	0.15 ± 0.01	48 ± 1	22 ± 1	109 ± 7	283 ± 5
	Final	138 ± 1	0.12 ± 0.03	48 ± 1	168 ± 6	118 ± 8	292 ± 5

† Measured by DLS and ELS (see **Chapter 9.5.1**); ‡ Measured by SDS-PAGE plus TGX by Dr. J. L. Corchero from IBB-UAB (Barcelona) (see **Chapter 9.6.3.1**); § Enzyme entrapment efficiency (EE%); || Measured by freezing-point (see **Chapter 9.5.3**).

Furthermore, both final nanoGLA prototypes showed nanovesicles with spherical morphology and mostly unilamellar, as shown by cryoTEM images acquired in collaboration with Prof. D. Danino from Technion (Israel) (**Figure 6.6**). Interestingly, GLA was clearly visible interacting with the vesicles (arrows). These structures can be distinguished inside and between the liposomal bilayers in accordance with previous cryoTEM images, in which similar findings were observed for liposomes with high GLA loading.

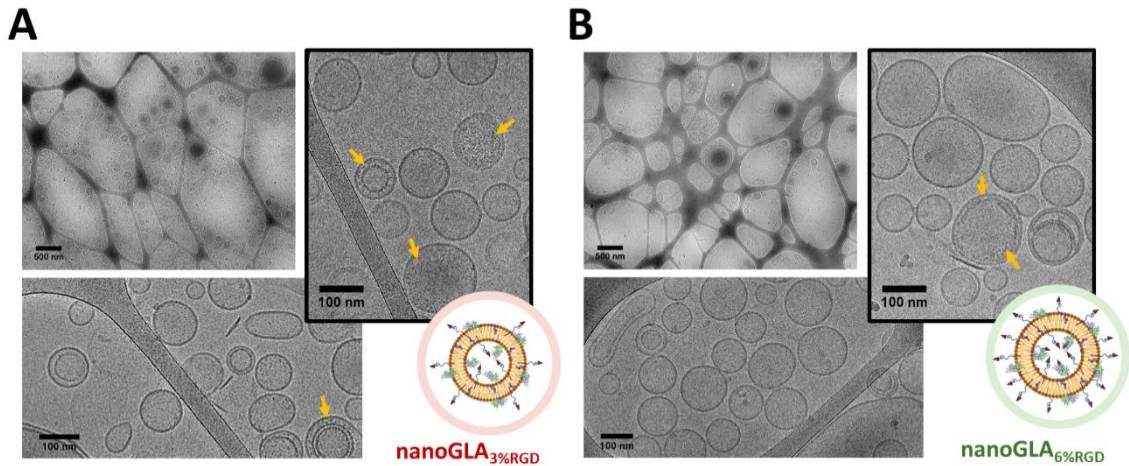


**Figure 6.6.** Morphology by cryoTEM of final (A) nanoGLA<sub>3%RGD</sub> and (B) nanoGLA<sub>6%RGD</sub>. Images acquired by Prof. D. Danino team from Technion (Israel).

Moving on biological behavior, specific enzymatic activity was determined in collaboration with Dr. I. Abasolo from VHIR (Barcelona). Although any of the samples showed an enzymatic activity superior to Replagal<sup>®</sup>, all the samples showed high GLA bioactivity, slightly lower for concentrated prototypes (**Figure 6.7**). Besides, similar behavior between nanoGLA<sub>3%RGD</sub> and nanoGLA<sub>6%RGD</sub> was observed, without appreciable impact of RGD density on GLA activity. Comparing rh-GLA-loaded liposomes with the previous GLAcmycHis-loaded ones, formulations with the new rh-GLA tend to show a slightly minor enzymatic activity, although in all the cases were above the 50 % of the specific enzymatic activity of Replagal<sup>®</sup>.

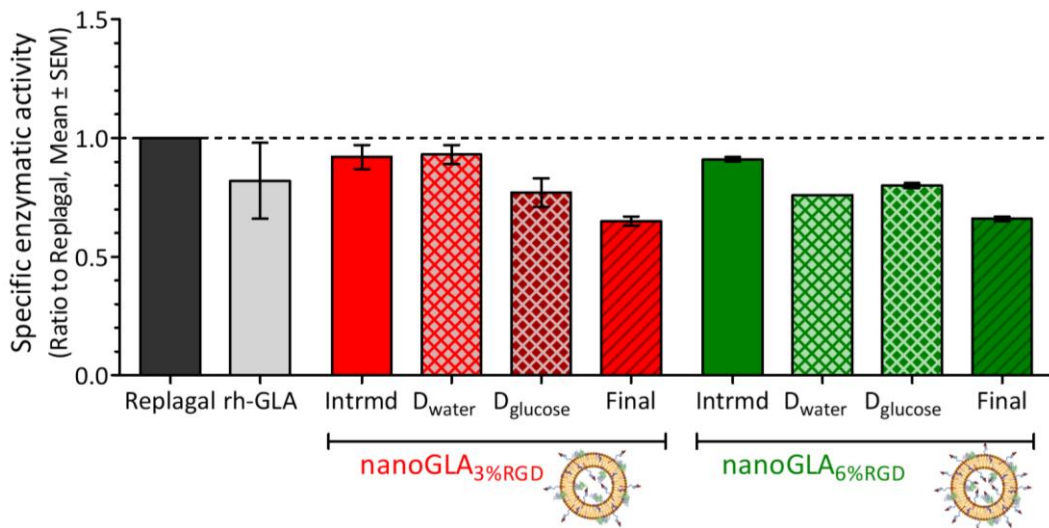


**Figure 6.7.** In vitro specific enzymatic activities in relation to the control (commercial Replagal<sup>®</sup> was normalized to 1) of free rh-GLA and final nanoGLA<sub>3%RGD</sub> and nanoGLA<sub>6%RGD</sub>, including the final concentrated form (Final), the intermediate after DELOS-susp (Intrmd), and two controls after diafiltration in water (D<sub>water</sub>) or in glucose 5 % (D<sub>glucose</sub>). Assay performed by Dr. I. Abasolo team from VHIR (Barcelona), < 1 week after production.

Besides, at least two months of colloidal stability were guaranteed (**Figure 6.8A and B**), indicating that the product development is mature enough to carry out longer studies, e.g., repeated efficacy studies and or 28-days GLP-toxicology studies, since the drug product stability allows covering the time period required for these studies. Regarding enzymatic activity, GLA in final nanoGLA liposomes retained its bioactivity for at least two months.

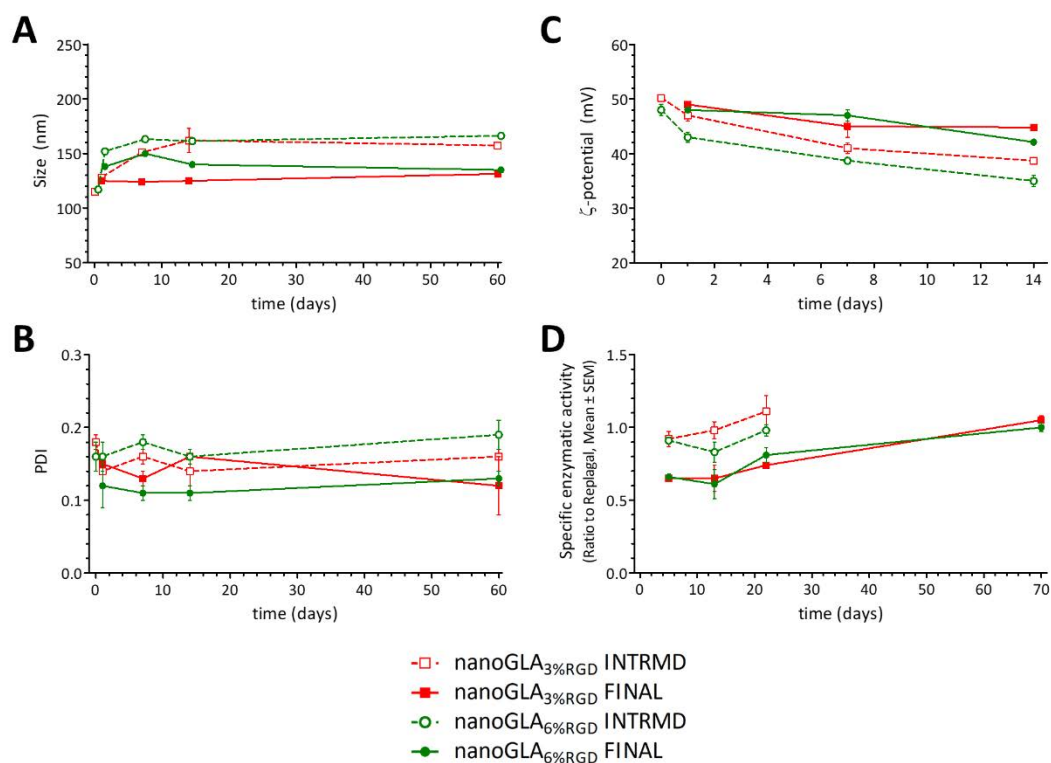


**Figure 6.8.** Evolution of intermediate (after DELOS-susp, dotted line, empty symbols) and final nanoGLA (after 7-fold concentration and diafiltration in glucose, solid line, solid symbols) after storage at 2 – 8 °C in terms of: (A) size and (B) PDI during 2 months, (C)  $\zeta$ -potential during 2 weeks, average mean  $\pm$  SD of three consecutive measurements per each time-point and sample; and (D) specific enzymatic activity (in relation to Replagal®, normalized to 1) during 2 months, measured by Dr. I. Abasolo team from VHIR (Barcelona).

### 6.3.2.3. In vitro safety of final nanoGLA<sub>3%RGD</sub> and nanoGLA<sub>6%RGD</sub>

Then, some safety in vitro assays were performed with the final nanoGLA<sub>3%RGD</sub> and nanoGLA<sub>6%RGD</sub>, in collaboration with Dr. I. Abasolo team from VHIR (Barcelona).

First, the impact of 3%-RGD and 6%-RGD nanoGLA samples on cell viability was assessed in two different cell lines, HeLa and HMEC-1 cells (**see Chapter 9.9.1**). As explained in previous sections, HeLa cell line is a well-established immortal cell line derived from cervical cancer human cells, typically and extensively used in cell culture laboratories, that is widely used as standard, and it is very useful for comparison purposes. On the other hand, HMEC-1 cell line is an immortalized human microvascular

endothelial cell line, with a high expression level of integrin  $\alpha_v\beta_3$  necessary for RGD targeting, and useful as in vitro endothelial cell model.<sup>13</sup>

Compared to the other viability assays presented in this Thesis, this assay was performed with final nanoGLA prototypes, thus after TFF 7-fold concentration and diafiltration in glucose 5 %. For this reason, it was possible to test lipid concentrations up to  $8.4 \text{ mg mL}^{-1}$  (the liposome concentration of the stock samples). The minimum tested concentration in this assay was  $0.07 \text{ mg mL}^{-1}$  of liposomes and corresponded to the maximum tested concentration in previous viability assays with non-concentrated samples, e.g., cell viabilities of Replagal<sup>®</sup>-loaded liposomes presented in **Chapter 3**.

Results showed a decrease on cell viability as lipid concentration was increased, with similar behavior for both systems, especially in HMEC-1 cells (**Figure 6.9**). NanoGLAs provoked a slightly higher cytotoxicity in HMEC-1 than in HeLa cell line, especially at lower lipid concentrations. In HeLa cell line, nanoGLA<sub>3%RGD</sub> showed a slightly higher cell viability than nanoGLA<sub>6%RGD</sub>, although this difference in general was not considered statistically significant. Therefore, in general, no relevant difference between the two nanoGLA samples, that contained different RGD densities (3 mol % and 6 mol % of chol-PEG<sub>400</sub>-RGD compared to the total mol of membrane components) was observed, suggesting the absence of correlation between RGD concentration and cell viability.

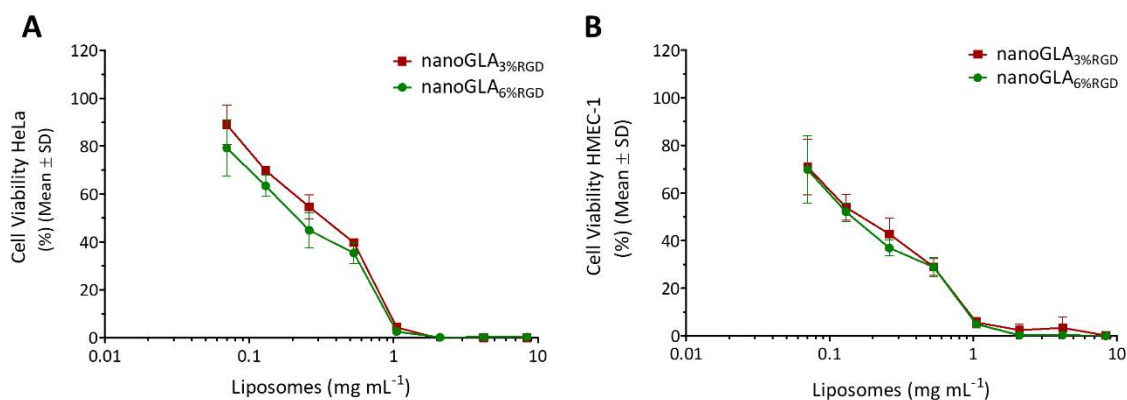


**Figure 6.9.** Cell viability by MTT assay in (A) HeLa cells, and in (B) HMEC-1 cells, treated during 72 h at 37 °C with up to  $8.4 \text{ mg mL}^{-1}$  of lipids. Values correspond to a single representative batch per each system. Assay performed by Dr. I. Abasolo team from VHIR (Barcelona).

Further, to ensure the safety of administering intravenously these nanoformulations, their hemocompatibility was also studied, through well-established assays already utilized during this Thesis (detailed in **Chapter 9.9.2**). First, the impact of final formulations in red blood cell fragility was studied by using hemolysis tests in human blood samples. Any of the two tested nanoGLA samples induced

significant hemolysis and values never surpassed 5 % of total hemolysis (**Figure 6.10**) to be considered hemolytic.

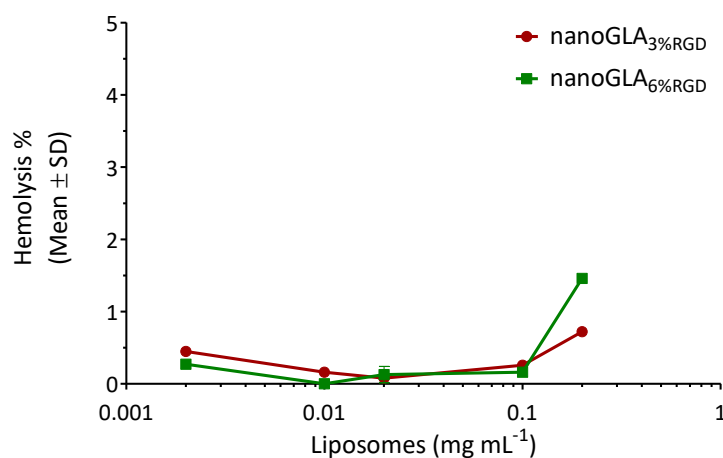


**Figure 6.10.** Hemolysis of human red blood cells incubated with nanoGLA formulations (1 h at 37 °C), at time 20 days after production. Assay corresponds to a single representative batch per each system, tested in duplicate. Assay performed by Dr. I. Abasolo team from VHIR (Barcelona). \*Nota: VHIR confirmar eix X

Later, in vitro plasma coagulation times after incubation of human plasma with nanoGLA samples were measured (**Chapter 9.9.2.2**). No significant variations in plasma coagulation times were detected after incubation with nanoGLA samples (**Table 6.4**), at a concentration of 0.1 mg mL<sup>-1</sup> of liposomes. Overall, both nanoGLA showed to be safe for intravenous administration since no hemolysis signs or alteration in plasma coagulation times were found.

**Table 6.4.** Plasma coagulation times measured as prothrombin time (PT), activated partial prothrombin time (APTT) and thrombin time (TT) after incubation with nanoGLA<sub>3%RGD</sub> and nanoGLA<sub>6%RGD</sub><sup>†</sup>.

Sample	PT (s) (± SD)	APTT (s) (± SD)	TT (s) (± SD)
Normal coagulation time range	≤ 13.4	≤ 34.1	≤ 21
Pathological coagulation time range	≥ 20	≥ 61	≥ 42
Control plasma	11.95 ± 0.07	35.70 ± 0.00	19.05 ± 0.07
Vehicle (PBS)	12.15 ± 0.21	35.3 ± 0.57	19.15 ± 0.07
nanoGLA <sub>3%RGD</sub>	11.55 ± 0.07	35.15 ± 0.07	19.20 ± 0.14
nanoGLA <sub>6%RGD</sub>	11.45 ± 0.07	35.0 ± 0.42	19.45 ± 0.07

<sup>†</sup> Incubation of human plasma with 0.1 mg mL<sup>-1</sup> liposomes (30 min, 37 °C) at time 20 days after production, tested in duplicate; Non-treated plasma (control plasma) and PBS were used as controls. Assay performed by Dr. I. Abasolo team from VHIR (Barcelona).

### 6.3.3. In vivo studies in a Fabry mouse model

The in vivo behavior of both nanoGLA (nanoGLA<sub>3%-RGD</sub> or nanoGLA<sub>6%-RGD</sub>, containing 3 mol % or 6 mol % of RGD, respectively) nanoformulations was assessed in Fabry mice and in collaboration with Dr. I. Abasolo's group from VHIR (Barcelona). Fabry mice (Gla<sup>tm1Kul</sup>) are characterized by the lack of endogenous GLA enzyme (KO for GLA) and, thus, by an increased level of Gb3 deposits. They allow to conduct efficacy studies by measuring the decrease of Gb3 levels, that can be directly correlated to the efficacy of exogenous administered GLA, since no endogenous GLA is present in these GLA-KO mice.

The objective of this study was to assess (i) the content of GLA in plasma and tissues analyzing the enzymatic activity at 1- and 30-min post-administration, and (ii) the efficacy in terms of reduction of Gb3 deposits one week after a single intravenous administration. Fabry mice were administered with both nanoGLAs or free rh-GLA. These results were compared to those obtained with the commercial GLA (agalsidase alfa, Replagal<sup>®</sup>) and non-treated animals (wild-type and KO mice). Thus, the design included: two non-treated control groups, i.e., WT mice (with endogenous GLA), and KO mice (without endogenous GLA), and four treated groups, i.e., KO mice administered with nanoGLA<sub>3%-RGD</sub>, nanoGLA<sub>6%-RGD</sub>, free GLA (rh-GLA), or Replagal<sup>®</sup> (currently approved for ERT).

The experimental design is schematized in **Figure 6.11** and detailed in **Chapter 9.10.1**. The four treated groups received GLA at 1 mg kg<sup>-1</sup> dose; nanoGLA dose was also based on GLA concentration, previously presented in **Table 6.3**, also at 1 mg kg<sup>-1</sup>. After one week, and before the euthanasia, mice received a second dose (same dosing, 1 mg kg<sup>-1</sup>). This second dose, allowed obtaining GLA activity in plasma at two time points, just after the second dose administration (1 min), and after 30 min. Then, animals were euthanized at 1 min or 30 min post-administration of the second dose (4 mice/group at each time point) and their organs (blood, kidneys, liver, spleen, heart, lungs, and brain) were collected.

Quantification of the Gb3 and lysoGb3 deposits in the different tissues by LC-MS/MS allowed the study of the efficacy of the GLA-containing formulations (**Chapter 9.15.4**). Besides, the analysis of the enzymatic activity in plasma and tissues allowed an estimation of the enzyme biodistribution 30 min post-administration.

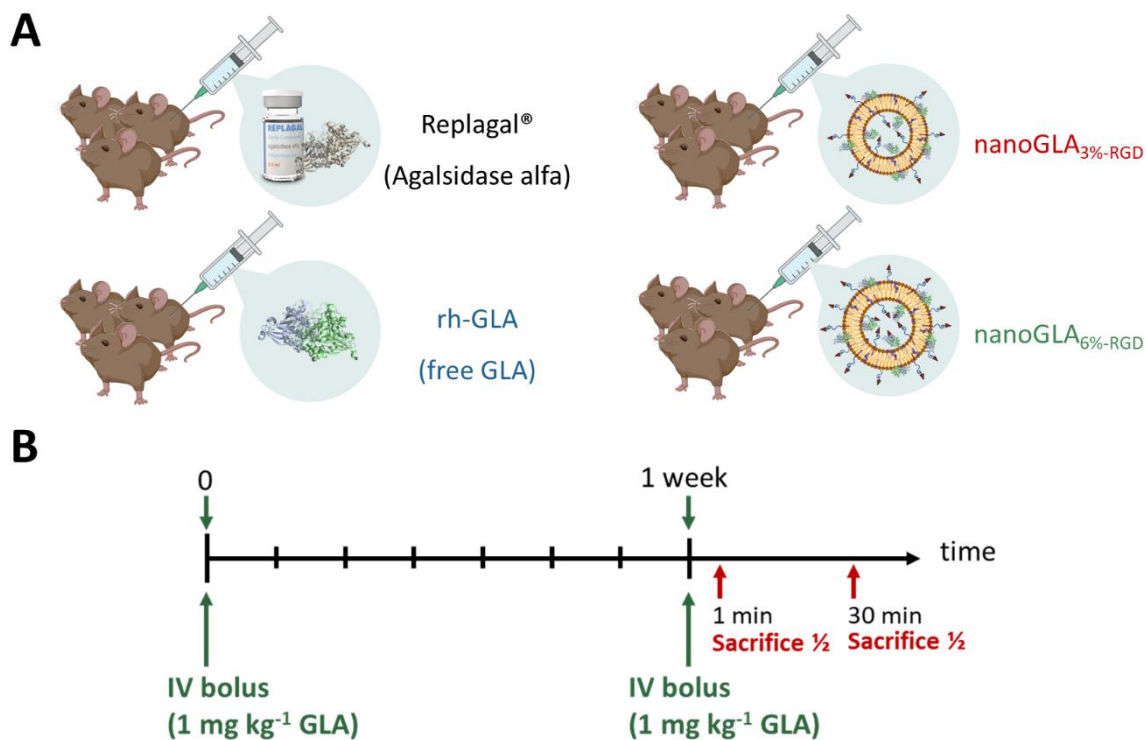


**Figure 6.11.** Scheme of the in vivo studies performed in a Fabry mouse model, including a single-dose efficacy study and the enzymatic activity assessment in plasma and tissues ( $n = 8$  mice/group). (A) Mice were IV (bolus) administered with nanoGLA<sub>3%RGD</sub>, nanoGLA<sub>6%RGD</sub>, free rh-GLA, or Replagal®, at  $1 \text{ mg kg}^{-1}$  dose of GLA. (B) Scheme of dosing and study design. Animals were sacrificed one-week post administration. Previously, mice were administered with a second dose in each group and then euthanized 1 or 30 min later (4 animals per group and time point) to determine the percentage of enzymatic activity in plasma and tissues. Assay performed by Dr. I. Abasolo's team from VHIR (Barcelona).

### 6.3.3.1. Biodistribution by enzymatic activity in plasma and tissues

First, results of GLA enzymatic activity in plasma and tissues allowed an estimation of the enzyme biodistribution 30 min post-administration. In this assay, it must be noted that a correlation between the GLA concentration and the preservation of its enzymatic activity after reaching the different organs was assumed, since GLA itself was not followed, but only its enzymatic activity. For this reason, enzymatic activity values at 30 min were presented as % of the injected dose (% ID), referred to the enzymatic activity at 1 min.

In plasma, nanoGLA systems (both nanoGLA<sub>3%RGD</sub> and nanoGLA<sub>6%RGD</sub>) increased the enzymatic activity levels over the free enzymes (rh-GLA or Replagal®) (**Figure 6.12**). In detail, plasma retained the ~ 18 % of the injected dose (% ID) of nanoGLAs after 30 min, referred to the enzymatic activity at 1 min, whereas free enzymes only maintained the ~ 3 % ID. Thus, the percentage of % ID at 30 min is higher when GLA is nanoformulated, indicating that the liposomal vehicle protects GLA and extends the GLA's activity in bloodstream.



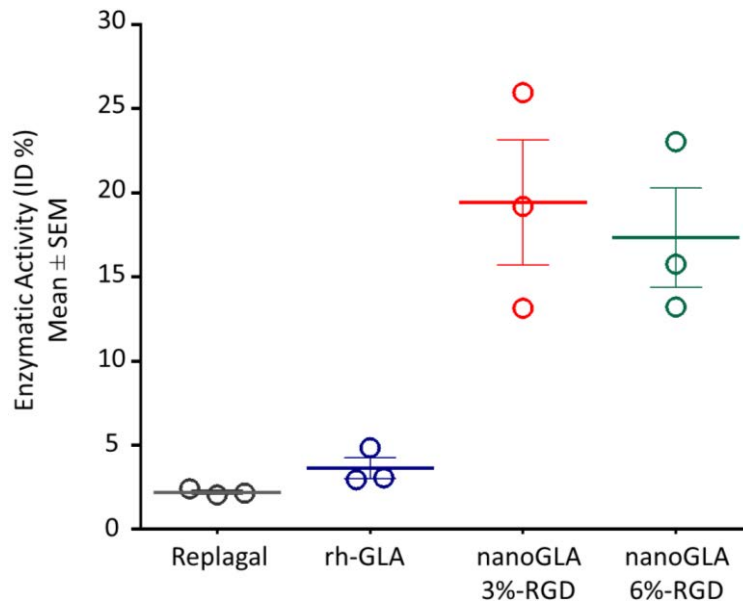


**Figure 6.12.** Enzymatic activity levels in plasma of nanoGLA<sub>3%-RGD</sub>, nanoGLA<sub>6%-RGD</sub>, rh-GLA, and Replagal<sup>®</sup>, 30 min post-administration and referred to activity at 1 min, to calculate the percentage of injected dose (% ID). Assay performed by Dr. I. Abasolo team from VHIR (Barcelona).

Next, the same enzymatic activity analysis was done in tissues. The biodistribution of enzymatic activity indicated that liver and spleen were the organs that received more enzyme activity, followed by distance with lungs and kidney. Heart received relative low quantities of enzyme activity (**Figure 6.13A**).

Nanoformulated GLA, as well as free enzymes, were mainly retained by liver (~ 40 – 80 % ID) and spleen (1.5 – 13 % ID). The enzymatic activity retention was higher for rh-GLA and both nanoGLA compared to Replagal<sup>®</sup> in liver and spleen. In addition, nanoformulated versions had a higher accumulation in spleen and lung, compared to free GLA.

In kidney and heart, nanoGLA reached these two of the target organs for ERT in a higher extent than the commercially available enzyme (Replagal<sup>®</sup>). No significant differences were observed between rh-GLA and nanoformulated GLA in terms of enzymatic activity in these two organs (**Figure 6.13B**).

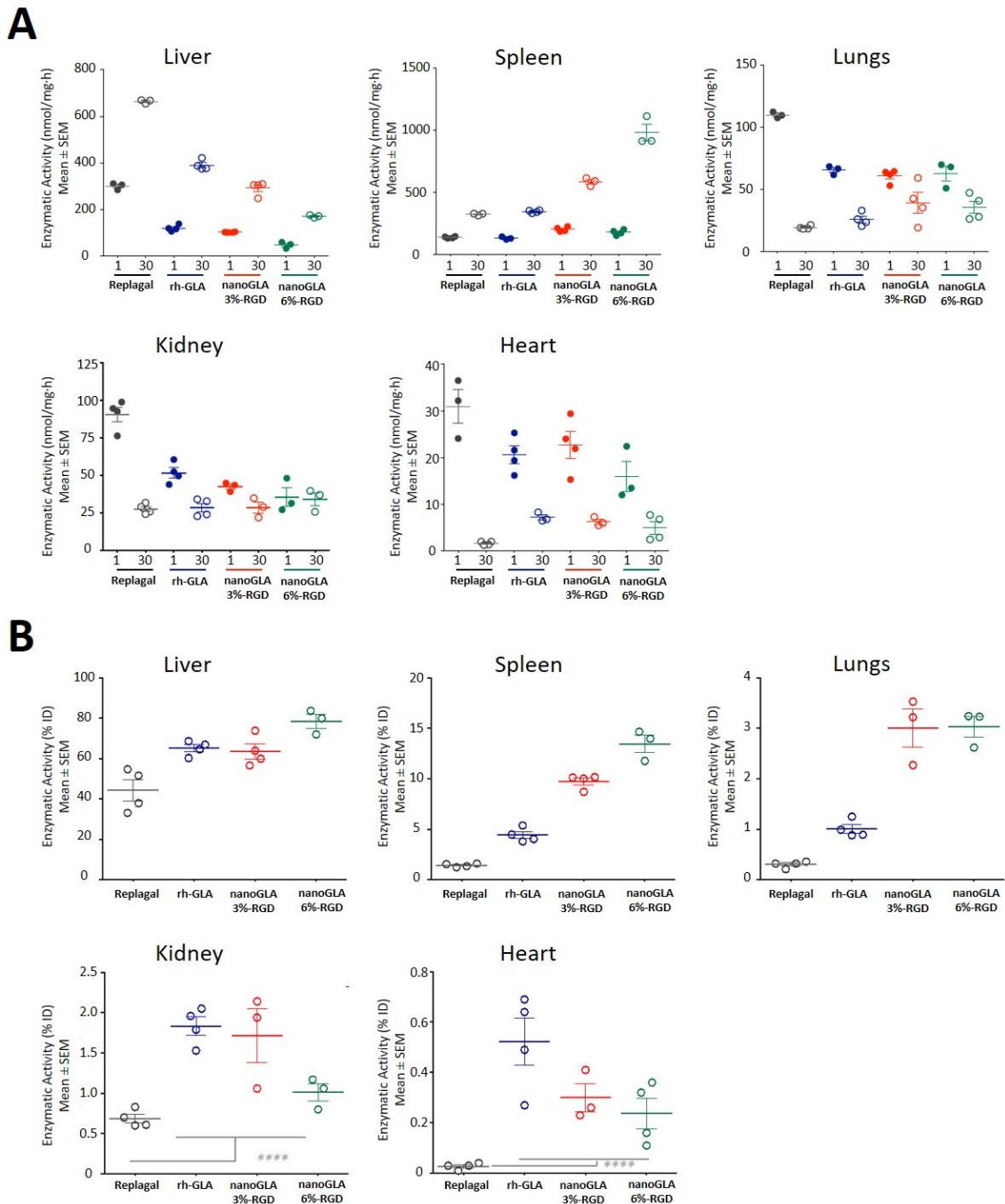


**Figure 6.13.** Enzymatic activity of nanoGLA<sub>3%-RGD</sub>, nanoGLA<sub>6%-RGD</sub>, free rh-GLA, and Replagal® in tissues, at (A) 1 min and 30 min, as absolute enzymatic activity, and at (B) 30 min post-administration referred to activity at 1 min (% ID). Assay performed by Dr. I. Abasolo's team from VHIR (Barcelona).

### 6.3.3.2. Single-dose efficacy

The Fabry KO mice model is the most widespread animal model for Fabry Disease and has a complete absence of the GLA gene.<sup>14</sup> These GLA-deficient mice exhibit typical lipid inclusions with concentric lamellar structures in the lysosomes and progressive accumulation of Gb3 in target tissues, e.g., kidneys,

following a similar pattern as in the human Fabry patients. Indeed, in Fabry patients, Gb3 accumulation in kidney can start very early in age and gradually increase, with direct correlation with early kidney damage and albuminuria,<sup>15</sup> although the Gb3 accumulation in renal cells is previous to the clinical manifestations (i.e., proteinuria), meaning that the cellular damage takes place before tissue damage becomes clinically evident.<sup>16</sup> This first Gb3 accumulation and later development of clinical symptoms seems to follow the same trend also in other organs, e.g., the heart.<sup>17</sup> In preclinical and clinical samples, Gb3 accumulation can be visualized and quantified using immunohistochemistry, thin layer chromatography, electronic microscopy, and mass spectroscopy (MS), being the last one the most quantitative and sensitive one.

Thus, as explained before, a single bolus of nanoGLAs (nanoGLA<sub>3%</sub>-RGD or nanoGLA<sub>6%</sub>-RGD), free rh-GLA, or commercial Replagal<sup>®</sup> were intravenously administered. All groups were administered at 1 mg kg<sup>-1</sup> of GLA to ease the comparison between among groups. This dosage was decided after literature reviewing of previous preclinical studies testing either a single dose or a dose-range of GLA in Gb3 clearance efficacy assays.<sup>18-22</sup> In all of them the doses of GLA in the range of 1 to 3 mg kg<sup>-1</sup> demonstrated to be efficacious after a single or a repeated administration.

One week after the administration, mice were euthanized and Gb3 levels in the different organs (liver, spleen, kidney, heart, lungs, and brain) were determined by Liquid Chromatography-Mass Spectrometry (LC-MS/MS) (see **Chapter 9.15.4**). Results of efficacy were based on the capability of the administered GLA of reducing the Gb3 deposits in Fabry mice. Results were expressed as % Gb3 levels. For calculation of the relative Gb3 loss, it was assumed that the difference in Gb3 levels between non-treated KO mice and WT counterparts corresponds to a 100% of Gb3 loss in WT. Then, the Gb3 levels in different treatment groups were referred to this total Gb3 loss in WT, meaning that those treatments with a higher percentage of Gb3 loss are the ones with a higher efficacy.

First, Gb3 levels varied significantly among tissues of non-treated Fabry mice (GLA-KO). The most affected tissues by the Gb3 accumulation were kidneys, spleen, and heart. **Table 6.5** gives an idea of the distinctive Gb3 levels in the collected organs: Gb3 levels in non-treated Fabry mice were high in kidney (~ 23,000 pmol mg<sup>-1</sup>) and spleen (~ 6,800 pmol mg<sup>-1</sup>), followed by lung (~ 2,500 pmol mg<sup>-1</sup>), heart (~ 700 pmol mg<sup>-1</sup>), and liver (~ 100 pmol mg<sup>-1</sup>).

**Table 6.5.** Gb3 levels (pmol eq./mg prot.) in the collected organs of non-treated Fabry mice (KO), Fabry mice treated with nanoGLA<sub>3%-RGD</sub> or nanoGLA<sub>6%-RGD</sub>, and non-treated wild type mice (WT), 1 week after single dose administration (1 mg kg<sup>-1</sup> of GLA).

Group	Gb3 levels*					
	Liver	Spleen	Lung	Plasma	Kidney	Heart
<b>KO</b>	100 ± 30	6,800 ± 500	2,500 ± 100	270 ± 20	23,000 ± 1000	700 ± 200
<b>nanoGLA<sub>3%-RGD</sub></b>	10.0 ± 0.7	92 ± 1	620 ± 50	68 ± 9	8,300 ± 700	100 ± 20
<b>nanoGLA<sub>6%-RGD</sub></b>	6.5 ± 0.9	1,380 ± 80	540 ± 40	59 ± 3	9,300 ± 600	95 ± 5
<b>WT</b>	1.4 ± 0.1	100 ± 1	148 ± 7	12 ± 1	6,200 ± 500	28 ± 1

\* Measured by LC-HRMS (see **Chapter 9.15.4**), by Dr. I. Abasolo's group from VHIR (Barcelona); Gb3 levels of Fabry mice administered with Replagal<sup>®</sup> or rh-GLA were quantified but are not reported in this table.

Results of GLA treated mice showed that nanoformulated GLA induced a Gb3 loss in all the tested tissues, comparable or even higher than the observed with free enzymes (rh-GLA or Replagal<sup>®</sup>) (**Figure 6.14**). Although no significant differences were found in liver or plasma, nanoGLAs outperformed free enzymes in kidney, heart, lung, and spleen. Among both nanoformulated GLAs, similar results were obtained in some tissues, although slightly better efficacy results were obtained for nanoGLA<sub>3%-RGD</sub> than for nanoGLA<sub>6%-RGD</sub>, especially in spleen, kidney, and heart. Actually, in heart, nanoformulated GLAs behaved more effectively than the commercial free GLA (Replagal<sup>®</sup>) in reducing Gb3 levels. Since the efficacy of classical ERT in cardiac tissue has been limited, the higher efficacy of nanoGLA in cardiac tissue after a single dose is promising. Further, in kidney, nanoGLA<sub>3%-RGD</sub> showed better efficacy than free rh-GLA and nanoGLA<sub>6%-RGD</sub>, which could be related to the higher enzymatic activity delivery noted in the biodistribution results (as previously seen in **Figure 6.13**). Although differences between nanoGLA<sub>3%-RGD</sub> and Replagal<sup>®</sup> in kidney were not statistically significant, it is worth mentioning that these assays were conducted after a single dose administration and in a small subset of animals, as well as kidneys have much higher basal levels of Gb3 than heart or spleen, so it is reasonable to think that more time and/or dose will be required to see the benefit of nanoGLA<sub>3%-RGD</sub> over Replagal<sup>®</sup>. These differences can be clearer after a repeated-dose efficacy assays, in which more than one dose are administered to animals.

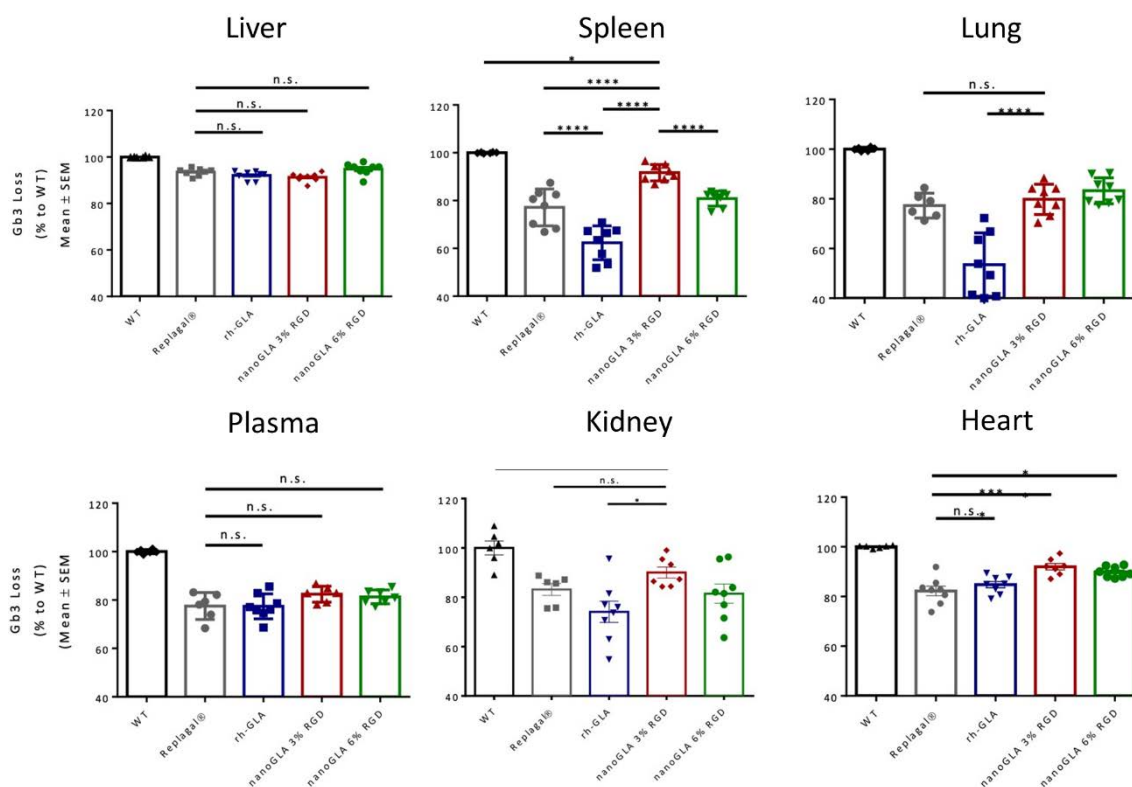


**Figure 6.14.** In vivo efficacy after single administration of  $1 \text{ mg kg}^{-1}$  of GLA, as Replagal®, free rh-GLA, nanoGLA<sub>3%-RGD</sub>, and nanoGLA<sub>6%-RGD</sub>, based on reduction of Gb3 levels in tissues, performed by Dr. I. Abasolo's group from VHIR (Barcelona). ANOVA test with multiple comparisons and t-test were performed to compare results (statistically significant when  $p \leq 0.05$ ).

Overall, for first time, it was possible to produce GLA-loaded liposomes (nanoGLA) meeting the established CQA specifications, including nanometric size, narrow vesicle size distribution, appropriate bioactivity, isosmolar, and with the required GLA concentration. Further, a new rh-GLA model protein was introduced in these experiments, consisting of a tag free GLA produced in CHO cell culture by stable production method, and with free-to-operate (FTO) status. The exchange of GLAcmycHis to rh-GLA as a protein model resulted in the improvement of the physicochemical characteristics. Besides, the potential of DELOS-susp technology combined with a tangential flow filtration (TFF) process as a flexible and robust preparation method to produce biological-nanovesicles conjugates involving few steps and with potential for easy scaling up was demonstrated. Two nanoGLA prototypes were produced, whose differences relied on the chol-PEG<sub>400</sub>-RGD density (3 mol % or 6 mol %, nanoGLA<sub>3%RGD</sub> or nanoGLA<sub>6%RGD</sub>, respectively), in enough quantities for carrying a preclinical in vivo single dose efficacy study in Fabry mice. Interestingly, the administration of an intravenous (bolus) single dose of the nanoGLA systems led to an enhanced reduction of Gb3 deposits in Fabry mice, when compared to free GLA, in tissues other than liver. Actually, nanoGLA showed superior efficacy results

than Replagal<sup>®</sup>, which is the current approved ERT treatment for Fabry disease, in several organs, including heart and spleen.

In conclusion, these promising results prompted us to continue with the preclinical development and testing of the nanoGLA, as explained in the following section. NanoGLA<sub>3%RGD</sub> was the selected prototype for further studies, since no important differences were observed in the in vivo single dose efficacy (actually, nanoGLA<sub>3%RGD</sub> showed a slightly better behavior in some organs, e.g., spleen and kidney). Therefore, further studies shown in this Chapter were performed with nanoGLA<sub>3%RGD</sub>, from here on named simplified named as “nanoGLA”.

#### 6.3.4. Implementation of HPLC quantification method for GLA quantification

Importantly, advancing towards further stages in the drug development process also requires a higher and robust control over the characteristics of the product, to ensure that the manufacturing process is well controlled. Therefore, the use of more accurate analytical techniques is strongly encouraged.

Until now, the amount of GLA present in the nanoGLA formulation has been determined by SDS-PAGE plus TGX. Although this technique is widely used and accepted for academic research proposes, SDS-PAGE plus TGX is a semi-quantitative technique and regulatory guidelines require the use of more precise and validate analytical techniques, such as chromatography methods. Therefore, a high-performance liquid chromatography (HPLC) method was implemented as the analytical method used for the determination of the GLA concentration in the nanoformulation, as an alternative to SDS-PAGE plus TGX method. This method was developed by LeanBio SL (Barcelona). For comparison and validation purposes, nanoGLA samples from the previous section were reanalyzed by the new HPLC method. **Table 6.6** summarizes the obtained results, and showed a good linearity between both techniques, since its ratio was very similar between all the quantified samples. Interestingly, SDS-PAGE plus TGX showed to slightly underestimate the GLA concentration in concentrated final samples, confirming the CQA requirement of GLA concentration ( $\geq 0.2 \text{ mg mL}^{-1}$ ).

**Table 6.6.** Comparison between GLA quantification methods, SDS-PAGE plus TGX and RP-HPLC.

Prototype		GLA by SDS-PAGE plus TGX <sup>†</sup> ( $\mu\text{g mL}^{-1}$ ) ( $\pm$ SD)	GLA by RP-HPLC <sup>‡</sup> ( $\mu\text{g mL}^{-1}$ ) ( $\pm$ SD)	Ratio RP-HPLC / SDS-PAGE plus TGX
NanoGLA 3% RGD	Intermediate	20 $\pm$ 1	27 $\pm$ 1	1.3
	Diaf. water	20 $\pm$ 1	30 $\pm$ 1	1.5
	Diaf. glucose	21 $\pm$ 1	31 $\pm$ 1	1.4
	Final	167 $\pm$ 6	216 $\pm$ 10	1.3
NanoGLA 6% RGD	Intermediate	23 $\pm$ 2	30 $\pm$ 1	1.3
	Diaf. water	24 $\pm$ 1	31 $\pm$ 1	1.3
	Diaf. glucose	22 $\pm$ 1	31 $\pm$ 1	1.4
	Final	168 $\pm$ 6	210 $\pm$ 8	1.3

<sup>†</sup> Assay performed by Dr. J. L. Corchero from IBB-UAB (Barcelona), as explained in **Chapter 9.6.3.1**;

<sup>‡</sup> Assay performed by Leanbio SL (Barcelona), as explained in **Chapter 9.6.3.3**.

## 6.4. Preparation of large nanoGLA batches with high quality level for non-regulatory and early GLP regulatory in vivo testing

The single-dose efficacy results, together with the extensively optimization of the physicochemical characteristics of the nanoGLA formulation, resulted in a drug delivery system with promising features as potential improved ERT for Fabry disease treatment. Therefore, next stages involved deeply preclinical testing regarding toxicology and efficacy at repeated dose, as well as an accurate characterization of the nanoGLA batches for ensuring the required quality.

Accordingly, two bigger nanoGLA productions were prepared, with the final objective of obtaining enough amount of nanoGLA to carry out in vivo studies which involve the use of high quantity of sample. Moreover, the same amount of empty-liposomes was also prepared, to evaluate the possible toxicity of the nanoliposomal vehicle by their self. Empty-liposomes were produced following the same process than for the preparation of the nanoGLA, with the only difference that rh-GLA was not added to the formulation.

The production of the required amount of nanoGLA and empty-liposomes supposed a big challenge, since until now, the maximum amount produced was around 300 mL DELOS-susp batch size and, although it already represented an increase over the initial production capacity of the system (around 25 mL),<sup>23</sup> it was still below the necessary quantities for carrying on more complex in vivo studies, where higher number of animals are involved.

Additionally, nanoGLA must accomplish with the required level of quality, meaning that a strong control on the manufacturing and characterization of their physicochemical features was necessary, to prepare an associate certificate of analysis for each batch confirming the meeting with the CQA specifications.

For sake of clarity, although the two independent productions (producing both nanoGLA and empty-liposomes in each run) were prepared separately in different time-lines, herein these are presented together. Later, after the introduction of the prepared systems, all the preclinical testing assays (non-regulatory and regulatory) are grouped and explained together.

#### 6.4.1. First large batch production of nanoGLA and empty-liposomes

The adopted strategy to produce high amounts of nanoGLA and empty-liposomes was to produce two identical batches (#1 and #2) of each system by DELOS-susp, followed by their mixing in a pool (obtaining a 1300 mL of each nanoformulation) before submitting them to the TFF process, consisting in a 7.5-fold concentration and a diafiltration in water with glucose 5 %. The process is schematized in **Figure 6.15**.

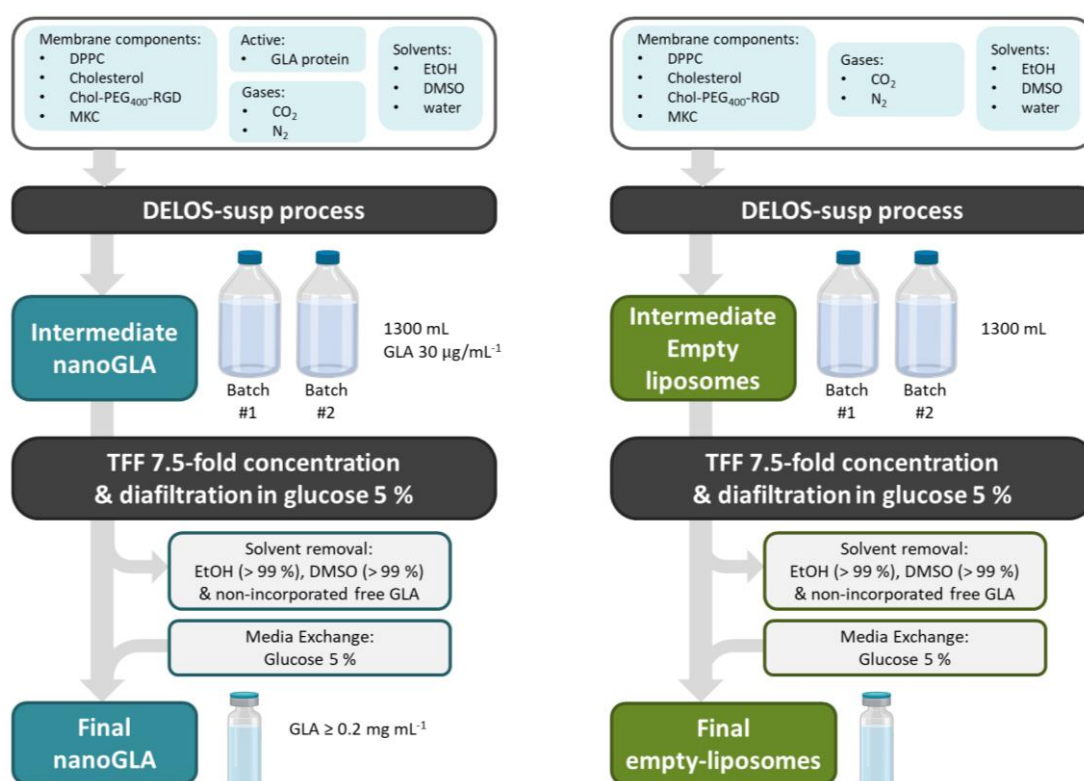


**Figure 6.15.** Process flow diagram to produce nanoGLA and empty-liposomes. Raw materials and the materials leaving the process are also represented.



### 6.4.1.1. Physicochemical characterization and biological activity

A good reproducibility between batches #1 and #2 was observed in terms of size, PDI, and  $\zeta$ -potential after DELOS-susp production (**Table 6.7**), both for nanoGLA and empty-liposomes. Intermediate nanoGLA samples showed a significant higher mean size ( $p = 0.027$ ,  $n = 2$ ) compared to intermediate empty liposomes samples, whereas PDI and  $\zeta$ -potential were similar. Both final nanoformulations (nanoGLA and empty-liposomes) showed very nice and narrow monomodal size distribution (**Figure 6.16**). Macroscopic appearance met specifications, being an opalescent dispersion without sedimentation, more whitish in the case of nanoGLA than the empty liposomes.

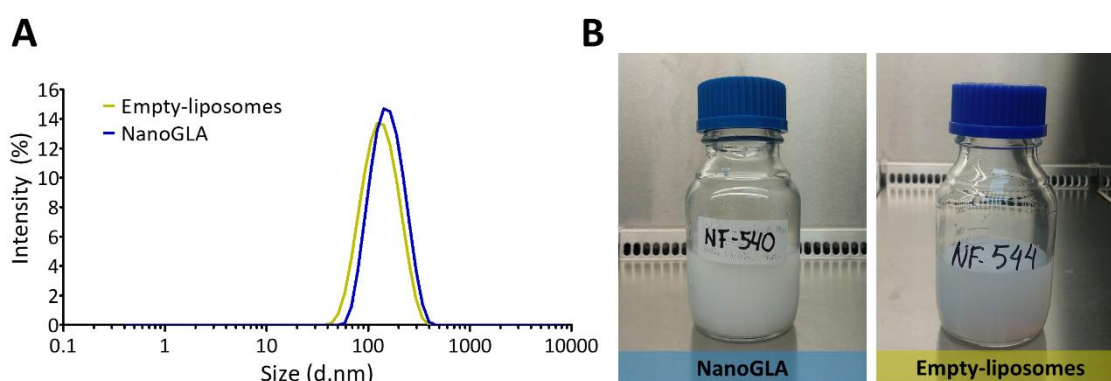


**Figure 6.16.** (A) Size distribution (by DLS, see **Chapter 9.5.1**) and (B) macroscopic appearance of final nanoGLA and empty liposomes.

**Table 6.7.** Physicochemical characteristics by DLS of intermediate and final samples of nanoGLA and empty-liposomes, at time one day after production.

Sample	Prototype	Size	PDI	$\zeta$ -pot
		(nm) ( $\pm$ SD)	( $\pm$ SD)	(mV) ( $\pm$ SD)
NanoGLA	Intermediate (batch #1)	133 $\pm$ 1	0.14 $\pm$ 0.01	44 $\pm$ 1
	Intermediate (batch #2)	134 $\pm$ 1	0.15 $\pm$ 0.01	42 $\pm$ 1
	Intermediate (pool #1 and #2)	140 $\pm$ 1	0.16 $\pm$ 0.01	43 $\pm$ 1
	Final nanoGLA	142 $\pm$ 2	0.13 $\pm$ 0.01	45 $\pm$ 1
Empty-liposomes	Intermediate (batch #1)	108 $\pm$ 1	0.19 $\pm$ 0.02	49 $\pm$ 2
	Intermediate (batch #2)	106 $\pm$ 1	0.19 $\pm$ 0.01	48 $\pm$ 1
	Intermediate (pool #1 and #2)	108 $\pm$ 1	0.19 $\pm$ 0.01	49 $\pm$ 1
	Final empty-liposomes	113 $\pm$ 3	0.20 $\pm$ 0.01	46 $\pm$ 1

The overall of nanoGLA samples (the two intermediate and the final sample) compared to the overall of empty liposomes samples confirmed the trend that nanoGLA liposomes presented higher sizes ( $p = 0.004$ ,  $n = 3$ ), smaller PDI values ( $p = 0.004$ ,  $n = 3$ ), and lower  $\zeta$ -potential charge ( $p = 0.033$ ,  $n = 3$ ). These results can be explained by the incorporation of GLA in the liposomal membrane: the addition of

GLA in the liposomal provoked a size increase; additionally, due to the electrostatic nature of the interaction between GLA and the liposomal membrane, this decrease on  $\zeta$ -potential is expected due to a charge neutralization effect. These two effects were also observed in previous work, but the most surprising fact is the significant decrease in the polydispersity index. It could be indicator of the proper positive association of the GLA with the lipid, as well as an indicator of the correct lipid/enzyme ratio.

A good reproducibility between produced batches was also obtained regarding GLA concentration (**Table 6.8**), and experimental values were quite close to the theoretical one ( $30 \mu\text{g mL}^{-1}$ ). The GLA concentration achieved in the final nanoGLA formulation met the established specifications ( $\geq 0.2 \text{ mg mL}^{-1}$  GLA), as shown in **Table 6.8**. Moreover, entrapment efficiency was very high, meaning that a majority of the added GLA remained incorporated into the liposomes after their purification by diafiltration, maintaining the desired physicochemical characteristics.

**Table 6.8.** GLA concentration and specific enzymatic activity of GLA in nanoGLA samples (intermediate and final).

NanoGLA sample	GLA <sup>†</sup> concentration ( $\mu\text{g mL}^{-1}$ ) ( $\pm$ SD)	EE% <sup>‡</sup> (%) ( $\pm$ SD)	EA <sup>§</sup> ( $\mu\text{mol h}^{-1} \text{ mg}^{-1}$ ) ( $\pm$ SD)	EA <sup>§</sup> ratio Replagal <sup>®</sup>
Free rh-GLA (tag-free)	–	–	109 $\pm$ 19	1.0 $\pm$ 0.3
Intermediate (batch #1)	34 $\pm$ 1	–	173 $\pm$ 20	1.5 $\pm$ 0.4
Intermediate (batch #2)	34 $\pm$ 2	–	175 $\pm$ 35	1.5 $\pm$ 0.6
Intermediate (pool #1 and #2)	36 $\pm$ 1	–	182 $\pm$ 25	1.6 $\pm$ 0.5
Final nanoGLA	262 $\pm$ 3	97 $\pm$ 1	132 $\pm$ 32	1.1 $\pm$ 0.5

<sup>†</sup> Measured by RP-HPLC (see **Chapter 9.6.3.3**) by LeanBio SL (Barcelona); <sup>‡</sup> Enzyme entrapment efficiency; <sup>§</sup> Specific enzymatic activity in absolute values and in relation to Replagal<sup>®</sup> (normalized to 1), assays performed by LeanBio SL (Barcelona), **Chapter 9.7.1**.

The osmolality of the nanoformulations were again assessed by freezing point osmometer, meeting with the specification range (260 – 300 mOsm  $\text{kg}^{-1}$ ). The pH of the formulations was also determined one week after production; final samples also met the specification range (pH = 6 – 7) (**Table 6.9**).

**Table 6.9.** Osmolality and pH of nanoGLA and empty-liposomes (intermediate and final prototypes).

Sample	Prototype	Osmolality <sup>†</sup> (mOsm kg <sup>-1</sup> ) (± SD)	pH <sup>‡</sup>
NanoGLA	Intermediate	–	5.90 ± 0.01
	Final	270 ± 5	6.58 ± 0.04
Empty-liposomes	Intermediate	–	4.86 ± 0.04
	Final	275 ± 5	6.73 ± 0.06
Specification range for final nanoformulations		260 – 300	6 – 7

<sup>†</sup> Measured by freeze-point (see **Chapter 9.5.3**); <sup>‡</sup> Measured by a pH meter at time 1 week after production (see **Chapter 9.5.2**).

#### 6.4.1.2. Stability of the first batch set

For the stability of the nanoGLA, the main physicochemical/biological attributes that are susceptible to change during storage and have a critical impact on the quality, safety, and efficacy have been controlled: mean vesicle size and vesicle size distribution (PDI),  $\zeta$ -potential, and specific enzymatic activity. Two storage temperatures were selected to generate real time stability data (at the storage temperature of 4 °C), and accelerate stability data (at room temperature, i.e., 25 °C). Monitoring the physicochemical characteristics, such as size, PDI, and  $\zeta$ -potential over time was conducted for intermediate (product after DELOS-susp) and final (after TFF 7.5-fold concentration and diafiltration in glucose 5% medium) samples, at two storage temperatures: 4 °C and 25 °C (**Figure 6.17**). This analysis was done both for nanoGLA and empty-liposomes.

First, regarding nanoGLA, a clear difference between intermediate and final samples was observed. Intermediate samples (dotted lines) clearly showed a slightly higher mean size and PDI than nanoGLA (solid lines). However, in all the cases formulations were within the established range of acceptance, and these values remained stable over time, at least for 12 weeks. No important differences were observed between both storage temperatures, suggesting very good physicochemical stability of nanoGLA. It is interesting to highlight the excellent low PDI obtained for final nanoGLA and maintained over time, always below 0.15. Then, regarding empty-liposomes, excellent stability was obtained, without important differences between intermediate and final samples or storage conditions. Only  $\zeta$ -potential of final empty-liposomes showed a smooth decrease from the sixth week.

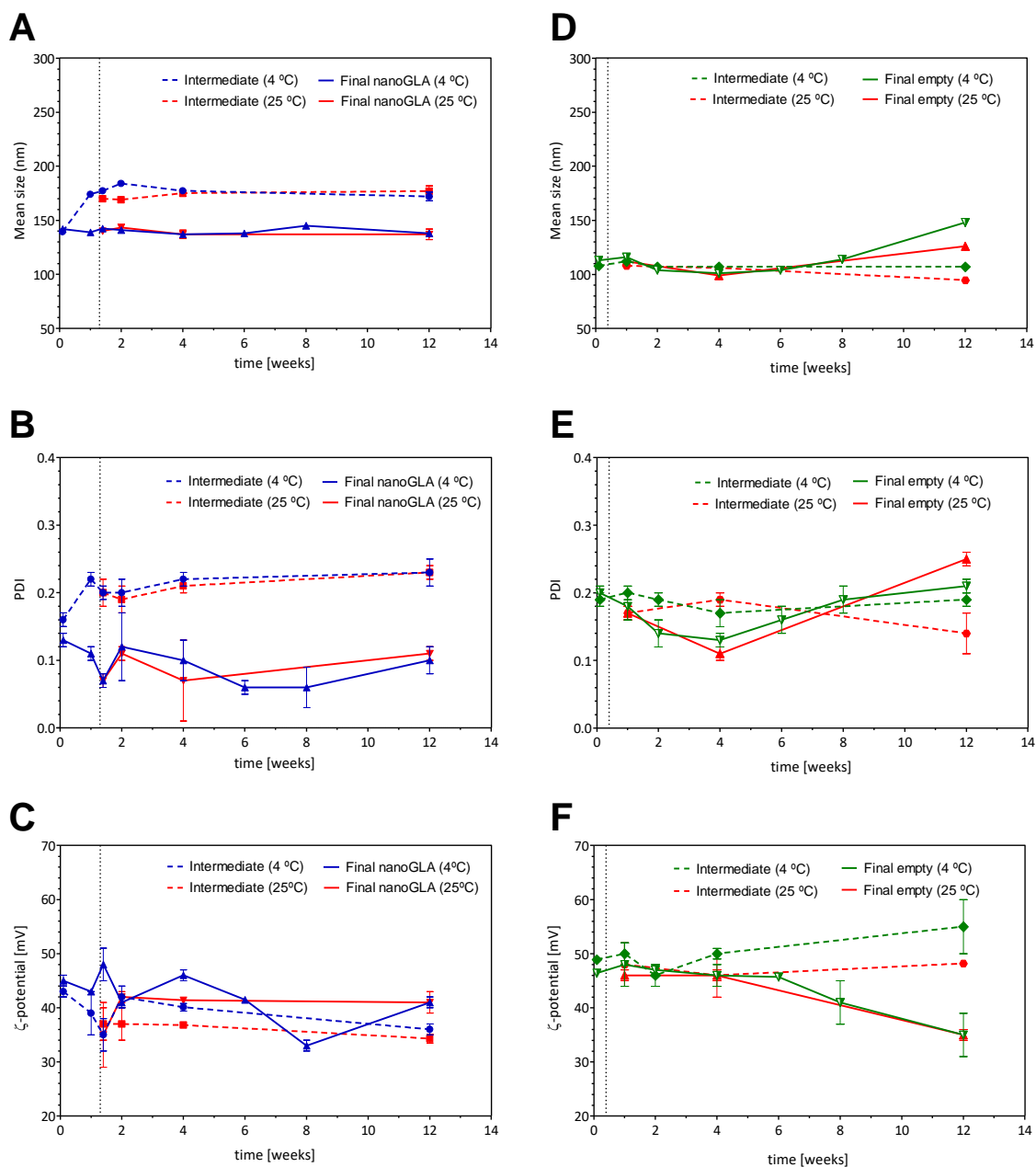


**Figure 6.17.** Monitoring of size, PDI, and  $\zeta$ -potential over time for intermediate (product after DELOS-susp, dotted line) and final (after 7.5-fold concentration and diafiltration in glucose medium, solid line) samples by DLS (see **Chapter 9.5.9.1**), at two storage temperatures: 4 °C (blue/green line) and 25 °C (red line), for (A-C) nanoGLA and (D-F) empty-liposomes.

Additionally, morphology checked three months after production confirmed the stability of these spherical and unilamellar vesicles, as shown in **Figure 6.18**.

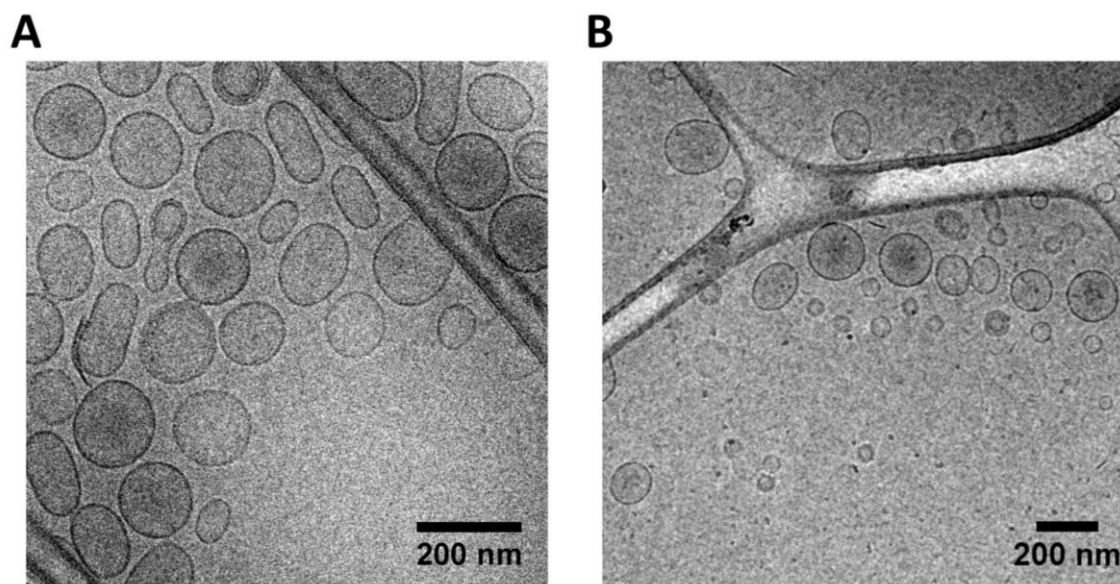


**Figure 6.18.** CryoTEM images of final (A) nanoGLA, and (B) empty-liposomes, 12 weeks after production.

On the other hand, not only good physical stability was important, but the preservation of the entrapped enzyme bioactivity over time. Therefore, monitoring of specific enzymatic activity over time was also conducted for intermediate (product after DELOS-susp) and final (after 7.5-fold concentration and diafiltration in glucose) nanoGLA samples, at two storage temperatures, 4 °C and 25 °C (**Figure 6.19**).

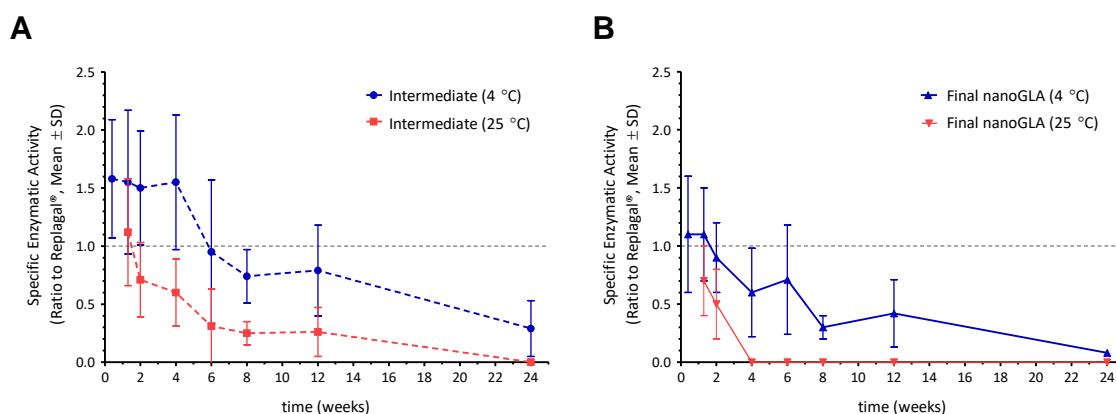


**Figure 6.19.** Specific enzymatic activity referred to Replagal® (normalized to 1) over time for (A) intermediate (product after DELOS-susp) and (B) final nanoGLA (after TFF 7.5-fold concentration and diafiltration in glucose) samples, monitored at two storage temperatures: 4 °C (blue line) and 25 °C (red line), for 24 weeks. Enzymatic assays performed by LeanBio SL (Barcelona)

Stability results showed that enzymatic activity of nanoformulated GLA maintained better at 4 °C, for both intermediate and final nanoGLA. Enzymatic activity of samples stored at 4 °C remained within the specification range, i.e., ratio of nanoGLA vs free GLA  $\geq 0.50$  (in this case, free GLA was considered

Replagal®) during the first 1 – 2 months. However, when samples were stored at 25 °C, enzymatic activity drastically decreased, especially after 4 weeks. Interestingly, again it was observed a higher enzymatic activity trend when comparing intermediate samples (just after DELOS-susp) with final nanoGLA samples (after TFF 7.5-fold concentration and diafiltration in glucose 5 %). These results confirm the acceptable stability data for at least two months, allowing the conductance of larger evaluations (such as repeated dose in vivo studies).

#### 6.4.2. Second large batch production of nanoGLA and empty-liposomes

After the satisfactory results obtained with the first high batch production presented in the previous section, the same strategy was adopted for the manufacturing of a second high batch production of nanoGLA and empty-liposomes for covering all the scheduled preclinical assays. However, bigger amounts of samples were required this time, resulting in the production of five identical batches of intermediate nanoGLA (#1, #2, #3, #4, #5) and four identical batches of intermediate empty-liposomes (#1, #2, #3, #4). The same TFF steps were performed for these samples, 7.5-fold concentration and diafiltration in glucose 5%, with the only difference of the challenge associated with the manipulation of such huge amount of sample, in the range of 2600 – 3500 mL. The whole process is schematized in **Figure 6.20**.

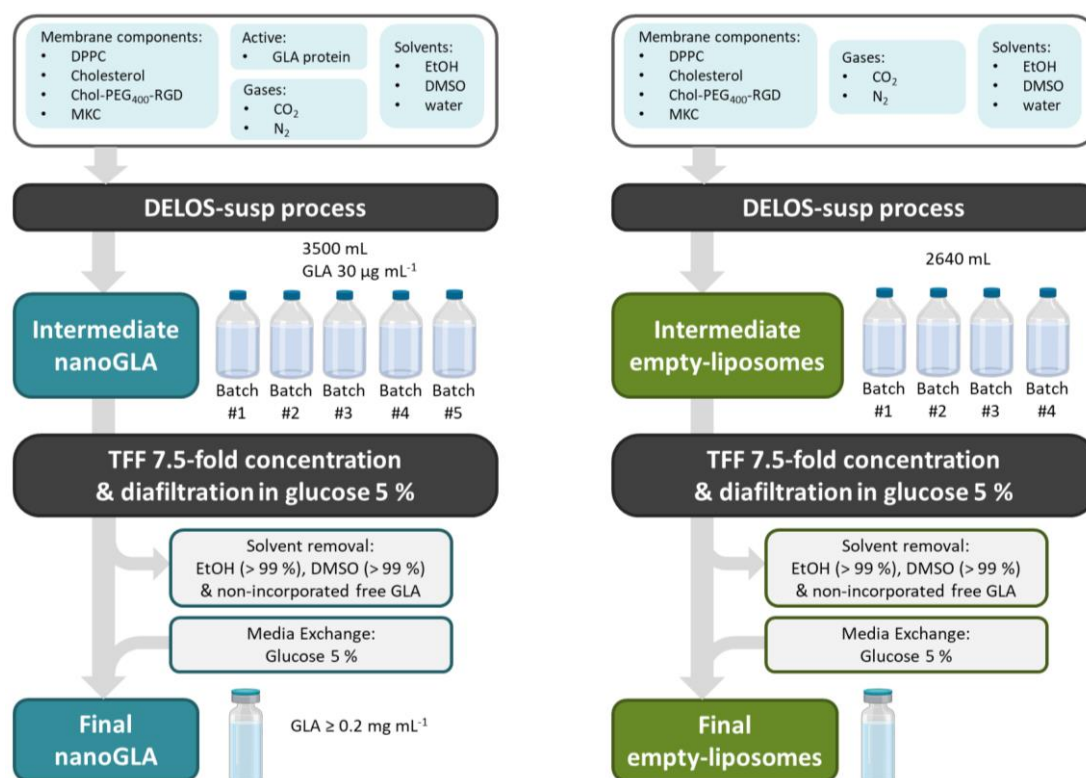


**Figure 6.20.** Process flow diagram to produce nanoGLA and empty-liposomes. Raw materials and the materials leaving the process are also represented.

#### 6.4.2.1. Physicochemical characterization and biological activity

Similar physicochemical characterization to the previous production was performed in this set of samples. Again, a good reproducibility between the different production batches (#) was observed in terms of size, PDI, and  $\zeta$ -potential after DELOS-susp production (**Table 6.10**). The same trend as in the previous section was observed at time zero: Intermediate nanoGLA samples (n = 5) showed a significant higher mean size (p = 0.001) compared to intermediate empty liposomes samples (n = 4), whereas PDI was similar. Moreover, in this experiment,  $\zeta$ -potential values of intermediate nanoGLA liposomes were significantly lower than intermediate empty-liposomes (p = 0.025). A monomodal size distribution and excellent macroscopic appearance were obtained for final nanoGLA and empty-liposomes systems, with vesicles in the nanometric range as shown by cryoTEM imaging (**Figure 6.21**), and especially uniform and mostly unilamellar for nanoGLA system.

**Table 6.10.** Physicochemical characteristics (by DLS) of intermediate and final samples of nanoGLA and empty-liposomes, at time one day after production.

Sample	Prototype	Size (nm) ( $\pm$ SD)	PDI ( $\pm$ SD)	$\zeta$ -potential (mV) ( $\pm$ SD)
<b>NanoGLA</b>	Intermediate (batch #1)	134 $\pm$ 1	0.15 $\pm$ 0.01	41 $\pm$ 1
	Intermediate (batch #2)	154 $\pm$ 2	0.19 $\pm$ 0.01	39 $\pm$ 1
	Intermediate (batch #3)	151 $\pm$ 2	0.18 $\pm$ 0.01	40 $\pm$ 1
	Intermediate (batch #4)	145 $\pm$ 3	0.17 $\pm$ 0.03	40 $\pm$ 2
	Intermediate (batch #5)	150 $\pm$ 2	0.16 $\pm$ 0.01	44 $\pm$ 1
	Intermediate (pool #1 – #5)	143 $\pm$ 4	0.17 $\pm$ 0.02	40 $\pm$ 2
	Final nanoGLA	143 $\pm$ 3	0.11 $\pm$ 0.02	44 $\pm$ 2
<b>Empty-liposomes</b>	Intermediate (batch #1)	110 $\pm$ 3	0.19 $\pm$ 0.01	60 $\pm$ 7
	Intermediate (batch #2)	110 $\pm$ 1	0.17 $\pm$ 0.01	52.7 $\pm$ 1
	Intermediate (batch #3)	104 $\pm$ 1	0.17 $\pm$ 0.01	49 $\pm$ 2
	Intermediate (batch #4)	111 $\pm$ 1	0.17 $\pm$ 0.01	49 $\pm$ 1
	Intermediate (pool #1 - #4)	108 $\pm$ 1	0.19 $\pm$ 0.01	51 $\pm$ 1
	Final empty-liposomes	114 $\pm$ 1	0.17 $\pm$ 0.01	47 $\pm$ 1

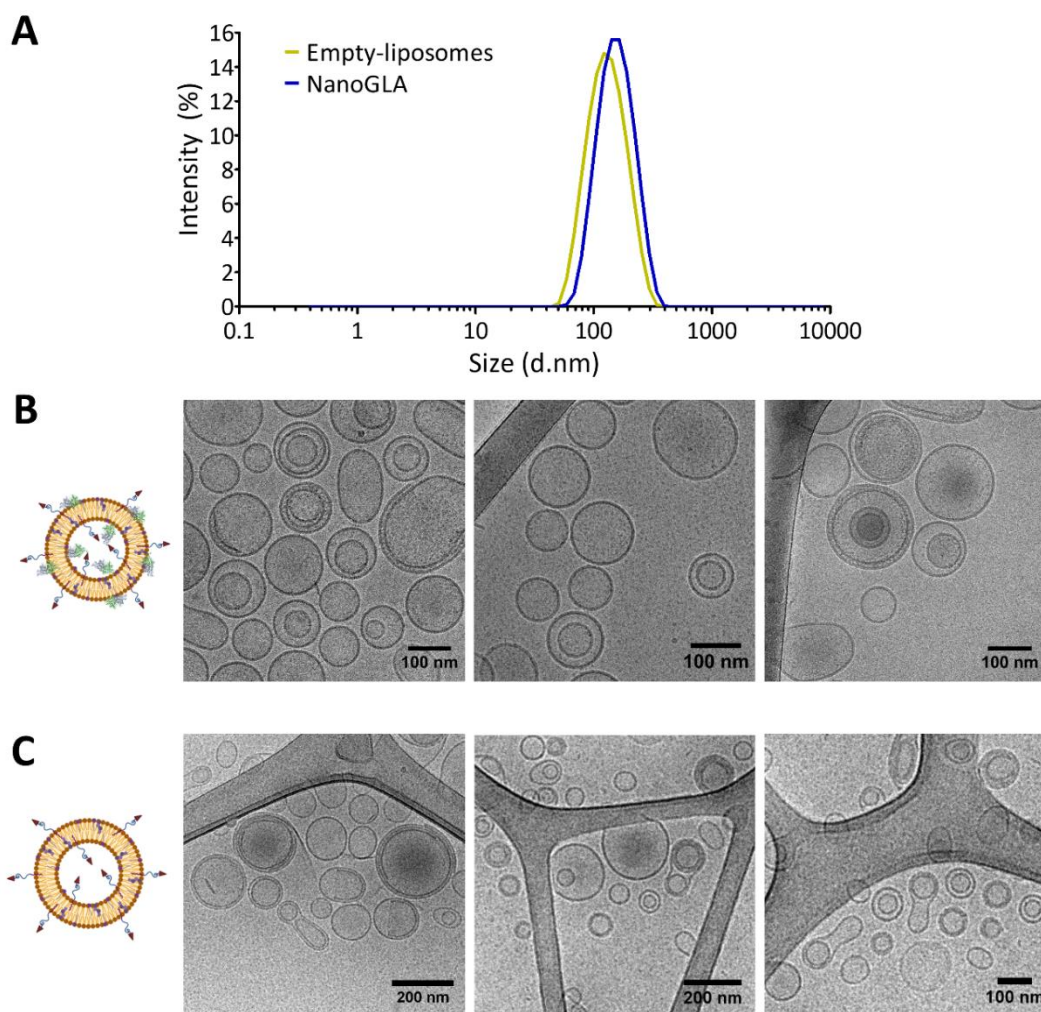


**Figure 6.21.** (A) Size distribution of final nanoGLA and empty liposomes just after production (by DLS, see **Chapter 9.5.1**), and morphology by cryoTEM of (B) nanoGLA, and (C) empty-liposomes, 1 week after production. Images were acquired by Prof. D. Danino team from Technion (Israel).

Both final nanoformulations were within the isosmotic specification range, as well as these presented a neutral pH (**Table 6.11**).

**Table 6.11.** Osmolality and pH of nanoGLA and empty-liposomes (intermediate and final prototypes).

Sample	Prototype	Osmolality <sup>†</sup> (mOsm kg <sup>-1</sup> )	pH <sup>‡</sup> (± SD)
NanoGLA	Intermediate	–	5.5 ± 0.2
	Final	265 ± 5	7.04 ± 0.04
Empty-liposomes	Intermediate	–	4.4 ± 0.1
	Final	261 ± 5	6.2 ± 0.1
Specification range for final nanoformulations		260 – 300	6 – 7

<sup>†</sup> Measured by freeze-point (see **Chapter 9**); <sup>‡</sup> Measured by a pH meter at time 1 week after production (see **Chapter 9**).



Expected results were also obtained in terms of GLA concentration in nanoGLA samples, good reproducibility between produced batches, and experimental values close to the theoretical ones ( $30 \mu\text{g mL}^{-1}$ ) (**Table 6.12**). The GLA concentration achieved in the final nanoGLA formulation met the established specifications ( $\geq 0.2 \text{ mg mL}^{-1}$  GLA for the final nanoGLA), as **Table 6.12** indicates. As shown, entrapment efficiency was again very high.

Similarly, enzymatic activity was comparable between the different batches ( $\text{CV}\% = 10.25\%$ ), confirming the aforementioned interbatch reproducibility. Nanoformulations met the established specification (ratio of nanoGLA vs Replagal<sup>®</sup>  $\geq 0.50$ ) and, therefore, were considered biologically active.

**Table 6.12.** GLA concentration and specific enzymatic activity of GLA in nanoGLA samples (intermediate and final).

NanoGLA sample	GLA concentration <sup>†</sup> ( $\mu\text{g mL}^{-1}$ ) ( $\pm$ SD)	EE% <sup>‡</sup> (%) ( $\pm$ SD)	EA <sup>§</sup> ( $\mu\text{mol h}^{-1} \text{mg}^{-1}$ ) ( $\pm$ SD)	EA <sup>§</sup> ratio Replagal <sup>®</sup>
Free rh-GLA (tag-free)	–	–	$1259 \pm 4$	$1.04 \pm 0.01$
Intermediate (batch #1)	$38 \pm 1$	–	$990 \pm 10$	$0.82 \pm 0.01$
Intermediate (batch #2)	$42 \pm 1$	–	$800 \pm 40$	$0.66 \pm 0.03$
Intermediate (batch #3)	$40 \pm 5$	–	$811 \pm 2$	$0.67 \pm 0.01$
Intermediate (batch #4)	$40.2 \pm 0.2$	–	$860 \pm 60$	$0.71 \pm 0.05$
Intermediate (batch #5)	$41 \pm 5$	–	$780 \pm 20$	$0.64 \pm 0.02$
Intermediate (pool #1 - #5)	$37 \pm 2$	–	$1020 \pm 10$	$0.84 \pm 0.01$
Final nanoGLA	$270.90 \pm 0.04$	$98 \pm 5$	$760 \pm 20$	$0.63 \pm 0.02$

<sup>†</sup> Measured by RP-HPLC (see **Chapter 9.6.3.3**) by LeanBio SL (Barcelona); <sup>‡</sup> Enzyme entrapment efficiency; <sup>§</sup> Specific enzymatic activity in absolute values and in relation to Replagal<sup>®</sup> (normalized to 1), assays performed by Dr. I. Abasolo group from VHIR (Barcelona), **Chapter 9.7.1**.

Next, the *in vitro* efficacy of nanoGLA, i.e., the capacity of the system to reduce NBD-Gb3 levels *in vitro*, using MAEC cells derived from KO Fabry mice (thus, without endogenous GLA) was evaluated in collaboration with Dr. I. Abasolo group from VHIR (Barcelona). Cells were faced against nanoGLA (both intermediate and final prototypes), empty-liposomes, free rh-GLA, and Replagal<sup>®</sup>, at the same concentration of GLA ( $0.25 \mu\text{g mL}^{-1}$ ).

*In vitro* efficacy assay showed that nanoGLA (both intermediate and final prototypes) reduced significantly better the levels of NBD-Gb3 than the free GLA. Moreover, nanoGLA also showed significant difference with Replagal<sup>®</sup> action. Here is also interesting to see that lower specific enzymatic activity resulted from 4-MUG substrate conversion by GLA action (**Figure 6.22A**), as it is the case of

final nanoGLA, can also result in higher in vitro efficacy by Gb3 reduction assay in MAEC cells (Figure 6.22B).

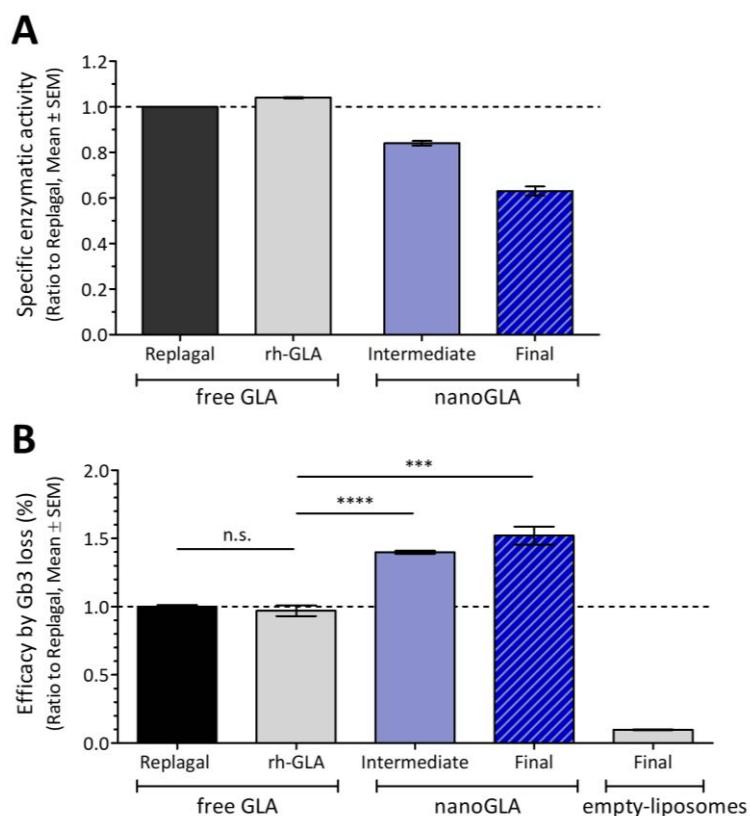


**Figure 6.22.** (A) Specific enzymatic activity of free GLA and nanoGLA, in relation to the control (commercial Replagal® normalized to 1); (B) In vitro efficacy assay measured as loss of Gb3 in MAEC cells derived from KO mice, incubation at  $0.25 \mu\text{g mL}^{-1}$  GLA (or at the equivalent liposome concentration for empty-liposomes), at  $37^\circ\text{C}$  for 48 h. Assays performed by Dr. I. Abasolo team from VHIR (Barcelona), as detailed in **Chapter 9.7.1** and **Chapter 9.7.2**.

#### 6.4.2.2. Stability of the second batch set

The same trend as observed with the first batch set was found with this second one. The mean vesicle size, PDI and  $\zeta$ -potential remained invariable for almost 12 weeks when nanoGLA was stored at  $4^\circ\text{C}$  (Figure 6.23).

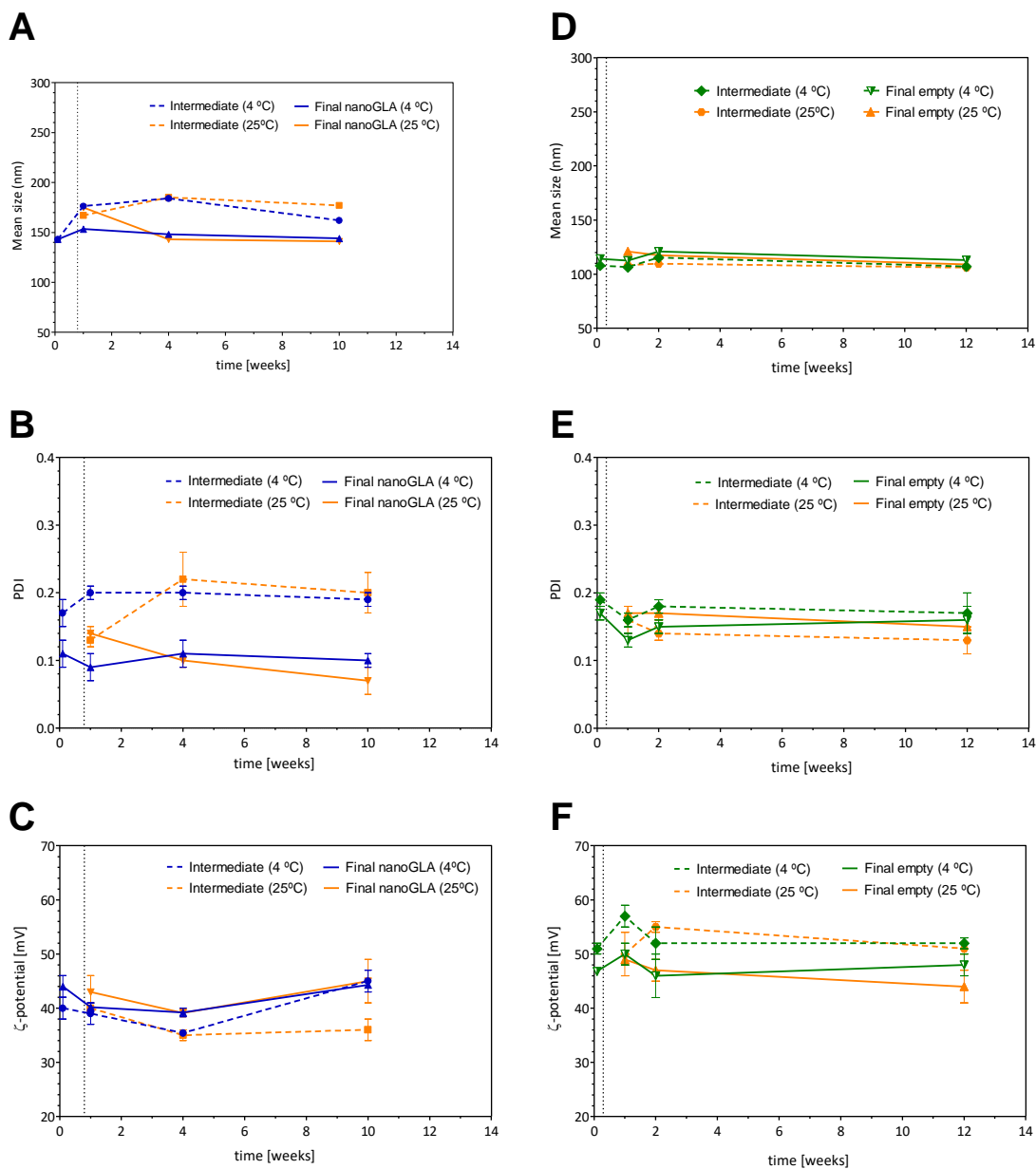


**Figure 6.23.** Monitoring of size, PDI, and  $\zeta$ -potential over time of the intermediate (product after DELOS-susp, dotted line) and final (after TFF 7.5-fold concentration and diafiltration in glucose, solid line) samples by DLS (see **Chapter 9.5.9.1**), after being stored at two temperatures: 4 °C (blue/green line) and 25 °C (orange line). Graphs A-C corresponds to nanoGLA and D-F corresponds to empty-liposomes.

From the bioactivity point of view, the enzymatic activity significantly decreased as a function of time, being this decrease more pronounced when the samples were stored at 25 °C (see **Figure 6.24**). Despite it, at fridge conditions the enzymatic activity remained within specifications ( $\geq 50\%$  to control).

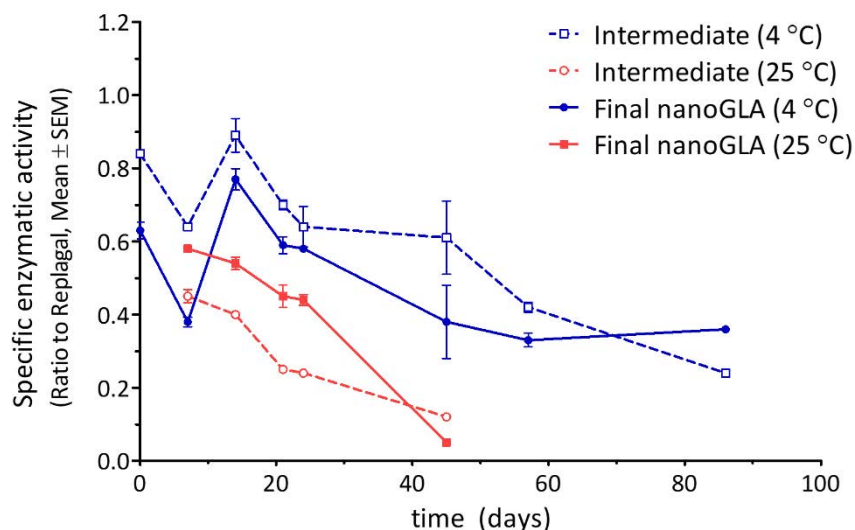


**Figure 6.24.** Specific enzymatic activity in relation to Replagal® (normalized to 1) over time for intermediate (product after DELOS-susp) and final nanoGLA (after TFF 7.5-fold concentration and diafiltration in glucose) samples, monitored at two storage temperatures: 4 °C (blue line) and 25 °C (red line), for 90 days. Assay performed by Dr. I. Abasolo group from VHIR (Barcelona).

To summarize, from these stability studies it can be concluded: (i) nanoGLA batches remained stable, maintained almost invariable the mean particle size, polydispersity index, and  $\zeta$ -potential for at least three months when stored at 4 °C; (ii) special attention must be paid with the activity of the entrapped GLA enzyme, since this decrease upon time and it is very sensitive to storage temperatures (> 4 °C); and (iii) the stability results demonstrate consistent batch-to-batch reproducibility and, thus, the robustness of the production process and the achievement of an optimal nanoformulation composition.

### 6.4.3. Chemical composition of both high batch productions

Although the supramolecular structure of drug delivery systems has a play role in their physicochemical and biological properties, chemical composition should be carefully controlled to guarantee the quality of liposomal pharmaceutical formulations. Among quantification techniques, high-performance liquid chromatography (HPLC) is one of the most recommended techniques in pharmaceutical analysis. HPLC is based on the separation of the different species along time, by a different distribution through two phases which depends on the chemical properties of the compounds, such as chain length, head groups, and polarity. Therefore, an HPLC procedure was developed and validated for the quantification of DPPC, cholesterol, cholesterol-PEG<sub>400</sub>-RGD, and MKC in nanoGLA samples (see **Chapter 9.5.4.2**).

Liposomal membrane components of intermediate and final samples for the previous two high productions (including empty-liposomes and nanoGLA) were quantified.

First, intermediate samples, i.e., after DELOS-susp production, showed a total lipid recovery with excellent agreement with the theoretical expected lipid concentration (i.e., 1.2 mg mL<sup>-1</sup>), as shown **Figure 6.25A**. Those high yields indicate the great performance of DELOS-susp technique. Furthermore, it is important to highlight the improvement of recovery in relation to previous quantifications (e.g., **Chapter 4**, total recoveries around 80 %), which can be related to work on bigger scale, since increased total batch size could reduce the material losses associated to the production (e.g., rests of materials in the walls of the vessel, tubing, etc.). Otherwise, concentrated final samples, i.e., after TFF process including 7.5-fold concentration and diafiltration in glucose medium, showed total lipid concentrations slightly above the expected ones (9.0 mg mL<sup>-1</sup>), but similar between all the samples (**Figure 6.25B**).

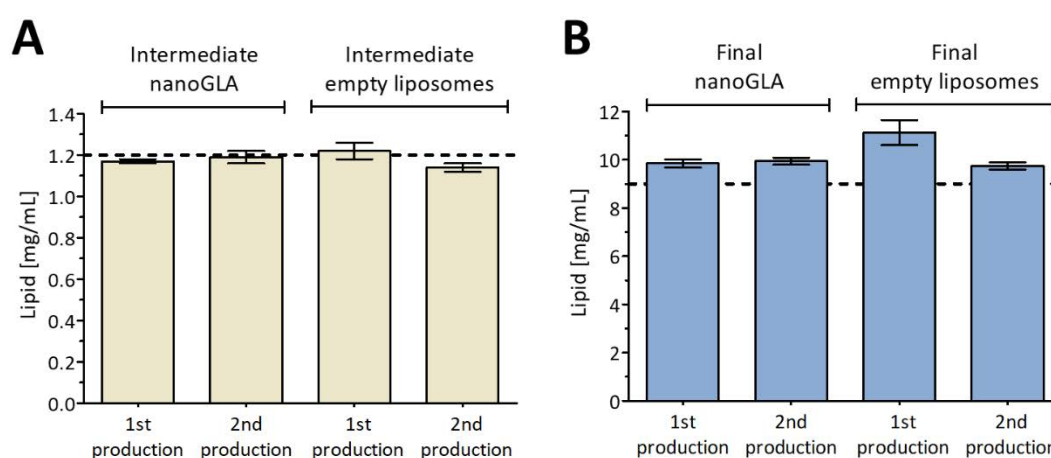


**Figure 6.25.** Total lipid concentration of (A) intermediate, and (B) final samples, including nanoGLA and empty-liposomes from both big productions. Dotted lines represent the theoretical expected concentration. Quantification by HPLC-ELDS (see **Chapter 9.5.1.2**).

Moving to the analysis of each component, high DELOS-susp recoveries were obtained for all the membrane components: > 95 % for DPPC and cholesterol, and > 87 % for MKC and chol-PEG<sub>400</sub>-RGD (**Figure 6.26A**). Then, the mol % ratio between components was calculated with the real quantified HPLC values and were compared to the theoretical ones. In the intermediate samples, ratios between components were close to the theoretical ones (**Figure 6.26B**), as well as in the final concentrated samples (**Figure 6.26C**). These results were especially relevant for chol-PEG<sub>400</sub>-RGD functionalization content, which values were near to 3 mol %, matching greatly with the theoretical ones. Moreover, RGD targeting functionalization was maintained after the TFF process, indicating a good incorporation in the liposomal membrane.

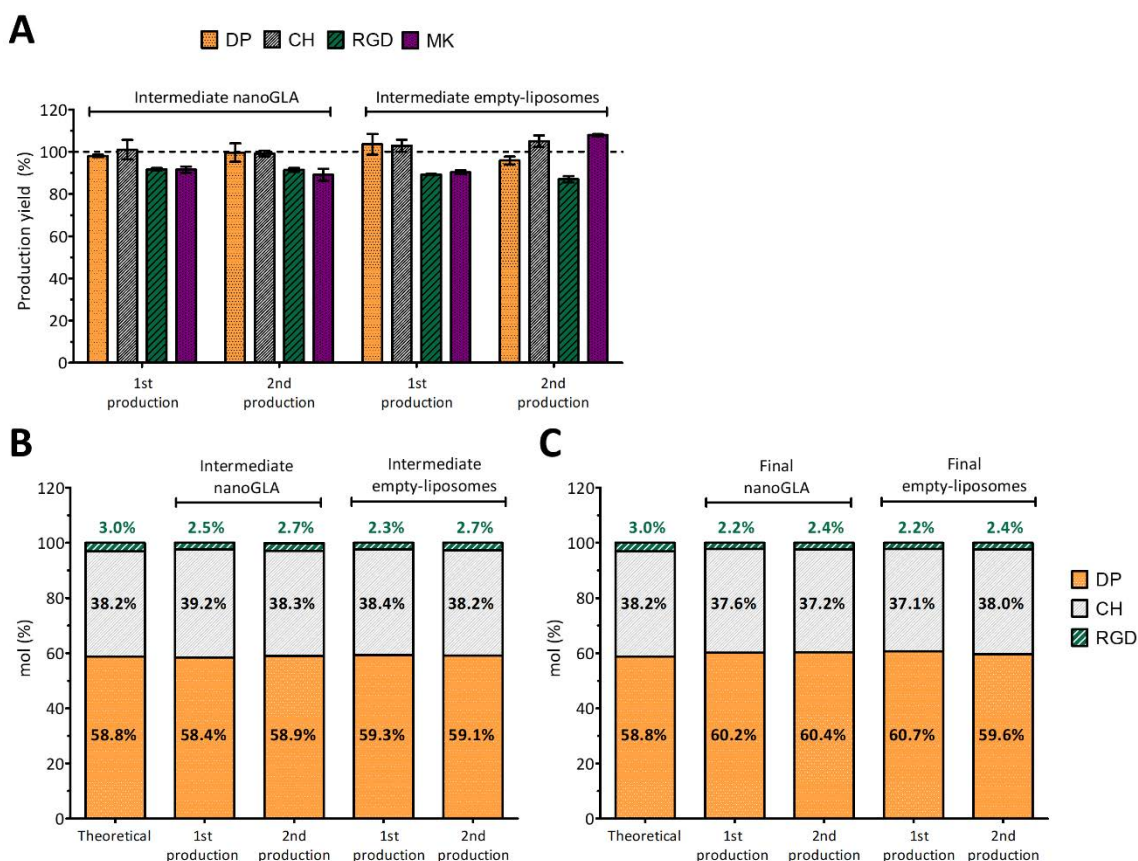


**Figure 6.26.** (A) Recovery yields of each membrane component (DPPC, i.e., DP; cholesterol, i.e., CH; chol-PEG<sub>400</sub>-RGD, i.e., RGD; and MKC, i.e., MK) from intermediate samples after DELOS-susp, quantified by HPLC and compared to the theoretical ones; mol % ratio between components measured by HPLC of intermediate and final samples from (A) the first production, and (B) from the second production.

#### 6.4.4. Analysis of the reproducibility between both large-batch productions

Interestingly, comparison between both independent productions showed an extremely good robustness of the DELOS-susp method. The coefficient variation was less than 10 % in majority of variables, including size, PDI,  $\zeta$ -potential, and GLA concentration (**Table 6.13**). This robustness degree in the production method is a very important milestone for translation of nanomedicines until the preclinical and clinical phases, and is an excellent result obtained at the academic level. The parameter that showed major variability was the enzymatic activity. Looking closer enzymatic activity values of both productions (**Table 6.8** and **Table 6.12**), different coefficient variation were obtained: 1 % for first run ( $n = 2$ ), and 10 % for second run ( $n = 5$ ). The difference based on enzymatic activity between runs was significant ( $p = 0.001$ ), however this could be associated to a possible interlaboratory variability since enzymatic activity in both large-batches productions were not assessed by the same laboratory team. Nevertheless, as aforementioned, in both cases met the specification for this CQA.

**Table 6.13.** Coefficient of variation (CV%) between the intermediate samples produced by DELOS-susp, produced in two different time-runs.

Sample	N batches <sup>†</sup>	Coefficient of variation (CV%)*				
		Size	PDI	ζ-potential	GLA concentration	EA <sup>‡</sup>
NanoGLA	7	6 %	11 %	5 %	8 %	43 %
Empty-liposomes	6	2 %	6 %	9 %	–	–

\* CV% as SD/mean ×100; † Sum of all the batches corresponding to two independent production series;

‡ Specific enzymatic activity.

#### 6.4.5. Aseptic-like processing, aliquoting, and generation of certificates of analysis

Drugs to be administered by IV route should be sterile and endotoxin free, as the regulatory agencies, e.g., EMA, recommend.<sup>24</sup> In the frame of nanoGLA development, several methods to provide terminal sterilization were explored, as detailed in **Annex I**. However, the terminal sterilization of liposomal formulations is still a major challenge in its pharmaceutical development process, since conventional sterilization techniques (e.g., steam or dry heat) can alter the physical and chemical properties of liposomal and biological containing samples.<sup>25</sup> Although several attempts were performed by the use of gamma radiation and membrane filtration, it was not possible to obtain a terminal sterility procedure for nanoGLA formulation with enough quality and able to maintain all their CQA (details in **Annex I**). Instead, an aseptic-like processing approach was carried out, i.e., related to the strategy of performing all the whole production in an almost sterile environment. First, several studies support the germicide effect of supercritical CO<sub>2</sub>,<sup>26,27</sup> meaning that DELOS-susp properties could allow working in sterile operation conditions.<sup>28</sup> Then, for keeping an aseptic-like environment, the TFF process was moved inside a laminar flow cabinet (see **Figure 27A**). Working in aseptic-like conditions was a provisional solution, although further efforts should be done in the future regarding terminal sterilization of the nanoformulation.



**Figure 6.27.** (A) Setting of the TFF process in a laminar flow cabinet to maintain a sterile environment, and (B) aliquoting of nanoGLA in sterile vials (see **Chapter 9.16.3**).

After completing the production, nanoGLA and empty-liposomes had to be aliquoted. Technical requirements such as the administration dose, the number of administrations per time-point, and the number of time-points, were considered for determining the sample volume per vial. It was decided to aliquot 5 mL per vial, as the better and most flexible option for administering, in 5 mL sterile glass vials assembled with butyl stoppers and aluminum seals (**Figure 27B**). Thus, 5 mL sterile glass vials were filled individually using a 5 mL syringe coupled to a 23G needle in a sterile laminar-low cabinet environment, as detailed in **Chapter 9.16.3**. No impact on sample macroscopic appearance, size, PDI,  $\zeta$ -potential, GLA concentration, and specific enzymatic activity was observed after aliquoting (**Table 6.14**).

**Table 6.14.** Critical quality attributes (CQA) of final nanoGLA before and after their passing through a syringe with needle.

CQA	NanoGLA	NanoGLA syringed with needle
Size (nm) ( $\pm$ SD) <sup>†</sup>	142 $\pm$ 2	140 $\pm$ 1
PDI ( $\pm$ SD) <sup>†</sup>	0.13 $\pm$ 0.01	0.14 $\pm$ 0.02
$\zeta$ -potential (mV) ( $\pm$ SD) <sup>†</sup>	44 $\pm$ 1	43 $\pm$ 1
GLA concentration ( $\mu\text{g mL}^{-1}$ ) ( $\pm$ SD) <sup>‡</sup>	262 $\pm$ 3	260 $\pm$ 7
Specific enzymatic activity (referred to Replagal <sup>®</sup> ) <sup>§</sup>	1.1 $\pm$ 0.5	1.1 $\pm$ 0.3

<sup>†</sup> By DLS; <sup>‡</sup> By RP-HPLC; <sup>§</sup> Performed by LeanBio SL (Barcelona) (see **Chapter 9.6.3.3** and **Chapter 9.7.2**).



Finally, to accomplish with the requirements to carry out GLP studies, the main characterized CQA of each final batch were collected in their corresponding Certificate of Analysis (CoA) (see **Annex II**). This documentation is a requirement for regulatory studies and must be sent to the GLP-compliant lab before the batch release.

Overall, the successful preparation of nanoGLA and empty-liposomal formulations were obtained, meeting the established requirements and with CQA within the specification range. Therefore, these batches were destined to carry out the preclinical in vivo studies summarized in **Table 6.15** and explained in the following sections. These in vivo experiments were performed in collaboration with Dr. I. Abasolo group from VHIR (Barcelona) and with Covance SL (UK), and were included in this Thesis to complete the work and show the in vivo performance of the optimized nanoGLA.

**Table 6.15.** Preclinical in vivo studies performed with the two large nanoGLA and empty productions described in the previous sections, in collaboration with Dr. I. Abasolo group from VHIR (Barcelona) and Covance SL (UK).

Study	Regulatory level	Animal model	ID of the large-batch production tested
Repeated dose efficacy	Non-GLP	Fabry mice	2 <sup>nd</sup> large batch production
Pharmacokinetic	Non-GLP	Rat	2 <sup>nd</sup> large batch production
One-week range-finding dose toxicology*	Non-GLP	Rat	1 <sup>st</sup> large batch production
28-days GLP-toxicology*	GLP	Rat	2 <sup>nd</sup> large batch production
Toxicokinetics*	GLP	Rat	2 <sup>nd</sup> large batch production

\* Not fully described in this Thesis.

## 6.5. Preclinical in vivo repeated dose efficacy in mice

After the positive results obtained in the single dose efficacy study, a repeated dose efficacy study was carried out in collaboration with Dr. I. Abasolo's group from VHIR (Barcelona) using Fabry KO mice. The aim of this study was to insight into the possible differences between the systems, at the time that a repeated administration is closer to the actual treatment for Fabry disease, in which repeated administrations of GLA are required for a sustained effect.

The objective was to compare the efficacy of free rh-GLA and commercial GLA against nanoformulated GLA (nanoGLA) in reducing the Gb3 levels. Thus, the design included: two non-treated control groups, i.e., WT mice (with endogenous GLA) and KO mice (without endogenous GLA), and three treated groups, i.e., KO mice administered with nanoGLA, free GLA (rh-GLA), or Replagal® (clinically approved for ERT).

The experimental design is schematized in **Figure 6.28** and detailed in **Chapter 9.10.2**. The 3 treated groups received GLA at  $1 \text{ mg kg}^{-1}$  dose; nanoGLA dose was also based on GLA concentration, previously presented in **Table 6.12**, also at  $1 \text{ mg kg}^{-1}$ . Mice were treated with 8 doses, distributed in two weeks. Then, animals were euthanized 24 h post-administration of the eighth dose and their organs (blood, kidneys, liver, spleen, heart, lungs, skin, and brain) collected. Organs were processed for Gb3 quantification by LC-MS/MS (see **Chapter 9.15.4**).

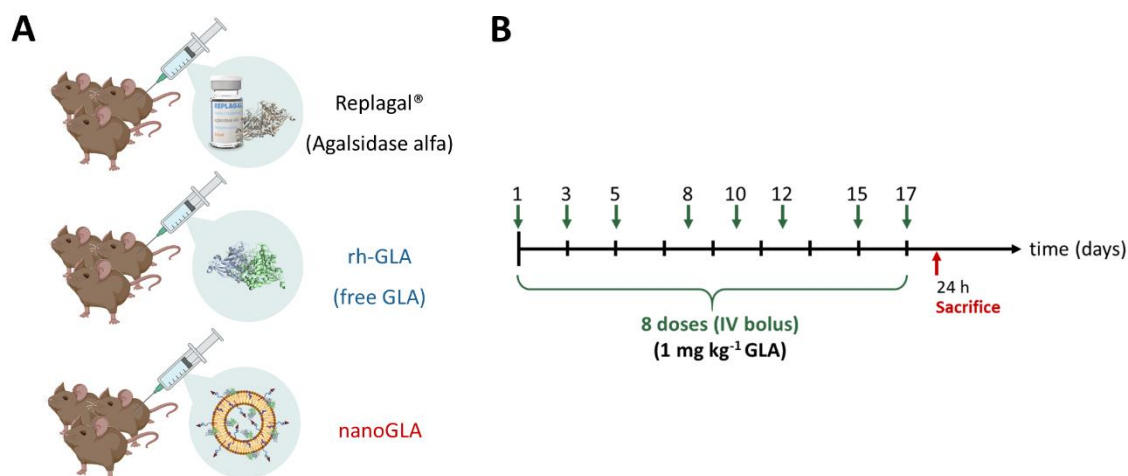


**Figure 6.28.** Scheme of the repeated-dose efficacy study. (A) Mice ( $n = 6$  per group) were IV administered with Replagal®, free rh-GLA, or nanoGLA, at  $1 \text{ mg kg}^{-1}$  dose of GLA up to 8 doses, distributed along two weeks. Mice were euthanized and tissues collected 24 h after the last administration (B). Assay performed by Dr. I. Abasolo's team from VHIR (Barcelona).

Efficacy results were based on the capability of GLA (dose  $1 \text{ mg kg}^{-1}$ ) on reducing the Gb3 deposits in Fabry KO mice. Results were expressed as % Gb3 levels. For calculation of the relative Gb3 loss, it was assumed that the difference in Gb3 levels between non-treated KO mice and WT counterparts corresponds to a 100% of Gb3 loss in WT. Then, the Gb3 levels in different treatment groups were referred to this total Gb3 loss in WT, meaning that those treatments with a higher percentage of Gb3 loss are the ones with a higher efficacy.

As already observed in the single dose efficacy study, Gb3 levels varied significantly among tissues of non-treated Fabry mice (GLA-KO) and were similar to those already reported, excepting liver which this time showed higher Gb3 levels. **Table 6.16** gives an idea of the distinctive Gb3 levels in the collected organs.

**Table 6.16.** Gb3 levels (pmol eq./mg prot.) in the collected organs of non-treated Fabry mice (KO), Fabry mice treated with nanoGLA, and wild type mice (WT), after 8 doses of 1 mg kg<sup>-1</sup> of GLA distributed along two weeks\*.

Group	Gb3 levels <sup>†</sup>							
	Liver	Spleen	Lung	Plasma	Kidney	Heart	Skin	Brain
<b>KO</b>	3,000 ± 90	6,000 ± 300	2,300 ± 100	260 ± 10	28,000 ± 3,000	880 ± 40	12,000 ± 1,000	600 ± 20
<b>nanoGLA</b>	76 ± 4	1,000 ± 90	580 ± 50	45 ± 3	4,600 ± 900	108 ± 9	1,485 ± 68	440 ± 20
<b>WT</b>	31 ± 1	90 ± 5	156 ± 6	20 ± 2	4,300 ± 400	23 ± 2	89 ± 13	39 ± 3

\* Tissues samples collected 24 h after the last administration. † Measured by LC-HRMS (see **Chapter 9.15.4**), by Dr. I. Abasolo group from VHIR (Barcelona); Gb3 levels of Fabry mice administered with Replagal<sup>®</sup> or rh-GLA were quantified but are not reported in this table.

Results showed a Gb3 loss induced by nanoGLA in all the tested tissues (**Figure 6.29**). Further, results showed a general superiority of nanoGLA compared to free rh-GLA and Replagal<sup>®</sup>. NanoGLA reduced more Gb3 than Replagal<sup>®</sup> in liver, lungs, plasma, kidneys, and heart, and more than the free rh-GLA in spleen. In heart, differences between nanoGLA and free rh-GLA were not statistically significant (opposite to what was found in the single dose efficacy assay), but both were more efficacious than Replagal. Moreover, nanoGLA was able to reduce in approximately 28 % the Gb3 deposits in brain, suggesting that the nanoformulation might cross the blood-brain barrier (BBB). This is an interesting finding since any of the current recombinant enzymes approved for ERT are able to reach this organ, suggesting a possible capacity of the nanoGLA for crossing the BBB. To confirm this result in brain, mice brains from the single-dose efficacy study (exposed in **Chapter 6.3.3**) were analyzed. In the previous single-dose experiment, although brains were also collected together with the rest of organs, Gb3 levels were not initially analyzed since no enzymatic activity was found 30 min post-administration (data not shown). However, after analyzed, a reduction of approximately 16 % of Gb3 deposits in brain was found. Therefore, the efficacy of nanoGLA in reducing Gb3 deposits in brain is evident after a single and repeated administration, although more studies should be performed to clarify the mechanism of BBB crossing.

Further, repeated dose regimen increased the difference in efficacy between the nanoGLA and GLA. Some non-statistically significant values obtained in the single dose, such as in kidney or lung, became significant in a repeated dose (**Figure 6.29**).

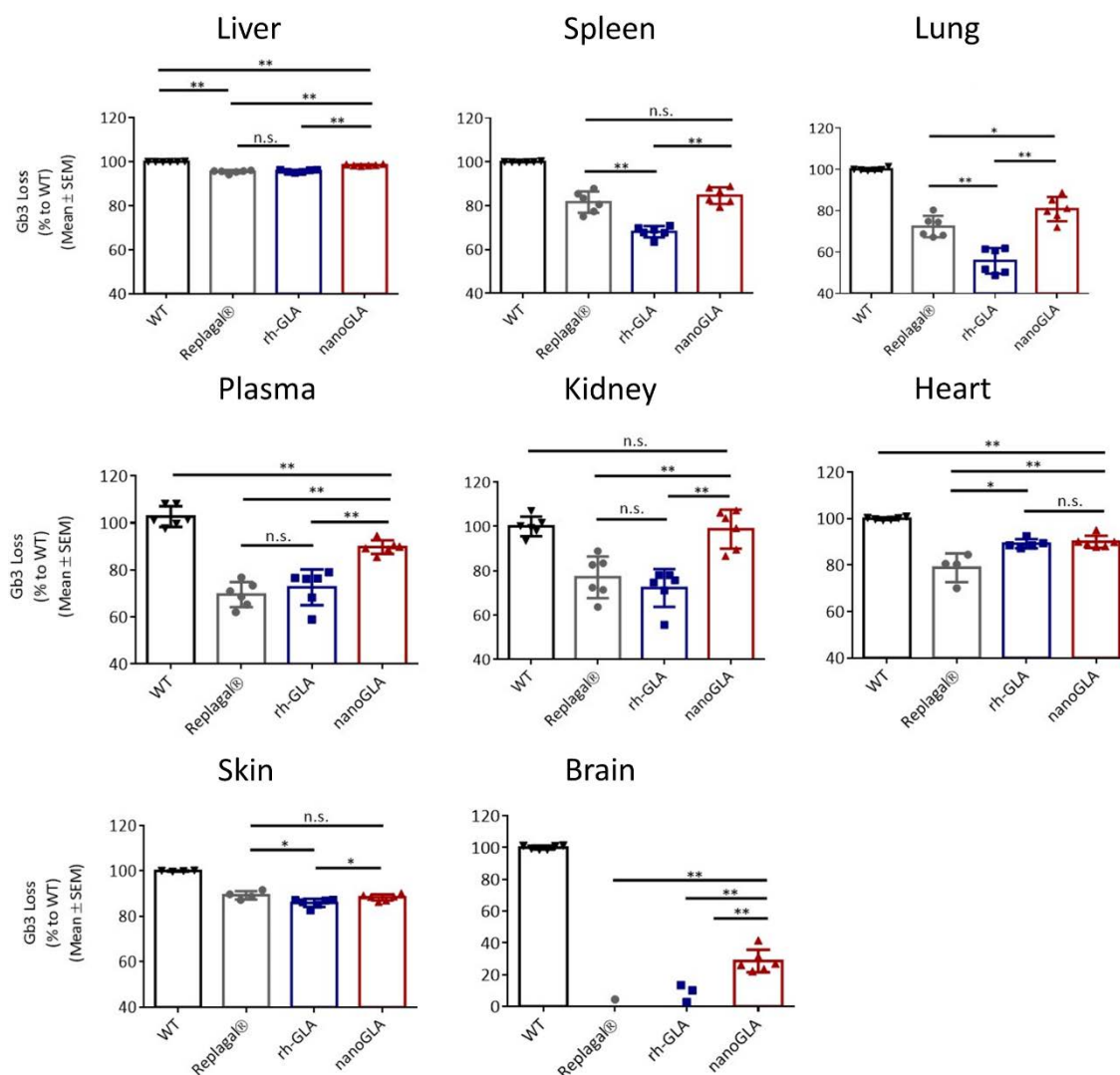


**Figure 6.29.** In vivo efficacy after repeated administration of 8 doses of 1 mg kg<sup>-1</sup> of GLA distributed along two weeks. Tissues samples were collected 24 h after the last administration. Results based on reduction of Gb3 levels in tissue. ANOVA test with multiple comparisons and t-test were performed to compare results (statistically significant when  $p \leq 0.05$ ). Assay performed by Dr. I. Abasolo's group from VHIR (Barcelona)

## 6.6. Pharmacokinetic profile in rat

Information of the pharmacokinetics (PK) of the test substance is required to confirm the increased half-life of GLA, predict the duration of its effects, and a further extrapolation of results from animal to human, when it is administered nanoformulated in liposomes (nanoGLA). Therefore, the objective of this study was to compare the pharmacokinetics of free GLA and nanoGLA following intravenous administration to rat, by blood sampling at different time points. This experiment was performed in collaboration with Covance SL (UK). Rat was selected as animal model since some issues were found

in mice after continuous blood sampling, due to limitations in having less total blood volume in these smaller animals.

Animals were divided in two dose groups and were administered with free rh-GLA or nanoGLA. Each animal received a single bolus intravenous administration, at 1 mg kg<sup>-1</sup> of GLA (Table 6.17). Blood samples were collected at different time points for 8 h (as detailed in Chapter 9.11), and MKC and GLA content were analyzed by LC-MS and ELISA, respectively (see Chapter 9.15.2, and Chapter 9.15.3).

**Table 6.17.** Designation of dose groups (n = 3 male rats/ group) and information about tested compounds.

Dose group	Test article	Concentration of GLA in test article	Dose level (mg GLA kg <sup>-1</sup> )	Nominal dose volume (mL kg <sup>-1</sup> )
A	rh-GLA	3.11 mg mL <sup>-1</sup>	1	0.32
B	nanoGLA	270.90 ± 0.04 µg mL <sup>-1</sup>	1	3.7

After IV bolus administration of either rh-GLA (Group A) or nanoGLA (Group B), total GLA mean concentrations readily declined and were measurable through 6 (rh-GLA) or 8 (nanoGLA) hours post-dose (Figure 6.30A).

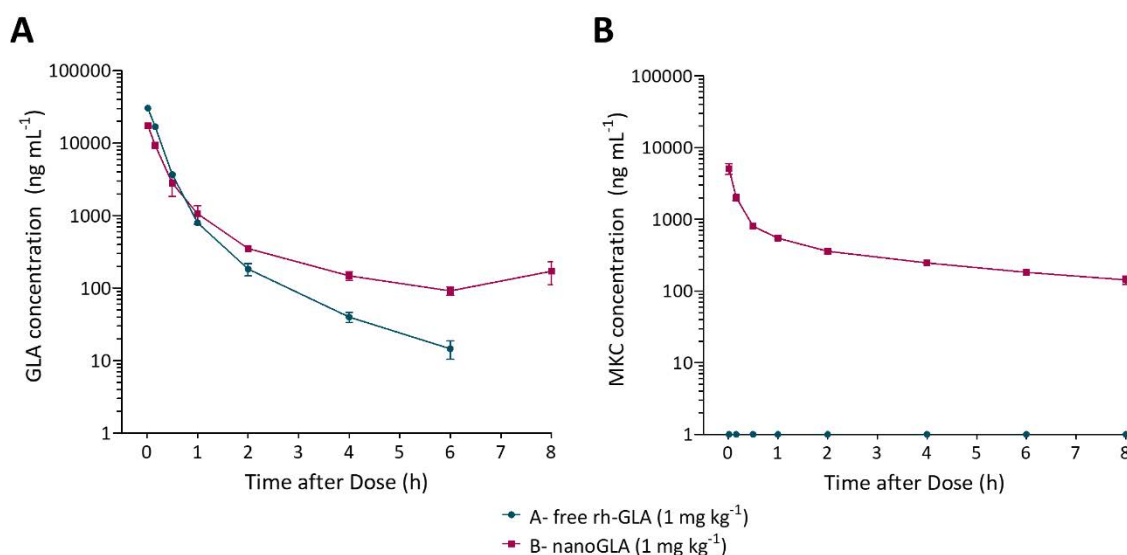


**Figure 6.30.** Mean ( $\pm$  SD) concentration of (A) total GLA, and (B) MKC, in male rat plasma following a single intravenous administration of free rh-GLA or nanoGLA (1 mg kg<sup>-1</sup> of GLA dosing). Assay performed by Covance SL (UK).

Concentration-time profiles of total GLA allow to obtain pharmacokinetic parameters (Table 6.18), such as half-life ( $t_{1/2}$ ) or clearance (CL) or  $V_{ss}$  (see Chapter 9.11). The conjugation of GLA in the

liposomal vehicle resulted in an increased half-life over the free GLA (1.80 h for nanoGLA against 1.11 h for free rh-GLA). Total GLA did not appear to be readily extracted by the liver following IV bolus administration of GLA or nanoGLA and was not highly distributed to the tissues. It is indicated by CL and  $V_{ss}$  values. CL values were less than liver blood flow in a 0.25 kg rat ( $3312 \text{ mL h}^{-1} \text{ kg}^{-1}$ ), meaning that total GLA is not readily extracted by the liver after the IV administration.  $V_{ss}$  values ranged from  $33.0 - 41.6 \text{ mL kg}^{-1}$  and did not exceed the total body water of a 0.25 kg rat ( $668 \text{ mL kg}^{-1}$ ), indicating that total GLA is not highly distributed to the tissues after IV administration.

**Table 6.18.** Pharmacokinetic parameters regarding total GLA (in rh-GLA and nanoGLA groups) and MKC (only nanoGLA group), including

Analyte	Dose Group	$C_0$ ( $\text{ng mL}^{-1}$ )	$C_{max}$ ( $\text{ng mL}^{-1}$ )	$t_{1/2}$ (h)	CL ( $\text{mL h}^{-1} \text{ kg}^{-1}$ )	$V_{ss}$ ( $\text{mL kg}^{-1}$ )
GLA	A- rh-GLA	$32400 \pm 2400$	$30400 \pm 2100$	$1.09 \pm 0.06$	$108 \pm 3$	$37.1 \pm 4$
	B- nanoGLA	$18600 \pm 1200$	$17400 \pm 1000$	$1.80^{\dagger}$	$141^{\dagger}$	$182^{\dagger}$
MKC	A- rh-GLA	NA	NA	NA	NA	NA
	B- nanoGLA	$5650 \pm 1070$	$5090 \pm 880$	$3.47^{\dagger}$	$258^{\dagger}$	$1040^{\dagger}$

NA = Not Applicable; Mean  $\pm$  SD of three animal ( $^{\dagger}$  Values from  $n \leq 2$ , due to a lack of a distinct elimination phase in some animals). Back-extrapolated concentration at time 0 ( $C_0$ ), maximum observed concentration ( $C_{max}$ ), elimination half-life ( $t_{1/2}$ ), clearance (CL), and volume of distribution at steady-state ( $V_{ss}$ ) (see **Chapter 9.11**). Assay performed by Covance SL (UK).

Besides, in the nanoGLA group, not only GLA was quantified at each time point, but also MKC, a membrane component of the nanoliposomal formulation and used as indicator of liposome exposure. After IV bolus administration of nanoGLA, concentrations readily declined and were measurable through 8 h post-dose (**Figure 6.30B**).

Again, concentration-time profiles of MKC allowed to obtain pharmacokinetic parameters (**Table 6.18**). Half-life values ranged  $3.34 - 3.61$  h, superior to the obtained values for GLA. MKC did not appear to be readily extracted by the liver following IV bolus administration of nanoGLA, since estimated CL values were less than liver blood flow ( $3312 \text{ mL h}^{-1} \text{ kg}^{-1}$  for a 0.25 kg rat), but MKC did appear to be highly distributed to the tissues (estimated  $V_{ss}$  were  $1030 - 1050 \text{ mL kg}^{-1}$ , which exceeded the total body water of a rat (0.25 kg rat,  $668 \text{ mL kg}^{-1}$ ). According to PK theoretical parameters, if  $V_{ss}$  is significantly higher than the rat volume of total body water ( $668 \text{ mL kg}^{-1}$ ), it means that the analyte appears to be dissolved in a volume higher than the total amount of water in the body. It can be only explained if an analyte is sequestered by some organs or tissues, although this distribution probably does not be uniform.

Overall, this circulation time differences between GLA and MKC in the nanoGLA, can be due to a GLA release from the liposomal vehicle, being the GLA cleared or uptaken by the cells.

## 6.7. NanoGLA designed as Orphan Drug by the European Medicines Agency

The outstanding results obtained with the nanoliposomal formulation of GLA (nanoGLA) permitted to request the orphan medicinal product designation to the European Medicines Agency (EMA) for the treatment of Fabry Disease. Contact with the EMA was conducted through the Smart-4-Fabry project, with the significant contribution of Drug Development & Regulation (DDR) SL (Barcelona), partner of the project.

Rare diseases overall considered as a group represents a serious health problem. As a case of example, around 30 million people living in the European Union suffer from a rare disease. Therefore, the EMA has put efforts in facilitating the development and authorization of medicines intended for rare diseases, which in the medical world are named “orphan medicines”. To qualify for orphan designation, a medicine must be intended for life-threatening or chronically debilitating diseases, with low prevalence (< 5 in 10,000), and with a new significant benefit if a satisfactory treatment already exists. Thus, designated orphan medicines can benefit from some incentives in the EU, such as protocol assistance specific for orphan medicines, fee reductions, and market exclusivity once the medicine is on the market.<sup>29</sup>

In the case of Fabry Disease (FD), it is reported to have an estimated birth prevalence of 1–5 per 10,000, according to Orphanet, which published on January 2020 a list of the prevalence and incidence of rare disease (ORPHA number: 324).<sup>30</sup> Moreover, as explained in the Introduction Chapter of this Thesis, three products are currently authorized in the EU as treatments for Fabry Disease: two GLA for enzymatic replacement therapy (ERT), i.e., Replagal<sup>®</sup> and Fabrazyme<sup>®</sup>, and the chaperone Galafold<sup>®</sup>.

On the one hand, both ERT medicinal products were granted with an orphan designation at the same time (August 2000), since there were not satisfactory treatments for Fabry Disease at the time of the Orphan Drug Designation (ODD) application. However, the ERT approach with these two products showed several disadvantages: (i) limited efficacy in patients with an advanced stage of the disease, (ii) short circulation time of the enzyme, due to the sequestration of the enzyme by the liver and the immune system, (iii) high cost of the treatment, (iv) no crossing of the BBB that precludes any reduction of Gb3 deposits in the brain. Finally, to note, the EU orphan status for these two ERT products, Replagal<sup>®</sup> and Fabrazyme<sup>®</sup>, have already expired. On the other hand, the chaperone Galafold<sup>®</sup> is in the EU market since 2016, and already has an orphan status for FD. However, this product is only beneficial for a

small number of FD patients (only those with residual GLA activity) and cannot be used in combination with ERT.

With our strategy of conjugating the GLA in liposomes, we intended to improve the current treatments and overcome some of the existing limitations. Thus, a selection of the above explained results obtained for nanoGLA (i.e., physicochemical characterization, in vitro evaluation, PK, and in vivo efficacy) were collected in a briefing document and submitted at the EMA to apply for orphan drug designation (ODD), since our results demonstrated an improved efficacy of nanoGLA over Replagal<sup>®</sup>, which can be considered appropriate for supporting the significant benefit. Replagal<sup>®</sup> was chosen as comparator for practical considerations, since as it is presented as a liquid solution stored at 2 – 8 °C its stability is more suitable from the experimental point of view, whereas Fabrazyme<sup>®</sup> is a lyophilized product and should be used immediately after reconstitution. Moreover, the two proteins were remarkably similar, suggesting that both GLA products could be good comparators.<sup>31</sup> Besides, Galafold<sup>®</sup> was not considered since its efficacy is limited to specific FD genetic variants, and nanoGLA is expected to be used in a wider range of population.

Finally, the Committee for Orphan Medicinal Products was in the opinion that the nanoGLA product satisfies the criteria for designation and recognized the significant potential benefit that nanoGLA can offer to Fabry disease patients. Therefore, nanoGLA medicinal product was designated as an orphan medicinal product for the orphan condition: treatment of Fabry disease (Designation number EU/3/20/2396),<sup>32</sup> achieving an important milestone in the process development of the nanoGLA. Additionally, these results were also filed in a IP protection of nanoGLA through a selection patent application (EP21382062).<sup>33</sup>

## 6.8. Toxicology studies

At this point, toxicity studies have been initiated at Covance SL (UK) in rodents (rats), as part of the toxicology package to support a first in human clinical trial. Reaching this preclinical stage is an important milestone in the pharmaceutical development of a drug product. According to ICH guideline S6 (R1) *Preclinical safety evaluation of biotechnology-derived pharmaceuticals* (EMA, EMA/CHMP/ICH/731268/1998, June 2011) nanoGLA's toxicology evaluation should include the use of relevant species. A relevant species is one in which the GLA will be pharmacologically active owing to the expression of its receptor. Rat is considered relevant for nanoGLA's toxicology assessment due to production of endogenous GLA (Galafold's EMA assessment report. EMA/272226/2016, April 2016). Additionally, the amino acid (aa) sequence homology of human  $\alpha$ -galactosidase A and that of the rat, i.e., 80 % sequence homology (determined by basic local alignment search tool (BLAST) from NCBI/NIH database), has been considered.



In these toxicology studies, two nanoGLA dose levels were assessed, as well as empty-liposomes at the equivalent highest dose were used as control to evaluate the effect of the liposomal vehicle. Doses have been expressed as the GLA content of the formulation, as indicated in **Table 6.19**. The high-dose level corresponds to the maximum feasible dose of nanoGLA that can be administered via this formulation (achieved by administering the maximum feasible volume in rat, i.e., 5 mL kg<sup>-1</sup>).<sup>1</sup> The low-dose level was an appropriate low-dose based on the potential efficacious dose. Detailed conditions can be found in **Chapter 9.13**.

First, a one-week range finding dose toxicology study has been performed to ensure that the proposed doses are well tolerated following intravenous (bolus) administration to the rat on days 1, 4 and 8 of the dosing phase. Then, once demonstrated the tolerability, studies have been moved to a 4-weeks toxicity and toxicokinetic study, which has been performed under GLP conditions with the aim to evaluate the toxicity and determine the toxicokinetic of nanoGLA when administered weekly via intravenous (bolus) to the rat for at least 4 weeks.

Results of these toxicology studies are not shown in this dissertation since part of the data have still not been included in the GLP- audited final report.

**Table 6.19.** Dosing of the four different groups, according to GLA content of the formulation\*.

	Group	Dose level	
		(mg GLA <sup>-1</sup> kg <sup>-1</sup> occasion)	(mL sample kg <sup>-1</sup> )
1	Control	NA	5
2	Empty-liposomes	NA	5
3	Low-nanoGLA*	0.4	1.5
4	High-nanoGLA*	1.3	5

\* see GLA concentration in **Table 6.8** and **Table 6.12**.

## 6.9. Summary and Conclusions

In this Chapter, final scale up production of nanoGLA was successfully achieved, in the required amount and quality for starting the preclinical evaluation in vivo. The previous GLAcmycHis used during the nanoGLA optimization presented in the previous **Chapter 5** was substituted by a new rh-GLA tag-free and FTO, which the potential to be used in further stages of the pharmaceutical development. This change of GLA version, indirectly improved the physicochemical characteristics of the nanoGLA liposomes, meeting all the established CQA within the specification range. NanoGLA and empty-liposomes in enough amounts were properly produced, by a first step using DELOS-susp followed by the TFF procedure, in two separately production runs.

Further, new analytical methodologies were also implemented, such as an RP-HPLC method for GLA quantification, or a LC-MS method for MKC determination in biological samples. The tracking of MKC from empty-liposomes in plasma showed an enhanced circulation time over the free MKC, confirming the suitability of the tracking of MKC as an indicator of liposomal presence in in vivo experiments.

In a single and a repeated-dose (twice per week up to 8 doses) efficacy study using a mice model of Fabry disease, this novel product has induced higher reduction of Gb3 levels in all tested tissues, including effects for the first time in brain, compared to the non-nanoformulated enzymes (included the commercially available agalsidasa alfa Replagal®).

Then, preclinical evaluation of nanoGLA showed an increased efficacy in reducing the Gb3 levels in several organs, including heart, spleen, kidney, and brain, after a single and repeated administration using a mice model of Fabry disease, as well as an increased blood circulation time in a pharmacokinetic study performed in rats. Overall, the results obtained with the nanoliposomal formulation of GLA (nanoGLA) were positive enough to be designated by the European Medicine Agency (EMA) as orphan medicinal product for the treatment of Fabry Disease.

Besides, the novel nanoGLA formulation achieved the regulatory preclinical stage of development with a first GLP toxicity study in rodents.

## 6.10. References

1. Boersen, N., Lee, T. & Hui, H. W. Development of Preclinical Formulations for Toxicology Studies. in *A Comprehensive Guide to Toxicology in Preclinical Drug Development* 69–86 (Elsevier Inc., 2013). doi:10.1016/B978-0-12-387815-1.00004-6.
2. Son, Y. W., Choi, H. N., Che, J. H., Kang, B. C. & Yun, J. W. Advances in selecting appropriate non-rodent species for regulatory toxicology research: Policy, ethical, and experimental considerations. *Regul. Toxicol. Pharmacol.* **116**, 104757 (2020).
3. Schrag, M. & Regal, K. Pharmacokinetics and Toxicokinetics. in *A Comprehensive Guide to Toxicology in Preclinical Drug Development* 31–68 (Elsevier Inc., 2013). doi:10.1016/B978-0-12-387815-1.00003-4.
4. Glassman, P. M. & Muzykantov, V. R. Pharmacokinetic and pharmacodynamic properties of drug delivery systems. *J. Pharmacol. Exp. Ther.* **370**, 570–580 (2019).
5. Fan, J. & De Lannoy, I. A. M. Pharmacokinetics. *Biochem. Pharmacol.* **87**, 93–120 (2014).
6. Andrade, E. L. *et al.* Non-clinical studies in the process of new drug development - Part II: Good laboratory practice, metabolism, pharmacokinetics, safety and dose translation to clinical studies. *Brazilian J. Med. Biol. Res.* **49**, e5646 (2016).
7. Syubaev, R. D. *et al.* Expert Evaluation of Preclinical Toxicokinetic Studies of Pharmaceuticals (Review). *Pharm. Chem. J.* **52**, 753–757 (2018).
8. Reigner, B. G. & Blesch, K. Estimating the starting dose for entry into humans: Principles and practice. *Eur. J. Clin. Pharmacol.* **57**, 835–845 (2002).
9. Kille, J. W. Regulatory Toxicology. in *A Comprehensive Guide to Toxicology in Preclinical Drug Development* 677–711 (Elsevier Inc., 2013). doi:10.1016/B978-0-12-387815-1.00028-9.
10. Raj, G. M. *Introduction to Basics of Pharmacology and Toxicology. Introduction to Basics of Pharmacology and Toxicology* vol. 1 (Springer, 2019).
11. Corchero, J. L. *et al.* Integrated approach to produce a recombinant, His-tagged human  $\alpha$ -galactosidase A in mammalian cells. *Biotechnol. Prog.* **27**, 1206–1217 (2011).
12. Khan, F. *et al.* Histidine affinity tags affect MSP1 42 structural stability and immunodominance in mice. *Biotechnol. J.* **7**, 133–147 (2012).
13. Beauvais, D. M., Ell, B. J., McWhorter, A. R. & Rapraeger, A. C. Syndecan-1 regulates  $\alpha$ v $\beta$ 3 and  $\alpha$ v $\beta$ 5 integrin activation during angiogenesis and is blocked by synstatin, a novel peptide inhibitor. *J. Exp. Med.* **206**, 691–705 (2009).

14. Ohshima, T. *et al.*  $\alpha$ -Galactosidase A deficient mice: A Model of Fabry Disease. *Proc. Natl. Acad. Sci. U. S. A.* **94**, 2540–4 (1997).
15. Najafian, B. *et al.* Progressive podocyte injury and globotriaosylceramide (GL-3) accumulation in young patients with Fabry disease. *Kidney Int.* **79**, 663–670 (2011).
16. Schiffmann, R. *et al.* Screening, diagnosis, and management of patients with Fabry disease: conclusions from a ‘Kidney Disease: Improving Global Outcomes’ (KDIGO) Controversies Conference. *Kidney Int.* **91**, 284–293 (2017).
17. Hsu, M. J. *et al.* Identification of lysosomal and extralysosomal globotriaosylceramide (Gb3) accumulations before the occurrence of typical pathological changes in the endomyocardial biopsies of Fabry disease patients. *Genet. Med.* **21**, 224–232 (2019).
18. Tian, W. *et al.* The glycosylation design space for recombinant lysosomal replacement enzymes produced in CHO cells. *Nat. Commun.* **10**, 1–13 (2019).
19. Shen, J. S. *et al.* Mannose receptor-mediated delivery of moss-made  $\alpha$ -galactosidase A efficiently corrects enzyme deficiency in Fabry mice. *J. Inherit. Metab. Dis.* **39**, 293–303 (2016).
20. Ioannou, Y. A., Zeidner, K. M., Gordon, R. E. & Desnick, R. J. Fabry disease: Preclinical studies demonstrate the effectiveness of  $\alpha$ -galactosidase a replacement in enzyme-deficient mice. *Am. J. Hum. Genet.* **68**, 14–25 (2001).
21. Togawa, T. *et al.* Tissue and plasma globotriaosylsphingosine could be a biomarker for assessing enzyme replacement therapy for Fabry disease. *Biochem. Biophys. Res. Commun.* **399**, 716–720 (2010).
22. Kodama, T. *et al.* Differences in cleavage of globotriaosylceramide and its derivatives accumulated in organs of young Fabry mice following enzyme replacement therapy. *Mol. Genet. Metab.* **120**, 116–120 (2017).
23. Cabrera, I. *et al.*  $\alpha$ -Galactosidase-A Loaded-Nanoliposomes with Enhanced Enzymatic Activity and Intracellular Penetration. *Adv. Healthc. Mater.* **5**, 829–840 (2016).
24. European Medicine Agency. ICH guideline Q8 (R2) on pharmaceutical development. *EMA/CHMP/ICH/167068/2004 Committee for Human Medicinal Products ICH* vol. 8 [http://www.ema.europa.eu/docs/en\\_GB/document\\_library/Scientific\\_guideline/2009/09/WC500002872.pdf](http://www.ema.europa.eu/docs/en_GB/document_library/Scientific_guideline/2009/09/WC500002872.pdf) (2009).
25. Toh, M.-R. & Chiu, G. N. C. Liposomes as sterile preparations and limitations of sterilisation techniques in liposomal manufacturing. *Asian J. Pharm. Sci.* **8**, 88–95 (2013).
26. Soares, G. C. *et al.* Supercritical CO<sub>2</sub> technology: The next standard sterilization technique?

- Mater. Sci. Eng. C* **99**, 520–540 (2019).
27. András, C. D. *et al.* A possible explanation of the germicide effect of carbon dioxide in supercritical state based on molecular-biological evidence. *Med. Hypotheses* **74**, 325–329 (2010).
  28. Cabrera, I. Nanovesicle-bioactive conjugates to be used as nanomedicines, prepared by a one-step scalable method using CO<sub>2</sub>-expanded solvents. *Tesis doctoral* (Universitat Autònoma de Barcelona (UAB), 2013).
  29. European Medicines Agency. Scientific advice and protocol assistance. <https://www.ema.europa.eu/en/human-regulatory/research-development/scientific-advice-protocol-assistance>.
  30. Orphanet. Fabry Disease Orpha number 324. [https://www.orpha.net/consor/cgi-bin/Disease\\_Search.php?lng=EN&data\\_id=94&Disease\\_Disease\\_Search\\_diseaseGroup=fabry&Disease\\_Disease\\_Search\\_diseaseType=Pat&Disease\(s\)/group\\_of\\_diseases=Fabry-disease&title=Fabry disease&search=Disease\\_Search\\_Simple](https://www.orpha.net/consor/cgi-bin/Disease_Search.php?lng=EN&data_id=94&Disease_Disease_Search_diseaseGroup=fabry&Disease_Disease_Search_diseaseType=Pat&Disease(s)/group_of_diseases=Fabry-disease&title=Fabry%20disease&search=Disease_Search_Simple) (2012).
  31. Lee, K. *et al.* A biochemical and pharmacological comparison of enzyme replacement therapies for the glycolipid storage disorder Fabry disease. *Glycobiology* **13**, 305–313 (2003).
  32. European Commission. Community Register of orphan medicinal products - Designation number: EU/3/20/2396. *EU/3/20/2396* <https://ec.europa.eu/health/documents/community-register/html/o2396.htm> (2021).
  33. Ventosa, N. *et al.* Liposomes and its use for enzyme delivery. *EP 21382062.4-1112* (2021).

” *Don't let anyone rob you of your imagination, your creativity or your curiosity. It's your place in the world; it's your life. Go on and do all you can with it, and make it the life you want to live*

— Mae Jemison

# 7

## **New targeted-liposomes for the transport across the Blood-Brain Barrier**

### **7.1. Intra-brain delivery of drugs: a real challenge for CNS disease treatment**

Brain controls a lot of multiple physiological processes that results critical in maintaining the functions of human body. Brain is the most complex and the most energy-consuming organ in all the vertebrate systems; it consumes 15 % of cardiac output and up to 60 % of blood glucose, despite its minimal body weight proportion (2 %).<sup>1</sup>

Unfortunately, these functions sometimes do not work properly, leading to central nervous system (CNS) diseases. Nowadays, there is a global prevalence of this type of diseases affecting brain and CNS, and their morbidity is continually rising. Currently, CNS disorders are the second cause of death in Europe, and the first cause of DALYs (i.e., disability adjusted life years) that refers to the years of life lost or lived with disability.<sup>2</sup>

The reason of this prevalence is the failure of current drugs due to the poor permeation of CNS drugs across the blood-brain barrier (BBB). The BBB acts as a very selective permeable barrier, that allows the entrance of nutrients but restricts the introduction of potentially harmful substances.<sup>3</sup> It is reported

that > 98 % of small molecule drugs and practically the 100% of the large-molecule pharmaceuticals, e.g., peptides, recombinant proteins, monoclonal antibodies, RNA interference (RNAi)-based drugs, and gene therapies, do not enter the brain via circulations, since they are not able to cross the BBB. Although there are few disorders treatable with small molecule drug therapy (e.g., depression, schizophrenia, chronic pain, and epilepsy), there are still a huge number of neurological disorders without effective drug treatment.<sup>4</sup> Some of these diseases are Alzheimer's disease, Parkinson's disease, Huntington's disease, amyotrophic lateral sclerosis, multiple sclerosis, brain cancer, stroke, or lysosomal storage disorders. Overall, intra-brain delivery of drugs has become a real challenge for CNS disease treatment.

### 7.1.1. Structure of brain and blood-brain barrier

Human brain is composed of four anatomical parts: cerebrum, cerebellum, brain stem, and the spinal cord, and it is surrounded by the calvarium or skull. The space between the brain and the skull is filled with cerebrospinal fluid (CSF), originated from the cerebral blood.

At the cellular level, the brain parenchyma is composed of several types of cells, that can be mainly divided in neurons, supporting glial cells, and a network of endothelial micro cerebral vessels. The complex interaction of these cells constitutes the neurovascular unit (NVU) (**Figure 7.1**).<sup>5</sup> Micro cerebral vessels are mainly composed by vascular endothelial cells enveloped by pericytes cells, which share a common basal lamina with them. They have specific functions, such as a structural role regulating the endothelial cell structure, and control of the blood flow and substance exchange. These cells (pericytes and vascular endothelial cells) are surrounded by other supporting glial cells, such as the astrocytes (which provide links to neurons), oligodendrocytes (involved in the myelination process), or microglia (related to the immune response).<sup>5</sup> The unoccupied parenchyma space between cells and microvasculatures (named brain extracellular space or ECS) is filled with confluent fluids from the cells, capillaries, and CSF, and receives the name of interstitial fluid (ISF).

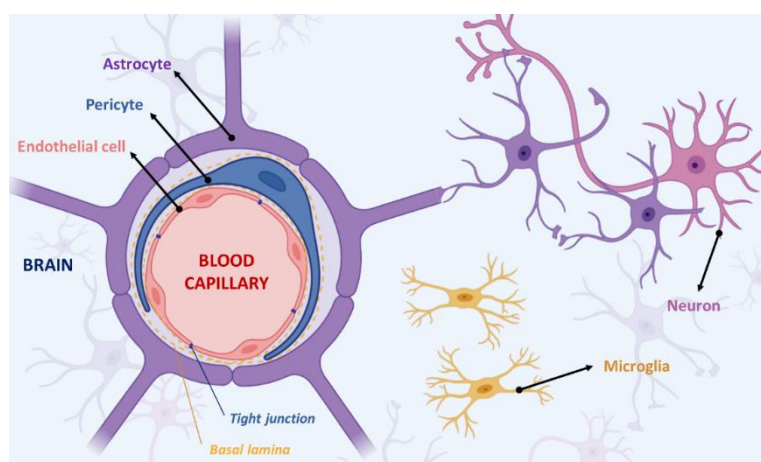


**Figure 7.1.** Cellular constituents of the neurovascular unit (NVU), formed by capillary endothelial cells and pericytes, surrounded by basal lamina and astrocytic end feet. Adapted from <sup>6,7</sup>.

As abovementioned, the transference of substance into the brain is a very well-controlled process, and it is mainly due to four kind of mass circulating ways: (i) CSF-blood exchange, (ii) CSF-ISF exchange, (iii) CSF-lymph exchange, (iv) ISF-blood exchange. Among them, the ISF-blood exchange, i.e., between the interstitial fluid and blood, is one of the most relevant transfer processes with special importance and strictly confined by the BBB.<sup>1</sup>

#### 7.1.1.1. Definition and role of blood-brain barrier

The blood-brain barrier (BBB) is a physiological barrier between blood and the interstitial fluid (ISF). It is composed of specific brain microvascular endothelial cells, characterized by having tight junctions (TJ) joining adjacent cells, surrounded by an outer layer of permeable basal membrane (**Figure 7.2**). Tight junctions are constituted by occludin, claudins, and junction associated molecules (JAMs) transmembrane protein families. TJ act as a packing physical barrier, restricting the paracellular access of soluble molecules, and forcing them to take a transcellular route across the BBB.<sup>6</sup> Besides the physical barrier, the BBB is also characterized by the expression of substrate-specific transporters for mediating, and limiting, the transport of substances from blood to the brain. Finally, BBB also shows an enzymatic barrier with metabolic enzymes able to metabolize non-desired molecules or drugs.<sup>1,6</sup>

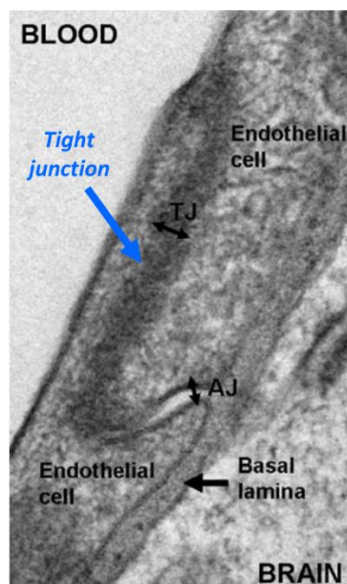


**Figure 7.2.** Electronic microscopy image of a rat brain section showing a tight junction (TJ) between two endothelial cells, from Weiss et al.<sup>8</sup>

#### 7.1.2. Transport pathways for nutrient delivery at the BBB

BBB plays an important role in the selectivity and permeability of substances, such as nutrients, metabolites, or drugs, from blood to CNS. However, the transport of necessary molecules to the brain is a very well-regulated process and can take place through the BBB via the following pathways (**Figure 7.3**):



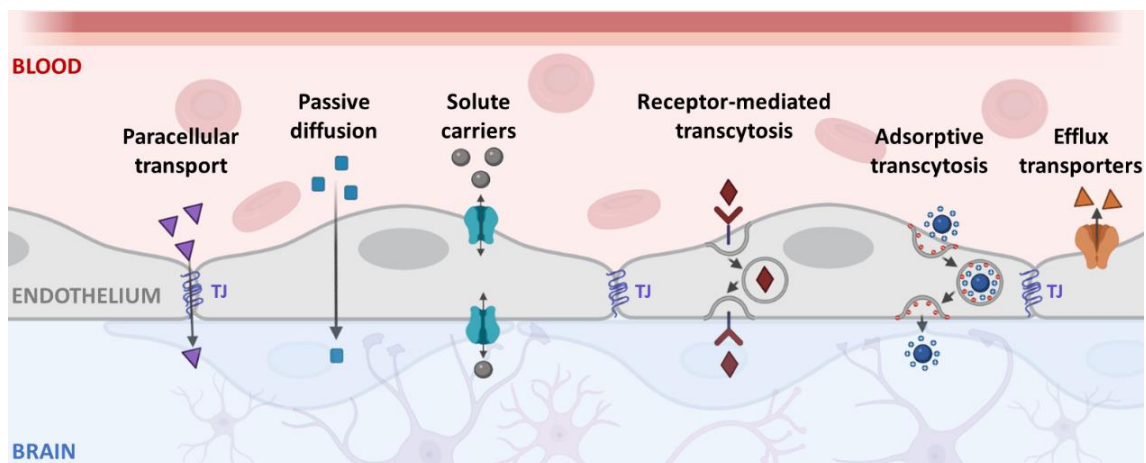


**Figure 7.3.** Transport pathways through the BBB. Adapted from <sup>9,10</sup>.

### 7.1.2.1. Passive diffusion

According to the high restriction function of the BBB, there are only very few molecules able to be up taken by passive diffusion, with strong dependence on their size and lipid solubility. Generally, BBB is only partially permeable for small compounds with lower molecular weight ( $MW < 400 - 600$  Da) and with high lipid-solubility, which is commonly estimated in the literature by the oil/water partition coefficient. **Figure 7.4** clearly illustrates the impact of lipid-solubility in the brain uptake, in which all the represented substances met the first requirement regarding small size for possible BBB crossing by passive diffusion. On the one hand, high permeability values are obtained for high lipid-soluble molecules such as ethanol, nicotine, iodoantipyrine, and diazepam.<sup>11</sup> On the other hand, polar molecules show significant lower brain uptake, such as glycine or catecholamines (e.g., epinephrine, morphine, dopamine). However, some molecules, such as D-glucose, showed unexpected high BBB permeability considering their high polar character. This phenomenon points out the existence of other transport pathways.

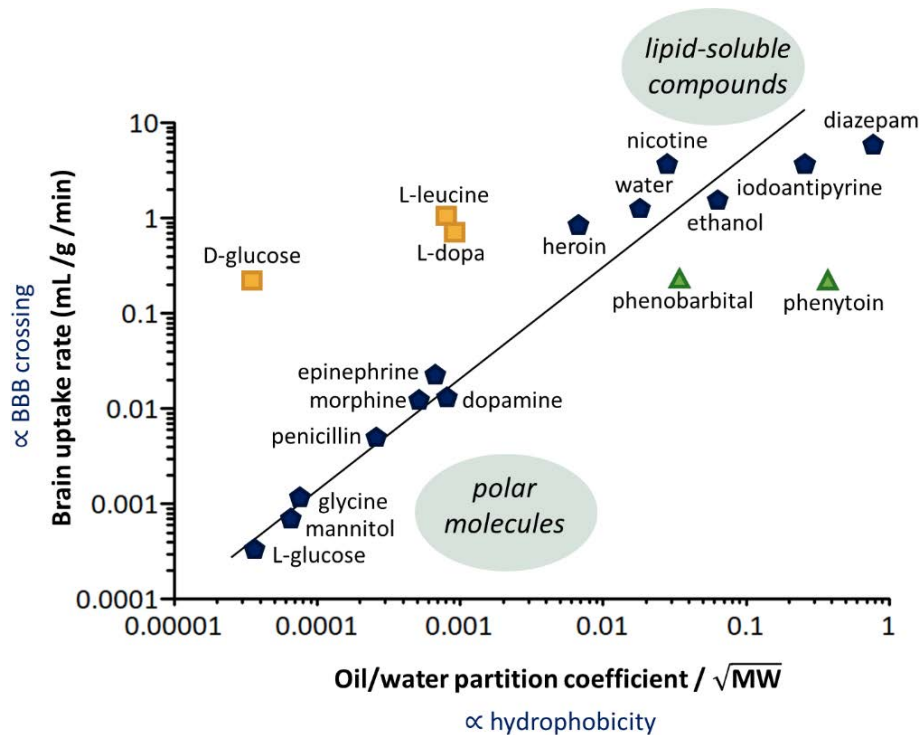


**Figure 7.4.** Brain uptake rate of some small molecules ( $\leq 400 - 600$  Da) in relation with their oil/water partition coefficient, as a measure of their lipid solubility, and adjusted for differences in MW. BBB crossing based on passive diffusion; some compounds showed higher values (square symbol) because of specific active transport, or lower values (triangle symbol) because of their binding to plasma proteins. Adapted from Laterra et al.<sup>11</sup>

### 7.1.2.2. Carrier-mediated transport

Some small-water soluble molecules (e.g., D-glucose, amino acids, lactic acid, ketone bodies, fatty acids, metal ions, vitamins, etc.) are transported by solute carriers (SLC), an especially important pathway for nutrient delivery to the CNS. SLC are proteins placed in the cell membrane able to transfer relatively small polar molecules.<sup>9</sup> Among them, it is worthy to highlight the glucose and the amino acid transporters.<sup>12</sup> Penetration of some drugs can be mediated by the conjugation of the drugs to the substrates of these transporters. However, this transport is sometimes inhibited by the endogenous substrates, that act as competitive ligands.<sup>1</sup>

### 7.1.2.3. Receptor-mediated transport

This transport pathway is very relevant for bigger macromolecules, and it is characterized by a regulated endocytosis process initiated by the interaction of the compound with its specific membrane receptor.<sup>1,9</sup> Briefly, a circulating ligand interacts with its specific receptor, placed at the membrane of the brain endothelium. Then, the endocytosis process of the receptor-ligand complex is initiated, including its clustering, endocytosis, and transcytosis, and finally released to the other side of the polarized endothelial cell.<sup>3</sup> Receptor-mediated transport is energy-dependent, bidirectional, and concentration-

independent, and it is the main transport pathway of peptide hormones (e.g., insulin, epidermal growth factor, leptin, and glucagon) and other proteins including transferrin, lactoferrin, and lipoproteins.<sup>1,9</sup>

#### **7.1.2.4. Adsorptive-mediated transport**

Some cationic species can interact with the overall negatively charged cell membrane of the brain capillary endothelial cells. Endocytosis can be facilitated by the formation of hydrogen bonds between the cell and the positively charged substances. This interaction is unspecific, and positive compounds can also have a high affinity to negative plasma proteins, leading to an early elimination by the RES and reducing the change of arriving to the brain.<sup>10</sup>

#### **7.1.2.5. Efflux transporters**

Finally, there are also active efflux carriers (e.g., ABC transporters family) able to intercept some of the lipophilic molecules diffused in a passive way, and pump them out of the endothelial cell, back again to the blood. This is a neuroprotectant and detoxifying function to remove some endogenous or exogenous potentially neurotoxic molecules.<sup>10,13</sup>

### **7.1.3. Nanocarriers as a strategy to enhance drug delivery to the brain**

This introduction to brain structure and nutrient transport highlights the fact that CNS drug development is hindered by the selective and restricted transport of drug candidates (especially for protein and nucleic acid) across the blood-brain barrier (BBB). To overcome this restriction, several strategies have been developed. Delivery of neurotherapeutic agents to the CNS can be divided into invasive and non-invasive drug delivery categories.<sup>13</sup> Invasive strategies are based on the physical penetration of the BBB, either for surgical procedures (e.g., implantation of a catheter followed by drug infusion) or for a transient opening of the BBB (e.g., BBB disruption using ultrasound with microbubbles). Invasive methods are not patient-friendly and show potential safety concerns. On the other hand, non-invasive strategies aim to penetrate the BBB exploiting its natural endogenous transport pathways, without BBB physical disruption (e.g., chemical modification of drugs or conjugation in drug delivery systems). In the recent years, the use of nanocarriers (e.g., liposomes, albumin nanoparticles, polymeric nanoparticles, dendrimers) has become an interesting strategy to overcome the limitation of drug transport to the brain. The development of nanocarriers has focused in the improvement of some safety, pharmaceutical, and pharmacology aspects.<sup>14</sup>

One benefit of using nanocarriers is the prolonged circulation of a drug in plasma, that usually leads in an improved therapeutic index and an increased plasma availability. The amount of encapsulated drug per nanoparticle is also important, since low encapsulation efficiencies results in poor therapeutic index and necessity of high doses, that can also result to an increase in side-effects and toxicity.<sup>14</sup> Finally, the conjugation of targeting ligands to the nanovehicle (e.g., antibodies, small molecules, peptides, etc.) can enhance the drug biodistribution in favor to the brain, as well as affect other pharmaceutical properties, such as stability, immunogenicity, pharmacokinetics, and safety.

As extensively mentioned in other sections of this thesis, liposomes are one of the drug delivery systems with strong presence in research and clinical use. This Chapter is focused on the exploration of their potential ability to cross the BBB and reach the brain, a challenge which could open the door to further transport and drug delivery studies.

Mostly all non-targeted liposomes are not able to cross the BBB in enough quantity or cannot release the entrapped drug in the brain area. There are only few non-targeted liposomal-drug systems with a moderately effectiveness to brain delivery when they are involved in disease in which the blood-brain barrier integrity is compromised (e.g., in some brain tumors). Pegylated liposomal doxorubicin (DOX) behaves as an example of moderately effective nanodrug to treat primary brain tumor.<sup>15</sup> Otherwise, their biodistribution can be influenced when targeted liposomes are used. For example, comparing non-targeted and glutathione-targeted pegylated DOX-liposomes, 3-fold higher DOX retention in brain was found for glutathione-targeted liposomes, despite non-targeted liposomes showed a major efficacy in the rest of organs.<sup>16,17</sup>

Other targeted ligands used in liposomal systems include larger proteins (e.g., antibodies against transferrin or insulin receptors),<sup>5</sup> peptides (e.g., angiopep-2, ApoE-mimetic peptide or COG133), sugars (e.g., glucose) or glycoproteins (e.g., lactoferrin).<sup>7,18</sup>

#### 7.1.4. Experimental methods to evaluate drug delivery across the BBB

Different approaches and analytical methods can be employed to study the transport across the BBB. Among them, the most reliable techniques are using live model animals, although the development of in vitro cell-culture models can enable the study of BBB transport at molecular or cellular level, in a more accessible, flexible, and reproducible way.<sup>19</sup>

##### 7.1.4.1. In vitro BBB cell models

Although different design, all the in vitro cell models tends to incorporate the following elements: (i) “barrier” cells grown on a semipermeable membrane or substrate dividing two (liquid) compartments, representing circulatory system and brain side, separated by the BBB; (ii) extracellular matrix deposited in-between cells and the semipermeable substrate; and (iii) inducing “brain microenvironment”.<sup>20</sup> Sometimes, the in vitro model can increase its complexity by the use of an induced flow, e.g. laminar flow (hollow fibers) or microfluidics (BBB on a chip), to mimic the in vivo sheer stress. The usual set up is represented in **Figure 7.5.** including some examples of each building part. The compound of interest is usually incubated in the upper compartment (representing blood circulating system), and their passage into the below compartment (representing brain parenchyma) is quantified over time.

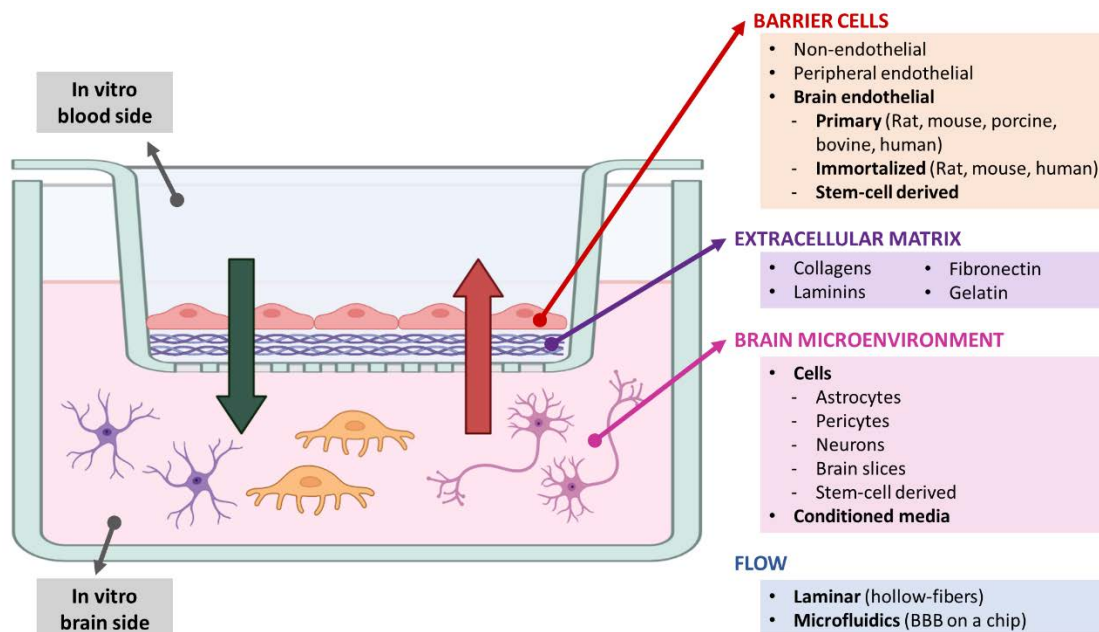


**Figure 7.5.** Main components of a standard in vitro BBB model. Adapted from Stanimirovic et al.<sup>20</sup>

Unfortunately, reliable in vitro models are in general still far away for substituting in vivo assays using animals. Representation of the in vivo condition regarding BBB barrier tightness and specific transporter expression is still poor represented. However, in vitro cell-culture models can be very useful as a first screening tool for finding potential drugs able to permeate the BBB, as well as studying transport properties.<sup>21</sup>

#### 7.1.4.2. In vivo methods

##### Intravenous Injection Method

The more used approach for evaluating the permeation of some substance across the BBB is the intravenous injection of the substance followed by the analyte concentration determination at different times in brain tissue, plasma, and cerebrospinal fluid. An advantage of this method is that the physiological system remains intact, allowing a realistic assessment since brain is not damaged or altered.<sup>20</sup> However, many animals need to be used to obtain statistically relevant data, i.e., a separate animal for each data point, since serial sampling from the same animal is not allowed and leading to less precision PK-PD studies.<sup>20,22,23</sup> Moreover, the discrimination between vascular and parenchymal or extracellular and intracellular analyte location is also difficult to evaluate.<sup>20</sup>

##### Brain Perfusion Technique

This technique developed by Smith & Allen and Takasato et al.<sup>22,24</sup> consists in the direct infusion of the compound of interest dissolved in a physiological media into the heart or a major vessel, that leads directly to the brain by the use of a perfusion pump. At a given time, the animal is sacrificed, and the

amount of substance in the brain is determined. For that purpose, radiolabeled substances are usually employed. An interesting advantage of this method is that the accurate modification of perfusate composition and flow rate allows the evaluation of solute concentrations larger than generally tolerated *in vivo*, as well as the avoidance of the compound transit to other organs.<sup>22,24</sup> However, although this technique allows higher sensitivity and more accurate modification of perfusate composition and flow rate, brain perfusion method again needs to involve a considerable number of animals.<sup>21</sup>

### **Non-invasive imaging techniques**

Tomographic methods, e.g., positron emission tomography (PET) and single-photon emission-computed tomography (SPECT), can be also employed to study brain uptake. The compound of interest is first labelled with a positron-emitting radionuclide, and then it is injected IV. The emitted  $\gamma$  radiation is measured in the different organ tissues and reconstructed in a 3D high-resolution image.<sup>23</sup> The advantages of this technique rely on the obtain of high spatial resolution drug distribution using a noninvasive method, also decreasing the number of animals per experiment. However, the instrumentation and equipment are expensive, and not always it is possible to synthesize radiolabeled analogs.

### **Micro-dialysis technique**

This method is based on the direct sampling of interstitial fluid (ISF) by a dialysis probe, consisting of a dialysis fiber membrane connected to inlet and outlet tubing, implemented into the brain parenchyma. A physiological solution is pumped slowly through the probe, small molecules of the brain diffuse across the probe membrane, and they are transported to a fraction collector.<sup>23</sup> Brain micro-dialysis allows the selectively sampling of brain ISF compartment using a semipermeable membrane.<sup>24</sup> Long-term sampling of multiple compounds can be done on a single animal, thus, this technique is extensively used to study the kinetics between blood and brain ISF, as well as for the quantification of neurotransmitters, neuropeptides, and hormones in the brain.<sup>25</sup> Some limitations include the possible local damage of brain tissue and BBB integrity, their suitability to be used only with small (i.e., enzymes and proteins are excluded) and hydrophilic substances, and the biofouling and clogging of membrane pores.<sup>21</sup>

#### **7.1.4.3. Cerebral Open Flow Microperfusion (cOFM) *in vivo* technique**

Cerebral open flow microperfusion (cOFM) is an *in vivo* technique which has been developed in the research group of Dr. Thomas Birngruber from Joanneum Research (Graz, Austria), with strong expertise in evaluating substance transport across the BBB. In collaboration with them and in the frame of Smart-4-Fabry project, the cOFM has been used for the *in vivo* evaluation of the BBB crossing of some nanoliposomal systems developed in this Thesis.

Cerebral open flow microperfusion (cOFM) is a new technology that overcomes some of the limitations of the above-explained *in vivo* methods, consisting in the continuous sampling of the unfiltered cerebral

interstitial fluid (ISF) through the implementation of a cerebral probe in brain parenchyma. First, the absence of membrane (in contrast of micro-dialysis) allows the sampling of virtually all substances, without limitation in molecular weight or solubility, providing a complete representation of ISF.<sup>26</sup> cOFM becomes an interesting and suitable strategy to conventional dialysis methods for testing nanovesicular systems, especially if they are protein-loaded, since the membrane cut-off in conventional dialysis methods restrict such bigger molecules/systems. Then, the use of this technique allows the distinction of the brain parenchyma space against the circulatory blood system, providing knowledge about the location of the compound of interest and its ability to cross the BBB and reach the ISF.

The working principle of cOFM is represented in **Figure 7.6**. First, the cOFM probe is inserted into the rat brain. A healing dummy is inserted inside the probe for 14 days to ensure the re-establishment of the BBB and to prevent tissue in-growth into guide tubing, since this implantation can cause a transitory disruption of the BBB due to its invasive character. After this time, the BBB permeability becomes intact and completely healed.<sup>27</sup> Then, after complete brain tissue regeneration, the healing dummy placed into the probe is replaced by an inflow/outflow tubing for experimental sampling. A perfusion fluid (usually a physiological media composed basically by salts, i.e., NaCl, MgCl<sub>2</sub>, CaCl<sub>2</sub>, KCl, NaH<sub>2</sub>PO<sub>4</sub>, Na<sub>2</sub>HPO<sub>4</sub>, glucose, and BSA) is then injected into brain tissue (pump 1) and withdrawn at the same flow rate (pump 2) (**Figure 7.6B**). At the tip of the probe, perfusate is directly exchanged with ISF and the mixture is collected at regular time intervals.

In this way, the compound of interest is independently administered by a common administration route, e.g., IV, it is biodistributed, and ISF is sampled over time. If the compound of interest can cross the BBB, it will be found in ISF samples. Quantification in ISF can be done by conventional quantification methods, e.g., fluorescence or LC-MS.

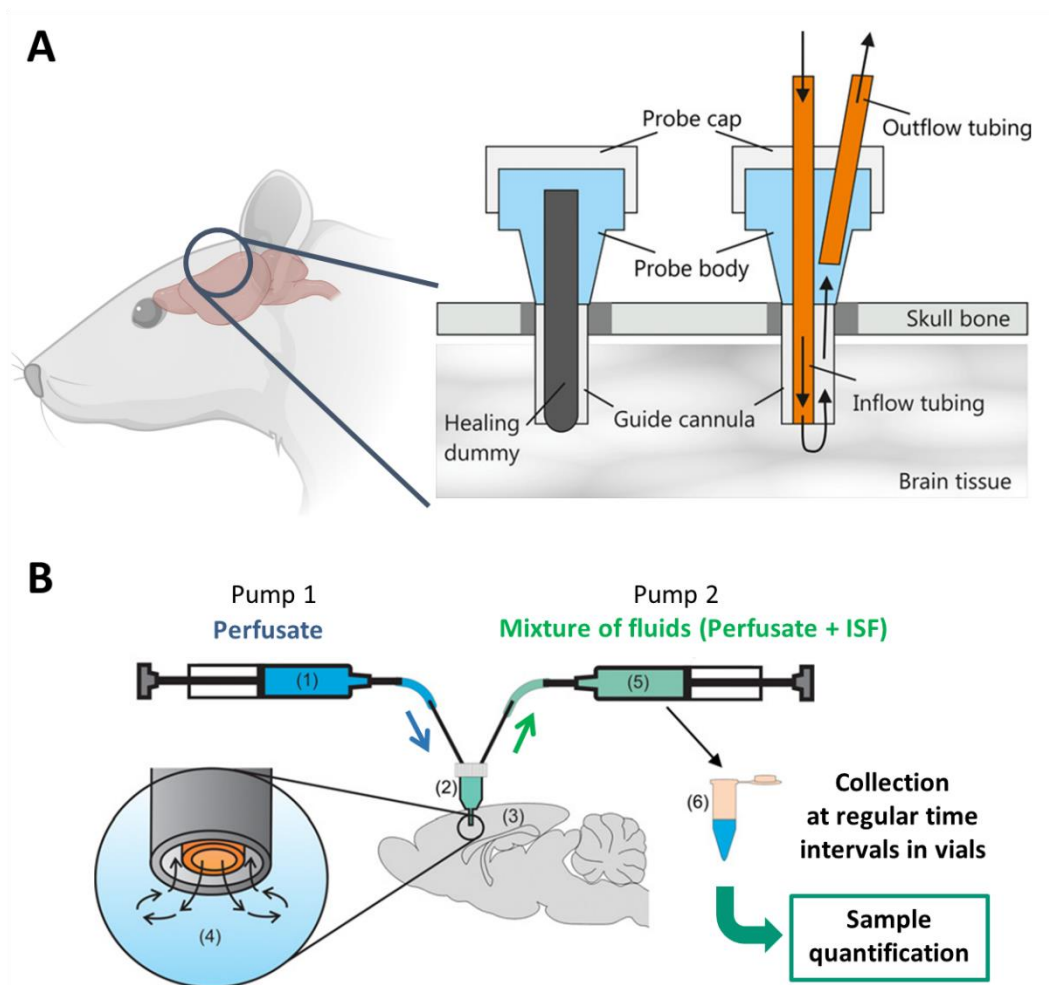


**Figure 7.6.** Representation of cOFM working principle. (A) cOFM probe inserted in the rat brain. Inside the probe, a healing dummy is inserted for 14 days until BBB re-establishment. Then, for experimental sampling, it is replaced by an in inflow and outflow tubing. (B) Scheme of cOFM process. Pump 1 pushes an external perfusate through the probe placed in the rat brain. At the tip of the probe, perfusate and ISF exchanged substances, and this mixture is withdrawn by Pump 2 and collected in vials at regular time intervals. Adapted from Birngruber et al.<sup>26</sup>

The cOFM technique has been used in other studies involving vesicular systems, for example for the evaluation of doxorubicin-loaded liposomes.<sup>17</sup> Birngruber et al.<sup>17</sup> evaluated two delivery systems, a glutathione-targeted PEGylated liposomes compared to the nontargeted version. In this case, doxorubicin present in brain ISF was sampling through cOFM and analyzed using HPLC-MS. Results showed differences between both systems and illustrate the suitability of this technique for sampling lipophilic substances in brain parenchyma. Moreover, this experimental design can be adapted for other brain drug small molecules<sup>28</sup> or delivery systems.<sup>17</sup>



In this Chapter, the behavior of unloaded targeted-liposomes as potential vehicles for brain delivery was explored. First, with a deeper and especial focus in the RGD-liposomal vehicle, extensively developed in the previous Chapters. Then, the incorporation of two additional new alternative ligands to the liposomes were also studied: the alanine amino acid (Ala) and a peptide ligand of the transferrin receptor (T7-peptide). These new ligands were developed and synthesized by Dr. Miriam Royo team from IQAC-CSIC (Barcelona). After their incorporation into liposomes, blood circulation time and presence in brain were evaluated using the cOFM technique, in collaboration with Dr. Thomas Birngruber team from Joanneum Research (Austria).

## 7.2. Evaluation of RGD-liposomes capability to cross the BBB

As introduced in Chapter 4, RGD peptides, whose functional domain is a tripeptide Arg-Gly-Asp, are a widely explored family ligand for enhancing cellular internalization, due to its targeting of  $\alpha v \beta_3$  integrins, overexpressed in neovasculature and especially in brain tumors.<sup>1,13</sup> Some examples illustrating also their availability of enhancing the BBB crossing and neurological diseases can also be found in the literature (e.g., RGD-modified nanocarrier for ischemic stroke,<sup>29</sup> or theranostic RGD-liposomes<sup>30</sup>), while it is true that usually the highest efficacy is obtained when RGD is simultaneously combined with other ligands, e.g., cell-penetrating peptides (CPP) such as the octa-arginine (R8).<sup>31</sup>

Moreover, in the frame of the previous Chapters related to nanoGLA for the improvement of the ERT in Fabry patients, RGD-liposomes loaded with the GLA enzyme showed an unexpected, but surprisingly great, capability to reduce some brain Gb3 deposits, an efficacy which was not obtained with the commercial GLA (agalsidase alfa, Replagal®). These results suggested that RGD-liposomes may be used as nanocarriers for brain targeting, although further exploration is required.

Therefore, the capability of unloaded RGD-liposomes to cross the BBB was evaluated by cOFM, a technique which allows the continuous sampling from the cerebral interstitial fluid (ISF). Similar to previous experiments introduced in **Chapter 6**, the presence of liposomes in biological samples, in this case the cerebral ISF, was evaluated by tracking the MKC, one of the membrane components of the nanoliposomes. Assuming MKC as a representative component of the whole liposomal vehicle, their presence in the ISF is indicator of liposome BBB crossing. Besides, the combination of cOFM for brain sampling with simultaneous blood sampling over time gives complementary information about the biodistribution of the liposomes in blood and in the brain.

### 7.2.1. PK of RGD-liposomes vehicle in plasma and cerebral ISF

As previously described in **Chapter 6.2**, plasma PK was assessed in rats administered with unloaded RGD-liposomes (composed by DPPC, cholesterol, chol-PEG<sub>400</sub>-RGD, and MKC) or free MKC at the equivalent concentration as control. Circulation times were completely different in liposomes ( $t_{1/2}$  =

96 min) and in free MKC ( $t_{1/2} < 15$  min), concluding that: (i) MKC component is retained in the nanoliposomes, and (ii) MKC can be used to monitor the in vivo exposition to the nanoliposomes.

In this experiment performed in collaboration with Dr. T. Birgnruber group from Joanneum Research (Austria), additionally to plasma sampling, the BBB crossing of unloaded RGD-liposomes was also evaluated by cOFM, as well as the BBB integrity after the administration of the nanoformulation (see **Chapter 9.14**). For that, animals were IV administered (bolus) with unloaded RGD-liposomes (30 mg kg<sup>-1</sup> liposome dose) or free MKC as control (at the equivalent amount, corresponding to the dose of 1 mg kg<sup>-1</sup>). Additionally, sodium fluorescein (Naf) was injected in two animals from the RGD-liposomes group, by an initial bolus (11 mg kg<sup>-1</sup>), followed by a constant intraperitoneal infusion during all the entire experiment (11 mg kg<sup>-1</sup> h<sup>-1</sup>). Naf is a known low molecular weight (376 Da) fluorescent marker widely used in permeability perfusion studies, e.g., to study BBB permeability in rodent models.<sup>27</sup> Naf crosses the intact BBB to a limited extent, and allows to detect changes in BBB permeability, for example if a partial opening happens at some point during the experiment.<sup>26,27</sup>

In animals administered with RGD-liposomes, Naf concentrations in plasma and cOFM samples were stable over the entire experiment (**Figure 7.7A**), indicating absence of BBB permeability alterations because of RGD-liposomes administration. Next, MKC content was measured in cerebral ISF samples obtained by cOFM technique. Unfortunately, no MKC could be measured during the first 5 h post-administration, since the obtained values were below the limit of quantification (LOQ < 15 ng mL<sup>-1</sup>) (**Figure 7.7B**). Therefore, the presence of RGD-liposomes could not be quantified in brain ISF.

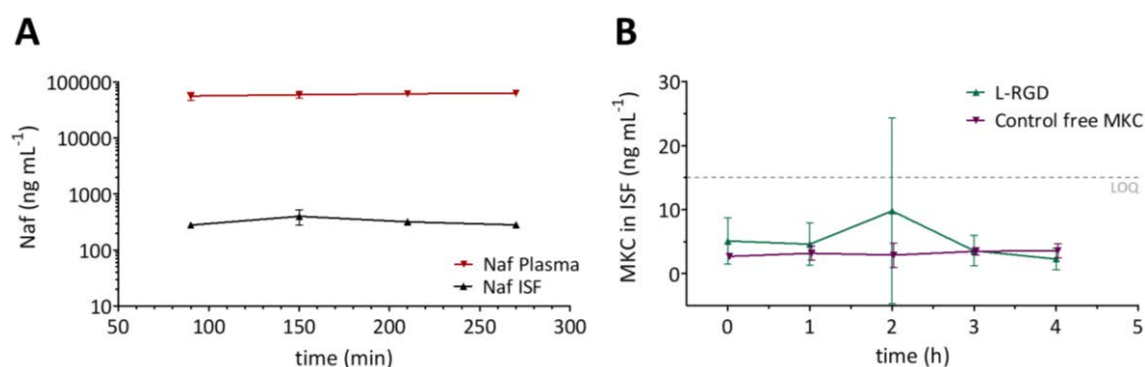


**Figure 7.7.** (A) Integrity of BBB, by Naf levels in plasma and in brain ISF after IV administration of unloaded RGD-liposomes (30 mg kg<sup>-1</sup> liposome dose, n = 2 rats). (B) MKC levels in brain ISF after administration of unloaded RGD-liposomes (30 mg kg<sup>-1</sup> liposome dose, n = 5) or free MKC as control (at the MKC equivalent dose, 1 mg kg<sup>-1</sup>, n = 3).

To sum up, the cOFM technique was set up for monitoring the presence of RGD-liposomes (containing MKC) in the brain ISF of alive rats. The MKC was used as surrogate of the liposomes, following the similar strategy used in the previous PK reported in **Chapter 6.6**. The MKC was assessed in ISF by LC-MS. However, results were below the limit of quantification of the technique, meaning that RGD-liposomes could not be quantified in brain ISF. Nevertheless, permeability of the BBB after RGD-liposome injection was monitored by Naf marker. Results discarded alterations in the BBB permeability due to the testing sample. Later, the LOQ of the LC-MS method used for MKC quantification was refined by Dr. T. Birngruber group, to improve its sensitivity. A lower LOQ, from 15 ng mL<sup>-1</sup> to 1 ng mL<sup>-1</sup>, was achieved, improving considerably the detection capacity, as seen in the next sections.

### 7.3. Development of alternative-ligand targeted-liposomes to enhance BBB crossing

Apart from RGD-peptide, the decoration of the nanoliposomes' surface with alternative targeting ligands was explored, with the aim of improving the brain targeting. Therefore, the incorporation of two alternative ligands into liposomes was studied: (i) the alanine amino acid (Ala) and (ii) a peptide ligand of the transferrin-1 receptor (TfR1) named as T7 (seq. HAIYPRH, i.e., Histidine-Alanine-Isoleucine-Tyrosine-Proline-Arginine-Histidine) (**Figure 7.8**)

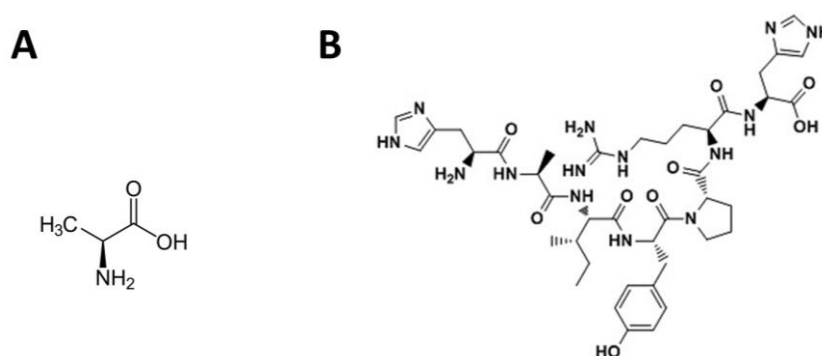


**Figure 7.8.** Chemical structure of (A) Alanine amino acid and (B) T7-peptide (His-Ala-Ile-Tyr-Pro-Arg-His), the two selected ligands to be explored as targeting for improving BBB crossing.

The first ligand selected for its incorporation into liposomes was the alanine amino acid. As explained for the carrier-mediated transport, a high number of solute carriers (SLCs) are responsible of transporting nutrients, and amino acids among them, across the BBB. Moreover, several clinically used small drugs are delivered via SLCs, such as the L-dopamine (L-DOPA) used as treatment for Parkinson's disease.<sup>9</sup> Amino acids, and with special attention to neutral amino acids (e.g. alanine, serine, and cysteine), could be considered as targeting molecules. This strategy starts to be reported in literature, but its exploration is still emerging, and few amino acids targeted nanoparticles for brain delivery are

still reported. To our best knowledge, there is only one reported system based on nanoparticles decorated with alanine as a targeting ligand for brain delivery application, and consists of niosomes vesicles decorated with alanine, developed by Mészáros et al.<sup>32</sup> In that work, niosomes functionalized with alanine and loaded with fluorescent-labeled bovine serum albumin as protein model resulted in an increased permeability across the BBB in culture model and mice, compared to naked niosomes. Studies in cellular uptake mechanism suggested an energy-dependent active process with endocytosis contribution.<sup>32</sup>

The second ligand selected for its incorporation into liposomes was the T7-peptide, ligand of transferrin receptor. Transferrin receptor (TfR) is a transmembrane protein that acts as a mainly receptor to transferrin (Tf) ligand. TfR has been reported to be overexpressed on tumor cells, and highly expressed in BBB. Although the feasibility of Tf as a targeting ligand has been demonstrated in several studies (REF), its use shows several limitations. Among them, there is its high molar weight ( $\approx 80$  kDa), that makes uncomfortable its conjugation in nanoparticles, as well as the receptor competition with endogenous transferrin, that inhibits the possible binding of Tf-nanoparticles.

Interestingly, in the last years a small peptide named T7 peptide has emerged as a unique targeting agent that has gained attention in the research field. The T7 is a seven amino acid peptide whose sequence is HAIYPRH (i.e., Histidine-Alanine-Isoleucine-Tyrosine-Proline-Arginine-Histidine) with high affinity for transferrin receptor (TfR1). Moreover, the binding site between T7 and Tf to TfR1 is different, meaning a possible potentially avoidance of the uptake inhibition by endogenous transferrin. Besides, its small size (only seven amino acids) makes easier the functionalization of nanoparticles with this peptide. Some examples found in literature show the successful targeting to the brain with T7-modified nanoparticles, compared to their non-targeted system, with especial attention in glioma brain therapy. For example, results showed a better drug brain accumulation with T7-targeted nanoparticles compared to non-targeted system, such as doxorubicin-loaded T7-peptide functionalized liposomes,<sup>33</sup> T7-peptide dendrimers for gene delivery applications,<sup>34</sup> or T7-decorated exosomes for microRNA delivery, for glioma brain targeting.<sup>35</sup>

### 7.3.1. Incorporation of Alanine and T7 ligands into nanoliposomes

Therefore, the functionalization of liposomes with the selected ligand candidates, (i) the alanine amino acid (Ala), and (ii) the T7 peptide (transferrin-receptor ligand), was explored to improve the penetration of the nanoliposomes through the BBB. Similar to the strategy used for the incorporation of the RGD moiety through chol-PEG<sub>400</sub>-RGD, the selected ligands were covalently linked to the cholesterol molecule through a polyethylene glycol chain (PEG 400 Da). These new cholesterol-derivative molecules, chol-PEG<sub>400</sub>-Ala and chol-PEG<sub>400</sub>-T7, were developed and synthesized for the first time by Dr. M. Royo group from IQAC-CSIC (Barcelona) (**Figure 7.9**). More chemical details of chol-PEG<sub>400</sub>-Ala and chol-PEG<sub>400</sub>-T7 can be found in **Chapter 9.6.1**.

Then, in the following section the incorporation of these resulting ligand-conjugates, ch-PEG<sub>400</sub>-Ala and ch-PEG<sub>400</sub>-T7, into the liposomal system is described. The objective was to obtain a system suitable for their administration *in vivo*, as well as the study of the circulation time and the BBB crossing capability by cOFM method in collaboration with Dr. T. Birngruber team from Joanneum Research (Austria).

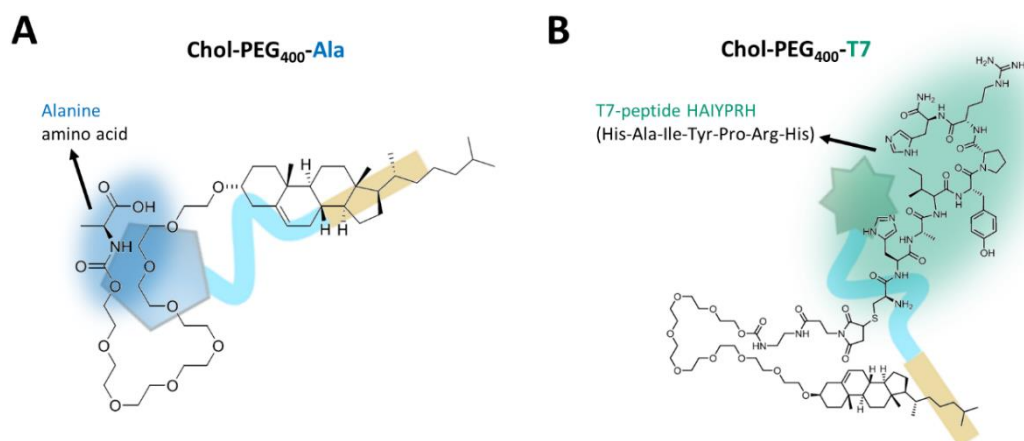


**Figure 7.9.** Chemical structure of (A) cholesterol-PEG<sub>400</sub>-Alanine, and (B) cholesterol-PEG<sub>400</sub>-T7, developed and synthesized by Dr. M. Royo team from IQAC-CSIC (Barcelona).

### 7.3.1.1. Preparation of Alanine- and T7-functionalized liposomes by DELOS-susp

On the one hand, nanoliposomes functionalized with this new alanine-ligand were produced, for first time, in the small lab-scale DELOS-susp equipment (7.5 mL reactor). The chol-PEG<sub>400</sub>-Ala could be easily dissolved in EtOH together with the rest of membrane components, making dispensable the use of DMSO (unlike RGD-liposomes) in the preparation of this formulation by DELOS-susp. Then, the depressurization step was performed as usually in water aqueous phase, obtaining for first time alanine functionalized liposomes (L-Ala).

Two different alanine-conjugate densities were used, based on previous experience with the RGD-liposomes: 3 mol % and 6 mol % of chol-PEG<sub>400</sub>-Ala in relation to the rest of membrane components. A small amount of the cationic surfactant MKC (5 mol %) was also added to the formulation, as a dispersion stabilizer and to provide positive charge to the liposomal membrane. Besides, without the addition of MKC, nanovesicles showed a sharp decrease on negative  $\zeta$ -potential compared to blank liposomes (**Figure 7.10C**). It could be attributed to the negative contribution of the alanine to the surface of the liposome, due to the terminal carboxyl group which provides negative charge. To switch into a positive  $\zeta$ -potential, it was needed the incorporation of the MKC in small amount.

L-Ala samples showed good macroscopic visual appearance, resulting in nanometric and narrow vesicle size distribution (**Figure 7.10A** and **B**). While plain liposomes, i.e., composed exclusively by DPPC, cholesterol, and a small amount of MKC, showed a remarkable positively surface charge, the incorporation of alanine provoked the progressive decrease of the  $\zeta$ -potential, being more negative as

more alanine content had. Therefore, the lower, but still positive,  $\zeta$ -potential of the higher alanine ratio ( $\sim 20$  mV for L-6%Ala) was also correlated with lower colloidal stability since a small amount of sedimentation was observed 4 – 5 days after production. This little sedimentation resuspended well after several inversion times of the vial, and good DLS values were still obtained. Otherwise, liposomes with lower alanine ratio (L-3%Ala) showed better stability, at least two weeks without macroscopic sedimentation or alteration of size distribution peak.

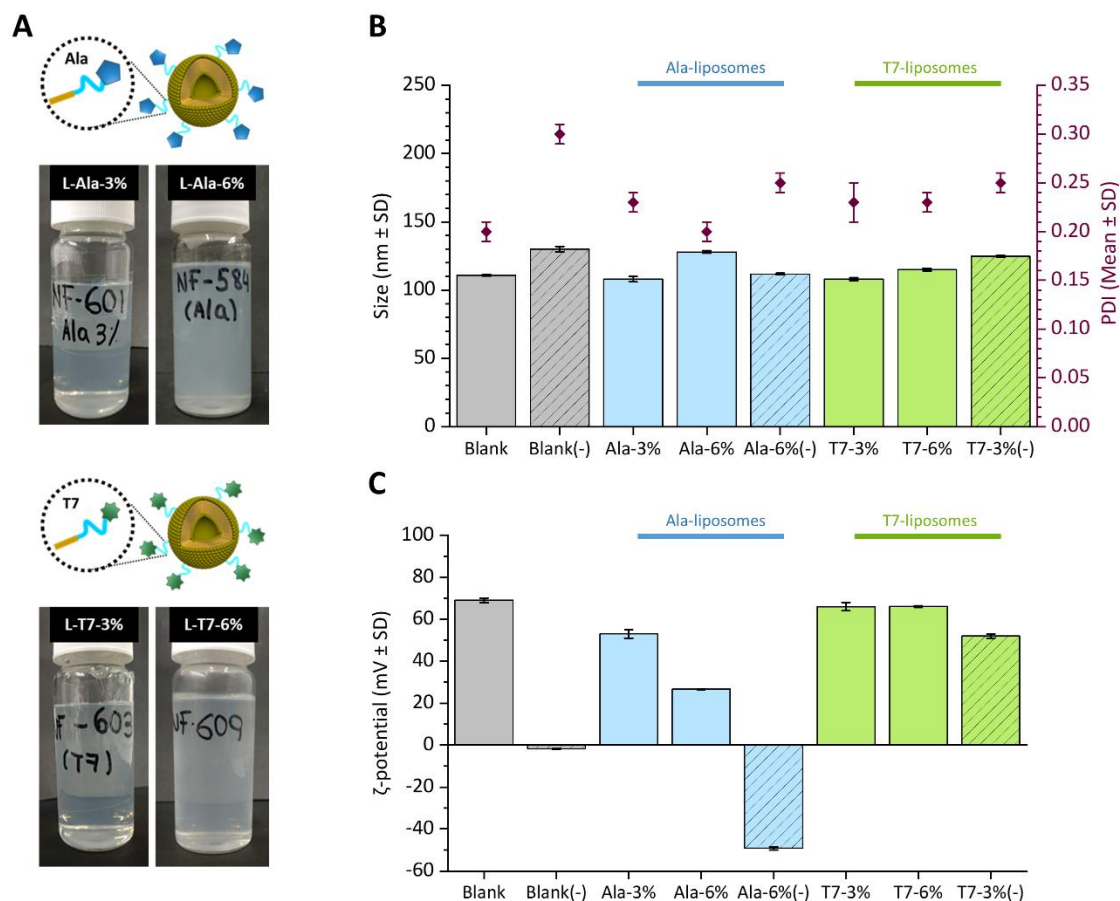


**Figure 7.10.** Physicochemical characteristics of new-targeted liposomes produced in the small lab-scale DELOS-susp plant, containing alanine and T7 as alternative targeting-ligands. (A) Macroscopic appearance, (B) size and PDI, and (B)  $\zeta$ -potential, the day of production. Both L-Ala and L-T7 were produced at two functionalization densities 3 mol % and 6 mol %, containing in all the cases 5 mol % of MKC. As control, blank liposomes (without functionalization) were also plotted. Control batches free of MKC are marked as (-).

On the other hand, nanoliposomes functionalized with the other targeting-ligand, the T7-peptide, were also produced for first time in the small lab-scale DELOS-susp equipment (7.5 mL reactor). This time, the chol-PEG<sub>400</sub>-T7 showed a worse solubility in the EtOH solution, so, similar as when working with chol-PEG<sub>400</sub>-RGD, the incorporation of DMSO was needed to obtain a transparent organic solution with all the membrane components dissolved, before adding the resulting mixture EtOH/DMSO into the small lab-plant DELOS-susp vessel. After the depressurization step in the aqueous phase (water), transferrin-ligand receptor (T7) functionalized liposomes (L-T7) were obtained for first time.

L-T7 liposomes were prepared, as well as two different T7-conjugate densities, 3 and 6 mol % of chol-PEG<sub>400</sub>-T7 in relation to the rest of lipid, were tested. Moreover, a small amount of MKC was also incorporated to the formulation (5 mol %), although L-T7 nanovesicles without it showed a high and positive  $\zeta$ -potential as well (**Figure 7.10C**). No significant difference in physicochemical characteristics was observed between the two T7-conjugate densities, 3 and 6 mol %.

L-T7 samples showed good macroscopic and quite transparent visual appearance, resulting in nanometric and narrow size distribution (**Figure 7.10A and B**). The incorporation of T7-peptide in the liposomal membrane provoked an increase of the  $\zeta$ -potential, obtaining values similar to those seen for RGD-liposomes in previous Chapters. The physicochemical parameters for both T7 densities, L-3%T7 and L-6%T7, remained stable and without sedimentation signs for at least 14 days.

Overall, it was possible to prepare for first time two new targeted-liposomal systems by DELOS-susp containing alanine amino acid or T7-peptide, by their incorporation through chol-PEG<sub>400</sub>-ligand conjugates. All the systems showed nanometric size and narrow particle distribution. The functionalization content impacts in the  $\zeta$ -potential of the systems, especially in the alanine formulation, whose colloidal stability was higher when containing 3 mol % of chol-PEG<sub>400</sub>-Ala. Therefore, the 3 mol % functionalization density was selected for the next experiments.

#### **7.3.1.2. Scale up to intermediate-lab plant and concentration by TFF**

After obtaining good and reproducible results in the small lab-scale DELOS-susp equipment, a first scaling to an intermediate lab-scale was performed to produce enough volume for reaching the required sample volumes for in vivo testing. It was possible to go from 25 mL batch size (obtained with the small lab-scale DELOS-susp equipment) to 150 mL batch size (intermediate lab-scale DELOS-susp equipment). No relevant change in size, PDI, and  $\zeta$ -potential was observed neither in alanine- nor T7-functionalized liposomes (**Figure 7.11**). However, in the case of T7-liposomes, some precipitate was found later in the reactor, probably because of a non-complete solubilization of the chol-PEG<sub>400</sub>-T7 in the CO<sub>2</sub>-expanded solution. This finding was not observable when working in the small lab-scale equipment, due to the smaller size of the high-pressure vessel. It suggests that the similar physicochemical characteristics obtained for the two previously tested chol-PEG<sub>400</sub>-T7 densities

(L-3% T7 and L-6% T7) may be attributed to a loss of chol-PEG<sub>400</sub>-T7 during the DELOS-susp process, resulting in a similar incorporation rate into the liposomal membrane.

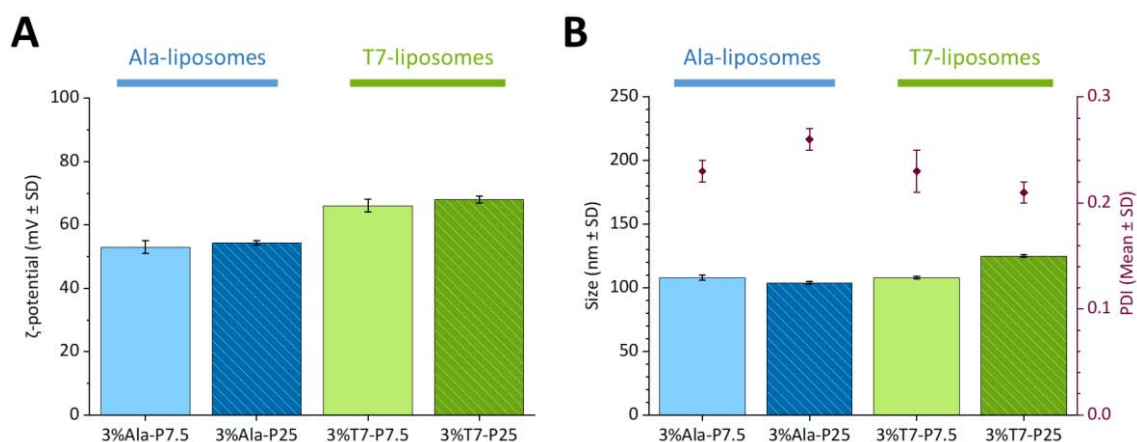


**Figure 7.11.** Comparison of batches obtained in the small (P7.5) and in the intermediate (P25) lab-scale DELOS-susp equipment, by (A) size and PDI, and (B)  $\zeta$ -potential.

Then, to reach doses compatible with in vivo intravenous administration, it was required a tangential flow filtration (TFF) concentration step (7.5-fold) followed by a diafiltration step in water, needed for the removal of the remained organic solvent and the non-incorporated small molecules.

Results showed no significant change after the TFF process, allowing the obtainment of a concentrated sample (9.0 mg mL<sup>-1</sup> liposomes), free of EtOH and DMSO, compatible with an in vivo dose. In all the cases, the size distribution showed a unique population, with an average size around 100 nm (**Figure 7.12**). CryoTEM images confirmed the low dispersity of the L-Ala and L-T7 concentrated samples, showing a predominance of small and unilamellar vesicles.



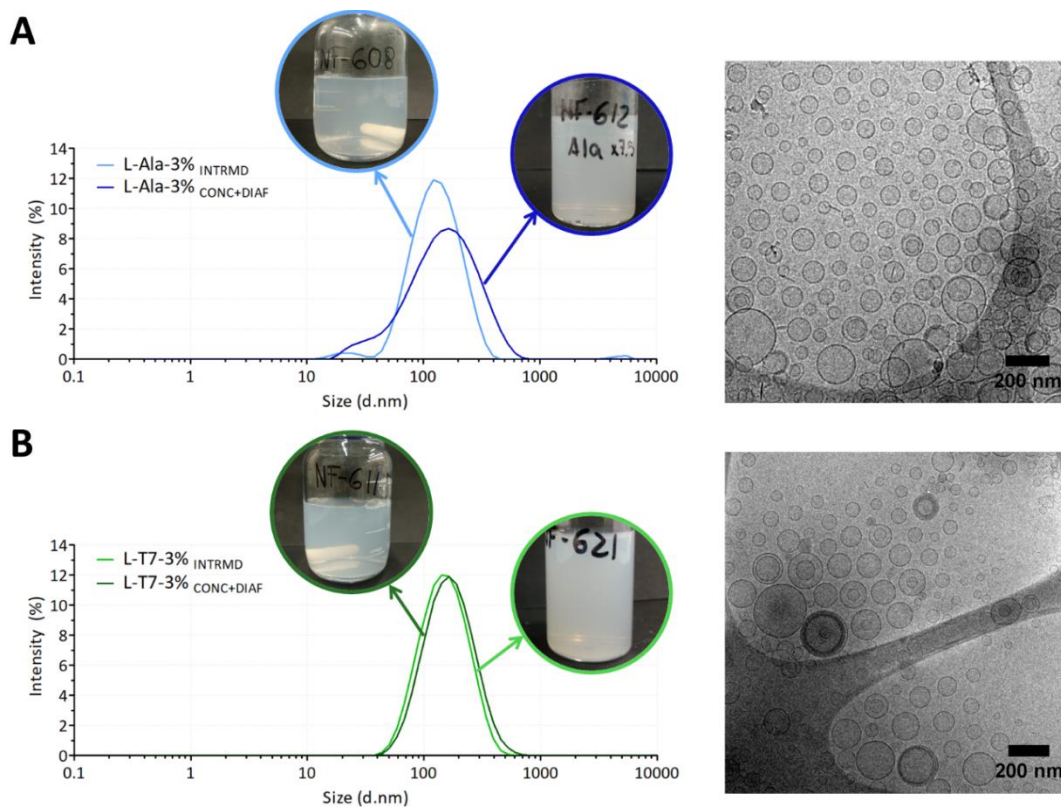


**Figure 7.12.** Size distribution, macroscopic appearance, and microscopic morphology of (A) alanine-liposomes and (B) T7-liposomes, after production by DELOS-susp (intrmd, 1.2 mg mL<sup>-1</sup> liposomes) and after TFF process (7.5-fold concentration and diafiltration in water, 9.0 mg mL<sup>-1</sup> liposomes).

As summary, a successfully incorporation of two new ligands, chol-PEG<sub>400</sub>-Alanine and chol-PEG<sub>400</sub>-T7, was achieved for first time. Then, it was possible to perform a first scaling up from the small to the intermediate lab-scale DELOS-susp plant, increasing the batch size from 25 mL to 150 mL. Further, it was possible to concentrate the sample by TFF up to 7.5-fold, from 1.2 mg mL<sup>-1</sup> to 9.0 mg mL<sup>-1</sup> of liposomes, reaching acceptable doses for in vivo administration. Overall, both final prototypes, L-Ala and L-T7, met the physicochemical requirements in terms of size (< 300 nm), PDI (< 0.35), and  $\zeta$ -potential (> +30 mV).

### 7.3.2. In vivo evaluation of Alanine-liposomes and T7-liposomes

Two batches containing the new targeting ligands (L-Ala and L-T7, 3% mol of functionalization), in enough quantity and with the appropriate quality for the intravenous administration (**Table 7.1**), were successfully prepared for their BBB crossing in vivo evaluation in collaboration with Dr. T. Birngruber team from Joanneum Research (Austria). Intermediate samples were submitted to a 7.5-fold concentration factor to obtain a liposome concentration of 9.0 mg mL<sup>-1</sup>.

**Table 7.1.** Physicochemical characteristics of the intermediate and final systems, the same day of production.

	L-Ala		L-T7	
	Intermediate	Final	Intermediate	Final
Size (nm) ( $\pm$ SD) <sup>†</sup>	111 $\pm$ 2	103 $\pm$ 1	121 $\pm$ 1	136 $\pm$ 1
PDI ( $\pm$ SD) <sup>†</sup>	0.30 $\pm$ 0.01	0.23 $\pm$ 0.01	0.20 $\pm$ 0.01	0.24 $\pm$ 0.01
$\zeta$ -potential (mV) ( $\pm$ SD) <sup>†</sup>	66 $\pm$ 1	60 $\pm$ 1	70 $\pm$ 8	76 $\pm$ 1
MKC (mg mL <sup>-1</sup> ) ( $\pm$ SD) <sup>‡</sup>	0.044 $\pm$ ND	0.155 $\pm$ 0.005	0.054 $\pm$ ND	0.148 $\pm$ 0.019
Solvent (% vol.)	EtOH 6%	Water	EtOH 5%/DMSO 1%	Water

<sup>†</sup> Measured by DLS and ELS (see **Chapter 9.5.1**); <sup>‡</sup> Measured by LC-MS by Dr. T. Birgruber from Joanneum Research (Austria) as explained in **Chapter 9.15.1**.

These batches also contain MKC, which was used later for tracking the nanovesicles. Before, MKC in stock samples was measured by LC-MS in collaboration to Dr. T. Birgruber group from Joanneum Research (Austria) (**Table 7.1**). The MKC concentration in intermediate samples was in quite good agreement with the theoretical one (0.04 mg mL<sup>-1</sup>), whereas in final samples the MKC concentration was half ( $\sim$  0.15 mg mL<sup>-1</sup>) of the expected (0.30 mg mL<sup>-1</sup>). This decrease can be attributed to a MKC loss during the diafiltration TFF process, in which non-incorporated small molecules were removed from the sample. In this case, about half of the added MKC was incorporated in the liposomal vesicle, although both systems L-Ala and L-T7 contained similar MKC content, which was relevant for comparison purposes.

Overall, the resulted concentrated systems showed a homogeneous and narrow size distribution, and very unilamellar morphology (**Figure 7.13A and B**), as well as they remained stable at least two weeks, fulfilling the time required for the in vivo experiment (**Figure 7.13C**).

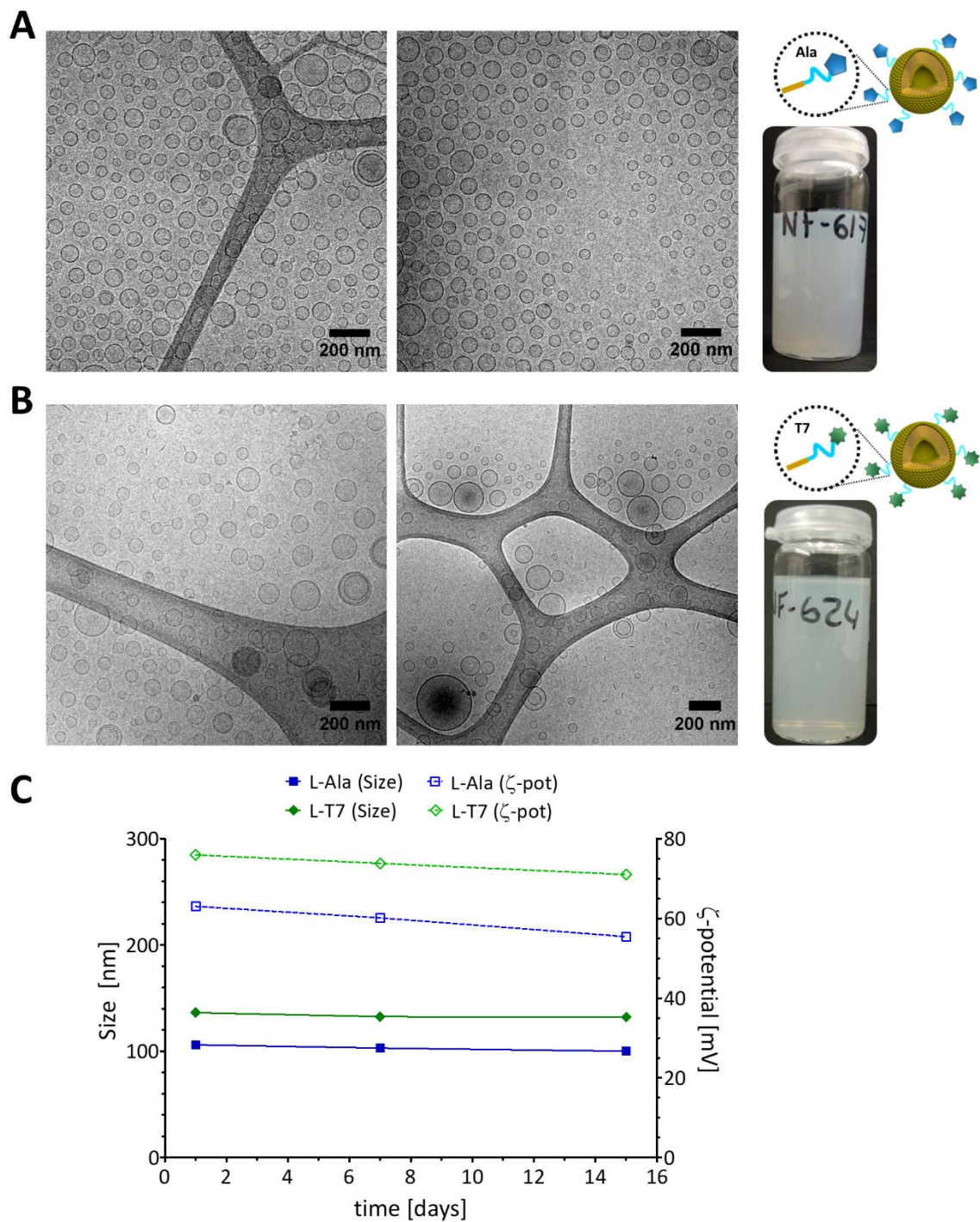


**Figure 7.13.** Macroscopic appearance and microscopic morphology by cryoTEM of (A) alanine-targeted and (B) T7-targeted liposomes, after 7.5-fold concentration and diafiltration in water. (C) Stability of final concentrated (7.5-fold) and diafiltrated L-Ala and L-T7 systems, in terms of size and  $\zeta$ -potential.

Then, the capability of the new targeted nanoliposomes to reach the brain was evaluated *in vivo*. The experiment was performed in collaboration with Dr. T. Birngruber team from Joanneum Research (Austria). Two different formulations were investigated and compared their ability to cross the intact blood-brain barrier (BBB) by cerebral open flow microperfusion (cOFM): (i) Alanine-functionalized liposomes (L-Ala), and (ii) T7-functionalized liposomes (L-T7).

Previously to the day of administration, two cOFM probes were implanted in the brain of each animal to have access to brain interstitial fluid (ISF). Two weeks after, BBB was completely healed and re-established, being ready for the sampling. Both formulations were administered through a bolus intravenous injection, dosed at  $30 \text{ mg kg}^{-1}$  of liposomes, in male Sprague-Dawley rats ( $n = 5$  rats per group). Continuing sampling of cerebral ISF and blood plasma in conscious animals was taken according to sampling regimen, schematized in **Figure 7.14**. The pharmacokinetics was assessed by following one of their membrane components, the MKC, as a representation of the whole liposome. Plasma and cerebral ISF were continuously sampled for 20 hours.

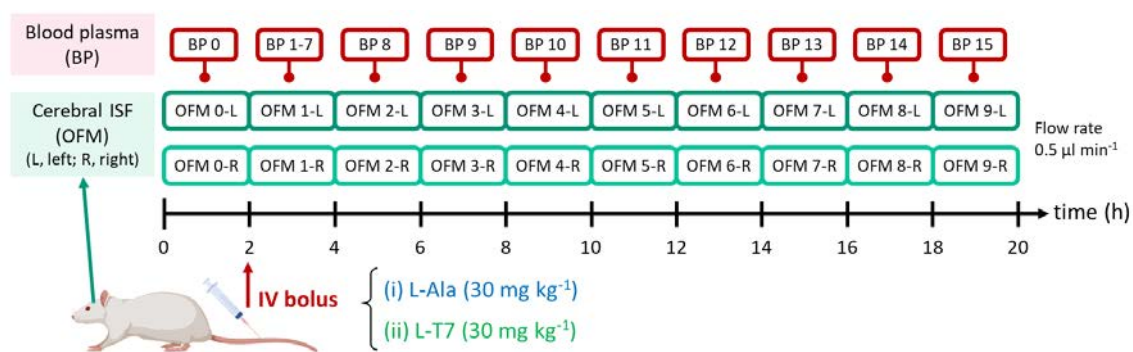


**Figure 7.14.** Dosing and sampling regimen of nanoliposomes with different targeting peptides for BBB crossing study. Study performed by Dr. Thomas Birngruber team from Joanneum Research (Austria).

Comparison of plasma PK showed an enhanced circulation half-life of both new-targeted liposomes, L-Ala and L-T7 (**Figure 7.15A**), compared to L-RGD (previously described **Chapter 6.2**). Therefore, Ala-targeted nanoliposomes (L-Ala) presented a  $t_{1/2}$  of 15 hours, whereas T7-targeted nanoliposomes (L-T7) showed a  $t_{1/2}$  of 8.5 hours (**Table 7.2**). Both systems stayed significantly longer in bloodstream than RGD-liposomes.

**Table 7.2.** Half-life ( $t_{1/2}$ ) following MKC from L-Ala and L-T7 after intravenous (bolus) administration ( $30 \text{ mg kg}^{-1}$  liposomes) in rats ( $n = 5/\text{group}$ ). L-RGD\* from **Chapter 6.2** is included for comparison purposes.

System	Dose of liposomes ( $\text{mg kg}^{-1}$ )	$t_{1/2}$ (h)
L-Ala	30	15.1
L-T7	30	8.5
L-RGD*	30	1.6

At the same time, by using cOFM for direct sampling in brain tissue, the presence of L-Ala and L-T7 in ISF was studied by MKC quantification. As mentioned before, this time the LOQ was improved until  $1 \text{ ng mL}^{-1}$  of MKC.

On the one hand, T7-targeted liposomes were detectable in cOFM samples, but levels were still too low for quantification, since remained below the LOQ (**Figure 7.15B**). In contrast, L-Ala, which showed the longest half-life in plasma, could be detected in cOFM samples around 4 h after administration (**Figure 7.15C**). The MKC presence in the cerebral ISF of animals administered L-Ala suggested that this system could be able to reach the brain. Although MKC was found in low content, this result represented a great finding, due to the challenge of developing nanocarriers able to cross the BBB.

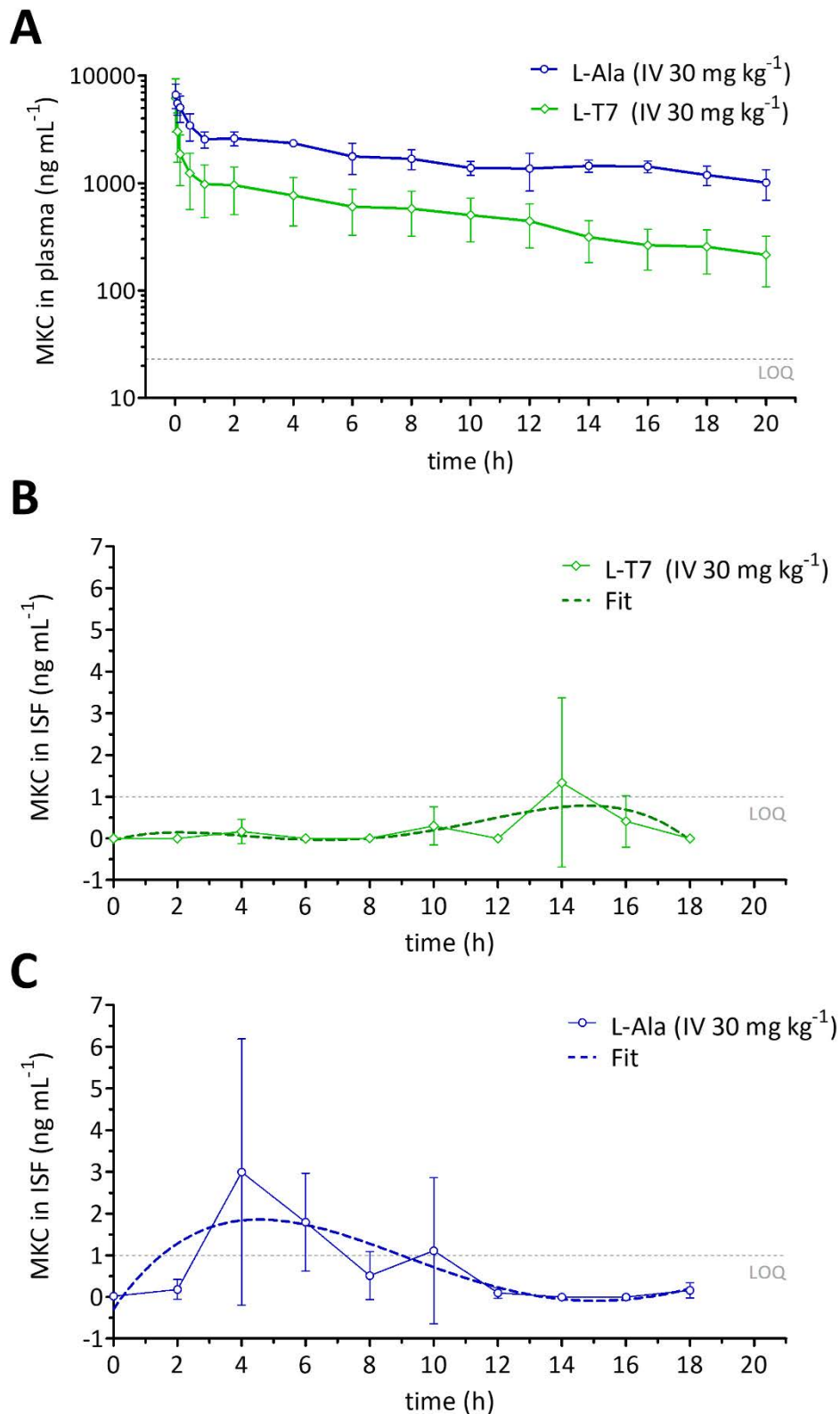


**Figure 7.15.** (A) Plasma PK profile of L-Ala and L-T7 nanoliposomes following MKC, in absolute MKC concentration, after intravenous (bolus) administration ( $30 \text{ mg kg}^{-1}$  liposomes) in rats ( $n = 5/\text{group}$ ). PK profile in brain cOFM samples of (B) L-Ala, and (C) L-T7. LOQ was  $23 \text{ ng mL}^{-1}$  and  $1 \text{ ng mL}^{-1}$  in plasma and cOFM samples, respectively. Assay performed by Dr. T. Birgnruber team from Joanneum Research (Austria).

## 7.4. Exploration of dual-targeted liposomes

The potential of these new alanine-functionalized liposomes was further studied. In literature, several examples of targeted nanoparticles for brain delivery showed higher BBB crossing when using dual-targeting, more than single-targeting.<sup>31,33</sup> It consists of decorating the surface of the nanocarrier with two targeting ligands, instead of one. Although a single peptide could enhance the BBB targeting, targeting only one receptor sometimes could lead to a limited uptake, because of the receptor saturation.<sup>33</sup> Thus, an approach to improve the efficacy of the targeting is this dual strategy. In many cases, the incorporation of two targeting units results in a synergic effect between both ligands, and the amount able to reach the brain is superior.<sup>32,33,36</sup>

Therefore, the possibility to functionalize the nanoliposomes' surface with two targeting ligands was explored. After the great results obtained independently with RGD and Alanine, the incorporation of both ligands to the liposomal surface composition was studied, with the aim to explore this attractive strategy for improving brain targeting. Accordingly, new dual-targeted liposomes composed of DPPC, cholesterol, and MKC (5 mol %), and containing both chol-PEG<sub>400</sub>-Ala and chol-PEG<sub>400</sub>-RGD were prepared in the small lab-scale DELOS-susp equipment. To optimize the concentration of each targeting ligand on the surface of the nanovesicles, three different molar ratios between chol-PEG<sub>400</sub>-Ala: chol-PEG<sub>400</sub>-RGD were tested: (i) 1.5: 1.5, (ii) 2.0: 1.0, and (iii) 2.5: 2.5 mol % (**Figure 7.16**).

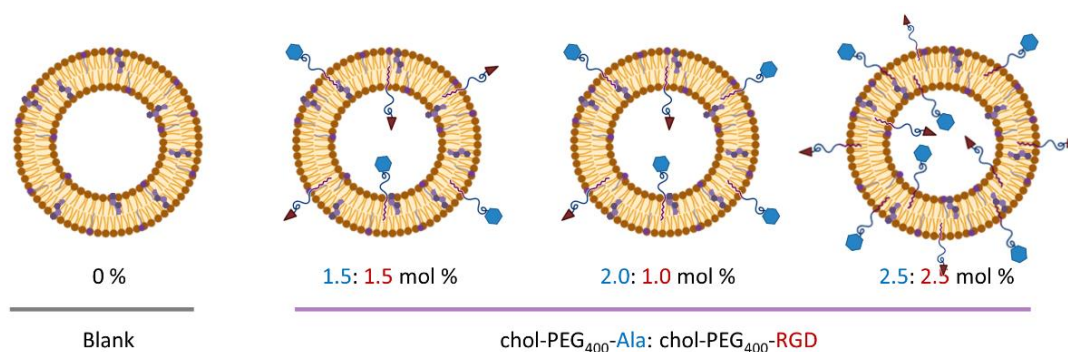


**Figure 7.16.** Scheme of the dual-targeted liposomal systems, containing different ratio of chol-PEG<sub>400</sub>-Ala and chol-PEG<sub>400</sub>-RGD (mol % in relation to the rest of mol % of membrane components).

For the DELOS-susp production, a mixture EtOH/DMSO was used to solubilize the components. After depressurization, the intermediate samples were submitted to a TFF diafiltration process in water to remove the organic solvents and other possible non-integrated components from the vesicles, obtaining the diafiltrated samples. As shown in **Figure 7.17A**, dual Ala/RGD-liposomes were obtained with optimal physicochemical properties: appropriate nanometric size, narrow PDI, and high positive  $\zeta$ -potential values. Besides, these systems presented good macroscopic appearance without sedimentation in the three tested combinations (**Figure 7.17B**).

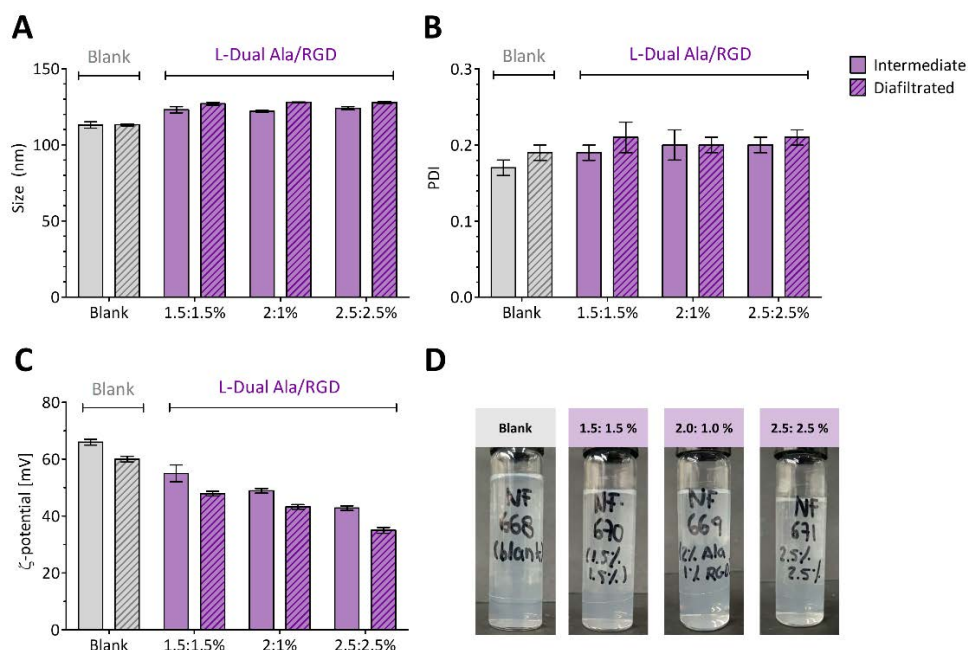


**Figure 7.17.** (A) Mean vesicle size, (B) PDI, and (C)  $\zeta$ -potential of dual Ala/RGD-liposomes, composed by DPPC, cholesterol, MKC, chol-PEG<sub>400</sub>-RGD, and chol-PEG<sub>400</sub>-RGD, in three chol-PEG<sub>400</sub>-RGD: chol-PEG<sub>400</sub>-RGD mol % ratios. Liposomes without functionalization (blank) were included as reference. Measures by DLS (see **Chapter 9.5.1**)

Whereas size and PDI resulted in similar values for all the three Ala/RGD ratios, once more,  $\zeta$ -potential values were more affected depending on the functionalization percentage. The more alanine, the lowest  $\zeta$ -potential values. Nevertheless, even the system with the highest percentage of functionalization (2.5: 2.5 %) showed  $\zeta$ -potential values  $> +30$  mV. Therefore, this system with the highest functionalization of both ligands (2.5 mol % chol-PEG<sub>400</sub>-Ala and 2.5 mol % chol-PEG<sub>400</sub>-RGD) was selected for further experiments.

## 7.5. Cell viability of targeted liposomes in HeLa cells

To check the impact of the new targeted-liposomes on cell viability, the best prototypes of each developed targeted system were selected: L-RGD (3 mol % RGD), L-Ala (3 mol % Ala), L-Dual Ala/RGD (2.5 mol % of Ala and 2.5 mol % of RGD), and a blank without functionalization as a control. All these systems were produced in the small lab-scale DELOS-susp equipment and submitted to a TFF diafiltration process in water to remove the organic solvent and the non-incorporated molecules.

Then, a MTT cell viability assay was performed in collaboration with Dr. I. Abasolo group (VHIR, Barcelona). HeLa cells were faced with a range of liposomes' concentrations, including L-RGD, L-Ala, L-Dual Ala/RGD, and liposomes without functionalization (blank). The four systems showed similar cell viability curves (**Figure 7.18**). Only at one concentration point (0.006 mg mL<sup>-1</sup>), the viability of L-RGD treated cells deviated slightly from the trend.



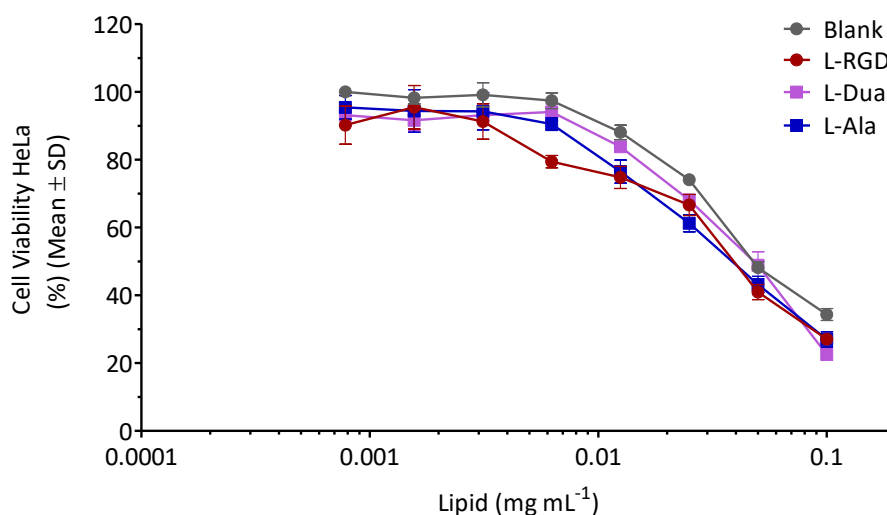


**Figure 7.18.** Cell viability by MTT assay in HeLa cells, treated during 72 h at 37 °C with up to 0.1 mg mL<sup>-1</sup> of L-RGD, L-Ala, L-Dual Ala/RGD, and blank liposomes (all systems after TFF diafiltration in water). Assay performed by Dr. I. Abasolo group from VHIR (Barcelona), as detailed in **Chapter 9.9.1**.

## 7.6. Optimization of ligand-targeted liposomes and in vitro hemocompatibility evaluation

Next, a new set of targeted liposomes were produced including, this time, the new dual Ala-RGD-liposomes. The objective of this new production is to study the impact of preparing these systems in an isosmotic media and to evaluate their hemocompatibility. Therefore, three systems were prepared: (i) RGD-liposomes, (ii) Ala-liposomes, and (iii) dual Ala/RGD-liposomes, containing both RGD and Ala targeting moieties (**Figure 7.19**).

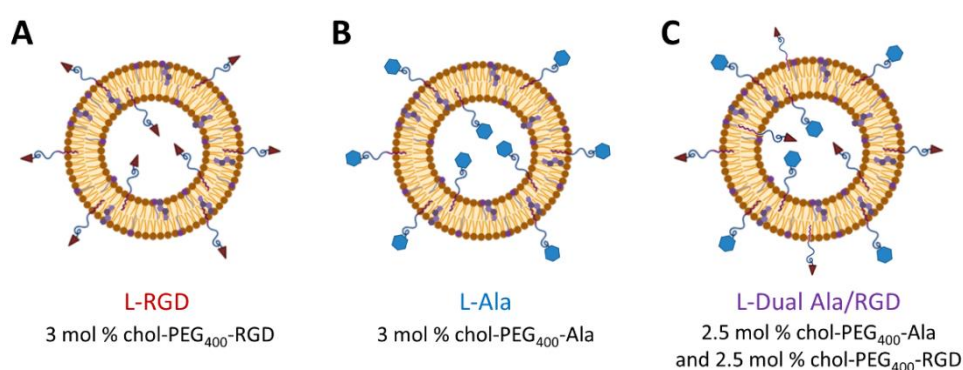


**Figure 7.19.** Systems prepared for in vitro hemocompatibility testing: (A) RGD-liposomes (L-RGD), (B) Alanine-liposomes (L-Ala), and (C) dual Ala/RGD-liposomes (L-Dual Ala/RGD).

All three systems were produced in the intermediate lab-scale DELOS-susp equipment, and then were submitted to a TFF concentration (7.5-fold) and diafiltration step. This time, water with glucose 5 % was used as medium instead of pure water, to obtain samples isosmotic to blood. In previous **Chapter 5** and **Chapter 6**, the suitability of this medium for L-RGD was demonstrated. However, this was the first time that L-Ala and L-Dual Ala/RGD were also prepared in this isosmotic medium. Results by DLS confirmed the suitability of glucose 5 % medium to be used for L-Ala and L-Dual, since nanometric and low disperse nanovesicles were obtained (**Figure 7.20A**), with good visual appearance and absence of sedimentation (**Figure 7.20B**). Additional morphological characterization by cryoTEM corroborated the DLS results. L-Ala liposomes in glucose showed small size and absence of aggregates, although this time vesicle morphology was a little more oval (**Figure 7.20C**) than when prepared in water. The same happened for L-Dual, where a mix of spherical and oval nanometric vesicles were found, with some non-predominant bigger structure (**Figure 7.20D**).

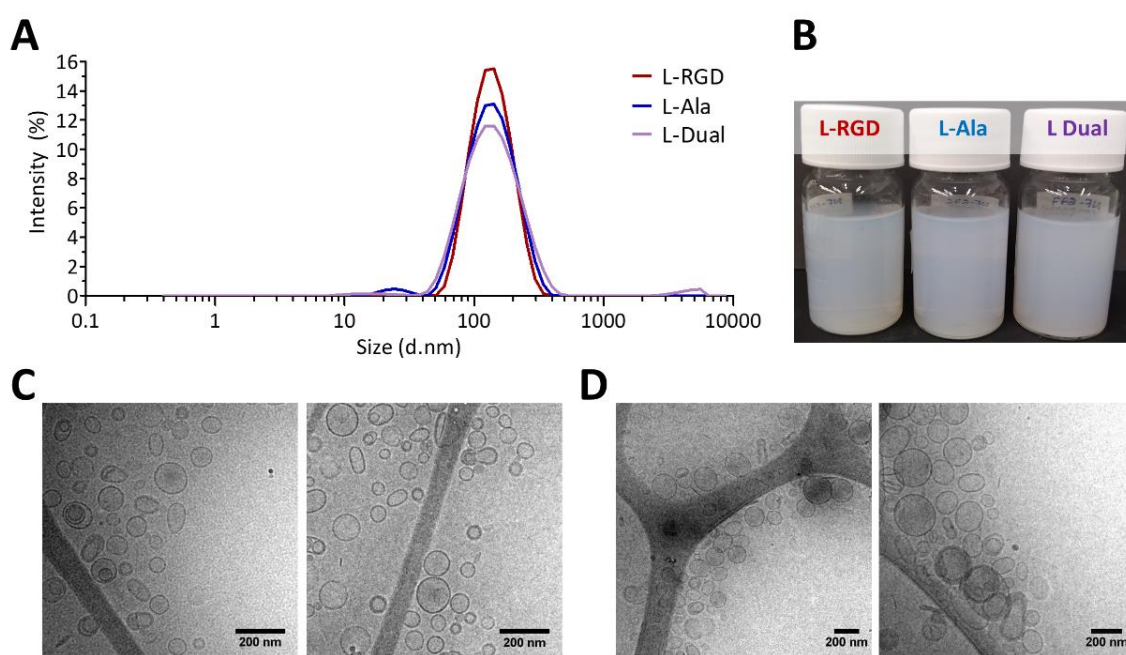


**Figure 7.20.** (A) Size distribution and (B) visual macroscopic appearance of L-RGD, L-Ala, and L-Dual after 7.5-fold concentration and diafiltration in water containing glucose 5% by TFF process. CryoTEM images of (C) L-Ala and (D) L-Dual.

**Table 7.3.** Physicochemical characteristics of the intermediate (after DELOS-susp, at time 1-day post-production) and final systems (after 7.5-fold concentration and diafiltration in glucose 5% medium, at time 1 week).

	L-RGD		L-Ala		L-Dual Ala/RGD	
	Intermediate	Final	Intermediate	Final	Intermediate	Final
Size (nm) ( $\pm$ SD) <sup>†</sup>	115 $\pm$ 2	116.8 $\pm$ 0.4	103.0 $\pm$ 0.1	108.2 $\pm$ 0.8	104.5 $\pm$ 0.8	115.0 $\pm$ 0.2
PDI ( $\pm$ SD) <sup>†</sup>	0.20 $\pm$ 0.01	0.19 $\pm$ 0.01	0.25 $\pm$ 0.01	0.24 $\pm$ 0.01	0.22 $\pm$ 0.01	0.25 $\pm$ 0.01
$\zeta$ -pot (mV) ( $\pm$ SD) <sup>†</sup>	57 $\pm$ 1	48.1 $\pm$ 0.3	55 $\pm$ 1	49 $\pm$ 1	43.4 $\pm$ 0.8	44.2 $\pm$ 0.2
Solvent	EtOH 5 % / DMSO 1 %	Glucose 5 %	EtOH 6 %	Glucose 5 %	EtOH 5 % /DMSO 1 %	Glucose 5 %

<sup>†</sup> Measured by DLS (see **Chapter 9.5.1**).

Finally, hemocompatibility of the liposomal systems was studied to ensure their biocompatibility. In vitro hemolysis test and plasma coagulation assays were performed in collaboration with Dr. I. Abasolo group from VHIR (Barcelona), as detailed in **Chapter 9.9.2**.

First, the incubation of L-RGD, L-Ala, and L-Dual with human blood samples did not induce hemolysis since values were below 5 % (threshold to be considered hemolytic) in all the tested concentrations, as shown in **Figure 7.21**. Besides, in vitro plasma coagulation times after incubation with liposomal samples were measured. No significant variations in plasma coagulation times were detected after incubation with liposomes at a concentration of 0.1 mg mL<sup>-1</sup> (**Table 7.4**). Overall, all liposomes showed to be safe for intravenous administration since no hemolysis signs or relevant alterations in plasma coagulation times were found.

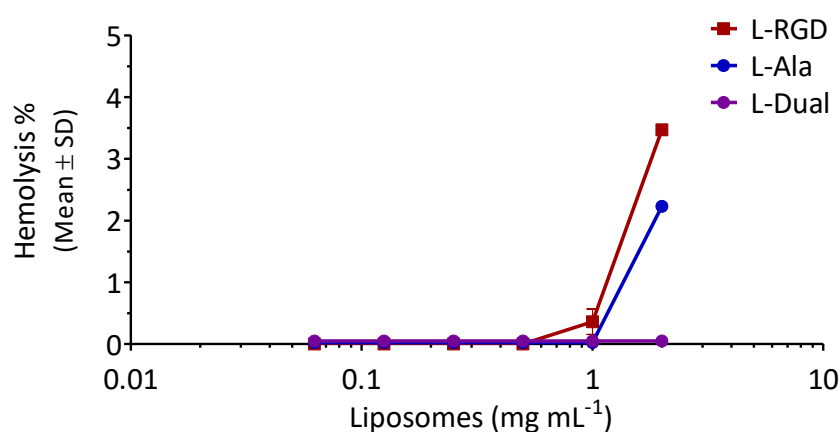


**Figure 7.21.** Hemolysis of human red blood cells incubated with liposomal formulations (systems after TFF 7.5-fold concentration and diafiltration in glucose 5%), for 1 h at 37 °C. Assay corresponds to a single representative batch per each system, performed by Dr. I. Abasolo group from VHIR (Barcelona).

**Table 7.4.** Plasma coagulation times measured as prothrombin time (PT), activated partial prothrombin time (APTT) and thrombin time (TT) after incubation of human plasma with L-RGD, L-Ala, and L-Dual Ala/RGD\*.

Sample	PT (s) (± SD)	APTT (s) (± SD)	TT (s) (± SD)
Normal coagulation time range	≤ 13.4	≤ 34.1	≤ 21
Pathological coagulation time range	≥ 20	≥ 61	≥ 42
Internal control plasma (healthy)	13.2 ± 0.2	31.7 ± 1.5	16.9 ± 0.2
Internal control plasma (pathological)	22.4 ± 0.2	59.6 ± 2.6	ND
Vehicle (PBS)	9.6 ± 1.2	32.3 ± 0.4	16.5 ± 0.8
L-RGD	9.9 ± 1.0	32.8 ± 0.0	16.9 ± 0.1
L-Ala	9.8 ± 1.4	32.2 ± 0.5	16.4 ± 0.6
L-Dual Ala/RGD	10.3 ± 1.5	36.3 ± 0.4	17.5 ± 0.6

\* Incubation at 0.1 mg mL<sup>-1</sup> liposomes (two weeks days after sample production), 30 min, 37 °C; Non-treated plasma and PBS were used as controls. Two independent measurements of the same batch, performed by Dr. I. Abasolo group from VHIR (Barcelona).

Overall, these results confirm the suitability of the implemented processing route, consisting in the production of the targeted liposomes by DELOS-susp and submitted to a TFF step for reaching doses suitable for intravenous dosing as well as for the incorporation of an isosmotic medium (water with glucose 5 %). The resulting systems meets the requirements for further in vivo BBB crossing studies.

## 7.7. Summary and Conclusions

In this Chapter, the development of new targeted liposomes for blood-brain barrier (BBB) crossing was studied.

First, new liposomes functionalized with novel ligands, including alanine amino acid (Ala) and transferrin ligand T7-peptide (T7), were successfully prepared by DELOS-susp technology. Both ligands were incorporated through chol-PEG<sub>400</sub>-derivative conjugates, i.e., chol-PEG<sub>400</sub>-Ala and chol-PEG<sub>400</sub>-T7, compounds specifically developed and synthesized by Dr. M. Royo group from IQAC-CSIC (Barcelona). The resulting liposomes showed great performance in terms of physicochemical characteristics, such as nanometric size, low dispersity, and spherical morphology. Additionally, exploratory studies for incorporating dual targeting (Ala and RGD) into liposomes were also performed. Liposomes functionalized with both alanine amino acid and RGD peptide were successfully developed. All new targeted liposomal systems could be obtained in liposome doses suitable for in vivo dosing and showed to be safe in vitro.

Then, the plasma circulation behavior and the BBB crossing capability of the new targeted liposomes were assessed by cerebral open flow microperfusion (cOFM), in collaboration with Dr. T. Birngruber from Joanneum Research (Austria). Ala-functionalized liposomes and T7-functionalized liposomes showed blood circulation times of several hours ( $> 6$  h), an interesting feature for exploring them in a future as drug nanocarriers. Besides, traces of MKC, a liposomal membrane component, could be found in brain of animals treated with Ala-functionalized nanoliposomes, opening the door to further exploration of these systems for brain targeting applications.

## 7.8. References

1. Mo, X., Liu, E. & Huang, Y. The intra-brain distribution of brain targeting delivery systems. in *Brain Targeted Drug Delivery System* (eds. Gao, H. & Gao, X.) 409–438 (Elsevier Ltd., 2019). doi:10.1016/b978-0-12-814001-7.00016-0.
2. Menken, M., Munsat, T. L. & Toole, J. F. The Global Burden of Disease Study: Implications for Neurology. *Arch. Neurol.* **57**, 418 (2000).
3. Jones, A. R. & Shusta, E. V. Blood-Brain Barrier Transport of Therapeutics via Receptor-Mediation. *Pharm. Res.* **24**, 1759–1771 (2007).
4. Pardridge, W. M. The Blood-Brain Barrier: Bottleneck in Brain Drug Development. *NeuroRx* **2**, 3–14 (2005).
5. Neuwelt, E. *et al.* Strategies to advance translational research into brain barriers. *Lancet Neurol.* **7**, 84–96 (2008).
6. Abbott, N. J., Rönnbäck, L. & Hansson, E. Astrocyte-endothelial interactions at the blood-brain barrier. *Nat. Rev. Neurosci.* **7**, 41–53 (2006).
7. Hammarlund-Udenaes, M., Lange, E. C. M. de & Thorne, R. G. *Drug delivery to the brain. Nanomaterials for Drug Delivery and Therapy* (American Association of Pharmaceutical Scientists, 2019). doi:10.1016/B978-0-12-816505-8.00005-9.
8. Weiss, N., Miller, F., Cazaubon, S. & Couraud, P. O. The blood-brain barrier in brain homeostasis and neurological diseases. *Biochim. Biophys. Acta - Biomembr.* **1788**, 842–857 (2009).
9. Campos-Bedolla, P., Walter, F. R., Veszelka, S. & Deli, M. A. Role of the Blood-Brain Barrier in the Nutrition of the Central Nervous System. *Arch. Med. Res.* **45**, 610–638 (2014).
10. Abbott, N. J., Patabendige, A. A. K., Dolman, D. E. M., Yusof, S. R. & Begley, D. J. Structure and function of the blood-brain barrier. *Neurobiol. Dis.* **37**, 13–25 (2010).
11. Lathera, J., Keep, R., Betz, L. A. & Goldstein, G. W. *Basic Neurochemistry: Molecular, Cellular and Medical Aspects*. (Philadelphia: Lippincott-Raven, 1999).
12. Zhang, E. Y., Knipp, G. T., Ekins, S. & Swaan, P. W. Structural biology and function of solute transporters: Implications for identifying and designing substrates. *Drug Metab. Rev.* **34**, 709–750 (2002).
13. Zhou, X., Smith, Q. R. & Liu, X. Brain penetrating peptides and peptide–drug conjugates to overcome the blood–brain barrier and target CNS diseases. *Wiley Interdiscip. Rev. Nanomedicine*

*Nanobiotechnology* 1–34 (2021) doi:10.1002/wnan.1695.

14. Khosa, A., Saha, R. N. & Singhvi, G. Blood-to-Brain Drug Delivery Using Nanocarriers. in *Drug Delivery to the Brain* (eds. Hammarlund-Udenaes, M., Lange, E. C. M. de & Thorne, R. G.) 433–454 (American Association of Pharmaceutical Scientists, 2019).
15. Glas, M. *et al.* Pegylated liposomal doxorubicin in recurrent malignant glioma: Analysis of a case series. *Oncology* **72**, 302–307 (2008).
16. Gaillard, P. J. *et al.* Pharmacokinetics, brain delivery, and efficacy in brain tumor-bearing mice of glutathione pegylated liposomal doxorubicin (2B3-101). *PLoS One* **9**, (2014).
17. Birngruber, T. *et al.* Enhanced Doxorubicin Delivery to the Brain Administered Through Glutathione PEGylated Liposomal Doxorubicin (2B3-101) as Compared with Generic Caelyx/Doxil - A Cerebral Open Flow Microperfusion Pilot Study. *J. Pharm. Sci.* **103**, 1945–1948 (2014).
18. Agrawal, M. *et al.* Recent advancements in liposomes targeting strategies to cross blood-brain barrier (BBB) for the treatment of Alzheimer's disease. *J. Control. Release* **260**, 61–77 (2017).
19. M. Fu, B. Experimental Methods and Transport Models for Drug Delivery Across the Blood-Brain Barrier. *Curr. Pharm. Biotechnol.* **13**, 1346–1359 (2012).
20. Stanimirovic, D. B., Bani-Yaghoub, M., Perkins, M. & Haqqani, A. S. Blood–brain barrier models: in vitro to in vivo translation in preclinical development of CNS-targeting biotherapeutics. *Expert Opin. Drug Discov.* **10**, 141–155 (2014).
21. Bickel, U. How to Measure Drug Transport across the Blood-Brain Barrier. *NeuroRx* **2**, 15–26 (2005).
22. Smith, Q. R. A Review of Blood–Brain Barrier Transport Techniques. in *The Blood-Brain Barrier: Biology and Research Protocols* (ed. Nag, S.) 193–208 (Humana Press, 2003).
23. Kuhnline Sloan, C. D. *et al.* Analytical and Biological Methods for Probing the Blood-Brain Barrier. *Annu. Rev. Anal. Chem.* **5**, 505–531 (2012).
24. Nag, S. *The Blood-Brain Barrier: Biology and Research Protocols. Methods in molecular medicine* vol. 89 (Humana Press, 2003).
25. Chefer, V. I., Thompson, A. C., Zapata, A. & Shippenberg, T. S. Overview of Brain Microdialysis. *Curr. Protoc. Neurosci.* 1–28 (2009) doi:10.1002/0471142301.ns0701s47.
26. Birngruber, T. & Sinner, F. Cerebral open flow microperfusion (cOFM) an innovative interface to brain tissue. *Drug Discov. Today Technol.* **20**, 19–25 (2016).

27. Birngruber, T. *et al.* Cerebral open flow microperfusion: A new in vivo technique for continuous measurement of substance transport across the intact blood-brain barrier. *Clin. Exp. Pharmacol. Physiol.* **40**, 864–871 (2013).
28. Ghosh, A. *et al.* Assessment of Blood-Brain Barrier Function and the Neuroinflammatory Response in the Rat Brain by Using Cerebral Open Flow Microperfusion (cOFM). *PLoS One* **9**, 3–9 (2014).
29. Deng, L. *et al.* RGD-Modified Nanocarrier-Mediated Targeted Delivery of HIF-1 $\alpha$ -AA Plasmid DNA to Cerebrovascular Endothelial Cells for Ischemic Stroke Treatment. *ACS Biomater. Sci. Eng.* **5**, 6254–6264 (2019).
30. Sonali *et al.* RGD-TPGS decorated theranostic liposomes for brain targeted delivery. *Colloids Surfaces B Biointerfaces* **147**, 129–141 (2016).
31. Liu, Y. *et al.* Paclitaxel loaded liposomes decorated with a multifunctional tandem peptide for glioma targeting. *Biomaterials* **35**, 4835–4847 (2014).
32. Mészáros, M. *et al.* Niosomes decorated with dual ligands targeting brain endothelial transporters increase cargo penetration across the blood-brain barrier. *Eur. J. Pharm. Sci.* **123**, 228–240 (2018).
33. Zong, T. *et al.* Enhanced Glioma Targeting and Penetration by Dual-Targeting Liposome Co-modified with T7 and TAT. *J. Pharm. Sci.* **103**, 3891–3901 (2014).
34. Kuang, Y. *et al.* T7 peptide-functionalized nanoparticles utilizing RNA interference for glioma dual targeting. *Int. J. Pharm.* **454**, 11–20 (2013).
35. Kim, G. *et al.* Systemic delivery of microRNA-21 antisense oligonucleotides to the brain using T7-peptide decorated exosomes. *J. Control. Release* **317**, 273–281 (2020).
36. Porkoláb, G. *et al.* Combination of Alanine and Glutathione as Targeting Ligands of Nanoparticles Enhances Cargo Delivery into the Cells of the Neurovascular Unit. *Pharmaceutics* **12**, 1–23 (2020).





“ You don't want to cover a subject; you want to uncover it.

— Eleanor Duckworth

# 8

## General Conclusions

From the work carried out in the present PhD. Thesis the following conclusions can be withdrawn:

1. New  $\alpha$ -galactosidase-loaded liposomes functionalized with RGD (nanoGLA) for the treatment of Fabry disease were properly developed and rationally optimized, using the compressed CO<sub>2</sub>-based DELOS-susp technology plus a tangential flow filtration process (TFF).
2. The strong impact of membrane composition of these vesicles on their physicochemical and biological characteristics was demonstrated by the incorporation of cationic miristalkonium chloride (MKC) surfactant to the formulation. Liposomes containing small amounts of MKC ( $\leq 5$  mol %) resulted in an important improving of the GLA entrapment efficiency and an enhancement of the colloidal stability and enzymatic activity.
3. The substitution of cholesterol-PEG<sub>200</sub>-RGD by cholesterol-PEG<sub>400</sub>-RGD as membrane component, allowed a more robust and reproducible functionalization of liposomes with RGD peptide.
4. Peptide density on liposomal surface could be finely tuned. Liposomes containing three different RGD densities on the liposomal surface were successfully prepared and deeply characterized, by changing the content of cholesterol-PEG<sub>400</sub>-RGD (0, 3, and 6 mol %) in the liposomal membrane. In vitro internalization studies in U2OS cells corroborated the functionality of cholesterol-PEG<sub>400</sub>-RGD containing liposomes for enhancing cellular internalization. Different nanoparticle-cell interactions were observed depending on the RGD

content on the liposomal surface, and higher cell internalization was obtained for liposomes containing a 3 mol % of cholesterol-PEG<sub>400</sub>-RGD.

5. NanoGLA formulation for the treatment of Fabry disease was successfully optimized to advance towards the preclinical development stage, including the establishment of the critical quality attributes and specifications, the study of the influence of critical parameters on nanoGLA quality by a DoE approach, the scale up to increase the batch-size, the addition of a concentration step using TFF in the manufacturing process to increase the total GLA content in the nanoformulation, and the selection of glucose 5 % as isosmotic dispersant medium.
6. Final scale up production of nanoGLA was successfully achieved, in the required amount and quality for starting the preclinical in vivo evaluation.
7. NanoGLA demonstrated superior efficacy compared to current treatment (Replagal®) and non-nanoformulated GLA in a Fabry KO mouse model. NanoGLA induced higher reduction of Gb3 levels in all tested tissues, included for the first time the brain. These results permitted to obtain the orphan medicinal product designation by the European Medicines Agency for the treatment of Fabry disease.
8. The regulatory preclinical stage of development was achieved for first time with this novel nanoGLA formulation, carrying out a first GLP toxicity study in rodents.
9. Alanine amino acid (Ala) functionalized nanoliposomes and transferrin-ligand (T7-peptide) functionalized nanoliposomes were successfully prepared by the CO<sub>2</sub>-based DELOS-susp technology. Both liposomal systems showed longer blood circulation time in rats than RGD-peptide functionalized nanoliposomes. Ala-functionalized nanoliposomes showed to be promising carriers for blood-brain barrier crossing and opens the door to further exploration of this system for brain targeting applications, nowadays a real challenge.

Based on these general conclusions, this Thesis demonstrates the strong potential of targeted liposomal systems for drug delivery application. The successful development and optimization of the nanoGLA product for improving the current enzymatic replacement therapy in Fabry disease especially contributes as an example of translational and interdisciplinary research.

” *I didn't want to just know names of things. I remember really wanting to know how it all worked.*

— Elizabeth Blackburn

# 9

## Experimental Methods

### 9.1. Materials

Cholest-5-en-3 $\beta$ -ol (cholesterol, chol, purity 95 %) was purchased from Panreac (Barcelona, Spain). 1,2-Dipalmitoyl-sn-glycero-3-phosphocholine (DPPC, MW 734.04, purity 99 %) was obtained from CordenPharma (Plankstadt, Germany). Miristalkonium chloride (MKC, MW 368.05, purity 99.2%) was acquired from US Biological Life Science (Salem, USA).

1,1'-dioctadecyl-3,3,3',3'-tetramethylindocarbocyanine perchlorate (DiI, MW 933.88, Ref. D282), and 1,1'-dioctadecyl-3,3,3',3'-tetramethylindodicarbocyanine perchlorate (DiD, MW 959.92, Ref. D307), were purchased from Invitrogen (Thermo Fisher Scientific, Waltham, USA).

The cholesterol-PEGn-peptide derivative molecules were specifically designed and synthesized by Dr. Miriam Royo group from the Institut de Química Avançada de Catalunya (IQAC-CSIC, Barcelona, Spain), and are explained in **Chapter 9.6.1**.

Agalsidase alfa (GLA, 1 mg mL<sup>-1</sup>, Replagal<sup>®</sup>) was purchased from Shire-Takeda. The other types of GLA (GLAcmycHis and rh-GLA) were produced by Dr. Jose Luís Corchero from the Institut de Biotecnologia i Biomedicina (IBB-UAB, Barcelona) and by LeanBio SL (Barcelona), and are explained in **Chapter 9.6.2**.

Ethanol (EtOH, HPLC grade, purity  $\geq$  99.5 %) was purchased from J.T.Baker (New Jersey, USA). Dimethyl sulfoxide (DMSO, ACS reagent, purity  $\geq$  99.9 %) was obtained from Sigma-Aldrich (Madrid, Spain). Methanol (MeOH, Optima™ LC/MS grade) was purchased from Fisher Scientific (Hampton, USA).

Carbon dioxide (CO<sub>2</sub>, purity 99.9 %) and nitrogen (N<sub>2</sub>, purity 99.9 %) were supplied by Carburos Metálicos S.A. (Barcelona, Spain). The water was always pre-treated with a Milli-Q® Advantage A10 water purification system (Millipore Ibérica, Madrid, Spain).

D-(+)-glucose (glucose, MW 180.16, purity ≥ 99.5 %), sodium phosphate dibasic (Na<sub>2</sub>HPO<sub>4</sub>, MW 141.96, purity 99.0 %), potassium chloride (KCl, ACS reagent, MW 74.56, purity ≥ 99 %), HEPES (MW 238.30, purity ≥ 99.5 %), calcium chloride (CaCl<sub>2</sub>, MW 110.98, purity 93.0 %), and glycine (bioultra, MW 75.07, purity ≥ 99.0 %) were supplied from Sigma-Aldrich (Saint Louis, USA). D-(+)-sucrose (sucrose, MW 342.30, purity ≥ 99.5 %), and sodium phosphate monobasic dihydrate (NaH<sub>2</sub>PO<sub>4</sub>·2H<sub>2</sub>O, MW 156.01, purity ≥ 99.0 %) were purchased from Fluka Biochemika (Germany). D-(+)-trehalose 2-hydrate (trehalose, BioChemica, MW 378.34, purity ≥ 98%), L-histidine (pharma grade, MW 155.16, purity ≥ 98.5 %), sodium chloride (NaCl, MW 58.44, purity 99.0 %), and sodium hydrogen carbonate (NaHCO<sub>3</sub>, MW 84.01, purity ≥ 99.7 %) were acquired from PanReac AppliChem (Castellar del Vallès, Spain). PBS 100 mM was prepared with sodium chloride (5.494 mg mL<sup>-1</sup>), sodium phosphate dibasic (0.44 mg mL<sup>-1</sup>), and sodium phosphate monobasic dihydrate (0.14 mg mL<sup>-1</sup>).

All the chemicals were used without further purification.

## 9.2. Preparation of nanovesicles by DELOS-susp

### 9.2.1. Equipment at lab-scale

Nanovesicles were prepared using DELOS-susp methodology, based on compressed CO<sub>2</sub> and developed by Nanomol group (ICMAB-CSIC) and Nanomol Technologies SL. Depending on the desired batch size, two different configurations were used: the small lab-scale equipment (7.5 mL high-pressure vessel, batch size 25 – 75 mL) or the intermediate lab-scale equipment (25 mL or 50 mL high-pressure vessel, batch size 150 – 900 mL) (see **Figure 9.1**)

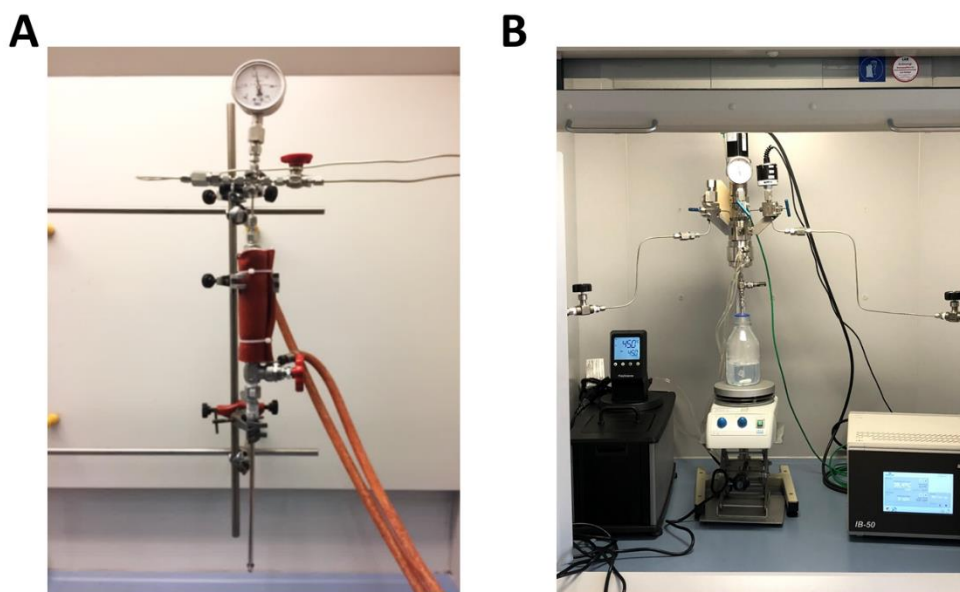


**Figure 9.1.** (A) Small lab-scale equipment (7.5 mL high-pressure vessel), and (B) Intermediate lab-scale equipment (25 mL/50 mL high-pressure vessel), used for the preparation of nanovesicles by DELOS-susp.

#### 9.2.1.1. Configuration of small lab-scale equipment (7.5 mL high-pressure vessel)

The small lab-scale equipment used to prepare nanovesicles using DELOS-susp is schematized in **Figure 9.2**. Briefly, the configuration consists of a 7.5 mL high pressure vessel (R), for which the temperature is maintained using an external fluid heating jacket. CO<sub>2</sub> is pumped into the reactor through a thermostatic syringe pump (model 260D, ISCO Inc., Lincoln, US) (P) to introduce CO<sub>2</sub> inside the vessel through valves V-02 and V-03 until reaching working pressure. Further, by using a manual depressurization valve (V-09), the expanded liquid solution contained in the vessel is depressurized into an aqueous phase placed in a collector (C) at atmospheric pressure, while at the same time, pressure of nitrogen (N<sub>2</sub>) is adjusted by a pressure regulator (V-05) and introduced through valves V-06 and V-07 directly from a pressurized reservoir to the vessel.

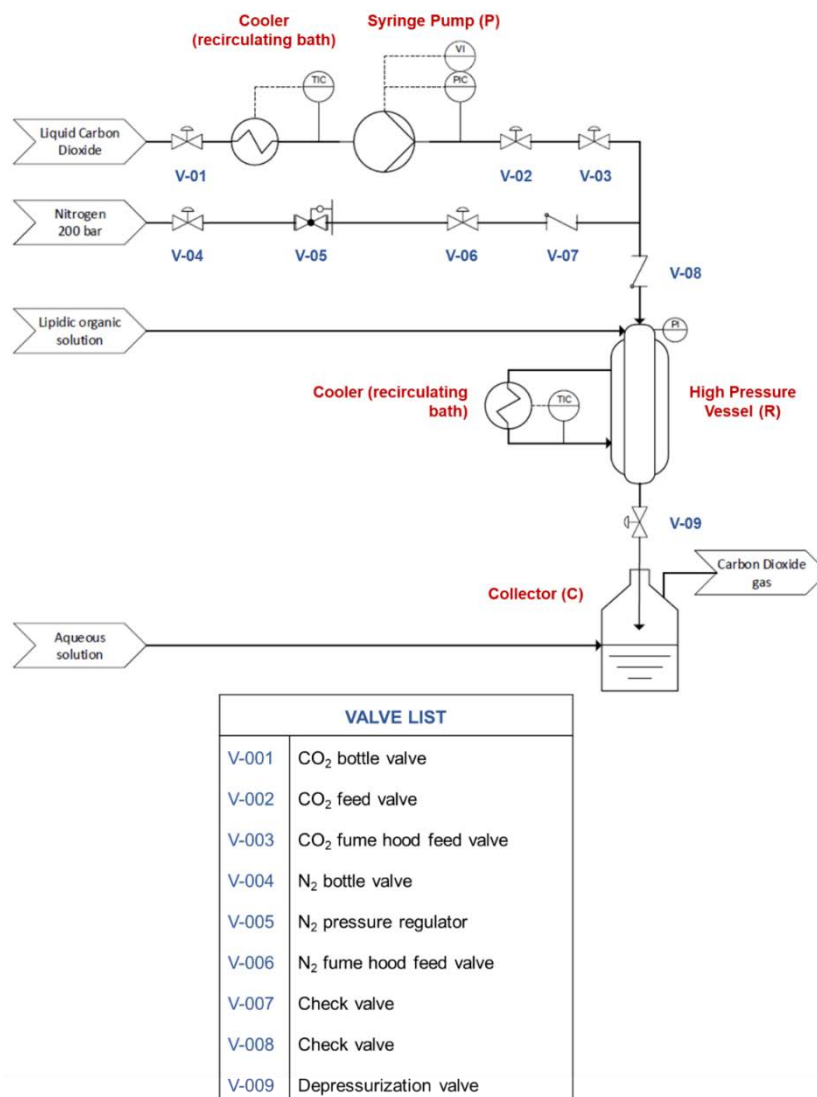


**Figure 9.2.** Process diagram of the small lab-scale equipment (7.5 mL high-pressure vessel) set-up used for the preparation of nanovesicles by DELOS-susp.

### 9.2.1.2. Configuration of intermediate lab-scale equipment (25/50 mL high-pressure vessel)

The intermediate lab-scale equipment used to prepare nanovesicles using DELOS-susp is schematized in **Figure 9.3**. Briefly, the configuration consists of a 25 mL or a 50 mL (independent and interchangeable) high-pressure vessel (R), for which the temperature is maintained using an external fluid heating jacket. Temperature and pressure inside R are monitored by a temperature indicator (TI) and a pressure indicator (PI). CO<sub>2</sub> is pumped into the reactor through a thermostatic syringe pump (model 260D, ISCO Inc., Lincoln, US) (P) to introduce CO<sub>2</sub> inside the vessel through valves V-01 and V-02 until reaching working pressure. A variable speed stirrer (S) inside R, ensures the homogeneity of the mixture in the volumetrically expanded phase. Further, by using a depressurization micrometric valve (V-07), the expanded liquid solution contained in the vessel is depressurized into an aqueous phase

placed in a collector (C) under magnetic agitation (SM) at atmospheric pressure, while at the same time, pressure of nitrogen (N<sub>2</sub>) is adjusted by a pressure adjustment valve (V-03) and introduced through valves V-04 and V-05 directly from a pressurized reservoir to the vessel.

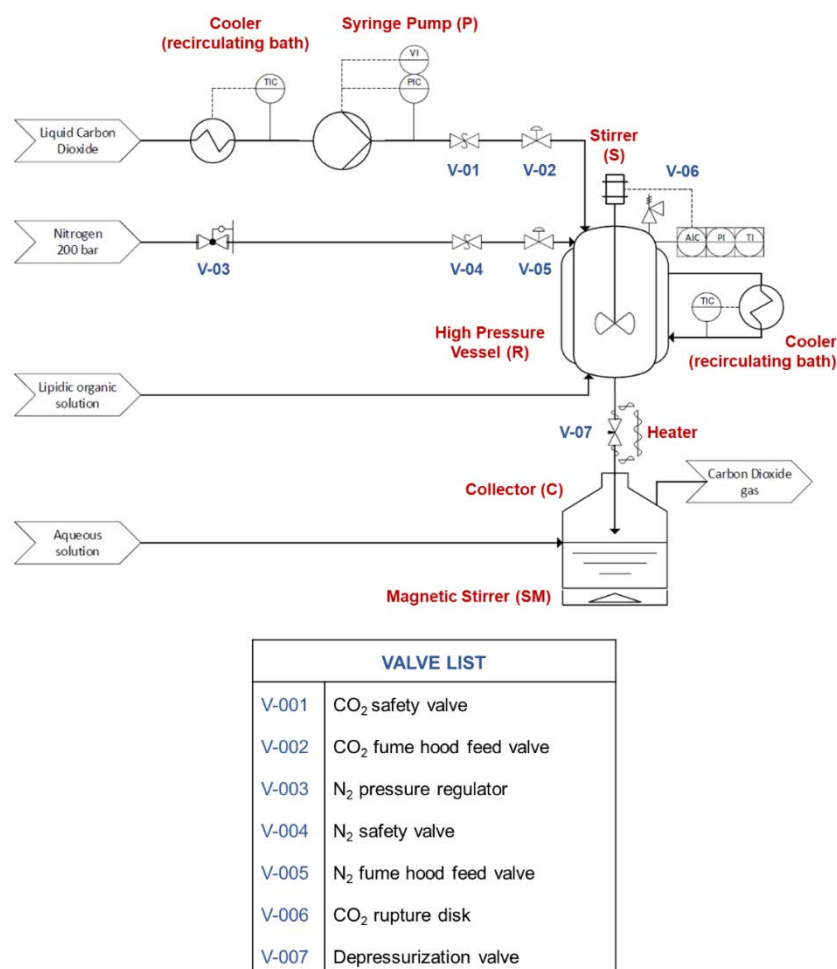


**Figure 9.3.** Process diagram of the intermediate lab-scale equipment (25/50 mL high-pressure vessel) set up used for the preparation of nanovesicles by DELOS-SUSP.

## 9.2.2. Experimental procedure

### 9.2.2.1. Experimental procedure in the small and intermediate lab-scale equipment

The preparation of nanovesicles by DELOS-susp was performed according to the following procedure, including:

- (iv) Loading of the organic solution consisting of a mixture of EtOH and DMSO containing hydrophobic membrane components (cholesterol, cholesterol-derivatives, DPPC, and/or MKC, previously sonicated 10 min at 40 °C) in the vessel R, at a working temperature ( $T_w = 35 - 40$  °C) and atmospheric pressure.
- (v) Addition of liquid compressed CO<sub>2</sub> and formation of a CO<sub>2</sub>-expanded solution with all the membrane components dissolved, at a given CO<sub>2</sub> molar fraction ( $X_{CO_2}$ ) between 0.50 and



0.85,  $T_w = 35\text{ }^\circ\text{C}$ , and working pressure  $P_w = 8.5 - 10\text{ MPa}$ ; The expanded-system was kept for 1 h in the small lab-scale equipment, or 15 min under stirring (500 rpm) in the intermediate lab-scale equipment, to achieve a complete homogenization and to attain thermal equilibration.

- (vi) Depressurization of the CO<sub>2</sub>-expanded solution into an aqueous solution (if not otherwise specified, purified water through a Milli-Q<sup>®</sup> Advantage A10 water purification system). A flow of nitrogen (N<sub>2</sub>) at a working pressure of  $P_w = 10 - 11\text{ MPa}$  is used to plunge the CO<sub>2</sub>-expanded solution from the reactor, maintaining a constant pressure inside the vessel during depressurization.

Average times per experiment were 1 h and 2 h for the small and intermediate lab-scale equipment, respectively. Nanovesicles were stored at  $2 - 8\text{ }^\circ\text{C}$  until further characterization.

#### **9.2.2.2. Encapsulation of GLA into nanovesicles by DELOS-susp**

The encapsulation of  $\alpha$ -galactosidase A (GLA) into nanovesicles by DELOS-susp, was performed following an identical experimental procedure as for the preparation of the unloaded nanovesicles, but just before the depressurization of the CO<sub>2</sub>-expanded solution, the free GLA was added into the aqueous solution (if not otherwise specified, purified water through a Milli-Q<sup>®</sup> Advantage A10 water purification system) at the desired concentration.

#### **9.2.3. Formulations prepared by DELOS-susp**

All nanovesicles samples were processed in the NANBIOSIS Soft Materials Service linked to Biomaterial Processing and Nanostructuring Unit (U6) at ICMAB-CSIC, or at Nanomol Technologies SL (Barcelona) facilities. The following **Table 9.1**, **Table 9.2**, **Table 9.3**, **Table 9.4**, and **Table 9.5** detail the composition and processing of the samples tested in the different Chapters.

**Table 9.1.** Preparation of samples by DELOS-susp\* and TFF† tested in **Chapter 3**.

Sample ID	Membrane components concentration (mM)	mol ratio	Aqueous phase	Vesicle concentration (mg mL <sup>-1</sup> )	Post-process
LP	DP:CH:CH-PEG200-RGD	10:6.0:1.0	water	1.5	TFF Diaf water
LP-GLA <sub>20</sub>	DP:CH:CH-PEG200-RGD	10:6.0:1.0	Replagal® in water	1.5	TFF Diaf water
MQ	MK:CH:CH-PEG200-RGD	17.5:7.5:1	water	3.5	TFF Diaf water
MQ-GLA <sub>20</sub>	MK:CH:CH-PEG200-RGD	17.5:7.5:1	Replagal® in water	3.5	TFF Diaf water
(0.4%MKC)-HLP	DP:CH:CH-PEG200-RGD (+ MK)	10:6.0:1.0 (0.4 mol %)	water	1.5	TFF Diaf water
(0.4%MKC)-HLP-GLA <sub>20</sub>	DP:CH:CH-PEG200-RGD (+ MK)	10:6.0:1.0 (0.4 mol %)	Replagal® in water	1.5	TFF Diaf water
(2.2%MKC)-HLP	DP:CH:CH-PEG200-RGD (+ MK)	10:6.0:1.0 (2.2 mol %)	water	1.5	TFF Diaf water
(2.2%MKC)-HLP-GLA <sub>20</sub>	DP:CH:CH-PEG200-RGD (+ MK)	10:6.0:1.0 (2.2 mol %)	Replagal® in water	1.5	TFF Diaf water
(2.2%MKC)-HLP-GLA <sub>8.5</sub>	DP:CH:CH-PEG200-RGD (+ MK)	10:6.0:1.0 (2.2 mol %)	Replagal® in water	1.5	TFF Diaf water
(4.3%MKC)-HLP	DP:CH:CH-PEG200-RGD (+ MK)	10:6.0:1.0 (4.3 mol %)	water	1.5	TFF Diaf water
(4.3%MKC)-HLP-GLA <sub>20</sub>	DP:CH:CH-PEG200-RGD (+ MK)	10:6.0:1.0 (4.3 mol %)	Replagal® in water	1.5	TFF Diaf water

\*P7.5/P25-DELOS-susp equipment ( $X_{CO_2} = 0.8$ ), final media water with EtOH (4 %) and DMSO (0.8 %); † TFF details: C02-E300-05-N, 10 mL min<sup>-1</sup> feed flow, TMP < 5, tubing #14. DP = DPPC, CH = cholesterol, CH-PEG200-RGD = cholesterol-PEG<sub>200</sub>-RGD, MK = MKC.

**Table 9.2.** Preparation of samples by DELOS-susp\* and TFF† tested in Chapter 4.

Sample ID	Composition	Membrane components mol ratio	Aqueous phase	Liposome concentration (mg mL <sup>-1</sup> )	Post-process
L-blank or L-0%RGD	DP:CH (+ MK)	10:7 (5 mol %)	water	1.2	TFF Diaf water
L-3%RGD	DP:CH:CH-PEG400-RGD (+ MK)	10:6.5:0.5 (5 mol %)	water	1.2	TFF Diaf water
L-6%RGD	DP:CH:CH-PEG400-RGD (+ MK)	10:6.0:1.0 (5 mol %)	water	1.2	TFF Diaf water
L-blank-DiD <sub>INCUB</sub>	DP:CH (+ MK)	10:7 (5 mol %)	water	1.2	Incub DiD (100 nM) + TFF Diaf water
L-blank-DiD <sub>DELOS</sub>	DP:CH (+ MK) (DiD)	10:7 (5 mol %) (0.004 mol %)	water	1.2	TFF Diaf water
L-RGD-DiD <sub>INCUB</sub>	DP:CH (+ MK)	10:6.5:0.5 (5 mol %)	water	1.2	Incub DiD (100 nM) + TFF Diaf water
L-RGD-DiD <sub>DELOS</sub>	DP:CH (+ MK) (DiD)	10:6.5:0.5 (5 mol %) (0.004 mol %)	water	1.2	TFF Diaf water
L-0%RGD	DP:CH (+ MK) (DiD)	10:7 (5 mol %) (0.004 mol %)	water	1.2	TFF Diaf water
L-3%RGD	DP:CH:CH-PEG400-RGD (+ MK) (DiD)	10:6.5:0.5 (5 mol %) (0.004 mol %)	water	1.2	TFF Diaf water
L-6%RGD	DP:CH:CH-PEG400-RGD (+ MK) (DiD)	10:6.0:1.0 (5 mol %) (0.004 mol %)	water	1.2	TFF Diaf water

\*P7.5-DELOS-susp equipment, 25.2 mL batch-size ( $X_{CO_2} = 0.8$ ), final media water with EtOH (5 %) and DMSO (1 %);

† TFF details: C04-E300-05-N, 27 mL min<sup>-1</sup> feed flow, TMP 5 – 10, tubing #14. DP = DPPC, CH = cholesterol, CH-PEG400-RGD = cholesterol-PEG<sub>400</sub>-RGD, MK = MKC.

**Table 9.3.** Preparation of samples by DELOS-susp\* and TFF† tested in Chapter 5.

Sample ID	Composition	Membrane components mol ratio	Aqueous phase	Post-process	TFF details
DOE‡	DP:CH:CH-PEG400-RGD (+ MK)	Variable (2.2 mol %)	GLAcmycHis in water	TFF Diaf water	C02-E300-05-N, 10, 1, 14
L-GLA <sub>INTRMED</sub>	DP:CH:CH-PEG400-RGD (+ MK)	10:6.5:0.5 (5 mol %)	GLAcmycHis in water	-	-
L-GLA <sub>DIAF</sub>	DP:CH:CH-PEG400-RGD (+ MK)	10:6.5:0.5 (5 mol %)	GLAcmycHis in water	TFF Diaf water	D02-E300-05-N, 50, 1 – 3, 14
L-GLA <sub>35</sub>	DP:CH:CH-PEG400-RGD (+ MK)	10:6.5:0.5 (5 mol %)	GLAcmycHis in water	-	-
L-GLA <sub>50</sub>	DP:CH:CH-PEG400-RGD (+ MK)	10:6.5:0.5 (5 mol %)	GLAcmycHis in water	-	-
L-GLA <sub>75</sub>	DP:CH:CH-PEG400-RGD (+ MK)	10:6.5:0.5 (5 mol %)	GLAcmycHis in water	-	-
L-GLA <sub>DIAF+CONC</sub>	DP:CH:CH-PEG400-RGD (+ MK)	10:6.5:0.5 (5 mol %)	GLAcmycHis in water	TFF Diaf water + Cx5-6	D02-E300-05-N, 50, 1 – 3, 14
L-GLA <sub>CONC</sub>	DP:CH:CH-PEG400-RGD (+ MK)	10:6.5:0.5 (5 mol %)	GLAcmycHis in water	TFF Cx5-6	D02-E300-05-N, 50, 1 – 3, 14

Sample ID (...continue)	Composition	Membrane components mol ratio	Aqueous phase	Post-process	TFF details
Optimized L-GLA <sub>DIAF+CONC</sub>	DP:CH:CH-PEG400-RGD (+ MK)	10:6.5:0.5 (5 mol %)	GLAcmycHis in water	TFF Diaf water + Cx7.5	C04-E300-05-N, 27, 10, 14
L-DELOS-water <sup>§</sup>	DP:CH:CH-PEG400-RGD (+ MK)	10:6.5:0.5 (5 mol %)	water	-	-
L-DELOS-PBS <sup>§</sup>	DP:CH:CH-PEG400-RGD (+ MK)	10:6.5:0.5 (5 mol %)	PBS 100 mM	-	-
L-DIAF-water	DP:CH:CH-PEG400-RGD (+ MK)	10:6.5:0.5 (5 mol %)	water	TFF Diaf water	C04-E300-05-N, 27, 6 – 8, 14
L-DIAF-PBS	DP:CH:CH-PEG400-RGD (+ MK)	10:6.5:0.5 (5 mol %)	water	TFF Diaf PBS 100 mM	C04-E300-05-N, 27, 6 – 8, 14
GLA-L <sub>DELOS-water</sub>	DP:CH:CH-PEG400-RGD (+ MK)	10:6.5:0.5 (5 mol %)	GLAcmycHis in water	-	-
GLA-L <sub>DIAF-water</sub>	DP:CH:CH-PEG400-RGD (+ MK)	10:6.5:0.5 (5 mol %)	GLAcmycHis in water	TFF Diaf water	C02-E300-05-N, 15, 2, 14
GLA-L <sub>DIAF-PBS</sub>	DP:CH:CH-PEG400-RGD (+ MK)	10:6.5:0.5 (5 mol %)	GLAcmycHis in water	TFF Diaf PBS 100 mM	C04-E300-05-N, 15, 6 – 8, 14
L-DELOS	DP:CH:CH-PEG400-RGD (+ MK)	10:6.5:0.5 (5 mol %)	GLAcmycHis in water	-	-
L-Water	DP:CH:CH-PEG400-RGD (+ MK)	10:6.5:0.5 (5 mol %)	GLAcmycHis in water	TFF Diaf water	C04-E300-05-N, 27, 6 – 8, 14
L-Glc	DP:CH:CH-PEG400-RGD (+ MK)	10:6.5:0.5 (5 mol %)	GLAcmycHis in water	TFF Diaf glucose (5%)	C04-E300-05-N, 27, 6 – 8, 14
L-Tre	DP:CH:CH-PEG400-RGD (+ MK)	10:6.5:0.5 (5 mol %)	GLAcmycHis in water	TFF Diaf Trehalose (10%)	C04-E300-05-N, 27, 6 – 8, 14
L-Suc	DP:CH:CH-PEG400-RGD (+ MK)	10:6.5:0.5 (5 mol %)	GLAcmycHis in water	TFF Diaf Sucrose (10%)	C04-E300-05-N, 27, 6 – 8, 14
L-Suc/His	DP:CH:CH-PEG400-RGD (+ MK)	10:6.5:0.5 (5 mol %)	GLAcmycHis in water	TFF Diaf Histidine (10 mM, pH 7) & Sucrose (10%)	C04-E300-05-N, 27, 6 – 8, 14
L-Suc/Gly	DP:CH:CH-PEG400-RGD (+ MK)	10:6.5:0.5 (5 mol %)	GLAcmycHis in water	TFF Diaf Sucrose (8.5%) & Glycine (0.4%)	C04-E300-05-N, 27, 6 – 8, 14
L-Gly	DP:CH:CH-PEG400-RGD (+ MK)	10:6.5:0.5 (5 mol %)	GLAcmycHis in water	TFF Diaf Glycine (2.5%)	C04-E300-05-N, 27, 6 – 8, 14
L-NaCl	DP:CH:CH-PEG400-RGD (+ MK)	10:6.5:0.5 (5 mol %)	GLAcmycHis in water	TFF Diaf NaCl (0.9%)	C04-E300-05-N, 27, 6 – 8, 14
L-LB	DP:CH:CH-PEG400-RGD (+ MK)	10:6.5:0.5 (5 mol %)	GLAcmycHis in water	TFF Diaf Buffer LB	C04-E300-05-N, 27, 6 – 8, 14
Optimized L-Glu x7	DP:CH:CH-PEG400-RGD (+ MK)	10:6.5:0.5 (5 mol %)	GLAcmycHis in water	TFF Diaf glucose (5%) + Cx7.5	C04-E300-05-N, 27, 6 – 8, 14

\* If not specified, all samples produced in the P25/P50-DELOS-susp equipment, 150 - 300 mL batch-size at 1.2 mg mL<sup>-1</sup>, final media water with EtOH (5 %) and DMSO (1 %); † TFF details: hollow fiber reference, feed flow, TMP, tubing. ‡ DOE samples according to **Table 5.3**,  $X_{CO_2} = 0.55$ ; § Samples produced in the P7.5-DELOS-susp equipment, 25.2 mL batch-size ( $X_{CO_2} = 0.8$ ) at 1.2 mg mL<sup>-1</sup>. DP = DPPC, CH = cholesterol, CH-PEG400-RGD = cholesterol-PEG<sub>400</sub>-RGD, MK = MKC.

**Table 9.4.** Preparation of samples by DELOS-susp\* and TFF† tested in **Chapter 6**.

Sample ID	Composition	Membrane components mol ratio	Aqueous phase	Post-process	TFF details	Final concentration (mg mL <sup>-1</sup> )
Empty liposomes	DP:CH:CH-PEG400-RGD (+ MK)	10:6.5:0.5 (5 mol %)	water	TFF Diaf glucose 5% + Cx7.5	C04-E300-05-N, 27, 5 – 10, 14	9.0
NanoGLA 3%RGD Intermediate	DP:CH:CH-PEG400-RGD (+ MK)	10:6.5:0.5 (5 mol %)	GLA-rh in water	-	-	1.2
NanoGLA 3%RGD Diaf. water	DP:CH:CH-PEG400-RGD (+ MK)	10:6.5:0.5 (5 mol %)	GLA-rh in water	TFF Diaf water	D04-E300-05-N, 159, 5 – 10, 16	1.2
NanoGLA 3%RGD Diaf. glucose	DP:CH:CH-PEG400-RGD (+ MK)	10:6.5:0.5 (5 mol %)	GLA-rh in water	TFF Diaf glucose 5%	D04-E300-05-N, 159, 5 – 10, 16	1.2
NanoGLA 3%RGD Final	DP:CH:CH-PEG400-RGD (+ MK)	10:6.5:0.5 (5 mol %)	GLA-rh in water	TFF Cx7.5 + Diaf glucose 5%	D04-E300-05-N, 159, 5 – 10, 16	8.4
NanoGLA 6%RGD Intermediate	DP:CH:CH-PEG400-RGD (+ MK)	10:6.0:1.0 (5 mol %)	GLA-rh in water	-	-	1.2
NanoGLA 6%RGD Diaf. water	DP:CH:CH-PEG400-RGD (+ MK)	10:6.0:1.0 (5 mol %)	GLA-rh in water	TFF Diaf water	D04-E300-05-N, 159, 5 – 10, 16	1.2
NanoGLA 6%RGD Diaf. glucose	DP:CH:CH-PEG400-RGD (+ MK)	10:6.0:1.0 (5 mol %)	GLA-rh in water	TFF Diaf glucose 5%	D04-E300-05-N, 159, 5 – 10, 16	1.2
NanoGLA 6%RGD Final	DP:CH:CH-PEG400-RGD (+ MK)	10:6.0:1.0 (5 mol %)	GLA-rh in water	TFF Cx7.5 + Diaf glucose 5%	D04-E300-05-N, 159, 5 – 10, 16	8.4
nanoGLA Intermediate (first set)	DP:CH:CH-PEG400-RGD (+ MK)	10:6.0:1.0 (5 mol %)	GLA-rh in water	-	-	1.2
nanoGLA Final (first set)	DP:CH:CH-PEG400-RGD (+ MK)	10:6.0:1.0 (5 mol %)	GLA-rh in water	TFF <sup>§</sup> Cx7.5 + Diaf glucose 5%	D04-E300-05-S, 159, 5 – 10, 16	9.0
Empty-liposomes Intermediate (first set)	DP:CH:CH-PEG400-RGD (+ MK)	10:6.0:1.0 (5 mol %)	water	-	-	1.2
Empty-liposomes Final (first set)	DP:CH:CH-PEG400-RGD (+ MK)	10:6.0:1.0 (5 mol %)	water	TFF <sup>§</sup> Cx7.5 + Diaf glucose 5%	D04-E300-05-S, 159, 5 – 10, 16	
nanoGLA Intermediate (second set)	DP:CH:CH-PEG400-RGD (+ MK)	10:6.0:1.0 (5 mol %)	GLA-rh in water	-	-	1.2

Sample ID (...continue)	Composition	Membrane components mol ratio	Aqueous phase	Post- process	TFF details	Final concentration (mg mL <sup>-1</sup> )
nanoGLA Final (second set)	DP:CH:CH- PEG400-RGD (+ MK)	10:6.0:1.0 (5 mol %)	GLA-rh in water	TFF <sup>§</sup> Cx7.5 + Diaf glucose 5%	D04-E300- 05-S, 159, 5 – 10, 16	9.0
Empty- liposomes Intermediate (second set)	DP:CH:CH- PEG400-RGD (+ MK)	10:6.0:1.0 (5 mol %)	water	-	-	1.2
Empty- liposomes Final (second set)	DP:CH:CH- PEG400-RGD (+ MK)	10:6.0:1.0 (5 mol %)	water	TFF <sup>§</sup> Cx7.5 + Diaf glucose 5%	D04-E300- 05-S, 159, 5 – 10, 16	9.0

\* All samples depressurized in water as aqueous phase, obtaining liposomes at 1.2 mg mL<sup>-1</sup> in water with EtOH (5 %) and DMSO (1 %); In general,  $X_{CO_2} = 0.5 - 0.8$ ; † TFF details: hollow fiber reference, feed flow, TMP, tubing. § Aseptic-like conditions, see **Chapter 9.3.1**.

**Table 9.5.** Preparation of samples by DELOS-susp\* and TFF† tested in **Chapter 7**.

Sample ID	Composition	Membrane components mol ratio	DELOS-susp equipment	Post-process	Final concentration (mg mL <sup>-1</sup> )
L-RGD	DP:CH:CH-PEG400-RGD (+ MK)	10:6.5:0.5 (5 mol %)	P25	TFF Diaf water + Cx7.5	9.0
Blank	DP:CH (+ MK)	10:7 (5 mol %)	P7.5	-	1.2
Blank(-)	DP:CH	10:07	P7.5	-	1.2
L-3%Ala <sup>‡</sup>	DP:CH:CH-PEG400-Ala (+ MK)	10:6.5:0.5 (5 mol %)	P7.5	-	1.2
L-6%Ala <sup>‡</sup>	DP:CH:CH-PEG400-Ala (+ MK)	10:6.0:1.0 (5 mol %)	P7.5	-	1.2
L-6%Ala(-) <sup>‡</sup>	DP:CH:CH-PEG400-Ala	10:6.0:1.0	P7.5	-	1.2
L-3%T7	DP:CH:CH-PEG400-T7 (+ MK)	10:6.5:0.5 (5 mol %)	P7.5	-	1.2
L-6%T7	DP:CH:CH-PEG400-T7 (+ MK)	10:6.0:1.0 (5 mol %)	P7.5	-	1.2
L-3%T7(-)	DP:CH:CH-PEG400-T7 (+ MK)	10:6.5:0.5	P7.5	-	1.2
L-3%Ala-P25 <sup>‡</sup>	DP:CH:CH-PEG400-Ala (+ MK)	10:6.5:0.5 (5 mol %)	P25	-	1.2
L-3%T7-P25	DP:CH:CH-PEG400-T7 (+ MK)	10:6.5:0.5 (5 mol %)	P25	-	1.2
L-3%Ala <sup>‡</sup> INTRMD	DP:CH:CH-PEG400-Ala (+ MK)	10:6.5:0.5 (5 mol %)	P25	-	1.2
L-3%Ala CONC+DIAF	DP:CH:CH-PEG400-Ala (+ MK)	10:6.5:0.5 (5 mol %)	P25	TFF Diaf water + Cx7.5	9.0

Sample ID (...continue)	Composition	Membrane components mol ratio	DELOS-susp equipment	Post-process	Final concentration (mg mL <sup>-1</sup> )
L-3%T7 <sup>INTRMD</sup>	DP:CH:CH-PEG400-T7 (+ MK)	10:6.5:0.5 (5 mol %)	P25	-	1.2
L-3%T7 <sup>CONC+DIAF</sup>	DP:CH:CH-PEG400-T7 (+ MK)	10:6.5:0.5 (5 mol %)	P25	TFF Cx7.5 + Diaf water	9.0
L-Ala <sup>‡</sup>	DP:CH:CH-PEG400-Ala (+ MK)	10:6.5:0.5 (5 mol %)	P25	TFF <sup>§</sup> Cx7.5 + Diaf water	9.0
L-T7	DP:CH:CH-PEG400-T7 (+ MK)	10:6.5:0.5 (5 mol %)	P25	TFF <sup>§</sup> Cx7.5 + Diaf water	9.0
L-Dual Ala/RGD	DP:CH:CH-PEG400- Ala:CH-PEG400-RGD (+ MK)	10:6.5:0.33:0.17 (5 mol %)	P7.5	TFF Diaf water	1.2
L-Dual Ala/RGD	DP:CH:CH-PEG400- Ala:CH-PEG400-RGD (+ MK)	10:6.5:0.25:0.25 (5 mol %)	P7.5	TFF Diaf water	1.2
L-Dual Ala/RGD	DP:CH:CH-PEG400- Ala:CH-PEG400-RGD (+ MK)	10:6.5:0.43:0.43 (5 mol %)	P7.5	TFF Diaf water	1.2
L-RGD	DP:CH:CH-PEG400-RGD (+ MK)	10:6.5:0.5 (5 mol %)	P25	TFF <sup>§</sup> Cx7.5 + Diaf glucose 5%	9.0
L-Ala <sup>‡</sup>	DP:CH:CH-PEG400-Ala (+ MK)	10:6.5:0.5 (5 mol %)	P25	TFF <sup>§</sup> Cx7.5 + Diaf glucose 5%	9.0
L-Dual Ala/RGD	DP:CH:CH-PEG400- Ala:CH-PEG400-RGD (+ MK)	10:6.5:0.43:0.43 (5 mol %)	P25	TFF <sup>§</sup> Cx7.5 + Diaf glucose 5%	9.0

\* All samples depressurized in water as aqueous phase, obtaining liposomes at 1.2 mg mL<sup>-1</sup> in water with EtOH (5 %) and DMSO (1 %) if not otherwise specified; † TFF details: C04-E300-05-N, 27 mL min<sup>-1</sup> feed flow, TMP 5 – 10, tubing #14. ‡ Depressurized in water as aqueous phase, obtaining liposomes at 1.2 mg mL<sup>-1</sup> in water with EtOH (6 %). In general,  $X_{CO_2} = 0.5 - 0.8$ . § Aseptic-like conditions (C04-E300-05-S), see **Chapter 9.3.1**. DP = DPPC, CH = cholesterol, CH-PEG400-RGD = cholesterol-PEG<sub>400</sub>-RGD, MK = MKC.

### 9.3. Microfiltration by Tangential Flow Filtration

After DELOS-susp production, nanovesicles were submitted to a purification step based on tangential flow filtration (TFF), using a KrosFlo Research Iii TFF System (Repligen, Waltham, USA) (**Figure 9.4**). Three different operating modes for the KrosFlo® Research Iii TFF system were used depending on the aimed objective: (i) diafiltration, (ii) buffer exchange, and (iii) batch concentration,<sup>1</sup> explained in more detail in **Chapter 1.4.4**. The TFF experimental procedure included the following steps.



**Figure 9.4.** Schematic set up of *KrosFlo Research Iii TFF System*, used for diafiltration purification step. Adapted from manufacturer’s operating instructions.<sup>1</sup>

To separate the free GLA homodimer (~ 100 kDa), samples obtained through DELOS-susp were recirculated through a modified polyethersulfone (mPES) filter hollow column 300 kDa cut-off. Depending on the sample volume, different filter hollow columns with a range of surface area were used, 20 cm<sup>2</sup>, 40 cm<sup>2</sup>, or 235 cm<sup>2</sup> (C02-E300-05-N, C04-E300-05-N, or D04-E300-05-N, respectively, from Repligen, USA). Components with a size below pore size were removed, such as free-GLA, the remaining organic solvent, or small molecules not incorporated into the nanovesicles.

To perform the diafiltration, the *KrosFlo® Research Iii TFF system* was set up following the manufacturer’s recommendations. Columns were hydrated with water accordingly to their surface (2 mL cm<sup>-2</sup>). A determined volume of sample ( $V_{\text{sample}}$ ) added to sample reservoir ( $R_{\text{sample}}$ ) and submitted to some cycles of diafiltration (5 – 6 cycles, according to manufacturer’s instructions) substituting the removed volume with new media placed in the buffer reservoir ( $R_{\text{buffer}}$ ), in order to maintain a constant concentration as free GLA and solvents were removed. After 6 diafiltration cycles, the process was stopped when the filtrated volume ( $V_{\text{permeate}}$ ) was 6-times the initial sample volume, resulting in the elimination of non-incorporated molecules and organic solvents from the dispersion. The buffer reservoir usually contained water (just for washing proposes) or a different buffer (for buffer exchange). The number of diafiltration cycles was reduced to 5 in some samples, obtaining the same results. For GLA-containing samples, the process was done in cold conditions (ice-water batch) to preserve GLA activity.

For samples’ concentration, the same process was followed, with the exception that in this case, the buffer reservoir was not connected to the system allowing the sample to become more concentrated as volume was being removed, until the desired concentration factor. In this thesis, concentration factor usually ranged from 7-fold to 12-fold.



Samples that were both concentrated and diafiltrated proceeded in the same way, one step followed by the other. The order of the diafiltration and concentration processes was interchangeable, since it was demonstrated no significant impact: diafiltration and concentration, or concentration and diafiltration.

Additional parameters were depending on the volume sample. The detailed operational parameters for each system were indicated in the previous **Chapter 9.2.3**. The duration of these processes depended on the volume sample as well as the size of the hollow fiber column, but they generally take about 15 min to 1.30 h. All nanovesicles samples were processed in the NANBIOSIS Soft Materials Service linked to Biomaterial Processing and Nanostructuring Unit (U6) at ICMAB-CSIC.

### 9.3.1. Aseptic-like conditions

Production in aseptic-like conditions was done using sterile material. According to literature, pressure and temperature levels achieved during the DELOS-susp process can have a sterilizing function,<sup>2,3</sup> inactivating microorganisms growth and reducing the contamination level associated to the production process. Further, the depressurization step was done in sterile autoclaved glass bottles.

TFF-based diafiltration and concentration process in aseptic-like conditions was performed moving the KrosFlo® Research Iii TFF system inside a class II laminar flow biological safety cabinet (Maxisafe 2020, Thermo Scientific). All the diafiltration material (tubes, reservoirs, volumetric glass recipients) was sterilized in an autoclave (Presoclave-III 50, J.P.Selecta) by pressurized saturated steam autoclave (121 °C, 20 min); plastic pieces (such as tubing connectors or reservoirs caps) were submerged overnight in ethanol. Filter hollow columns (D04-E300-05-S or C04-E300-05-S) and pressure transducers were purchased directly in a sterile packaging (Repligen, USA). Obtained samples were always manipulated and aliquoted inside the laminar flow cabinet.

## 9.4. Freeze-drying of nanovesicles

Lyophilization or freeze-drying process allows the removal of water and solvents from liposomal samples. It works by freezing the material and then sublimating the ice directly from solid to gaseous state under vacuum (**Figure 9.5**). The process can be divided in three steps: freezing, primary drying, and second drying.

**Freezing phase:** First, samples were cooled until their freezing. It was done at atmospheric pressure and  $-80\text{ °C}$  (nominal temperature) for 2 h.

**Primary drying (sublimation) phase:** Then, pressure was decreased from the atmospheric pressure (1 atm,  $10^5\text{ Pa}$ ) to  $5 \times 10^{-5}\text{ atm}$  (5 Pa), a value below their critical temperature. This pressure reduction induces the sublimation of the sample water, allowing a phase transition from solid to gas under vacuum. These conditions ( $-80\text{ °C}$ , 5 Pa) were maintained for 3 days, in which most of the solvent content was eliminated.

**Second drying (adsorption) phase:** In this phase, ionically bound water molecules are removed by raising the temperature above than in the primary drying temperature. Here, first the vacuum was broken until samples returned to atmospheric pressure. They were stored at 2 – 8 °C until characterization.

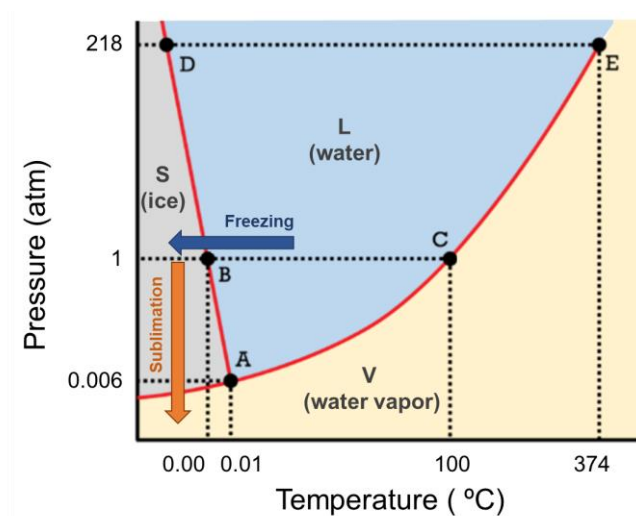


**Figure 9.5.** Water phase diagram. Sample freeze-drying process consists of a freezing process at atmospheric pressure, followed by a sublimated process by reduction of pressure.

In this Thesis, a precise volume of liposomal sample was placed into a 4 mL glass vial (**Table 9.6**) and then covered by aluminum foil. Using a needle, tiny holes were made in the aluminum foil, to allow the water to escape but preventing the loss of sample mass. Samples were then lyophilized with a LyoQuest™ Plus –85 °C (Telstar®, Spain).

**Table 9.6.** Lyophilized volume depending on their intended characterization.

Liposome concentration (mg mL <sup>-1</sup> )	Goal	Lyophilized volume (mL)
~ 1	Concentration for DiD quantification	2.000 – 2.500
~ 1	Lipid quantification	1.000
~ 8 – 9	Lipid quantification	0.500

## 9.5. Physicochemical characterization of nanovesicles

### 9.5.1. Size, PDI, ζ-potential, and particle concentration

These measures were performed in the NANBIOSIS Soft Materials Service linked to Biomaterial Processing and Nanostructuring Unit (U6) at ICMAB-CSIC.

#### **9.5.1.1. Dynamic Light Scattering (DLS) and Electrophoretic Light Scattering (ELS)**

Particle size distribution, polydispersity index (PDI), and  $\zeta$ -potential of all the produced vesicles were measured using a dynamic light scattering (DLS) and electrophoretic light scattering (ELS) analyzer combined with non-invasive backscatter technology (NIBS) (Malvern Zetasizer Nano ZS, Malvern Instruments, U.K.). The equipment was equipped with a 4 mW “red” He-Ne laser ( $\lambda = 632.8$  nm), and with a thermostatic sample chamber. The detector was set at  $173^\circ$  for particle size distribution measurements, and  $13^\circ$  for  $\zeta$ -potential measurements.

Samples (1 mL) were placed in a disposable polystyrene cuvette (for DLS measurements) or in a disposable folded capillary cell (for  $\zeta$ -potential measurements, applied voltage 40 mV) and were analyzed without any previous modification or dilution. Only concentrated samples were diluted in water just before analysis, the same dilution than the concentration factor (usually 1:7 vol.).

All reported values correspond to the average result of three consecutive measurements at  $20^\circ\text{C}$  on the same sample. Data was recorded using the Zetasizer Software 7.13 (Malvern Panalytical, UK). Size data was based on intensity size-distribution and corresponds to z-average  $\pm$  SD between the three measurements. The use of scattered intensity is the most recommendable data when using DLS, since it comes from the original data provided by the analyzer, without further processing or involved assumptions for calculating particle size. The  $\zeta$ -potential data was based on Smoluchowski model and corresponds to  $\zeta$ -potential average  $\pm$  SD between the three measurements.

#### **9.5.1.2. Nanoparticle tracking analysis (NTA)**

Particle size distribution and particle concentration were also measured using a Nanoparticle Tracking Analysis (NTA) (Nanosight NS300, Malvern Panalytical, U.K.), equipped with a sCMOS camera and a  $\lambda = 488$  nm laser. A video of particles moving under Brownian motion and visualized through their scattering signal was recorded in a field of view of  $100\ \mu\text{m} \times 80\ \mu\text{m} \times 10\ \mu\text{m}$  and analyzed by the NTA software. NTA tracks particles individually and uses the Stokes- Einstein equation for calculating their hydrodynamic diameters as well as the particle concentration. NTA data was based on the average of three independent videos (1 min per video). Just before the measurement, samples were diluted between 1/1,000 and 1/100,000 in water to reach the optimum number of particles/frame (from 50 to 90) recommended by the manufacturer.

#### **9.5.1.3. Multi-Angle Dynamic Light Scattering (MADLS)**

Particle size distribution and particle concentration were also measured using a multi-angle dynamic light scattering (MADLS), based on the combination of the light dispersion of three different detectors located at different angles ( $173^\circ$ ,  $13^\circ$ , and  $90^\circ$ ). The equipment (Malvern Zetasizer Ultra, Malvern Panalytical, U.K.) was equipped with a He-Ne laser ( $\lambda = 633$  nm). Samples (1 mL) were placed in a disposable polystyrene cuvette (with the four walls transparent) were analyzed without any previous modification or dilution. Only concentrated samples were diluted in water just before analysis, the same

dilution than the concentration factor (usually 1:7 vol.). All reported values correspond to the average result of three consecutive measurements at 20 °C on the same sample. Data was recorded using the ZS Xplorer Software 1.3.2.27 (Malvern Panalytical, UK). Particle concentration data corresponds to average  $\pm$  SD between the three measurements, excluding those values corresponding to particles below 30 nm.

### 9.5.2. pH measurements

The determination of pH was measured using a HI5221-02 pH meter (Hanna Instruments, USA). Samples were left from at least 15 minutes at room temperature before performing the measurement, at least per triplicated of the same sample, cleaning the electrode between measurements. The resulted value was expressed as the average of the different measurements  $\pm$  standard deviation (SD). No stirring was used to avoid sample disturbing. Sometimes, pH was estimated by pH indicator strips (indicator strips pH 0 – 14, 1x4.8m, Filter-Lab), in those cases in which it was not necessary a very accurate measurement.

### 9.5.3. Osmolality measurements

Osmolality, expressed as number of osmoles (Osm) of solute per kilogram of solvent ( $\text{Osm kg}^{-1}$ ), can be measured using an osmometer, which measures colligative properties such as freezing-point depression, vapor pressure or boiling-point elevation. In this thesis, it has been used an Osmomat-030 (Gonotec, Germany) based on freezing-point determination. The principle of working is based on a comparison between the freezing-point of the pure water (0 °C) with the sample to measure, since a solution of 1  $\text{Osm kg}^{-1}$  leads to a decrease of the freezing-point  $-1.858$  °C.

First, the equipment was calibrated using pure water (calibration of the zero), as well as using a standard calibration solution, corresponding to 300  $\text{mOsm kg}^{-1}$ . A 0.9 % NaCl (w/v) solution was used as a standard reference, from commercially available preparation (physiological solution NaCl 0.9 %, Stada, Germany) or prepared from the manufacture's protocol (9.463 g NaCl per kg of water). Each solution (50  $\mu\text{l}$ ) was placed in a small 0.5 mL Eppendorf and introduced in the equipment for their measurement, ensuring there were no visible air bubbles. Next, samples (50  $\mu\text{l}$ ) were measured under the same conditions.

### 9.5.4. Quantification of membrane components

#### 9.5.4.1. Membrane components by gravimetric analysis

The mass of liposomes was measured by gravimetric analysis after freeze-drying (see **Chapter 9.4**). Previously to lyophilization, vials were weighted, both empty, after placing the sample, with the aluminum foil, and finally with the vial cap, using an XA105 DualRange analytical balance (Mettler Toledo, USA). After lyophilization, the lyophilized mass product was also weighted and converted to a

concentration considering the initial lyophilized sample volume. This analysis was performed at least in two independent duplicates.

#### **9.5.4.2. Membrane components by HPLC-ELSD**

The determination of the main liposomal components was performed by High-Performance Liquid Chromatography (HPLC) analysis, using a HPLC equipment (Agilent Technologies 1260 Infinity II), equipped with a reverse phase Symmetry300 C4 (5  $\mu\text{m}$ , 250 x 4.6 mm) column (Waters, USA) as stationary phase coupled with an ELSD detector (evaporative light scattering detector), allowing the quantification of each membrane component, as well as the molar ratio between them. Moreover, it also allows the determination of the degree of purity.

The HPLC-ELSD method for the matrix containing DPPC, cholesterol, cholesterol-PEG<sub>400</sub>-RGD, MKC, and tag free rh-GLA free tag in glucose media was validated, thus the obtained output values can be considered quantitative. Otherwise, the other similar matrix but with small changes in composition (e.g., absence of GLA, MKC, chol-PEG<sub>400</sub>-RGD, or glucose) should be considered semi-quantitative, since their matrix were not validated.

**Sample preparation:** Liposomal samples were first freeze-dried in order to remove the solvent. Then, they were resuspended in 3 mL of methanol (MeOH) and completely dissolved by sonicating (15 min), and precisely leveled up to 5 mL using a volumetric flask. All the dissolved samples were filtered with a hydrophilic 0.2  $\mu\text{m}$  PTFE Millex-LG membrane syringe filter (Merck KGaA, Darmstadt, Germany) before their injection into the HPLC system.

Due to the high difference in concentration between components, each sample was analyzed in three independent replicates and each replicate was injected at two volumes: 1  $\mu\text{L}$  for DPPC and cholesterol quantification, and 20  $\mu\text{L}$  for chol-PEG<sub>400</sub>-RGD and MKC quantification. Additionally, standard curves containing each of the analytes were also prepared in methanol and injected in each sequence.

The mobile phase A (MPA<sub>Lipid</sub>) was composed by 0.01% formic acid (FA, HCOOH) in water; the mobile phase B (MPB<sub>Lipid</sub>) was composed by 0.07% formic acid (FA, HCOOH) in acetonitrile (ACN). Separation was done using a multistep gradient (33 min) at a controlled temperature (25 °C) (**Table 9.7**). Injection sample volume was 1  $\mu\text{l}$  or 20  $\mu\text{l}$ , and flow rate 1 mL min<sup>-1</sup>. Good quality signal intensities were recovered by ELSD maintaining the temperature of the evaporator and the nebulizer at 80 °C and 40 °C respectively, the nitrogen flow at 1 L min<sup>-1</sup>, and the gain set at 8.

**Table 9.7.** Gradient elution method for liposomal composition analysis.

Time (min)	% MPA <sub>Lipid</sub>	% MPB <sub>Lipid</sub>
0.0	60	40
17	5	95
23	60	40
33	60	40

### 9.5.5. Morphological analysis by cryoTEM

The morphology of the systems was studied using cryogenic transmission electron microscopy (cryoTEM), after sample plunge freezing. It allows the direct investigation of colloidal systems, such as liposomes, in the vitrified, frozen-hydrated state, so their structure is quite well preserved, and very close to their native state. During all the procedure, it is necessary to work at cryogenic temperatures, reached using liquid nitrogen (N<sub>2</sub>), to avoid damaging the sample by phase transition of the vitrified water into crystalline ice.

Images were obtained at Servei de Microscopia de la UAB, equipped with a JEOL 2011 (JEOL LTD, Tokyo, Japan) operating at 200 kV. Vitrified samples were prepared using a controlled environment vitrification system (CEVS) Leica EMCP (Leica Microsystems, Germany). A 2-4 µl drop of sample was placed in a copper grid coated with a lacey carbon film and blotted with a filter paper (Whatman® grade 1), obtaining a thin film of 20-400 nm. Then, the grid was plunged into a liquid ethane held at a temperature just above its freezing point (−179 °C), using a Leica EM GP automatic plunge freezer (Leica, Wetzlar, Germany). The vitrified sample was transferred to the microscope using a cryo-transfer holder (Gatan 626, Gatan, Pleasanton, USA). To prevent sample perturbation and the formation of crystals, samples were always kept at −196 °C using liquid N<sub>2</sub> during the transfer and the viewing procedure. Images were recorded on a CCD Gatan 895 USC 4000 camera (Gatan, Pleasanton, USA) analyzed with the Digital Micrograph 1.8 software. No image processing was applied except for background subtraction.

Additionally, for deeper cryoTEM analysis samples were sent to Prof. Dganit Danino group and analyzed in the CryoEM Laboratory of Soft Matter from Technion (Israel). Vitrified specimens were prepared in a similar way. First they were equilibrated for 30 min at 25 °C and then vitrified from this temperature in a controlled specimen preparation chamber following well established procedures<sup>4</sup> and examined in a T12 G2 Tecnai (FEI) and a Talos F200C (Thermo Fisher) microscopes at cryogenic temperatures. Perforated Ted Pella grids were used; vitrified specimens' temperature was always kept below −170 °C. Images were recorded with a Gatan UltraScan 2kx2k CCD camera or a Ceta camera at low dose operation, as previously described. No image processing was applied except for background subtraction.

If not otherwise specified, cryoTEM images were acquired at Servei de Microscopia de la UAB.

### 9.5.6. Lamellarity determination by SAXS

Quantitative information about the liposomes' bilayer thickness and profile, degree of lamellar structure, and amount of incorporated GLA was investigated with small-angle X-ray scattering (SAXS). Analysis of SAXS were performed by Prof. Jan Skov Pedersen group from Aarhus University (Denmark), using an optimized NanoSTAR SAXS instrument<sup>5</sup> from Bruker AXS set up at Aarhus University and equipped with a liquid Ga metal jet X-ray source (Excillum)<sup>6</sup> and scatterless slits.<sup>7</sup>

#### 9.5.6.1. Lamellarity of Liposomes and Hybrid-Liposomes from Chapter 3

Briefly, GLA in water (1 mg mL<sup>-1</sup>) and liposomes or hybrid-liposomes (1.5 mg mL<sup>-1</sup>) in their dispersant medium (water or water with a mixture of EtOH (4 % v/v) and DMSO (0.8 % v/v)) were measured, the matching backgrounds subtracted, and water was used for absolute scale calibration. Note that prior to the measurements, the samples were checked for changes during shipment by performing DLS in Aarhus on an ALV instrument (ALV, Langen, Germany) with an ALV/CGS-8F goniometer equipped with an ALV-6010/EPP multi-tau digital correlator.

The protein scattering was modelled using the PDB structure of  $\alpha$ -galactosidase (PDB: 1r46)<sup>8</sup> using home-written programs<sup>9</sup> to calculate the solution scattering of a protein which includes a surrounding hydration layer, a background constant, and the concentration on absolute scale as fitting parameters. A random search rigid-body refinement algorithm was used to create the most plausible dimer structure.

A model based on Pabst et al.<sup>10,11</sup> with some modifications was used to model the liposome scattering. The intensity can be written as a product of the membrane cross-section form factor  $|F(q)|^2$ , which is related to the cross-section excess electron density of the membrane, a structure factor  $S(q)$ , which in case of multilamellar vesicles describes how the membranes are ordered in the direction perpendicular to the membrane, and  $P_v(q)$ , which is the average form factor related to the larger dimensions of the vesicles:

$$I(q) = S(q)|F(q)|^2P_v(q) \quad (\text{Eq. 9.1})$$

In this, the modulus of the scattering vector is defined as:  $q = 4\pi \sin\theta / \lambda$ , where  $2\theta$  is the scattering angle and  $\lambda$  the X-ray wavelength.

For the structure factor, the para-crystalline model was used.<sup>12</sup> In this model, there is random disorder between the layers, which follows a Gaussian distribution. For a finite number of layers:

$$S(q, N) = 1 + \frac{2}{N} \sum_{k=1}^{N-1} (N-k) \cos(kqD) \exp(-k^2 q^2 \sigma_D^2 D^2 / 2) \quad (\text{Eq. 9.2})$$

where  $D$  is the distance between the centers of the layers and  $\sigma_D$  is the sigma value of the relative disorder distribution. To be able to fit the number of layers, it was used for a non integer value  $P$  a mixture of  $N$  and  $N + 1$  the expression:

$$S(q, P) = (1 - w)S(q, N) + w S(q, N + 1) \quad (\text{Eq. 9.3})$$

where  $w = P - \text{int}[P]$ , where  $N = \text{int}[P]$  is the largest integer smaller than  $P$ . For **LP** and **LP-GLA**, the optimized  $D$  value was 74.4 Å, but since most of the remaining samples contained mainly single layered liposomes, it was not possible to fit  $D$ , and thus it was kept constant at a value of 74.4 Å.

Polydispersity is also included in the number of layers. The distribution is described by a Gaussian truncated at  $\pm 3\sigma_N$  where  $\sigma_N$  is the sigma value of the Gaussian. Since the number of layers in a stack cannot be lower than  $N = 2$ , the Gaussian was furthermore truncated at this value if it reaches below this value, while the numerical integration range was kept at  $6\sigma_N$ .

The expression for the excess electron density on arbitrary scale for the asymmetric profile described by three Gaussians (of which the two are proposed to be related to the head groups) is:

$$\Delta\rho(z) = A_1 \left[ \exp\left(-\frac{(z-z_{H,1})^2}{2(\sigma_{H,1})^2}\right) + \exp\left(-\frac{(z+z_{H,1})^2}{2(\sigma_{H,1})^2}\right) \right] - \exp\left(-\frac{z^2}{2(\sigma_t)^2}\right) \quad (\text{Eq. 9.4})$$

where  $z_{H,1}$  is the positions of the head-group contributions relative to the center of the membrane and  $\sigma_{H,1}$  and  $\sigma_t$  are the width of the tail and central tail parts, respectively. The head group contribution has the amplitude  $A_1$  relative to the tail amplitude, which is set to  $-1$ .

The Fourier transform is:

$$F(q) = \sqrt{2\pi} \left[ A_1 2\sigma_{H,1} \exp\left(-\frac{\sigma_{H,1}^2 q^2}{2}\right) \cos(qz_{H,1}) - \exp\left(-\frac{\sigma_t^2 q^2}{2}\right) \right] \quad (\text{Eq. 9.5})$$

To reduce the number of parameters  $\sigma_{H,1} = \sigma_t = z_{H,1} / 4$  was used. This gives only two parameters for describing the cross-section structure of the vesicles ( $z_{H,1}$ ,  $A_1$ ). The bilayer thickness ( $T$ ) is hereafter defined as  $T = 2(z_{H,1} + \sigma_{H,1})$ .

It turns out that the ordered lamellae are coexisting with single layers and therefore the total expression becomes:

$$I(q) = Sc[f + (1 - f) S(q)] |F(q)|^2 P_v(q) \quad (\text{Eq. 9.6})$$

Where  $f$  is the fraction of layers which are present as single layers and  $Sc$  is an overall scale factor.

The average form factor related to the larger dimensions of the vesicles was described by:

$$P_v(q) = \int_0^\infty D(R, R_{av}, \sigma_R) \left( \frac{\sin(qR)}{qR} \right)^2 dR \quad (\text{Eq. 9.7})$$



Where  $D(R, R_{av}, \sigma_R)$  is a Gaussian function centered at  $R_{av}$  with a relative sigma value of  $\sigma_R$ , which describes the intensity distribution, so that  $R_{av}$  is a Z-average value.

In the final model, a scattering contribution from Gaussian chains<sup>13</sup> was included to fit the data. This polymer scattering likely arise from the flexible PEG-RGD in the cholesterol-PEG<sub>200</sub>-RGD moieties. For the modelling, the polymer radius of gyration was kept constant at 0.8 nm while the overall contribution was fitted. It turned out that the polymer scattering to some degree anti-correlated with fitting of a constant background, and a background was therefore not fitted for the liposomes.

The presence of GLA also gives rise to additional scattering, which we added as a background contribution through a linear combination. The scattering from pure GLA was added with a scale factor to the intensity of the lamellar structures to mimic the additional scattering from unbound GLA incorporated into the liposomes.

MKC has an electron density close to that of water and, therefore, it was not possible to get good data for samples with high MKC concentrations. Thus, the **MQ** and **MQ-GLA<sub>20</sub>** systems were therefore not fully analyzed with SAXS. Moreover, reliable size data cannot be extracted from samples showing instability issues (i.e., **LP-GLA<sub>20</sub>** system), and consequently the number of GLA units per liposome was not calculated either.

#### **9.5.6.2. Lamellarity of unloaded RGD-liposomes from Chapter 4**

Similar procedure and data analysis were performed for the analysis of systems from **Chapter 4**. the  $z$  *head* parameter is referred to the distance from center of bilayer to modelled maximum intensity of the headgroup, and from it the total bilayer thickness ( $T$ ) could be approximated as  $T = z \cdot \sigma_N$ . Measurements were performed 10 days after production.

#### **9.5.6.3. Lamellarity of intermediate nanoGLA from DoE experiment from Chapter 5**

Similar procedure and data analysis were performed for the determination of the fraction of single-layered vesicles in DoE experiments from **Chapter 5**. This time, the model was expressed so that the fraction of bilayers presented as single-layered vesicles,  $f_{single}$ , was a fit parameter. Additionally, the  $z$  *head* parameter was represented. As explained before, it referred to the distance from center of bilayer to modelled maximum intensity of the headgroup, although this time it was not calculated the  $T$  parameter. The wavelength was  $\lambda = 1.34 \text{ \AA}$  and the measurements were performed 2 weeks after production.

### **9.5.7. Theoretical number of GLA per vesicle**

An approximated theoretical calculation of the number of GLA units per vesicle was performed in **Chapter 3**. Human GLA is a homodimeric enzyme with a monomer weight of 48.8 kDa, so the whole GLA shows an approximated molecular weight of 100 KDa. A theoretical number of homodimer GLA units per nanovesicle was calculated in an approximated approach, using the following theoretical

(Table 9.8) and experimental (Table 9.9) data of the systems after purification by diafiltration (Loaded prototype), since non-incorporated GLA was removed. It was only possible to perform these calculations for HLP-GLA hybrid-liposomes, due to LP-GLA instability issues and unsuitability of SAXS technique for MQ-GLA quatsomes.

**Table 9.8.** Theoretical data of hybrid-liposomes.

GLA parameters (homodimer)	
Molecular weight ( <i>MW</i> )	100 kDa (100,000 g mol <sup>-1</sup> )
Liposome's parameters	
Theoretical lipid concentration ( <i>C</i> ) <sup>†</sup>	1.5 mg mL <sup>-1</sup>
Bilayer Thickness ( <i>T</i> ), from SAXS <sup>‡</sup>	5 nm
Theoretical lipid bilayer density ( <i>d</i> ) <sup>§</sup>	1 g cm <sup>-1</sup>

<sup>†</sup> Theoretical amount of lipid used in the initial preparation by DELOS-susp procedure;

<sup>‡</sup> Estimated from SAXS analysis of blank HLP systems; <sup>§</sup> From T. Miyoshi et al. <sup>3</sup>

**Table 9.9.** Experimental data of hybrid-liposomes and final calculation of number of GLA (homodimer) per vesicle.

System	GLA <sup>a)</sup> (μg mL <sup>-1</sup> )	No. GLA <sup>b)</sup> (mL <sup>-1</sup> )	Size (D) <sup>c)</sup> (nm)	Lipid volume per liposome (V) <sup>d)</sup> (cm <sup>3</sup> )	No. liposomes <sup>e)</sup> (mL <sup>-1</sup> )	No. GLA per vesicle <sup>f)</sup>
(0.4%MKC)- HLP-GLA <sub>20</sub>	2.8	1.68 × 10 <sup>13</sup>	140	3.08 × 10 <sup>-16</sup>	4.87 × 10 <sup>12</sup>	3.4
(2.2%MKC)- HLP-GLA <sub>20</sub>	6	3.60 × 10 <sup>13</sup>	124	2.42 × 10 <sup>-16</sup>	6.21 × 10 <sup>12</sup>	5.8
(2.2%MKC)- HLP-GLA <sub>8.5</sub>	4.6	2.76 × 10 <sup>13</sup>	112	1.97 × 10 <sup>-16</sup>	7.61 × 10 <sup>12</sup>	3.6
(4.3%MKC)- HLP-GLA <sub>20</sub>	12	7.20 × 10 <sup>13</sup>	123	2.38 × 10 <sup>-16</sup>	6.31 × 10 <sup>12</sup>	11.4

<sup>a)</sup> Determined by SDS-PAGE plus TGX (see Chapter 9.6.3.1); <sup>b)</sup> Calculated using Eq. 9.8, where  $N_A$  is the Avogadro's number; <sup>c)</sup> From DLS measurement, mean size based on intensity; <sup>d)</sup> Lipid volume per liposome, calculated using Eq. 9.9; <sup>e)</sup> Number of liposomes, calculated using Eq. 9.10; <sup>f)</sup> Ratio between number of GLA dimers (No. GLA) and number of liposomes (No. liposomes).

$$\text{No. GLA (mL}^{-1}\text{)} = [\text{GLA}] / M_w \times N_A \quad (\text{Eq. 9.8})$$

$$V \text{ (cm}^3\text{)} = \text{Surface vesicle} \times T = 4\pi (D/2)^2 \times T \quad (\text{Eq. 9.9})$$

$$\text{No. liposomes (mL}^{-1}\text{)} = C / V \times d \quad (\text{Eq. 9.10})$$

## 9.5.8. Optical characterization of DiD-labeled liposomes

### 9.5.8.1. DiD quantification by UV-vis spectroscopy

Absorption spectra for samples placed in cell was acquired using a V-780 UV-Visible/Near Infrared Spectrophotometer (Jasco) or a Varian Cary 5000 UV-Vis-NIR spectrophotometer (Agilent Technologies, Santa Clara, USA), belonging to NANBIOSIS Soft Materials Service linked to Biomaterial Processing and Nanostructuring Unit (U6) at ICMAB-CSIC. Samples were placed in a micro (500  $\mu\text{L}$ ) or in a macro (2.5 – 3.0 mL) quartz SUPRASIL<sup>®</sup> precision cell (Hellma Analytics, Müllheim, Germany), both cells with a 1 cm light path length.

Data was recorded using the Spectra Manager<sup>™</sup> software (Jasco), using 1.0 nm of data interval, 1000  $\text{nm min}^{-1}$  of scan speed. Baseline correction was applied measuring and resting the absorbance of the media of the sample alone.

### 9.5.8.2. Fluorescence spectroscopy

Fluorescence emission and excitation spectra were collected with a Varian Cary Eclipse (Agilent Technologies, Santa Clara, USA) fluorescence spectrophotometer.

For fluorescence spectra recording of DiD-labelled liposomes (DiD ~ 100 nM), samples (50  $\mu\text{L}$ ) were placed in a quartz SUPRASIL<sup>®</sup> precision cell (Hellma Analytics, Müllheim, Germany), and were analyzed directly, without any modification or dilution, unless otherwise noted.

Excitation spectra was recorded using the following parameters:  $\lambda_{\text{em}} = 700$  nm, scanning from 500 nm to 690 nm, excitation/emission slit 5/10 nm, scan rate 60  $\text{nm min}^{-1}$ , averaging time 1 s, data interval 1 nm, PMT detector voltage High option.

Emission spectra was recorded using the following parameters:  $\lambda_{\text{exc}} = 585$  nm, scanning from 620 nm to 800 nm, excitation/emission slit 5/10 nm, scan rate 60  $\text{nm min}^{-1}$ , averaging time 1 s, data interval 1 nm, PMT detector voltage High option, S/N mode with S/N 1000 and time out 1.000 s.

## 9.5.9. Stability studies

### 9.5.9.1. Stability of vesicles by size, PDI, and $\zeta$ -potential evolution with time

The stability at the desired temperature (4 °C or 25 °C) of the liposomal systems was followed by measuring the size, polydispersity index (PDI) and  $\zeta$ -potential of the nanovesicles at different time points after production using a DLS equipment (Malvern Zetasizer Nano ZS, Malvern Panalytical, U.K.) as described previously. Samples were stored at fridge (4 °C) or at room temperature (25 °C).

### 9.5.9.2. Stability of vesicles by turbidimetry

Stability of liposomal systems obtained in the design of experiments (DoE) of **Chapter 5** was evaluated by means of the Turbiscan Stability Index (TSI), determined by static multiple light scattering (S-MLS) using a Turbiscan Lab Expert (Formulation, France). Samples (20 mL) were placed in a Tturbiscan

reservoir at 20 °C and analyzed two weeks after production, during 8 h. The TSI at given time is a specific parameter to compare the stability of the suspensions. In a general way, TSI below 3 are considered acceptable, whereas TSI above 10 indicate important destabilization.

### 9.5.9.3. Stability of hybrid-liposomes in human serum

The 12-fold concentrated (**2.2%MKC**)-HLP system was incubated with two different concentrations of human serum (H4522, Sigma-Aldrich), 75 % and 90 % (vol. %), in triplicates in a 48-well plate. Samples were then incubated at 37 °C in orbital shaker agitation, and analyzed at 0 min, 15 min, 30 min, 60 min, 90 min, and 120 min. At each time-point the absorbance of samples was read at  $\lambda = 300$  nm (Microplate reader Infinite 200 Pro, Tecan) with the corresponding amount of serum alone as reference. Relative turbidity was determined dividing the sample turbidity by the turbidity at time zero (**Eq. 9.11**).

$$\text{Turbidity } \lambda_{300} \text{ change (\%)} = \frac{\frac{Abs_{HLP \text{ in serum}}(t)}{Abs_{HLP \text{ in serum}}(t_0)}}{\frac{Abs_{serum}(t)}{Abs_{serum}(t_0)}} \quad (\text{Eq. 9.11})$$

Additionally, concentrated (**2.2%MKC**)-HLP was incubated with 50 % (vol. %) of human serum (1 h, 37 °C, agitation by orbital shaker) and liposome integrity was assessed by cryoTEM imaging.

## 9.6. Synthesis and characterization of bioactive compounds

### 9.6.1. Production of cholesterol-PEG<sub>n</sub>- derivatives

The cholesterol-PEG<sub>n</sub>-derivative molecules were specifically designed and synthesized by Dr. Miriam Royo group from the Institut de Química Avançada de Catalunya (IQAC-CSIC, Barcelona). Chemical details of the synthesized molecules are summarized below.

#### 9.6.1.1. Chemical details of cholesterol-PEG<sub>200</sub>-RGD

The cyclic c-RGDfK peptide (simplified here as RGD) was synthesized and incorporated to a previously produced cholesterol-PEG<sub>200</sub> intermediate, obtaining the cholesterol-PEG<sub>200</sub>-RGD (**Figure 9.6**).

Chemical formula: C<sub>63</sub>H<sub>101</sub>N<sub>9</sub>O<sub>13</sub> (MW 1192).

Chemical purity > 95%, determined by HPLC-PDA-MS. Column: Symmetry300, C4, 5  $\mu$ m, 4.6 x 250 mm; Elution system: A = 0.1 % HCOOH in H<sub>2</sub>O, and B = 0.1 % HCOOH in CH<sub>3</sub>CN; Gradient: 5 % B to 100 % B, 30 min, 50 °C, 1 mL min<sup>-1</sup>;  $\lambda = 210$  nm; RT: 17.3 min.

HR-MS (ESI): Calculation for [M+H]<sup>+</sup>: 1192.75916; found: 1192.75932.

Amino acid analysis (HPLC-UV, AccQTag Waters pre-column derivatization method):  $\geq 80$  % peptide content (Asp, Gly, Arg, Lys, Phe).

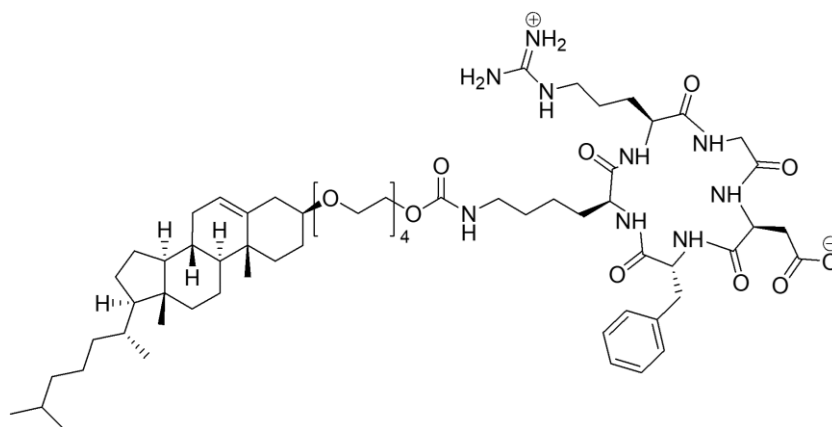


**Figure 9.6.** Chemical structure of cholesterol-PEG<sub>200</sub>-cRGDfk (chol-PEG<sub>200</sub>-RGD).

#### 9.6.1.2. Chemical details of cholesterol-PEG<sub>400</sub>-RGD

The cyclic c-RGDfK peptide (simplified here as RGD) was synthesized and incorporated to a previously produced cholesterol-PEG<sub>400</sub> intermediate, obtaining the cholesterol-PEG<sub>400</sub>-RGD (**Figure 9.7**).

Chemical formula: C<sub>71</sub>H<sub>117</sub>N<sub>9</sub>O<sub>17</sub> (MW 1369).

Chemical purity > 95 %, determined by HPLC-PDA-MS. Column: Symmetry300, C4, 5 μm, 4.6 x 250 mm; Elution system: A = 0.1 % HCOOH in H<sub>2</sub>O, and B = 0.07 % HCOOH in CH<sub>3</sub>CN; Gradient: 5 % B to 100 % B, 30 min, 50 °C, 1 mL min<sup>-1</sup>; λ = 210 nm; RT: 17.7 min.

HR-MS (ESI): Calculated mass for [M+H]<sup>+</sup>: 1368.86402; found: 1368.87080

Amino acid analysis (HPLC-UV, AccQTag Waters pre-column derivatization method): ≥ 85 % peptide content (Asp, Gly, Arg, Lys, Phe).

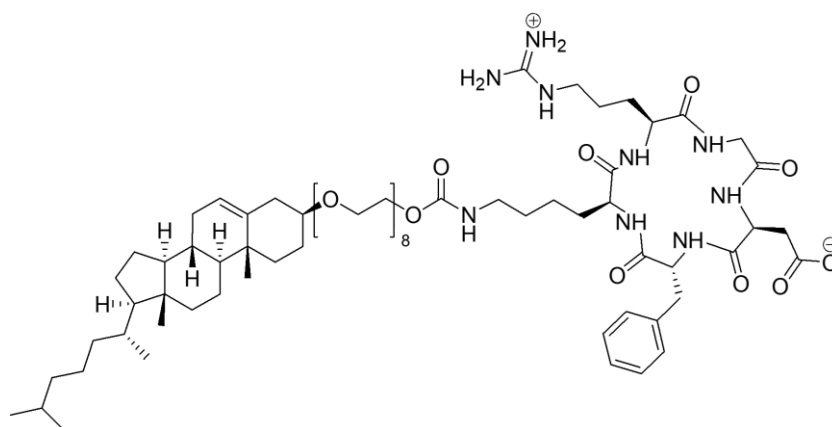


**Figure 9.7.** Chemical structure of cholesterol-PEG<sub>400</sub>-cRGDfk (chol-PEG<sub>400</sub>-RGD).

### 9.6.1.3. Chemical details of cholesterol-PEG<sub>400</sub>-Alanine

Alanine was incorporated to a previously produced cholesterol-PEG<sub>400</sub>-(4-nitrophenyl) carbonate intermediate, obtaining the cholesterol-PEG<sub>400</sub>-Alanine (**Figure 9.8**).

Chemical formula: C<sub>47</sub>H<sub>83</sub>NO<sub>12</sub> (MW 853.59).

Chemical purity 99%, determined by HPLC-PDA-MS. Column: Symmetry300, C4, 5 μm, 4.6 x 250 mm; Elution system: A = 0.1 % HCOOH in H<sub>2</sub>O, and B = 0.1 % HCOOH in CH<sub>3</sub>CN; Gradient: 5 % B to 100 % B, 27 min, 50 °C, 1 mL min<sup>-1</sup>; λ = 210 nm; RT: 21.1 min.

HR-MS (ESI): Calculated mass for [M+H]<sup>+</sup>: 854.59; found 854.8.

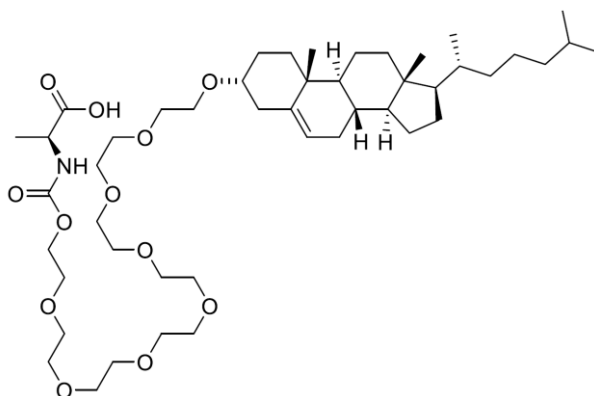


**Figure 9.8.** Chemical structure of cholesterol-PEG<sub>400</sub>-alanine (chol-PEG<sub>400</sub>-Ala).

### 9.6.1.4. Chemical details of cholesterol-PEG<sub>400</sub>-T7

The peptide ligand T7 (sequence His-Ala-Ile-Tyr-Pro-Arg-His) was incorporated to a previously produced cholesterol-PEG<sub>400</sub>-Maleimide, obtaining the cholesterol-PEG<sub>400</sub>-T7 (**Figure 9.9**).

Chemical formula: C<sub>97</sub>H<sub>155</sub>N<sub>19</sub>O<sub>22</sub>S (without considering counterions, MW 1971.48) and C<sub>105</sub>H<sub>159</sub>F<sub>12</sub>N<sub>19</sub>O<sub>30</sub>S (Considering 4 x TFA, MW 2427.57).

Chemical purity: > 98 %, determined by HPLC-PDA. Column: Symmetry300, C4, 5 μm, 4.6 x 250 mm; Elution system: A = 0.1 % HCOOH in H<sub>2</sub>O, and B = 0.07 % HCOOH in CH<sub>3</sub>CN; Gradient: 5 % B to 100 % B, 27 min, 50 °C, 1 mL min<sup>-1</sup>; λ = 210 nm; RT: 14.6 min.

HR-MS (ESI): Calculated mass for [M+2H]<sup>2+</sup>: 986.1; found 986.6.

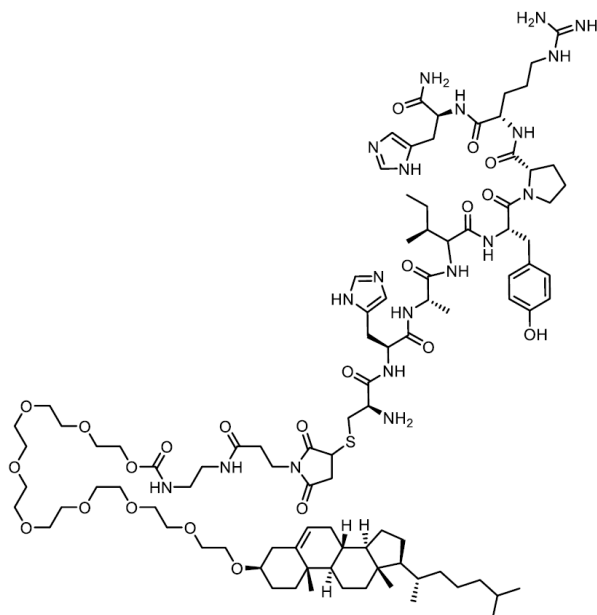


**Figure 9.9.** Chemical structure of cholesterol-PEG<sub>400</sub>-T7 (chol-PEG<sub>400</sub>-T7)

## 9.6.2. Synthesis of GLAcmycHis and rh-GLA enzymes

Apart from the commercial agalsidase alfa (Replagal<sup>®</sup>, Shire-Takeda), in this Thesis two additional types of GLA were used for formulating: the GLAcmycHis (with two additional tags, “c-myc” and “His”), and the rh-GLA tag free and with freedom-to-operate (FTO) status.

### 9.6.2.1. Synthesis of GLAcmycHis

GLAcmycHis (a GLA containing c-myc and His-tag) was produced using a non-FTO stable expression-based production method, developed by Dr. José Lu s Corchero from the IBB-UAB (Barcelona), and scaled-up by LeanBio S.L. (Barcelona).

#### Plasmids and *E. coli* strains

The GLA gene was obtained from the commercial vector pReceiver-M10 (OmicsLink ORF Expression Clone, ref. EX-Q0172-M10), that encodes a cDNA version of the GLA gene (primary gene accession number: NM\_000169), in which both c-myc and 6xHis tags are fused (for further detection and purification purposes) to the C-terminus. For further steps, the pOptiVEC<sup>TM</sup>-TOPO<sup>®</sup> TA Cloning Kit (12744-017, Invitrogen) was used following the vendor protocol. The PCR product was cloned into the pOptiVEC<sup>TM</sup>-TOPO<sup>®</sup> plasmid, and the resulting plasmid (pOptiVec-GLA) was transformed into TOP10 *E. coli* cells. Positive clones were selected by ampicillin and confirmed by restriction analysis. The pOptiVec-GLA plasmid was purified by “gigaprep” method, and finally linearized before transfection, as recommended by the vendor, with restriction enzyme PvuI. All plasmids were purified from their corresponding overnight bacterial cultures, using the EndoFree Plasmid Giga Kit (Qiagen, ref. 12391). For their quantification, absorbance at 260 nm and 280 nm were measured.

## **Mammalian cell line, transfection, and selection of positive clones**

For the transfection and further selection of CHO cells overexpressing the human GLA enzyme, the OptiCHO™ Express Kit (12745-014, Invitrogen) was used. This kit provides CHO DG44 cells, media and transfection reagent needed. DG44 dhfr- CHO cells were grown in CD DG44 medium with L-glutamine (8 mM), at 37 °C in 8% CO<sub>2</sub> using standard techniques. Transfection of CHO DG44 cells and selection of positive GLA-DHFR cells were performed following the vendor protocol. At 28 days post-transfection, stepwise selection for dhfr amplification was started, using two-fold increments of methotrexate hydrate (MTX, A6770, Sigma) starting at 50 nM up to 4 μM. Finally, and in order to obtain a single clone, the pool of stably transfected and MTX-amplified cells (4 μM) was serially diluted and seeded at 1 – 2 cells per well in a 96-well plate. As suggested by vendor, to grow CHO DG44 cells under adherent conditions, the specific medium Gibco® CD-CHO-A was used. After this process, a single clone (namely CHO-DG44-GLA<sub>clone#3</sub>) was isolated and cryopreserved.

### **Cryopreservation of CHO-DG44-GLA clone #3**

CHO-DG44-GLA<sub>clone#3</sub> was cultured in complete CD OptiCHO medium (supplemented with L-Glutamine 8 mM) to  $2 \times 10^6$  cells mL<sup>-1</sup> and then centrifuged (100 g, 5 min). Cell pellets were then resuspended in fresh medium containing DMSO (10%) to a final cell concentration of  $10 \times 10^6$  cells mL<sup>-1</sup>. Cells were aliquoted into 1 mL cryovials (Nalgene) and stored in the vapor phase of liquid nitrogen.

### **Production and purification of extracellular GLAcmycHis protein**

Cryovials of CHO-DG44-GLA<sub>clone#3</sub> were thawed under standard procedures, rapidly thawed at 37 °C and resuspended in 15 mL of pre-warmed complete CD OptiCHO medium. Cells were expanded by subculturing them up to the desired volume. In each passage, cells were diluted into pre-warmed complete CD DG44 Medium to give a final cell density of  $2 \times 10^5$ – $3 \times 10^5$  viable cells mL<sup>-1</sup>. Finally, supernatant containing extracellular GLAcmycHis was harvested by centrifuging the cell culture (14,000 rpm, 15 min). This supernatant was purified in an ÄKTA Pure system (GE Healthcare) by using an affinity chromatography column (HisTrap Excel 5 mL, Ref 17-3712-06, GE Healthcare) following the vendor protocol. Finally, the eluted protein was dialyzed in acetic buffer (0.01 M, pH 5.5) and stored at –20 °C until use.

#### **9.6.2.2. Production of freedom-to-operate rh-GLA (tag-free and FTO)**

For the preparation of the nanoGLA batches for the preclinical studies, including non-regulatory in vivo efficacy studies and regulatory toxicology testing, a new tag free recombinant human GLA (rh-GLA) was developed by Dr. Jose Luís Corchero from the IBB-UAB (Barcelona) and LeanBio S.L. (Barcelona). This rh-GLA enzyme was produced by a CHO-derived stable clone, free of tags since any



tag (e.g. –myc or –His) was included, and without restrictions in terms of intellectual property (i.e. considered as freedom-to-operate FTO rh-GLA).

For the cell line development of tag free rh-GLA (FTO), the suspension-adapted cell line CHO-K1 (ATCC CCL-61) was used to produce a recombinant human GLA by means of stable-expression-based production. Briefly, synthetic gene coding for human GLA enzyme (no tags included) was synthesized and cloned into plasmids coding either for hygromycin and geneticin resistance. Then, the plasmid was transfected into CHO cells by means of polyethyleneimine (PEI)-mediated transfection. Two days after transfection, positive cells were selected (by selective pressure using hygromycin and geneticin) and GLA production of the pool was confirmed by Western-blot. Sequential dilutions to 2,500 and 25,000 cells mL<sup>-1</sup> were performed and seeded into 24-well plates (500 µl well<sup>-1</sup>). Supernatants of the different pools were analyzed by Western-blot ten days after, and the best ones were expanded and isolated. From the best producers, it was selected the best individual clones to produce the rh-GLA FTO.

Then, the production of higher batches of rh-GLA was manufactured at higher scale in LeanBio SL facilities. Cells were expanded, and the process was transferred to a 50 L bioreactor, fed-batch, and harvested. Next, cell culture was clarified by centrifugation and 0.22 µm filtration, followed by a 10-fold concentration by tangential flow filtration (TFF). Finally, rh-GLA was purified using chromatographic techniques (IEX, i.e., ion exchange chromatography, and HIC, i.e., hydrophobic interaction chromatography), obtaining around 350 mg (at 3.11 mg mL<sup>-1</sup>) of rh-GLA with high purity (> 90 %) FTO and tag free, and was stored at –20 °C until use. The test certificate of the released batch appeared in **Table 9.10**.

**Table 9.10.** Test certificate of the 50 L batch, including the results of the analytical characterization.

Purpose	Attribute	Analytical method	Results
<b>Content</b>	Protein concentration	Absorbance at 280 nm	3.11 mg mL <sup>-1</sup>
<b>Identity</b>	Immunological detection	Western Blot	Consistent with reference material
	Isoelectric point determination	cIEF	5.11
<b>Potency</b>	Enzyme activity	Fluorescence detection at 0.2 mg mL <sup>-1</sup>	30 IU
<b>Purity</b>	Non-reducing SDS-PAGE		93.14 %
	Reducing SDS-PAGE		91.62 %
	SEC-HPLC		85.91 %
	RP-HPLC		89.96 %
	cIEF		99.4 %
<b>Safety</b>	Microbial Contamination	Bioburden	< 10 CFU mL <sup>-1</sup>
	HC-DNA	Picogreen	71.86 ng mg <sup>-1</sup>
	Endotoxins	LAL	< 80.4 EU mg <sup>-1</sup>

### 9.6.3. Quantification of GLA and Entrapment Efficiency (EE%) calculation

#### 9.6.3.1. Quantification of GLA by SDS-PAGE plus TGX acrylamide gels

Detection and quantification analysis of GLA concentration in nanoformulations was performed in collaboration with Dr. José Luís Corchero from the IBB-UAB (Barcelona) by SDS-PAGE (sodium dodecyl sulphate-polyacrylamide gel electrophoresis) using TGX (Tris-Glycine eXtended) Stain-Free™ FastCast™ acrylamide 12 % gels (Bio-Rad, ref. 161-0185). This stain-free imaging technology utilizes proprietary polyacrylamide gel chemistry to make proteins fluorescent directly in the gel after a short (45 s) photoactivation period, allowing immediate visualization of proteins. To visualize the fluorescent bands, a ChemiDoc™ Touch Imaging System (Bio-Rad) was used. GLA protein amounts were estimated by densitometric analysis after SDS-PAGE and photoactivation, using as standards known amounts of a control His-tagged GLA produced, purified, and quantified in-house. Samples and standards, to be quantitatively compared, were run in the same gel, and processed as a data set. Densitometric analysis of the bands were performed with the Image Lab™ software (version 5.2.1., Bio-Rad).

#### 9.6.3.2. Quantification of GLA by UV

Quantification of rh-GLA produced by LeanBio SL were quantified by spectrophotometry. The rh-GLA was diluted in the formulation buffer (mannitol 3 %,  $\text{NaH}_2\text{PO}_4 \cdot \text{H}_2\text{O}$  0.275 %,  $\text{Na}_2\text{HPO}_4 \cdot 7\text{H}_2\text{O}$  0.8 %, pH 7) at three different dilutions: 1:5, 1:10 and 1:20, and were measured by UV ( $\lambda_{\text{Abs}} = 280 \text{ nm}$ ), without further modification or filtration.

#### 9.6.3.3. Quantification of GLA present in nanoGLA liposomes by RP-HPLC

Quantification of GLA concentration in each sample (i.e., when GLA is in presence with the nanoliposomal product) was performed by LeanBio S.L. by using a Reversed-Phase High-Performance Liquid Chromatography (RP-HPLC) method.

For the preparation of the reference standard curve, reference standard (free commercial GLA, Replagal®) was diluted in a liposomal matrix. Liposomal matrix corresponded to empty liposomes (without GLA) disgregated in methanol and acetic acid (AcOH, 0.010 M, pH 5.5), in a volume ratio of 1:1:1 (sample: MeOH: AcOH) and filtered by 0.22  $\mu\text{m}$  polytetrafluoroethylene (PTFE) filter. Calibration curve was prepared in a range  $5.0 \mu\text{g mL}^{-1} - 40 \mu\text{g mL}^{-1}$  of GLA (Table 9.11).

**Table 9.11.** Example of a calibration curve preparation.

Dilution	C final GLA ( $\mu\text{g mL}^{-1}$ )	C stock GLA ( $\mu\text{g mL}^{-1}$ )	V stock ( $\mu\text{L}$ )	V matrix ( $\mu\text{L}$ )	V final ( $\mu\text{L}$ )
A	40.0	500.0	24.0	276	300
B	25.0	250.0	30.0	270	300
C	15.0	250.0	18.0	282	300
D	10.0	100.0	30.0	270	300
E	5.0	100.0	15.0	285	300

Then, for the preparation of samples, GLA-containing liposomal suspensions were first dispersed in an organic mixture, containing acetic acid (AcOH, 0.010 M, pH 5.5) and methanol (MeOH) in a proportion 1:1:1 volume (sample:AcOH:MeOH) in order to break up the liposomes. Samples were filtered with a 0.22  $\mu\text{m}$  PTFE filter before HPLC injection. Two independent preparations were made for each tested sample. Samples containing an estimated GLA concentration higher than 40  $\mu\text{g mL}^{-1}$  were previously diluted in water to get an approximate concentration of 20 – 30  $\mu\text{g mL}^{-1}$ , and then submitted to the same procedure.

In detail, GLA quantification was done using an Infinity 1260 II HPLC system (Agilent Technologies, USA), with a Zorbax 300SB-C18 (3.5  $\mu\text{m}$ , 4.6 x 150 mm) column (Agilent Technologies, USA) at 60  $^{\circ}\text{C}$ , and equipped with a UV-detector ( $\lambda = 215 \text{ nm}$ ). The mobile phase A (MPA<sub>GLA</sub>) was composed by water 95 %, acetonitrile 5 %, and trifluoroacetic acid 0.1 %; the mobile phase B (MPB<sub>GLA</sub>) was composed by water 5 %, acetonitrile 95 %, and trifluoroacetic acid 0.09 %. Separation was done using a linear gradient from 0 to 60 % MPB<sub>GLA</sub> (30 min) and cleaning step of 100 % of MPB<sub>GLA</sub> (5 min) (Table 9.12). Injection volume was 100  $\mu\text{L}$  and the flow rate 1  $\text{mL min}^{-1}$ .

**Table 9.12.** Gradient elution method for GLA quantification in liposomal samples.

Time (min)	% MPA <sub>GLA</sub>	% MPB <sub>GLA</sub>
0.0	100	0
35.0	40	60
40.0	0	100
40.5	100	0
45.0	100	0

#### 9.6.3.4. Entrapment efficiency (EE%) and GLA loading

The entrapment efficiency (EE%) was determined by comparing the amount of the enzyme encapsulated in the nanovesicles after removing the free GLA by diafiltration with the amount of initial GLA present in the raw batch obtained just after their production, see **Eq. 9.12**. The GLA loading was calculated by comparing the amount of GLA loaded on liposomes after elimination of free GLA with the total amount of membrane components of the vesicles, see **Eq. 9.13**. Statistics were done by two-sample t-test using *Minitab*<sup>®</sup> 17 statistical software (2013).

$$\text{EE\%} = (\text{mass GLA after diafiltration} / \text{mass GLA initial}) \times 100 \quad (\text{Eq. 9.12})$$

$$\text{GLA loading} = \text{mass GLA after diafiltration} / \text{mass membrane components} \quad (\text{Eq. 9.13})$$

## 9.7. Biological activity of GLA

### 9.7.1. Specific enzymatic activity

Specific enzymatic activity assays were performed in collaboration with Dr. Ibane Abasolo group from VHIR (Barcelona).

GLA enzymatic activity was assayed as previously described,<sup>14,15</sup> using fluorometric methods initially described by Desnick et al.<sup>16</sup> with the modifications of Mayes et al.<sup>17</sup> The enzymatic activity assay is based on the conversion of a non-fluorescent substrate (4-MUG) in a fluorescent product (4-MU) when active GLA is present. The protocol included the use of 4-methylumbelliferyl  $\alpha$ -D-galactopyranoside (4-MUG, M-7633 Sigma Aldrich) as substrate ( $2.46 \times 10^{-3}$  M) in assay buffer (0.01 M acetic acid, 0.01 M acetate, pH 4.5). A typical assay reaction mixture contains 100  $\mu$ L of 4-MUG and 25  $\mu$ L of the sample. Enzymatic reactions took place in agitation (GLS Aqua 12 Plus, USA) at 25 rpm, 37 °C for 1 h. The reaction was stopped by glycine buffer (1.25 mL, 0.2 M, pH 10.4) and the released product (4-methylumbelliferone or 4-MU) was determined by fluorescence measurement ( $\lambda_{\text{exc}} = 365$  nm,  $\lambda_{\text{em}} = 450$  nm) using a microplate fluorescence reader (96 dark well-plate, 200  $\mu$ L/well, FLx800<sup>™</sup>, Biotek<sup>™</sup>, USA).

Samples of commercial product 4-MU (Sigma Aldrich) ranging from 5 to 500 ng mL<sup>-1</sup> in glycine-NaOH buffer (0.2 M, pH 10.4) were used to obtain a calibration curve to transform fluorescence readings into product 4-MU concentration. Measurements were adjusted per time and protein quantity. Specific enzymatic activity was expressed as [ $\mu$ mol 4-MU mg<sup>-1</sup> GLA h<sup>-1</sup>]. In some experiments, enzymatic activity values were referred to enzymatic activity of free GLA, agalsidase alfa (Replagal<sup>®</sup>), included always in all the assays as reference. Assays usually corresponded to a single representative experiment, replicated in three independent assays. The error is the standard error of the mean (SEM) of the three replicates.

Additionally, to discard a matrix effect of these compounds in presence of the tested GLA-nanoformulations, the fluorescent emission of 4-MUG and 4-MU was recorded in presence of liposomal nanovesicles (**Figure 9.10**). Both fluorescence spectra of 4-MUG and 4-MU products used in the enzymatic activity assay were not altered by the presence of the nanovesicles.

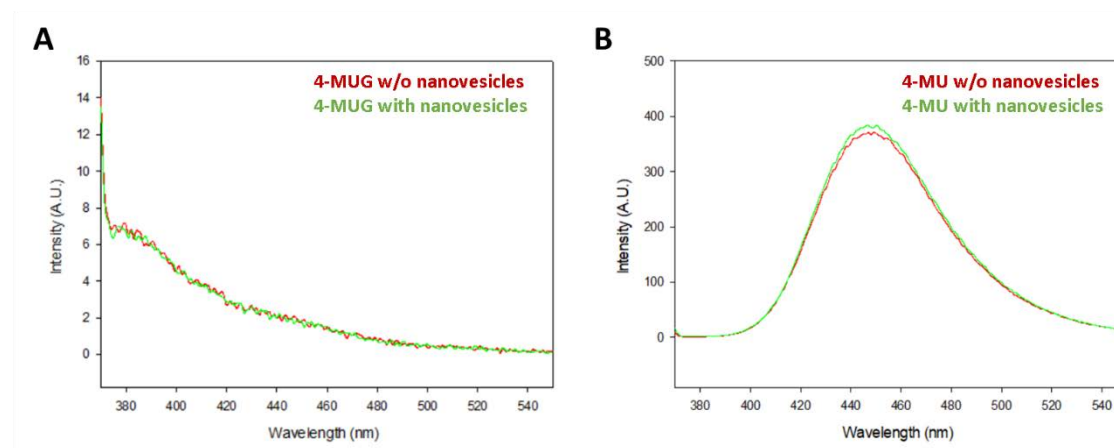


**Figure 9.10.** (A) 4-MUG (enzymatic assay substrate) fluorescence emission spectra with and without the presence of the nanovesicles; (B) 4-MU (enzymatic activity assay product) fluorescence emission spectra with and without the presence of liposomes;  $\lambda_{\text{exc}} = 365 \text{ nm}$ ,  $\lambda_{\text{em}} = 450 \text{ nm}$ .

For stability studies, liposomal systems were stored at fridge ( $4 \text{ }^{\circ}\text{C}$ ) or at room temperature ( $25 \text{ }^{\circ}\text{C}$ ). An aliquot was taken at the established time points and the specific enzymatic activity was determined. In **Chapter 6**, some enzymatic activity assays were carried out by LeanBio SL (Barcelona), as specified in the corresponding footnote.

### 9.7.2. In vitro enzymatic efficacy by Gb3 reduction in MAEC

In vitro Gb3 reduction efficacy assays were performed in collaboration with Dr. Ibane Abasolo group from VHIR (Barcelona). The ability of GLA-loaded nanovesicles to reach the lysosomes and hydrolyze Gb3 was tested in primary cultures of mouse aortic endothelial cells (MAEC) from GLA deficient mice ( $\text{Gla}^{\text{tmKul1}}$ ).<sup>18</sup> These cells were isolated at the in vivo Experimentation Platform/U20 of ICTS NANBIOSIS and grown as previously described<sup>14</sup> in RPMI media supplemented with non-essential amino acids (Gibco), heparin ( $0.1 \text{ mg mL}^{-1}$ , Sigma Aldrich), endothelial cell growth supplement (ECGS) ( $0.05 \text{ mg mL}^{-1}$ , BD), hydrocortisone ( $1 \text{ } \mu\text{g mL}^{-1}$ , Sigma Aldrich) and fetal bovine serum (10 – 20 %, Gibco) to allow the growth of endothelial cells. Cells ( $100,000/\text{well}$ ) in passages 2 – 5 were seeded in 24-well plates to 60 – 80 % of confluence and incubated with Gb3-NBD ( $0.8 \times 10^{-6} \text{ M}$ , Matreya) along with the specified concentrations of tested compounds. Samples were added to each well to reach the desired GLA concentrations (as specified in each figure footnote). GLA concentrations are usually in the range of  $0.001 - 1 \text{ } \mu\text{g mL}^{-1}$ , when a complete curve of GLA concentration against Gb3

loss is measured, or 0.01 and 0.25  $\mu\text{g mL}^{-1}$  when only one concentration of GLA is evaluated. After 48 h, Gb3-NBD fluorescent signal was analyzed by flow cytometry (FacsCalibur, Beckton Dickinson) in viable cells (negative to 7-aminoactinomycin D staining). The fluorescent signal in control cells (without treatment) was established as 100 % and the rest of values were normalized accordingly. The efficacy of GLA in reducing the Gb3 deposits was obtained as the percentage of Gb3 loss (**Eq. 14**).

$$\% \text{ Gb3 loss} = 100 - \% \text{ Gb3-NBD signal} \quad (\text{Eq. 14})$$

## 9.8. In vitro cell internalization of RGD-liposomes in U2OS cells

Cell adhesion experiments with human osteosarcoma cells (U2OS) were done in close collaboration with Dr. Imma Ratera and Dr. Judit Guasch team from the ICMAB-CSIC (Barcelona).

### 9.8.1. Preparation of substrates: Cleaning and Fibronectin coating

First, glass substrates (borosilicate glass, 20 x 20 mm, Divers BioLab) were cleaned for removing all the organic material. Substrates were placed in a substrate support and submerged in piranha solution (1 part of water and 3 parts of sulfuric acid, 45 min), then they were extensively rinsed with water, and finally they were ultrasonicated (5 – 10 min). Substrates were kept submerged in water until their use.

Fibronectin 10  $\mu\text{g mL}^{-1}$  solution (Fibronectin bovine plasma, F1141, Sigma Aldrich, stock 1  $\text{mg mL}^{-1}$ ) was prepared in PBS (1:10 volume). Substrates were incubated with fibronectin (100  $\mu\text{L}$  per substrate) overnight in a wet chamber.

### 9.8.2. Cell culture, Seeding, and Immunostaining

Human osteosarcoma cells (U2OS) were obtained from the American Type Culture Collection (ATCC; Manassas, USA). Cells were routinely cultured in Dulbecco's Modified Eagle Medium (DMEM 1X + GlutaMAX, Gibco, Thermo Fisher Scientific, USA) medium, supplemented with 10 % FBS (Fetal Bovine Serum, qualified, Brazil, Gibco) and 1 % of penicillin/streptomycin (100x, Gibco), and were incubated in a humidified atmosphere at 37 °C and 5 %  $\text{CO}_2$ .

Before cell seeding, substrates were rinsed three times with sterile PBS (DPBS 1X, Dulbecco's Phosphate Buffered Saline, Gibco) and placed into a 6-well plate (Nunc™ Non-Treated Multidishes, 150239, Thermo Scientific). Thereafter, 45,000 cells were seeded onto each substrate and wells were filled with cell medium (3 mL final volume). Substrates were incubated overnight at 37 °C and 5 %  $\text{CO}_2$  for allowing the cell adhesion and spreading out. Next, each well was treated with a volume of DiD-labelled liposomes sample (final concentration 0.1  $\text{mg mL}^{-1}$  per well). Cells were incubated with liposomes for 3 h (37 °C and 5 %  $\text{CO}_2$ ), before cell fixation and immunostaining.

Then, cells were rinsed with sterile PBS and fixed by addition of 4% paraformaldehyde in PBS (PFA, Servei de Microscopia de la UAB, stock at 20%) (3 mL/sample, RT, 20 min). Then, substrates were

rinsed 2–3 times with PBS. After cell fixation, cells were permeabilized by adding 0.1% v/v Triton (Triton™ X-100, Sigma Aldrich) prepared in PBS (3 mL/sample, RT, 5 min). After this time, samples were treated with a blocking solution (1% w/v bovine serum albumin in PBS, filtered by 0.22 µm nylon syringe filter) for 30 min to prevent non-specific binding.

After blocking, substrates were incubated with antibodies for the immunostaining. First, an antibodies solution was prepared, diluting 1:100 the antibody Alexa Fluor™ 488 Phalloidin (A12379, Invitrogen, Thermo Fisher) and 1:1000 the Hoechst (Hoechst 33342, Invitrogen, Fisher Scientific, stock at 10 mg mL<sup>-1</sup>) in 1% w/v BSA in PBS. Samples were covered with the antibody's solution (100 µL per sample) for 45 min at RT in a wet chamber (in dark, covering them with aluminum foil).

Finally, substrates were placed in a clean 6-well plate and washed with fresh PBS (10 min on shaker). They were transferred into a standard glass microscope slide and mounted in antifading oil (ProLong™ Gold antifade reagent, P36930, Invitrogen, Thermo Fisher) (100 µL per sample) covered with a cover slip. Samples were left to dry (at least 24 h) and stored at RT in dark until the image acquisition.

### 9.8.3. Confocal Imaging

#### 9.8.3.1. Confocal image acquisition

Confocal images were acquired with a Leica TCS SP5 AOBS spectral confocal microscope (Leica Microsystems, Germany) equipped with a HCX PL APO lambda blue 63.0x1.40 OIL UV objective (pinhole 95.5 µm, airy 1; numerical aperture 1.40; refraction index 1.52). A green laser (488 nm) was used for excitation of phalloidin-Alexa-488 (emission recorded between 500 – 590 nm, HyD detector, gain 30, offset 0), a red laser (633 nm, 15 % potency in all the images) for excitation of DiD (emission recorded between 640 – 750 nm, gain 695 nm, offset -1), and a blue UV laser (405 nm) for Hoechst (emission recorded between 415 – 495 nm, gain 650, offset -1), in a sequential way. Captures were taken at 63X magnifications (no zoom, scan speed at 400 Hz) to obtain detailed pictures of few cells with good resolution. Images (acquired at 8-bit, line-average 2, 1024 x 1024 px, 246.27 x 246.27 µm, z-step size 0.13 nm) were treated and analyzed using the ImageJ software (National Institutes of Health, USA).

#### 9.8.3.2. Confocal analysis using ImageJ software

The following protocol was used for image processing, to quantify the cell area and some parameters related to DiD signal, including area and intensity per cell, as well as number of particles per cell.

- a) Open the RAW image selecting split channels, colorized, and auto-scale options.
- b) Start working with the Green channel:
  1. Image/Stacks/Z-project/Sum slices.
  2. Image/Adjust/Brightness&Contrast/Auto.

3. Process/Filters/Gaussian Blur/Sigma 2.0.
  4. Image/Adjust/Threshold (Lower limit until reaching a uniform covering of all the cells)/Apply.
  5. Analyze/Set measurements/ Select the options: Area, Min&Max gray value, Integrated density, Mean gray value, Limit to Threshold, and Decimal places: 5.
  6. Analyze/Analyze particles/ Select the options: 1-Infinity, show Outlines, Display results, Summarize, Add to Manager, Include holes.
  7. The obtained data is presented in the ROI manager (the contour of each cell area in a separated measure), and Results window shows the specific measured values (each cell area).
- c) Continue working with the Red channel:
8. Image/Stacks/Z-project/Sum slices.
  9. Image/Adjust/Threshold (Until uniform covering of all the cells)/NO Apply. Threshold value must be fixed for all the images (319).
  10. Analyze/Set measurements/ Select the options: Area, Min&Max gray value, Integrated density, Mean gray value, Limit to Threshold, and Decimal places: 5.
  11. ROI manager/Select area of one cell/Measure.
  12. Results window showed the corresponding measure for the selected cell.
  13. Analyze/Analyze Particles (0-Infinity, show Outlines, Summarize).
  14. The obtained data is presented in the Results window and shows the specific corresponding measures of each individual detected particle for the selected cell (the sum is the previous result).
  15. Repeat the last two steps for the other cells (ROI manager...)
  16. Export results window to excel

In some cases, if the green labelling is not allowing the automatic selection of cell area, contour of each cell is delimited manually with the Freehand selection. Overall, liposome-cell interactions were evaluated in terms of: (i) area of DiD signal divided by cell area (x100), (ii) DiD intensity (integrated density value) per cell, and (iii) number of particles (from the Analyze Particles function) per cell.

## 9.9. In vitro safety assays

### 9.9.1. Cytotoxicity in HeLa and HMEC-1

Cell viability assays were performed in collaboration with Dr. Ibane Abasolo group from VHIR (Barcelona). Cell cytotoxicity was tested by a MTT assay, using 3-(4,5-dimethylthiazol-2-yl)-2,5-diphenyltetrazolium bromide (MTT) on HeLa or HMEC-1 cells.<sup>19,20</sup> Briefly, 2,000 – 3,000 cells were seeded in 96-well plates, let to adhere, and then exposed to different doses of the nanovesicles for 72 h



at 37 °C (generally 6 replicates per point). Negative control corresponded to no-treated cells, and positive control to cells with DMSO (10 %). Then, an MTT solution (5 mg mL<sup>-1</sup>) in PBS was added to the wells and incubated during 4 additional hours. Formazan crystals resulted from the MTT reduction by active mitochondria were dissolved with DMSO and spectrophotometrically measured at 590 nm (Biotek ELx800 Absorbance Microplate Reader, Izasa Scientific). The data are expressed as the percentages of viable cells compared to the cell survival of negative (non-treated cells) and positive (DMSO-treated cells) control groups.

## 9.9.2. Hemocompatibility

Two types of assays were performed to test the hemocompatibility of the nanosystems. On the one hand, their effect on the integrity of red blood cells was measured using a hemolysis test.<sup>15</sup> On the other hand, their potential interference with blood coagulation was studied by analyzing the plasma coagulation times. Both assays were performed in collaboration with Dr. Ibane Abasolo group from VHIR (Barcelona).

### 9.9.2.1. Hemolysis test

For the hemolysis test, red blood cells (RBC) (isolated from wild type C57BL6 mice or human blood, as specified in each figure footnote) were resuspended in 2 % (v/v) of PBS and exposed to different concentrations of test compounds during 1 h at 37 °C in duplicates. The amount of released hemoglobin was measured in a spectrophotometer at 405 nm (Biotek ELx800) after centrifugation (1000 g, 10 min). Absorbance values were referred to a positive control of 100 % hemolysis obtained after incubating RBC with 1 % of Triton-X. According to manufacturer's protocol, samples showing hemolysis values below 5 % can be considered non-hemolytic.

### 9.9.2.2. Plasma coagulation times

The effect of the nanovesicles in plasma coagulation was tested as previously reported<sup>21</sup> using the Start4 equipment (Stago, France) and following the manufacturer's protocol to determine the activated partial thromboplastin time (APTT), the prothrombin time (PT), and the thrombin time (TT). Values were compared to the normal reference time ranges. The APTT assay is used to assess the intrinsic pathway, while the prothrombin time (PT) assay is a measure of the extrinsic pathway. Extrinsic and intrinsic pathways converge into the common pathway. Thrombin time (TT) is an indicator of the functionality of the final common pathway. For most of control samples, normal coagulation time is in the range of PT assay ≤ 13.4 s, APTT ≤ 34.1 s, and TT ≤ 21 s. Generally, prolongation ≥ 2-fold versus untreated control is considered physiologically significant. If not otherwise specified, testing samples (0.1 mg mL<sup>-1</sup>) were incubated with human plasma (30 min, 37 °C) in duplicates.

## 9.10. In vivo studies in Fabry mouse model

### 9.10.1. Single dose efficacy study and enzymatic activity biodistribution in tissue

The in vivo efficacy after a single dose and enzymatic activity biodistribution of the nanoGLA 30 min post administration was tested in Fabry KO mice (GlatmKul in C57BL6 background), characterized by the complete absence of GLA gene and widely used as animal model for Fabry disease.<sup>18</sup> This assay was performed in collaboration with Dr. I. Abasolo group from VHIR (Barcelona).

Male GLA Fabry KO mice (n = 8/group) with ages ranging from 2 to 4 months were treated with nanoGLA<sub>3%RGD</sub>, nanoGLA<sub>6%RGD</sub>, free rh-GLA, or the clinically available Replagal<sup>®</sup> by tail vein injection (bolus) at 1 mg kg<sup>-1</sup> GLA dose. C57BL6 WT mice and non-treated Fabry KO mice were also included as controls and received the corresponding volume of serum. One week later, animals were administered with a second dose and euthanized 1 min (n = 4/group) or 30 min (n = 4/group) post-administration, and organ and tissues samples were collected (blood, kidneys, liver, spleen, heart, lungs, and brain). Enzymatic activity of GLA in plasma and tissues from samples taken at 1 min and at 30 min post-administration of the second dose was determined as explained in **Chapter 9.7.1**. Quantification of the Gb3 deposits in the different tissues was determined as described in **Chapter 9.14.4**.

### 9.10.2. Repeated dose efficacy study

The in vivo efficacy after a repeated dose of nanoGLA was tested in Fabry KO mice in collaboration with Dr. I. Abasolo group from VHIR (Barcelona). Animals (n = 6/group) were treated with nanoGLA, free rh-GLA, or the clinically available Replagal<sup>®</sup>. Testing compounds were administered by tail vein injection (bolus) at 1 mg kg<sup>-1</sup> GLA dose with a total of 8 doses, distributed in two weeks (days 1, 3, 5, 8, 10, 12, 15, 17). Animals were euthanized 24 h after the eighth dose, and organ and tissues samples were collected. Tissue samples were snap frozen and kept at – 80 °C upon analysis. Gb3 levels were determined as described in **Chapter 9.14.4**.

## 9.11. Pharmacokinetics of nanoGLA and free rh-GLA in rat

Pharmacokinetic of nanoGLA and free rh-GLA was performed in collaboration with Covance SL (UK) in Han Wistar healthy rats (n = 6, Charles River UK) with ages ranging from 63 to 70 days and target weight ranging from 210 to 290 g at dosing. Rats were kept in thermostatically maintained rooms (19 – 25 °C temperature, 40 – 70 % relative humidity), and exposed to fluorescent light (nominal 12 h) each day. All animals will be allowed free access to mains water from bottles attached to the cages. All procedures to be carried out on live animals as part of this study will be subject to provisions of United Kingdom National Law, in particular the Animals (Scientific Procedures) Act 1986.

Each animal received a single intravenous administration, as a bolus injection via a lateral tail vein, at a nominal dose volume of 0.32 mL kg<sup>-1</sup> for tag free rh-GLA (group A, n = 3 rats), or 3.7 mL kg<sup>-1</sup> for nanoGLA (group B, n = 3 rats). Serial blood samples (300 µL) were collected from all the animals at 7 time points (0.016, 0.16, 0.5, 1, 2, 4, 6, and 8 h post-dose), by venepuncture from the jugular vein, except for the final sample which was collected by cardiac puncture whilst under terminal inhalation anesthesia (isoflurane in oxygen). All animals were observed at the beginning and the end of the working day and at each blood sampling occasion for any abnormal signs.

Blood was collected into tubes containing K2-EDTA (ethylenediaminetetraacetic acid) anticoagulant and centrifuged (800 g, 10 min, 4 °C) to produce plasma for analysis, and residual blood cells were discarded. The resultant plasma samples were split into two aliquots of approximately equal volume. Samples were processed to plasma within 30 min of collection, and snap-frozen on dry ice within 60 min (< -50 °C)

Samples were analyzed for MKC content as a measure of nanoliposomal exposure, and for GLA content as bioactive exposure, using qualified methods (**Chapter 9.15.2** and **Chapter 9.15.3**).

Reported pharmacokinetic parameters included in **Table 9.13**, after noncompartmental analysis.

**Table 9.13.** Description of reported parameters in PK study.

Parameter	Description
C <sub>0</sub>	Back-extrapolated concentration at time 0.
C <sub>max</sub>	Maximum observed concentration.
DN C <sub>max</sub>	Dose normalized maximum concentration, calculated as C <sub>max</sub> /dose.
T <sub>max</sub>	Time of maximum observed concentration.
AUC <sub>0-t</sub>	Area under the curve from time 0 to the time of the last measurable concentration, calculated using the linear trapezoidal rule.
AUC <sub>0-24</sub>	Area under the curve from time 0 to hour 24, calculated using the linear trapezoidal rule.
DN AUC <sub>0-24</sub>	Dose normalized AUC <sub>0-24</sub> , calculated as AUC <sub>0-24</sub> /dose.
AUC <sub>0-inf</sub>	Area under the curve from time 0 to infinity, calculated as AUC <sub>0-t</sub> + C <sub>t</sub> / λ <sub>z</sub> , where C <sub>t</sub> is the last observed quantifiable concentration and λ <sub>z</sub> is the elimination rate constant.
t <sub>1/2</sub>	Elimination half-life, calculated as ln(2) / λ <sub>z</sub> .
CL	Clearance, calculated as Dose / AUC <sub>0-inf</sub> (reported for parent only).
V <sub>ss</sub>	Volume of distribution at steady-state, calculated as CL * MRT <sub>0-inf</sub> (reported for parent only), where MRT is defined as the mean residence time

## 9.12. Preliminary toxicity of MKC-liposomes in mice

This assay was performed in collaboration with Dr. Ibane Abasolo team from VHIR (Barcelona). In order to test the feasibility of repeated administration of MKC containing nanovesicles, the effect of 8 intravenous (bolus) administrations of hybrid-liposomes at three different doses (0.37, 1.22 and 3.67 mg lipid per administration) were tested in wild type C57BL6 female mice (22 – 38 g, n = 3 mice/group) obtained from their GLA transgenic colony maintained in heterozygosity (Gla<sup>tmKul1</sup>).<sup>18</sup> Injection of PBS media (vehicle) was used as control. Animal care was handled in accordance with the Guide for the Care and Use of Laboratory Animals of the Vall d'Hebron University Hospital Animal Facility and followed the EU Directive 2010/63/EU for animal experiments. Precise experimental procedures were approved by the Animal Experimentation Ethical Committee at the institution and the regional government (ref. 9572). All studies using animals or samples derived from animals, including MAEC obtaining and hemocompatibility assays, were performed by the ICTS NANBIOSIS, at the CIBER-BBN's in vivo Experimental Platform of the Functional Validation & Preclinical Research (FVPR) area (Barcelona, Spain).

## 9.13. Toxicology studies in rat

A regulatory assessment regarding toxicology was performed by Covance SL (UK). These studies were carried out in male and female Crl:WI(Han) rats (Charles River Laboratories, UK). Two studies were carried out: first, it was conducted a dose range-finding toxicity study (one-week of duration); later, after its completion and analysis, the 4-weeks toxicity study under GLP was performed. The certificate of analysis (CoA) of the nanoGLA and empty-liposomes batches tested in these studies can be found in **Annex II**.

## 9.14. BBB crossing studies

BBB crossing studies were performed in collaboration with Dr. Thomas Birngruber team from Joanneum Research (Austria).

The cOFM probe implantation into the striatum (CP) of the rat's brain was performed as described in surgery. Each animal received one probe per hemisphere (two probes per animal). Sampling started 2 weeks after surgery. Then, animals were connected to an awake-animal sampling system to allow assessment of BBB transport of test drug in conscious animals. Dosing of test drug according to dosing regimen (flow rate 0.5  $\mu\text{L min}^{-1}$ ). Samples were taken according to sampling regimen, specified in each experiment. Samples were stored on  $-20\text{ }^{\circ}\text{C}$  until analytical measurement. PK of nanoliposomes was assessed by following MKC, a membrane component of nanoliposomes.

**Animals:** All animal protocols used in this study were approved by the Austrian Ministry for Science and Research Ref.II/10b, Vienna. After cOFM probe implantation, Male Sprague-Dawley rats with a weight of 400 – 800 g (Charles River Lab., Germany) were housed individually in acrylic glass cages with a 12:12 h light: dark cycle, and food and water available ad libitum.

**Surgery:** Animals were anesthetized by isoflurane (1.5 – 2 %, O<sub>2</sub> 1.8 L min<sup>-1</sup>), prepared for surgery and placed in a stereotaxic frame. Pain treatment during surgical procedure was maintained by fentanyl (5 µg kg<sup>-1</sup>) and carprofen (Rimadyl). Skull was exposed by mid-line incision. Holes for both probe implantation and anchor screws were drilled by a surgical drill (drill bit diameter 0.7 mm). Prior to probe insertion, dura was punctured by hypodermic needle (30 Ga). Probe was carefully inserted into brain (1 mm min<sup>-1</sup>). After anchor screws were placed, area around probe and anchor screws was covered by UV-light curing dental cement. Animal received an injection of glucose, carprofen and enrofloxacin (antibiotic) for post-surgical treatment on three consecutive days post-surgery.

**Perfusate for in vivo sampling:** cOFM standard perfusate with test compound was used for adsorption testing. Perfusate composition: 123 mM NaCl, 0.4 mM MgCl<sub>2</sub> (purity ≥ 98 %), 0.7 mM CaCl<sub>2</sub> (purity ≥ 93 %), 4.3 mM KCl, 1.3 NaH<sub>2</sub>PO<sub>4</sub>, 21 mM Na<sub>2</sub>HPO<sub>4</sub>, 4 mM glucose and 0.2 % BSA. All reagents were dissolved in sterile water. BSA was add after filtration.

**Analysis:** Samples were analysed by LC-MS/MS method for determining the MKC content in stock samples, plasma and ISF samples, as described in **Chapter 9.15.1**.

## 9.15. Quantification of analytes in biological samples

### 9.15.1. Quantification of MKC in plasma and cOFM samples by LC-MS

The amount of MKC present in plasma or cOFM samples was quantified by Dr. Thomas Birngruber team from Joanneum Research (Austria) by using a Liquid Chromatography-Mass Spectroscopy (LC-MS). This technique combines the physical separation capabilities of liquid chromatography with the mass analysis of mass spectroscopy, allowing the identification of the MKC in complex samples. As internal standard solution (ISTD), a solution of cetyltrimethylammonium bromide (CTAB) (160 ng mL<sup>-1</sup> in acetonitrile, CH<sub>3</sub>CN) was used, which is a compound that also belongs to the quaternary ammonium surfactant family.

Then, biological samples containing MKC-liposomes were prepared as following. Plasma samples (10 µL) were diluted with ISTD (10 µL) in CH<sub>3</sub>CN (10 µL). The mixture was vortexed and then centrifuged (5 min, 3000g). The supernatant was then analyzed by LC-MS.

For cOFM samples, cOFM samples (10 µL) were diluted with the ISTD (5 µL) in CH<sub>3</sub>CN (50 µL). The mixture was evaporated to dryness (RT, N<sub>2</sub>), and CH<sub>3</sub>CN (25 µL) was added.

For the preparation of the calibration standards, a similar procedure was followed, diluting known amounts of MKC in an artificial CSF matrix containing 0.2 % w/v of BSA in buffer for obtaining a calibration curve in the range of 25 to 600 ng mL<sup>-1</sup> for plasma samples and 0.5 to 100 ng mL<sup>-1</sup> for cOFM samples.

HPLC was done using a HPLC equipment (Vanquish, Thermo Scientific), equipped with an Atlantis T3 (3 µm, 150 x 2.1 mm) column (Waters, USA) at 25 °C. The mobile phase A (MPA<sub>MKC</sub>) was composed by 0.3 % of formic acid (HCOOH) in water; the mobile phase B (MPB<sub>MKC</sub>) was composed by 0.3 % of HCOOH in CH<sub>3</sub>CN. Separation was done using a multistep gradient (5.1 min) (Table 9.17). Injection sample volume was 4 µL for plasma samples and 10 µL for cOFM samples, and flow rate of 200 µL min<sup>-1</sup>. Approximated retention times were 3.2 and 3.6 min for MKC and CTAB, respectively.

**Table 9.17.** Gradient elution method for MKC analysis.

Time (min)	% MPA <sub>MKC</sub>	% MPB <sub>MKC</sub>
0.0	20	80
1.0	20	80
2.0	5	95
3.0	5	95
3.1	20	80
5.1	20	80

Then, mass spectrometry was done using a triple quadrupole mass spectrometer equipment (TSQ Ultra AM, Thermo Scientific). The ionization method was done by positive electrospray ionization (ESI) or heated-electrospray ionization (HESI). Typical ionization parameters were the following: spray voltage 3.0 kV, sheath gas 15 AU, auxiliary gas 5 AU, transfer capillary temperature 320 °C. The selected scan mode was SRM (selected reaction monitoring), that allows the selection of an ion of a particular mass in the first stage of the tandem MS, that then is used as precursor of the second fragmentation reaction (Table 9.18). Detection parameters were the following: scan width 0.4, scan time 0.1, positive polarity, peak width 0.7.

**Table 9.18.** Typical scan-parameters, in SRM mode for MKC quantification in plasma or cOFM biological samples.

Compound	Parent mass (Da)	Product mass (Da)	Collision energy level (eV)
MKC (Analyte)	332.3	240.2	18
CTAB (Internal reference)	284.3	60.24	28

### 9.15.2. Quantification of MKC from nanoGLA samples in PK study

The amount of MKC present in rat plasma was quantified by protein precipitation and liquid chromatography followed by tandem mass spectrometric detection (LC-MS/MS) at Covance SL (UK), in a similar method than the previously described. As reference materials, MKC (US Biological Life Sciences) and MKC-d7 (ref. B276287, Toronto Research Chemicals) compounds were used. Method was validated in a 10.0 – 5000 ng mL<sup>-1</sup> range, using a quadratic regression as calibration model, and weighting factor 1/x. Each sample (10 µL) was analyzed in duplicate.

### 9.15.3. Quantification of GLA from nanoGLA samples in PK study

The amount of rh-GLA present in rat plasma was quantified by an ELISA (enzyme-linked immunosorbent assay) method performed by Covance SL (UK) and Unilabs York Bioanalytical Solutions (UK). Briefly, mouse anti-GLA antibodies solution (mouse polyclonal antibody to GLA, ref. 169315, Abcam, UK) was added into a 96-well immunoplate (50 µL/well, Nunc MaxiSorp, Thermo) and incubated for 14 – 24 h at 4 °C. After washing (3 x 300 µL/well of PBS solution containing 0.05 % v/v Tween-20), the plate was blocked (200 µL) using SuperBlock (ref. 37515, Thermo Fisher, USA) for 1 – 2 h. After another wash step (3 x 300 µL), plasma samples diluted 1.5 in buffer (low cross buffer, ref. 100500, Candor Biosciences) containing Triton X-100 (2 % w/v) were then added to the plate and incubated for 1 h. The use of Triton X-100 was required to disrupt the nanoliposomes and allow GLA release for quantification. After a further wash step, sheep anti-GLA antibodies solution (sheep polyclonal antibody to GLA, ref. AF6146, R&D Systems, USA) was added to the plate (50 µL/well) and incubated for 1 h. After a further wash step, anti-sheep-peroxidase conjugate solution (anti-sheep IgG peroxidase, ref. A3415, Sigma, USA) was added to the plate (50 µL/well) and incubated for 1 h. After a final wash step, a TMB substrate (ref. T4444, Sigma, USA) was added (50 µL/well). Reaction was stopped after 20 min, adding the stop solution (0.5 M, sulphuric acid, ref. 07208, Sigma). Absorbance was read within 15 min of the reaction being stopped in a suitable plate reader (Tecan Infinite 200 Pro), at  $\lambda_{\text{Abs}} = 450 \text{ nm}$  with a reference  $\lambda_{\text{Ref}} = 620 \text{ nm}$ . Besides, calibration standards were also prepared in rat plasma, using known amounts of rh-GLA, and following the same protocol.

### 9.15.4. Quantification of Gb3 levels in tissue samples by LC-HRMS

Gb3 levels were determined by Dr. I. Abasolo group from VHIR (Barcelona). Gb3 levels were quantified with LC-HRMS at the IQAC-CSIC, as reported in Seras-Franzoso et al.<sup>22</sup> Results of efficacy were based on the capability of the administered GLA of reducing the Gb3 deposits in Fabry mice. Results were expressed as % Gb3 levels. For calculation of the relative Gb3 loss, it was assumed that the difference in Gb3 levels between non-treated KO mice and WT counterparts corresponds to a 100 % of Gb3 loss in WT. Then, the Gb3 levels in different treatment groups were referred to this total Gb3 loss in WT, meaning that those treatments with a higher percentage of Gb3 loss are the ones with a higher efficacy.

## 9.16. Sterilization studies

### 9.16.1. Gamma-radiation of nanovesicles

Samples (both free GLA and GLA-loaded liposomes) were placed in a polyurethane box, prepared with 5 cold-accumulators (2 in the bottom, 1 in the middle and 2 in the upper part) inside, for keeping a cold environment during all the process, and full of packing chips. They were sent to Aragogamma S.L. and  $\gamma$ -irradiated ( $^{60}\text{Co}$  source, 25 kGy dosis, 9 – 10 h of irradiation). The obtained monitored dose was 30.78 kGy (real monitored value). Cold conditions were kept during all the process, since the interior of the box remained cold after recovery of the samples from the box. Each sample was compared to its control (same sample without irradiation). For each condition, two independent samples were aliquoted and analyzed.

### 9.16.2. Syringe filtration of nanovesicles

Samples were filtered using membrane syringe filter of different pore size, i.e., 0.8, 0.45, and/or 0.22  $\mu\text{m}$ , and materials, i.e., polyethersulfone (PES), polyvinylidene fluoride (PVDF), and cellulose acetate (CA). Membrane syringe filters were purchased from MILLEX<sup>®</sup>-GV or Sterlitech Corporation (sterile package, 25 mm).

### 9.16.3. NanoGLA aliquoting in sterile vials for preclinical studies

It was decided to aliquot 5 mL per vial, in 5 mL sterile glass vials assembled with butyl stoppers and aluminum seals (Thermo Scientific, Ref 15193508). Thus, 5 mL sterile glass vials were filled individually using a 5 mL syringe coupled to a 23G needle (Terumo Agani, G 23, 0.6 x 25 mm), in a sterile laminar flow cabinet environment.

## 9.17. Statistical analysis

All results are expressed as the mean  $\pm$  standard deviation (SD) of several experimental replicates, unless otherwise specified. ANOVA tests, student's t-tests or equivalent non-parametric tests were used to investigate the differences between different formulations, using *Prism 6.02* software (GraphPad Software, Inc., CA, USA) or *Minitab<sup>®</sup> 17* statistical software (2013). Statistical differences were accepted as significant ( $p \leq 0.05$ , \*), very significant ( $p \leq 0.01$ , \*\*) or as highly significant ( $p \leq 0.001$ , \*\*\*) according to the obtained p-value.

### 9.17.1. Design of experiments (DoE) and data processing

This experiment was performed in collaboration with MSc., Eng. Josep Merlo, from Nanomol Technologies SL (Bellaterra, Spain). An experimental design with 4 factors and 2 levels with 2 central points (resulting in a total of 10 experimental runs) was constructed to study the influence of the formulation parameters ( $X_n$ , independent factors) on the properties (CQA, or responses) of intermediate



nanoGLA. The selected experimental design was a Fractional Factorial design, and it was developed using Modde 12 Pro software (Umetrics, Sweden). Data fitting and calculation of statistical parameters were performed by partial least squares (PLS) method. The experimental design used in this study allowed fitting the data with a linear regression interaction model. The acceptance of the responses obtained was evaluated by means of the statistical parameters predicted by the software  $R^2$ ,  $Q^2$  model validity and model reproducibility. The design space for nanoGLA was determined using Design Space Explorer option from the Optimizer module of Modde 12 Pro software.

## 9.18. Figures

Figures showed in this Thesis were created with PowerPoint (Microsoft Office), Origin 2019, GraphPad Prism 5, and Biorender.com.

## 9.19. References

1. Spectrum Labs. KrosFlo Research Iii TFF System: Product Information and Operating Instructions.
2. Ribeiro, N. *et al.* A new era for sterilization based on supercritical CO<sub>2</sub> technology. *J. Biomed. Mater. Res. - Part B Appl. Biomater.* **108**, 399–428 (2020).
3. Soares, G. C. *et al.* Supercritical CO<sub>2</sub> technology: The next standard sterilization technique? *Mater. Sci. Eng. C* **99**, 520–540 (2019).
4. Danino, D. Cryo-TEM of Soft Molecular Assemblies. *Curr. Opin. Colloid Interface Sci.* **17**, 316–329 (2012).
5. Pedersen, J. S. A Flux- and Background-Optimized Version of the NanoSTAR Small-Angle X-Ray Scattering Camera for Solution Scattering. *J. Appl. Crystallogr.* **37**, 369–380 (2004).
6. Schwamberger, A. *et al.* Combining SAXS and DLS for Simultaneous Measurements and Time-Resolved Monitoring of Nanoparticle Synthesis. *Nucl. Instruments Methods Phys. Res. Sect. B Beam Interact. with Mater. Atoms* **343**, 116–122 (2015).
7. Li, Y., Beck, R., Huang, T., Choi, M. C. & Divinagracia, M. Scatterless Hybrid Metal-Single-Crystal Slit for Small-Angle X-Ray Scattering and High-Resolution X-ray Diffraction. *J. Appl. Crystallogr.* **41**, 1134–1139 (2008).
8. Garman, S. C. & Garboczi, D. N. The Molecular Defect Leading to Fabry Disease: Structure of Human  $\alpha$ -Galactosidase. *J. Mol. Biol.* **337**, 319–335 (2004).
9. Steiner, E. M. *et al.* The Structure of the N-terminal Module of the Cell Wall Hydrolase RipA and its Role in Regulating Catalytic Activity. *Proteins Struct. Funct. Bioinforma.* **86**, 912–923 (2018).
10. Pabst, G., Rappolt, M., Amenitsch, H. & Laggner, P. Structural Information from Multilamellar Liposomes at Full Hydration: Full q-range Fitting with High Quality X-ray Data. *Phys. Rev. E - Stat. Physics, Plasmas, Fluids, Relat. Interdiscip. Top.* **62**, 4000–4009 (2000).
11. Pabst, G. *et al.* Structural Analysis of Weakly Ordered Membrane Stacks. *J. Appl. Crystallogr.* **36**, 1378–1388 (2003).
12. Hosemann, R. & Bagchi, S. N. Direct Analysis of Diffraction by Matter. *Science* **141**, (1963).
13. Debye, P. Molecular-weight determination by light scattering. *J. Phys. Colloid Chem.* **51**, 18–32 (1947).
14. Cabrera, I. *et al.*  $\alpha$ -Galactosidase-A Loaded-Nanoliposomes with Enhanced Enzymatic Activity

- and Intracellular Penetration. *Adv. Healthc. Mater.* **5**, 829–840 (2016).
15. Giannotti, M. I. *et al.* Highly Versatile Polyelectrolyte Complexes for Improving the Enzyme Replacement Therapy of Lysosomal Storage Disorders. *ACS Appl. Mater. Interfaces* **8**, 25741–25752 (2016).
  16. Desnick, R. J. Fabry's Disease: Enzymatic Diagnosis of Hemizygotes and Heterozygotes. *J. Lab. Clin. Med.* **81**, 157–171 (1973).
  17. Mayes, J. S., Scheerer, J. B., Sifers, R. N. & Donaldson, M. L. Differential Assay for Lysosomal Alpha-Galactosidases in Human Tissues and its Application to Fabry's Disease. *Clin. Chim. Acta* **112**, 247–251 (1981).
  18. Ohshima, T. *et al.*  $\alpha$ -Galactosidase A deficient mice: A Model of Fabry Disease. *Proc. Natl. Acad. Sci. U. S. A.* **94**, 2540–4 (1997).
  19. Bomati-Miguel, O. *et al.* Ex vivo Assessment of Polyol Coated-Iron Oxide Nanoparticles for MRI Diagnosis Applications: Toxicological and MRI Contrast Enhancement Effects. *J. Nanoparticle Res.* **16**, (2014).
  20. Botella, P. *et al.* Surface-modified Silica Nanoparticles for Tumor-targeted Delivery of Camptothecin and its Biological Evaluation. *J. Control. Release* **156**, 246–257 (2011).
  21. Rafael, D. *et al.* Efficient EGFR Mediated siRNA Delivery to Breast Cancer Cells by Cetuximab Functionalized Pluronic® F127/Gelatin. *Chem. Eng. J.* **340**, 81–93 (2018).
  22. Seras-Franzoso, J; Díaz-Riascos, ZV; Corchero, JL; González, P; García-Aranda, N; Mandaña, M; Riera, R; Boullosa, A; Mancilla, S; Grayston, A; Moltó-Abad, M; Garcia-Fruitós, E; Mendoza, R; Pintos-Morell, G; Albertazzi, L; Rosell, A; Casas, J; Villaverde, I. Extracellular Vesicles from Recombinant Cell Factories Improve the Activity and Efficacy of Enzymes Defective in Lysosomal Storage Disorders. *J. Extracell. Vesicles* (2021) doi:10.1002/jev2.12058.

# Scientific Contributions

## Patents

N. Ventosa, J. Veciana, M. Royo, J. Tomsen-Melero, I. Abasolo, S. Schwartz, J. L. Corchero Nieto, D. Pulido, E. Cristóbal-Lecina, E. González-Mira, S. Sala Vergés, A. Córdoba, J. Merlo-Mas, A. Soldevila, A. Font. *Liposomes and its use for enzyme delivery*. EU patent Application No 21382062.4 – 1112. Date of filing: 27.01.21. Applicant/Property: Consejo Superior de Investigaciones Científicas (CSIC), Centro de Investigación Biomédica en Red (CIBER), Vall d'Hebron Institut de Recerca, Nanomol Technologies SL, and LeanBio SL.

## Publications

### Publications within the scope of this Thesis

J. Tomsen-Melero, E. González-Mira, N. Segovia, J. Veciana, N. Ventosa. European Smart-4-Fabry project to develop a new nanomedicine for the treatment of Fabry disease. *Rev. la Soc. Catalana Química* 18, 100–110 (2019).

J. Tomsen-Melero, S. Passemar, N. García-Aranda, Z.V. Díaz-Riascos, R. González-Rioja, J. N. Pedersen, J. Lyngsø, J. Merlo-Mas, E. Cristóbal-Lecina, J.L. Corchero, D. Pulido, P. Cámara-Sánchez, I. Portnaya, I. Ionita, S. Schwartz, J. Veciana, S. Sala, M. Royo, A. Córdoba, D. Danino, J.S. Pedersen, E. González-Mira, I. Abasolo, and N. Ventosa. Impact of Chemical Composition on the Nanostructure and Biological Activity of  $\alpha$ -Galactosidase-Loaded Nanovesicles for Fabry Disease Treatment. *ACS Appl. Mater. Interfaces* 13, 7825–7838 (2021).

J. Merlo-Mas, J. Tomsen-Melero, J.L. Corchero, E. González-Mira, A. Font, J.N. Pedersen, N. García-Aranda, E. Cristóbal-Lecina, M. Alcaina-Hernando, R. Mendoza, E. Garcia-Fruitós, T. Lizarraga, S. Resch, C. Schimpel, A. Falk, D. Pulido, M. Royo, S. Schwartz Jr., I. Abasolo, J. S. Pedersen, D. Danino, A. Soldevila, J. Veciana, S. Sala, N. Ventosa, and A. Córdoba. Application of Quality by Design to the

robust preparation of a liposomal GLA formulation by DELOS-susp method. *J. Supercrit. Fluids* 173, 105204 (2021).

### **Publications outside the scope of this Thesis**

M. Martínez-Miguel, M. Castellote, M. Köber, A. R. Kyvik, J. Tomsen-Melero, G. Vargas-Nadal, J. Muñoz, D. Pulido, S. Passemard, M. Royo, M. Mas-Torrent, J. Veciana, M. I. Giannotti, J. Guasch, N. Ventosa, and I. Ratera. Impact of hierarchical Quatsome-RGD nanostructured surfaces on integrin-mediated cell adhesion. *In Preparation*.

### **Presentations at International Congresses**

Oral Communication “Design of peptide targeted nanovesicles for the  $\alpha$ -galactosidase A enzyme delivery” in the 17<sup>th</sup> European Student Colloid Conference (ESC2019), Varna, Bulgaria, June 2019. Recognized as «Best Oral Presentation» by Langmuir awards. (Presenter: Judit Tomsen-Melero)

Oral Communication “Design of peptide targeted nanovesicles for the  $\alpha$ -galactosidase A enzyme delivery” in the 33<sup>rd</sup> European Colloid and Interface Society Conference (ECIS2019), Leuven, Belgium, September 2019. (Presenter: Judit Tomsen-Melero)

Oral Communication “ $\alpha$ -Galactosidase Enzyme Nanoformulated in Multifunctional Nanoliposomes for Fabry Disease Treatment” in the 7<sup>th</sup> International Symposium on SupraBiomolecular Systems (SUPRABIO2021), Virtual Edition, May 2021. (Presenter: Judit Tomsen-Melero)

### **Contributions in Scientific Projects**

Research activities presented in this manuscript have been mainly conducted in the framework of the European project H2020 *Smart-4-Fabry* (S4F, Ref. ID720942).

### **Other Contributions**

Orphan drug designation (Designation number EU/3/20/2396). Orphan condition: *Alpha galactosidase A for treatment of Fabry disease*. Sponsor: Consejo Superior de Investigaciones Científicas (CSIC) (2021).

# Annex I – Sterilization study

## Sterilization of nanoGLA liposomes

Nowadays, liposomes are one of the most used carriers to be used for drug delivery of biomolecules in the field of nanomedicine. For translation of a nanomedicine from the bedside to the clinics, not only it is important to prove safety and higher efficacy, but also to fulfill all the regulatory requirements that will be mandatory in future clinical phases. In this sense, formulations must be sterile, especially for parenteral administration (such as the intravenous administration). Sterility ensures a minimum level of undesirable biological agents.

Conventional sterilization techniques include physical methods, such as irradiation, filtration, or autoclaving, and chemical methods, such as hydrogen peroxide, gas plasma, ethylene oxide and chemical vapor. However, sterilization of liposomes remains an unresolved issue in the manufacturing of liposome-based formulations, since there is not a widely applicable techniques to use, and each technique presents its own limitations.<sup>1</sup> Many of these conventional techniques, such as steam or dry heat, are unsuitable for the sterilization of liposomal formulations, since they alter the physical and chemical properties of the liposomes, as well as they can denature the proteins.<sup>2</sup> Among all these techniques, terminal sterilization by filtration and aseptic manufacturing are the most recommended methods for the preparation of sterile liposomal-based nanomedicines,<sup>1</sup> despite there are studies of sterilization of liposomes using other techniques such as irradiation.<sup>3-5</sup> Terminal sterilization usually takes place at the end, or near, of the manufacturing process; instead, aseptic processing refers to the combination when the products or components are sterilized separately, and then combined in a sterile environment for the production, obtaining a final sterile product.<sup>6</sup>

In this Thesis, a first exploration on sterilization methods for GLA-loaded liposomes was performed. Two terminal sterilization methods were evaluated: sterilization by gamma radiation and filtration using syringe filters.

## Sterilization by Gamma radiation

Irradiation is a sterilization technique used in the field of healthcare, specially focused in pharmaceuticals, cosmetics, and medical equipment industry. Recently, ionizing radiation, such as gamma-rays, has gained importance as an alternative sterilization in recent years.<sup>4</sup> Gamma-rays are emitted by a radioisotope, usually cobalt-60 or cesium-137 as a source. For sterilization by gamma-radiation ( $\gamma$ -rad), the recommended irradiation dose is 25 kGy.

In the pharmaceutical field, gamma-radiation has been used for the sterilization of nanoparticles, such as topical drug delivery systems, nanospheres, niosomes, and liposomes.<sup>3-5</sup>

The suitability of this technique for the sterilization of GLA-loaded liposomes was investigated. Free GLA (Replagal<sup>®</sup> and GLAcmycHis) as well as GLA-loaded liposomal samples (**Table I.1**) were sent to an external company for gamma-radiation ( $\gamma$ -rad), at the recommended dose (25 kGy) for 9-10 hours (**Chapter 9.16.1**). Cold conditions were kept during all the process, since the interior of the box remained cold after recovery of the samples from the box.

**Table I.1.** Detail of samples irradiated.

Sample ID	Description
GLA Replagal <sup>®</sup>	Free GLA. Stock 1 mg mL <sup>-1</sup> (nominal)
GLAcmycHis	Free GLA. Stock 0.280 mg mL <sup>-1</sup>
nanoGLA	GLA-loaded liposomes*

\* Composition: DPPC, cholesterol, chol-PEG<sub>400</sub>-RGD, MKC (2.2 mol %), GLAcmycHis (5.6  $\mu$ g mL<sup>-1</sup>).

First, a visual change on irradiated samples were that the glass vial containing them turned yellowish. This effect was expected after sterilization by gamma-radiation.

Gamma radiation caused a decrease of the PDI (from 0.18 to 0.11) in GLA-loaded liposomes (**Figure I.1**), compared to the non-irradiated sample. No variation in size or  $\zeta$ -potential was observed. Macroscopic appearance did not change, but irradiated samples presented a change on their olfactometric characteristics, since irradiated samples presented a very unpleasant odor. This effect could be indicator of changes on the composition of the liposomes, for example the degradation of the membrane components or the production of radical species.<sup>4,5</sup> Analysis of GLA-loaded liposomes by ELSD-HPLC (**Chapter 9.5.4.2**) indicated a difference in the acquisition time chromatogram between non-radiated and  $\gamma$ -radiated GLA-loaded liposomes (**Figure I.1E** and **I.1F**). In irradiated samples, the well-known peaks corresponding to DPPC, cholesterol, and cholesterol-PEG<sub>400</sub>-RGD, appeared altered.

Additionally, GLA enzymatic activity assay done in collaboration with Dr. I. Abasolo team from VHIR (Barcelona) few days after  $\gamma$ -radiation showed a completely loss of GLA enzymatic activity in all the

radiated samples, both formulated (GLA-loaded liposomes) and non-formulated (Replagal® and GLAcmycHis) (**Figure I.1D**). Moreover, the irradiated samples showed an interference in the well-established protocol assays for quantification by BCA (i.e., bicinchoninic acid protein assay). BCA is a widely used assay for quantification of the total protein in a sample, and it is based on the reduction of copper ( $\text{Cu}^{+2}$  to  $\text{Cu}^{+1}$ ). It was finding that the addition of the BCA reactive to the radiated non-formulated GLA resulted in a sudden increase of color, indicating a potential interference of the irradiated samples with the BCA technique.

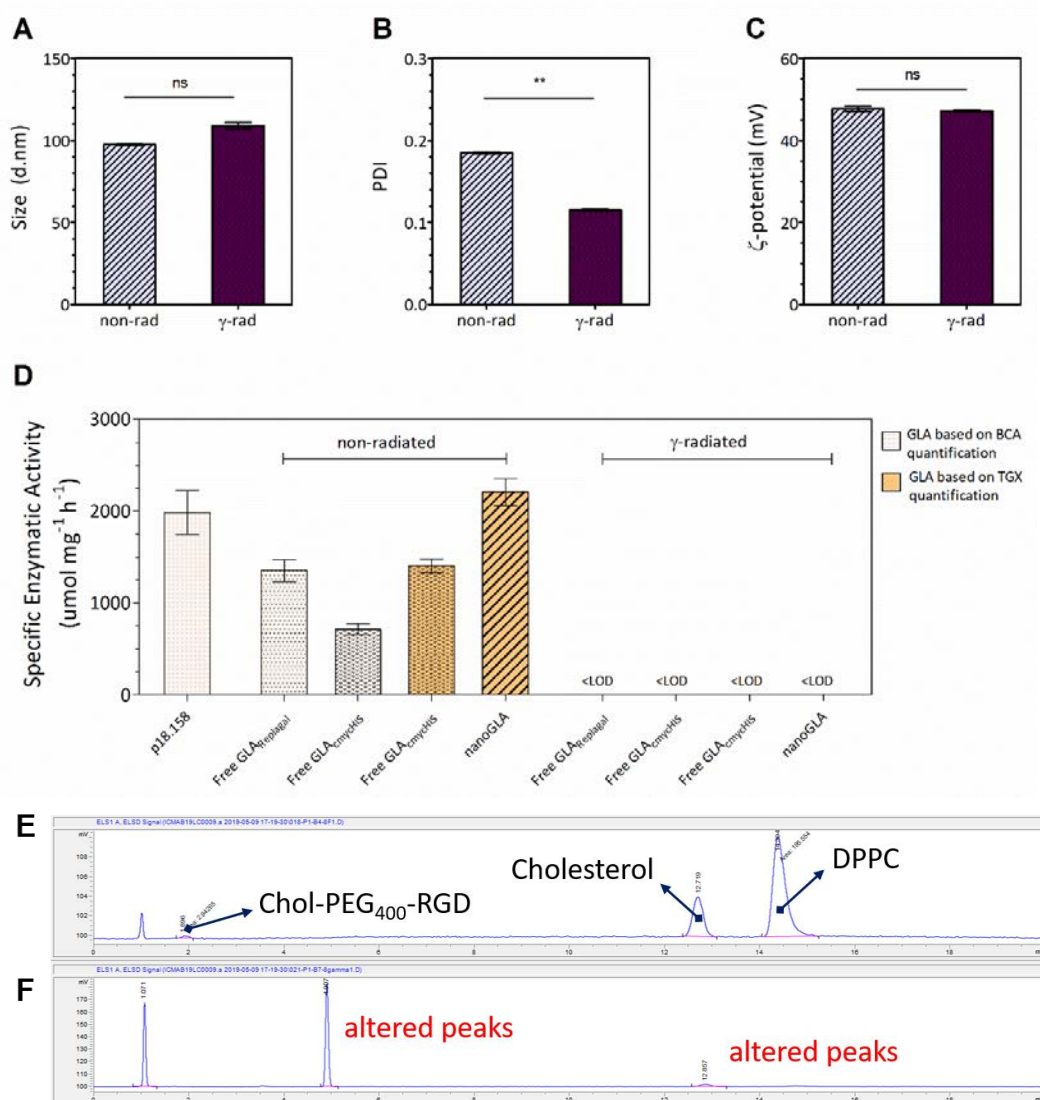


**Figure I.1.** (A) Size, (B) PDI, and (C)  $\zeta$ -potential of non-radiated compared to  $\gamma$ -radiated GLA-loaded liposomes. Each bar corresponds to the average DLS result of two independent aliquots of the same sample, see **Chapter 9.5.1**. (D) Specific enzymatic activity of free GLA (both Replagal® and GLAcmycHis) and GLA-loaded liposomes (nanoGLA), without irradiating and after  $\gamma$ -radiation; Legend indicates the technique used for GLA quantification, a value used in the correction of the results. Acquisition time (in minutes) for (E) non-radiated and (F)  $\gamma$ -radiated GLA-loaded liposomes, analyzed by HPLC-ELSD (**Chapter 9.5.4.2**).



Based on these results,  $\gamma$ -radiation was discarded as feasible sterilization method for GLA-loaded liposomes, since gamma radiation provoked degradation of the liposomal membrane components, as well as an inactivation of the GLA enzymatic activity.

### Sterilization by Filtration

Another terminal sterilization approach accepted to sterilize pharmaceutical products is by microfiltration using membrane filters. It consists of the passage of a mixture of fluids and particles through a porous medium capable of retaining the particles on their surface and/or trapping them in their matrix. For sterilization propose, the effective sterilizing filter must have a pore size of 0.22  $\mu\text{m}$ , to retain microorganism such as bacteria that normally have bigger sizes. A strategy to improve its effectiveness at moderate costs, is to first use bigger pore sizes to remove larges particles, followed later by a high efficiency filtration with membrane filters. Material of the filter should also be considered, to prevent undesired interaction or retention of sample (specially in protein-containing samples) with the filter.

Therefore, the sterilization of nanoGLA liposomes by filtration was addressed. Two different strategies were followed, differing in the moment in which samples are filtered: (i) filtration of the intermediate nanoGLA sample, just after de DELOS-susp procedure, or (ii) filtration of the final nanoGLA sample, after the TFF 7.5-fold and diafiltration process in glucose. The total amount of lipid and protein in liposome samples is different in intermediate and final products and can have an impact when filtering (**Table I.2**). By the strategy (i) it could be ensured a sterile intermediate product, although the later TFF process must be conducted in sterile conditions. However, samples are less concentrated in terms of lipid and GLA, so may be easy the filtration. Besides, by the strategy (ii) a terminal sterilization of the end product could be achieved, although samples are more concentrated, and this can hinder the filtration process.

**Table I.2.** Typical liposome and GLA concentration in intermediate and final nanoGLA samples\*.

Prototype	Description	Liposome concentration (mg mL <sup>-1</sup> )	GLA concentration (μg mL <sup>-1</sup> )
Intermediate	After DELOS-susp	1.2	30
Final	After TFF process	9.0	≥ 200

\* Containing DPPC, cholesterol, chol-PEG400-RGD, MKC, and rh-GLA.

Therefore, samples were submitted to filtration using syringe filters, as detailed in **Chapter 9.16.2**. Several membrane syringe filter of different pore size, i.e., 0.8 and 0.22  $\mu\text{m}$ , and materials, i.e., polyethersulfone (PES), polyvinylidene fluoride (PVDF), were used (see **Figure I.2**.)

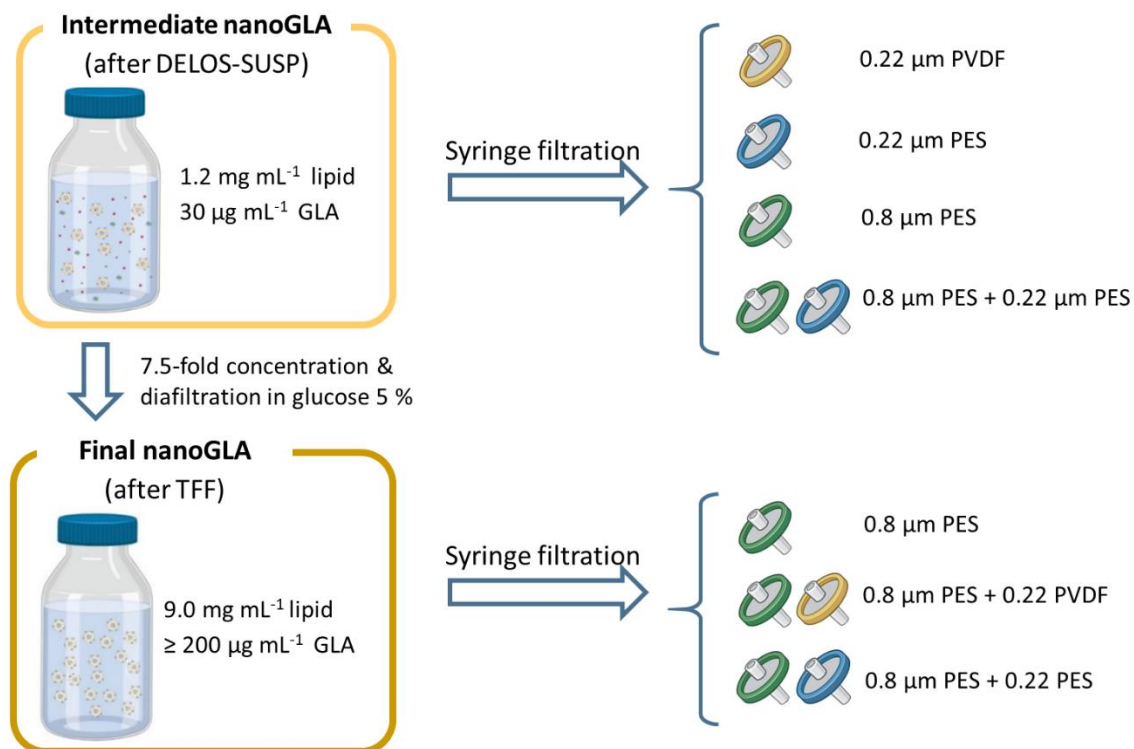


**Figure I.2.** Scheme of the experimental design for nanoGLA filtration using several sizes (0.8 or 0.22  $\mu\text{m}$ ) and material (PES, i.e., polyethersulfone, or PVDF, i.e., polyvinylidene fluoride) syringe filters.

Lipid concentration was quantified by HPLC-ELDS, as described in **Chapter 9** and **Chapter 9**. Furthermore, GLA concentration was quantified by RP-HPLC by LeanBio SL (Barcelona) as explained in **Chapter 9**.

Results showed a similar trend for both intermediate and final nanoGLA products after filtration. In general, important lipid loss were observed for all the samples, although lipid recoveries were higher when using PES instead of PVDF (**Figure I.3A** and **I.3B**). In terms of GLA concentration, similar GLA recoveries were found after 0.22  $\mu\text{m}$  filtration independently of the filter material (**Figure I.3C** and **I.3D**). These GLA recoveries were significantly lower than lipid recoveries, indicating that a large part of protein was lost during the filtration process, probable retained in the filter (**Figure I.3E**).

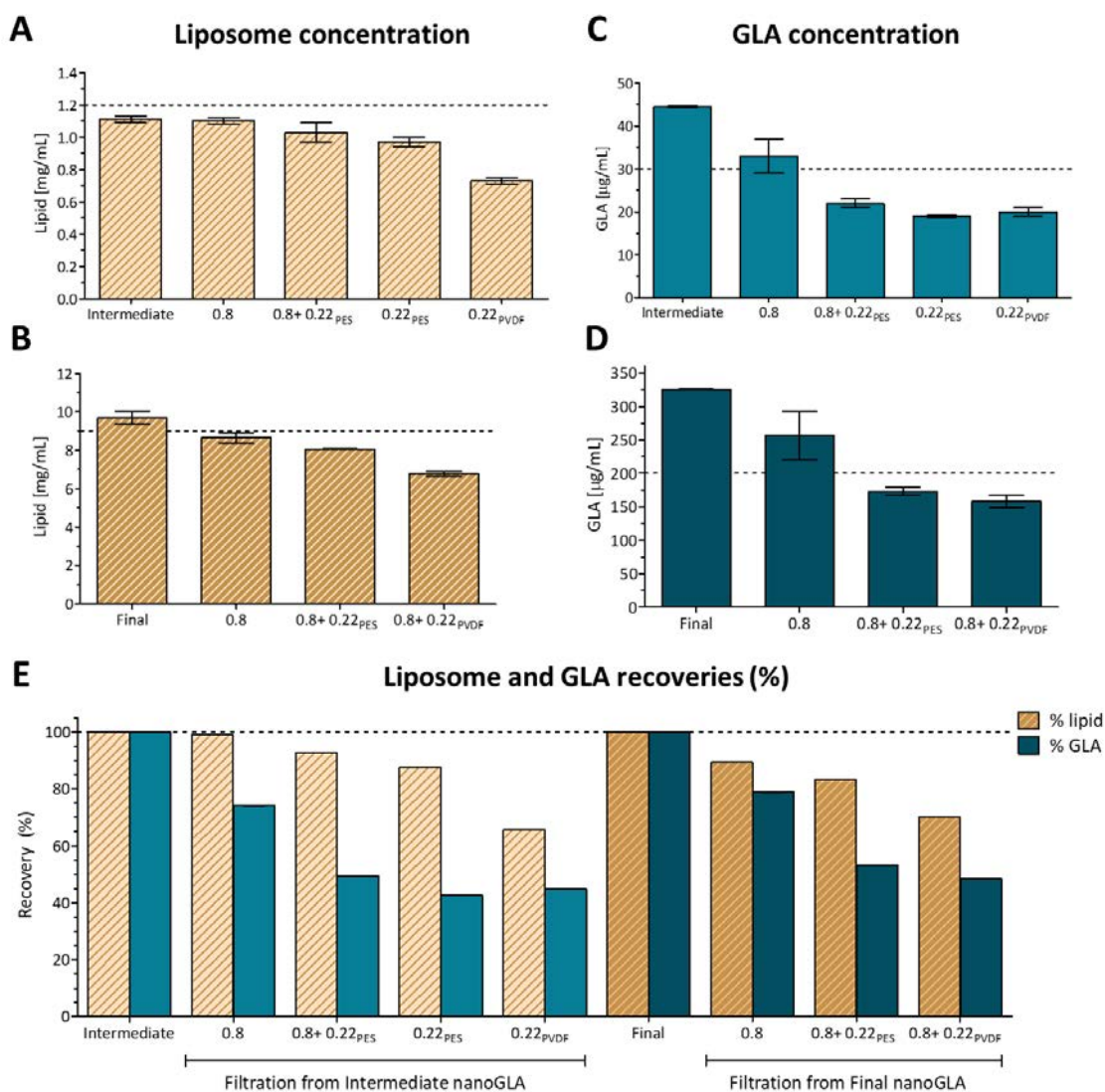


**Figure I.3.** Lipid concentration in (A) intermediate nanoGLA and (B) final nanoGLA samples after syringe filtration, measured by HPLC-ELSD (see **Chapter 9**). GLA concentration in (C) intermediate nanoGLA and (D) final nanoGLA samples after syringe filtration, measured by RP-HPLC (see **Chapter 9**). (E) Summary of recoveries (%) referred to the quantification values before filtering.

In conclusion, there was a general material loss after syringe filtration, higher for GLA than for lipid, in both intermediate and final product. Regarding filter material, PES showed better results than PVDF. In any case, GLA concentration required for in vivo testing (> 0.2 mg/mL) was maintained. Therefore, further optimization is needed to achieve sterile samples.



## References

1. Toh, M.-R. & Chiu, G. N. C. Liposomes as sterile preparations and limitations of sterilisation techniques in liposomal manufacturing. *Asian J. Pharm. Sci.* **8**, 88–95 (2013).
2. Zielińska, A. *et al.* Nanopharmaceuticals for eye administration: Sterilization, depyrogenation and clinical applications. *Biology (Basel)*. **9**, 1–18 (2020).
3. Abuhanoglu, G. & Özer, A. Y. Radiation sterilization of new drug delivery systems. *Interv. Med. Appl. Sci.* **6**, 51–60 (2014).
4. Sakar, F. *et al.* Nano drug delivery systems and gamma radiation sterilization. *Pharm. Dev. Technol.* **22**, 775–784 (2017).
5. Zuidam, J. N. Gamma-Irradiation of Non-Frozen, Frozen and Freeze-Dried Liposomes. *Pharm. Res.* **12**, (1995).
6. Lambert, B. J., Mendelson, T. A. & Craven, M. D. Radiation and ethylene oxide terminal sterilization experiences with drug eluting stent products. *AAPS PharmSciTech* **12**, 1116–1126 (2011).



## **Annex II – CoA**

# Certificate of analysis first large-batch production

  SMART4FABRY	NanoGLA Batch for <i>in vivo</i> testing – Smart4Fabry Project	Code: NT-COA-12.01
	<b>Certificate of Analysis</b>	Version: 01
Replaces: NA		
Page 1 of 2		Product: nanoGLA

## General information

Product: nanoGLA	Code/Batch: S4F-nanoGLA_NF-540
Batch size: 138 mL	Manufacturing date: 17/03/2020
Certificate No: -	Analysis Date: 27/03/2020



## Results

Test	Results	Specification range
Appearance	Homogeneous whitish aqueous dispersion without sediment and opalescent appearance macroscopically	Homogeneous aqueous dispersion without sediment and opalescent appearance macroscopically
Particle size	142 ± 2 nm	50 - 300 nm
Polydispersity Index	0.13 ± 0.01	≤ 0.45
Z-potential	45 ± 1 mV	> +20 mV
Potency - Specific enzymatic activity	1.2 ± 0.5 ratio of nanoGLA vs freeGLA	Ratio of nanoGLA vs freeGLA ≥ 1
HPLC: Total GLA content	262 ± 3 µg/mL	≥ 200 µg/mL
pH	6.5 ± 0.2	6.0 – 7.0

## Remarks

- Batch of process under development
- Not for use in humans
- Methods under development

**CONFIDENTIAL**

  SMART4FABRY	Nano GLA Batch for <i>in vivo</i> testing – Smart4Fabry Project	Code: NT-COA-13.01
	<b>Certificate of Analysis</b>	Version: 01
Replaces: NA		
Page 1 of 2		Product: empty liposomes

### General information

Product: empty liposomes	Code/Batch: S4F-nanoGLA_NF-544
Batch size: 138 mL	Manufacturing date: 23/03/2020
Certificate No: -	Analysis Date: 27/03/2020

### Results

Test	Results	Specification range
Appearance	Homogeneous whitish aqueous dispersion without sediment and opalescent appearance macroscopically	Homogeneous aqueous dispersion without sediment and opalescent appearance macroscopically
Particle size	113 ± 3 nm	50 - 300 nm
Polydispersity Index	0.20 ± 0.01	≤ 0.45
Z-potential	46 ± 1 mV	> +20 mV
pH	6.5 ± 0.2	6.0 – 7.0



### Remarks

- Batch of process under development
- Not for use in humans
- Methods under development

**CONFIDENTIAL**



# Certificate of analysis second large-batch production

  SMART4FABRY	NanoGLA Batch for <i>in vivo</i> testing – Smart4Fabry Project	Code: NT-COA-15.02
	<b>Certificate of Analysis</b>	Version: 02
Replaces: 01		
Page 1 of 2		Product: nanoGLA

## General information

Product: nanoGLA	Code/Batch: S4F-nanoGLA_NF-566
Batch size: 387 mL	Manufacturing date: 14/07/2020
Certificate No: -	Analysis Date: 11/08/2020



## Results

Test	Results	Specification range
Appearance	Homogeneous whitish aqueous dispersion without sediment and opalescent appearance macroscopically	Homogeneous aqueous dispersion without sediment and opalescent appearance macroscopically
Particle size	153 ± 1 nm	50 – 300 nm
Polydispersity Index	0.09 ± 0.02	≤ 0.45
Z-potential	40 ± 1 mV	> +20 mV
Potency - Specific enzymatic activity	Bioactive (ratio of nanoGLA vs freeGLA: 0.63 ± 0.2)	Bioactive (ratio of nanoGLA vs freeGLA ≥ 0.50)
Total GLA content (by RP-HPLC-UV)	270.90 ± 0.04 µg/mL	≥ 200 µg/mL
pH	7.04 ± 0.04	6.0 – 7.0
Osmolality	265 ± 2 mOsm/Kg	260 – 300 mOsm/Kg
MKC content	0.190 ± 0.002 mg/mL	≥ 0.2 mg/mL

## Remarks

- Batch of process under development
- Not for use in humans
- Methods under development

**CONFIDENTIAL**

  SMART4FABRY	Nano GLA Batch for <i>in vivo</i> testing – Smart4Fabry Project	Code: NT-COA-14.02
	<b>Certificate of Analysis</b>	Version: 02
Replaces: 01		
Page 1 of 2		Product: empty liposomes

### General information

Product: empty liposomes	Code/Batch: S4F-nanoGLA_NF-559
Batch size: 287 mL	Manufacturing date: 30/06/2020
Certificate No: -	Analysis Date: 11/08/2020

### Results

Test	Results	Specification range
Appearance	Homogeneous whitish aqueous dispersion without sediment and opalescent appearance macroscopically	Homogeneous aqueous dispersion without sediment and opalescent appearance macroscopically
Particle size	113 ± 1 nm	50 – 300 nm
Polydispersity Index	0.13 ± 0.01	≤ 0.45
Z-potential	50 ± 2 mV	> +20 mV
pH	6.2 ± 0.1	6.0 – 7.0
Osmolality	261 ± 3 mOsm/Kg	260 – 300 mOsm/Kg
MKC content	0.290 ± 0.006 mg/mL	≥ 0.2 mg/mL

### Remarks

- Batch of process under development
- Not for use in humans
- Methods under development

**CONFIDENTIAL**



# **Annex III – Scientific contributions**

# Impact of Chemical Composition on the Nanostructure and Biological Activity of $\alpha$ -Galactosidase-Loaded Nanovesicles for Fabry Disease Treatment

Judit Tomsen-Melero, Solène Passemard, Natalia García-Aranda, Zamira Vanessa Díaz-Riascos, Ramon González-Rioja, Jannik Nedergaard Pedersen, Jeppe Lyngsø, Josep Merlo-Mas, Edgar Cristóbal-Lecina, José Luis Corchero, Daniel Pulido, Patricia Cámara-Sánchez, Irina Portnaya, Inbal Ionita, Simó Schwartz, Jr., Jaume Veciana, Santi Sala, Miriam Royo, Alba Córdoba, Dganit Danino, Jan Skov Pedersen, Elisabet González-Mira,\* Ibane Abasolo,\* and Nora Ventosa\*



Cite This: *ACS Appl. Mater. Interfaces* 2021, 13, 7825–7838



Read Online

ACCESS |



Metrics & More



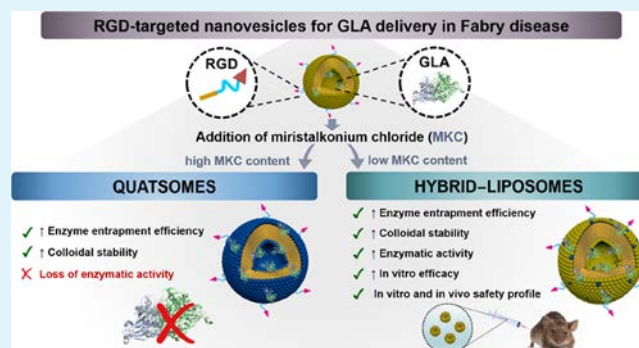
Article Recommendations



Supporting Information

**ABSTRACT:** Fabry disease is a rare lysosomal storage disorder characterized by a deficiency of  $\alpha$ -galactosidase A (GLA), a lysosomal hydrolase. The enzyme replacement therapy administering naked GLA shows several drawbacks including poor biodistribution, limited efficacy, and relatively high immunogenicity in Fabry patients. An attractive strategy to overcome these problems is the use of nanocarriers for encapsulating the enzyme. Nanoliposomes functionalized with RGD peptide have already emerged as a good platform to protect and deliver GLA to endothelial cells. However, low colloidal stability and limited enzyme entrapment efficiency could hinder the further pharmaceutical development and the clinical translation of these nanoformulations. Herein, the incorporation of the cationic miristakonium chloride (MKC) surfactant to RGD nanovesicles is explored, comparing two different nanosystems—quatsomes and hybrid liposomes. In both systems, the positive surface charge introduced by MKC promotes electrostatic interactions between the enzyme and the nanovesicles, improving the loading capacity and colloidal stability. The presence of high MKC content in quatsomes practically abolishes GLA enzymatic activity, while low concentrations of the surfactant in hybrid liposomes stabilize the enzyme without compromising its activity. Moreover, hybrid liposomes show improved efficacy in cell cultures and a good in vitro/in vivo safety profile, ensuring their future preclinical and clinical development.

**KEYWORDS:** nanovesicles, RGD targeting, Fabry disease,  $\alpha$ -galactosidase A (GLA), miristakonium chloride (MKC)



## 1. INTRODUCTION

Fabry disease (FD) is a lysosomal storage disorder (LSD) disease caused by a deficiency or absence of the  $\alpha$ -galactosidase A (GLA) lysosomal enzyme. GLA is a glycosylated enzyme produced in the endoplasmic reticulum, modified with mannose-6-phosphate recognition markers in the Golgi apparatus, packed into secretory vesicles, and delivered to the late endosomes/lysosomes.<sup>1–3</sup> Moreover, after their passage through the Golgi apparatus, a variable fraction of the newly synthesized GLA can also be secreted from the cell and be endocytosed and transported to the lysosomes of neighboring cells through plasma membrane-located mannose-6-phosphate receptors.<sup>2</sup> Glycosylation is essential for GLA water solubility, activity, stability, and correct transport to the lysosome.<sup>4</sup>

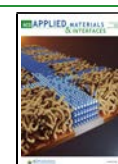
The missing GLA activity leads to the accumulation of its neutral glycosphingolipid substrates, mainly globotriaosylceramide (Gb3), within lysosomes of a wide variety of cell types

including vascular endothelial cells, podocytes, cardiomyocytes, and nerve cells.<sup>5</sup> Endothelial cells are among the most affected cell types, playing an important role in the disease pathophysiology. Substrate accumulation in endothelial cells impairs multiple cellular activities such as energy metabolism, oxidative stress, and transport across ions channels, leading to multiorgan pathologies and the early death of untreated patients.<sup>6</sup> The principal treatment of Fabry patients is enzyme replacement therapy (ERT), which relies on the intravenous infusion of

Received: September 18, 2020

Accepted: January 25, 2021

Published: February 15, 2021



exogenous recombinant GLA every other week.<sup>7,8</sup> Currently, there are two enzymes approved for ERT in FD: agalsidase beta (Sanofi-Genzyme) and agalsidase alfa (Shire-Takeda) administered at 1 and 0.2 mg kg<sup>-1</sup>, respectively. Although both compounds reduce Gb3 accumulation in tissues,<sup>9,10</sup> neither treatment seems to completely reverse the disease, especially in advanced stages. The poor biodistribution of GLA (liver sequestration), a short plasma half-life, and the immunogenic response to the naked enzyme might be among the causes of this impaired efficacy. Novel formulations should protect the active biomolecules from degradation, reduce enzyme immunogenicity, enhance enzyme cellular internalization, and significantly improve the treatment efficacy.<sup>11,12</sup> Currently, a modified version of the GLA with attached chains of 2 kDa polyethylene glycol (PEG) (pegunigalsidase alfa, Protalix Biotherapeutics) showed a significant extension of the enzyme's half-life and a lower generation of antidrug antibodies (ADAs).<sup>13</sup> This clearly indicates that there is still room to improve ERT formulations for treating Fabry disease, as well as other LSDs.

One attractive strategy to improve an ERT formulation is to design a robust enzyme delivery nanoformulation. In the field of nanomedicine, biomolecules can be encapsulated in different types of delivery systems with the aim to improve the efficacy and reduce the adverse effects of the treatment.<sup>8</sup> Widely used nanocarriers are vesicular systems, especially liposomal systems, which have shown promising *in vitro* and *in vivo* results.<sup>14,15</sup>

Within the frame of a multidisciplinary project, we previously developed a liposomal nanovesicle system containing an in-house-produced recombinant GLA.<sup>16,17</sup> This liposomal system (LP) was composed of the phospholipid DPPC, cholesterol, and an RGD unit (tripeptide Arg-Gly-Asp) linked to the cholesterol moiety (chol-PEG<sub>200</sub>-RGD)<sup>18</sup> to favor the recognition of  $\alpha_v\beta_3$ -integrins, expressed in endothelial cells. Considering that injured endothelial cells overexpress  $\alpha_v\beta_3$ -integrins<sup>19</sup> and their levels are increased in kidneys of Fabry disease patients,<sup>20</sup> the RGD-mediated internalization pathway is a promising alternative to the mannose-6-phosphate (M6P) one. Among the different types of RGD peptides available, the cRGDfk was chosen to functionalize the nanoliposomes due to the advantages brought by its cyclic structure (e.g., improved selectivity and stability).<sup>21</sup> The incorporation of a PEG<sub>200</sub>-RGD moiety within the nanoliposomes translated into a higher cellular uptake compared to the plain liposomes with the same membrane composition but without RGD, emphasizing the importance of incorporating this targeting unit.<sup>16</sup> The addition of this peptide did not alter the enzymatic activity of the GLA but improved its delivery into lysosomes of target cells since the incorporation of the RGD contributed to a significant enhancement of the cell functionality in comparison with the free drug.<sup>16</sup> Theoretical analysis with atomistic resolution of the interaction of the GLA protein with the liposomes pointed out that such enzymatic activity increase was caused by the enzyme-liposome association through electrostatic interactions, which oriented the enzyme in a "site-specific" manner in the lipid bilayer, exposing its active site to the exterior aqueous phase.<sup>16</sup> In this GLA-loaded liposomal system (LP-GLA), the enzyme entrapment efficiency was around 40% (i.e., the amount of GLA attached and/or contained inside nanoliposomes compared with the total amount of added GLA), resulting in an insufficient drug concentration for achieving *in vivo* therapeutic doses.

Accordingly, to continue with the preclinical development of the liposomal GLA system and guarantee the arrival of this innovative enzyme nanoformulation to the clinics, GLA

entrapment, as well as the colloidal stability of the nanoformulation, must be improved. A higher percentage of drug entrapment could potentially reduce the manufacturing cost and increase the GLA concentration in the final nanoformulation, allowing therefore for greater flexibility in dosing.<sup>22</sup> Additionally, a high enzyme entrapment efficiency implies a reduced or null presence of free enzyme in the liposomal formulation, which might induce unwanted destabilization phenomena, e.g., liposome aggregation and/or formation of enzyme aggregates. Both types of instabilities may contribute to the activation of the complement system *in vivo* that could, in turn, reduce the bioavailability of the nanomaterial<sup>23</sup> and induce hypersensitivity (allergic) reactions and anaphylaxis,<sup>24</sup> as previously shown for other types of liposomes.<sup>25,26</sup>

In this work, we examined if an increase in the cationic character of the nanovesicles could promote a better electrostatic interaction with the negatively charged GLA at the pH in which the nanovesicles are self-assembled. This would lead to higher enzyme entrapment as previously described for other proteins,<sup>27–29</sup> and enhanced colloidal stability of the nanoformulation. Indeed, human GLA, a homodimeric enzyme with a monomer weight of 48.8 kDa and one active site per monomer, is an unstable protein having a negative net charge close to neutral pH and a theoretical pI of 5.1.<sup>30</sup>

In this work, two different RGD-targeted lipid-based nanovesicles for the intracellular delivery of GLA were explored: (i) nonliposomal nanovesicles, known as quatsomes,<sup>31,32</sup> and (ii) liposomes with various concentrations of a cationic surfactant in their membrane, named here hybrid liposomes. Both systems contain the quaternary ammonium surfactant miristalkonium chloride (MKC) in high (>50 mol % of the total membrane components, h-MKC) and low (<5 mol % of the total membrane components, l-MKC) amounts, respectively, and they were produced using the DELOS-SUSP method based on the use of compressed CO<sub>2</sub>.<sup>18,33,34</sup> Importantly, DELOS-SUSP allows the preparation of nanovesicles with high batch-to-batch consistency and easy scalability, in comparison to other nanovesicle processing techniques, which are essential requirements for clinical translation.<sup>16,35</sup>

MKC is the C14 homolog of a benzalkonium chloride. Surfactants of the benzalkonium chloride family are widely used as antimicrobial preservatives in many medicinal products with different administration routes. For example, they are found in approved parenteral formulations of corticosteroids (Celestone Soluspan, Schering-Plough) at a concentration of 0.02% w/v, as well as in products for the enteral route that are used to ease the penetration of drugs, such as lorazepam.<sup>36,37</sup>

In addition, quatsomes with high MKC levels were shown to be stable for several years, keeping stability upon rising temperature and dilution and displaying high homogeneity in terms of nanovesicle size and lamellarity.<sup>31,38</sup> However, there are no studies on the impact of high MKC concentrations on the stability and activity of enzymes such as GLA.

Our objective was to compare h-MKC-based quatsomes (MQ) with hybrid liposomes (HLP) containing low MKC levels as vehicles for GLA delivery. From a regulatory perspective, HLP could present an advantage over MQ since their formulations are closer to the well-studied LP and, additionally, because lower MKC concentrations will preclude future safety concerns. Our results clearly show that incorporation of small amounts of MKC into the liposomal formulation improves colloidal stability and enzyme entrapment capacity of the nanovesicles without compromising the enzymatic activity of

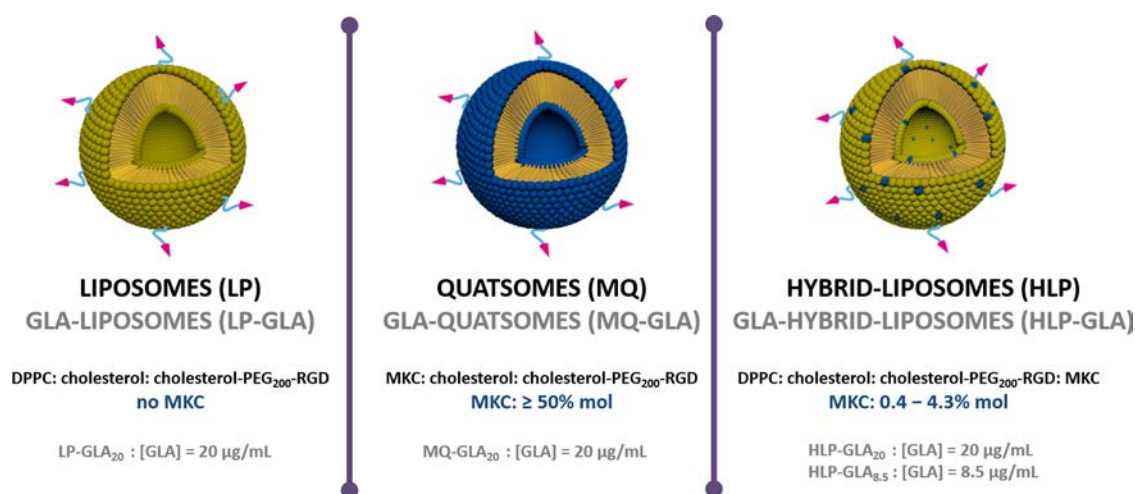


**Figure 1.** Nomenclature and chemical composition of the different nanovesicle systems: liposomes, quatsomes, and hybrid liposomes, in which MKC is contributing in different ways for each system. Moreover, for each system, the blank prototype (without GLA) and the GLA-loaded version (with GLA) were produced. For hybrid liposomes, two different GLA concentrations (i.e., 20 and 8.5 µg mL<sup>-1</sup>) were tested, resulting in **HLP-GLA<sub>20</sub>** and **HLP-GLA<sub>8.5</sub>**, respectively.

**Table 1.** Physicochemical Characteristics of the GLA Nanoformulations, the Next Day after Production<sup>d</sup>

nanovesicle system	mean size [nm]	PDI	ζ-potential [mV]	GLA [µg mL <sup>-1</sup> ]	theor. GLA per vesicle <sup>a</sup>	GLA per membrane component [µg µmol <sup>-1</sup> ] <sup>b</sup>
LP	152 ± 1	0.41 ± 0.02	26 ± 1			
LP-GLA <sub>20</sub>	550 ± 40 <sup>c</sup> (310 ± 20) <sup>c</sup>	0.77 ± 0.02 <sup>c</sup> (0.50 ± 0.10) <sup>c</sup>	-6.3 ± 0.2 (-25.2 ± 0.8)	20 ± 1 (7 ± 2)	ND	8.3
MQ	69 ± 1	0.19 ± 0.01	64.2 ± 0.7			
MQ-GLA <sub>20</sub>	69 ± 3 (65 ± 3)	0.19 ± 0.02 (0.20 ± 0.01)	61.0 ± 0.9 (58.0 ± 0.6)	18 ± 1 (15.1 ± 0.3)	ND	3.4
(0.4%MKC)-HLP	107 ± 1	0.23 ± 0.02	36 ± 4			
(0.4%MKC)-HLP-GLA <sub>20</sub>	141 ± 6 (140 ± 4)	0.18 ± 0.02 (0.17 ± 0.01)	17 ± 1 (17 ± 1)	12 ± 2 (2.8 ± 0.2)	3	8.3
(2.2%MKC)-HLP	112 ± 1	0.24 ± 0.01	59 ± 2			
(2.2%MKC)-HLP-GLA <sub>20</sub>	123 ± 1 (124 ± 3)	0.17 ± 0.01 (0.17 ± 0.02)	36 ± 2 (42.3 ± 0.1)	11 ± 2 (6 ± 1)	6	8.3
(2.2%MKC)-HLP-GLA <sub>8.5</sub>	108 ± 2 (112 ± 1)	0.18 ± 0.01 (0.20 ± 0.01)	51 ± 2 (46 ± 1)	4.9 ± 0.4 (4.6 ± 0.2)	4	3.4
(4.3%MKC)-HLP	113 ± 1	0.23 ± 0.02	63.6 ± 0.7			
(4.3%MKC)-HLP-GLA <sub>20</sub>	126 ± 1 (123 ± 1)	0.19 ± 0.01 (0.17 ± 0.01)	46.8 ± 0.7 (49 ± 1)	12.1 ± 0.9 (12 ± 1)	11	8.3

<sup>a</sup>Theoretical number of GLA per vesicle (see Section 5, Supporting Information). <sup>b</sup>Theoretical ratio mass of GLA per mole of membrane component. <sup>c</sup>Not reliable data; the sample showed some sedimentation. <sup>d</sup>Values in parentheses are for diafiltrated nanoformulations. Results are shown as the average of two independent productions for each system (mean ± SD, *n* = 2).

the cargo. Moreover, *in vitro* and *in vivo* studies with the **HLP** formulation confirmed not only the safety of the system but also a therapeutic benefit in cellular models of Fabry disease.

## 2. RESULTS AND DISCUSSION

**2.1. MKC Improves the Colloidal Stability and GLA Entrapment Efficiency of the Nanovesicles.** GLA-nanovesicle systems were prepared using three different membrane compositions (Figure 1). All were functionalized with chol-PEG<sub>200</sub>-RGD to allow the recognition of α<sub>v</sub>β<sub>3</sub>-integrins overexpressed in endothelial cells.<sup>16,18</sup> The first formulation was constituted of DPPC, cholesterol, and chol-PEG<sub>200</sub>-RGD yielding liposomes (**LP**). The second formulation was composed of cholesterol, chol-PEG<sub>200</sub>-RGD, and h-MKC that forms quatsomes (**MQ**). For the third system, a small amount of MKC was added to the liposome formulation at three different l-

MKC concentrations, 0.4, 2.2, and 4.3 mol %, allowing the generation of hybrid liposomes (**HLP**) with positively charged membranes. All the GLA-loaded systems (named **LP-GLA<sub>20</sub>**, **MQ-GLA<sub>20</sub>**, and **HLP-GLA<sub>20</sub>**, respectively) were prepared using the same initial theoretical GLA concentration, i.e., 20 µg mL<sup>-1</sup>. An additional **HLP-GLA<sub>8.5</sub>** system was prepared at the lower GLA concentration of 8.5 µg mL<sup>-1</sup> to yield the same enzyme and membrane components ratio of 3.4 µg µmol<sup>-1</sup>, as in **MQ-GLA<sub>20</sub>** (see Table 1). All the nanovesicles were prepared with the DELOS-SUSP production route described in Section 4 and in the Supporting Information (Section 1).

The physicochemical characteristics of blank vesicles and GLA-loaded vesicles were assessed by measurements of the particle size, size distribution, and ζ-potential using DLS. The results are summarized in Table 1.

First, GLA-loaded liposomes (LP-GLA<sub>20</sub>) similar to those described by Cabrera et al.<sup>16</sup> were prepared, but using the commercially available agalsidase alfa (Replagal) as the model enzyme of high-quality, tag-free, and already approved and commercialized GLA instead of the in-house-produced His tag GLA, obtaining similar low enzyme entrapment efficiency but less stability than the previously reported system. Entrapping the commercial GLA, LP-GLA<sub>20</sub> showed a higher mean particle size and wider size distribution compared to LP and the previous evaluated systems, also reflected by a notably higher polydispersity index. In addition, LP-GLA<sub>20</sub> showed low-negative  $\zeta$ -potential values, a fact that had a direct negative impact on their stability. Specifically, these LP-GLA<sub>20</sub> liposomes sedimented a few days after production, indicating the necessity of improvement.

In comparison, MQ formulations showed a narrow size distribution and a considerable smaller mean size of around 70 nm. Notably, their physicochemical properties were also maintained when GLA was incorporated into the system (MQ-GLA<sub>20</sub>).

All three HLP systems (see Table 1) formed small vesicles around 110 nm in diameter, slightly larger than the MQ vesicles but still with a narrow size distribution. The  $\zeta$ -potential values directly correlated with the MKC concentration, increasing when more MKC was added to the structures. The addition of MKC maintained high and positive  $\zeta$ -potential values even when the GLA was entrapped (HLP-GLA<sub>20</sub> systems), although values were slightly below those obtained in the absence of GLA (HLP). This decrease in the  $\zeta$ -potential value could reflect the electrostatic nature of the interaction between the negatively charged enzyme and the positively charged vesicle. The  $\zeta$ -potential represents the electrical charge on the nanovesicle surface, which is also an important parameter that allows prediction of the physical stability. In theory, higher  $\zeta$ -potential values, either positive or negative, tend to stabilize particle dispersions. Usually, particle aggregation is less likely to occur for charged particles with a pronounced  $\zeta$ -potential due to the electrostatic repulsion between particles with the same electrical charge.<sup>39</sup> This effect on the nanoformulation stability was clearly observed when MQ-GLA<sub>20</sub> and HLP-GLA<sub>20</sub> containing the cationic MKC surfactant were compared with the non-MKC-containing LP-GLA<sub>20</sub> system since no vesicle sedimentation was observed up to 1 month after production for the first systems. The remarkable stability of MKC-containing systems could also be observed by monitoring the evolution of their size, PDI, and  $\zeta$ -potential over time (Figure 2).

Next, the concentration of GLA in the nanovesicles was quantified by SDS-PAGE and densitometry analysis (GLA concentration for each nanovesicle system is shown in Table 1) and, based on it, the entrapment efficiency (EE%) and GLA loading were determined (see Section 4). The correlation between both parameters, the EE and GLA loading, and the MKC content is represented in Figure 3.

As expected, MKC played an important role in the integration capacity of GLA into the nanoformulations. Significantly higher entrapment efficiency was achieved in MQ-GLA<sub>20</sub> (EE > 80%) in comparison to the MKC-free LP-GLA<sub>20</sub> (EE  $\approx$  30%). As aforementioned, the quaternary ammonium surfactant MKC was the main membrane component of MQ-GLA<sub>20</sub> formulations, and consequently, it led to higher cationic surface charge in the membrane, which induces higher entrapment of GLA by electrostatic interactions.

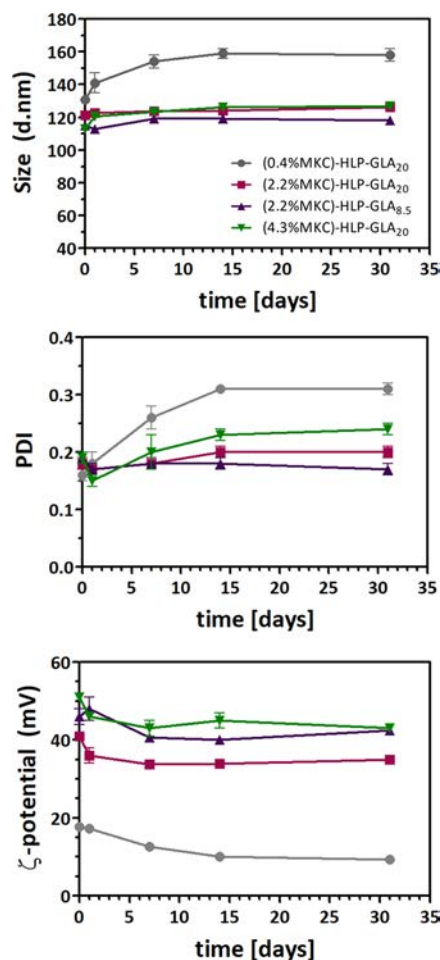


**Figure 2.** Stability of HLP-GLA nanovesicles in terms of diameter size, PDI, and  $\zeta$ -potential measured at different time points (day 0, 1, 7, 14, and 31 after production) after being stored at  $5 \pm 2$  °C. The shown data corresponds to the mean  $\pm$  SD of three independent measurements of the same batch per each system.

Similar effects were found in the hybrid-liposomal systems as shown in Figure 3; in HLP-GLA<sub>20</sub> systems, EE and GLA loading directly correlated with the amount of MKC present. For the (0.4%MKC)-HLP-GLA<sub>20</sub> (the lowest MKC concentration), an entrapment efficiency of  $23 \pm 5\%$  was obtained, comparable to LP-GLA<sub>20</sub>, suggesting that despite the improvement of physicochemical characteristics (size, PDI, and stability) given by MKC addition, more electrostatic interactions are needed to achieve the improvement of EE. In the formulations with higher MKC levels, (2.2%MKC)-HLP-GLA<sub>20</sub> and (4.3%MKC)-HLP-GLA<sub>20</sub>, with considerably improved EE values of up to  $60 \pm 20$  and  $100 \pm 20\%$ , respectively, were detected. However, the difference between EE% of (4.3%MKC)-HLP-GLA<sub>20</sub> and MQ-GLA<sub>20</sub> was not statistically significant at this specific GLA concentration of  $20 \mu\text{g mL}^{-1}$ , indicating that the electrostatic interactions provided by MKC concentrations  $\geq 4.3$  mol % are more than enough to entrap this amount of GLA.

Interestingly, as shown in Figure 3, both (2.2%MKC)-HLP-GLA<sub>20</sub> and (2.2%MKC)-HLP-GLA<sub>8.5</sub> showed similar GLA loading despite being formulated at two different GLA concentrations, suggesting that, at this MKC concentration, nanovesicles reach the maximum enzyme loading capacity with  $8.5 \mu\text{g mL}^{-1}$  GLA. These findings provide a better understanding of the effect of MKC.



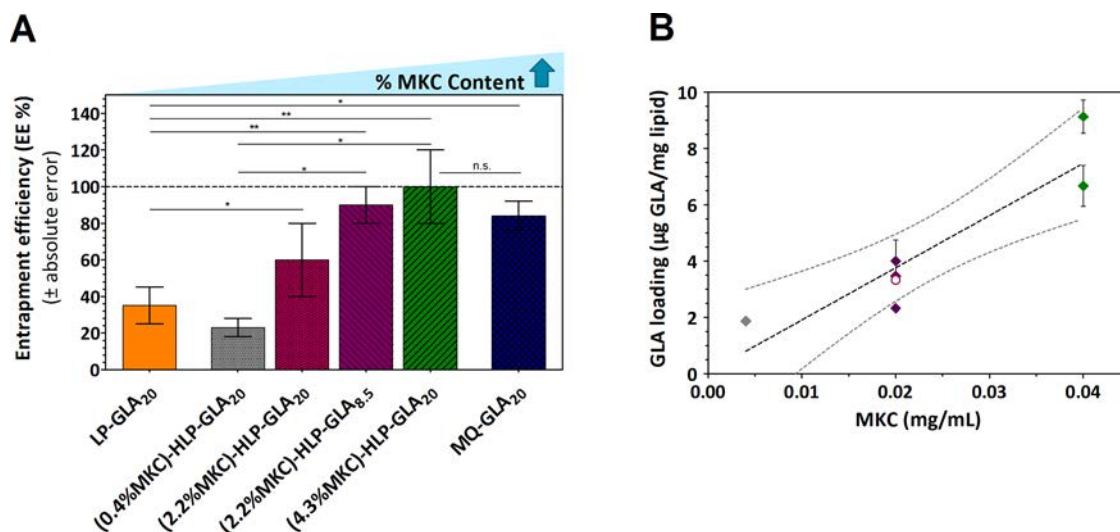


**Figure 3.** (A) GLA entrapment efficiency of all the tested systems and (B) GLA loading in relation to MKC amount (in  $\text{mg mL}^{-1}$  of formulation) for hybrid liposomes. Samples represented with bulk symbols correspond to systems prepared with the same GLA initial concentration (HLP-GLA<sub>20</sub>). The empty circle corresponds to the system with lower GLA initial concentration (HLP-GLA<sub>8.5</sub>). The results correspond to the average of two or three independent assays.

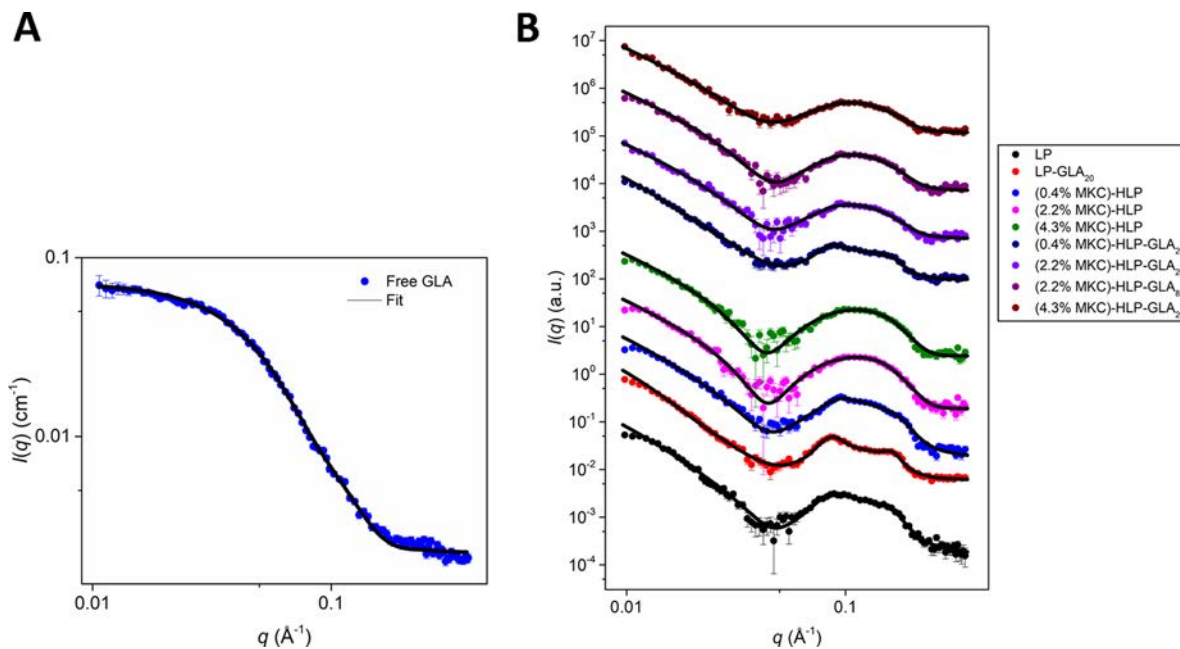


**Figure 4.** (A) SAXS data of free GLA and (B) the nanoformulation samples. Assay corresponds to a single representative experiment for each system, replicated in three independent assays. Solid lines are model fits to the SAXS data.

We then turned to SAXS to gain further understanding of changes in the liposome morphology. First, the scattering from the free GLA was investigated since GLA contributes significantly to the total scattering signal in the loaded liposome samples. The SAXS data of the pure enzyme could be fitted with a rigid-body refined dimer structure<sup>40</sup> based on the known dimeric crystal structure of GLA (PDB: 1r46,<sup>30</sup>  $\chi^2 = 1.8$ ) (Figure 4A). Fitting was done on an absolute scale, yielding a concentration estimate of  $1.10 \text{ mg mL}^{-1}$  (assuming that all GLA is on dimer form), which was slightly higher than the concentration of  $1 \text{ mg mL}^{-1}$  for the commercial stock GLA sample. A small increase in intensity at low scattering vector moduli,  $q$ , could suggest slight aggregation in the sample, resulting in a somewhat elevated concentration estimate.

For the nanoformulations, the SAXS data showed a characteristic minimum at intermediate  $q$ , typical for liposomes, arising from the variations in electron density across the cross-section profile of the bilayer membranes. The data was fitted with a paracrystalline model<sup>41</sup> based on Pabst et al.<sup>42,43</sup> where the average number of layers ( $N_{\text{layers}}$ ) and the bilayer thickness ( $T$ ) can be determined. When fitting the data, it was observed that an additional contribution from polymer scattering had to be included to obtain good fits (Figure 4B and Table 2). For the samples without GLA (LP and HLP), this scattering contribution was constant and probably arises from the flexible chol-PEG<sub>200</sub>-RGD on the membrane surface. For samples containing GLA, the polymer scattering was therefore fixed at an average value obtained from the GLA-free fits. In LP-GLA<sub>20</sub> and

Table 2. SAXS Modeling Results for the Nanoformulations<sup>e</sup>

nanovesicle system	$\chi^2$ <sup>a</sup>	polymer scale ( $10^{-4}$ )	[GLA] <sub>theo.</sub> [ $\mu\text{g mL}^{-1}$ ]	[GLA] <sub>fitted</sub> [ $\mu\text{g mL}^{-1}$ ]	$N_{\text{layers}}$ <sup>b</sup>	$T^c$ [ $\text{\AA}$ ]
LP	1.1	$4.6 \pm 0.8$			$1.5 \pm 0.1$	$51.5 \pm 0.3$
LP-GLA <sub>20</sub>	1.1	$4.2^{cd}$	20	$13 \pm 2$	$2.0 \pm 0.1$	$51.0 \pm 0.2$
(0.4%MKC)-HLP	2.2	$4.2 \pm 0.8$			$1.3 \pm 0.1$	$48.9 \pm 0.3$
(2.2%MKC)-HLP	1.5	$3.4 \pm 0.7$			$1.0 \pm 0.1$	$48.6 \pm 0.3$
(4.3%MKC)-HLP	1.5	$4.4 \pm 0.8$			$1.0 \pm 0.1$	$48.5 \pm 0.4$
(0.4%MKC)-HLP-GLA <sub>20</sub>	1.2	$4.2^{cd}$	20	$22 \pm 3$	$1.1 \pm 0.1$	$50.7 \pm 0.3$
(2.2%MKC)-HLP-GLA <sub>20</sub>	1.5	$4.2^{cd}$	20	$18 \pm 3$	$1.1 \pm 0.1$	$50.2 \pm 0.5$
(2.2%MKC)-HLP-GLA <sub>8.5</sub>	1.6	$4.2^{cd}$	8.5	$8 \pm 4$	$1.1 \pm 0.1$	$49.9 \pm 0.4$
(4.3%MKC)-HLP-GLA <sub>20</sub>	0.9	$4.2^{cd}$	20	$16 \pm 3$	$1.1 \pm 0.1$	$49.3 \pm 0.3$

<sup>a</sup> $\chi^2$  is the reduced weighted chi-square. <sup>b</sup>Average number of layers in liposomes. <sup>c</sup>Bilayer thickness defined as  $T = 2(z_{H,1} + \sigma_{H,1})$ , where  $z_{H,1}$  is the distance from the center of the bilayer to the center of the Gaussian used to describe the headgroup and  $\sigma_{H,1}$  is the width of this Gaussian. <sup>d</sup>Not fitted value. <sup>e</sup>Assay corresponds to a single representative experiment for each system, replicated in three independent assays. Values correspond to the mean  $\pm$  SD.

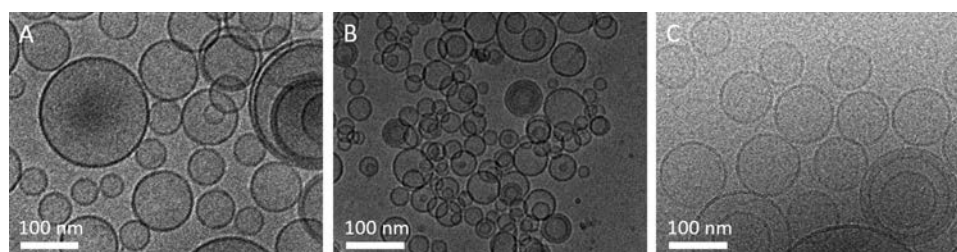


Figure 5. Cryo-TEM images of the three different nanoformulations: (A) non-MKC-containing liposomes (LP-GLA<sub>20</sub>), (B) quatsomes (MQ-GLA<sub>20</sub>), and (C) hybrid liposomes (HLP-GLA<sub>8.5</sub>).

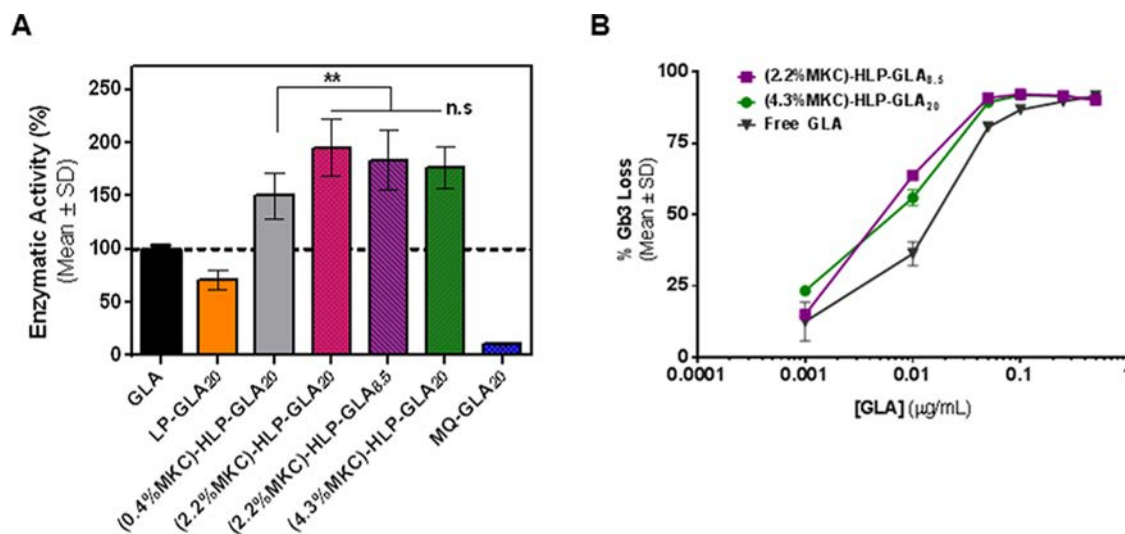


Figure 6. Enzymatic activity and in vitro cell activity of different GLA-nanovesicle conjugates. (A) Specific enzymatic activity in liposomes (LP-GLA), quatsomes (MQ-GLA), and hybrid liposomes containing MKC (HLP-GLA). All values were normalized by their GLA concentration and referred to the enzymatic activity of the free GLA as a reference. Measurements were run at 37 °C for 1 h, and results were corrected for incubation time, as detailed in Section 4. The results correspond to the average of three independent assays using two different batches per each system. (B) In vitro efficacy assays measured as loss of Gb3 (due to its hydrolysis by GLA) in primary endothelial cells derived from Fabry KO mice. Incubation with GLA or liposomal systems was performed at 37 °C for 48 h. Assay corresponds to a single batch per system, replicated in three independent assays.

HLP-GLA<sub>20</sub>, GLA also contributed to the scattering patterns and, thus, the theoretical signal from free GLA was added to the liposome scattering through a linear combination with its own individual scale factor. Even though the scattering contributions from the polymer and GLA were small and, to some extent, correlated, it was still possible by this approach to determine the GLA concentrations with SAXS, which corresponded fairly well with the theoretically calculated GLA concentrations (Table 2).

Increasing MKC concentrations decreased the bilayer thickness ( $T$ ) slightly for both GLA-containing (from 51.0  $\text{\AA}$  to 49.3  $\text{\AA}$ ) and GLA-free (from 51.5  $\text{\AA}$  to 48.5  $\text{\AA}$ ) liposomes. Furthermore, for samples with MKC,  $T$  was slightly higher when GLA was added, suggesting that the protein possibly binds to the positively charged liposome surface and therefore increases the apparent bilayer thickness. Both LP and LP-GLA<sub>20</sub> showed some multilamellarity that diminished as MKC was introduced into the liposomes, probably an effect of the

general lower stability and early sedimentation observed for LP and LP-GLA<sub>20</sub> in comparison with HLP and HLP-GLA<sub>20</sub>.

Direct analysis of the nanovesicles with cryo-TEM was fully consistent with the SAXS analysis. Figure 5 presents as examples characteristic data for the LP-GLA<sub>20</sub>, MQ-GLA<sub>20</sub>, and HLP-GLA<sub>8.5</sub> systems. The nanoformulations are largely unilamellar as expected and rather uniform in size. LP-GLA and HLP-GLA<sub>8.5</sub> nanovesicles are about 120 nm in diameter, and MQ-GLA<sub>20</sub> nanovesicles are smaller and, on average, 60–70 nm in diameter, all in excellent agreement with the DLS data shown in Table 1. Because cryo-TEM is showing individual nanovesicles, certain polydispersity with some double-layer structures is recognized, but overall and in agreement with the SAXS analysis, vesicles show a high degree of unilamellarity.

Overall, the physicochemical properties showed that both quatsomes and hybrid liposomes are promising systems for further exploration as potential carriers of the GLA enzyme. The increase in their membrane positive charge due to the presence of the cationic surfactant leads to a narrower and more monodisperse size distribution, with a marked improvement in the colloidal stability. This amends the earlier destabilization phenomena seen in the MKC-free system (LP-GLA<sub>20</sub>) and makes MQ-GLA<sub>20</sub> and HLP-GLA systems suitable for further examination. Especially important is the two-fold increase in GLA entrapment efficiency compared with LP-GLA<sub>20</sub>. This is a major advancement in enzyme nanoformulations, where it is often very challenging to obtain high or full incorporation of big biomacromolecules into the nanovesicles.

**2.2. The Specific Enzymatic Activity of GLA Is Increased in HLP-GLA Systems.** The specific enzymatic activity of the GLA enzyme conjugated to the nanovesicles was measured using a fluorescence assay following Cabrera et al.<sup>16</sup> Since the GLA is a lysosomal enzyme, the enzymatic activity assay needs to occur at low pH values. To be sure that the enzyme activity was measured over the nonaltered encapsulation patterns, we confirmed the stability of the nanostructured formulations in the acidic media of the assay conditions before performing the enzyme assays (Figure S9, Supporting Information).

The results in Figure 6A indicate that the presence of MKC in the nanovesicles had a dramatic impact on the protein enzymatic activity. The use of h-MKC in MQ-GLA<sub>20</sub> provoked a considerable reduction in the activity of the enzyme of up to 80%.

On the other hand, when no MKC was used (LP-GLA<sub>20</sub> system), enzymatic activities were about half of those of the commercially available GLA, which is formulated as a solution with a series of excipients (polysorbate-20, sodium chloride, sodium hydroxide, and sodium phosphate monobasic) in its final pharmaceutical form.<sup>44</sup> The entrapment of the commercialized GLA formulation into non-MKC-containing liposomes possibly destabilizes the enzyme, initially stabilized in its original formulation with the 0.2 μg mL<sup>-1</sup> nonionic polysorbate-20 surfactant. These results contrast those obtained with an in-house-produced recombinant GLA in an acetate buffer solution free of excipients, as reported by Cabrera et al.<sup>16</sup> In that case, the stabilizing function of the liposomal system was more than evident with this in-house-produced recombinant GLA.

Interestingly, in the case of HLP-GLA, the presence of l-MKC in the liposomal membrane helped substantially increase the enzyme activity in the nanoformulation since the enzymatic activity of all hybrid liposomes were above those of the

commercial free enzyme and LP-GLA<sub>20</sub> without MKC in the membrane.

Statistical comparison between LP-GLA and HLP-GLA or LP-GLA and MQ-GLA was highly significant (\*\**p* = 0.0001) and very significant (\*\**p* = 0.004), respectively (not shown inside the graph in Figure 6A for the sake of clarity). Statistical comparisons on enzymatic activity among HLP-GLA were only significant when comparing (0.4%MKC)-HLP-GLA<sub>20</sub> to other HLP-GLA containing higher MKC content (\*\**p* = 0.004).

As previously mentioned, molecular dynamics calculations pointed out that GLA-liposome association occurs through electrostatic interactions, which could orient the enzyme in a “site-specific” manner in the lipid bilayer, exposing its active site to the exterior aqueous phase.<sup>16</sup> So, it seems reasonable that the presence of small amounts of the cationic MKC surfactant in the HLP-GLA membrane enhances this effect in comparison to LP-GLA, with similar membrane composition but free of MKC. The enzymatic activity of GLA, measured in the presence of pure MKC at equivalent surfactant concentrations to those in HLP-GLA formulations, was lower than the one measured for the corresponding formulations (see Figure S10, Supporting Information). This result points out that the enzymatic activity enhancement is related to the entrapment of GLA in HLP-GLA liposomes, containing l-MKC in their membrane, and not only due to the presence of this surfactant in the formulation. The LP-GLA and HLP-GLA liposomes used in the present work for the encapsulation of GLA are constituted by DPPC phospholipids and have a high content of cholesterol, which, as it is well known, yields rigid liposomal nanovesicles with mechanically stable gel-phase bilayers.<sup>45</sup> In a recent work, we have reported that quatsome nonliposomal lipid nanovesicles, although having also a high cholesterol content, are flexible nanovesicles, formed by a bilayer membrane with comparable structural properties to fluid-like lipid bilayers.<sup>46</sup> These differences on the membrane phase state between liposomes and quatsomes might cause a different type of enzyme-nanovesicle association and explain the different enzyme activities under different types of encapsulation patterns. It has been reported that the way proteins interact with lipid membranes depends not only on the surface charge of the membrane but also on the phase state.<sup>47</sup>

Although quatsomes were shown to be appropriate nano-carriers for other drug models,<sup>38</sup> the loss of enzymatic activity made them unfit for GLA delivery. Thus, further biological studies were only performed with the hybrid-liposomal systems due to their promising results, in terms of improved GLA loading and physicochemical stability, as well as the higher enzymatic activity of conjugated GLA.

**2.3. HLP-GLA Hybrid Liposomes Increase the In Vitro Efficacy of the GLA Enzyme while Keeping a Safe In Vivo Toxicological Profile.** The capacity of HLP-GLA to enter cells and reduce the Gb3 deposits within the lysosomes was measured by adding a fluorescent-labeled Gb3 (NBD-Gb3).<sup>16,48</sup> In this assay, mouse aortic endothelial cells (MAECs) from Fabry KO mice, with no endogenous GLA activity, were challenged with different concentrations of HLP-GLA. Consequently, total Gb3 loss was solely attributed to the action of the enzyme carried by the nanovesicles after cell internalization and lysosomal localization, where the low pH allowed enzyme activity. Results showed better efficacy of nanoformulated enzymes compared to experiments with free GLA (Figure 6B), in accordance with the previously described increase in the intrinsic specific enzymatic activity.

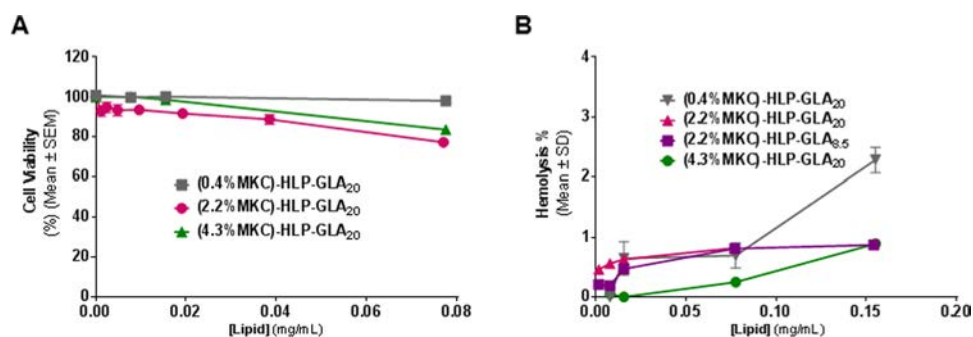


**Figure 7.** In vitro safety assays of different HLP-GLA formulations. (A) Cell viability in HeLa cells treated during 72 h at 37 °C with up to 0.08 mg mL<sup>-1</sup> in lipids. The mean  $\pm$  SEM values of three independent experiments of a single representative batch per each system are shown. (B) Hemolysis of mouse red blood cells with different HLP-GLA systems, incubated 1 h at 37 °C. Assay corresponds to a single representative batch per each system. Mean  $\pm$  SD values are also represented.

Therefore, these new HLP-GLA systems with enhanced colloidal stability and higher EE ( $\geq 90\%$ ) and, thus, of better quality have demonstrated to be as effective in vitro as the previous published GLA-loaded liposomal system.<sup>16</sup> These results validate this nanoformulation optimization work since the present developed hybrid liposomes overall fulfill the physicochemical and biological requirements to warrant their progress to an advanced stage of preclinical development.

The higher efficacy of nanoformulated GLA compared to experiments with free GLA could be explained by (i) the enzyme conjugation to nanoliposomes, which are well-known nanocarriers for intracellular delivery, and (ii) the presence of RGD peptide in the nanoliposomal membrane, which we previously demonstrated allows a rapid mediated-internalization in endothelial cells.<sup>16,49</sup> The impact of GLA nanoformulation on efficacy was also observed when using other types of nanoparticles, such as ICAM-1-targeted polystyrene nanocarriers.<sup>50</sup>

To characterize the safety and toxicological profile of the HLP-GLA systems, several in vitro assays were performed. First, HeLa cells were exposed to different concentrations of HLP-GLA and cell viability was measured after 72 h incubation by the MTT assay (Figure 7A). Cell viabilities were kept above 75% in all cases, indicating that integration of MKC into the hybrid liposomes was not inducing any dose-dependent cytotoxicity.

Further, it was also tested whether the HLP-GLA could be safely administered intravenously using well-established hemocompatibility studies. First, the impact of different nanoformulations in red blood cell fragility was studied by using hemolysis tests in murine blood samples. We find that none of the tested HLP-GLA systems induced significant hemolysis and the values measured never surpassed 5% total hemolysis (see Figure 7B).

Similarly, no significant variations in plasma coagulation times were detected after incubating human plasma with 0.154 mg mL<sup>-1</sup> (2.2%MKC)-HLP-GLA<sub>20</sub>. Thus, the results were within the normal expected range (Table S4, Supporting Information).

Once the HLP-GLA demonstrated to be safe in vitro, an in vivo repeated dose toxicity assay was performed with just the vehicle (without GLA). The rationale behind this preliminary in vivo study was to evaluate the plausibility of using MKC-containing liposomes and thus identify potential toxicities caused by the vehicle in vivo. Accordingly, C57BL6 wild-type mice were treated twice a week during 4 weeks with three different doses (0.37, 1.22, and 3.67 mg of lipid per injection, which corresponded approximately to 12, 41, and 105 mg kg<sup>-1</sup>

lipid) of non-GLA (2.2%MKC)-HLP hybrid liposomes. Prior to administration, the concentration of the liposomal system was needed to reach the desired doses, mimicking the concentration factor that is required to reach the sufficient GLA concentration in the nanoformulation for achieving a therapeutic dose in vivo. This step did not induce any significant change in physicochemical properties of the system and 12-fold concentrated samples were obtained (details in Section 2, Supporting Information). Additionally, the stability of this system in human serum (37 °C) was assessed by turbidity measurements (Section 3, Supporting Information). No significant changes in turbidity were observed (Figure S6), and vesicle integrity was also confirmed by cryo-TEM (Figure S7).

The treatment schedule was aimed at mimicking that of efficacy assays with GLA in Fabry mice, where repeated administrations of the enzyme are required to ensure a sustained effect. The overall welfare of the animals (general appearance, drinking/eating behavior, and response to stimuli) as well as weight was monitored during 5 weeks (4 weeks of treatment plus an additional week of surveillance), with no significant alterations of any of the monitored parameters (see Figure 8 for body-weight monitoring), demonstrating a good tolerability of the HLP system upon repeated administrations.

### 3. CONCLUSIONS

In this work, we explored the use of two different RGD-targeted lipid-based nanovesicles for GLA enzyme entrapment, with distinct MKC content, i.e., nonliposomal nanovesicles, known as quatsomes, which contain high MKC concentrations ( $>50$  mol % of the total membrane components), and hybrid liposomes that contain low MKC concentrations ( $<5$  mol % of the total membrane components). Both systems were successfully prepared using the DELOS-SUSP procedure, confirming the suitability of this technique for the preparation of multifunctional nanovesicles with a high level of homogeneity.

Membrane composition of these vesicles strongly impacted both the physicochemical and biological characteristics of the nanoformulations. As expected, the addition of positive charges to the membrane by incorporating MKC improved the colloidal stability of the nanoformulation. Moreover, the amount of positive charge added to the system had a direct impact on the ability to entrap the enzyme, which is negatively charged at neutral pH. Consequently, quatsomes showed high entrapment efficiencies, but surprisingly, hybrid liposomes, with lower levels of MKC, achieved enzyme entrapment efficiencies similar to

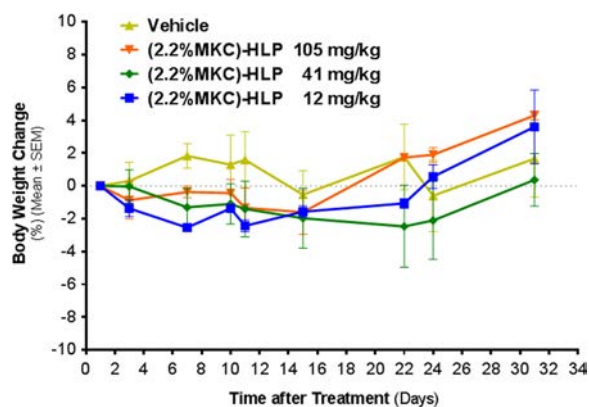


**Figure 8.** Body-weight changes in animals administered with concentrated (2.2%MKC)-HLP. Mice ( $n = 3$  per group) were treated repeatedly with a total of eight intravenous administrations over 4 weeks, with three different doses of (2.2%MKC)-HLP (0.37, 1.22, and 3.67 mg of lipid, corresponding to 12, 41, and 105 mg kg<sup>-1</sup> lipid per administration). Injection of PBS media (vehicle) was used as a control. Weight gain on day 31 of the different treatment groups was not significantly different ( $p = 0.3747$ , by Kruskal–Wallis test).

quatsomes. However, despite the high entrapment efficiency and good colloidal stability, quatsomes completely abolished the activity of the GLA enzyme. This underlines the relevance of obtaining a good balance between physicochemical properties of the carrier and the biological activity of the encapsulated drug, which must be tuned for each type of nanocarrier/drug combination.

In vitro, l-MKC hybrid liposomes (0.4–4.3 mol % of the total membrane components) were shown to be noncytotoxic and nonhemolytic. Moreover, the entrapment of GLA into these hybrid liposomes enhanced the efficacy of the enzyme and showed greater reduction of lysosomal Gb3 than the free administered GLA. Good tolerability and no adverse side effects were observed in mice after repeated administrations of MKC-containing liposomes, paving the way for future in vivo efficacy assays of such systems. Overall, the improvements in the colloidal stability, entrapment efficiency, and biological activity of GLA described in this work would allow a reduction in dose and volume of GLA-conjugated liposomes to be administered in vivo, a necessary step to demonstrate the significant benefit of these systems versus the current enzymatic replacement therapy in Fabry patients. The final purpose is to ensure a future effective translation of this promising nanoformulation into a novel product for Fabry disease treatment.

## 4. EXPERIMENTAL SECTION

**4.1. Materials.** Cholest-5-en-3 $\beta$ -ol (cholesterol; purity, 95%) was purchased from Panreac (Barcelona, Spain). 1,2-Dipalmitoyl-*sn*-glycero-3-phosphocholine (DPPC) was obtained from CordentPharma (Plankstadt, Germany). Miristalkonium chloride (MKC) was purchased from US Biological (Salem, United States). Cholesterol-PEG<sub>200</sub>-RGD was prepared as described previously by Cabrera et al.<sup>18</sup> or by Cristóbal-Lecina et al.<sup>51</sup> Agalsidase alfa (GLA, 1 mg mL<sup>-1</sup>, Replagal) was purchased from Shire-Takeda. Ethanol (HPLC grade; Teknocrroma Sant Cugat del Vallès, Spain) was purchased with high purity and used without further purifications. Dimethyl sulfoxide (DMSO; ACS reagent; purity, 99.9%) was obtained from Sigma-Aldrich (Madrid, Spain). Carbon dioxide (purity, 99.9%) was supplied by Carbueros Metálicos S.A. (Barcelona, Spain). The water used was pretreated with a Milli-Q Advantage A10 water purification system (Millipore Ibérica, Madrid, Spain).

**4.2. Preparation of Nanovesicles.** All formulations (Table 1 and Figure 1) were prepared using the same preparative route with the DELOS-SUSP methodology (see the Supporting Information). The physicochemical parameters such as size, shape, charge, short-term stability, and GLA loading were carefully considered before selecting the best design.

**4.3. Quatsome (MQ and MQ-GLA) Preparation.** For GLA-unloaded quatsomes (MQ), chol-PEG<sub>200</sub>-RGD was dissolved in DMSO before adding dropwise an ethanolic solution of cholesterol and MKC, obtaining a solution with DMSO and EtOH in a 2:5 volume ratio. The mixture was loaded into a 25 mL high-pressure vessel and volumetrically expanded with compressed CO<sub>2</sub> to reach a working pressure ( $P_w$ ) of 10 MPa. The system was kept at 308 K and 10 MPa for approximately 15 min to achieve complete homogenization and thermal equilibration. For GLA-loaded quatsomes (MQ-GLA<sub>20</sub>), GLA was added to water for injection (type I) to reach the desired final enzyme concentration (20  $\mu$ g mL<sup>-1</sup>). To form the nanovesicles, the expanded organic phase was depressurized over the cold aqueous solution. In this step, a flow of N<sub>2</sub> at the working pressure was used as a plunger to push down the CO<sub>2</sub>-expanded solution from the vessel and to maintain a constant pressure of 11 MPa inside the vessel during depressurization. Dispersions of nanovesicles in a total concentration of 3.6 mg mL<sup>-1</sup> (detailed final molar concentrations of the components were 0.35, 2.59, and 5.87  $\mu$ mol mL<sup>-1</sup> for chol-PEG<sub>200</sub>-RGD, cholesterol, and MKC, respectively) in the aqueous media containing low amounts of DMSO and EtOH (3% and 7% v/v, respectively) were obtained and stored at 4 °C until characterization.

**4.4. Liposome (LP and LP-GLA) Preparation.** Liposomes (LP) were prepared following the described procedure<sup>16</sup> with slight modifications. Briefly, chol-PEG<sub>200</sub>-RGD was dissolved in DMSO before adding dropwise an ethanolic solution of cholesterol and DPPC, obtaining a solution with DMSO and EtOH in a 1:5 volume ratio. The mixture was loaded into a 25 mL high-pressure vessel and volumetrically expanded with compressed CO<sub>2</sub> to reach a working pressure of 10 MPa. The system was kept at 308 K and 10 MPa for approximately 15 min to achieve a complete homogenization and thermal equilibration. For GLA-loaded liposomes (LP-GLA<sub>20</sub>), GLA was diluted in water for injection (type I) to reach the desired final enzyme concentration (20  $\mu$ g mL<sup>-1</sup>). To form the nanovesicles, the expanded organic phase was depressurized over the aqueous solution at room temperature. The next steps followed the same order as for quatsome preparation. Dispersions of nanovesicles in a total concentration of 1.5 mg mL<sup>-1</sup> (detailed final molar concentrations of the components were 0.10, 0.91, and 1.45  $\mu$ mol mL<sup>-1</sup> for chol-PEG<sub>200</sub>-RGD, cholesterol, and DPPC, respectively) in an aqueous media containing low amounts of DMSO and EtOH (0.8% and 4% v/v, respectively) were obtained and stored at 4 °C until characterization.

**4.5. Hybrid Liposome (HLP and HLP-GLA) Preparation.** For the preparation of hybrid liposomes, a similar preparative route to that for liposomes was used. MKC (0.4, 2.2, or 4.3 mol % of the total moles of membrane components) was incorporated to the ethanolic solution before loading into the reactor. Next steps followed the same order as for liposomes preparation, obtaining (0.4%MKC)-HLP, (2.2%MKC)-HLP, and (4.3%MKC)-HLP systems. For GLA-loaded hybrid liposomes, as it was described previously, GLA was diluted in water for injection (type I) to reach the final enzyme concentrations: 20  $\mu$ g mL<sup>-1</sup> for (0.4%MKC)-HLP-GLA<sub>20</sub>, (2.2%MKC)-HLP-GLA<sub>20</sub>, and (4.3%MKC)-HLP-GLA<sub>20</sub> and 8.5  $\mu$ g mL<sup>-1</sup> for (2.2%MKC)-HLP-GLA<sub>8.5</sub>. Hybrid liposomes in a total lipid concentration of 1.5 mg mL<sup>-1</sup> (detailed final molar concentrations of the components were 0.10, 0.91, and 1.45  $\mu$ mol mL<sup>-1</sup> for chol-PEG<sub>200</sub>-RGD, cholesterol, and DPPC, respectively, and 0.01, 0.06, or 0.11  $\mu$ mol mL<sup>-1</sup> MKC for (0.4%MKC)-HLP, (2.2%MKC)-HLP, or (4.3%MKC)-HLP, respectively) in an aqueous media containing low amounts of DMSO and EtOH (0.8% and 4% v/v, respectively) were obtained and stored at 4 °C until characterization.

**4.6. Diafiltration and Concentration.** The nonconjugated GLA enzyme was separated from the GLA-loaded liposomes using the KrosFlo Research Iii TFF diafiltration system (KR2i) following the procedure already described by Cabrera et al.<sup>16</sup> with slight

modifications (detailed in Section 2, Supporting Information). Briefly, to separate the free GLA ( $\approx 100$  kDa), a 300 kDa cut-off mPES hollow fiber column was used. For each GLA-containing formulation, 10 mL of the nanovesicle dispersion was submitted to six cycles of diafiltration with cold pure water for injection (type I) (60 mL), resulting in the elimination of nonincorporated GLA and the organic solvents from the dispersion.

To reach the dose for in vivo testing, the (2.2%MKC)-HLP hybrid-liposome system was concentrated using the KrosFlo Research Ili TFF diafiltration system (KR2i) with a 300 kDa cut-off mPES filter column. An initial volume of 74 mL was submitted to a concentration factor of  $\times 12$ , resulting in 6 mL of the final nanoformulation. Three independent batches were produced following the same procedure to ensure the administration of a fresh formulation throughout the in vivo study, with no significant difference in physicochemical properties (see the Supporting Information).

**4.7. Size, Polydispersity Index, and  $\zeta$ -Potential Characterization.** The size, polydispersity index (PDI), and  $\zeta$ -potential of all the vesicles produced were measured using a dynamic light scattering (DLS) and electrophoretic light scattering (ELS) analyzer combined with noninvasive backscatter technology (NIBS) (Malvern Zetasizer Nano ZS, Malvern Instruments, U.K.). The samples (1 mL) were analyzed without any previous modification or dilution. All reported values were the average result of three consecutive measurements at 20 °C on the same sample using Zetasizer software, the day after production. Size data were based on intensity size distribution and corresponded to  $z$ -average  $\pm$  standard deviation between the three measurements.

**4.8. Morphology Characterization by Cryo-TEM.** Nanoformulations were examined by cryo-TEM to directly analyze vesicle morphology and learn on their uniformity (heterogeneity) and coexistence of structures. Information about size, shape, number of bilayers, and bilayer distribution was gathered. Vitriified specimens were prepared after a few days of nanoformulation production and two to three times in the following month to learn about the short-term stability. Nanoformulations were stored at 4 °C until cryo-TEM analysis. For that, they were equilibrated for 30 min at 25 °C, then vitriified from this temperature in a controlled specimen preparation chamber following well-established procedures,<sup>52</sup> and examined in T12 G2 Tecnai (FEI) and Talos F200C (Thermo Fisher) microscopes at cryogenic temperatures. Perforated Ted Pella grids were used; vitriified specimens' temperature was always kept below  $-170$  °C. Images were recorded with a Gatan UltraScan 2k  $\times$  2k CCD camera or a Ceta camera at low dose operation, as previously described.<sup>52</sup> Images were recorded at various magnifications (from 8.8 K to 53 K) to properly capture all structures, namely, at different length scales, ranging from a few nanometers to a few hundreds. No image processing was applied except for background subtraction. All measurements were performed at the CryoEM Laboratory of Soft Matter at the Technion (Israel Institute of Technology, Israel).

**4.9. Morphology Characterization of Liposomes Using Small-Angle X-ray Scattering (SAXS).** Quantitative information about the liposomes' bilayer thickness and profile, degree of lamellar structure, and amount of incorporated GLA was investigated with small-angle X-ray scattering (SAXS) on an optimized NanoSTAR SAXS instrument<sup>53</sup> from the Bruker AXS setup at Aarhus University and equipped with a liquid Ga metal jet X-ray source (Excillum)<sup>54</sup> and scatterless slits.<sup>55</sup> GLA in water (1 mg mL<sup>-1</sup>) and liposomes or hybrid liposomes (1.5 mg mL<sup>-1</sup>) in their dispersant medium (water or water with 4% EtOH and 0.8% DMSO v/v) were measured, the matching backgrounds were subtracted, and water was used for absolute-scale calibration. Note that prior to the measurements, the samples were checked for changes during shipment by performing DLS at Aarhus University on an ALV instrument (ALV, Langen, Germany) equipped with an ALV/CGS-8F goniometer and an ALV-6010/EPP multi-tau digital correlator.

**4.10. Nanovesicle Stability.** The stability at 4 °C of the liposomal systems was followed by measuring the size, polydispersity index (PDI), and  $\zeta$ -potential of the nanovesicles at different time points (0, 1, 7, 14,

and 31 days after production) using a DLS equipment (Malvern Zetasizer Nano ZS; Malvern Instruments) as described previously.

**4.11. Enzyme Quantification and Entrapment Efficiency.** The entrapment efficiency (EE%) was determined by comparing the amount of the enzyme encapsulated in the nanovesicles after removing the free GLA by diafiltration (named prototype Loaded, L) with the amount of initial GLA present in the raw batch obtained just after their production (named prototype Total, T); see eq 1. The GLA loading was calculated by comparing the amount of GLA loaded on liposomes after elimination of free GLA with the total amount of membrane components of the vesicles; see eq 2. Statistics were done by two-sample  $t$ -test using Minitab 17 statistical software (2013).

$$EE\% = (\text{mass GLA Loaded} / \text{mass GLA Total}) \times 100 \quad (1)$$

$$\text{GLA loading} = \text{mass GLA Loaded} / \text{mass membrane components} \quad (2)$$

To detect and quantify the recombinant enzyme concentration in each of these samples, SDS-PAGE was performed by using TGX Stain-Free FastCast acrylamide 12% gels (Bio-Rad, ref. 161-0185). This stain-free imaging technology utilizes proprietary polyacrylamide gel chemistry to make proteins fluorescent directly in the gel after a short photoactivation period, allowing immediate visualization of proteins. To visualize the fluorescence bands, a ChemiDoc Touch Imaging System (Bio-Rad) was used. GLA protein amounts were estimated by densitometry after SDS-PAGE and photoactivation, with known amounts of a control His-tagged GLA produced, purified, and quantified in-house. Samples and standards, to be quantitatively compared, were run in the same gel and processed as a data set. Densitometric analysis of the bands was performed with ImageLab software (version 5.2.1, Bio-Rad).

**4.12. In Vitro Specific Enzymatic Activity.** GLA enzymatic activity was assayed as previously described<sup>16,48</sup> using fluorometrical methods initially described by Desnick et al.<sup>56</sup> with the modifications of Mayes et al.<sup>57</sup> The protocol included the use of 4-methylumbelliferyl  $\alpha$ -D-galactopyranoside (4-MUG, M-7633 Sigma-Aldrich) as a substrate ( $2.46 \times 10^{-3}$  M) in assay buffer (0.01 M acetic acid and 0.01 M acetate, pH 4.5) at 37 °C in a water bath with agitation for 1 h. The reaction was stopped by glycine buffer (0.1 M, pH 10.4) and the released product (4-methylumbelliferone or 4-MU) was determined by fluorescence measurement ( $\lambda_{\text{exc}} = 365$  nm and  $\lambda_{\text{em}} = 450$  nm), and fluorescence measurements were transformed into 4-MU  $\mu\text{mol}$  using a regression plot and adjusted per time and protein quantity. Enzymatic activity values were normalized by GLA concentration and referred to enzymatic activity of free GLA as a reference.

**4.13. In Vitro Efficacy Assay.** The ability of GLA-loaded nanovesicles to reach the lysosomes and hydrolyze Gb3 was tested in primary cultures of mouse aortic endothelial cells (MAECs) from GLA-deficient mice (Gla<sup>tmKul1</sup>).<sup>58</sup> These cells were isolated at the In Vivo Experimentation Platform/U20 of ICTS NANBIOSIS and grown as previously described<sup>16</sup> in RPMI media supplemented with nonessential amino acids (Gibco), heparin (0.1 mg mL<sup>-1</sup>, Sigma-Aldrich), endothelial cell growth supplement (ECGS) (0.05 mg mL<sup>-1</sup>, BD), hydrocortisone (1  $\mu\text{g}$  mL<sup>-1</sup>, Sigma-Aldrich), and fetal bovine serum (10–20%, Gibco) to allow the growth of endothelial cells. Cells in passages 2–5 were seeded in 24-well plates to 60–80% of confluence and incubated with Gb3-NBD ( $0.8 \times 10^{-6}$  M, Matreya) along with the specified concentrations of tested compounds. After 48 h at 37 °C, the Gb3-NBD fluorescence signal was analyzed by flow cytometry (FacsCalibur, Beckton Dickinson) in viable cells (negative to 7-aminocincomycin D staining). The fluorescence signal in control cells (without treatment) was established as 100% and the percentage of Gb3 loss (%Gb3 loss =  $100 - \% \text{Gb3-NBD signal}$ ) was used to plot the results.

**4.14. In Vitro Toxicity.** Cell cytotoxicity was tested using 3-(4,5-dimethylthiazol-2-yl)-2,5-diphenyltetrazolium bromide (MTT) on HeLa cells.<sup>59,60</sup> Briefly, 2000 cells were seeded in 96-well plates, let to adhere, and then exposed to different doses of the nanovesicles for 72 h. Then, an MTT solution (5 mg mL<sup>-1</sup>) in PBS was added to the wells and incubated during 4 additional hours. Formazan crystals resulted

from the MTT reduction by active mitochondria were dissolved with DMSO and spectrophotometrically measured at 590 nm (Biotek ELx800 Absorbance Microplate Reader, Izasa Scientific). The data are expressed as the percentages of viable cells compared to the cell survival of a nontreated control group.

**4.15. In Vitro Hemocompatibility.** Two types of assays were performed to test the hemocompatibility of the nanosystems. On the one hand, their effect on the integrity of red blood cells was measured using a hemolysis test.<sup>48</sup> On the other hand, their potential interference with blood coagulation was studied by analyzing the plasma coagulation times.

In detail, for the hemolysis test, mouse red blood cells (RBCs) were isolated from three wild-type C57BL/6 mice, resuspended in 2% (v/v) of PBS, and exposed to different concentrations of test compounds during 1 h at 37 °C in duplicates. The amount of released hemoglobin was measured in a spectrophotometer at 405 nm (Biotek ELx800) after centrifugation (1000g, 10 min). Absorbance values were referred to a positive control of 100% hemolysis obtained after incubating RBCs with 1% of Triton-X. Samples with <5% hemolysis are considered nonhemolytic.

The effect of the nanovesicles in plasma coagulation was tested as previously reported<sup>61</sup> using the Start4 equipment (Stago, France) and following the manufacturer's protocol to determine the activated partial thromboplastin time (APTT), the prothrombin time (PT), and the thrombin time (TT). Values were compared to the normal reference time ranges. The APTT assay is used to assess the intrinsic pathway, while the prothrombin time (PT) assay is a measure of the extrinsic pathway. Extrinsic and intrinsic pathways converge into the common pathway. Thrombin time (TT) is an indicator of the functionality of the final common pathway.

**4.16. In Vivo Toxicity.** To test the feasibility of repeated administration of MKC-containing nanovesicles, the effect of eight intravenous (i.v.) administrations of hybrid liposomes at three different doses (0.37, 1.22, and 3.67 mg of lipid per administration) was tested in wild-type C57BL/6 female mice (22–38 g) obtained from our GLA transgenic colony maintained in heterozygosity (Gla<sup>tmKull1</sup>).<sup>58</sup> Animal care was handled in accordance with the Guide for the Care and Use of Laboratory Animals of the Vall d'Hebron University Hospital Animal Facility and followed the EU Directive 2010/63/EU for animal experiments. Precise experimental procedures were approved by the Animal Experimentation Ethical Committee at the institution and the regional government (ref. 9572).

All studies using animals or samples derived from animals, including MAEC-obtaining and hemocompatibility assays, were performed by the ICTS NANBIOSIS at the CIBER-BBN's In Vivo Experimental Platform of the Functional Validation & Preclinical Research (FVPR) area (<http://www.nanbiosis.es/portfolio/u20-in-vivo-experimental-platform/>) (Barcelona, Spain).

**4.17. Statistical Analysis.** All results are expressed as the mean ± standard deviation (SD) of several experimental replicates, with individual or several batches as detailed in each table and figure legend. ANOVA tests, Kruskal–Wallis tests, Student's *t*-tests, or equivalent nonparametric tests were used to investigate the differences between different formulations using Prism 6.02 software (GraphPad Software, Inc., CA, USA). Statistical differences were accepted as significant ( $*p \leq 0.05$ ), very significant ( $**p \leq 0.01$ ), or highly significant ( $***p \leq 0.001$ ) according to the obtained *p*-value.

## ■ ASSOCIATED CONTENT

### SI Supporting Information

The Supporting Information is available free of charge at <https://pubs.acs.org/doi/10.1021/acsami.0c16871>.

Equipment configuration and DELOS-SUSP methodology; separation of free GLA by diafiltration; concentration of the sample for in vivo testing; stability of the sample in human serum; composition of nanovesicles; theoretical number of GLA per vesicle; morphology of liposomes using SAXS; enzymatic activity assay con-

ditions; in vitro cell viability in endothelial HMEC-1; plasma coagulation times (PDF)

## ■ AUTHOR INFORMATION

### Corresponding Authors

**Elisabet González-Mira** – Institut de Ciència de Materials de Barcelona, ICMAB-CSIC, 08193 Bellaterra, Spain; Centro de Investigación Biomédica en Red–Bioingeniería, Biomateriales y Nanomedicina (CIBER-BBN), 28029 Madrid, Spain; [orcid.org/0000-0003-2502-225X](https://orcid.org/0000-0003-2502-225X); Phone: +34 935 801 853; Email: [egonzalez@icmab.es](mailto:egonzalez@icmab.es); Fax: 34 935 805 729

**Ibane Abasolo** – Centro de Investigación Biomédica en Red–Bioingeniería, Biomateriales y Nanomedicina (CIBER-BBN), 28029 Madrid, Spain; Drug Delivery and Targeting, and Functional Validation and Preclinical Research (FVPR), CIBBIM-Nanomedicine, Vall d'Hebron Institut de Recerca (VHIR), Universitat Autònoma de Barcelona, 08035 Barcelona, Spain; [orcid.org/0000-0001-5970-6276](https://orcid.org/0000-0001-5970-6276); Phone: + 34 934 893 000; Email: [ibane.abasolo@vhir.org](mailto:ibane.abasolo@vhir.org); Fax: +34 932 746 708

**Nora Ventosa** – Institut de Ciència de Materials de Barcelona, ICMAB-CSIC, 08193 Bellaterra, Spain; Centro de Investigación Biomédica en Red–Bioingeniería, Biomateriales y Nanomedicina (CIBER-BBN), 28029 Madrid, Spain; [orcid.org/0000-0002-8008-4974](https://orcid.org/0000-0002-8008-4974); Phone: +34 935 801 853; Email: [ventosa@icmab.es](mailto:ventosa@icmab.es); Fax: 34 935 805 729

### Authors

**Judit Tomsen-Melero** – Institut de Ciència de Materials de Barcelona, ICMAB-CSIC, 08193 Bellaterra, Spain; Nanomol Technologies SL, 08193 Bellaterra, Spain; Centro de Investigación Biomédica en Red–Bioingeniería, Biomateriales y Nanomedicina (CIBER-BBN), 28029 Madrid, Spain; [orcid.org/0000-0002-2837-8107](https://orcid.org/0000-0002-2837-8107)

**Solène Passemard** – Institut de Ciència de Materials de Barcelona, ICMAB-CSIC, 08193 Bellaterra, Spain; Centro de Investigación Biomédica en Red–Bioingeniería, Biomateriales y Nanomedicina (CIBER-BBN), 28029 Madrid, Spain

**Natalia García-Aranda** – Centro de Investigación Biomédica en Red–Bioingeniería, Biomateriales y Nanomedicina (CIBER-BBN), 28029 Madrid, Spain; Drug Delivery and Targeting, and Functional Validation and Preclinical Research (FVPR), CIBBIM-Nanomedicine, Vall d'Hebron Institut de Recerca (VHIR), Universitat Autònoma de Barcelona, 08035 Barcelona, Spain

**Zamira Vanessa Díaz-Riascos** – Centro de Investigación Biomédica en Red–Bioingeniería, Biomateriales y Nanomedicina (CIBER-BBN), 28029 Madrid, Spain; Drug Delivery and Targeting, and Functional Validation and Preclinical Research (FVPR), CIBBIM-Nanomedicine, Vall d'Hebron Institut de Recerca (VHIR), Universitat Autònoma de Barcelona, 08035 Barcelona, Spain

**Ramon González-Rioja** – Institut de Ciència de Materials de Barcelona, ICMAB-CSIC, 08193 Bellaterra, Spain; Centro de Investigación Biomédica en Red–Bioingeniería, Biomateriales y Nanomedicina (CIBER-BBN), 28029 Madrid, Spain; [orcid.org/0000-0002-3699-9691](https://orcid.org/0000-0002-3699-9691)

**Jannik Nedergaard Pedersen** – Interdisciplinary Nanoscience Center (iNANO) and Department of Chemistry, Aarhus University, DK-8000 Aarhus C, Denmark; [orcid.org/0000-0003-1416-5626](https://orcid.org/0000-0003-1416-5626)

**Jeppe Lyngso** – Interdisciplinary Nanoscience Center (iNANO) and Department of Chemistry, Aarhus University,

DK-8000 Aarhus C, Denmark; [orcid.org/0000-0002-6301-1300](https://orcid.org/0000-0002-6301-1300)

**Josep Merlo-Mas** – Nanomol Technologies SL, 08193

Bellaterra, Spain; [orcid.org/0000-0002-3698-6655](https://orcid.org/0000-0002-3698-6655)

**Edgar Cristóbal-Lecina** – Centro de Investigación Biomédica en Red–Bioingeniería, Biomateriales y Nanomedicina (CIBER-BBN), 28029 Madrid, Spain; Institut de Química Avançada de Catalunya (IQAC-CSIC), 08034 Barcelona, Spain;

[orcid.org/0000-0003-3270-9340](https://orcid.org/0000-0003-3270-9340)

**José Luis Corchero** – Centro de Investigación Biomédica en Red–Bioingeniería, Biomateriales y Nanomedicina (CIBER-BBN), 28029 Madrid, Spain; Departament de Genètica i de Microbiologia, Institut de Biotecnologia i de Biomedicina (IBB), Universitat Autònoma de Barcelona, 08193 Bellaterra, Spain; [orcid.org/0000-0002-6109-144X](https://orcid.org/0000-0002-6109-144X)

**Daniel Pulido** – Centro de Investigación Biomédica en Red–Bioingeniería, Biomateriales y Nanomedicina (CIBER-BBN), 28029 Madrid, Spain; Institut de Química Avançada de Catalunya (IQAC-CSIC), 08034 Barcelona, Spain;

[orcid.org/0000-0002-2841-194X](https://orcid.org/0000-0002-2841-194X)

**Patricia Cámara-Sánchez** – Centro de Investigación Biomédica en Red–Bioingeniería, Biomateriales y Nanomedicina (CIBER-BBN), 28029 Madrid, Spain; Drug Delivery and Targeting, and Functional Validation and Preclinical Research (FVPR), CIBBIM-Nanomedicine, Vall d'Hebron Institut de Recerca (VHIR), Universitat Autònoma de Barcelona, 08035 Barcelona, Spain; [orcid.org/0000-0003-1958-9735](https://orcid.org/0000-0003-1958-9735)

**Irina Portnaya** – CryoEM Laboratory of Soft Matter, Faculty of Biotechnology and Food Engineering, Technion-Israel Institute of Technology, 32000 Haifa, Israel

**Inbal Ionita** – CryoEM Laboratory of Soft Matter, Faculty of Biotechnology and Food Engineering, Technion-Israel Institute of Technology, 32000 Haifa, Israel

**Simó Schwartz, Jr.** – Centro de Investigación Biomédica en Red–Bioingeniería, Biomateriales y Nanomedicina (CIBER-BBN), 28029 Madrid, Spain; Drug Delivery and Targeting, CIBBIM-Nanomedicine, Vall d'Hebron Institut de Recerca (VHIR), Universitat Autònoma de Barcelona, 08035 Barcelona, Spain; [orcid.org/0000-0001-8297-7971](https://orcid.org/0000-0001-8297-7971)

**Jaume Veciana** – Institut de Ciència de Materials de Barcelona, ICMAB-CSIC, 08193 Bellaterra, Spain; Centro de Investigación Biomédica en Red–Bioingeniería, Biomateriales y Nanomedicina (CIBER-BBN), 28029 Madrid, Spain;

[orcid.org/0000-0003-1023-9923](https://orcid.org/0000-0003-1023-9923)

**Santi Sala** – Nanomol Technologies SL, 08193 Bellaterra, Spain

**Miriam Royo** – Centro de Investigación Biomédica en Red–Bioingeniería, Biomateriales y Nanomedicina (CIBER-BBN), 28029 Madrid, Spain; Institut de Química Avançada de Catalunya (IQAC-CSIC), 08034 Barcelona, Spain;

[orcid.org/0000-0001-5292-0819](https://orcid.org/0000-0001-5292-0819)

**Alba Córdoba** – Nanomol Technologies SL, 08193 Bellaterra, Spain; [orcid.org/0000-0002-2726-5119](https://orcid.org/0000-0002-2726-5119)

**Dganit Danino** – CryoEM Laboratory of Soft Matter, Faculty of Biotechnology and Food Engineering, Technion-Israel Institute of Technology, 32000 Haifa, Israel; Faculty of Biotechnology and Food Engineering, Guangdong Technion-Israel Institute of Technology, Shantou 515063, Guangdong Province, China

**Jan Skov Pedersen** – Interdisciplinary Nanoscience Center (iNANO) and Department of Chemistry, Aarhus University, DK-8000 Aarhus C, Denmark; [orcid.org/0000-0002-7768-0206](https://orcid.org/0000-0002-7768-0206)

Complete contact information is available at:

<https://pubs.acs.org/10.1021/acsami.0c16871>

## Author Contributions

J.T.-M. and S.P. were involved in the work design, production and characterization, acquisition, data analysis and interpretation, and writing of the original draft. R.G.-R. carried out the production and data interpretation. E.G.-M., N.V., and J.V. performed the work conception, data analysis and writing and review of the manuscript, project administration, and funding acquisition. N.G.-A. carried out the enzymatic activity assays and data processing and curation. P.C.-S. conducted the in vitro toxicity assays and data processing and curation. Z.V.D.-R. obtained the primary cells and blood samples for in vitro assays, in vivo assays, and data processing and curation. I.A. and S.S.Jr. carried out the data analysis, data curation, writing, review, and editing of the manuscript, project administration, and funding acquisition. J.N.P., J.L., and J.S.P. were involved in the SAXS measurements and methodology development, data analysis, and writing, review, and editing of the manuscript. I.I. conducted the cryo-TEM methodology development, imaging, and data analysis. I.P. performed the physicochemical characterization and data analysis. D.D. carried out the physicochemical and cryo-TEM analysis supervision and writing, review, and editing of the manuscript. J.M.-M. provided the 25 mL DELOS-SUSP equipment design and setup and was involved in the production and physicochemical characterization, data analysis and interpretation, and writing, review, and editing of the manuscript. S.S. carried out the funding acquisition, project administration, and experimental activity supervision. A.C. provided the work design and conducted the data interpretation, project administration, experimental activity supervision, and writing, review, and editing of the manuscript. E.C.-L. performed the highly pure chol-PEG<sub>200</sub>-RGD synthesis and characterization. D.P. conducted the chol-PEG<sub>200</sub>-RGD method of synthesis development. M.R. was involved in the chol-PEG<sub>200</sub>-RGD synthesis supervision and writing, review, and editing of the manuscript. J.L.C. conducted the enzyme quantification and writing, review, and editing of the manuscript. All authors have given approval to the final version of the manuscript.

## Funding

This work was supported by the financial support from European Commission through the H2020 program (Smart-4-Fabry project, ID 720942). The Networking Research Centre on Bioengineering, Biomaterials, and Nanomedicine (CIBER-BBN) is financed by the Instituto de Salud Carlos III (ISCIII) with assistance from the European Regional Development Fund (ERDF). This work was also financed by the Ministerio de Ciencia e Innovación (PID2019-105622RB-I00). The work was also partially funded by ISCIII (PI18\_00871 cofounded by ERDF) and CIBER-BBN (EXPLORE) granted to I.A. We also acknowledge the ICTS “NANBIOSIS”, more specifically, the support from the Protein Production Platform of CIBER-BBN/IBB, at the UAB SepBioES scientific-technical service (<https://www.nanbiosis.es/portfolio/u1-protein-production-platform-ppp/>), the Soft Materials Service linked to Biomaterial Processing and Nanostructuring Unit (U6) at ICMAB-CSIC ([www.nanbiosis.es/portfolio/u6-biomaterial-processing-and-nanostructuring-unit/](http://www.nanbiosis.es/portfolio/u6-biomaterial-processing-and-nanostructuring-unit/)), the Synthesis of Peptide Unit (U3) at the IQAC-CSIC ([www.nanbiosis.es/portfolio/u3-synthesis-of-peptides-unit/](http://www.nanbiosis.es/portfolio/u3-synthesis-of-peptides-unit/)), and the In Vivo Experimental Platform of the Functional Validation & Preclinical Research (FVPR) area (<http://www.nanbiosis.es/portfolio/u20-in-vivo-experimental-platform/>). We also thank the denomination of the consolidated



group from Generalitat de Catalunya: 2017-SGR-1439 (M.R.) and 2017-SGR-918 (J.V.). J.T.-M. thanks the financial support by the FI-AGAUR grant by the Generalitat de Catalunya, especially the Secretary of Universities and Research of the Department of Business and Knowledge of the Generalitat de Catalunya and the European Social Fund (ESF—Investing in your future) of the European Union. This work has been done in the framework of the J.T.-M. doctorate in Materials Science of the Universitat Autònoma de Barcelona. N.G.-A. is supported by a PERIS grant from the Catalan Government (SLT006/17/270). Authors acknowledge financial support from the Agencia Estatal de Investigación-Ministerio de Ciencia e Innovación through the “Severo Ochoa” Programme for Centres of Excellence in R&D (CEX2019-000917-S).

## Notes

The authors declare the following competing financial interest(s): The following authors declare the following financial interests/personal relationships which may be considered as potential competing interests: Jos Luis Corchero, Daniel Pulido, Sim Schwartz Jr., Miriam Royo, Ibane Abasolo, Jaume Veciana, Santi Sala, and Nora Ventosa: Inventor of patent WO/2014/001509 licensed to Biopraxis Resarch AIE. Jaume Veciana, Santi Sala, and Nora Ventosa: Inventor of patent WO/2006/079889 owned by Nanomol Technologies SL, and stock-owner ship in Nanomol Technologies SL.

## ACKNOWLEDGMENTS

We are thankful to Sandra Mancilla-Zamora and Ana M. Boullosa for their technical support on the in vitro cell-based assays and in vivo animal handling. We are thankful to Aida Carreño for her help with the enzymatic activity assays. We thank Ellina Kesselman, Mingming Zhang, and Luba Kolik for the technical support with cryo-TEM and Carsten Pedersen, from Aarhus University, for helping with DLS measurements.

## REFERENCES

- (1) Kornfeld, S.; Mellman, I. The Biogenesis of Lysosomes. *Annu. Rev. Cell Biol.* **1989**, *5*, 483–525.
- (2) Beck, M. New Therapeutic Options for Lysosomal Storage Disorders: Enzyme Replacement, Small Molecules and gene Therapy. *Hum. Genet.* **2007**, *121*, 1–22.
- (3) Coutinho, M. F.; Prata, M. J.; Alves, S. Mannose-6-phosphate Pathway: A Review on its Role in Lysosomal Function and Dysfunction. *Mol. Genet. Metab.* **2012**, *105*, 542–550.
- (4) Ioannou, Y. A.; Zeidner, K. M.; Grace, M. E.; Desnick, R. J. Human  $\alpha$ -Galactosidase A: Glycosylation Site 3 is Essential for Enzyme Solubility. *Biochem. J.* **1998**, *332*, 789–797.
- (5) Zarate, Y. A.; Hopkin, R. J. Fabry's Disease. *Lancet* **2008**, *372*, 1427–1435.
- (6) Anastasakis, A.; Papatheodorou, E.; Steriotis, A. Fabry Disease and Cardiovascular Involvement. *Curr. Pharm. Des.* **2013**, *19*, 5997–6008.
- (7) Alipourfetrati, S.; Saeed, A.; Norris, J. M.; Sheckley, F.; Rastogi, A. A Review of Current and Future Treatment Strategies for Fabry Disease: A Model for Treating Lysosomal Storage Diseases. *J Pharmacol Clin. Toxicol* **2015**, *3*, 1051.
- (8) Solomon, M.; Muro, S. Lysosomal Enzyme Replacement Therapies: Historical Development, Clinical Outcomes, and Future Perspectives. *Adv. Drug Delivery Rev.* **2017**, *118*, 109–134.
- (9) Ferverza, F. C.; Torra, R.; Warnock, D. G. Safety and Efficacy of Enzyme Replacement Therapy in the Nephropathy of Fabry Disease. *Biol.: Targets Ther.* **2008**, *2*, 823–843.
- (10) Siatskas, C.; Medin, J. A. Gene Therapy for Fabry Disease. *J. Inherited Metab. Dis.* **2001**, *24*, 25–41.
- (11) Ibraheem, D.; Elaissari, A.; Fessi, H. Administration Strategies for Proteins and Peptides. *Int. J. Pharm.* **2014**, *477*, 578–589.
- (12) Bosio, V. E.; Islan, G. A.; Martínez, Y. N.; Durán, N.; Castro, G. R. Nanodevices for the Immobilization of Therapeutic Enzymes. *Crit. Rev. Biotechnol.* **2016**, *36*, 447–464.
- (13) Schiffmann, R.; Goker-Alpan, O.; Holida, M.; Giraldo, P.; Barisoni, L.; Colvin, R. B.; Jennette, C. J.; Maegawa, G.; Boyadjiev, S. A.; Gonzalez, D.; Nicholls, K.; Tuffaha, A.; Atta, M. G.; Rup, B.; Charney, M. R.; Paz, A.; Szlaifer, M.; Alon, S.; Brill-Almon, E.; Chertkoof, R.; Hughes, D. Pegunigalsidase Alfa, a Novel PEGylated Enzyme Replacement Therapy for Fabry Disease, Provides Sustained Plasma Concentrations and Favorable Pharmacodynamics: A 1-year Phase 1/2 Clinical Trial. *J. Inherited Metab. Dis.* **2019**, *42*, 534–544.
- (14) Torchilin, V. P. Recent Advances with Liposomes as Pharmaceutical Carriers. *Nat. Rev. Drug Discovery* **2005**, *4*, 145–160.
- (15) Bulbake, U.; Doppalapudi, S.; Kommineni, N.; Khan, W. Liposomal Formulations in Clinical Use: An Updated Review. *Pharmaceutics* **2017**, *9*, 12.
- (16) Cabrera, I.; Abasolo, I.; Corchero, J. L.; Elizondo, E.; Gil, P. R.; Moreno, E.; Farauo, J.; Sala, S.; Bueno, D.; González-Mira, E.; Rivas, M.; Melgarejo, M.; Pulido, D.; Albericio, F.; Royo, M.; Villaverde, A.; García-Parajo, M. F.; Schwartz, S., Jr.; Ventosa, N.; Veciana, J.  $\alpha$ -Galactosidase-A Loaded-Nanoliposomes with Enhanced Enzymatic Activity and Intracellular Penetration. *Adv. Healthcare Mater.* **2016**, *5*, 829–840.
- (17) Ventosa Rull, L.; Veciana Miró, J.; Cabrera Puig, I.; Elizondo Saez De Vicuña, E.; Melgarejo Diaz, M.; Royo Expósito, M.; Albericio Palomera, F.; Pulido Martinez, D.; Sala Vergés, S.; Corchero Nieto, J. L.; Schwartz Navarro, S.; Abasolo Olaortua, I.; Villaverde Corrales, A. P. & (BioPraxis Research Institute S.A.). Functionalised Liposomes Useful for the Release of Bioactive Compounds. WO2014/001509, 2012.
- (18) Cabrera, I.; Elizondo, E.; Esteban, O.; Corchero, J. L.; Melgarejo, M.; Pulido, D.; Córdoba, A.; Moreno, E.; Unzueta, U.; Vazquez, E.; Abasolo, I.; Schwartz, S., Jr.; Villaverde, A.; Albericio, F.; Royo, M.; García-Parajo, M. F.; Ventosa, N.; Veciana, J. Multifunctional Nanovesicle-Bioactive Conjugates Prepared by a One-Step Scalable Method Using CO<sub>2</sub>-Expanded Solvents. *Nano Lett.* **2013**, *13*, 3766–3774.
- (19) Sajid, M.; Stouffer, G. A. The Role of  $\alpha_v\beta_3$  Integrins in Vascular Healing. *Thromb. Haemostasis* **2002**, *87*, 187–193.
- (20) Utsumi, K.; Sakuraba, H.; Iino, Y.; Katayama, Y. Urinary Excretion of the Vitronectin Receptor (integrin  $\alpha_v\beta_3$ ) in Patients with Fabry Disease. *Clin. Chim. Acta* **1999**, *3*, 41–45.
- (21) Temming, K.; Schifferers, R. M.; Molema, G.; Kok, R. J. RGD-based Strategies for Selective Delivery of Therapeutics and Imaging Agents to the Tumour Vasculature. *Drug Resist. Updates* **2005**, *8*, 381–402.
- (22) Porfire, A.; Achim, M.; Barbalata, C.; Rus, I.; Tomuta, I.; Cristea, C. Pharmaceutical Development of Liposomes Using the QbD Approach. *Liposomes - Adv. Perspect.* **2019**, 1–20.
- (23) Dobrovolskaia, M. A.; Aggarwal, P.; Hall, J. B.; McNeil, S. E. Preclinical Studies To Understand Nanoparticle Interaction with the Immune System and Its Potential Effects on Nanoparticle Biodistribution. *Mol. Pharmaceutics* **2008**, *5*, 487–495.
- (24) Szebeni, J. Complement Activation-related Pseudoallergy: A New Class of Drug-Induced Acute Immune Toxicity. *Toxicology* **2005**, *216*, 106–121.
- (25) Barenholz, Y. Doxil® - The First FDA-approved Nano-drug: Lessons Learned. *J. Controlled Release* **2012**, *160*, 117–134.
- (26) Szebeni, J.; Bedőcs, P.; Rozsnyay, Z.; Weiszhar, Z.; Urbanics, R.; Rosivall, L.; Cohen, R.; Garbuzenko, O.; Báthori, G.; Tóth, M.; Bünger, R.; Barenholz, Y. Liposome-induced Complement Activation and Related Cardiopulmonary Distress in Pigs: Factors Promoting Reactogenicity of Doxil and AmBisome. *Nanomed. Nanotechnol. Biol. Med.* **2012**, *8*, 176–184.
- (27) Colletier, J.-P.; Chaize, B.; Winterhalter, M.; Fournier, D. Protein Encapsulation in Liposomes: Efficiency Depends on Interactions Between Protein and Phospholipid Bilayer. *BMC Biotechnol.* **2002**, *2*, 9.
- (28) Shimizu, T.; Mori, T.; Tomita, M.; Tsumoto, K. pH Switching That Crosses over the Isoelectric Point (pI) Can Improve the

Entrapment of Proteins within Giant Liposomes by Enhancing Protein–Membrane Interaction. *Langmuir* **2014**, *30*, 554–563.

(29) Hwang, S. Y.; Kim, H. K.; Choo, J.; Seong, G. H.; Hien, T. B. D.; Lee, E. K. Effects of Operating Parameters on the Efficiency of Liposomal Encapsulation of Enzymes. *Colloids Surf., B* **2012**, *94*, 296–303.

(30) Garman, S. C.; Garboczi, D. N. The Molecular Defect Leading to Fabry Disease: Structure of Human  $\alpha$ -Galactosidase. *J. Mol. Biol.* **2004**, *337*, 319–335.

(31) Ferrer-Tasies, L.; Moreno-Calvo, E.; Cano-Sarabia, M.; Aguilera-Arzo, M.; Angelova, A.; Lesieur, S.; Ricart, S.; Faraudo, J.; Ventosa, N.; Veciana, J. Quatsomes: Vesicles Formed by Self-Assembly of Sterols and Quaternary Ammonium Surfactants. *Langmuir* **2013**, *29*, 6519–6528.

(32) Grimaldi, N.; Andrade, F.; Segovia, N.; Ferrer-Tasies, L.; Sala, S.; Veciana, J.; Ventosa, N. Lipid-based Nanovesicles for Nanomedicine. *Chem. Soc. Rev.* **2016**, *45*, 6520–6545.

(33) Elizondo, E.; Veciana, J.; Ventosa, N. Nanostructuring Molecular Materials as Particles and Vesicles for Drug Delivery, Using Compressed and Supercritical Fluids. *Nanomedicine* **2012**, *7*, 1391–1408.

(34) Ventosa, N.; Veciana, J.; Sala, S.; Cano, M. & (Nanomol Technologies SL). Procedure for the Obtainment of Micro- and Nano-disperse Systems. WO2006/079889, 2005.

(35) Eaton, M. A. W. Improving the Translation in Europe of Nanomedicines (a.k.a. Drug Delivery) from Academia to Industry. *J. Controlled Release* **2012**, *164*, 370–371.

(36) European Medicines Agency. Benzalkonium Chloride Used as an Excipient. *Comm. Hum. Med. Prod. EMA/CHMP/495737/2013* (2017).

(37) Pramanick, S.; Singoidia, D.; Chandel, V. Excipient Selection In Parenteral Formulation Development. *PharmaTimes* **2013**, *45*, 65–77.

(38) Vargas-Nadal, G.; Muñoz-Úbeda, M.; Álamo, P.; Mitjans, M.; Céspedes, V.; Köber, M.; Gonzalez, E.; Ferrer-Tasies, L.; Vinardell, M. P.; Mangués, R.; Veciana, J.; Ventosa, N. MKC-Quatsomes: a Stable Nanovesicle Platform for Bio-imaging and Drug-Delivery Applications. *Nanomed. Nanotechnol. Biol. Med.* **2020**, *24*, 102136.

(39) Moore, T. L.; Rodriguez-Lorenzo, L.; Hirsch, V.; Balog, S.; Urban, D.; Jud, C.; Rothen-Rutishauser, B.; Lattuada, M.; Petri-Fink, A. Nanoparticle Colloidal Stability in Cell Culture Media and Impact on Cellular Interactions. *Chem. Soc. Rev.* **2015**, *44*, 6287–6305.

(40) Steiner, E. M.; Lyngsø, J.; Guy, J. E.; Bourenkov, G.; Lindqvist, Y.; Schneider, T. R.; Pedersen, J. S.; Schneider, G.; Schnell, R. The Structure of the N-terminal Module of the Cell Wall Hydrolase RipA and its Role in Regulating Catalytic Activity. *Proteins: Struct., Funct., Bioinf.* **2018**, *86*, 912–923.

(41) Hosemann, R.; Bagchi, S. N. *Direct Analysis of Diffraction by Matter*; North-Holland Publishing Company: 1963, 141.

(42) Pabst, G.; Rappolt, M.; Amenitsch, H.; Laggner, P. Structural Information from Multilamellar Liposomes at Full Hydration: Full  $q$ -range Fitting with High Quality X-ray Data. *Phys. Rev.* **2000**, *62*, 4000–4009.

(43) Pabst, G.; Koschuch, R.; Pozo-Navas, B.; Rappolt, M.; Lohner, K.; Laggner, P. Structural Analysis of Weakly Ordered Membrane Stacks. *J. Appl. Crystallogr.* **2003**, *36*, 1378–1388.

(44) Agency European Medicines, Replagal - EMEA/H/C/000369 - IAIN/0096, <https://www.ema.europa.eu/en/medicines/human/EPAR/replagal#product-information-section>, accessed November 2019.

(45) Redondo-Morata, L.; Giannotti, M. I.; Sanz, F. Influence of Cholesterol on the Phase Transition of Lipid Bilayers: A Temperature-Controlled Force Spectroscopy Study. *Langmuir* **2012**, *28*, 12851–12860.

(46) Gumí-Audenis, B.; Illa-Tuset, S.; Grimaldi, N.; Pasquina-Lemonche, L.; Ferrer-Tasies, L.; Sanz, F.; Veciana, J.; Ratera, I.; Faraudo, J.; Ventosa, N.; Giannotti, M. I. Insights into the Structure and Nanomechanics of a Quatsome Membrane by Force Spectroscopy Measurements and Molecular Simulations. *Nanoscale* **2018**, *10*, 23001–23011.

(47) Crespo-Villanueva, A.; Gumí-Audenis, B.; Sanz, F.; Artzner, F.; Mériadec, C.; Rousseau, F.; Lopez, C.; Giannotti, M. I.; Guyomarc'h, F. Casein Interaction with Lipid Membranes: Are the Phase State or Charge Density of the Phospholipids Affecting Protein Adsorption? *Biochim. Biophys. Acta - Biomembr.* **2018**, *1860*, 2588–2598.

(48) Giannotti, M. I.; Abasolo, I.; Oliva, M.; Andrade, F.; García-Aranda, N.; Melgarejo, M.; Pulido, D.; Corchero, J. L.; Fernández, Y.; Villaverde, A.; Royo, M.; García-Parajo, M. F.; Sanz, F.; Schwartz, S., Jr. Highly Versatile Polyelectrolyte Complexes for Improving the Enzyme Replacement Therapy of Lysosomal Storage Disorders. *ACS Appl. Mater. Interfaces* **2016**, *8*, 25741–25752.

(49) Abasolo, I.; Seras-Franzoso, J.; Moltó-Abad, M.; Díaz-Riascos, V.; Corchero, J. L.; Pintos-Morell, G.; Schwartz, S., Jr. Nanotechnology-based Approaches for Treating Lysosomal Storage Disorders, a Focus on Fabry Disease. *Wiley Interdiscip. Rev.: Nanomed. Nanobiotechnol.* **2020**, 1–18.

(50) Hsu, J.; Serrano, D.; Bhowmick, T.; Kumar, K.; Shen, Y.; Kuo, Y. C.; Garnacho, C.; Muro, S. Enhanced Endothelial Delivery and Biochemical Effects of  $\alpha$ -Galactosidase by ICAM-1-Targeted Nanocarriers for Fabry Disease. *J. Controlled Release* **2011**, *149*, 323–331.

(51) Cristóbal-Lecina, E.; Pulido, D.; Martín-Malpartida, P.; Macias, M. J.; Albericio, F.; Royo, M. Synthesis of Stable Cholesteryl-Polyethylene Glycol-Peptide Conjugates with Non-Disperse Polyethylene Glycol Lengths. *ACS Omega* **2020**, *5*, 5508–5519.

(52) Danino, D. Cryo-TEM of Soft Molecular Assemblies. *Curr. Opin. Colloid Interface Sci.* **2012**, *17*, 316–329.

(53) Pedersen, J. S. A Flux- and Background-Optimized Version of the NanoSTAR Small-Angle X-Ray Scattering Camera for Solution Scattering. *J. Appl. Crystallogr.* **2004**, *37*, 369–380.

(54) Schwamberger, A.; De Roo, B.; Jacob, D.; Dillemans, L.; Bruegemann, L.; Seo, J. W.; Locquet, J. P. Combining SAXS and DLS for Simultaneous Measurements and Time-Resolved Monitoring of Nanoparticle Synthesis. *Nucl. Instrum. Methods Phys. Res., Sect. B* **2015**, *343*, 116–122.

(55) Li, Y.; Beck, R.; Huang, T.; Choi, M. C.; Divinagracia, M. Scatterless Hybrid Metal-Single-Crystal Slit for Small-Angle X-Ray Scattering and High-Resolution X-ray Diffraction. *J. Appl. Crystallogr.* **2008**, *41*, 1134–1139.

(56) Desnick, R. J.; Allen, K. Y.; Desnick, S. J.; Raman, M. K.; Bernlohr, R. W.; Krivit, W. Fabry's Disease: Enzymatic Diagnosis of Hemizygotes and Heterozygotes. Alpha-galactosidase activities in plasma, serum, urine, and leukocytes. *J. Lab. Clin. Med.* **1973**, *81*, 157–171.

(57) Mayes, J. S.; Scheerer, J. B.; Sifers, R. N.; Donaldson, M. L. Differential Assay for Lysosomal Alpha-Galactosidases in Human Tissues and its Application to Fabry's Disease. *Clin. Chim. Acta* **1981**, *112*, 247–251.

(58) Ohshima, T.; Murray, G. J.; Swaim, W. D.; Longenecker, G.; Quirk, J. M.; Cardarelli, C. O.; Sugimoto, Y.; Pastan, I.; Gottesman, M. M.; Brady, R. O.; Kulkarni, A. B.  $\alpha$ -Galactosidase A deficient mice: A Model of Fabry Disease. *Proc. Natl. Acad. Sci. U. S. A.* **1997**, *94*, 2540–2544.

(59) Bomati-Miguel, O.; Miguel-Sancho, N.; Abasolo, I.; Candiota, A. P.; Roca, A. G.; Acosta, M.; Schwartz, S., Jr.; Arus, C.; Marquina, C.; Martínez, G.; Santamaria, J. Ex vivo Assessment of Polyol Coated-Iron Oxide Nanoparticles for MRI Diagnosis Applications: Toxicological and MRI Contrast Enhancement Effects. *J. Nanopart. Res.* **2014**, *16*, 1.

(60) Botella, P.; Abasolo, I.; Fernández, Y.; Muniesa, C.; Miranda, S.; Quesada, M.; Ruiz, J.; Schwartz, S., Jr.; Corma, A. Surface-modified Silica Nanoparticles for Tumor-targeted Delivery of Camptothecin and its Biological Evaluation. *J. Controlled Release* **2011**, *156*, 246–257.

(61) Rafael, D.; Martínez, F.; Andrade, F.; Seras-Franzoso, J.; García-Aranda, N.; Gener, P.; Sayós, J.; Arango, D.; Abasolo, I.; Schwartz, S., Jr. Efficient EFGR Mediated siRNA Delivery to Breast Cancer Cells by Cetuximab Functionalized Pluronic® F127/Gelatin. *Chem. Eng. J.* **2018**, *340*, 81–93.



Contents lists available at ScienceDirect

## The Journal of Supercritical Fluids

journal homepage: [www.elsevier.com/locate/supflu](http://www.elsevier.com/locate/supflu)

## Application of Quality by Design to the robust preparation of a liposomal GLA formulation by DELOS-susp method

Josep Merlo-Mas<sup>a,1</sup>, Judit Tomsen-Melero<sup>a,b,c,1</sup>, José-Luis Corchero<sup>c,d</sup>, Elisabet González-Mira<sup>b,c</sup>, Albert Font<sup>e,2</sup>, Jannik N. Pedersen<sup>f</sup>, Natalia García-Aranda<sup>c,g</sup>, Edgar Cristóbal-Lecina<sup>c,h</sup>, Marta Alcaina-Hernando<sup>a,1</sup>, Rosa Mendoza<sup>c,d</sup>, Elena Garcia-Fruitós<sup>c,d,3</sup>, Teresa Lizarraga<sup>e,2</sup>, Susanne Resch<sup>i</sup>, Christa Schimpel<sup>i</sup>, Andreas Falk<sup>i</sup>, Daniel Pulido<sup>c,h</sup>, Miriam Royo<sup>c,h</sup>, Simó Schwartz Jr.<sup>c,g</sup>, Ibane Abasolo<sup>c,g</sup>, Jan Skov Pedersen<sup>f</sup>, Dganit Danino<sup>j</sup>, Andreu Soldevila<sup>e,2</sup>, Jaume Veciana<sup>b,c</sup>, Santi Sala<sup>a,1</sup>, Nora Ventosa<sup>b,c,\*</sup>, Alba Córdoba<sup>a,\*,\*,1</sup>

<sup>a</sup> Nanomol Technologies S.L., 08193 Cerdanyola del Vallès, Spain

<sup>b</sup> Institut de Ciència de Materials de Barcelona, ICMA-B-CSIC, 08193 Bellaterra, Spain

<sup>c</sup> Centro de Investigación Biomédica en Red – Bioingeniería, Biomateriales y Nanomedicina (CIBER-BBN), 28029 Madrid, Spain

<sup>d</sup> Institut de Biotecnologia i Biomedicina (IBB-UAB), 08193 Cerdanyola del Vallès, Spain

<sup>e</sup> Leanbio S.L., 08028 Barcelona, Spain

<sup>f</sup> Department of Chemistry and Interdisciplinary Nanoscience Center (iNANO), Aarhus University, 8000, Aarhus, Aarhus C Denmark

<sup>g</sup> Functional Validation and Preclinical Research, Drug Delivery & Targeting, CIBBIM-Nanomedicina, Vall d'Hebron Institute of Research (VHIR), Universitat Autònoma de Barcelona (UAB), 08035 Barcelona, Spain

<sup>h</sup> Institut de Química Avançada de Catalunya (IQAC-CSIC), 08034 Barcelona, Spain

<sup>i</sup> BioNanoNet Forschungsgesellschaft mbH, 8010 Graz, Austria

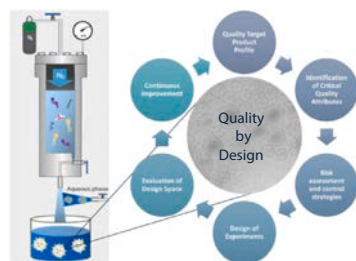
<sup>j</sup> CryoEM Laboratory of Soft Matter, Faculty of Biotechnology and Food Engineering, Technion – Israel Institute of Technology, 32000 Haifa, Israel



## HIGHLIGHTS

- Robust preparation of liposomal formulation by DELOS-susp method.
- Implementation of Quality by Design methodology to liposomes preparation.
- Influence of critical parameters on quality was studied through DoE analysis.
- Design Space was obtained for GLA-loaded liposomes formulation.

## GRAPHICAL ABSTRACT



**Abbreviations:** BCA, Bicinchoninic acid assay; Chol, Cholesterol; Chol-PEG<sub>400</sub>-RGD, Cholesterol pegylated with arginyl-glycyl-aspartic (RGD) acid peptide; CMA, Critical Material Attributes; CO<sub>2</sub>, Carbon dioxide; CoA, Certificate of Analysis; CPP, Critical Process Parameters; CQA, Critical Quality Attribute; Cryo-TEM, Cryogenic Transmission Electron Microscopy; DELOS-susp, Depressurization of an Expanded Liquid Organic Solution into aqueous solution; DLS, Dynamic Light Scattering; DMSO, Dimethyl sulfoxide; DoE, Design of Experiments; DPPC, 1,2-Dipalmitoyl-sn-glycero-3-phosphocholine; EA, Enzymatic Activity; EE, Entrapment Efficiency; EHS, Environment, Health and Safety; EMA, European Medicines Agency; ERT, Enzyme Replacement Therapy; EtOH, Ethanol; FDA, Food and Drug Administration;  $f_{\text{single}}$ , Ratio of monolayered liposomes; GLA,  $\alpha$ -galactosidase A enzyme; H<sub>2</sub>O, Water; HPLC, High Performance Liquid Chromatography; ICH, Council for Harmonisation of Technical Requirements for Pharmaceuticals for Human Use; LSD, Lysosomal storage disorders; MKC, Myristalkonium chloride; N<sub>2</sub>, Nitrogen; nanoGLA, GLA-loaded nanoliposomes; NTA, Nanoparticle Tracking Analysis; PEG, Polyethylene Glycol; PLS, Partial Least Squares; PdI, Polydispersity Index; PIC, Pressure Indicator Controller; Pw, Working pressure; QbD, Quality by Design; RGD, Arginine-Glycine-Aspartic acid; SAXS, Small-Angle X-ray Scattering; SbD, Safe by Design; SDS-PAGE, Sodium Dodecyl Sulfate Polyacrylamide Gel Electrophoresis; S-MLS, Static Multiple Light Scattering; TFF, Tangential Flow Filtration; TGX, Trys-Glycine eXtended; TIC, Temperature Indicator Controller; TSI, Turbiscan Stability Index; Tw, Working temperature; USP, United States Pharmacopeia; X<sub>CO<sub>2</sub></sub>, Carbon dioxide molar fraction

\* Corresponding author at: Institut de Ciència de Materials de Barcelona, ICMA-B-CSIC, 08193 Bellaterra, Spain.

\*\* Correspondence to: Nanomol Technologies SL, Mòdul de Recerca B, Edifici IBB, Campus de la UAB, 08193 Cerdanyola del Vallès, Spain.

E-mail addresses: [ventosa@icmab.es](mailto:ventosa@icmab.es) (N Ventosa), [acordoba@nanomol-tech.com](mailto:acordoba@nanomol-tech.com) (A Córdoba).

<sup>1</sup> ([www.nanomol-tech.com](http://www.nanomol-tech.com)).

<sup>2</sup> ([www.leanbiopro.com](http://www.leanbiopro.com)).

<sup>3</sup> Department of Ruminant Production, Institut de Recerca i Tecnologia Agroalimentàries (IRTA), 08140 Caldes de Montbui, Spain.

<https://doi.org/10.1016/j.supflu.2021.105204>

Received 26 October 2020; Received in revised form 12 February 2021; Accepted 14 February 2021

Available online 19 February 2021

0896-8446/© 2021 Published by Elsevier B.V.

## ARTICLE INFO

**Keywords:**  
Quality by Design  
DELOS  
Scale-up  
Protein-loaded liposomes  
Fabry disease  
 $\alpha$ -galactosidase

## ABSTRACT

Fabry disease is a lysosomal storage disease arising from a deficiency of the enzyme  $\alpha$ -galactosidase A (GLA). The enzyme deficiency results in an accumulation of glycolipids, which over time, leads to cardiovascular, cerebrovascular, and renal disease, ultimately leading to death in the fourth or fifth decade of life. Currently, lysosomal storage disorders are treated by enzyme replacement therapy (ERT) through the direct administration of the missing enzyme to the patients.

In view of their advantages as drug delivery systems, liposomes are increasingly being researched and utilized in the pharmaceutical, food and cosmetic industries, but one of the main barriers to market is their scalability.

Depressurization of an Expanded Liquid Organic Solution into aqueous solution (DELOS-susp) is a compressed fluid-based method that allows the reproducible and scalable production of nanovesicular systems with remarkable physicochemical characteristics, in terms of homogeneity, morphology, and particle size. The objective of this work was to optimize and reach a suitable formulation for in vivo preclinical studies by implementing a Quality by Design (QbD) approach, a methodology recommended by the FDA and the EMA to develop robust drug manufacturing and control methods, to the preparation of  $\alpha$ -galactosidase-loaded nanoliposomes (nanoGLA) for the treatment of Fabry disease.

Through a risk analysis and a Design of Experiments (DoE), we obtained the Design Space in which GLA concentration and lipid concentration were found as critical parameters for achieving a stable nanoformulation. This Design Space allowed the optimization of the process to produce a nanoformulation suitable for in vivo preclinical testing.

## 1. Introduction

One of the main challenges to produce advanced materials such as enzyme-loaded liposomes is the successful implementation of new manufacturing nanotechnologies at industrial scale. The DELOS-susp method is a compressed fluid-based technology that allows the reproducible preparation of different nanovesicular systems with remarkable physicochemical characteristics, in terms of homogeneity, morphology and particle size, as well as a high versatility to integrate different active compounds, that can lead to innovative nanomedicines with enhanced efficiency [1–3].

Lysosomal storage disorders (LSD) are diseases caused by lysosomal dysfunction usually as a consequence of deficiency of a single metabolic enzyme. In the case of Fabry disease, the lack of  $\alpha$ -galactosidase A (GLA) enzyme causes the accumulation of glycosphingolipids leading to multiple organ pathology [4]. Enzyme replacement therapy (ERT), which is the main current treatment, exhibits several drawbacks mainly related to protein instability and low efficacy [5].

To overcome the main limitations of the current ERTs (e.g. rapid enzyme degradation, high immunogenicity, short circulation half-life, poor biodistribution, and limited efficacy among others [6]) a strategy under development consists in the encapsulation of the GLA enzyme into nanoliposomes. Such encapsulation aims to protect the enzyme, decrease the degradation and immunogenicity of GLA, and increase its plasma half-life. Moreover, the addition of a targeting peptide on the liposomal membrane can facilitate cellular up-take via peptide receptors recognition and could help to improve GLA biodistribution. Thus, GLA-loaded nanoliposomes (nanoGLA) functionalized with Arginine-Glycine-Aspartic acid (RGD) peptide and prepared by DELOS-susp, have recently been reported to increase enzymatic activity and intracellular penetration, showing the great potential of this CO<sub>2</sub>-based methodology for the simple production of protein-nanoliposome therapeutic conjugates [4,7]. Fig. 1 shows the DELOS-susp process and the starting materials used to obtain the nanoGLA liposomal formulation.

The results obtained in earlier stages of nanoGLA development, although being biocompatible and showing interesting in vitro activity, presented some limitations regarding formulation characteristics for continuing with their translation towards the clinics. In first place, the concentration of GLA enzyme we could load into the nanoliposomes, with robust particle size and PDI, was around 20  $\mu$ g/mL, far below the minimum required for reaching those doses that will allow to perform

efficacy studies in mice (200  $\mu$ g/mL). Besides, the enzyme entrapment efficiency in the liposomes was below 40% [4]. The addition of cationic surfactant myristalkonium chloride (MKC) into the formulation in low concentration allowed to increase the drug entrapment efficiency as well as the colloidal stability of the system [7]. However, further work was required in order to obtain a stable formulation with the proper protein concentration.

In this work we applied the Quality by Design (QbD) approach to determine formulation and process parameters that could have an important impact on nanoGLA attributes when prepared by DELOS-susp. The QbD methodology is described in Guidelines of the International Council for Harmonisation of Technical Requirements for Pharmaceuticals for Human Use (ICH) [8–10] and it is strongly encouraged by the Food and Drug Administration (FDA) and the European Medicines Agency (EMA) to develop robust drug manufacturing and control methods. Pharmaceutical QbD is a systematic approach to development that aims to ensure the quality of medicines, identifying characteristics that are critical to quality from the patient's perspective, translating them into the product Critical Quality Attributes (CQAs), and establishing a relationship between manufacturing variables and CQAs through a Design of Experiments (DoE). The goals of the pharmaceutical QbD may include the achievement of meaningful product quality specifications as well as the reduction of product variability and defects, to increase efficiencies and to enhance root cause analysis [11].

Another systematic methodology used in pharmaceutical design is the Safe by Design (SbD) approach, which aims to eliminate possible risks to the human health and the environment at early innovation stages, i.e., during the design or planning stage [12]. SbD requires a full life cycle perspective combined with nanomaterial sustainability (environmental, social, and economic) [13] improvements, to avoid the shifting of potential risks across development stages.

In this framework, we report here the implementation of the QbD approach to develop a robust process for the preparation of nanoGLA. In the present work, the process was scaled-up from previous work [4] by a 7-fold factor, and the liposomal prototype was optimized increasing 10-times (i.e. from around 20 to 200  $\mu$ g/mL) the final concentration of GLA enzyme in the nanoformulation. Its physicochemical stability was improved while meeting the defined quality specifications in order to fulfill the required therapeutic doses for advanced preclinical testing. Besides, a SbD evaluation of the nanoGLA manufacturing process by DELOS-susp is also presented.

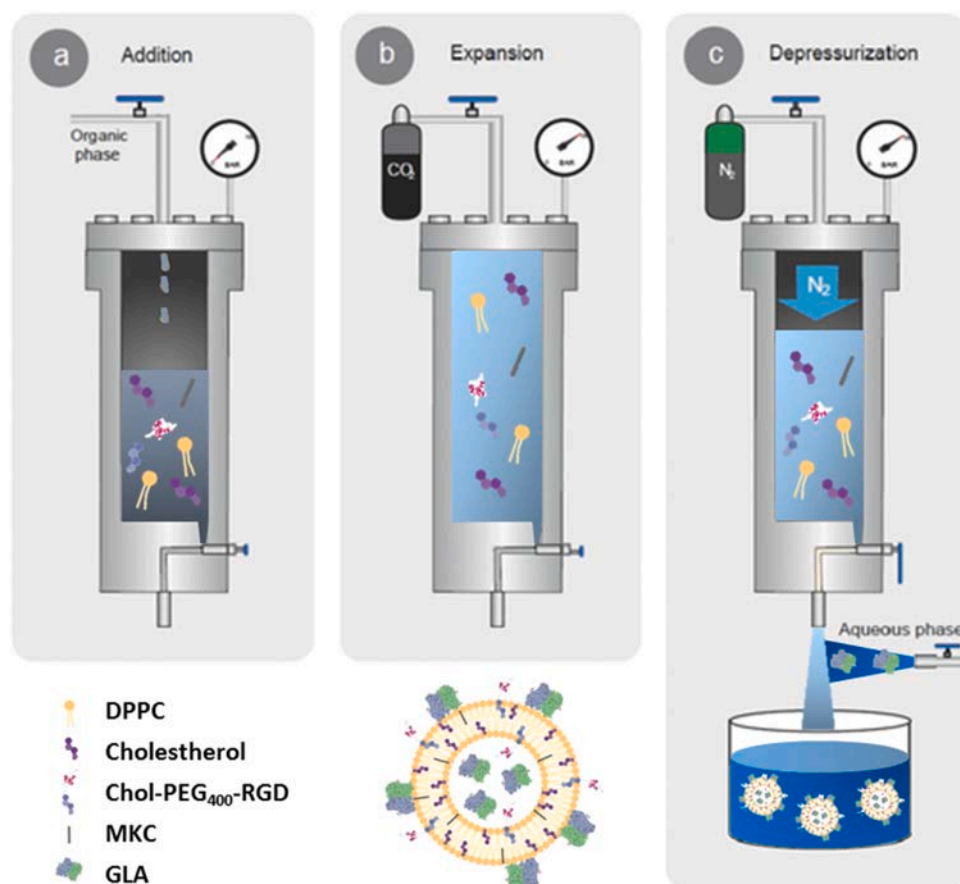


**Fig. 1.** Schematic representation of the DELOS-susp method for the preparation of GLA loaded nanoliposomes (nanoGLA). The procedure includes: a) Loading of an organic solution containing the liposome membrane components (Cholesterol, DPPC, Cholesterol-PEG<sub>400</sub>-RGD, MKC) into the high pressure vessel; b) Addition of compressed CO<sub>2</sub> until a certain pressure to produce a CO<sub>2</sub>-expanded solution, where all membrane components remain dissolved in a single liquid phase; and c) Depressurization of the expanded solution over an aqueous solution containing the GLA enzyme at atmospheric pressure, obtaining the protein-liposomes nanoconjugates. Figure adapted from [4].

## 2. Materials and methods

### 2.1. Materials

GLAcmycHis protein (GLA) was synthesized as explained in [Appendix A](#). 1,2-Dipalmitoyl-sn-glycero-3-phosphocholine (DPPC) was purchased from Cordem Pharma (Liestal, Switzerland), cholesterol was purchased from Panreac Química (Castellar del Vallès, Spain), and myristalkonium chloride (MKC) from United States Biological (Salem, US). Cholesterol pegylated with arginyl-glycyl-aspartic acid peptide (Chol-PEG<sub>400</sub>-RGD) was synthesized as described by E. Cristóbal-Lecina et al. [14]. Ethanol (EtOH) was purchased from Scharlab (Sentmenat, Spain), dimethyl sulfoxide (DMSO) from Sigma-Aldrich (St. Louis, US), carbon dioxide (CO<sub>2</sub>) and nitrogen (N<sub>2</sub>) from Carburros Metálicos (Cornellà de Llobregat, Spain). Diafiltration column modules of 300 kDa cut-off were purchased from Repligen (Waltham, US). Ultrapure Type I water (H<sub>2</sub>O), purified using Milli-Q Advantage A10 equipment from Millipore Corporation (Burlington, US), was used for all studies.

### 2.2. Methods

#### 2.2.1. NanoGLA preparation

DELOS-susp methodology was used for the nanoGLA preparation ([Fig. 1](#)). An EtOH:DMSO solution (volume ratio EtOH:DMSO 4:1) containing DPPC (from 0.86 to 3.46 mg/mL), cholesterol (from 0.30 to 1.24 mg/mL), Chol-PEG<sub>400</sub>-RGD (from 0.03 to 0.31 mg/mL), and MKC (from 0.02 to 0.07 mg/mL) at a working temperature (Tw) of 308 K was loaded into a 50 mL high pressure vessel at atmospheric pressure. The solution was, then, volumetrically expanded with compressed CO<sub>2</sub> until a molar fraction ( $X_{CO_2}$ ) of 0.55 was achieved, reaching a working pressure (Pw) of 9 MPa. The system was kept at 308 K and 9 MPa under

stirring for approximately 15 min to achieve a complete homogenization and to attain thermal equilibration. A given volume of GLA stock solution at 0.28 mg/mL, measured by SDS-PAGE, was dissolved in ultrapure water to reach the desired enzyme concentration (7, 17 or 27 µg/mL). To form the nanoconjugates, the volumetrically expanded organic phase was depressurized over the aqueous solution containing the GLA. In this way, nanoGLA DELOS-susp batches of 290–500 mL were obtained. In this step, a flow of compressed N<sub>2</sub> was used as a plunger to push down the CO<sub>2</sub>-expanded solution from the vessel and to maintain a constant pressure of 10 MPa inside the vessel during depressurization. Average time per experiment was 60 min and the resulting dispersions of nanoconjugates were stored at 4 °C until their characterization. The process parameters that were kept constant for all experiments are listed in [Appendix B](#).

#### 2.2.2. Separation of the free GLA from the nanoGLA liposomal dispersion by diafiltration and concentration process

The non-conjugated GLA enzyme (with a molecular weight between 90 and 110 kDa in its dimer form) was separated from the GLA-loaded liposomes obtained by DELOS-susp using a KrossFlo Research Iii Tangential Flow Filtration (TFF) System with mPES hollow fiber modules of 300 kDa cut-off, in order to determine the GLA entrapment efficiency (EE) [4]. A volume of 10 mL of liposomal sample was added to the sample container, which was connected to the column and the buffer reservoir. Six diafiltration cycles were performed with ultrapure Type I water to eliminate the free molecules and the organic solvent present in the liposomal samples.

Concentration of the intermediate nanoGLA during the optimization step was performed using the same equipment, materials, and conditions. A volume of 50 mL of diafiltrated sample was added to the sample container and submitted to a 7.5 concentration factor, evacuating ca. 87% of water.

2.2.3. Characterization of liposomes

2.2.3.1. Mean particle size, PDI and ζ-potential. Liposomal mean size, polydispersity index (PDI) and ζ-potential were determined by Dynamic Light Scattering (DLS), using a Zetasizer Nano ZS analyzer (Malvern Instruments, Malvern, UK). The measurements were performed at 20 °C with a scattering angle of 173°, immediately after liposomes' preparation, and 1 and 2 weeks after the production.

2.2.3.2. Turbiscan Stability Index. Turbiscan Stability Index (TSI) was determined by Static Multiple Light Scattering (S-MLS), using a Turbiscan Lab Expert (Formulation, Toulouse, France), at 20 °C and 2 weeks after liposomes production.

2.2.3.3. Morphology. The morphology of the systems was studied using Cryogenic Transmission Electron Microscopy (Cryo-TEM). Images were obtained with a FEI Tecnai G2 12 microscope (FEI, The Netherlands) operating at 120 kV, as described in [15]. The analysis was performed 1 week after samples production.

2.2.3.4. Uni-lamellarity. Quantitative information on the liposomes degree of lamellar structure and bilayer thickness was investigated with small-angle X-ray scattering (SAXS) on an optimized NanoSTAR SAXS instrument (Bruker AXS, Karlsruhe, Germany) equipped with a

liquid Ga metal jet X-ray source (Excillum AB, Sweden) and scatterless slits. The wavelength was λ = 1.34 Å and the measurements were performed 1 week after production. The data were analyzed by a model similar to the one described in [16,17]. The model was expressed so that the fraction of bilayers presented as single-layered vesicles, f<sub>single</sub>, was a fit parameter.

2.2.3.5. Entrapment efficiency. The entrapment efficiency (EE) was determined by comparing the amount of enzyme encapsulated in the nanovesicles after removal of free enzyme by diafiltration (Loaded prototype) with the amount of initial GLA present in the DELOS-susp batch just after its production (Total prototype), see Eq. (1) (Entrapment efficiency calculation):

$$EE = \frac{\text{mass GLA}_{\text{Loaded}}}{\text{mass GLA}_{\text{Total}}} \cdot 100 \tag{1}$$

To detect and quantify the enzyme in each of these samples, SDS-PAGE was performed by using gels TGX Stain-Free™ FastCast™ acrylamide 12% (Bio-Rad, ref. 161-0185). To visualize the fluorescent bands, a ChemiDoc™ Touch Imaging System (Bio-Rad) was used. Samples and standards to be quantitatively compared were run in the same gel and processed as a set. Densitometric analysis of the bands were performed with the Image Lab™ software (version 5.2.1., Bio-Rad).

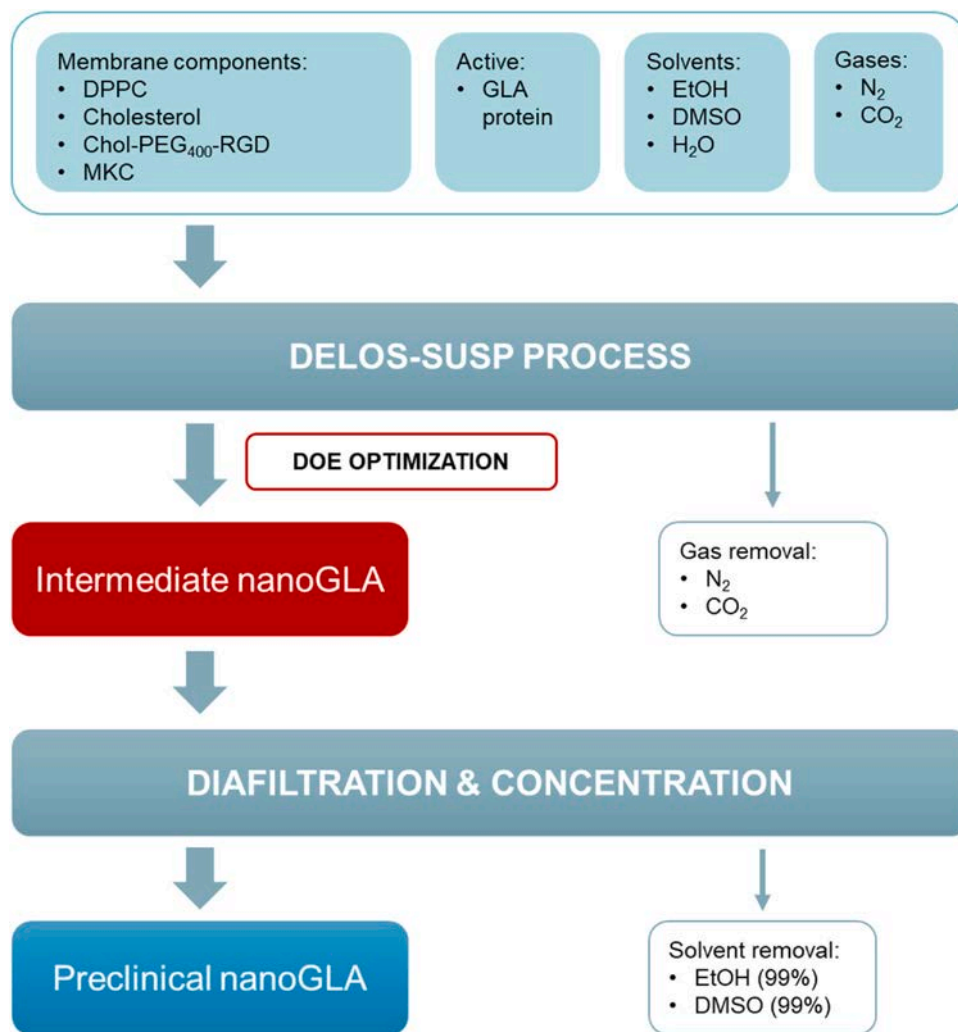


Fig. 2. Process Flow Diagram to produce the nanoGLA. Raw materials and the materials leaving the process are also represented. In red, the intermediate nanoGLA formulation obtained by DELOS-susp that has been studied in the QbD implementation. Diafiltration and concentration processes are necessary to remove the remaining free GLA and organic solvents from the nanoformulation and to maximize the enzyme concentration in the final nanoformulation for preclinical studies, respectively.

**2.2.3.6. Enzymatic activity.** The  $\alpha$ -galactosidase specific enzymatic activity (EA) of liposomal formulations was assayed using 4-Methylumbelliferyl  $\alpha$ -D-galactopyranoside (4-MUG, Sigma Chemical) as substrate, at a concentration of 2.46 mM in assay buffer (0.01 M acetic acid, pH 4.5) as previously described [18]. The released product (4-methylumbelliferone) was determined by fluorescence measurement ( $\lambda_{exc} = 365$ ,  $\lambda_{em} = 450$  nm) and final specific enzymatic activities were shown as 4-methylumbelliferone  $\mu$ mol per time and protein quantity. Measurements were performed 1 week after production of the samples.

#### 2.2.4. Experimental design and data processing

An experimental design with 4 factors at 2 levels with 2 central points (resulting in a total of 10 experimental runs) was constructed in order to study the influence of formulation parameters (independent variables or factors) on the properties (dependent variables or responses) of nanoGLA dispersion. The selected experimental design was a Fractional Factorial design, and it was developed using Modde 12 Pro software (Umetrics, Sweden). Data fitting and calculation of statistical parameters were performed by partial least squares (PLS) method. The experimental design used in this study allowed fitting the data with a linear regression interaction model. The acceptance of the responses obtained was evaluated by means of the statistical parameters predicted by the software  $R^2$ ,  $Q^2$  model validity, and model reproducibility. The design space for nanoGLA was determined using Design Space Explorer option from the Optimizer module of Modde 12 Pro software.

### 3. Results and discussion

The process flow diagram of the whole nanoGLA optimized manufacturing process is presented in Fig. 2. Membrane components, solvents, and gases, as well as the GLA protein, were processed using DELOS-susp (see Section 2) obtaining an intermediate nanoGLA dispersion, whose quality was studied by QbD. Then, the optimized intermediate nanoGLA was diafiltrated and concentrated by TFF in order to remove the organic solvents and to reach the target enzyme

concentration, which cannot be directly achieved in the DELOS-susp step because of the limited solubility of the liposome membrane components in the organic phase, while keeping the nanoformulation quality.

#### 3.1. Identification of the Critical Quality Attributes (CQAs)

During the development of liposomal drug products, the identification and pertinent characterization of CQAs of liposomal drug products is one of the main challenges from the quality point of view, together with the definition of proper control strategies. Liposomal products are complex formulations and small changes in their physicochemical attributes can have notable effects in their in vivo performance. Thus, a suitable definition of CQAs and control strategies may allow a faster and more efficient drug product development [19]. Table 1 shows the CQAs selected for QbD implementation related to the intermediate nanoGLA liposomal dispersion. The definition of the quality attributes has considered the ICH recommendations, as well as FDA and EMA guidelines [10].

As a parenteral dosage form, liposomal products must be sterile and pyrogen-free. These parameters are not considered as CQAs at this stage of formulation development since it is an intermediate product, but they must be considered as CQAs in the final formulation.

#### 3.2. Risk assessment and control strategies

Risk assessment is a valuable science-based process used in quality risk management that can aid in identifying which material attributes and process parameters potentially influence product CQAs [11,22]. The potential risk factors which might influence the quality of the product were identified through risk analysis, creating the Ishikawa diagram for each CQA defined for nanoGLA (see Appendix C, where the detailed risk analysis assessment is presented). As a result, 4 formulation factors were considered relevant to be included in the subsequent DoE analysis: GLA concentration, lipid concentration, peptide content in the liposomal membrane, and ethanol concentration. The justification regarding the

**Table 1**  
CQAs defined for the intermediate nanoGLA liposomal dispersion obtained by DELOS-susp and their justification.

Quality Attribute	Justification [19–21]
Macroscopic Appearance	It must be a homogeneous opalescent dispersion without sedimentation. Sedimentation could indicate poor colloidal stability.
Mean Particle Size	Particle size and particle size distribution are major CQAs for nanoparticle-based systems, playing an important role in determining their in vivo absorption and distribution, drug loading, drug release, and targeting ability. Therefore, robust control of particle size is one of the crucial parameters for further in vivo application of liposomal drug products. Values below 300 nm are considered acceptable for nanoGLA.
Polydispersity Index (PDI)	PDI reflects the heterogeneity of the particle size, indicating how wide is the particle size distribution. The lower the PDI, the higher the homogeneity of the dispersion. To meet specification, PDI should be below 0.45.
$\zeta$ -potential	Important parameter in the evaluation of colloidal system's stability. Particles with a high negative or positive $\zeta$ -potential value repel each other, indicating that the colloidal system is stable. On the contrary, decreasing the $\zeta$ -potential value to nearly neutral could lead to liposomal aggregation. The liposome surface charge can also influence drug loading, cellular uptake, tissue distribution, and clearance. $\zeta$ -potential values higher than + 30 mV are considered inside the specification range for nanoGLA.
Particle morphology and lamellarity	Vesicles must be spheroidal and, mostly, uni-lamellar. Lamellarity can affect drug loading and release, thus, impacting the enzyme delivery.
GLA Entrapment Efficiency (EE) /Free drug substance	Free drug substance may have side effects and impact into pharmacokinetic profile. Besides, a high and reproducible percentage of drug entrapment could reduce manufacturing costs and increase drug concentration in the final formulation allowing greater flexibility in dosing. Depending on the pharmacokinetics, higher drug concentration can result in increased dosing intervals and hence improved patient compliance.
Specific Enzymatic Activity (EA)	The bioactivity of the integrated enzyme must be preserved in the nanoformulation. EA ratio to control should be higher than 0.8, referred to the EA of a commercially available GLA (agalsidase alfa, Replagal®).
Integration efficiency of Chol-PEG <sub>400</sub> -RGD in the vesicular membrane	The amount of targeting peptide moiety integrated in the nanoliposomal membrane must be in the proper ranges to allow the nanoGLA to interact with cells and facilitate intracellular penetration.
pH	pH can affect dispersion stability, drug loading and release, and cell uptake among others. A suitable pH range is from 6.0 to 7.0.
Dispersion stability	The intermediate formulation must be stable at least until the diafiltration and concentration step. In terms of Turbiscan stability, the TSI should be less than 10.0 at 24 h.
Lipid and GLA degradation products	Chemical stability of the lipid components in the liposome as well as the chemical stability of the contained drug substance is important. These will be considered at further stages of development.

selection of these factors and their range of investigation is detailed in Table 2.

Although the depressurization flow rate during the DELOS-susp could be considered as a factor [30], it was not included in the present work since an accurate flow rate range variation could not be carried out in the used set-up. Due to limitations of the available in-house synthesized starting materials (GLA and Chol-PEG<sub>400</sub>-RGD), an intermediate laboratory plant was selected for performing the DoE. Thus, for this first QbD study the depressurization flow rate was kept constant at  $6.3 \pm 0.7$  g/min because it can be controlled within narrow values where the formulation requirements are ensured. So, despite not being able to introduce the flow rate as a factor in the present study, this parameter was defined as a controlled variable that was kept constant for all experiments. QbD is based on the principle of continuous improvement, thus, by gathering knowledge during early development, it is possible to avoid potential manufacturing problems as the drug product evolves through the development pipeline. Thus, the knowledge obtained in the present study will allow to concisely define further scale-up studies. The influence of DELOS-susp depressurization flow rate variation on the nanoGLA quality will be more accurately evaluated in future studies at pilot plant scale, where it is possible to control and register this parameter. Taking the present results as the basis for refining the Design Space of the nanoGLA will ease this transition from the lab to the pilot plant.

### 3.3. Experimental design and development

An experimental design was constructed to study the influence of the formulation (independent variables or factors) on the physico-chemical properties (dependent variables or responses) of intermediate nanoGLA obtained by DELOS-susp, as shown in Table 3. Low and high levels for each factor (Table 2) were selected based on previous experiments and studies [4,7].

All process parameters, including depressurization flowrate at 10 g/min, were kept constant for all experiments. The responses of the experimental design were the CQAs of the intermediate nanoGLA dispersion: particle mean size, polydispersity index,  $\zeta$ -potential, Turbiscan stability index, ratio of monolayered liposomes, entrapment efficiency, enzymatic activity, and pH. Furthermore, macro and microscopic appearance (i.e. particle morphology) were analyzed, but these two CQAs were not included in the design because of their qualitative nature. The matrix of the experimental design is presented in Table 3.

All experiments were produced following DELOS-susp method at the laboratory scale, as explained in Section 2. All 10 experiments were produced in 2 consecutive days.

**Table 2**

Factors included in the DoE to optimize the intermediate nanoGLA formulation, their potential impact into CQAs and the ranges of investigation.

Factor	Potential impact into CQAs	Factor Range studied in DoE
GLA concentration	Protein concentration plays a key role on dispersion stability. It has been reported that increasing the loading and charge of protein will impact on size distribution and aggregation rate of the liposomal system [23].	From 7 to 27 $\mu\text{g}/\text{mL}$ of enzyme. Defined according to the viability of performing the subsequent diafiltration and concentration step up to the 200 $\mu\text{g}/\text{mL}$ required for in vivo doses.
Lipid concentration	Besides the molar ratio between membrane components (cholesterol and phospholipid), the total lipid concentration in liposomal systems will impact on its mean size, particle distribution and stability, as well as on its loading capacity [24–27].	From 1.2 to 5.0 mg/mL, moving almost 2 mg/mL up and down of previously tested concentrations in similar nanoformulations (3.0 mg/mL).
Chol-PEG <sub>400</sub> -RGD molar ratio	PEGylation of liposomes improves not only the stability and circulation time, but also the passive targeting ability on tumoral tissues, through a process known as the enhanced permeation retention effect, able to improve the therapeutic effects and reduce the toxicity of encapsulated drug [28].	From 1% to 3% mol of molar ratio in relation to the total amount of lipid components, according to previous studies.
EtOH concentration	Solvent concentration could have a direct impact on shape, solubility and electrostatic interactions between the liposomal bilayer and the loaded protein [29].	From 5% to 10% v/v, folding the standard 5% v/v since higher quantities are not recommended for intravenous administration [4].

### 3.4. Characterization of the intermediate nanoGLA obtained

A high variability on the stability of the samples was observed among the different experimental conditions tested. Thus, some characterizations were performed at the production day ( $t = 0$ ) and followed until 14 days.

Regarding the macroscopic appearance, all DELOS-susp batches presented a homogenous, whitish, opalescent appearance without presence of sediment, except for DOE-001, DOE-006, and DOE-009.

A summary of the microscopy analysis of the nanoGLA samples by cryo-TEM is presented in Fig. 3, indicating that for all experiments nanovesicles were obtained, being mostly uni-lamellar and spherical, and ranging between 100 and 200 nm, with the presence of some larger vesicles around 500 nm.

Table 4 shows a summary of the characterization results of the DoE samples, which were considered for the statistical analysis. The three out of ten batches (DOE-001, DOE-006, and DOE-009) that presented small sedimentation also showed a higher TSI indicating the dispersion instability.

Besides, samples in which aggregation and sedimentation were observed presented also higher size and PDI, and lower uni-lamellarity. Furthermore, the mean particle size and PDI of DOE-001, DOE-006, and DOE-009 significantly increased with time after production (Appendix D). On the other side,  $\zeta$ -potential, EE, and EA values did not correlate with macro and microscopical characteristics of the samples.

All the formulations showed enzymatic activity, varying from 0.8 to 1.7 ratio to control referred to the enzymatic activity of a commercially available free GLA (Agalsidase alfa, Replagal® from Shire-Takeda) included in the analysis, as also shown in Table 4. These results indicate an excellent enzymatic activity in all cases, compliant with preliminary specifications.

### 3.5. Analysis of the influence of the factors on CQAs

The influence of the factors was studied for the rest of dependent variables or CQAs. An analysis and discussion for each quantifiable CQA is described below. From the characterized CQAs, mean particle size,  $\zeta$ -potential, and uni-lamellarity could be statistically fitted and were included in the prediction model (see Appendix E for modeling and data fitting) while for the rest of attributes a bad correlation was obtained and thus a poor predictive ability of the model.

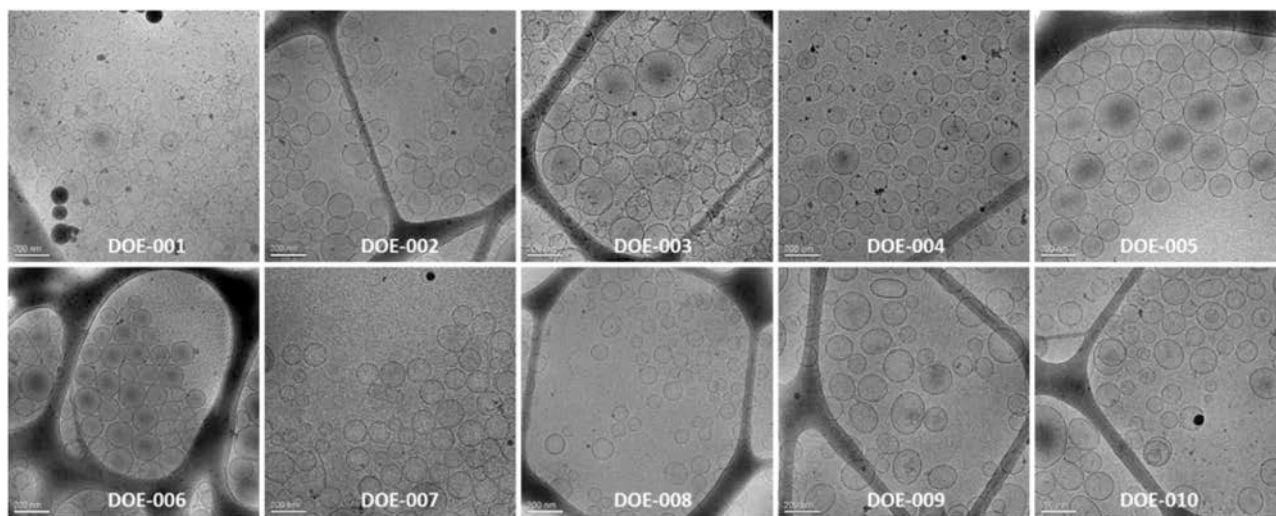
According to the data presented in Table 4, the mean particle size of the nanoGLA dispersions varied from 90 to 200 nm. These differences could be explained because of the aggregation and fusion of liposomal vesicles that could occur 1 week after preparation. The coefficients of the equation describing the influence of the factors on nanoGLA particle



**Table 3**

Matrix of experimental design. The sample codes consider the randomized order of experiments.

Experimental run	GLA concentration ( $\mu\text{g/mL}$ )	Lipid concentration ( $\text{mg/mL}$ )	Chol-PEG <sub>400</sub> -RGD molar ratio to lipids (% mol)	EtOH concentration (% v/v)
DOE-001	27	1.2	1	10.0
DOE-002	7	1.2	3	10.0
DOE-003	17	3.1	2	7.5
DOE-004	27	5.0	1	5.0
DOE-005	7	5.0	3	5.0
DOE-006	27	1.2	3	5.0
DOE-007	17	3.1	2	7.5
DOE-008	7	1.2	1	5.0
DOE-009	27	5.0	3	10.0
DOE-010	7	5.0	1	10.0

**Fig. 3.** Representative cryo-TEM images of nanoGLA DoE samples at 1 week after production. Scale bar 200 nm.**Table 4**Characterization of intermediate nanoGLA CQAs after 1 week of production. Uncertainties are calculated from the standard deviation of measurement for Size, PDI,  $\zeta$ -potential, and EE; and from standard error of the mean for uni-lamellarity and EA.

Sample ID	Size (nm)	PDI	$\zeta$ -potential (mV)	TSI	Uni-lamellarity, $f_{\text{single}}$	EE (%)	EA (ratio to control)
DOE-001 <sup>a</sup>	143 $\pm$ 6	0.45 $\pm$ 0.08	35 $\pm$ 2	11.5	0.88 $\pm$ 0.01	60 $\pm$ 1	1.7 $\pm$ 0.1
DOE-002	88 $\pm$ 2	0.17 $\pm$ 0.01	36 $\pm$ 2	0.6	0.99 $\pm$ 0.01	53 $\pm$ 1	1.2 $\pm$ 0.0
DOE-003	142 $\pm$ 3	0.12 $\pm$ 0.05	34 $\pm$ 0	1.2	0.95 $\pm$ 0.00	59 $\pm$ 1	1.4 $\pm$ 0.0
DOE-004	175 $\pm$ 1	0.32 $\pm$ 0.05	45 $\pm$ 0	8.2	0.93 $\pm$ 0.00	45 $\pm$ 1	1.6 $\pm$ 0.1
DOE-005	158 $\pm$ 4	0.24 $\pm$ 0.03	45 $\pm$ 6	1.9	0.93 $\pm$ 0.00	42 $\pm$ 1	0.8 $\pm$ 0.1
DOE-006 <sup>a</sup>	202 $\pm$ 4	0.46 $\pm$ 0.05	32 $\pm$ 1	6.6	0.85 $\pm$ 0.02	68 $\pm$ 1	1.5 $\pm$ 0.0
DOE-007	146 $\pm$ 2	0.11 $\pm$ 0.05	35 $\pm$ 1	1.2	0.99 $\pm$ 0.01	53 $\pm$ 1	1.2 $\pm$ 0.2
DOE-008	100 $\pm$ 1	0.17 $\pm$ 0.02	38 $\pm$ 1	1.8	1.00 $\pm$ 0.01	84 $\pm$ 1	0.8 $\pm$ 0.0
DOE-009 <sup>a</sup>	172 $\pm$ 5	0.22 $\pm$ 0.02	38 $\pm$ 1	12.0	0.94 $\pm$ 0.01	53 $\pm$ 1	1.1 $\pm$ 0.1
DOE-010	134 $\pm$ 2	0.13 $\pm$ 0.02	46 $\pm$ 2	0.6	0.93 $\pm$ 0.00	84 $\pm$ 1	1.4 $\pm$ 0.1

<sup>a</sup> DOE-001, DOE-006, and DoE-009 presented sedimentation.

size are shown in Fig. 4a (left). According to this figure, the size of nanoGLA liposomes is significantly influenced by GLA concentration (X1) and the lipid concentration (X2). Thus, a significant increase in size is obtained when the concentration of GLA and lipid increase. The increase in size with the increase of GLA and lipid concentrations could be explained by the occurrence of physical aggregation of the vesicles. The influence of GLA and lipid concentration is also illustrated by the contour plot for size in Fig. 4a (right).

As shown in Table 4,  $\zeta$ -potential ranged from 32 to 46 mV for non-diafiltrated liposomes. The influence of studied factors on  $\zeta$ -potential is shown as coefficients of the regression equation plot in Fig. 4b (left). According to this plot, lipid concentration (X2) was the only factor that had a significant positive effect on the  $\zeta$ -potential of the dispersions obtained. This could be explained because when lipid concentration

increases, MKC surfactant (used as excipient in the nanoformulation) concentration also increases, giving more positive charges to the liposomal system. The influence of lipid concentration is also illustrated by the contour plot for size in Fig. 4b (right).

Monolayered liposomes fractions varied from 0.88 to 1.00, as shown in Table 4 by  $f_{\text{single}}$  values. According to Fig. 4c (left), lipid concentration was the only factor affecting this CQA significantly, showing a larger difference in comparison to the rest of factors. As can be seen in Fig. 4c (right), GLA concentration had an insignificant influence on the monolayer ratio of liposomes, but it was strongly affected by the lipid concentration. The explanation can be the same as the effect of lipid concentration on vesicle size: aggregation and fusion of the vesicles when lipid concentration increases could be responsible of this behavior.

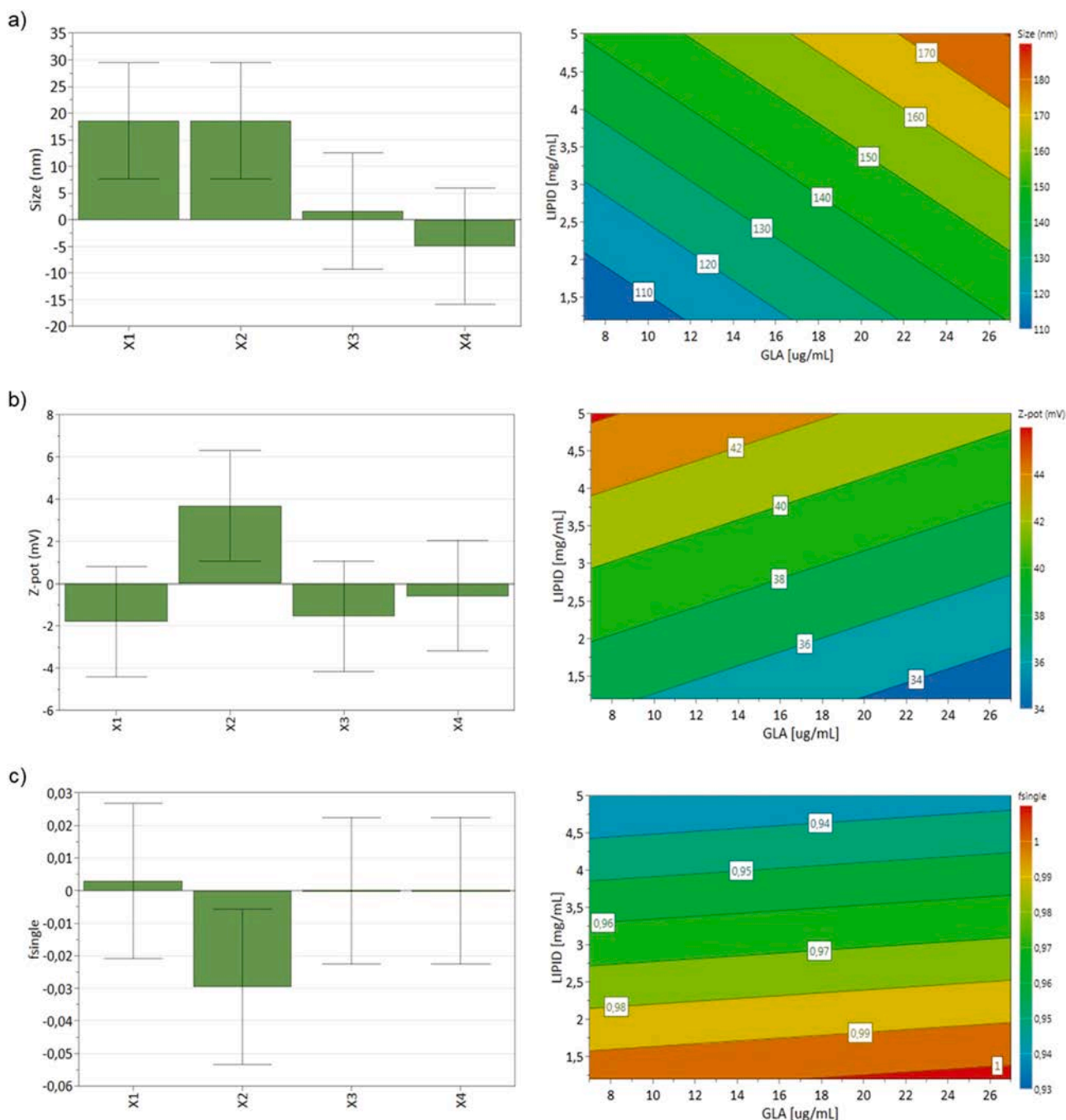


Fig. 4. Left side: scaled and centered coefficients of the regression equations describing the influence of formulation parameters X1-GLA concentration, X2-lipid concentration, X3-Chol-PEG<sub>400</sub>-RGD molar ratio, X4-EtOH concentration, on the liposomes size,  $\zeta$ -potential, and uni-lamellarity of nanoGLA intermediate dispersion. Right side: contour plots for the same CQAs of the nanoGLA intermediate dispersion. Molar ratio of chol-PEG<sub>400</sub>-RGD to lipid and EtOH concentration were kept constant at 2% mol and 7.5% v/v, respectively.

### 3.6. Evaluation of the design space

Among all the factors studied, GLA concentration and lipid concentration were found to have a significant influence on some of the responses. Thus, the Design Space for intermediate nanoGLA was constructed using these factors which significantly influenced the quality of the nanoformulation. On the one hand, increase of GLA and lipid concentration had a negative influence on liposomal mean particle size because of the size increase promoted by aggregation. On the other hand, as the lipid concentration increased, and consequently, the amount of MKC surfactant was higher,  $\zeta$ -potential (which is related to the electrical charge at the liposomes surface) also increased due to the formal positive

charge provided by this cationic surfactant. Nevertheless, this  $\zeta$ -potential increase was not correlated with a higher colloidal stability of the nanoformulation as also confirmed by an uni-lamellarity decrease. It seems that this MKC amount is not enough to stabilize such highly concentrated samples. However, higher MKC concentrations, although could improve the stability of these concentrated samples, it also could entail a toxicological concern as well as the abolishment of the enzymatic activity of the GLA, as reported by Tomsen-Melero et al. [7].

The other CQAs such as polydispersity index, TSI, GLA entrapment efficiency, and enzymatic activity could not be fitted in any reliable model because of the sedimentation of some batches and the high characterization variability, due to the use of SDS-PAGE plus TGX as a reference method for

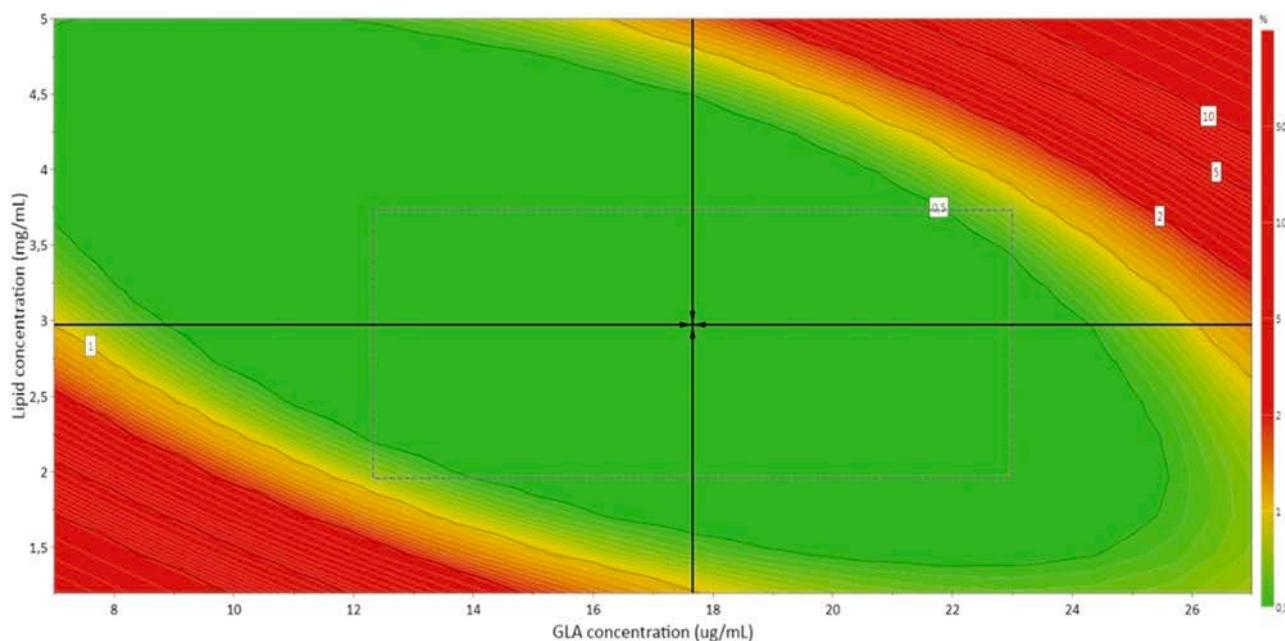


Fig. 5. The Design Space for intermediate nanoGLA liposomal dispersion that meets the specifications in terms of CQAs, expressed as the probability of failure (%). Molar ratio of chol-PEG<sub>400</sub>-RGD to lipid and EtOH concentration have been optimized in the run at 1.16% mol and 6.2% v/v, respectively.

Table 5

The desired CQAs of nanoGLA introduced in the Design Space explorer and their values.

Response	Criterion	Min.	Target	Max.
Size (nm)	Target	50	150	250
ζ-potential	Excluded	-	-	-
Uni-lamellarity ( $f_{single}$ )	Maximize	0.95	1.00	-

GLA quantification. Results could be improved in the future using a HPLC method for the quantification of GLA. Hence, the Design Space was determined using particle size, ζ-potential, and uni-lamellarity.

The Design Space obtained is shown as the green region in Fig. 5, and shows the combination of factors for which the nanoGLA intermediate obtained by DELOS-susp will meet the specifications in terms of CQAs, specified in Table 5, with a probability of failure less than 1%. The combination inside the design space which is pointed out by the black arrows indicates the robust setpoint (17.7 μg/mL GLA concentration, 2.97 mg/mL lipid concentration, 1.3% mol Chol-PEG<sub>400</sub>-RGD, and 6.2% v/v EtOH) corresponding to the formulation for which the prediction errors are the lowest.

To our knowledge, there are no similar results reporting the relationship between lipid and protein concentration affecting size, ζ-potential, and uni-lamellarity in this way. We could expect that at low concentration of lipid and GLA, we would also obtain a nanoGLA within the established acceptance limits, so it could be possible that the red zone showed in Fig. 5 around the lowest concentrations belongs to a range that remained unexplored. In addition, the finding of a model which indicates that formulation will escape from the acceptance limits

Table 6

Critical Quality Attributes for optimized intermediate nanoGLA, diafiltrated and concentrated around 10-fold.

Attributes	After DELOS-susp (Intermediate nanoGLA)	After concentration (Preclinical nanoGLA)
Stability	NA	> 2 weeks
Particle mean size (nm)	138 ± 7	165 ± 3
Polydispersity Index	0.38 ± 0.03	0.41 ± 0.02
ζ-potential (mV)	40 ± 1	35 ± 1
Enzymatic activity (ratio to control)	1.11 ± 0.08	0.93 ± 0.04
GLA (μg/mL)	34 ± 2	330 ± 20

if both factor concentrations are high is due to aggregation effect of liposomes caused by a change of interaction between them, provoked by the high load of components in the membrane [24,31].

### 3.7. Optimization of the nanoGLA formulation

The challenge was to obtain a stable nanoGLA concentrated formulation containing 200 μg/mL of GLA, suitable doses for in vivo testing. To do so, a batch of nanoGLA was prepared by DELOS-susp and diafiltrated and concentrated following the trend of the preliminary Design Space: the lipid concentration was reduced to 1.2 mg/mL so that the GLA concentration could be increased up to 35 μg/mL, obtaining an intermediate nanoGLA by DELOS-susp meeting all the CQAs.

Physicochemical properties are shown in Table 6 and Fig. 6. Particle mean size, polydispersity index, ζ-potential, and GLA concentration – all meet the requirements to go to future in vivo preclinical trials (<300 nm, ≤0.45, >30 mV, and >200 μg GLA/mL, respectively). A good colloidal stability was observed for the concentrated final nanoGLA, composed mainly by single lamellar liposomes (Fig. 6). Some structural effects were noticeable by cryo-TEM after over-concentrating the GLA-loaded liposomes. Images revealed the formation of some multilamellar complexes, where the GLA can be identified between liposomal layers as well as inside the vesicles (Fig. 6, arrows), forming structures resembling lipoplexes [32]. Interestingly, the high concentration of GLA (330 μg/mL) after the concentration process where these structures were identified was quite above the minimum required value for in vivo trials (200 μg/mL).

In addition, the final prototype dispersion was stable for more than 2 weeks.

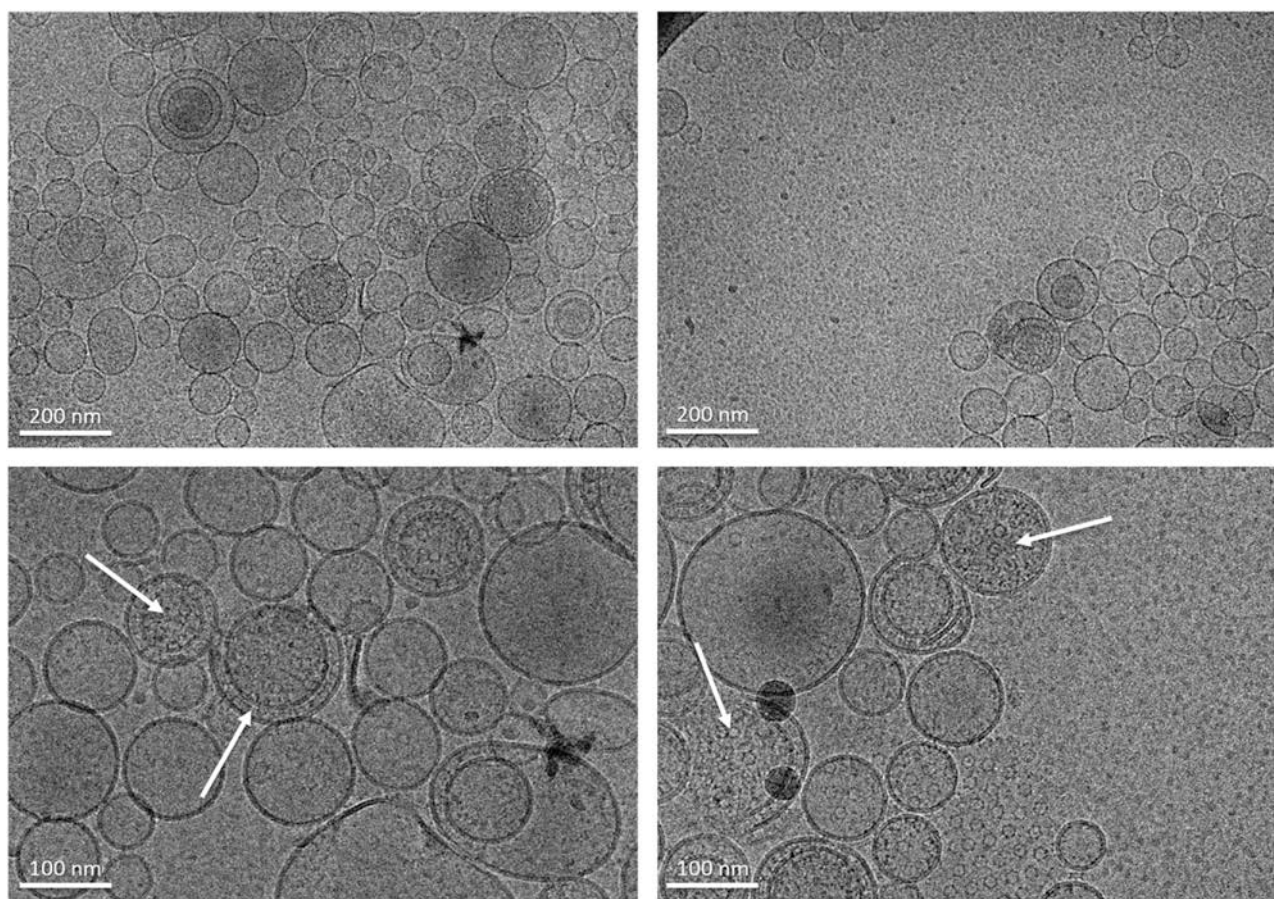


Fig. 6. Cryo-TEM images of optimized nanoGLA prototype after concentration. The images were acquired 2 weeks after production.

### 3.8. Safe-by-Design implementation

The implementation of the SbD approach followed the strategy reported by [33] and was specifically tailored to complement the QbD work, to prevent hazards from the developed components and processes, and to support the redesign of technical workflows where the need is identified. Each individual process step was evaluated to identify possible exposure scenarios and safety issues.

For the used DELOS-susp methodology (see Fig. 2), four specific issues that pose a potential risk were identified:

1. DMSO/EtOH in the nanoformulation
2. Aerosol exposition due to organic compounds, vapors, streams from the organic phase
3. Carbon dioxide poisoning
4. Cold burn during lyophilization

All the identified possible risks during the DELOS-susp methodology are rated on low respectively medium risk level and are controlled (see Appendix F), thus the DELOS-susp process can be considered as safe. To fully cover the entire innovation process towards its final product application, immunogenicity, endotoxicity, and impurities of the nano-formulation will be evaluated at later stage.

## 4. Conclusions

The current work brings a new contribution in the preparation of GLA loaded liposomes through the successful application of the QbD approach to DELOS-susp production method. Thanks to this methodology a

prototype of nanoGLA suitable for in vivo testing could be optimized. The influence of some formulation parameters was determined by using a DoE. Thus, among the formulation factors, GLA concentration and lipid concentration were the most important parameters for the quality of nanoGLA obtained by compressed fluid processing.

This study also enabled the obtaining of a preliminary design space to produce nanoGLA intermediate dispersion, in which the established quality requirements of the product are met.

Through the design space analysis, it could be predicted that for achieving a higher (10-fold), concentration of enzyme in the final formulation the concentration of lipid in the DELOS-susp step could be reduced in order to obtain a good quality product in terms of particle size and uni-lamellarity, and to avoid aggregation and sedimentation.

### Declaration of Competing Interest

The authors declare the following financial interests/personal relationships which may be considered as potential competing interests: J.L.-C., D.P., S.Sch., M.R., I.A., J.V., S.Sa. and N.V. are inventors of patent WO/2014/001509 licensed to Biopraxis Research AIE. J.V., S.Sa. and N.V. are inventors of patent WO/2006/079889 owned by Nanomol Technologies SL, and stock-owners in Nanomol Technologies SL. J.M.-M., J.T.-M., A.F., E.G.-M., J.-L.C, E.C.-L., D.P., M.R., S.Sch., I.A., A.S., S.Sa., J.V., N.V. and A.C. are inventors of patent application EP21382062.4.

### Acknowledgments

The authors acknowledge the financial support from European Commission through H2020 program of the Smart-4-Fabry project (ID 720942).

We acknowledge financial support to our research from Instituto de Salud Carlos III, through “Acciones CIBER”. The Networking Research Center on Bioengineering, Biomaterials, and Nanomedicine (CIBER-BBN) is 2008–2011, financed by the Instituto de Salud Carlos III with assistance from the European Regional Development Fund. Authors acknowledge financial support from the Agencia Estatal de Investigación-Ministerio de Ciencia e Innovación through the “Severo Ochoa” Programme for Centres of Excellence in R & D (CEX2019-000917-S). This work was also financed by 1084 the Ministerio de Ciencia e Innovación (PID2019-105622RB-1085 I00). We also thank the denomination of the 1101 consolidated group from Generalitat de Catalunya: 2017-1102 SGR-1439 (M.R.) and 2017-SGR-918 (J.V.).

We also acknowledge the ICTS “NANBIOSIS”, more specifically the support from the Protein Production Platform of CIBER-BBN/IBB, at the

UAB SepBioES scientific-technical service ([www.nanbiosis.es/unit/u1-proteinproduction-platform-ppp/](http://www.nanbiosis.es/unit/u1-proteinproduction-platform-ppp/)), the Soft Materials Service linked to Biomaterial Processing and Nanostructuring Unit at ICMAB-CSIC ([www.nanbiosis.es/portfolio/u6-biomaterial-processing-and-nanostructuring-unit/](http://www.nanbiosis.es/portfolio/u6-biomaterial-processing-and-nanostructuring-unit/)) and the Peptide Synthesis unit at the IQAC-CSIC ([www.nanbiosis.es/portfolio/u3-synthesis-of-peptides-unit/](http://www.nanbiosis.es/portfolio/u3-synthesis-of-peptides-unit/)).

N. A-G. is supported by a PERIS grant from the Catalan Government (SLT006/17/270).

J. T-M. is supported by a FI-AGAUR grant from the Catalan Government and the European Social Fund (ESF-Investing in your future) of the European Union. This work has been done in the framework of the JT-M. doctorate in Materials Science of the Universitat Autònoma de Barcelona.

The technical assistance of Inbal Ionita, Ella Kesselman and Mingming Zhang from Technion - Israel Institute of Technology; and Ramon González from ICMAB-CSIC is acknowledged.

## Appendix A. Synthesis of GLAcmycHis

### *Plasmids and E. coli strains*

The GLA gene was obtained from the commercial vector pReceiver-M10 (OmicsLink ORF Expression Clone, ref. EX-Q0172-M10), that encodes a cDNA version of the GLA gene (primary gene accession number: [NM\\_000169](https://www.ncbi.nlm.nih.gov/nuccore/NM_000169)), in which both c-myc and 6xHis tags are fused (for further detection and purification purposes) to the C-terminus.

For further steps, the pOptiVEC™-TOPO® TA Cloning Kit (Catalog Number 12744-017, Invitrogen, by Life Technologies) was used following the vendor protocol. The PCR product was cloned into the pOptiVEC™-TOPO® plasmid, and the resulting plasmid (pOptiVec-GLA) was transformed into TOP10 *E. coli* cells. Positive clones were selected by ampicillin and confirmed by restriction analysis. The pOptiVec-GLA plasmid was purified by “gigaprep” method, and finally linearized before transfection, as recommended by the vendor, with restriction enzyme *PvuI*. All plasmids were purified from their corresponding overnight bacterial cultures, using the EndoFree Plasmid Giga Kit (Qiagen, ref. 12391). For their quantification, absorbances at 260 nm (A260) and 280 nm (A280) were measured.

### *Mammalian cell line, transfection and selection of positive clones*

For the transfection and further selection of CHO cells overexpressing the human GLA enzyme, the OptiCHO™ Express Kit (Catalog number 12745-014, Invitrogen, by Life Technologies) was used. This kit provides CHO DG44 cells, media and transfection reagent needed. DG44 dhfr- CHO cells were grown in CD DG44 medium with 8 mM L-glutamine, at 37 °C in 8% CO<sub>2</sub> using standard techniques.

Transfection of CHO DG44 cells and selection of positive GLA-DHFR cells were performed following the vendor protocol. At 28 days post-transfection, stepwise selection for dhfr amplification was started, using two-fold increments of methotrexate hydrate (MTX, Sigma, catalog number A6770) starting at 50 nM up to 4 μM. Finally, and in order to obtain a single clone, the pool of stably transfected and 4 μM MTX-amplified cells were serially diluted and seeded at 1–2 cells per well in a 96-well plate. As suggested by vendor, to grow CHO DG44 cells under adherent conditions, the specific medium Gibco® CD-CHO-A was used. After this process, a single clone (namely CHO-DG44-GLA clone #3) was isolated and cryopreserved.

### *Cryopreservation of CHO-DG44-GLA clone #3*

CHO-DG44-GLA clone #3 was cultured in complete CD OptiCHO medium (supplemented with L-Glutamine 8 mM) to  $2 \times 10^6$  cells per milliliter and then centrifuged at 100 g for 5 min. Cell pellets were then resuspended in fresh medium containing 10% DMSO to a final cell concentration of  $10 \times 10^6$  cells/mL. Cells were aliquoted into 1 mL cryovials (Nalgene) and stored in the vapor phase of liquid nitrogen.

### *Production and purification of extracellular GLAcmycHis protein*

Cryovials of CHO-DG44-GLA clone #3 were thawed under standard procedures. Briefly, cryovial was rapidly thawed at 37 °C and resuspended in 15 mL of prewarmed complete CD OptiCHO medium. Cells were expanded by subculturing them up to the desired volume. In each passage, cells were diluted into pre-warmed complete CD DG44 Medium to give a final cell density of  $2 \times 10^5$ – $3 \times 10^5$  viable cells/mL. Finally, supernatant containing extracellular GLAcmycHis was harvested by centrifuging the cell culture at 14,000 rpm for 15 min. This supernatant was purified in an ÄKTA Pure system (GE Healthcare) by using an affinity chromatography column (HisTrap Excel 5 mL, Ref 17-3712-06, GE Healthcare) following the vendor protocol. Finally, the eluted protein was dialyzed in acetic buffer 0.01 M pH 5.5 and stored at –20 °C until used.

Appendix B. DELOS-susp methodology for the preparation of nanoGLA

Table B.1 summarizes the process parameters that were kept constant for all DELOS-susp experiments; and also includes the control strategies since some of them could have an impact on some CQAs. The 10 experiments carried out in this study were produced in 2 consecutive days.

Table B.1  
DELOS process parameters kept constant in all DoE experimental runs.

Process Parameter	Value	Control
Working temperature, Tw	35 °C	Heating jacket
High pressure stirring	500 rpm	Magnetic stirrer controller
Working pressure, Pw	9 MPa	Syringe pump for CO <sub>2</sub>
Depressurization pressure in the autoclave	10 MPa	Manometer and N <sub>2</sub> pressure regulator
Collector Stirring	300 rpm	Plate with magnetic stirrer
CO <sub>2</sub> molar fraction, X <sub>CO2</sub>	0.55	Solvent volume in the reactor
Depressurization flowrate	10 g/min	Manually controlled due to scale, averaged
Collector temperature	23 °C	Monitored, room temperature

Appendix C. Risk analysis assessment

Fig C.1 represents a summary of Critical Material Attributes (CMAs) and Critical Process Parameters (CPPs) that may impact the CQAs of the intermediate nanoGLA using Ishikawa methodology.

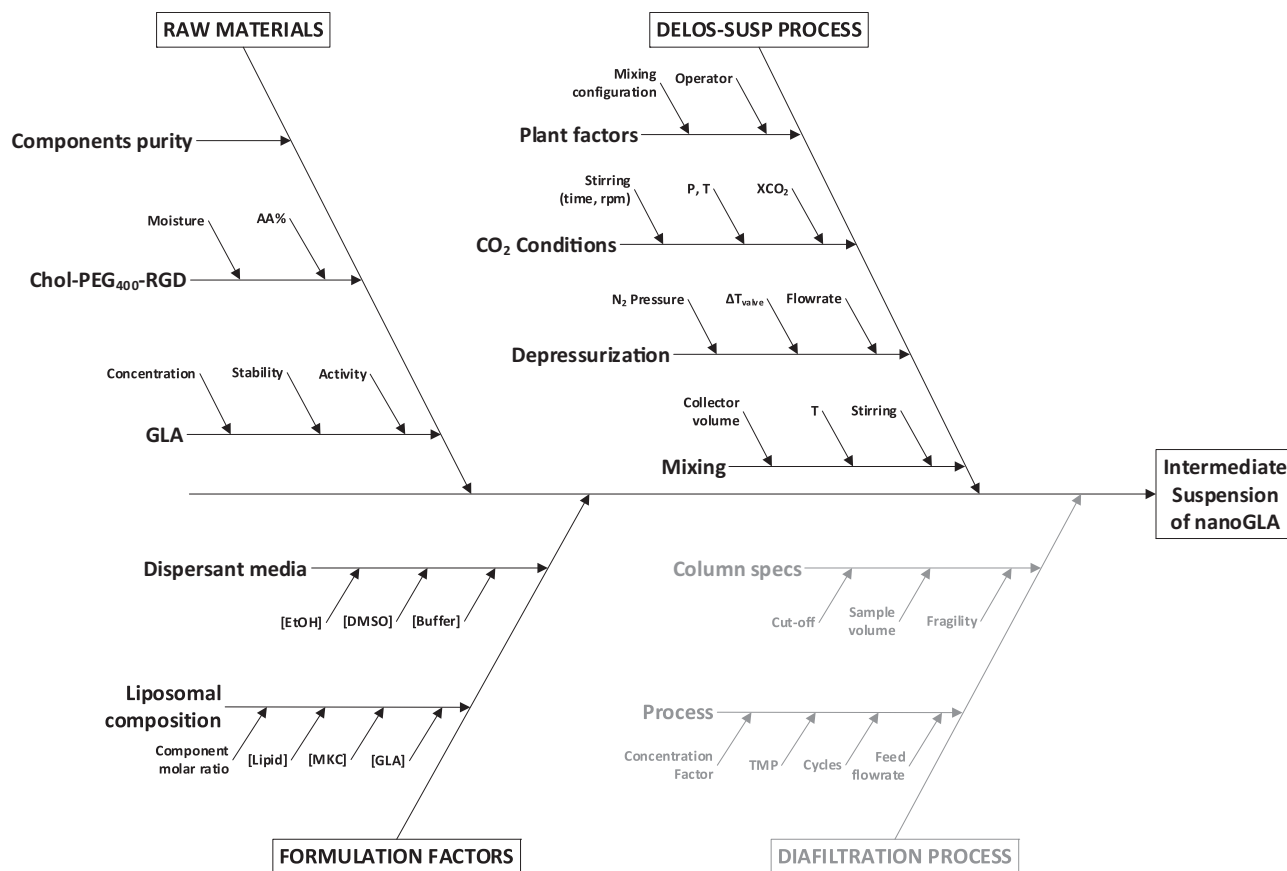


Fig. C.1. Ishikawa diagram illustrating the summary of CPPs and CMAs that may impact on each selected CQA of intermediate nanoGLA dispersion.

A control strategy is designed to ensure that a product of required quality will be produced consistently. These controls are based on product, formulation and process understanding and should include, at a minimum, control of the critical process parameters and material attributes. The risk assessment and the definition of control strategies serve to evaluate which CMAs and CPPs must be studied in a DoE.

In Table C.1 the risk analysis assessment of the potential CMAs and CPPs on the DELOS-susp process is presented.

**Table C.1**

Risk analysis assessment and control strategies of CMAs and CPPs for intermediate nanoGLA production by DELOS-susp.

CMA or CPP	Impact on CQA	Risk	Control strategy
Components purity	Low	Change in composition	CoA from supplier
Raw GLA	High	Change in morphology, nanoGLA stability an activity	CoA from supplier and check analysis by TGX, BCA or HPLC.
Chol-PEG <sub>400</sub> -RGD AA%	Low	Affect biological activity	CoA from supplier and check analysis
Chol-PEG <sub>400</sub> -RGD moisture	Low	Uni-lamellarity and morphology could be affected.	CoA from supplier and check analysis
EtOH concentration	High	To be evaluated in DoE.	To be included in DoE.
DMSO concentration	Medium	Stability, enzymatic activity	Previously defined.
Buffer concentration	Medium	To be studied in further steps.	To be defined in further steps of the project.
Membrane components molar ratio	High	Morphology, stability	Previously defined.
Lipid concentration	High	Entrapment efficiency, stability of the solution.	To be included in DoE.
Chol-PEG <sub>400</sub> -RGD concentration	High	Morphology, stability, intracellular penetration	To be included in DoE.
MKC concentration	High	Higher concentration, higher stability and Entrapment.	Previously defined.
GLA concentration	High	Stability, enzymatic activity	To be included in DoE.
Mixing configuration	High	Morphology, stability	Previously defined.
Operator	Low	Low control of the flowrate	Lab scale: Follow the standard protocol and practice on depressurization. Pilot scale: automatic control of depressurization valve.
Stirring of vessel	Low	Enough to obtain a single phase inside the high pressure vessel.	Previously defined, servocontrolled by high pressure stirrer.
Pressure of vessel	Low	Enough to obtain a liquid phase inside the high pressure vessel.	Previously defined, servocontrolled by pump and PIC.
Temperature of vessel	Low	Enough to obtain a liquid phase inside the high pressure vessel.	Previously defined, controlled by heating jacket and TIC.
CO <sub>2</sub> molar fraction	Low	Inside the range of cosolvency.	Previously Defined and controlled by volume, P and T of the pump.
N <sub>2</sub> pressure	Low	10 bar higher than pressure of the vessel, could affect the flowrate.	Defined and controlled by a pressure regulator and PIC
Flowrate	High	Morphology and uni-lamellarity. To be evaluated in DoE.	To be included in DoE.
Collector volume	Medium	Change in flow and mixing between phases.	Previously defined.
Collector temperature	High	GLA degradation depends on temperature and exposition time	Previously defined. Controlled by TIC.
Stirring of the collector	Medium	Change in flow and mixing between phases.	Previously defined.

#### Appendix D. Samples time evolution of mean particle size, PdI, and $\zeta$ -potential

Fig D.1 shows the analysis in time by DLS of the samples. As the Fig D.1. Evolution shows, the mean size of some samples increased during time, mainly explained by the aggregation of the nanovesicles, showing clearly that DOE-006 and DOE-009 were going to sediment. PdI values, remained constant except for the two samples previously mentioned.  $\zeta$ -potential maintained mostly constant with time, although the decrease observed in some cases could be explained because of the change in pH during time caused by the release of dissolved CO<sub>2</sub>.

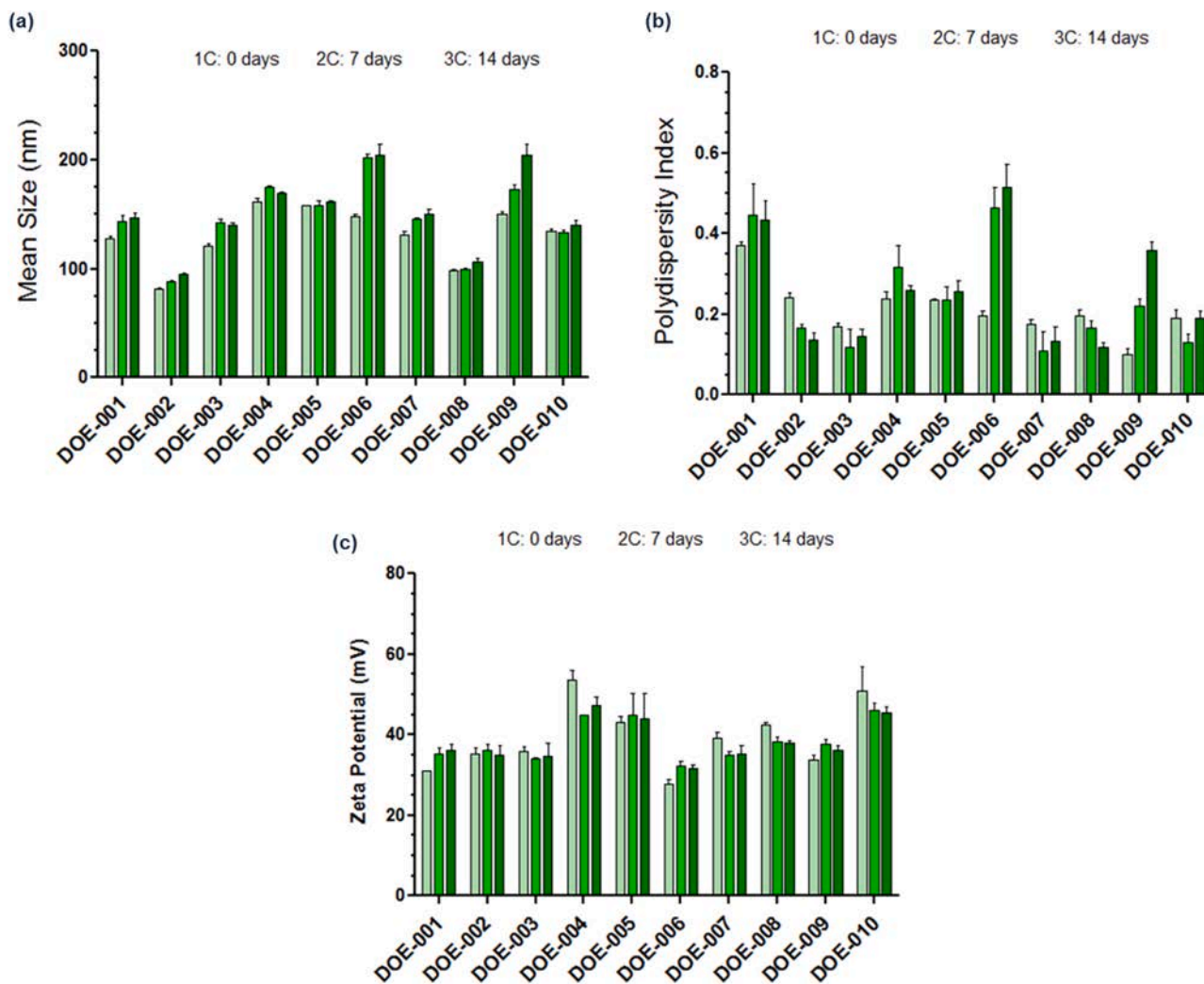


Fig. D.1. Evolution of a) mean particle size, b) PDI, and c)  $\zeta$ -potential over time during 14 days after the production of the samples.

### Appendix E. Modeling and data fitting

The acceptance of the responses obtained was evaluated by means of the statistical parameters predicted by the software  $R^2$ ,  $Q^2$  model validity, and model reproducibility: (i)  $R^2$ : it represents the percent of the variation of the response explained by the model, that is, how well the model fits the data; (ii)  $Q^2$ : it is the percent of the variation of the response predicted by the model according to cross validation. It gives information about how well the model predicts new data. In Table E.1, the values of these statistical parameters are summarized, indicating if the data collected from the experimental results is fitting into a model. Only those CQAs that could be fitted (mean particle size,  $\zeta$ -potential and uni-lamellarity) were included in the model.

**Table E.1**  
Statistical parameters and fitting for the investigated intermediate nanoGLA CQAs.

CQA	$R^2$	$Q^2$	Fitting and model (if applies)
Mean particle size	0.937	0.661	Yes, Size = $2.0 X_1 + 10.6 X_2 + 11.7 X_3 - 2.2 X_4 + 86$
Polydispersity	0.437	0.200	No, a bad correlation and a poor predictive ability of the model were obtained.
$\zeta$ -potential	0.791	0.550	Yes, $\zeta$ -pot = $-19 X_1 + 2.1 X_2 - 10.9 X_3 - 24.5 X_4 + 41$
TSI	0.636	0.200	No, a bad correlation and a poor predictive ability of the model were obtained.
Uni-lamellarity	0.858	0.498	Yes, $f_{single} = 3.3 \cdot 10^{-4} X_1 - 1.8 \cdot 10^{-2} X_2 - 1.1 \cdot 10^{-7} X_3 - 5.7 \cdot 10^{-9} X_4 + 1.0$
Entrapment efficiency	0.420	0.200	No, a bad correlation and a poor predictive ability of the model were obtained.
Enzymatic activity	0.625	0.040	No, it could be explained by the high measurement related variability

### Appendix F. Identified safety issues

Occupational exposure scenarios as well as environmental exposure scenarios were registered, considering different operational conditions. Table F.1 shows the obtained risk rating key for the specific activity and/or process in the DELOS-susp methodology for the preparation of the nanoGLA intermediate, and lists relevant methods to manage the possible risk and decrease its possibility to take place.



Table F.1

Identified safety issues in relation to their severity and likelihood leads to risk rating key.

Activity/Process	Associated Risk(s): Safety issue(s) associated with the activity	Severity: Level of impact	Likelihood: The chances of that risk happening	Method(s) to Manage the Risk: A list of methods you will use to minimize the chances of the risk happening
<b>Preparation of the organic solution</b>	EtOH/DMSO in the nanoformulation	Acceptable	Low	Related to the environment: Solvents to the non-chlorinated solvents waste container. Cholesterol, Chol-PEG <sub>n</sub> -RGD, MKC, and DPPC to the solid chemical waste container.
<b>Weighing solids and preparation of a solution</b>	Dermal/occu pational safety issues during cleaning	Acceptable	Low	Related to workers: Fume hood. Mask, gloves, glasses and lab coat.
<b>Cleaning the laboratory material</b>				Related to workers: Fume hood. Mask, gloves, glasses, and lab coat. Vent and safety valves present in the equipment in case of overpressure
<b>Loading of the vessel, closing and pressurization by adding CO<sub>2</sub></b>	Dermal/occupational safety issues during loading the vessel	Acceptable	Low	Related to workers: Fume hood. Mask, gloves, glasses, and lab coat.
<b>Preparation of aqueous solution</b>	Dermal safety issues during cleaning of the material	Acceptable	Low	Related to workers: Fume hood. Mask, gloves, glasses, and lab coat.
<b>Depressurization and mixing of the organic and aqueous phases</b>	Carbon dioxide poisoning during valve opening	Tolerable	Low	Related to workers: Fume hood. Mask, gloves, glasses and lab coat. Vent and safety valves. Filters for carbon dioxide exhaust expelled to the environment have to be considered in larger scales.
<b>Collecting the final product and storage</b>	Cold Burn during lyophilization	Acceptable	Low	Fume hood. Mask, gloves, glasses and lab coat.

## References

- [1] N. Ventosa, J. Veciana, S. Sala, M. Cano, Patent Application EP 1843836, 2012.
- [2] I. Cabrera, E. Elizondo, O. Esteban, J.L. Corchero, M. Melgarejo, D. Pulido, A. Córdoba, E. Moreno, U. Unzueta, E. Vazquez, I. Abasolo, S. Schwartz, A. Villaverde, F. Albericio, M. Royo, M.F. García-Parajo, N. Ventosa, J. Veciana, Multifunctional nanovesicle-bioactive conjugates prepared by a one-step scalable method using CO<sub>2</sub>-expanded solvents, *Nano Lett.* 13 (2013) 3766–3774, <https://doi.org/10.1021/nl4017072>
- [3] N. Grimaldi, F. Andrade, N. Segovia, L. Ferrer-Tasies, S. Sala, J. Veciana, N. Ventosa, Lipid-based nanovesicles for nanomedicine, *Chem. Soc. Rev.* 45 (2016) 6520–6545, <https://doi.org/10.1039/c6cs00409a>
- [4] I. Cabrera, I. Abasolo, J.L. Corchero, E. Elizondo, P.R. Gil, E. Moreno, J. Faraudo, S. Sala, D. Bueno, E. González-Mira, M. Rivas, M. Melgarejo, D. Pulido, F. Albericio, M. Royo, A. Villaverde, M.F. García-Parajo, S. Schwartz, N. Ventosa, J. Veciana,  $\alpha$ -Galactosidase-A loaded-nanovesicles with enhanced enzymatic activity and intracellular penetration, *Adv. Healthc. Mater.* 5 (2016) 829–840, <https://doi.org/10.1002/adhm.201500746>
- [5] S. Alipourfetrati, A. Saeed, J.M. Norris, A review of current and future treatment strategies for fabry disease: a model for treating lysosomal storage diseases, *J. Pharmacol. Clin. Toxicol.* 3 (2015).
- [6] M. Solomon, S. Muro, Lysosomal enzyme replacement therapies: historical development, clinical outcomes, and future perspectives, *Adv. Drug Deliv. Rev.* 118 (2017) 109–134, <https://doi.org/10.1016/j.addr.2017.05.004>
- [7] J. Tomsen-Melero, S. Passemard, N. García-Aranda, Z.V. Díaz-Rascos, R. González-Rioja, J.N. Pedersen, J. Lyngso, J. Merlo-Mas, E. Cristóbal-Lecina, J.L. Corchero, D. Pulido, I. Portnaya, E. Crist, L. Corchero, D. Pulido, P. Cámara-Sánchez, I. Portnaya, I. Ionita, S. Schwartz, J. Veciana, S. Sala, M. Royo, A. Córdoba, D. Danino, J.S. Pedersen, E. González-Mira, I. Abasolo, N. Ventosa, Impact of chemical composition on the nanostructure and biological activity of  $\alpha$ -galactosidase-loaded nanovesicles for fabry disease treatment: impact of chemical composition on the nanostructure and biological activity of galactosidase-loaded nanovesicles for fabry disease treatment, *ACS Appl. Mater. Interfaces* 13 (7) (2021) 7825–7838, <https://doi.org/10.1021/acsami.0c16871>
- [8] International Council of Harmonisation, Q9 - Pharmaceutical Development, 2009.
- [9] International Council of Harmonisation, Q9 - Quality Risk Management, 2005.
- [10] International Council of Harmonisation, Q10 - Pharmaceutical Quality System, 2008.
- [11] A. Porfire, D.M. Muntean, L. Rus, B. Sylvester, I. Tomuță, A quality by design approach for the development of lyophilized liposomes with simvastatin, *Saudi Pharm. J.* 25 (2017) 981–992, <https://doi.org/10.1016/j.jsps.2017.01.007>
- [12] I. van de Poel, Z. Robaey, Safe-by-design: from safety to responsibility, *Nanoethics* 11 (2017) 297–306, <https://doi.org/10.1007/s11569-017-0301-x>
- [13] R. Purohit, A. Mittal, S. Dalela, V. Warudkar, K. Purohit, S. Purohit, Social, environmental and ethical impacts of nanotechnology, *Mater. Today Proc.* 4 (2017) 5461–5467, <https://doi.org/10.1016/j.matpr.2017.05.058>
- [14] E. Cristóbal-Lecina, D. Pulido, P. Martín-Malpartida, M.J. Macias, F. Albericio, M. Royo, Synthesis of stable cholesteryl-polyethylene glycol-peptide conjugates with non-disperse polyethylene glycol lengths, *ACS Omega* 5 (2020) 5508–5519, <https://doi.org/10.1021/acsomega.0c00130>
- [15] D. Danino, Cryo-TEM of soft molecular assemblies, *Curr. Opin. Colloid Interface Sci.* 17 (2012) 316–329, <https://doi.org/10.1016/j.cocis.2012.10.003>
- [16] G. Pabst, M. Rappolt, H. Amenitsch, P. Laggnner, Structural information from multilamellar liposomes at full hydration: full q-range fitting with high quality X-ray data, *Phys. Rev. E - Stat. Phys. Plasmas Fluids Relat. Interdiscip. Topics* 62 (2000) 4000–4009, <https://doi.org/10.1103/PhysRevE.62.4000>
- [17] R. Hosemann, S.N. Bagchi, The interference theory of ideal paracrystals, *Acta Cryst.* 5 (1952) 612–614.
- [18] M.I. Giannotti, I. Abasolo, M. Oliva, F. Andrade, N. García-Aranda, M. Melgarejo, D. Pulido, J.L. Corchero, Y. Fernández, A. Villaverde, M. Royo, M.F. García-Parajo, F. Sanz, S. Schwartz, Highly versatile polyelectrolyte complexes for improving the enzyme replacement therapy of lysosomal storage disorders, *ACS Appl. Mater. Interfaces* 8 (2016) 25741–25752, <https://doi.org/10.1021/acsami.6b08356>
- [19] M. Kapoor, S.L. Lee, K.M. Tyner, Liposomal drug product development and quality: current US experience and perspective, *AAPS J.* 19 (2017) 632–641, <https://doi.org/10.1208/s12248-017-0049-9>
- [20] FDA, Liposome Drug Products Chemistry, Manufacturing, and Controls; Human Pharmacokinetics and Bioavailability; and Labeling Documentation, 2018.
- [21] European Medicine Agency, Reflection Paper on the Data Requirements for Intravenous Liposomal Products Developed with Reference to an Innovator Liposomal Product, *EMA/Committee Hum. Med. Prod.*, 2013, pp. 1–13 806058/2009/Rev. 02. 44.
- [22] X. Xu, M.A. Khan, D.J. Burgess, A quality by design (QbD) case study on liposomes containing hydrophilic API: II. Screening of critical variables, and establishment of design space at laboratory scale, *Int. J. Pharm.* 423 (2012) 543–553, <https://doi.org/10.1016/j.ijpharm.2011.11.036>
- [23] I.C. Pintre, S.J. Webb, Binding and Reactivity at Bilayer Membranes, 1st ed., Elsevier Ltd, 2013, <https://doi.org/10.1016/B978-0-12-407754-6.00003-X>
- [24] S. Shaker, A. Gardouh, M. Ghorab, Factors affecting liposomes particle size prepared by ethanol injection method, *Res. Pharm. Sci.* 12 (2017) 346–352, <https://doi.org/10.4103/1735-5362.213979>
- [25] G. Pamunuwa, V. Karunaratne, D.N. Karunaratne, Effect of lipid composition on in vitro release and skin deposition of curcumin encapsulated liposomes, *J. Nanomater.* 2016 (2016) 1–9, <https://doi.org/10.1155/2016/4535790>
- [26] N.S. Awad, V. Paul, M.S. Mahmoud, N.M. Al Sawafah, P.S. Kawak, M.H. Al Sayah, G.A. Hussein, Effect of pegylation and targeting moieties on the ultrasound-mediated drug release from liposomes, *ACS Biomater. Sci. Eng.* 6 (2019) 48–57, <https://doi.org/10.1021/acsbomaterials.8b01301>
- [27] M.L. Briuglia, C. Rotella, A. McFarlane, D.A. Lamprou, Influence of cholesterol on liposome stability and on in vitro drug release, *Drug Deliv. Transl. Res.* 5 (2015) 231–242, <https://doi.org/10.1007/s13346-015-0220-8>
- [28] P. Milla, F. Dosio, L. Cattel, PEGylation of proteins and liposomes: a powerful and flexible strategy to improve the drug delivery, *Curr. Drug Metab.* 13 (2011) 105–119, <https://doi.org/10.2174/138920012798356934>
- [29] S. Guner, M.H. Oztop, Food grade liposome systems: effect of solvent, homogenization types and storage conditions on oxidative and physical stability, *Colloids Surf. A Physicochem. Eng. Asp.* 513 (2017) 468–478, <https://doi.org/10.1016/j.colsurfa.2016.11.022>
- [30] D. Carugo, E. Bottaro, J. Owen, E. Stride, C. Nastruzzi, Liposome production by microfluidics: potential and limiting factors, *Sci. Rep.* 6 (2016) 1–15, <https://doi.org/10.1038/srep25876>
- [31] X. Xu, A. Costa, D.J. Burgess, Protein encapsulation in unilamellar liposomes: High encapsulation efficiency and a novel technique to assess lipid-protein interaction, *Pharm. Res.* 29 (2012) 1919–1931, <https://doi.org/10.1007/s11095-012-0720-x>
- [32] N. Dan, D. Danino, Structure and kinetics of lipid-nucleic acid complexes, *Adv. Colloid Interface Sci.* 205 (2014) 230–239, <https://doi.org/10.1016/j.cis.2014.01.013>
- [33] C. Schimpel, S. Resch, G. Flament, D. Carlander, C. Vaquero, I. Bustero, A. Falk, A methodology on how to create a real-life relevant risk profile for a given nanomaterial, *J. Chem. Heal. Saf.* 25 (2018) 12–23, <https://doi.org/10.1016/j.jchas.2017.06.002>